The Origin and Geochemistry of the Metalliferous Sediments of the Troodos Massif, Cyprus

John F. Boyle BSc

THESIS SUBMITTED FOR THE DEGREE OF DOCTOR OF PHILOSOPHY
AT THE UNIVERSITY OF EDINBURGH
JUNE 1984

CONTENTS

		PAGE
ACKNOWLEDGEMENTS		1
ABSTRACT		4
CHAPTER 1	Metalliferous sediments and the Troodos Ophiolite.	5
CHAPTER 2	Ocean crustal setting of the Troodos Metalliferous sediments.	8
2.1	Tectonic setting - a geochemical debate	8
2.2	Environment of formation	11
2.3	Oceanic metamorphism of the igneous complex	12
2.3.1	Mid-Ocean ridge metamorphism	13
2.3.2	Layered metamorphism in the Troodos Ophiolite	14
2.3.3	Bulk chemical changes during alteration of the Troodos igneous basement	15
2.3.4	Conclusion	17
2.4	An ocean origin for the Troodos metalliferous sediments: a conclusion	18
CHAPTER 3	The relationship of the metalliferous sediments with the extrusive sequence	19
3.1	The geology of the Mathiati-Margi area	19
3.1.1	Introduction	19
3.1.2	Lithostratigraphy	21
3.1.3	Lava morphology	21
3.1.4	Interlava sediments	23
3.1.5	Supralava sediments	25
3.1.6	Fault stages	25
3.2	Discussion	28
3.2.1	Stages of spreading	28
3.2.2	Metallogenesis of modern mid-ocean ridges	30
3.2.3	Implications for the Troodos	31
3.3	Conclusion	34

PAGE

CHAPTER 4 The interlava metalliferous sediments of the Troodos Ophiolite 36

4.1 The sulphide ore bodies 36

4.1.1 Introduction 36

4.1.2 Ore body location with respect to the volcanic stratigraphy 37

4.1.3 The relationship of mineralisation to structure. 38

4.1.4 Lateral distribution of sulphide ore 38

4.1.5 Ore texture, mineralogy and chemistry 39

4.1.6 Summary 41

4.2 The oxide sediments 42

4.2.1 Definitions of umber and ochre 42

4.2.2 Field relations and petrography 43

4.2.2.1 Ochre 44

4.2.2.2 Interlava umbers 45

4.2.2.3 Interpillow oxide sediments 47

4.2.3 Mineralogy 51

4.2.4 Chemical characteristics and variations of the oxide facies sediments 54

4.2.4.1 General statement 54

4.2.4.2 Ochres 54

4.2.4.3 Interpillow oxide sediment 54

4.2.4.4 Interlava umber 56

4.2.5 Simplification of chemical variation : identification of independent chemical components 57

4.2.6 Vertical and horizontal distribution of chemical components 61

4.2.7 Factor analysis and multiple regression 61

4.2.8 Trace element distribution 62

4.2.8.1 Interelement relationships 63

4.2.8.2 Trace element composition of major element components 68

PAGE

4.3 Discussion : Inter-relationships and origin of the interlava sediments 69

4.3.1 Sources for the compositional components 69

4.3.2 Relative accumulation rates 73

4.3.3 Secondary modification of mineralogy and chemistry 74

4.3.4 Inter-relationship of sediment types 76

4.3.5 Distribution of metalliferous sediments in the Troodos Massif 77

4.3.6 Dispersal of hydrothermal effluent 77

4.4 Conclusions 78

CHAPTER 5 Supra-lava metalliferous sediments 80

5.1 Introduction 80

5.2 Succession and physical characteristics of the supra-lava metalliferous sediment 81

5.2.1 Succession 81

5.2.2 Lithological types 82

5.2.2.1 Umber 83

5.2.2.2 Clay-rich umber 85

5.2.3 Sites of metalliferous sediment accumulation 87

5.2.4 Modification of umber through loading compaction 88

5.2.5 Origin of the MnO_2 - palygorskite veins 91

5.2.6 Origin of the secondary cherts 91

5.2.7 Manganese depleted umber 92

5.2.8 Sub-umber bleaching of lava 93

5.2.9 Sediment inter-relationships 93

5.3 Mineralogy of the umber 94

5.3.1 Techniques 95

5.3.2 Mineral characteristics 96

5.3.3 Lateral variation of mineral abundance 104

5.4 Geochemistry of the supra-lava metalliferous sediments 106

5.4.1 Bulk composition of the sediments 106

5.4.2 Inter-deposit variation 107

PAGE

5.4.3 Intra-locality variations 108
5.4.4 Defocused beam electron micro-probe study 110
5.4.5 Chemical variations of the Margi umber deposit : inter-element correlations 112
5.4.6 Major element component compositions 115
5.4.7 Trace element geochemistry. Studies from Skouriotissa, Analiondas and Margi 117
5.4.7.1 Selective leaching studies 118
5.4.7.2 Inter-element correlations - The Margi umber 120
5.4.7.3 Trace elements in relation to the major element phases 130
5.4.8 Isotope geochemistry 132
5.5 Discussion 134
5.5.1 Modern oceanic metalliferous sediments 134
5.5.2 Models for the origin of the umber 136
5.5.3 Variations in trace element enrichment in the manganese phase : The origin of the manganese 138
5.5.4 Trace element enrichment of the phosphate 139
5.5.5 The iron-rich component : composition and origin 140
5.5.6 Origin of lithogenous component 141
5.5.7 Diagenesis 142
5.5.8 Comparison with modern metalliferous sediments 145
5.5.9 Relationships of umber with sulphide 148
5.5.10 Depositional model for the umber 148
5.6 Conclusions 152

CHAPTER 6 Geochemistry and mineralogy of the non-metalliferous cover sediments 154
6.1.1 Introduction 154
6.1.2 Nomenclature of the cover sediments 154
6.2 Sedimentary cover succession and lateral variations 155
6.2.1 Volcaniclastic sediments 155
6.2.2 Radiolarites and radiolarian mudstones 156
6.2.3 Upper Cretaceous chalks 156
6.3 Mineralogy and petrography 157

		Page
6.3.1	Sandstones of the Paphos District	157
6.3.2	Bentonitic clays	157
6.3.3	Radiolarian cherts	160
6.3.4	Basal chalks	160
6.4	Geochemistry of the sediments	161
6.4.1	Mean chemical composition of the sediments	161
6.4.2	Regionl variations in composition	161
6.4.3	Inter-element correlation study: Margi sediments	162
6.4.3.1	Major element components	162
6.4.3.2	Factor analysis	163
6.4.3.3	Trace element associations - Margi sediments	163
6.4.3.4	Trace element associations - a summary	170
6.5	Discussion	172
6.5.1	Chemical composition of the lithogenous component. Possible terrigenous sources	172
6.5.2	Vertical changes in accumulation rate	173
6.5.3	The composition of the manganese component. Accumulation rates of the bentonitic clays	173
6.5.4	Siliceous sediments - composition and origin	175
6.5.5	Carbonate-bearing sediments	176
6.5.6	Diagenesis	176
6.6	Conclusions	178
CHAPTER 7	The sedimentary geochemistry of the Troodos Ocean	180
7.1	Palaeogeographical aspects of the Troodos Ocean	180
7.2	Sediment sources	181
7.3	Geochemistry of the oceanic sediments	184
7.4	Discussion	188
7.4.1	Major elements	188
7.4.2	Trace elements	190
7.4.3	Hydrothermal contribution	190
7.5	Conclusions	191
CHAPTER 8	The origin and geochemistry of the Troodos metallifeorus sediments : a conclusion	193
APPENDIX		198
BIBLIOGRAPHY		

Publication: Boyle, J.F. and Robertson, A.H.F. 1984. Evolving metallogenesis of the Troodos Spreading Axis.

ACKNOWLEDGEMENTS

I am greatly indebted to my supervisors, Drs A.H.F. Robertson and N.B. Price, for their encouragement and assistance during this project. I thank Professors G.Y. Craig, Sir Frederick Stewart and B.G.J. Upton for their backing and making the resources of the geology department at Edinburgh freely available.

Of the others with whom I have had profitable discussion, I particularly thank the following:- Mr G. Aktas (Edinburgh), Dr J.P.N. Badham (Selection Trust), Prof J.R. Cann (Newcastle), Mr T. Clube (Edinburgh), Mr D. Cooper, (Edinburgh), Mr J.A. Craven (Edinburgh), Dr J.E. Dixon (Edinburgh), Mr S. Eaton (Edinburgh), Prof I.G. Gass (Open University),Mr K.M. Greig (Edinburgh) Mr A.E.S. Kemp (Edinburgh), Mr A.R. Martin (Edinburgh), Mr N.R. Moles (Edinburgh), Mr D.R.M. Pattison (Edinburgh), Dr J.A. Pearce (Newcastle), Mr S.C.R. Rainey (Edinburgh), Prof M.J. Russell (Strathclyde), Mr G.B. Shimmield (Edinburgh), Pauline L. Smedley (Edinburgh), Mr A. Walker (Edinburgh), Dr P. Williams (Goldsmith's College), Dr D.A. Winter (B.P. Exploration).

I am greatful to Dr. H. Friedrichson and the technicians of the ABT Geochemie, Mineralogisches Institut, Tubingen, for undertaking oxygen isotope determinations.

In addition I would like to thank the various members of the International Crustal Research Drilling Group, for assistance in the field and helpful discussion, particularly Mr J.M. Mehegan (Dalhousie), Prof P.T. Robinson (Dalhousie) and Prof F.J. Vine (East Anglia).

I am indebted to Dr G. Constantinou, Dr A. Panayotou, Dr C. Xenofontos, of the Cyprus Geological Survey Department, and Dr N Adamides (Hellenic Mining Company), for guidance in the field, and and for friendly support for the duration of my work in Cyprus.

In the laboratory, I have received invaluable assistance from Mr G.R. Angell with X-ray diffraction, Dr P.G. Hill and Mr D. Russell with electron micro-probe, Mrs D.E. James and Dr J.G. Fitton with X-ray fluorescence, Aruna Varma, of the Department of Chemistry with the TGA and Dr J. Miller with cathode luminescence. I am particularly indebted to Mr M.J Saunders, for assistance with wet chemical analyses and for stimulating discussion on a variety of topics. For thin section preparation and general technical advice I thank Mr C. Chaplin and Mr K. Cameron and Mrs F.M. Tullis. For photography I thank Mrs D. Baty and Mr C. Chaplin and Mr R. Brown.

The preparation of this thesis has been greatly aided by the skill and enterprise of my typist, Heather A. Hooker.

This work was carried out under the tenure of a Natural Environment Research Council Grant, and completed with the assistance of the Department of Health and Social Security, both are gratefully acknowledged.

Note on co-authorship

Chapter 3 was jointly written with A.H.F. Robertson. The field work, the literature survey concerning modern mid-ocean ridge morphology, and diagram preparation, were undertaken by J.F. Boyle.

DECLARATION

I declare that this thesis has been composed by myself, and that the work is my own except where otherwise indicated and duly acknowledged.

John F. Boyle

"Well, yes: he may have done all that, but there's no proof that he did: I am beginning to believe that nothing can ever be proved. These are reasonable hypotheses which take the facts into account: but I am only too well aware that they come from me, that they are simply a way of unifying my own knowledge. Not a single glimmer comes from Rollebon's direction. Slow, lazy, sulky, the facts adapt themselves at a pinch to the order I wish to give them, but it remains outside of them. I have the impression of doing a work of pure imagination. And even so, I am certain that characters in a novel would appear more realistic, or in any case would be more amusing."

Nausea

Jean-Paul Sartre

ABSTRACT .

The Troodos ophiolite includes a diverse assemblage of metalliferous sediments which are very similar in field relations and chemistry to those observed presently forming at modern oceanic spreading axes. Sulphide-producing hydrothermal vents were initiated at the axis of a narrow well-defined median valley, and persisted off axis, almost to the limits of the volcanically active zone. Direct oxidative erosion of the sulphide deposits led to nearby formation of iron oxide sediments locally rich in sulphide detritus (ochres). Iron in the discharging vent fluids became oxidised in the water column, and was more widely dispersed. In volcanically active regions, erupting lava disrupted the sediment, dispersing it through cooling-fractures and pillow interstices. This local rapid burial prevented total dissolution of pelagic carbonate, but generally caused chemical reduction with loss of manganese oxides. Ferromanganese sediments extremely similar to those observed at the crest of the East Pacific Rise were preserved (umbers) in fault-hollows within the lavas during longer quiescent periods. Individual source vents were of limited life, ceasing abruptly after periods of relatively stable activity. Away from the axis, non-metalliferous sediments accumulated free of admixed hydrothermal material.

Subsequent alteration of the sediment was promoted by two processes. First, ageing and gradual burial of the basal sediment, and secondly, exposure of the deeper sediments to both widespread low temperature, and localised high temperature, hydrothermal alteration. Temperatures did not normally exceed 100°C, but in the vicinity of high temperature hydrothermal conduits(up to c. 350°C), silicification has taken place (jaspers).

The chemical composition of the sediment can be described in terms of mixing of the various sediment sources, with modification of some trace element abundances through diagenetic processes.

A great similarity to modern mid-ocean ridge sediments is observed both in terms of geometric relationship to the palaeo-ridge, and in chemical and mineralogical composition. Minor deviations may be explained by the different basement composition, ocean circulation, relative position of the carbonate compensation depth, and aluminosilicate accumulation rates. In Cyprus the well exposed relationships thus contribute directly to an understanding of mid-ocean ridge processes.

CHAPTER 1

METALLIFEROUS SEDIMENTS AND THE TROODOS OPHIOLITE

This study is concerned with the origin of the various metalliferous sediments which occur within and as part of the sedimentary cover of the Troodos ophiolite complex Cyprus, a subject inseparable from the problem of the origin of the ophiolite as a whole. The geology of the Troodos massif and current views concerning its genesis are outlined below.

The Troodos massif comprises Upper Cretaceous basic and ultrabasic igneous rocks (Vine et al., 1973; Mantis, 1970) with a cover of Upper Cretaceous and younger sedimentary rocks. A complete ophiolite sequence is present ranging downwards from pelagic sediments, through pillow lavas, a sheeted dyke complex, cumulate gabbros and peridotites, to tectonised harzburgites. The succession is presently exposed in a crudely concentric outcrop pattern, as a result of the late uplift of the central portion (Fig. 1.1). The extrusive sequence within, and above, which the metalliferous sediments are found, is thus exposed at the periphery of the exposure.

A schematic cross-section of the igneous sequence is shown in Fig. 1.1. The extrusive rocks at the top of the succession, designated "pillow lavas" on the cross-section are a heterogeneous assemblage of pillow lavas (the predominant morphology), sheetflows, hyaloclastics, with numerous small intrusive bodies and dykes. The total thickness is between 1000 and 1500 metres (Wilson, 1959; Gass, 1960; Schmincke et al., 1983). The lavas fall compositionally into two lava suites: an andesite-dacite-rhyolite assemblage, and a basalt-basaltic andesite assemblage (Robinson et al., 1983). Downwards the dykes increase in abundance, passing into a zone of sheeted dykes in which there are no intervening host rocks (Kidd, 1977). Passing downwards again, screens of plutonic rocks appear between the dykes, and after a zone of transition, a region composed of isotropic gabbroic, ferrogabbroic, dioritic, tonalitic and trondhjemitic intrusives is entered. These overlie gabbros and

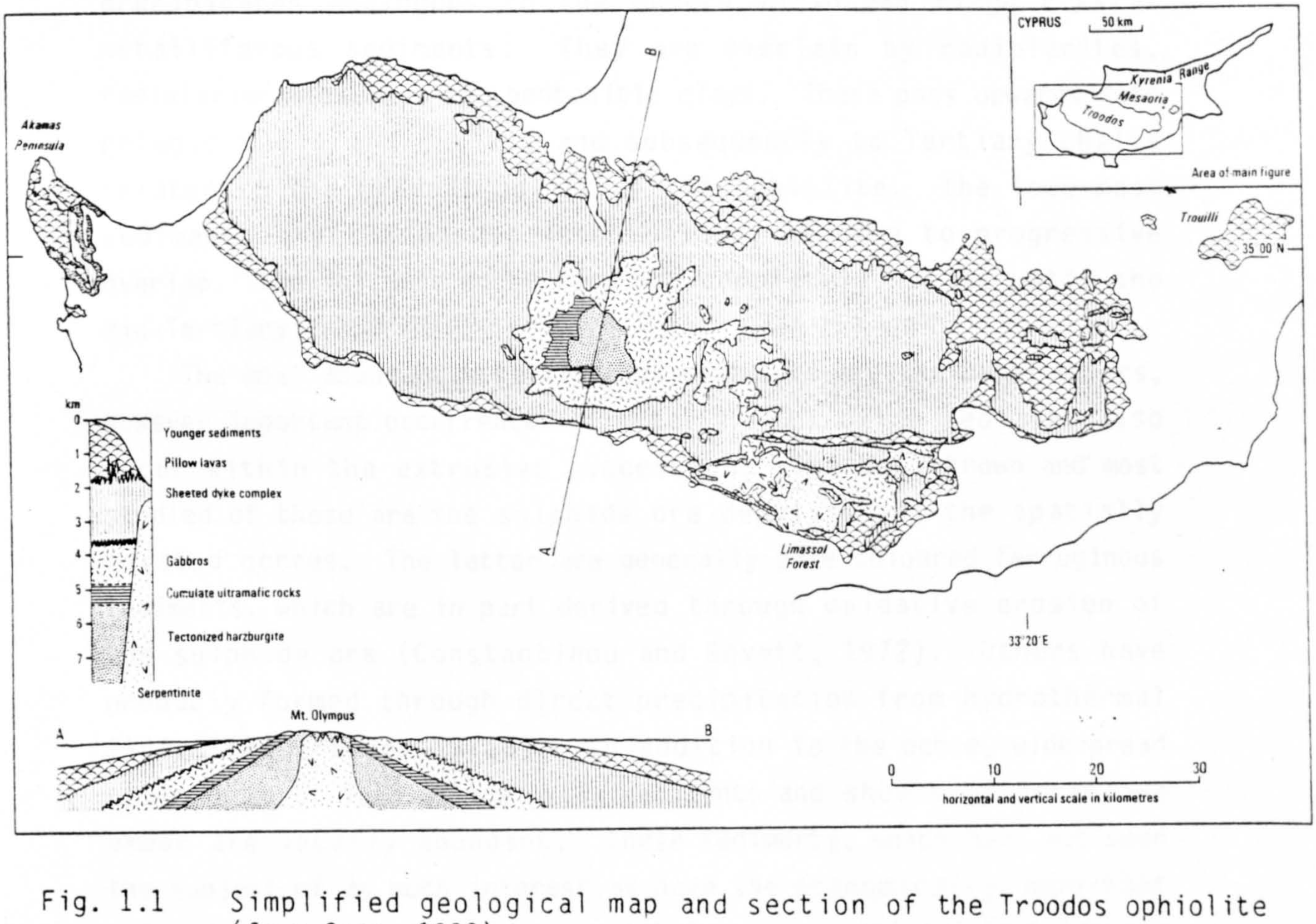

Fig. 1.1 Simplified geological map and section of the Troodos ophiolite (from Gass, 1980).

peridotites of cumulate origin, and below these, tectonised harzburgites with a gneissic foliation and lineation, incorporating lenticular pods of dunite. The chemical composition of the igneous rocks and aspects of the hydrothermal metamorphism are discussed in Chapter 2 sections 2.1, 2.3.1. Contained in the upper parts of the extrusive sequence are massive sulphide ore bodies, with stockwork zones passing to deeper levels in the lavas (Constantinou, 1980).

The pelagic sedimentary cover to the ophiolite is described by Robertson and Hudson (1974). A simplified cross-section is shown in Fig. 1.2. The first deposits to accumulate on the irregular volcanic basement, are the ferromanganese umbers, chemical precipitates analogous to the modern mid-ocean ridge crestal metalliferous sediments. They are overlain by radiolarites, radiolarian mudstones and bentonitic clays. These pass upwards into pelagic marls and chalks, and subsequently to Tertiary chalks related to the gradual uplift of the ophiolite. The lowermost sediments are all ponded into hollows, leading to progressive overlap. The volcanic rocks were not completely buried until the mid-Tertiary.

The most abundant metalliferous sediments are the basal umbers, however important occurrences of metalliferous oxide sediment also occur within the extrusive succession. The best known and most studied of these are the sulphide ore deposits and the spatially related ochres. The latter are generally pale coloured ferruginous sediments, which are in part derived through oxidative erosion of the sulphide ore (Constantinou and Govett, 1972). Others have probably formed through direct precipitation from hydrothermal fluids (Robertson, 1976a). In addition to the ochre, widespread occurrences of interpillow oxide sediments and sheets of interlava umber are locally abundant. These sediments, which have not been the subject of as much interest as have the economically important sulphides or related ochres, constitute a compositional link between the latter and the supralava umbers.

Interest in the geochemistry and origin of the Cyprus oxide metalliferous sediments stems from their striking similarity in both composition and geological setting to the iron and manganese rich sediments found at modern mid-ocean ridges. That accumulation of

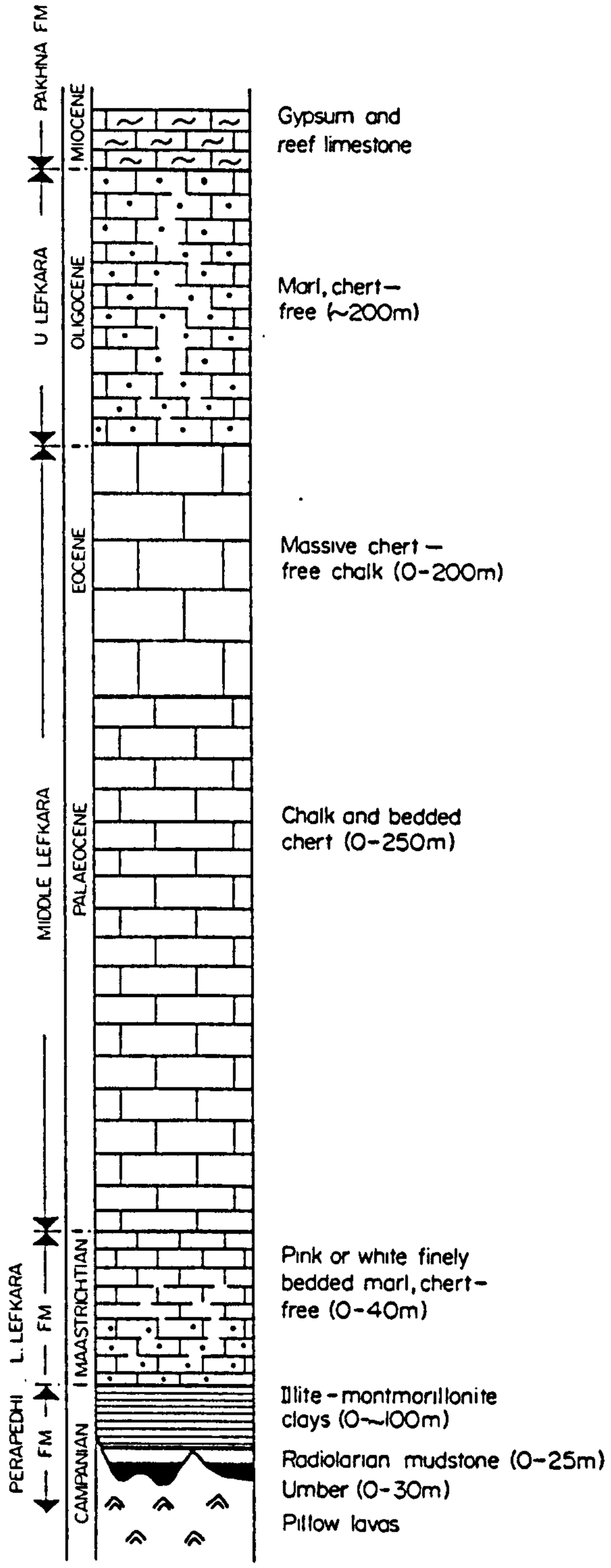

Fig. 1.2

Generalised stratigraphic section of the Troodos supralava sediments. (After Robertson and Hudson, 1974)

such sediments at mid-ocean ridges occurred in the geological past is indicated by the existence of basal metal enrichments in sediments as old as mid Cretaceous (Cronan, 1976) in the eastern Pacific. These older sediments can only be sampled by drilling, and though the modern crestal sediments are accessible by comparison, diving, drilling or dredging are necessary. In Cyprus, Upper Cretaceous crestal metalliferous sediments, of the Tethyan ocean, are well exposed. In contrast with most ophiolites uplift has not involved metamorphism of the overlying sediments - minor loading compaction being the only observable deformation. Thus the Troodos ophiolite is an ideal location in which to examine the field relations and chemical variations, of mid-ocean ridge metalliferous sediments.

Before describing and discussing the metalliferous sediments, the problem of just how "oceanic" the Troodos ophiolite was, must be addressed, and this is the subject of the following chapter. In Chapter 3, the relationship of the metalliferous sediments to the extrusive sequence is examined. In Chapters 4, 5 and 6, the interlava metalliferous sediments, supralava metalliferous sediments, and the supralava pelagic sediments, respectively are described and discussed. Each of these chapters involves a description of field data, mineralogy and chemistry. In Chapter 7, the chemical variations of all the sediments, and the controls over these variations are discussed.

CHAPTER 2

OCEAN CRUSTAL SETTING OF THE TROODOS METALLIFEROUS SEDIMENTS

Introduction

It is now widely accepted that the Troodos ophiolite complex is a fragment of an ancient oceanic lithospheric plate (Gass and Masson-Smith, 1963; Gass, 1968; Moores and Vine, 1971). There is however much debate as to the precise original tectonic setting (Gass and Smewing, 1973; Miyashiro, 1973; Pearce 1975, 1980; Smewing et al., 1975; Cameron et al., 1980; Robinson et al., 1983; Schmincke et al., 1983). Before describing and discussing the various metalliferous sediments it is important that their environment of formation is properly evaluated.

The discussion is divided into two parts. The first deals with arguments concerning the original tectonic setting. After reviewing the development of ideas, current interpretations are compared, and points relevant to the metalliferous sediments are considered. In the second part, more general geological aspects of the environmental setting, such as water depth, sediment type, and basement heat flow are examined.

2.1 TECTONIC SETTING - A GEOCHEMICAL DEBATE

An oceanic spreading axis model for the Troodos ophiolite was first suggested by Gass and Masson-Smith (1963) and received support from Gass (1968) and Moores and Vine (1971). Critical evidence comprised the broad chemical similarity with mid-ocean ridge basalts, and the presence of a sheeted dyke complex requiring 100% extension. An alternative interpretation was offered by Miyashiro (1973) who showed that the major element composition of one third of the analysed samples fell on a calc-alkaline trend, and suggested an island arc origin. This was severely criticised by Gass et al. (1975) on the grounds that the well documented metasomatic alteration of the lavas invalidated the use of major element

variation diagrams, and that the interpretation was incompatible with all the geological and geophysical data, notably the presence of the sheeted dyke complex.

Gass and Smewing (1973) were the first to suggest that the Upper Pillow Lavas might have been erupted in a different tectonic setting. They noted the chemical affinities of the Lower Pillow Lavas with the intrusive complex, and termed these together the Axis Sequence, but suggested that the Upper Pillow Lavas might have been erupted as off axis volcanism akin to that of ocean islands. Pearce (1975) applied an empirical chemical discriminant method to the lavas, based on alteration resistant trace elements (after Pearce and Cann, 1973). The interpretation was similar to Gass and Smewing (1973) in placing the two lava suites in different tectonic settings, but importantly identified a chemical affinity with island arc tholeiites. The axis sequence was found to lie compositionally between mid-ocean ridge basalt and island arc tholeiite, and the Upper Pillow Lavas more strongly like the latter. This chemical evidence was reconciled with the geological data by invoking back arc spreading with partial melts influenced by water released from a subducting plate. The Upper Pillow Lavas were interpreted as an incipient island arc, forming in response to hydrous melting of depleted mantle.

Smewing et al. (1975) recognised that in places a complete continuum of composition existed through the lavas, and argued on the strength of this, and on the constancy of dyke directions through the sequence, that all eruption had occurred in a single tectonic setting - whatever that might actually be.

Both Pearce (1975) and Smewing et al. (1975) emphasise the importance of hydrous melting to produce the compositions required. Pearce (1975) suggests that the early lavas were derived by water-undersaturated partial melting, and that the Upper Pillow Lavas were derived later by water-oversaturated partial melting of the already depleted source region. It is difficult to reconcile this model with eruption of both lava suites in the same tectonic setting. Smewing et al. (1975) propose a petrogenetic model involving sequential extraction of partial melts from a progressively depleted source region migrating away from the axis.

They are in agreement with Pearce (1975) in regarding the original setting as a marginal basin.

Cameron et al. (1980) draw attention to the petrographic and chemical similarity of some of the Troodos lavas with boninites. They agree with the petrogenetic model of Smewing et al. (1975), though further emphasising the importance of water, and cite in support the experimental work of Green (1976). Green obtained boninite-like compositions during hydrous melting of pyrolite at 1200°C and 10 kbars. There is unfortunately some uncertainty over the original tectonic setting of boninite occurrences, both incipient island arcs and fore-arc regions being possible.

The major element chemistry of the lavas, neglected since the early 1970's, has been re-investigated by several parties working in association with the International Crustal Research Drilling Group. Importantly, samples of petrographically fresh glass - subsequently proved to be unaltered using oxygen and strontium isotopes - were analysed using electron micro-probe. The study identified two suites of lavas, a lower andesite-dacite-rhyolite assemblage, and an upper basalt-basaltic andesite assemblage with high MgO and low TiO_2 contents (Robinson et al., 1983). The former is interpreted as an evolved arc-tholeiite suite, and the similarities of the latter with boninites is confirmed. In the area first studied, the presence of the more primitive lavas on top of those more fractionated led Schmincke et al. (1983) to suggest eruption in a broad zone of accretion located above a subduction zone. However results from other areas (J. Malpas and J.A. Pearce, conference report 1984) indicate that these two lava suites may be erupted in the reverse order. This suggests that two independent magma sources exist; sequential extraction from a single source as proposed by Smewing et al. (1975) is unlikely.

The interpretation favoured by the geochemists is that the Troodos ophiolite formed by back-arc spreading within a larger normal ocean basin in response to the early stages of northward subduction. It is argued that the newly formed hot atypical crust was obducted, and that the cooler more normal ocean crust was preferentially destroyed (J.A. Pearce, pers. comm.). From the geological point of view, it is noteworthy that the Mesozoic

sedimentary sequences in SW Turkey, Syria, the Levant and Egypt are of passive margin type. Evidence for subduction and hence pre-existence of a large oceanic plate is not forthcoming.

In conclusion there are several generally accepted observations and some points of uncertainty.

1) The Axis Sequence and the Upper Pillow Lavas were erupted together at some form of spreading axis.
2) At least two separate magma sources are required.
3) Hydrous melting of the source region is required to explain the chemical characteristics of the lavas.
4) There is no consensus over the tectonic setting, except that it was not a large ocean basin.

With reference to the metalliferous sediments the most important point is that a spreading axis origin is inferred from all studies.

2.2 ENVIRONMENT OF FORMATION

The chemical composition of the basement is peculiar, but its physical structure is that of a spreading axis. In the following section other physical characteristics, as can be inferred from studies of the ophiolite, are compared with those of modern spreading axes.

Water Depth

A near 2.6 km water depth is observed at mid-ocean ridges (Sclater et al., 1971). In the past a shallow water depth was favoured for the Troodos ophiolite. Wilson (1958) suggested that some of the volcanic rocks were subaerial implying a shallow water depth for the whole. The highly vesicular character of the lavas supported this (Robertson, 1975). However a greater depth is suggested by fluid inclusion studies and isotopic temperature data. Fluid inclusion homogenisation temperatures for hydrothermal quartz in stockwork zone lavas of 310-350°C were obtained by Spooner and Bray (1977). These temperatures are supported by isotopic studies of the stockwork zones (Heaton and Sheppard, 1977). At Mathiati a

mixed assemblage of fluid and vapour dominated inclusions, all homogenising near to 370°C, indicate that phase separation had occurred at this temperature (Spooner, 1980). Spooner suggests that a confining pressure equivalent to 2.5 km of seawater would be compatible with this phenomenon, though noting that a high gas content would facilitate phase separation and lower the depth estimate. In conclusion, the inferred water depth is that of a normal mid-ocean ridge. The highly vesicular character of the lavas may be explained by the high observed volatile content of the lavas (H.-U. Schmincke, Conference Report, 1984).

Sediment cover

Mid-ocean ridges have a cover of deep-sea pelagic sediments, in addition to any locally derived detrital material, and hydrothermal precipitates. The basal iron enrichment in Cyprus is typical of mid-ocean ridges, but it is important to consider how oceanic in character is the non-metalliferous sediment fraction. Owing to the poor resolution of the biostratigraphical data, a good estimate of the accumulation rate of the overlying sediments has not been obtained. However, it is clear that the non-metalliferous sediments, comprising finely laminated bentonitic clays, with numerous sharks teeth did not accumulate rapidly. They show chemical characteristics of pelagic sediments (Chapter 6, section 6.5.3). In contrast with modern mid-ocean ridges, the Cyprus basal sediments are carbonate-free. Evidence from the interlava sediments and the basal parts of the overlying chalks suggest that this is due to formation of the ophiolite just beneath the carbonate compensation depth (section 4.3.1). This contrast, though interesting, does not rule out an oceanic origin to the massif, as carbonate compensation depths were variable during the end of the Mesozoic and the Tertiary (Robertson and Hudson, 1974).

2.3 OCEANIC METAMORPHISM OF THE IGNEOUS COMPLEX

Mid-ocean ridges have a very characteristic style of metamorphism resulting from the high heat flow and cooling of the crust by hydrothermal circulation. In the following section, ocean floor metamorphic characteristics are summarised, and a comparison

is made with observations from Cyprus. A brief study of the lava alteration in the Akaki River section was undertaken during the beginning of this project to examine a possible relationship between pervasive alteration and areas of mineralisation. The study was abandoned when it became clear that the pervasive low-temperature alteration was not relevant to the umber question. However some interesting results did emerge, and these are briefly described in part of the following section.

2.3.1 Mid-Ocean Ridge Metamorphism

The character of the metamorphism at mid-ocean ridges has been investigated through direct sampling of altered igneous rocks, both dredged and drilled, and through observations of hydrothermal vent waters and their products. Steep geothermal gradients are evidenced by finds of amphibolite facies gabbro exposed along normal faults at the Mid-Atlantic Ridge (Miyashiro et al., 1971; Cann, 1971), and by heat flow measurements (Lister, 1972) which fit simple sea floor spreading models indicating gradients of 500°C/km (Cann, 1974). The dominant heat transfer mechanism is hydrothermal convection, predicted from geophysical measurements (Lister, 1972) and subsequently proven by the discovery of high temperature (c.350°C) hot springs at ridge axes (Spiess et al., 1980; Edmond et al., 1979; Normark et al., 1983).

The hydrothermal activity is responsible for metasomatic alteration of the crust, both by rapid high temperature reactions at depth in the intrusives and along fluid escape channels (Cann, 1979); Edmond et al., 1982) and by slow low-temperature alteration of the higher level extrusives (Baragar et al., 1977; Robinson et al., 1977; Scarfe and Smith, 1977; Pritchard et al., 1979). In addition to this hydrothermal alteration, lavas exposed to the cold ocean water are subject to slow "weathering" (Muehlenbachs and Clayton, 1972; Robinson et al., 1977; Cann, 1979).

A summary of metamorphic facies, is given by Cann (1979). In order of increasing grade these are: brownstone, zeolite, greenschist, amphibolite and gabbro. The brownstone facies, newly defined after recent studies of DSDP drill cores (Cann, 1979) comprises an alteration assemblage of saponites and proto-celad-

onites (high-K high-Fe saponites with chemistry resembling celadonite), occurring in fractures and vesicles and replacing olivines. It is a facies of low temperature ocean floor weathering or cool hydrothermal alteration, which proceeds very slowly.

The formation of these alteration assemblages results in chemical exchange with the reacting fluids. The nature of this exchange differs greatly depending upon the mineral assemblage. The net chemical exchange with seawater can be estimated by considering the composition and volume of exhaled hydrothermal fluids (Edmond, et al., 1982). Thus overall, Mg is lost from the ocean, and Si, Fe, Mn, K and Ca are gained, but locally the reverse may be true. For example in the brownstone facies, Mg is gained by the water and K, Na and Fe are lost (Pritchard, et al., 1979).

2.3.2 Layered metamorphism in the Troodos ophiolite

In the Troodos massif a broadly layered hydrothermal metamorphic sequence is observed, grading from amphibolite facies in the upper part of the plutonic complex, though greenschist facies in the bulk of the sheeted dyke complex, into zeolite facies and low-temperature weathering in the pillow lavas (Wilson, 1959; Gass and Smewing, 1973; Spooner, et al., 1973; Heaton and Sheppard, 1977; Spooner, 1977). Superimposed upon this layering are subvertical zones passing up through the sequence where the high temperature metamorphic assemblages occur surrounded by less altered rocks. The two forms of alteration: the general layered, and the localised, represent respectively areas of downward migrating seawater, and of exiting high-temperature chemically modified seawater.

Throughout most of the extrusive sequence low temperature mineral assemblages are observed, and the downward decrease in degree of oxidation indicates that water was moving downwards (Spooner, 1977). In the uppermost lavas the mineral assemblage is dominated by very fine grained grey and pale-green to brown saponites. Chemically these lie on a trend from pure saponites to a potassium and iron enriched smectite (Fig. 2.1). The latter is chemically identical to celadonite but the X-ray diffraction pattern reveals that it has a smectite- rather than an illite-structure. These minerals are characteristic of the brownstone facies defined

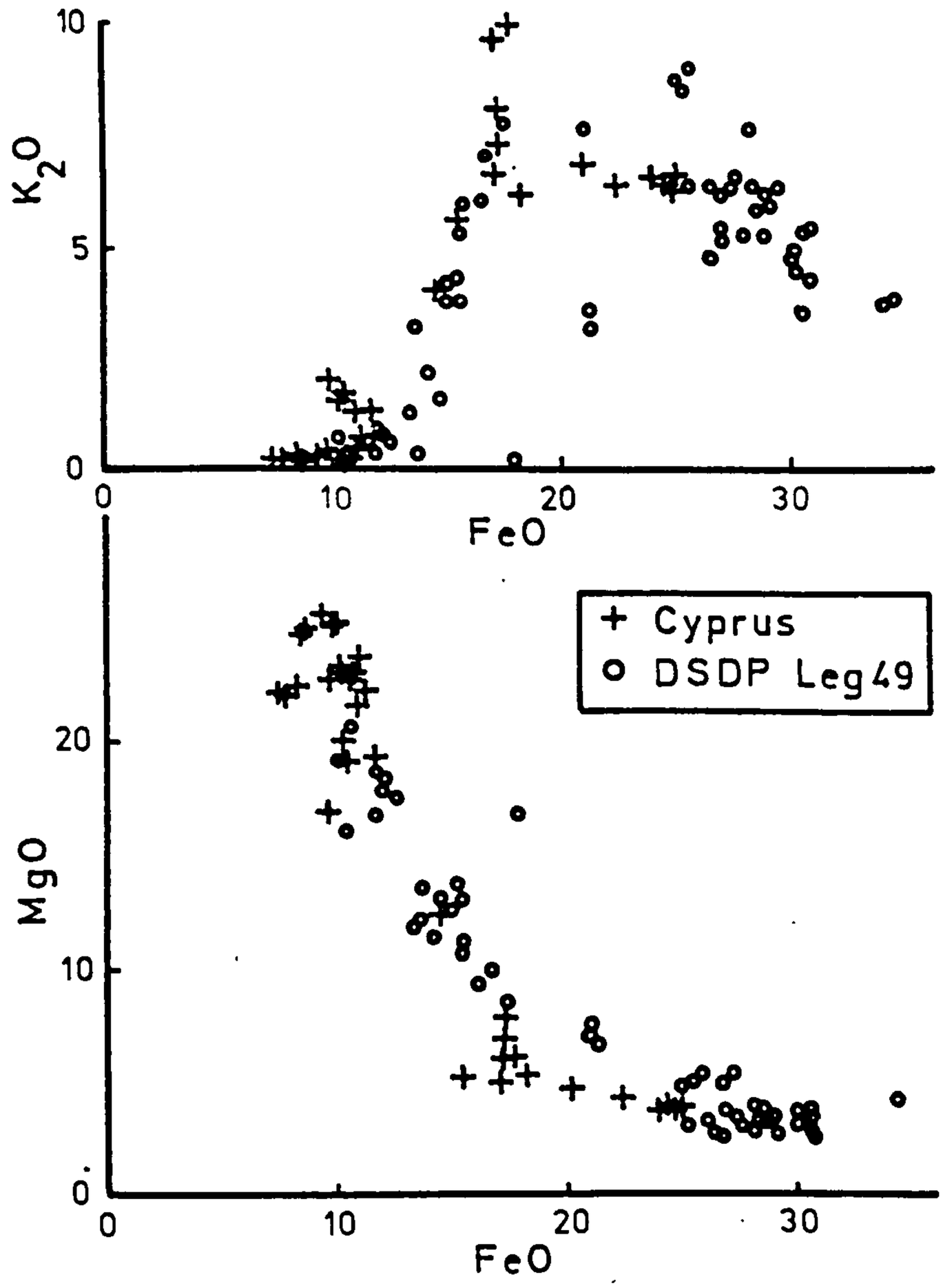

Fig. 2.1 Chemical variation in saponites, proto-celadonites and celadonites, occurring in low-temperature altered lavas. DSDP data from Pritchard et al., (1979). Troodos data are from the Akaki River and the Margi area.

by Cann (1979) from studies of alteration in DSDP drill core. Deeper in the section where chalcedony and zeolites become abundant (Gass and Smewing, 1973) the clays become more coarsely crystalline, and fall clearly into two categories: rosettes of brown saponite crystals, and aggregates of blue-green well crystalline celadonite. These are characteristic of the zeolite facies. The extremely close match of the chemical trends of these clays, to those found in altered ocean crust in the eastern Pacific (Fig. 2.1) (Pritchard, et al., 1979), argue for a very similar environment of formation.

Beneath the sulphide ore bodies, and aligned with faults elsewhere are zones of high temperature alteration, surrounded by brownstone or zeolite facies alteration. The greenschist mineral assemblages in these (Constantinou and Govett, 1973), isotopic equilibrium data (Heaton and Sheppard, 1977) and fluid inclusions studies (Spooner and Bray, 1975) indicate that temperatures of up to 350°C were involved. Fluids of this temperature can only have come from the sheeted dyke complex or deeper, where similar assemblages and palaeo-temperatures are found. The high temperature zones must represent exit pathways for the hydrothermal fluids (Constantinou and Govett, 1973). The temperatures indicated are identical to those observed at the 21° N site on the East Pacific Rise (Spiess, et al., 1980).

The fluid inclusion data (Spooner and Bray, 1975) and the isotope data (Heaton and Sheppard, 1977; Gale et al., 1980) demonstrate that the aqueous fluid was in these respects identical to Cretaceous seawater.

The average geothermal gradient has been estimated from the metamorphic temperatures (Gass and Smewing, 1973) and a minimum value of 150°C/km has been obtained. They conclude that the metamorphism must have occurred within 100km of the ridge axis.

2.3.3 Bulk chemical changes during alteration of the Troodos Ophiolite

Heaton and Sheppard (1977) compared average major element compositions for the altered lavas in the Sheeted Dyke Complex and pillow lavas, with supposed fresh compositions. They observed loss from the rock of Si, Al, Fe, Mg and Ca, and gain in Na, K and water.

This result is surprising in the cases of K and Mg: studies of hydrothermal fluids in the Pacific show that Mg should be gained by the lava and K lost. They emphasise however the problem concerning uncertainty over initial compositions, and in the light of new data on the chemistry of the lavas their reservations have proved well founded. Importantly their choice of a fresh lava composition: an analysis of a glassy rim from the Kambia area (Bear, 1960), is of the low-titanium high-magnesium type described by Robinson et al. (1983) and Schmincke et al. (1983), and is thus not comparable with the altered lavas chosen for the study. Using new data concerning fresh glass compositions (Robinson et al., 1983) and 35 XRF analyses of altered lavas from the Akaki River section, the chemical balance calculations are re-evaluated.

Data

The 35 sample data set from the Akaki River have been subdivided into three groups according to whether they are of the high- or low-titanium lava suites, and type of alteration. The distribution of these lava types along the Akaki River is discussed by Schmincke, et al. (1983). Of the high titanium lavas, none are of the brownstone facies. The greenschist data are taken from Heaton and Sheppard (1977).

Results

In Table (2.1) the compositions of the various subsets are compared. The differences on a weight per cent basis are also shown. Heaton and Sheppard (1977) calculated the differences using a constant volume model (correcting for density differences) but this policy has not been adopted here. The rationale for using a constant volume model is to allow for increasing compaction with depth. However this effect is negligible in comparison with the density variation resulting from inhomogeneous vesicularity. If a density correction were applied in comparing the vesicular margin of a fresh pillow with its core, then large spurious differences would be observed.

Brownstone facies. A significant loss of Si and Ca and gain of Mg and K is observed. This results from the replacement of the lava by smectites which are rich in the latter elements and depleted in the former.

TABLE 2.1

Chemical changes during alteration of the Troodos lavas

Chemical composition of fresh and altered Troodos lavas.

	Low-Ti lavas			High-Ti lavas		
	Fresh N=23	Brownstone N=10	Zeolite N=10	Fresh N=28	Zeolite N=10	Greenschist N=44
SiO_2	55.3 ± 1.4	47.6 ± 1.7	51.3 ± 1.9	59.3 ± 2.9	54.8 ± 4.8	53.0 ± 5.8
Al_2O_3	15.9 ± 0.5	15.7 ± 0.6	14.8 ± 0.5	14.8 ± 0.3	14.8 ± 0.6	14.6 ± 1.3
FeO*	8.4 ± 0.9	8.4 ± 1.0	7.5 ± 0.8	10.6 ± 1.2	9.4 ± 1.5	7.6
MgO	6.4 ± 1.2	7.9 ± 1.6	6.8 ± 1.1	2.7 ± 0.7	3.4 ± 1.0	5.2 ± 1.6
CaO	10.8 ± 1.0	6.8 ± 1.8	9.1 ± 1.2	7.3 ± 1.0	7.0 ± 0.8	6.8 ± 2.9
Na_2O	2.0 ± 0.4	2.0 ± 0.7	2.2 ± 0.7	3.1 ± 0.5	3.1 ± 0.4	3.3 ± 1.4
K_2O	0.15 ± 0.06	1.8 ± 1.3	0.4 ± 0.5	0.43 ± 0.23	0.36 ± 0.40	0.5 ± 0.3

Table of differences

	Brownstone	Zeolite	Zeolite	Greenschist
SiO_2	-7.7 ± 2.2	-4.0 ± 2.4	-4.6 ± 5.6	-6.3 ± 6.5
Al_2O_3	-0.2 ± 0.8	-1.1 ± 0.7	0.0 ± 0.7	-0.2 ± 1.3
FeO*	0.0 ± 1.3	-0.9 ± 1.2	-1.2 ± 1.9	-3.0 ± 1.2
MgO	1.5 ± 1.6	0.4 ± 1.6	0.7 ± 1.2	2.5 ± 1.7
CaO	-4.0 ± 2.1	-1.7 ± 1.6	-0.3 ± 1.3	-0.5 ± 3.1
Na_2O	0.0 ± 0.8	0.2 ± 0.8	0.0 ± 0.6	0.2 ± 1.5
K_2O	1.65 ± 1.3	0.25 ± 0.50	-0.07 ± 0.5	0.07 ± 0.4

Significant changes
At a 95% confidence level

	Brownstone	Zeolite (upper)	Zeolite (lower)	Greenschist
SiO_2	-	-	-	-
Al_2O_3	0	-	0	0
FeO*	0	-	-	-
MgO	+	0	+	+
CaO	-	-	0	0
Na_2O	0	0	0	0
K_2O	+	+	0	0

* Total iron expressed as FeO

Zeolite facies. The two estimates obtained for the different lava suites yield slightly different results. In part this may be caused by the fact that the high-Ti suite lavas occur deeper in the section. In both, Si and Fe show significant losses. For the remaining elements changes are small. Mg shows a gain in both, but is not significant in the low-Ti suite. Ca shows the reverse. The weak gain in K in the low-Ti suite, may indicate the effect of the K-rich smectites.

Greenschist facies. A significant loss in both Si and Fe, and gain in Mg is observed. All other changes are insignificant.

Discussion

The composition of the 350°C water emerging from the hot springs at 21°N on the East Pacific Rise, indicate that a net gain in Mg and loss of Si, Ca, K and Fe should be occurring in the igneous basement. This is broadly what is observed in the lavas from Troodos, with the notable exception of K which nowhere shows a loss. However it is clearly unreasonable to compare the net changes in composition of the Troodos rocks, with the composition of the 21°N fluids which represent only the early stage of alteration. The brownstone facies and zeolite facies alteration proceeds very slowly owing to the relatively low temperatures involved (Muehlenbachs and Clayton, 1972). Thus it is more reasonable only to consider the greenschist facies alteration. Differences still exist as significant changes in Ca and K are not observed. Presumably the greenschist facies rocks have undergone a long period of cooling, during which, considering the ample supply of water, retrogressive alteration may have occurred modifying the chemical composition. Thus although there is some disagreement with the 21°N data, there is no reason to suppose that the chemical reactions involved were different.

2.3.4 Conclusions

The metamorphism of the Troodos Ophiolite can be attributed to processes operative at a mid-ocean ridge. The critical evidence for this conclusion is as follows:

1) A broadly layered metamorphic sequence is observed in which the metamorphic facies are identical to those of mid-ocean ridges. The inferred geothermal gradient is compatible.
2) The agent of metamorphism was Cretaceous seawater driven by hydrothermal convection. The resulting alteration was caused by widespread downward migration of cold seawater, and localised discharge of this after heating and chemical modification. Discharged water was of the same temperature as is observed in the Pacific.
3) Chemical exchange of the seawater with the igneous rocks is compatible with that inferred for the East Pacific Rise, except in the case of potassium which may have been influenced by later retrogressive alteration.

2.4 AN OCEANIC ORIGIN FOR THE TROODOS METALLIFEROUS SEDIMENTS: A CONCLUSION

The geochemical data for the Troodos igneous rocks indicate that they are significantly different from normal mid-ocean ridge basalts. Similarities with arc lavas, and petrogenetic considerations suggest that a subduction zone may have influenced the formation. However there is no doubt that physically the ophiolite was formed at a spreading axis, even if the precise plate tectonic setting is not fully understood.

The inferred water depth is indistinguishable from that of modern spreading axes. The pelagic sedimentary cover differs in respect to the absence of carbonate, but is otherwise also compatible. The metamorphic imprint is also similar to that of a mid-ocean ridge, and the inferred thermal characteristics are identical.

In short, were it not for the peculiarities of the chemical and mineralogical composition of the lavas, there would be no reason to suspect that the Troodos ophiolite was not formed in a normal mid-ocean ridge setting. It is in this framework that interpretation of the metalliferous sediments will be considered.

CHAPTER 3

THE RELATIONSHIP OF THE METALLIFEROUS SEDIMENTS TO THE EXTRUSIVE SUCCESSION

Introduction

It is now firmly established that the various metalliferous sulphide- and oxide-deposits of the Troodos massif were formed by hydrothermal processes at a Late Cretaceous oceanic spreading axis (Constantinou and Govett, 1972, 1973; Robertson, 1976a; Spooner, 1977; Heaton and Sheppard, 1977). An important remaining question is how exactly the oxide- and sulphide-sediments can be related to the stages of construction of a spreading axis. The approach here has been to map the lava succession of a selected area in sufficient detail to identify the main phases of metalliferous accumulation, and to relate these to the structural and volcanic development of the ridge. This is timely in view of the recent upsurge of interest in the Troodos ophiolite, stimulated by the work of the International Deep Crustal Research Group (IDCRG).

Over the last few years new deep ocean exploration techniques have immeasurably increased knowledge of hydrothermal processes at spreading ocean ridges (e.g. Ballard and van Andel, 1977; Lonsdale, 1977a, b). The extremely close parallels which can now be drawn with ophiolites like the Troodos facilitate interpretation of the latter; conversely detailed mapping of ophiolites can add a depth dimension not readily available in the oceans.

3.1 THE GEOLOGY OF THE MATHIATI-MARGI AREA

3.1.1 Introduction

The Troodos massif has long been recognised as an intact ophiolite succession created at some form of Late Cretaceous spreading axis (Gass 1968; Moores and Vine, 1971), although the exact tectonic setting remains controversial (e.g. Pearce, 1980;

Robertson and Woodcock, 1980). The sheeted dykes, which constitute the key evidence of a spreading genesis are orientated overall N-S in the Troodos (Kidd and Cann, 1974), but complications exist, particularly in the east where the present study is located.

The extrusive succession has been subdivided into the Lower Pillow Lavas and the Upper Pillow Lavas (Wilson, 1959), the former being largely basaltic andesites and the latter mostly olivine basalts. The boundary between these two units is unconformable in some areas, but transitional in others (Wilson, 1959; Bear, 1960; Gass, 1960), leading to uncertainty over the location and significance of this subdivision. More recent attempts to divide the lavas have been based upon other criteria, for example metamorphic grade (Gass and Smewing, 1973; Smewing et al, 1975) and petrochemistry (current work by the International Deep Crustal Research Group). In the absence of a generally accepted definition of the Upper and Lower Pillow Lava units, we have simply mapped the lavas as local units and assigned letters to them.

An area on the eastern margin of the Troodos massif in the vicinity of the well known Mathiati mine (Fig. 3.1) was chosen for mapping because both sulphide- and oxide-metalliferous sediments are abundant and because regionally low dips and fault repetitions allow the individual units to be traced substantial distances laterally. In this area the dyke trend is consistently NW-SE deviating from the regional N-S direction. The sedimentary cover dips at 10-20° to the NE defining the mean dip of the lavas, but locally within the lavas dips range up to 30-40°, where rotation on normal faults has taken place. The distinctive ferromanganiferous oxide-sediments, the umbers, occur in small hollows along the contact between the stratigraphically highest lavas and the overlying sedimentary cover. Mostly ferruginous metal-oxide sediments are disseminated throughout the lava pile, largely in pillow interstices. The Mathiati massive sulphide ore body (Constantinou and Govett, 1973) is located within the lava pile towards the southern end of the area mapped (Fig. 3.1).

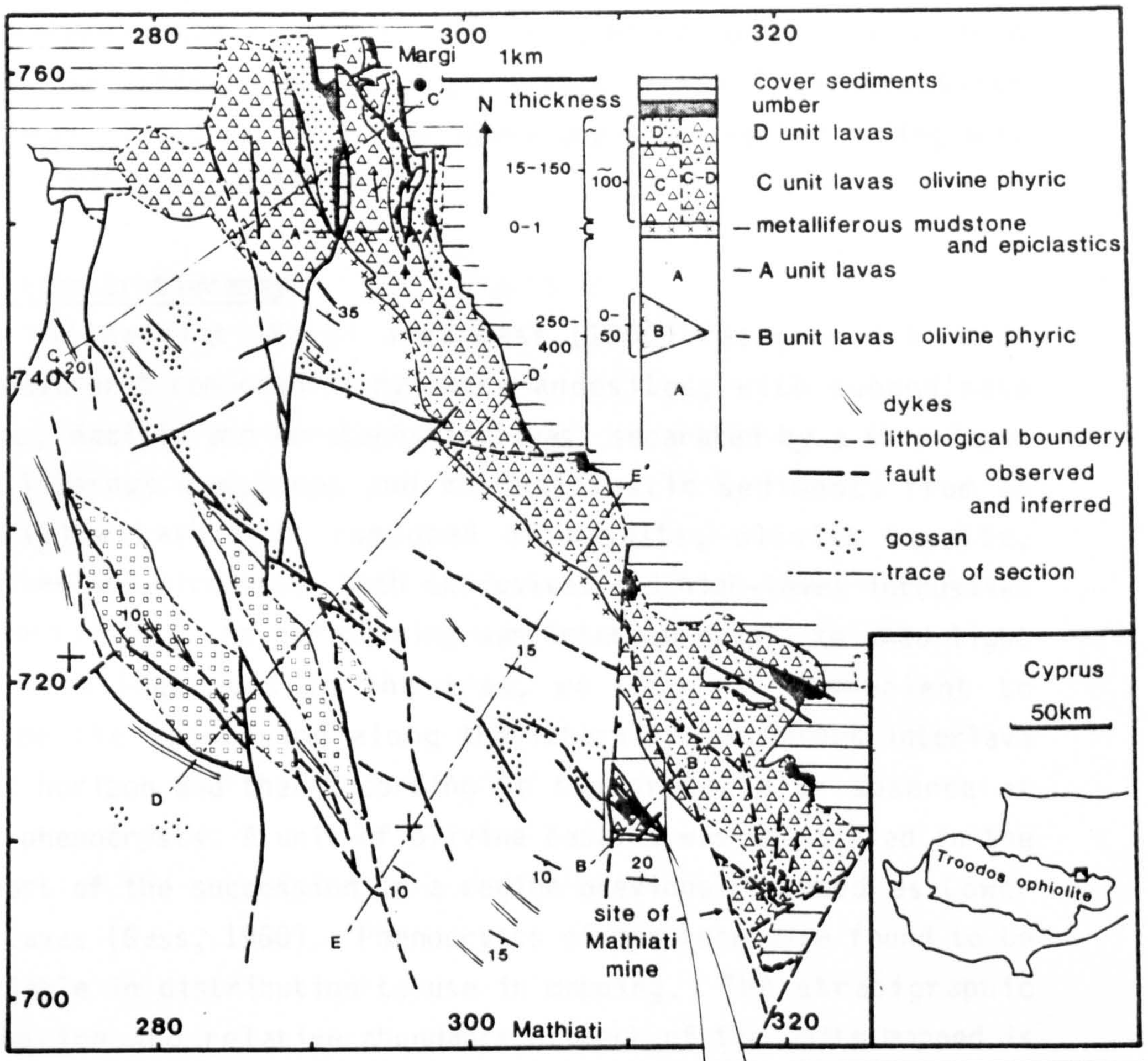

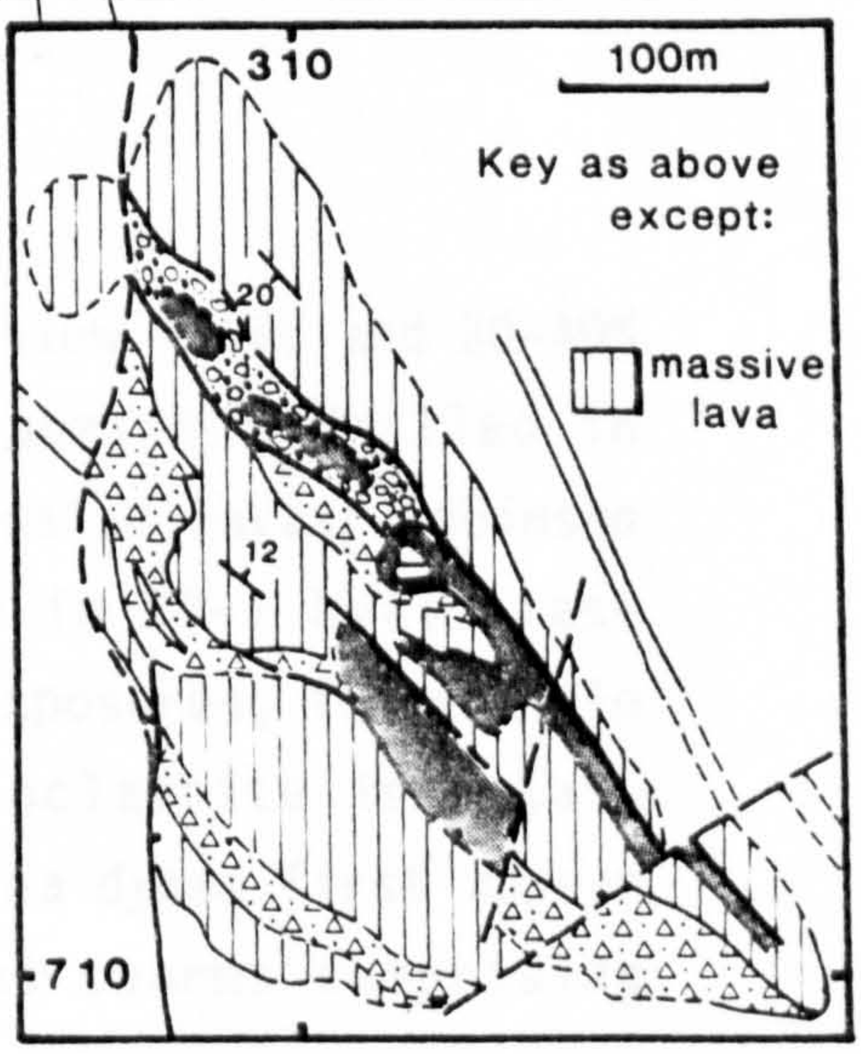

Fig.3.1 Geological map of the Mathiati–Margi area. Based on field mapping of selected areas using Cyprus series D.L.S.17 1:5000 topographical maps, aerial photographs and the Cyprus Geological Survey Department 1:31,680 map (Gass,1960).

The Mathiati-Margi area contains a higher proportion of both sulphide- and oxide-sediments at all levels of the lava succession than adjacent areas except the SE where there is the Sha mining area (1km SE of Map. Fig. 3.1).

3.1.2 Lithostratigraphy

In the Mathiati-Margi area Gass (1960) recognised a Lower Pillow Lava unit composed of pyroxene andesites, with subordinate basaltic, dacitic and keratophyric lavas, separated by a thin layer of metalliferous mudstones and volcaniclastic sediments from an Upper Pillow Lava unit composed of basalts, olivine basalts, limburgites and picrites. Both extrusives and high-level intrusives were identified. As our mapping was intended mainly to shed light on the metallogenesis in the area, we found it convenient to subdivide the succession along the laterally continuous interlava sediment horizon and then according to the presence or absence of olivine phenocrysts. A unit of olivine basalts was identified in the lower part of the succession in a region previously mapped as Lower Pillow Lavas (Gass, 1960). Phenocrysts of pyroxene were found to be too variable in distribution to use in mapping. The stratigraphic distribution and relative abundance of each of the units mapped is shown in Fig. 3.1.

3.1.3 Lava Morphology

The area mapped consists of ca. 60-70% pillow lavas and 30-40% massive lavas. This is comparable with the proportions drilled in CY-I of the IDCRG (69.9% pillow lava, 28.4% massive lavas; Robinson and Gibson, 1983). In both the area mapped and in CY-I hyaloclastite is very subordinate, although in some exposures, for example the Akaki River section of North Troodos, hyaloclastite is relatively more abundant. In the Mathiati-Margi area dykes first appear in the lower part of the succession locally as swarms comprising >50% of the outcrop.

The original eruptive morphology of the extrusives in the area can be interpreted in the light of observations from modern spread-

ing axes (Ballard et al., 1981, 1982; Ballard and Moore, 1977). Steep sided pillowed flows form topographic highs around eruptive centres which are located along fissures at the ridge axis. The early flows of each eruptive cycle tend to be sheet-like, travelling further than the pillowed flows (ca. 1km), pouring down slope and ponding in fault hollows. All except the most recent lavas are dissected by minor ridge-parallel fractures.

In the mapped area in Cyprus differential erosion has tended to reverse the original sea floor topography; the more resistant high-level intrusions and the massive flows form the high ground while the pillow lavas and the fragmented extrusives now form depressions (relief 20-50m). The original relationships can however still be observed, for example near Mathiati (Fig 3. 1, inset; Fig. 3.3, Section B-B), where massive flows of the C-D lava units dip in opposite directions on either sides of a valley. Older A unit pillow lavas on the floor of the intervening valley are cut by a 4m thick dyke which could have a fed a pillow volcano originally located between the oppositely dipping massive flow units.

In outcrop most of the lava pillows are relatively uniform in size and shape (ca. 1m across), but locally throughout the succession some of the lava pillows are conspicuously elongated as 'bolsters', or larger still as 'mega-pillows'. The 'mega-pillows', which range up to 10m across, commonly possess pillow-lobed lateral and upper contacts and are thought to represent sites of lava transport and extrusion (Schmincke and Rautenschlein, 1982). The 'mega-pillows' often occur in groups capping small hills of more normal pillow lavas. Although hard to measure, the apparently radiating dips of these lavas suggest that they originated as small pillow lava volcanos.

Two• types of fragmental extrusive rocks are recognised, hyaloclastites and pillow breccias. Small elongate lenses of hyaloclastite up to 5m thick are present associated with both massive and pillowed extrusives throughout the lava pile and are best exposed in stream sections. The hyaloclastites are typically

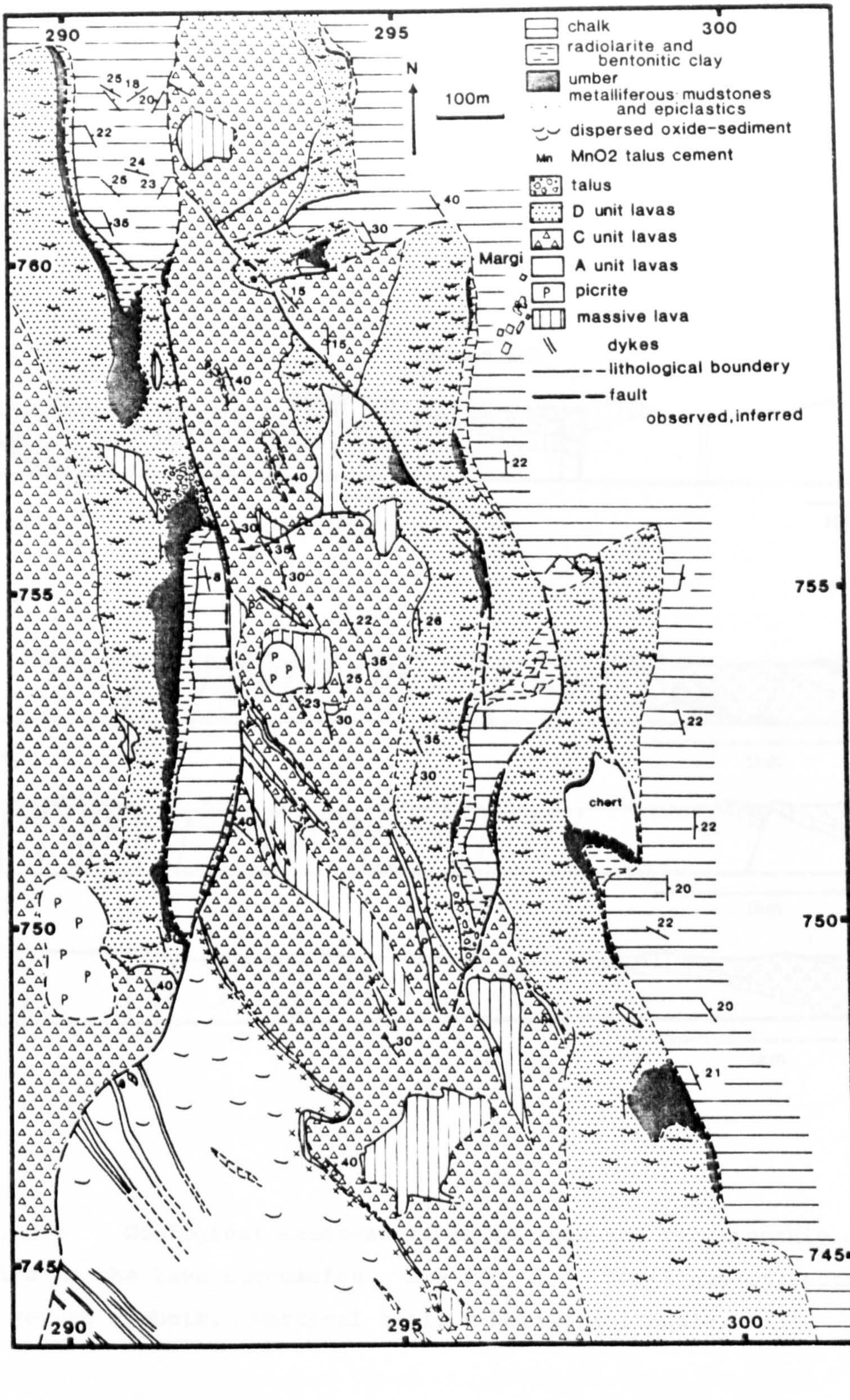

Fig. 3.2 Geological map of the area south of the Margi village showing the relationship of the metalliferous sediments to the lava units and faults. See figure 5.1 for location and details of the volcanic succession. Base map: 1:5000 topographical series D.L.S. 17 sheets 39/V, 30/XXXIX.

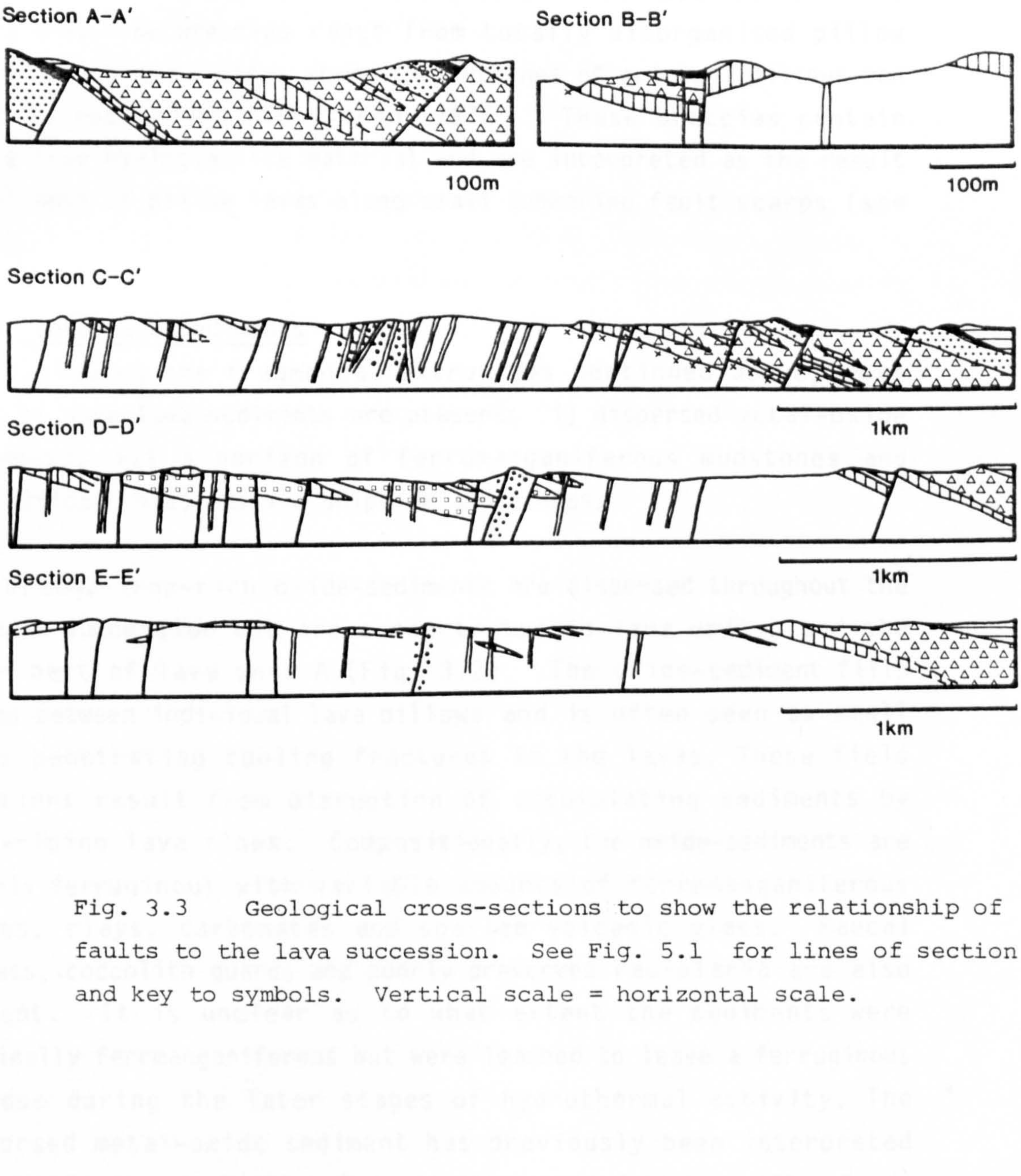

Fig. 3.3 Geological cross-sections to show the relationship of faults to the lava succession. See Fig. 5.1 for lines of section and key to symbols. Vertical scale = horizontal scale.

green to brown, weakly bedded to massive, consisting of poorly sorted glassy fragments and small intact pillows ca. 10cm in diameter. In the oceans hyaloclastite is seen to form particularly on steep flow fronts (Ballard and Moore, 1977), and a similar origin is favoured in Cyprus.

The pillow breccias are concentrated in the upper parts of the D lava unit. The breccias range from totally disorganised pillow segments, to some cases where the outlines of original pillows can still be recognised (Robertson, 1975). These breccias contain little true hyaloclastite material and are interpreted as the result of collapse of pillow lavas along small submarine fault scarps (see below).

3.1.4 Interlava Sediments

Excluding the fragmental extrusives mentioned above, three types of interlava sediments are present: i) dispersed metal-oxide sediments; ii) a horizon of ferromanganiferous mudstones and epiclastics; iii) massive sulphide and ochres.

Orange iron-rich oxide-sediments are dispersed throughout the volcanic succession but are concentrated in lava unit D and the upper part of lava unit A (Fig. 3.2). The oxide-sediment fills spaces between individual lava pillows and is often seen as small veins penetrating cooling fractures in the lavas. These field relations result from disruption of accumulating sediments by over-riding lava flows. Compositionally, the oxide-sediments are largely ferruginous with variable amounts of ferromanganiferous oxides, clays, carbonates and spalled volcanic glass. Faecal pellets, coccolith guards and poorly preserved radiolaria are also present. It is unclear as to what extent the sediments were originally ferrmanganiferous but were leached to leave a ferruginous residue during the later stages of hydrothermal activity. The dispersed metal-oxide sediment has previously been interpreted regionally as a hydrothermal precipitate ponded in the pillow lavas during the later stages of lava eruption (Robertson, 1975; Robertson and Fleet, 1976). The present work now shows that in the Margi area

the dispersed sediment is more widespread within the lava pile, defining broad horizons extending several kilometres around Margi and to the SE (Fig. 3.2). A possible source for this oxide-material would be oxidation of sulphide precipitates drifting away from more axial vents, and this would adequately explain their widespread dispersed character. This process has been observed at Pacific spreading axes (Edmond et al., 1982). The downward decrease in abundance of dispersed oxide-sediment within the lava pile could result either from reduced sedimentation rates, or more probably from more rapid eruption of the earlier pillow lavas.

At the contact between the A and C lava units there is a laterally continuous horizon of ferromanganiferous mudstones underlain by epiclastic sediments. The epiclastics are fine to medium grained, poorly bedded, generally massive and contain altered lava fragments in a muddy matrix which is commonly iron- and manganese-rich. Thickness varies from 0-1m. The ferromanganiferous horizon above is 0-1m thick, very fine grained, either massive or finely laminated and generally resembles the umbers above the highest lavas. This sediment is interpreted as a mixture of background pelagic and hydrothermal oxide-sediment which accumulated above the epiclastics, during a pause in lava eruption. The laterally continuous, unponded character of these sediments indicates that the seafloor was relatively flat and had not undergone significant tilting at this stage.

The formerly economic Mathiati sulphide ore body and stockwork mineralisation in the south of the area mapped (Fig. 3.1) now exists as a tilted horst overlain by unmineralised lavas (Constantinou and Govett, 1973). Until recent quarrying the massive ore was seen to be overlain by ferruginous ochres. These formed by a combination of submarine oxidation of massive sulphide (submarine gossans) and as hydrothermally precipitated ferruginous metal-oxide sediment; ochre of erosive origin is minimal (Robertson, 1976a). Constantinou (1980) reports that the sulphide occurs at the contact between the Lower and Upper Pillow Lavas, which places it at the same stratigraphic level as the ferromanganiferous mudstone horizon described above.

Later faulting has obscured the seafloor topography in the vicinity of the mineralisation, but a stratigraphic association with the sediment horizon would indicate that it formed prior to the major faulting. The inferred depositional geometry of the ore body suggests it was probably formed in a fault-controlled bathymetric depression (Constantinou, 1980).

3.1.5 Supralava Sediments

In the area mapped the stratigraphically highest lavas are overlain by ferromanganiferous oxide-sediments (umbers), metal-enriched clays, radiolarites and mudstones of the Perapedhi Formation, dated as Campanian. In turn these are overlain by Maastrichtian pelagic chalks of the Lefkara Formation (Robertson and Hudson, 1973, 1974). The umbers commonly occur in faulted depressions on the original lava surface where underlying lavas have locally undergone extensive low temperature hydrous alteration indicating a local source for the hydrothermal fluids. Robertson (1976a) interpreted the umbers as hydrothermal precipitates ponded in hollows during and after the waning stages of volcanism. The pelagic chalk cover accumulated later in gradually shallowing seas up to a Mid-Tertiary emergence.

3.1.6 Fault Stages

A major objective of this work has been to determine the relationships of metalliferous sediment accumulation to faulting of the extrusive sequence and to use this as a basis for comparisons with modern spreading axes.

In the mapped area a major transverse fault and two generations of normal faults, predate pelagic sediments above the umbers. The transverse fault is at the SE end of the area and trends NE-SW, perpendicular to the dykes (Fig. 3.1). An earlier generation of normal faults trends parallel to the dykes (NW-SE) and a later one trends both N-S and NW-SE (Fig. 3.1). The earliest sediments, the umbers, are found ponded in grabens and half-grabens created by this faulting. The umbers, after allowing for differential compaction,

have the same dip as the overlying chalks, showing that faulting and tilting was mostly before umber accumulation.

The transverse fault

The most prominent fault in the area runs close to the southern edge of the Mathiati opencast at a high angle to both generations of normal faults and is also perpendicular to the orientation of dykes in the area mapped. None of the normal faults can be traced across this fault. To the south outside the area mapped, the dykes swing round to parallel this NE-SW trending fault suggesting that it may have been active early. Since this fault is at right angles to the local dyke trends, we suggest it may have operated as a minor transform fault.

The normal faults

The normal faults are of two generations here termed <u>type 1</u> and <u>type 2</u>. The type 1 faults displace only the A and B lava units. The type 2 faults displace the type 1 faults and were coeval with eruption of the C and D lava units.

<u>Type 1: earlier normal faults</u>

The earlier normal faults, which cut the A and B lava units, are parallel to the NW-SE dyke trend (Fig. 3.1). The maximum observed vertical fault offset is ca. 160m, determined by displacement of the B lava unit (Fig. 3.3, Section D-D), but offsets could possibly have been as great as 400m. These earlier faults are parallel to those which bound the Mathiati sulphide body and have often been extensively gossanised. Shearing, which has taken place along these fault planes, is compatible with post-mineralisation movement. The field relations discussed above show that the laterally continuous horizon of ferromanganiferous and epiclastic sediment above the A lava unit, accumulated on an almost flat sea floor, thus the type 1 faulting cannot have involved significant differential vertical motion prior to this stage. Although the type 1 faults may have existed as fractures from a very early stage, major movement on them is constrained to an interval following the deposition of the sediment blanket, and prior to eruption of the C

and D unit lavas.

Type 2: Later normal faulting

The C lava and the type 1 faults are displaced by later faults, mostly trending N-S, but some, particularly in the south of the area, follow the pre-existing NW-SE trend. Several lines of evidence suggest that the N-S faulting took place over a short time interval during eruption of the C and D lavaunits. First, there is a marked upward decrease in dip and change in direction of strike through the C and D lava units (Fig. 3.2). Secondly, thin sheet and pillowed flows of the lower part of the ca. 150m thick succession give way upward to disrupted pillow lavas intercalated with lava breccia and hyaloclastite, indicating a steeper palaeoslope. Thirdly, upfaulted C unit lavas are locally overlain by the D unit with an unfaulted extrusive contact (Fig. 3.3). The D lavas did not entirely fill the half-grabens, leaving fault hollows which subsequently became sites of umber accumulation.

There are also the type 2 faults which cut the C-D lava units but are parallel to the NW-SE trend of the earlier type 1 faults. These are best exposed as an outlier of C-D unit lavas, umbers and cover sediments located in the south of the area mapped, 1km N of Mathiati (Fig. 3.1, inset; Fig. 3.3). These faults form small grabens in the C-D unit lavas which also later became sites of umber accumulation. No cross-cutting relations with the N-S trending type 2 faults have been observed.

It is important to note that although there is a clear relative age difference between the type 1 and the type 2 normal faults this need not imply a large time separation. The volcaniclastic and metal-oxide blanket beneath the C unit lavas could well record a significant time interval, followed by the normal faulting and extrusion of the C and D lava units.

3.2 DISCUSSION

In the following sections the field evidence presented above is viewed in the context of a simple model for the process of construction of the volcanic pile. Comparisons with modern spreading axes are made, and inferences steming from these are discussed.

3.2.1 Stages of spreading axis construction

The field relations of the Mathiati-Margi area can now be considered in the context of new crust forming and moving away from a spreading axis.

The following stages are recognised:

1) Most of the lava volume was rapidly extruded as pillowed and massive flows very close to the spreading axis. The rapidity of this earlier eruption restricted interlava sediment to minor dispersed oxide-sediment. During a subsequent hiatus, volcaniclastic material, was eroded, presumably by seafloor currents, and accumulated on a more or less flat sea floor.

2) The sulphide sediments and a halo of metal-oxide sediments were then deposited in an area close to the minor transform fault. Numerous fractures parallel to the spreading axis were mineralised, and the sulphide probably formed in a related shallow graben.

3) Blocks of lava 0.5-3km wide were rapidly rotated parallel to the spreading axis, with vertical throws in the order of 160m. The sulphide orebody was also dissected and rotated at this stage.

4) Basaltic eruptions resumed partially smoothing the topography. At the same time N-S faults became active and blocks up to 0.5km across were rotated up to 30°. Metal-oxide sediments accumulated during eruption and were dispersed throughout the upper part of the lava succession. Restricted to the south of the area mapped the later faulting continued after the end of volcanism forming a series of grabens.

5) The newly formed grabens, and the half-grabens of the north of the area which were not completely filled by the later lavas, were flanked by lava talus and then progressively filled by umber. During low temperature off axis hydrothermal activity the umbers and the associated lavas were veined by palygorskite and poorly crystalline MnO_2.

6) Later, after the spreading axis had migrated away, metalliferous clays accumulated with a greater hydrogenous component (Chapter 5, section 5.5.3), then the remaining hollows were progressively filled with radiolarites, mudstones and pelagic carbonates, although the basement remained exposed in places for up to 20 Ma.

The question which then arises is how typical these stages are of the Troodos massif as a whole. This excludes the Arakapas fault zone, which is interpreted as a fossil transform fault (Simonian and Gass, 1978), with its own distinctive hydrothermal metalliferous oxide-sediments (Robertson, 1978). The gross lava succession, the position of the sulphide ore bodies and the style of faulting in the Mathiati-Margi-area is very similar to many other parts of the Troodos massif. There is often an abrupt upward change to more mafic compositions in the lavas (Gass, 1980). The major sulphide ore bodies are mostly, if not all, located beneath these more mafic lavas (Constantinou and Govett, 1973). Also Adamides (1980) has demonstrated that the major sulphide mineralisation of Kalavasos was controlled by early faulting, although this area is complicated by the close proximity to the Arakapas fault zone. The Mathiati-Margi area is peculiar in its richness of mineralisation and metalliferous sediments throughout the lava succession. Away from mining districts hydrothermal sediments are generally scarce and are completely absent from some areas, for example, the Akaki River section on the northern margin of the Troodos massif.

One remaining puzzle is why some of the later (type 2) faults were orientated ca. 40° clockwise from the trend of the earlier

faults (type 1) which had parallelled the inferred spreading axis. This change took place during the later stages of the principal tectonic event, which corresponds to the construction of the rift valley walls, and was coincident with eruption of the later more mafic lavas.

3.2.2 Metallogenesis at modern spreading axes

We now review the main morphological, structural and metallogenic features of the Atlantic and Pacific spreading axes, which are relevant to interpretation of the Troodos ophiolite.

Atlantic (Slow spreading rate: c. 20mm/yr total)

The Mid-Atlantic Ridge in the TAG area (26°N) is topographically rugged with a median valley ca. 20-30km across and 1-2km deep. Normal faults along the walls of the median valley are inferred to possess throws up to 1km, locally exposing gabbros (Rona et al., 1976). The TAG hydrothermal field comprising manganese deposits, is situated on the inner wall of the rift, 10-12km from the axis.

In the FAMOUS area (37°N) the axial graben is still 20-30km across, but shallower (1km relief). The topography of the inner rift valley floor is subdued and is controlled by eruption with relatively little faulting. The walls of the median valley are dissected by normal faults spaced 0.5 to 8km across with inferred displacements up to 500m (Ballard and van Andel, 1977). Only in transform fault 'A' have hydrothermal deposits been found, these comprising nontronite and manganese oxides (Hoffert et al., 1978).

Pacific

At the Galapagos rift, which has an intermediate spreading rate (60mm/yr total), there is a narrow median valley 3-8km across with a total relief of 100-250m (Lonsdale, 1977a; Ballard et al., 1982). Normal faults spaced 1-6km apart, with inferred throws of ca. 100m, are formed in a tectonically active zone at the margin of the median valley (ca. 4km from the axis). Inactive sulphide deposits are located at 85° 49-50'W along a fault associated with the southern boundary of the north rift valley (Skirrow and Coleman, 1982) and at

86° 0-15'W located along both the northern and southern scarps of the rift valley. Active hydrothermal fields, none of high temperature type, are located immediately on the axis. The hydrothermal mounds, composed of MnO_2 and nontronite, are situated on the sedimentary cover above basement fractures, 20-30km south of the axis.

The Juan de Fuca ridge, which is also an intermediate rate spreading axis, (60mm/yr total) is morphologically similar to the Galapagos rift, with a well defined median valley ca. 3km across and ca. 100m deep (Normark et al., 1983). The inner walls are composed of low terraces bounded by steep normal faults (throws ca. 30m) and define an axial volcanic floor about 1km across. Along the centre of the valley, which is largely flat and unfaulted, there is a nearly continuous depression 50-200m across and about 25m deep. Four of the known sulphides occur in this median depression, and one is located against the scarp at the foot of the eastern inner wall. Low-temperature active vents occur along the median depression.

The much faster spreading East Pacific Rise at 3°25'S (150mm/yr total) differs from the Galapagos by the absence of a well defined axial graben. Most of the faulting takes place in a zone of extension 1-15km from the ridge axis (Lonsdale, 1977b). In contrast to the Atlantic and the Galapagos, the fault blocks are symmetrical horsts and grabens rather than asymmetrical half-grabens (Lonsdale, 1977b). Numerous sulphide deposits of high temperature origin (ca. 370°C) have been discovered on the EPR at 21°N. The active vents are located in a linear zone 200-300m wide right on the spreading axis. The sulphide sampled by Francheteau et al. (1979) were found in small faulted depressions about 700m from the axis, with notional ages of 10-20,000 years.

3.2.3 Implications for the Troodos

Profiles of basement topography on the rift flanks are compared in Fig. 3.4. The slow spreading TAG area, with huge fault throws and exposed plutonic rocks, and the fast spreading EPR, with symmetrical block-faulting are not compatible with the area mapped. The FAMOUS

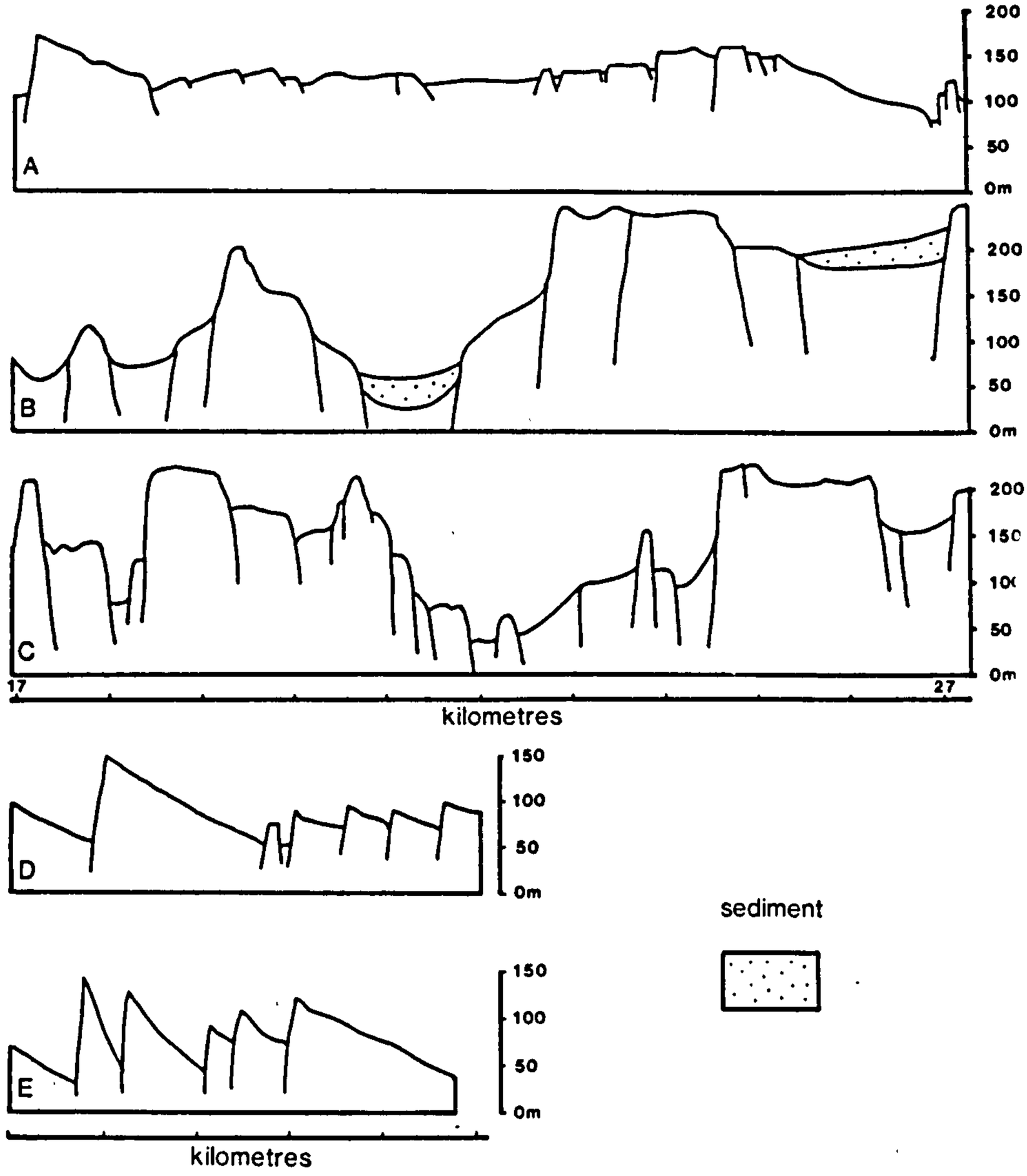

Fig. 3.4 Comparisons of the topography of modern spreading axes with those inferred for the Mathiati-Margi area of Cyprus. a) Galapagos (Lonsdale 1977a); b) FAMOUS area (Macdonald and Luyendyk 1977); c) East Pacific Rise (Lonsdale 1977b). A-C are shown for 17-27km from the spreading on the ridge flanks. D-E style of basement topography inferred for Cyprus at an equivalent distance from the axis. In each case the ridge is to the left.

area, and the intermediate spreading axes of the Galapagos and Juan de Fuca ridges which have asymmetri-cal block-faulting and lower relief compare more closely. The maximum estimated fault-controlled relief of ca. 160m for the mapped area compares with 500m for the FAMOUS area, ca. 100m for the Galapagos and 30m for the Juan de Fuca spreading axes. In modern spreading axes the median valley walls are uplifted on ridge-parallel faults, that apparently contrast with the two directions of faulting in the Mathiati-Margi area. It is however clear that the area mapped is not large enough to allow a more confident comparison with modern ridge morphology to be made.

On modern spreading axes the bulk of the lava pile is produced in a narrow relatively unfaulted volcanically active zone around 2km across where topography is largely controlled by volcanism (Lonsdale, 1977a, b; Ballard and van Andel, 1977; Ballard et al., 1981, 1982). Consistent with earlier interpretations (Smewing et al., 1975; Robertson and Fleet, 1976) we envisage the A and B lava units of the Mathiati-Margi area (Lower Pillow Lavas) as having been erupted in a similar narrow volcanically-controlled axial zone. The massive and pillowed flows were erupted there from fissures with little vertical relief. Eruption rates were high enough to preclude much accumulation of pelagic sediments, in contrast for example, with the higher levels of the extrusive succession of the Semail ophiolite, Oman, which contains pelagic chalks in addition to metalliferous oxide-sediments (Fleet and Robertson, 1980). The dispersed sediments in Cyprus consist of mixed background pelagic sediment and metalliferous oxide-sediment which was precipitated from vent fluids, possibly originating as fine sulphide particles. Volcanism ceased, and as the area moved off the axis still within the axial valley, currents were sufficiently active to erode lava to form a laterally continuous thin blanket of volcaniclastic sediment over a wide area of relatively flat sea floor.

Massive sulphides in the ocean have to date only been discovered on the Pacific spreading axes. All of the high temperature vents (ca. 370°C) are located on the youngest lavas on the spreading axis. Some inactive sulphides are found near major scarps at the

edges of the median valley as in the Galapagos rift (Skirrow and Coleman, 1982); and the Juan de Fuca ridge (Normark et al., 1983). These could either be fossil sulphides transported away from the axis, or else could have formed near the the walls of the median valley where greater fracturing and permeability might have favoured hydrothermal discharge (Normark et al., 1983). Sulphides formed at the spreading axis are likely to be rapidly buried by later lavas and thus would be expected to be located low in a hypothetical vertical succession of axial lavas. This contrasts with the Mathiati-Margi area, where the massive sulphides are located on top of the lavas interpreted as having formed in the axial valley prior to major faulting. In this regard the sulphides seem to differ somewhat in location from the known 'black smokers', which are more axial. Constraints on the actual distance from the axis that the Cyprus massive sulphides were deposited can be inferred from modern examples, assuming that they were deposited beyond the axial volcanic zone but inside the axial valley. Maximum development of the rift valley walls is achieved at 10km from the axis at the FAMOUS area, ca. 4km at the Galapagos rift, and ca. 1.5km at the Juan de Fuca rift. No sulphides have been found on the slow spreading axes, so a realistic maximum distance for sulphide formation is ca. 4km.

The later C and D unit lavas in the Mathiati-Margi area were erupted during a period of intense fault rotation and differential uplift which can be interpreted as the construction of the rift valley walls. The site of eruption would thus be at the margins of the axial graben rather than for example some distance out on the flanks of the ridge. To date off-axis extrusion has been reported only in the FAMOUS area, but these extrusions are more evolved than their axial counterparts (Bryan and Moore, 1977), in contrast with the Troodos. In many parts of the Troodos massif the traditional Upper Pillow Lava - Lower Pillow Lava break is less marked or apparently absent which could imply either that the later lavas were more nearly axial or that the median valley was less well defined.

The question remains as to why the Mathiati-Margi area is one of a number of areas of the Troodos which are metal-enriched at all levels of the extrusives. Although these sediments accumulated close to a major fault, there are plenty of other highly faulted areas of the Troodos which are devoid of mineralisation. Modelling of convective circulation by Spooner (1977) has demonstrated the need for local thermal anomalies to impose spatial stability, and he pointed out that large magma chambers would act in this way. Theoretical considerations of the thermal budget of the hydrothermal 'smokers' indicate that the heat source needed to sustain hydrothermal discharge at 370°C must involve magma crystallisation (Strens and Cann, 1982), which thus implies the existence of magma chambers under the 'smokers'. Even after freezing, magma chambers would remain thermal anomalies which could localise cooler hydrothermal circulation after they had moved off-axis. Unfortunately, no relationship between the plutonic rocks and extrusive sequence can be established in the area mapped. Regardless of the mechanism, however, the localisation of hydrothermal sediments at particular sites in the Troodos ophiolite indicates a local persistence of hydrothermal metallogenesis not yet demonstrated at modern spreading axes.

A further point is that the close integration now possible of all the Troodos lavas and sediments into the evolution of spreading axis offers no obvious support for earlier suggestions that the Upper Pillow Lavas formed in some separate tectonic setting from the Lower Pillow Lavas, for example, as an off-axis seamount (Gass and Smewing, 1973) or as an incipient island arc (Pearce, 1975).

3.3 CONCLUSIONS

The combined field observations and the comparisons with the modern oceans show that the volcanic and structural development of the Mathiati-Margi area of the eastern Troodos massif (Upper Cretaceous) is compatible with formation at an intermediate spreading rate axis with a well defined axial graben. The bulk of the

lava pile was erupted on an area of relatively flat seafloor in the axial part of the median valley (traditional Lower Pillow Lavas). During a pause in volcanism submarine erosion produced a thin layer of volcaniclastic sediments. The massive sulphides accumulated in small fault-controlled depressions towards the walls of the axial graben, with a halo of Fe-Mn oxide-sediments. Ferruginous oxides dispersed throughout the lava pile are possibly drifted products of high temperature sulphide vents.

The walls of the median valley were constructed by two phases of normal faulting, of which the second accompanied the eruption of the later more mafic lavas, (traditional Upper Pillow Lavas). The Fe-Mn oxide-sediments, the umbers, then accumulated in small fault-controlled hollows near the crest of the ridge flanks. Later as the spreading axis migrated away pelagic clays accumulated which where enriched in metals by hydrogenous processes, followed by pelagic chalk deposition.

Analogy with modern intermediate rate spreading axes suggests an axial volcanic zone ca. 2km across within an 3-8km wide rift valley. The inferred origin of most, if not all, the Cyprus massive sulphides above the highest axial lavas differs some what from the 'smokers' of modern Pacific spreading axes which mostly appear to have formed immediately on the axis.

CHAPTER 4

THE INTERLAVA METALLIFEROUS SEDIMENTS OF THE TROODOS OPHIOLITE

Introduction

Metalliferous sediments are locally interbedded with the extrusive volcanic rocks of the Troodos ophiolite. These sediments may be divided into two compositional groups: sulphide facies; and oxide facies.

The sulphide sediments are composed predominantly of iron sulphide, but also contain variable amounts of copper- and zinc-sulphides.

The oxide sediments are of more diverse morphological, mineralogical and chemical character. Morphologically they comprise lensoid bodies, sheets laterally continuous over distances of 1km and, more important volumetrically, infillings of interpillow interstices and cooling-fractures. Iron oxide enrichment, principally in the form of goethite, is common to all the interlava oxide sediments. In addition to this, extremely variable amounts of carbonate, analcite, manganese oxides and quartz occur.

Previous work has concentrated upon the sulphide sediments and the ochre directly associated with these. In this work effort has been directed towards those sediment types largely neglected in the earlier work, and to the relationship of the sediments with each other and with processes of construction of the ophiolite.

4.1 THE SULPHIDE ORE BODIES

4.1.1 Introduction

The mineralogy, chemistry and morphology of the sulphide ore bodies of Cyprus have been described in detail (Adamides, 1975; Adamides, 1980; Constantinou, 1972, 1976, 1980; Constantinou and Govett, 1973; Oudin and Constantinou, 1984). Of the following description only the discussion of the association of mineralisation with the structural development of the ophiolite, introduces any new data. The reasons for including a section on the sulphide ore

bodies are two-fold. First, for the sake of completeness sulphides must be included in any description of Troodos interlava sediments. Secondly, in the light of new evidence concerning both the formation of the Troodos ophiolite, and the origin of deep ocean sulphide sediments, a review seems called for. Three questions must be addressed. First, how does the existing metallogenic model stand up to new interpretations of the lava sequence? Secondly, how were the sulphides related spatially to the palaeo-ridge axis? Thirdly, how does the texture, mineralogy and chemistry of the ore compare with those of modern ocean floor sulphide deposits?

4.1.2 Ore body location with respect to the volcanic stratigraphy

The model of Constantinou (1972) for the formation of the sulphide ore bodies has them accumulating from hydrothermal vents during the break in eruption between the Lower Pillow Lavas and Upper Pillow Lavas. With the subsequent revision and redefinition of this much-discussed subdivision of the extrusive succession (Gass and Smewing, 1973; Smewing et al., 1975; Robinson et al., 1983) it is important to re-examine the evidence for this interpretation.

Central to Constantinou's interpretation is the observation that more mafic, olivine-bearing lavas predominate in the upper part of the lava pile, and that the sulphide mineralisation always occurs beneath this. Further, none of the olivine-bearing uppermost lavas, nor their feeder dykes are mineralised, even where the latter are seen to cross-cut sulphide stockworks. These observations are not affected by redefinition of the lava subdivision. The required existence of an accompanying break in eruption prior to accumulation of the more mafic lavas, is supported independently on two counts. First, interstratification of the olivine basalts with the underlying andesitic lavas is rarely seen. This is true also of the two lava suite of Robinson et al. (1983). Secondly, specific examples can be observed in the field, for example in the Margi-Mathiati area, where a period of submarine erosion has occurred prior to synchronous block-faulting and eruption of olivine basalts (Chapter 3, section 3.1.6).

4.1.3 The relationship of mineralisation to structure

Constantinou (1972, 1980) demonstrated that the ore bodies are of saucer-shape if post-depositional faults are removed, suggesting that they accumulated in small fault-bounded bathymetric depressions. Adamides (1975, 1980) however concludes that much of the normal faulting which Constantinou (1972) regarded as post-mineralisation in fact predates ore formation. He suggests that both the Limni and Kalavasos ore bodies accumulated in topographically steep half-grabens orientated parallel to the ridge axis. The evidence cited to support early faulting, is the occurrence of extensive propylitisation and mineralisation (now gossanised) along the bounding dyke-parallel faults. This evidence is equally compatible with sulphide accumulation in the vicinity of ridge-parallel fractures, which were subsequently exploited during a period of block-rotation. The latter interpretation is favoured by the presence of extensive shearing of the gossanised faults (Adamides, 1980), and by the widespread thin layers of interlava umber at the same horizon as the sulphide, which shows no signs of ponding into deep faulted hollows. A similar situation is observed in the vicinity of the Mathiati Mine. A series of dyke-parallel normal faults with throws of several hundreds of metres are extensively gossanised and sheared, yet overlying thin interlavas umbers and epiclastic sediments extend for more than 1km laterally. During mineralisation sea-floor gradients must have been low.

In summary, it is suggested that sulphide sediment accumulated in shallow depressions on a relatively horizontal sea-floor, in the vicinity of ridge-parallel fractures. Exploitation of these fractures during block-rotation at the margins of a rift valley was responsible for the final disposition. Accumulation of the ore prior to basement block rotation, places the location of formation of the ores more nearly axial (Chapter 3, section 3.2.3).

4.1.4 Lateral distribution of sulphide ore

Constantinou (1980), notes that the ore bodies occur in five clusters of four or more. Possible controls on the distribution of the ore bodies are discussed in Chapter 3, section 3.2.3.

4.1.5 Ore texture, mineralogy and chemistry

Subsequent to Constantinou's (op. cit.) work on the Cyprus ore bodies, sulphide sediments have been discovered on the ocean floor (Francheteau et al., 1979; Spiess et al., 1980; Normark et al., 1983). Recently, samples collected by Constantinou have been re-examined and hydrothermal vent fragments similar to those of the Pacific have been identified (Oudin and Constantinou, 1984).

There are two textural varieties observed in Cyprus, a conglomeratic ore generally underlain by a less abundant compact ore. The compact variety comprises hard massive sulphide dissected into blocks by fractures filled with sugary pyrite. The conglomeratic ore comprises a matrix of gritty sugary pyrite containing spheroidal or pillow-shaped bodies, which increase in size and abundance downwards. Cavities in these bodies, from 1-10mm are common, and collomorphic banding is characteristic.

Pyrite, the most abundant mineral, can be divided into three paragenetic types:

Pyrite I — The most common type in the compact ore. Euhedral to subhedral, zoned, containing inclusions of copper and zinc sulphides. (0.2-0.6 wt% copper, 0.08-0.2 wt% zinc)

Pyrite II — Also most abundant in the compact ore. This is unzoned, of variable size and shape, but consistently truncates pyrite I.

Pyrite III — Occurs as collomorphic bands and framboids in the conglomeratic ore. Truncates the other pyrites.

Chalcopyrite and sphalerite occur variably, but are most abundant in the upper parts of the ore as cavity fillings in the pyrite III.

Constantinou originally interpreted this in terms of a progressive downward oxidation of a sediment which would originally have comprised solely compact ore, and leading ultimately to the formation of in situ ochre. The conglomeratic texture was seen as resulting from dissolution collapse (Constantinou, 1976).

Previous interpretations of the conglomeratic ore: replacement of lava breccias (Bear, 1963; Cullis and Edge, 1927; Jarrel, 1947; Moussoulos, 1957; Pantazis, 1967); tectonic brecciation (Cullis and Edge, 1922; Moussoulos, 1957); collapse of ancient workings (Moussoulos, 1957); or autobrecciation of banded sulphides by final explosive escape of gas (Hutchinson, 1965), were dismissed by Constantinou and Govett (1973). The importance of dissolution and reprecipitation of sulphide led them to the above interpretation. However, Robertson (1976a) emphasised the sedimentary character of the upper parts of the ore where sulphide and ochre are interbedded,and subsequently textural similarities with modern mid-ocean ridge sulphide chimney and mound deposits have been observed (Oudin and Constantinou, 1984).

Sulphide deposits at the East Pacific Rise comprise mounds up to 15 x 30 metres in plan and more than 2 metres thick which have formed through collapse of chimney structures (Hekinian et al., 1980; Haymon and Kastner, 1981). The growth of the chimneys involves a series of precipitation and replacement stages, during which both euhedral and botryoidal massive sulphides are produced. The mounds formed this way contain large chimney fragments, but are often ochreous in character through oxidation of the sulphide. The resulting deposits are smaller than those in Cyprus and are chemically distinct, containing much greater abundances particularly of zinc, but also of copper (For a comparison see table 4.1). Further, they differ from the Cyprus deposits in the absence of the less stable minerals such as Zn-bearing isocubanite, pyrrhotite and wurtzite. However these differences are considered to have resulted from early sea-floor diagenesis and ageing (Oudin and Constantinou, 1984). Base metal enrichment of the small modern sulphides may result from fractionation of these towards the edges of the hydrothermal system (Normark et al., 1983). This hypothesis is supported

TABLE 4.1

Comparison of sulphide sediment compositions between modern Pacific and Cyprus

		East Pacific Rise (21 N)*					Juan de Fuca**			
Cu	Wt%	0.28	0.40	1.16	0.28	1.51	0.32	0.24	0.07	<0.0003
Fe	Wt%	8.9	1.37	12.60	45.40	1.28	8.0	22.5	1.8	50.5
Zn	Wt%	49.7	22.87	49.7	0.05	ND	54.0	29.7	59.2	0.63
Ag	ppm	380	480	290	320	83	290	124	230	<3
Pb	ppm	640	ND	330	520	ND	2500	1800	600	1100
Co	ppm	<10	ND	500	500	ND	-	-	-	-

		Mathiati	Skouriotissa Conglom.	Skouriotissa Compact	Agrokipia	Kokkinoyia
		N=12	N=6	N=1	N=5	N=3
Cu	Wt%	0.29	2.78	0.30	3.12	3.78
Zn	Wt%	0.11	0.02	0.10	2.73	0.26
Ni	ppm	44	20	44	33	63
Co	ppm	53	359	610	33	55

*Data from Hekinian et al. (1980) **Data from Normark et al. (1983)
Cyprus data from Constantinou and Govett (1973)

ND = Not detected - = Not determined

by the discovery of a large (several million tonnes?) sulphide deposit at the Galapagos rift which is predominantly composed of iron sulphide (Malahoff et al., 1981). More rapid accumulation of sulphide at a more active vent field would reduce the degree of oxidation of early formed mound material, and would result in accumulation of sediment less ochreous in character than that found in the East Pacific Rise mounds. Later, as activity declined, the abundance of oxidized degradation products would increase.

4.1.6 Summary

At individual mine sites ore deposition has been controlled by ridge-parallel faulting. The distribution of ore bodies about the Troodos massif as a whole: clusters separated by unmineralized regions, indicates an important regional control which may be related to magma emplacement (Chapter 3, section 3.2.3).

The sulphides all occur within the deeper parts of the lava pile, predating the more mafic lavas characteristic of the upper part of the lava pile. The presence of thin, laterally continuous, sediment horizons deposited in the vicinity of the sulphide ore bodies suggests that they accumulated on untilted lava basement close to the axis of the palaeo-rift.

The conglomeratic texture of much of the ore, the presence of chimney-like structures, the paragenesis of the sulphide minerals and the presence of increasingly abundant interbeds of ochreous material towards the uppermost parts of the sediments, are closely comparable with deposits accumulating from high temperature vents on the Pacific spreading axes.

The differences in chemistry and mineralogy between the Cyprus and the Pacific sulphide sediments, may be the result only of the difference in size of the examples which are compared, and the ageing process.

4.2 THE OXIDE SEDIMENTS

4.2.1 Definition of umber and ochre

There are at present two different definitions for both umber and ochre. Constantinou and Govett (1972) defines ochre as a manganese-poor, iron-rich bedded deposit with varying proportions of interbedded chert, volcaniclastic material and limestone, commonly containing bands of sulphide, which is spatially associated with sulphide ore. Robertson (1976a) recognising a chemical gradation between the ochres and umbers, qualifies the definition by the statement "generally manganese-poor" and re-emphasises the spatial association with sulphide ore. Umbers, on the other hand, Constantinou and Govett (1972) define as post-volcanic iron- and manganese-rich sediments occurring as the lowermost member of the Perapedhi Formation. Robertson (1976a) qualifies this again to "generally manganese rich" and replaces the stratigraphic constraint by stating that they "are genetically associated with the later stages of eruption of the Upper Pillow Lavas". The complication of having two definitions is further compounded by the original descriptive use of the terms, which may carry unintended genetic connotations. Further, some rock types, such as the ferruginous and ferromanganiferous oxide-sediments, which may occur deep in the lava pile, and which do not necessarily bear a spatial relationship to sulphides, do not fit either classification. Further redefinition of the terms would complicate the issue, but some kind of review is necessary.

With regard to the definition of the terms umber and ochre, there are three possible criteria: field appearance; chemical composition and spatial associations.

The terms are both of descriptive origin, ochre deriving ultimately from the Greek Okhros (yellow) and umber from the Latin Umbra (shade). When describing these natural pigments in the field, the useful adjectives umberous and ochreous spring to mind, and would be unambigously interpreted by the reader. To use the nouns umber and ochre in this descriptive sense, however desirable, would inevitably lead to misinterpretation. The chemical composition of a bedded "ochre" lying on top of a sulphide ore body is very different from that of a supralava "umber", but a complete gradation of composition occurs in between (Robertson, 1976a). Further,

post-depositional manganese removal can convert a sediment which is umber-like into one which is ochre-like. An arbitrary separation based upon a Mn/Fe ratio is possible, but this would be no more useful than a field separation based largely on colour, and would suffer from the same drawbacks.

Spatial association is important in the definitions from both Robertson (1976a) and Constantinou and Govett (1972). This has the advantage of being related to origin, but has disadvantages where spatial associations are unknown or ambiguous.

The terms used in this discussion of the Cyprus metalliferous sediments are defined as follows:

Ochre

Used in the sense of both Constantinou and Govett (1972) and Robertson (1976a) to refer only to those bedded, predominantly ferruginous sediments which are found immediately at the sites of the sulphide orebodies.

Umbers

Brown ferromanganiferous oxide sediments which are carbonate-free and with insufficient clay to impart a shaly fissility. Umberous limestone or mudstone may be used for non-pure varieties. The only deviation from this definition concerns umber which is manganese depleted through secondary removal.

Interpillow oxide sediment

Umberous or ochreous oxide-rich sediments occurring in interpillow interstices or cooling fractures, admixed with varying proportions of volcaniclastic or carbonate material.

4.2.2 Field Relations and Petrography

The interlava oxide sediments can be divided into three categories:-

1) Ochres - which have a close spatial association with ore bodies.
2) Umbers - laterally persistent horizons of pure umber.
3) Interpillow oxide sediments - predominantly ochreous but also

umberous mudstones, limestones and cherts occurring in fractures and interpillow interstices..

4.2.2.1 Ochre

Ochre has been reported at Apliki, Mavrovouni and Agrokipia, but is best exposed at Mousoulos, Mathiati and Skouriotissa (Constantinou and Govett, 1972). Several sediment types comprise the ochre group.

1) Massive ochre

Un-banded and without obvious bedding, comprising widely varying blocks of very porous pyrite embedded in a matrix of yellow ochre. The ochre-ore contact is gradational, both on the metre scale as abundance of pyrite blocks increase downwards into pure ore, and on the microscale as goethite progressively replaces pyrite. The thickness of ochre varies upto 5 metres. This massive ochre, which is best exposed at Mousoulos (Kalavasos mining district) and Mathiati, was formed by in situ oxidative attack of sulphide ore (Constantinou and Govett, 1972).

2) Interbedded ochre and ore

Alternating bands of brown to yellow ochre and massive sulphide ore. Individual ochre beds may comprise alternating dark to yellow laminations, the colour variation resulting from changes in grain size and crystallinity. Elsewhere beds of homogeneous yellow ochre occur. The massive sulphide is in sharp contact with the ochre, and comprises blocks of pyrite in a matrix of soft friable sulphide. Some of the interbedded ochre and sulphide occurrences are red in colour owing to the presence of maghemite either intimately associated with goethite in the ochre, or replacing sulphide in the ore.

Graded bedding and washout channels attest to the sedimentary origin of this type of ochre, which is best exposed at Skouriotissa.

3) Finely-laminated ochre

At Mathiati and Skouriotissa very finely laminated lenses of ochreous sediment, locally rich in derived

sulphide fragments occur either interbedded with or on top of the conglomeratic ore, or mineralised lavas (Robertson, 1976a). Conformable contacts with the overlying dark umber indicate that these were not originally manganiferous umbers. These differ markedly from the coarse clastic or replacive ochres described above. Their fine-grained character and fine lamination is suggestive of slow accumulation from suspension.

4) Siliceous limestones, volcaniclastic sediments and cherts

At Mathiati siliceous limestone is commonly interbedded with volcaniclastic sediment, and at one locality rests directly on the ore. The volcaniclastic sediments are commonly cemented by quartz and calcite. At Skouriotissa, volcaniclastic sediment occurs both interbedded with the ochre, and admixed in varying proportions with it. Also at Skouriotissa, cherts are exposed above the massive ore, where they comprise silicified brecciated ore, and above the altered lavas where they comprise fine alternating bands of sulphide-quartz mixtures. Fine laminations result from the variable dispersion of iron oxide.

The intimate association of the ochre with the sulphide ore bodies suggests a genetic relationship (Constantinou and Govett, 1972). Increasing abundance of interbedded ochre towards the top of the orebodies, and the presence of corroded pyrite argue strongly for derivation of the former by oxidation and erosion of the latter.

4.2.2.2 Interlava Umbers

Sandwiched between lava flows in three areas occur thin laterally continuous bodies of dark brown to black laminated or massive umber, varying in thickness from a few tens of centimetres up to a couple of metres.

Margi-Mathiati area

Interlava manganiferous sediments near Margi were first

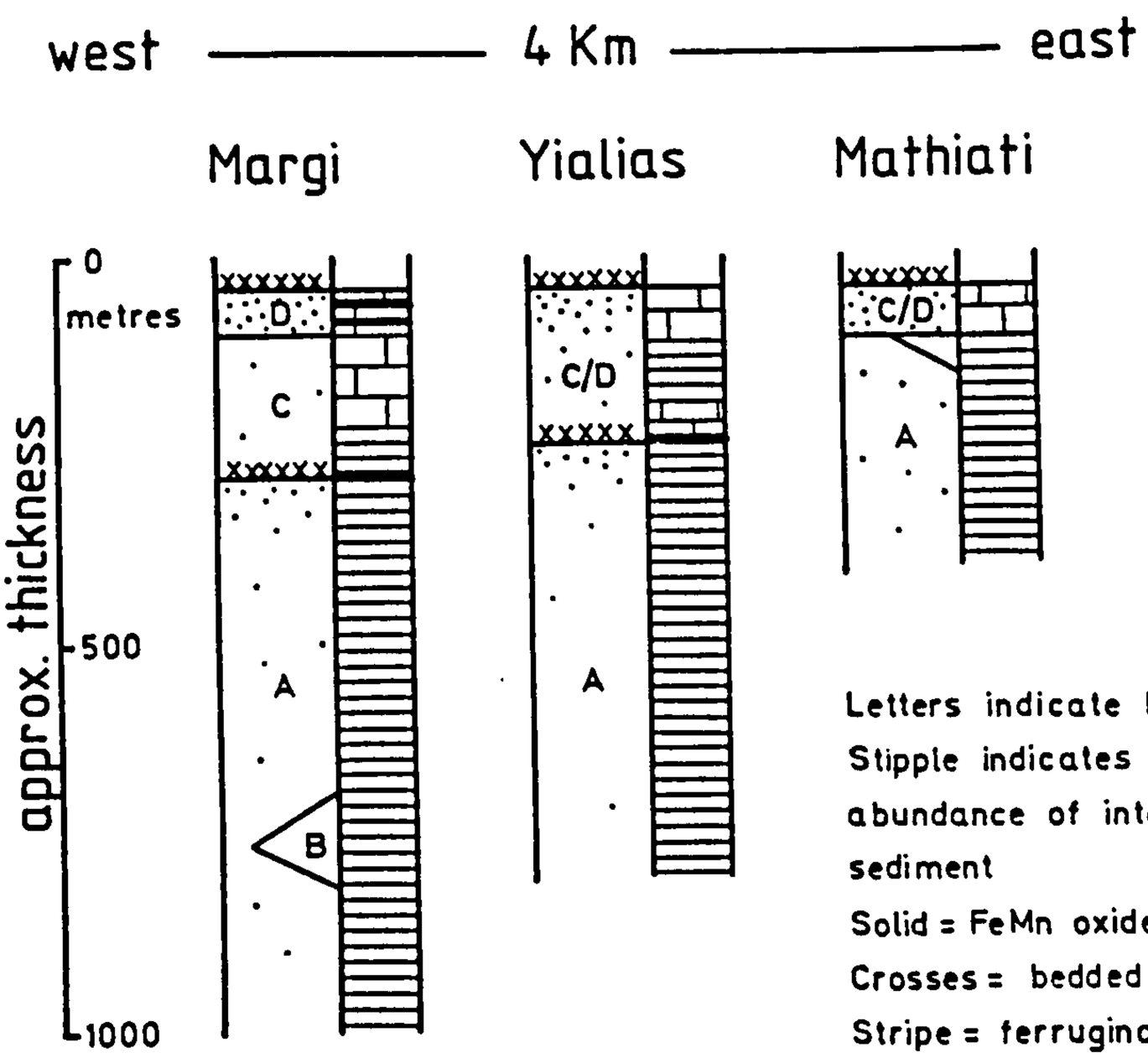

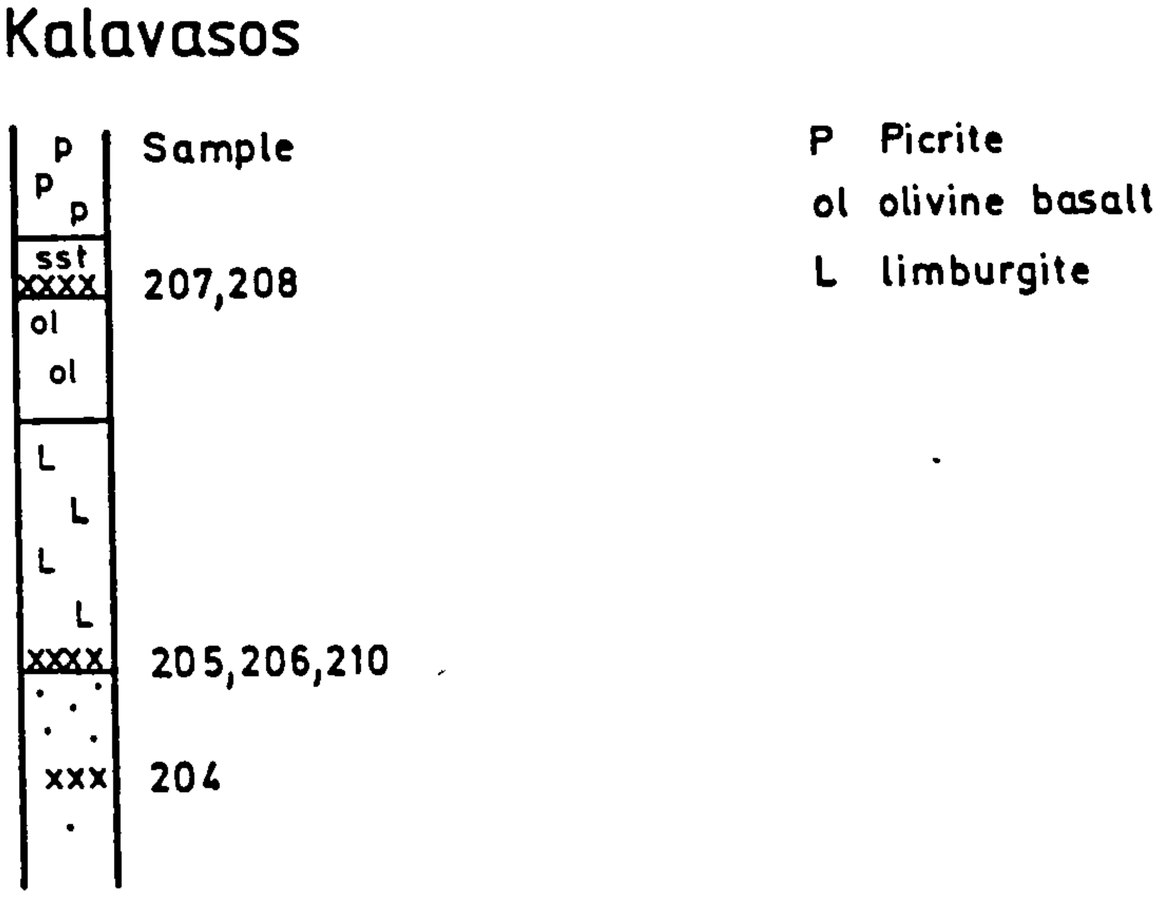

Fig. 4.1 Distribution of interlava sediments in the Mathiati-Margi and Kalavasos areas. a) Compiled sections from the Mathiati-Margi area. Siliceous varieties resulting from hydrothermal alteration are not included. Of each double column, the lefthand side shows the lava unit and the relative abundance of interlava sediment, and the righthand unit shows the type of sediment. b) Schematic section from the Kalavasos mining district. The section is that of 1/2 km east of the mine offices, but is closely similar to the generalised section described by Adamides (1980).

described by Gass (1960). Their distribution is shown on Figs. 3.1, 3.2. The rock is finely laminated and varies in thickness from 0 m to 1m (Plate 4.2A). The mudstone is underlain by a sheet of fine epiclastic sediments and overlain by the lowermost olivine basalt flows of the C unit lavas. Beneath the umber in the A unit lavas is the lower horizon of interpillow oxides. The high manganese content results in the rock being very nearly opaque in thin section. The texture is similar to that of the interpillow sediments (Plate 4.4C). Veins and nodular patches of pyrolusite (Plate 4.4C, 4.3F) testify to the oxidative recrystallisation of some of the primary manganese.

Kambia

Interlava umbers exposed in the Pedhios River in the vicinity of Kambia, were first described by Bear (1960). They comprise a discontinuously exposed band of manganiferous shales. Beneath the shales occur yellow and orange interpillow oxides (Robertson, 1975).

Kalavasos

Thin black manganiferous shales are exposed widely in the banks of the Vasilikos River and its tributaries in the vicinity of the Kalavasos mines. The distribution is indicated on the map of Adamides (1980). These occur at three different horizons (Fig. 4.1B). The middle horizon occurs at the contact between the aphyric lavas and the overlying limburgites (Plate 4.2B) which is the same horizon as the sulphide ore bodies (Adamides, 1980). In thin section, these rocks are seen to be particularly rich in volcaniclastic debris (Plate 4.4D). Interbedded with the volcanic breccias which comprise the upper part of the lava succession, are disrupted horizons of black manganiferous umber (Robertson, 1975). Thus at Kalavosos umbers occur throughout most of the lava succession, as well as occurring on top of them.

In the case of the interlava umbers, secondary removal of manganese is rarely seen. In this they differ from the interpillow oxide sediments which in many cases have been leached of manganese. The umber is distributed widely in the areas in which it is found, indicating that manganese phases were both deposited and preserved

over the whole area of the mineralised terrains. This latter point is important when considering the possible initial distribution of manganese in the interpillow oxide sediments.

4.2.2.3 Interpillow oxide sediments

General statement.

Ferruginous oxide sediment is found filling cooling-fractures in lava flows, in interpillow interstices and as the matrix to breccias. The sediment, which may contain green angular fragments of spalled volcanic glass, varies from a soft ochreous or rarely, umberous, mudstone to paler coloured limestones and vitreous red jaspers. Varying proportions of volcaniclastic material are present.

Regional distribution:

Interpillow oxide sediments are not evenly distributed about the Troodos massif, but are concentrated in the uppermost lavas in regions up to 6km across. Areas of concentration are observed in the vicinity of Skouriotissa, Kambia, Mathiati-Margi, Lymbia, Kalavasos and Limni. In between these areas interpillow oxides are scarce or absent. The association with known ore bodies at all but one of these sites is supported by the almost ubiquitous occurrence of jaspers (of sedimentary origin, see below) in stockwork zones. An important observation is the general up-sequence increase in abundance of sediment. The variation in oxide sediment content in the lavas is illustrated in Fig. 4.1A, which shows three sections through the area between Margi and Mathiati. At depth in the A unit lavas, oxide becomes very scarce.

Mechanism of incorporation

In the vicinity of Margi interpillow oxide sediments are particularly abundant, and clear field relations indicate the mode of formation. Most commonly the sediment occurs in interpillow interstices and is of homogeneous texture. Spalled glass fragments are abundant (Plate 4.1A). Also abundant are vein-like infills of cooling-fractures (Plate 4.1B). These locally contain microfossils. Fractures or pockets occasionally contain bedded sediment. Some of these occur in steep-sided fractures or interpillow pockets, and must have been deposited after eruption by downward percolating

sediment. Others occur as lenses from which the upper parts have been stripped by overriding lava flows (Plate 4.1C). Garrison (1972) describes mechanisms of incorporation of interpillow limestones, and identifies three categories. First, disruption and incorporation of deposited sediment by overriding lava flows. Secondly, eruption of pillowed flows into soft sediment. Thirdly, post-eruptive downward percolation of material. The unlaminated character of the vast majority of the examples suggests that the post-eruptive mechanism is unimportant. The field relations discussed by Garrison (op. cit.), where partially preserved sediment lenses, and vertical variation in sediment abundance feature, are not observed. The regular vertical distribution of interpillow sediment in the Margi area, and absence of lithoclasts, suggests that the originally deposited sediment was less lithified than Garrison's limestone, and was more easily transported through the overriding lavas.

The rarity of "neptunian' fills argues against the possibility that sediment was derived by downward percolation from the umbers as was suggested by Gass (1960).

The uneven distribution of interpillow sediment on the metre scale contrasts with the wider scale variation. The sediment is seen to occur in diffuse horizons within the sequence (Fig. 3.2). In the Margi area two horizons are observed, one in the upper part of the A unit lavas and one in the D unit lavas (Chapter 3, section 3.1.4). Both horizons are richest in their upper parts, achieving a maximumabundance beneath the umbers. The distribution of interpillow sediment is not pipe-like beneath the umbers, in the manner described by Robertson (1975). The lateral persistence of the diffuse horizons over distances of several kilometres argues against isolated local sources as was previously suggested (Robertson op. cit.).

The sediments can be divided into four compositional types: ferruginous mudstones, ferruginous limestones, jasper and manganese-rich varieties.

Ferruginous oxide sediment (Margi-Mathiati area)

The most common sediment type is soft and ochreous, free of carbonate and quartz, and is manganese depleted. This becomes less

volumetrically important towards the upper part of the lava pile, where ferruginous limestones predominate. In thin section a mottled matrix is observed in which scarce fragments of palagonite and microfossils are found. The mottled appearance results from the presence of small 20μm orange to dark brown fragments (Plate 4.3A, B). This texture is the same as that observed in the umber. In the umber the fragments tend to be flattened through compaction, but the pillow lava framework protects the interpillow sediments, and the texture remains largely isotropic. Near circular cross-section of replaced radiolaria are commonly seen in thin section (Plate 4.3B).

Ferruginous limestones

The abundance of carbonate found in the sediment varies from none to nearly one hundred per cent, in the latter case yielding a pale pink to white rock. In the Margi-mathiati area the carbonates are most common in the upper part of the lava succession in the C and D unit lavas (see Chapter 3, Section 3.1.2 for a description of the lava succession). The carbonate is recrystallised imparting to the rock a hardness which is not otherwise seen. Crystals of carbonate can be seen overgrowing matrix textures (Plate 4.3C). In some cases induration by carbonate is marginal to veins of calcite, suggesting a secondary origin. However the occurrence of foraminifera, and vermiform textures (see below) suggests that a proportion of the carbonate is primary.

Jaspers

Cutting the lava pile are a number of normal faults adjacent to which the rock is extensively altered and mineralised. The alteration consists principally of replacement of primary volcanic minerals by silica. As a consequence of this faults form prominent upstanding features. As these faults are approached a progressive alteration of the interpillow sediments is observed. The yellow mudstone may become silicified without dehydration of the goethite, giving rise to a compact yellow/brown chert, but this is relatively scarce. More commonly alteration of the goethite to haematite, produces a strong red colour, yielding the jaspers characteristic of the hydrothermally altered zones. In bedded specimens alternations of quartz, quartz + haematite, and quartz + epidote, the latter presumably after volcaniclastic material are observed (Plate 4.3D).

In the central parts of these altered zones, and in stockworks beneath the sulphides, pyrite crystals appear in fractures, and in the matrix adjacent to the fractures. Even in the sulphide-rich jasper of the stockworks, the characteristic mottled matrix texture, and silicified remains of ostracods are observed in thin section. (Plate 4.3E).

Manganese-rich varieties•

The great majority of the interpillow oxide sediments are of a uniform ochreous colour. However in the upper parts of the lava pile scarce umberous interpillow sediments are found. In almost all cases these umberous sediment bodies have been leached at their margins and there is a sharp irregular boundary between marginal ochreous sediment and an umberous core. The cores to these sediments, when marginal leaching has occurred, are extremely dark, and have manganese concentrations far greater than is is observed in the umber.

Fossil occurrences

In the interpillow sediments faunal remains are scarce and localised. The most abundant forms are poorly preserved radiolaria. Less common are fragments of phosphatised cuticle attributable to ostracods and, rarely, intact ostracod shells, visible in thin section. In one specimen foraminifera and faecal pellets occur, and in another a single coccolith. Vermiform structures attributable to organic activity are found in some of the limestones.

Radiolaria

Radiolaria are found in the form of partially flattened spheres with long axes up to 100μm. Rare tridendate spicules are observed. In the jaspers these are most commonly infilled with quartz or quartz plus epidote, and in the mudstones by goethite.

Ostracods

Scarce fragments of phosphatised cuticle identical to that found in the supralava sediments occur. In the jaspers these are replaced by quartz but the characteristic shape is preserved. These fragments are illustrated and described in Chapter 5 Section 5.2.2.1. More rarely, complete shells are found (Plate 4.5A, B).

Faecal pellets

In two samples taken from the C unit lavas near the Margi-Kataliondas road, faecal pellets were found. These are cigar-shaped, up to 0.5 mm in diameter and 2.5 mm long. They are characterised by four axially symmetrical channels (Plate 4.5C, D, E). The pellets resemble those of some modern decapod crustaceans and are possibly referable to Favreina (C.G. Adams, British Museum, Pers. Comm. 1982).

Foraminifera

In one sample, poorly preserved planktonic foraminifera are found (Plate 4.5E). Some vestige of coarse surficial ornamentation is preserved, but further identification is not possible.

Vermiform structures

Elongate winding cylinders of carbonate overgrow the muddy matrix in some of the limestones (Plate 4.4B). The rhomb-shaped outlines may have been formed during recrystallisation of the carbonate (Plate 4.4A). The vermiform shape is strongly suggestive of an organic origin.

4.2.3 Mineralogy

In Table 4.2 the mineralogies of the various interlava oxide sediments are contrasted. The data for this table were obtained largely through X-ray diffraction studies, owing to the fine grained character of the sediments.

Goethite. Goethite occurs in all sediment type except jasper where it has been transformed into haematite. Constantinou and Govett (1972) note that goethite in the dark fine-grained ochre is less crystalline than that of the coarsely-crystalline yellow or orange yellow ochre. No significant variation in crystallinity of goethite through the sequence is observed. However, the goethite is significantly more crystalline in the interlava sediments than in the supralava umber. This may reflect a higher temperature of diagenesis.

Haematite. Haematite is abundant in the jasper where it is presumably derived by dehydration of goethite. This interpretation is supported by the similarity in texture of the jaspers to the unaltered mudstones.

Table 4.2

Table of interlava sediment mineralogy

Mineral	Ochre	Interlava umber	Interpillow oxide sediment Mudstone	Limestone	Jasper
Goethite	A	A	A	A	-
Hematite	L	-	-	-	A
Quartz	P	-	-	-	A
Carbonate	L	-	-	A	-
Smectite	L	P	P	P	-
Illite	P	-	-	-	-
Analcite	-	-	A	L	-
Apatite	-	P	S	S	-
Manganese	L	A	L	L	-
Sulphide	L	-	-	-	L
Others	Local Gypsum	Chlorite Palygorskite	Rare Natrolite feldspar Native Cu		Locally Epidote

A = Abundant P = Present L = Local - = Absent S = Scarce

Quartz. Quartz, which is an abundant mineral in the supra-lava sediments is present only in the ochre and in the hydrothermally altered sediments. In the ochre, quartz, which is not of secondary origin, may have been derived from quartz associated with the sulphide ore. The absence of quartz from the interpillow oxide sediments, even those in the vicinity of the orebodies, sets them apart compositionally from the ochre.

Carbonate. Constantinou and Govett (1972) report the occurrence of both calcite and siderite in the calcareous ochre at Mathiati. The calcite was found to contain no FeO, from which it was deduced that the environment of formation was oxidising. The interpillow ferruginous limestones contain more or less coarsely-crystalline calcite. No probe determinations have been made, but the whole-rock chemical data indicate that the mineral is low-Mg calcite.

Sheet silicates. Locally in the ochre are found beds of grey-green volcaniclastic debris now altered to smectite. The ochre away from these bands contains little basaltic material. In both the interpillow oxide, and the interlava umber, smectite is ubiquitous and is locally abundant. The major-element chemistry of the alumino-silicate component of the rock is comparable with the iron rich saponites of the lavas. Illite, which is observed in the ochre (Constantinou and Govett, 1972) is absent from the other interlava sediments. Chlorite was identified in small quantities in two samples of interlava umber from near Kotchiati. Palygorskite occurs in small quantities in the umber, as it does in all supralava sediments. Some of the volcaniclastic rich sediments of the Skouriotissa ochres are rich in palygorskite, possibly resulting from hydrothermal alteration of the basaltic debris (Robertson, 1976a).

Analcite. Analcite, not reported in the ochre, is almost ubiquitous in the interpillow oxides from the A unit lavas. In stratigraphically higher lavas it becomes increasingly scarce. Locally euhedral analcite is visible in vugs and veins cutting the sediment, but more commonly it is microcrystalline and dispersed throughout the matrix.

Apatite. Apatite is found in all of the sediments except the ochres, but is most abundant in the interlava umbers. It is rarely visible in thin section, but shows up in XRD traces. In contrast to

the supra-lava umbers, there is at least one Ca bearing phase other than apatite, so the Ca/P ratio is always greater than that of apatite.

Manganese minerals. Constantinou and Govett (1972) conclude from the evidence of electron microprobe scans that there are no discrete Mn minerals in the brown ochre. They found however anhedral manganese-rich grains in the yellow coarsely-crystalline ochre.

In the interlava umbers and in some of the interpillow oxide sediments pyrolusite occurs commonly as small spherules and fracture fills. These are undoubtedly of secondary origin. No other manganese minerals have been identified, but the large amounts of manganese indicated by the whole rock chemistry requires there to be a manganese-bearing phase. The X-ray diffraction pattern using CuKα radiation, rule out birnessite or todorokite. Poorly crystalline δ-MnO_2 remains a strong possibility. Veins of this mineral identified by XRD are present in the lavas, demonstrating that it can be preserved. The two δ-MnO_2 X-ray diffraction peaks are coincident with the main goethite peaks, so the latter is an effective mask.

Sulphide. Sulphides are found only in the ochre and in sediments which have been subjected to intense hydrothermal alteration. In the ochre the principal mineral is pyrite, but covellite, commonly intergrown with digenite, is found as well as rare.chalcopyrite (Constantinou and Govett, 1972).

Other minerals. Gypsum is reported in the calcareous ochre at Mathiati, (Constantinou and Govett, 1972), but this is all apparently of secondary origin (Robertson, 1976a).

Feldspar and pyroxene of basaltic origin occur in some of the interlava sediments, particularly in the interlava umbers which are associated with the epiclastic sediments.

Native copper is found as veins and wires passing through the interpillow oxide sediment found in the vicinity of the Mathiati mine. The proximity to the ore body suggests that this may be the source of the copper. Some of the inter-pillow sediments may thus have become significantly enriched in copper during this veining.

Epidote is found in the bedded jasper where it occurs as small euhedral needles up to 100μm long and 25um across surrounded by recrystallised quartz.

4.2.4 Chemical characteristics and variations of the oxide facies sediments

4.2.4.1 General statement

The average chemical compositions of ochre, interpillow oxide, and interlava umber are shown on Table 4.3A. All of the interlava sediments are enriched in Fe, V, Cu, Zn and Y with respect to deep-sea clay. Mn, Ni, Pb and Sr are enriched in the interlava umbers, and locally enriched in the interpillow lava oxides. The ochres are characterised by particularly high Fe, Cu and Zn concentrations. The interpillow oxides and interlava umbers both differ from the ochre in their high content of aluminosilicate elements. The interlava umbers are distinguished by higher concentrations of Mn, Pb, Sr, Ba, La and Nd.

4.2.4.2 Ochres

The ochres contain on average greater than 40% Fe, a concentration higher than is observed in the other oxide metalliferous sediments. Cu and Zn concentrations and Cu/Fe Zn/Fe ratios are also significantly higher than in the other sediments, and are extremely variable. The broad correlation between the copper content of the ochre and the spatially associated sulphide ore supports the view that the two are genetically related (Constantinou and Govett, 1972). These authors also note a sympathetic increase in Mn and Ni values in ochre occurring progressively further from the ore. Bedded ochres well above the ochre/sulphide contact contain concentrations of Ni similar to the interpillow oxides.

4.2.4.3 Interpillow oxide sediment

The four compositional types; ferruginous mudstones, limestones, and cherts, and ferromanganiferous sediments, are compared in Table 4.4.

The ferruginous mudstones have been sub-divided into those with or without analcite as a component mineral. Those containing analcite have higher Na, Al and Si than those which do not. Evidence presented below (Section 4.2.5) indicates that analcite has resulted from addition of components rather than isochemical alteration.

TABLE 4.3A

MEAN OCHRE COMPARED WITH OTHER INTERLAVA SEDIMENTS.

Rock type	Ochre					Interpillow oxide sediment	Interlava umber	Ochre mean
Locality	Skouriotissa Mathiati	Skouri-otissa	Mathiati	Mathiati	Kambia	Mathiati-Margi	Mathiati-Margi-Kalavasos	
Data source	C	R	R	G	B	B	B	
	N=4	N=7	N=1	N=1	N=1	N=34	N=13	N=14
Si				6.73	4.80	10.85 ± 6.55	10.72 ± 5.52	
Al	0.92 ± 0.41	3.7	4.0	2.40	0.72	4.69 ± 2.89	3.92 ± 1.75	2.62
Fe	42.65 ± 8.76	47.6	51.1	39.51	47.63	14.53 ± 10.18	25.62 ± 7.90	45.82
Mg		0.5	4.8	2.38	0.34	2.35 ± 2.33	1.55 ± 0.62	
Ca		0.8	0.02	0.56	0.02	11.86 ± 14.10	2.68 ± 1.14	
Na				0.17	0.02	1.95 ± 2.71	0.66 ± 0.77	
K		0.6	0.7	0.33	0.02	0.57 ± 0.51	1.07 ± 0.99	
Ti		0.05	0.10	0.26	0.09	0.07 ± 0.05	0.21 ± 0.21	
Mn	0.59 ± 0.49	0.76	1.96	1.93	1.56	1.32 ± 2.98	7.69 ± 7.23	0.94
P					0.49	0.11 ± 0.07	0.59 ± 0.42	
Ba		51	16		600	120 ± 451	130 ± 85	105
Ce					*	*	16 ± 26	
Co	168 ± 109	79	47	159		37 ± 20(N=6)	50(N=1)	110
Cr		15	38	45	14	30 ± 24	25 ± 15	20
Cu	7890 ± 9500	556	1600	5000	1028	923 ± 1072	827 ± 810	3077
La					15	14 ± 15	92 ± 40	
Nd					*	12 ± 13	64 ± 33	
Ni	38 ± 10	309	126	321	130	132 ± 94	206 ± 94	207
Pb		219	59		31	20 ± 33	110 ± 60	180
Rb					*	10 ± 10	20 ± 13	
Sr		31	63	60	36	83 ± 160	179 ± 89	38
V		432	872	254	763	1048 ± 751	873 ± 422	491
Y					12	39 ± 22	100 ± 47	
Zn	491 ± 454	448	592		2259	141 ± 103	242 ± 60	535
Zr		644	272		89	42 ± 34	60 ± 20	

*Not detected

Data sources: C = Constantinou and Govett (1972); R = Robertson (1976a); G = Guillemot and Nesteroff (1980); B = This work.

TABLE 4.3B

ELEMENT/FE RATIOS FOR AVERAGE OCHRES COMPARED WIHT OTHER CYPRUS METALLIFEROUS SEDIMENTS.

	Av. Ochre	Av. Interpillow oxide sedidment	Av. Interlava umber	Av. Margi Supra lava umber	Av. Dhrapia umber
Mn	0.021	0.091	0.30	0.24	0.17
x10^4 V	10.7	72	34	40	33
x10^4 Ba	2.3	8.3	5.1	46	3.6
x10^4 Cu	67	64	32	28	23
x10^4 Ni	4.5	9.1	8.0	13	4.0
x10^4 Zn	12	9.7	9.5	16	8.4
x10^4 Pb	3.9	1.4	4.3	17	2.8
x10^4 Sr	0.83	5.7	7.0	56.8	7.1

Element/Fe ratios are however very similar, so the addition of analcite has not resulted in significant alteration of the pre-existing composition. The ferruginous mudstones contain greater amounts of aluminosilicate elements, and thus lower abundances of the hydrothermal elements, than the ochre. They resemble the ochre however in having a high and variable copper content.

The ferruginous limestones are composed predominantly of $CaCO_3$. They are depleted in all trace elements but Sr with respect to the carbonate free interlava oxide, but in most cases have similar element/Fe ratios to the latter. They have slightly higher Mn, Pb and Ni ratios, and very much higher Sr.

The cherts are composed predominantly of silica, but are significantly enriched in Fe. Element/Fe ratios are low, suggesting that silicification has resulted in loss of trace elements.

The ferromanganiferous sediments cannot be sharply separated from the remainder, as a gradation exists. The two analyses presented in Table 4.4 are slightly carbonate enriched. Both have significantly higher Ni, Pb, Sr and Ba than the other sediments, in this respect resembling the interlava umbers. One of the samples is also enriched in La and Nd, which is a characteristic of the umbers.

The clear field evidence that manganese has been leached from the margins of some of the large interpillow sediment bodies raises the possibility that many or all of the manganese-free interpillow sediments were originally manganiferous. In Table 4.7, an analysis is shown of a paired sample taken from either side of a leach front in the manganiferous interlava sediments. The leached sediment has lost Mn ,Ba and Sr. The trace element/Fe ratios are compared with those of the mean ferruginous mudstone, and mean ferruginous limestone. The leached sub-sample falls within or marginal to one standard deviation for the mean ferruginous limestone. Thus the chemical data are compatible with leaching of manganese from all interlava sediments.

Table 4.5 shows the mean compositions of interpillow oxide sediment (not subdivided into compositional types) from three sample traverses between Margi and Mathiati. The location of the traverses

TABLE 4.4A

AVERAGE COMPOSITIONS FOR INTERPILLOW OXIDE SEDIMENT TYPES FROM THE MARGI - MATHIATI AREA.

	FERRUGINOUS MUDSTONE Analcite Free	FERRUGINOUS MUDSTONE All samples	FERRUGINOUS Limestone	Ferro-manganese-rich 81-44	Ferro-manganese-rich 81-48	FERRUGINOUS Chert Brown 82-55	FERRUGINOUS Chert Red 80-226
	N=6	N=18	N=7	N=1	N=1	N=1	N=1
Si	12.30 ± 2.38	14.86 ± 3.50	2.09 ± 2.21	4.01	7.73	37.63	43.19
Al	5.46 ± 0.85	6.74 ± 1.60	0.77 ± 0.64	1.86	4.15	0.43	0.10
Fe	28.24 ± 6.00	21.79 ± 7.82	2.83 ± 1.12	17.66	12.01	10.38	4.71
Mg	3.20 ± 1.81	2.61 ± 1.61	0.88 ± 0.59	0.92	3.69	0.08	0.10
Ca	1.19 ± 0.36	1.12 ± 0.82	33.51 ± 3.86	13.65	7.43	0.19	0.03
Na	0.69 ± 0.40	3.30 ± 2.90	*	0.03	0.18	0.04	0.05
K	0.90 ± 0.25	0.59 ± 0.37	0.20 ± 0.31	0.74	0.88	0.01	*
Ti	0.12 ± 0.04	0.09 ± 0.04	0.02 ± 0.02	0.06	0.05	0.02	0.01
Mn	0.93 ± 0.24	0.71 ± 0.30	0.26 ± 0.13	11.28	14.73	0.13	*
P	0.18 ± 0.07	0.14 ± 0.06	0.04 ± 0.04	0.27	0.09	0.06	0.01
Ba	36 ± 9	27 ± 10	2 ± 52	2609	71	30	11
Ce	*	*	*	11	*	*	*
Cr	43 ± 19	41 ± 19	14 ± 21	*	*	10	*
Cu	1061 ± 785	1176 ± 1050	140 ± 112	683	3543	122	74
La	19 ± 7	16 ± 9	7 ± 2	87	*	12	*
Nd	14 ± 14	11 ± 12	10 ± 3	61	*	7	*
Ni	235 ± 73	169 ± 72	35 ± 15	363	317	22	*
Pb	20 ± 5	14 ± 6	*	197	78	*	*
Rb	17 ± 2	11 ± 6	*	8	11	*	*
Sr	36 ± 11	30 ± 11	81 ± 9	964	245	11	*
V	1560 ± 433	1499 ± 551	163 ± 125	1561	626	188	*
Y	60 ± 24	50 ± 19	18 ± 5	82	33	27	*
Zn	246 ± 62	198 ± 93	23 ± 10	236	206	22	*
Zr	81 ± 35	61 ± 31	*	55	38	*	*

* Not detected

TABLE 4.4B

Element/Fe ratios for average interpillow oxide sediment types.

		FERRUGINOUS MUDSTONE Analcite free	FERRUGINOUS MUDSTONE All samples	FERRUGINOUS Limestone	Ferro-manganese-rich 81-44	Ferro-manganese-rich 81-48	FERRUGINOUS chert 82-55	FERRUGINOUS chert 80-226
	Mn	0.033	0.033	0.092	0.639	1.226	0.013	*
x10^4	V	55.2	68.8	57.6	88.4	52.1	18.1	*
	Ba	1.29	1.27	0.89	148	5.91	2.89	2.34
	Cu	37.6	53.9	49.6	38.7	295	11.8	15.7
	Ni	8.34	7.76	12.4	20.6	26.4	2.12	*
	Zn	8.73	9.11	8.34	13.4	17.2	2.12	*
	Pb	0.71	0.69	3.08	11.2	6.49	0.87	*
	Sr	1.30	1.40	28.9	54.6	3.16	1.06	*

TABLE 4.5A

AVERAGE COMPOSITION OF INTERPILLOW SEDIMENTS OF THE MARGI-MATHIATI AREA DIVIDED GEOGRAPHICALLY.

Host lava unit	MARGI C/D lavas	YIALIAS RIVER C/D lavas	MARGI A lavas	YIALIAS RIVER A lavas	MATHIATI MINE A lavas
	N=10	N=8	N=1	N=11	N=6
Si	7.57 ± 6.69	6.75 ± 5.94	13.79	13.99 ± 4.14	16.13 ± 2.03
Al	2.83 ± 2.35	3.08 ± 2.67	7.12	6.01 ± 2.03	7.47 ± 0.94
Fe	8.92 ± 6.82	15.12 ± 12.68	23.36	18.71 ± 8.88	16.83 ± 8.52
Mg	3.31 ± 3.67	1.77 ± 1.56	0.63	2.49 ± 1.46	1.78 ± 0.50
Ca	19.31 ± 14.51	17.78 ± 16.96	0.72	4.56 ± 6.31	3.18 ± 5.01
Na	0.39 ± 0.67	0.48 ± 0.84	5.33	2.58 ± 3.13	5.11 ± 2.13
K	0.43 ± 0.35	0.52 ± 0.46	0.15	0.80 ± 0.64	0.37 ± 0.23
Ti	0.05 ± 0.03	0.05 ± 0.04	0.09	0.10 ± 0.06	0.11 ± 0.05
Mn	2.86 ± 5.13	0.85 ± 0.55	1.23	0.67 ± 0.32	0.48 ± 0.21
P	0.10 ± 0.08	0.09 ± 0.05	0.07	0.11 ± 0.06	0.14 ± 0.09
Ba	260 ± 783	132 ± 233	24	19 ± 8	38 ± 32
Ce	*	*	*	*	*
Cr	9 ± 20	28 ± 21	29	43 ± 18	46 ± 13
Cu	606 ± 1029	418 ± 290	217	2011 ± 4050	2410 ± 962
La	18 ± 25	11 ± 4	13	12 ± 6	16 ± 10
Nd	16 ± 18	7 ± 5	9	7 ± 8	18 ± 12
Ni	146 ± 125	106 ± 77	115	146 ± 81	117 ± 48
Pb	36 ± 57	14 ± 6	27	13 ± 4	11 ± 4
Rb	6 ± 5	8 ± 9	*	15 ± 12	6 ± 4
Sr	180 ± 266	68 ± 49	15	28 ± 13	30 ± 9
V	473 ± 465	936 ± 659	993	1325 ± 710	1698 ± 460
Y	37 ± 25	28 ± 16	52	43 ± 14	51 ± 25
Zn	109 ± 95	104 ± 87	175	186 ± 110	179 ± 74
Zr	22 ± 19	39 ± 35	73	44 ± 30	78 ± 27

* Not detected

TABLE 4.5 B

Element/Fe ratio for average interpillow oxide sediments.

		MARGI	YIALIAS RIVER	MARGI	YIALIAS RIVER	MATHIATI MINE
	Mn	0.32	0.056	0.053	0.036	0.029
x10^4	V	53	62	43	71	101
	Ba	29	9.0	1.0	1.0	2.3
	Cu	68	28	9.3	107	143
	Ni	16	7.0	5.0	7.8	7.0
	Zn	12	7.0	7.5	9.9	10.6
	Pb	4.1	0.9	1.2	0.7	0.7
	Sr	20	4.6	0.7	1.5	1.8

are shown in Fig. 3.1. Each traverse has been divided at the A unit/C unit lava contact where possible, into an upper and lower part. Significant lateral and vertical variation is apparent.

Vertical variation is influenced strongly by the high carbonate content, and corresponding dilution of the metalliferous component, of the upper part. Further, the addition of analcite to sediments in the lower part elevates Na, Al and Si. Recalculation on a carbonate and analcite free basis, described below, clarifies the vertical variation in sediment components. However, the element/Fe ratios illustrate the important changes in the metalliferous component. The sediments of the upper lava units have a higher element/Fe ratio in the cases of Mn, Ba, Pb and Sr. As in the ochre, Cu is extremely variable.

Horizontal variations are again obscured by variable dilution by carbonate and analcite, and are more fully discussed below (Section 4.2.6). However, an increase with lateral distance from the Mathiati ore body of Mn/Fe and Pb/Fe ratios, and a complementary decrease in Cu/Fe and V/Fe ratios is observed.

4.2.4.4 Interlava umber

The interlava sediments are all free of carbonate, and contain little analcite, and consequently dilution effects are less important. Table 4.6 compares chemical data for interlava umbers from the Pedhios River Kambia, the Margi Mathiati area and Kalavasos. Compared with the ochres and inter-pillow oxides, the interlava umbers of Margi, Yialias and Kalavasos are enriched in Mn, Ba, Pb, Sr, La and Nd. The concentration of Mn is variable but similar to that of the supralava umber. Ba, Pb, Sr and REE are at lower concentration than in the mean supralava umber but are well within the range observed. The most significant difference between the interlava and supralava umber is in the composition of the lithogenous component which is for the former derived by local erosion of the lavas (Section 4.3.1). With the exception of Cu, which is very variable, and P, which is more enriched in the Kalavasos area, the interlava umbers are of remarkably constant composition.

TABLE 4.6A

MEAN INTERLAVA UMBER COMPOSITIONS - MARGI, MATHIATI, KAMBIA AND KALAVASOS.

Locality	KAMBIA	MARGI	YIALIAS RIVER	MATHIATI	KALAVASOS
Data source	R	B	B	B	B
	N=4	N=3	N=2	N=2	N=6
Si	No major	16.31 ± 5.39	7.54 ± 1.60	4.67 ± 0.13	11.00 ± 4.40
Al	element	5.57 ± 1.90	2.13 ± 0.26	2.36 ± 0.08	4.21 ± 1.22
Fe	data	23.94 ± 8.92	26.28 ± 0.60	37.22 ± 6.37	22.37 ± 5.00
Mg		1.95 ± 0.52	1.11 ± 0.33	0.99 ± 0.05	1.68 ± 0.64
Ca		2.52 ± 1.09	1.32 ± 0.11	1.95 ± 0.27	3.46 ± 0.87
Na		1.24 ± 0.94	0.10 ± 0.01	*	0.79 ± 0.63
K		0.23 ± 0.72	0.61 ± 0.08	0.25 ± 0.03	1.42 ± 1.19
Ti		0.50 ± 0.27	0.11 ± 0.01	0.06 ± 0.01	0.15 ± 0.06
Mn		1.63 ± 1.11	14.72 ± 3.68	7.39 ± 5.59	8.48 ± 7.90
P		0.20 ± 0.12	0.23 ± 0.00	0.62 ± 0.12	0.90 ± 0.39
Ba	87 ± 24	107 ± 19	126 ± 2	310 ± 423	56 ± 10	168 ± 109
Ce		6 ± 2	75 ± 5		5 ± 1	4 ± 8
Co	65 ± 9		50(N=1)	72 ± 11		
Cr	18 ± 5	9 ± 4	35 ± 5	30 ± 8	42 ± 3	24 ± 14
Cu	1020 ± 942	202 ± 121	1379 ± 348	370 ± 152	1817 ± 1183	626 ± 495
La		55 ± 25	155 ± 0		123 ± 18	81 ± 23
Nd		48 ± 37	104 ± 13		96 ± 26	49 ± 12
Ni	364 ± 58	185 ± 98	308 ± 56	280 ± 81	325 ± 35	144 ± 25
Pb	134 ± 34	105 ± 40	149 ± 22	91 ± 77	37 ± 2	125 ± 65
Rb		21 ± 8	21 ± 4		*	25 ± 14
Sr	61 ± 9	175 ± 96	221 ± 23	491 ± 331	86 ± 24	197 ± 91
V	892 ± 494	1142 ± 357	708 ± 117	683 ± 146	1269 ± 90	661 ± 415
Y		79 ± 48	143 ± 8		166 ± 40	74 ± 11
Zn	330 ± 47	261 ± 25	303 ± 25	194 ± 123	313 ± 5	189 ± 35
Zr	563 ± 43	87 ± 6	78 ± 5	316 ± 84	50 ± 2	44 ± 7

* Not detected. R = A H F Robertson, unpublished data; B = J F Boyle

TABLE 4.6B

Element/Fe ratios for interlava umbers (all data from J F Boyle)

		MARGI	YIALIAS RIVER	MATHIATI	KALAVASOS
	Mn	0.068	0.560	0.199	0.379
$\times 10^4$	V	47.7	26.9	34.1	29.5
	Ba	4.47	4.79	1.50	7.51
	Cu	8.4	52.5	48.8	28.0
	Ni	7.7	11.7	8.7	6.4
	Zn	10.9	11.5	8.4	8.4
	Pb	4.39	5.67	0.99	5.59
	Sr	7.31	8.41	2.31	8.81

TABLE 4.7a

PAIRED SAMPLES ACROSS A MANGANESE LEACH FRONT.

	82-52B	82-52A
Si	0.48	0.32
Al	0.28	0.17
Fe	3.29	2.18
Mg	0.26	0.19
Ca	35.03	36.01
Na	0.02	0.02
K	0.07	0.06
Ti	0.01	0.01
Mn	0.45	2.08
P	0.05	0.04
Ba	52	744
Ce	34	*
Cr	9	6
Cu	352	680
La	*	*
Nd	16	*
Ni	33	35
Pb	*	*
Rb	*	*
Sr	75	185
V	391	295
Y	13	10
Zn	18	13
Zr	*	*

* Not detected

TABLE 4.7b

Element/Fe ratios for sample pair.

		82-52B	82-52A	Mean analcite-free ferruginous mudstone		Mean ferruginous limestone	
	Mn	0.137	0.954	0.033	0.011	0.092	0.059
$\times 10^4$	V	119	135	55.2	19.3	57.6	49.7
	Ba	15.8	341	1.29	0.44	0.89	18.7
	Cu	107	312	37.6	28.9	49.6	44.3
	Ni	10.0	16.0	8.34	3.13	12.4	7.42
	Zn	5.5	4.6	8.73	2.87	8.34	4.92
	Sr	22.8	84.9	1.30	0.5	28.9	11.9

4.2.5 Simplification of chemical variation : Identification of independent chemical components

The interlava oxide sediments are of very diverse composition. However, the compositional types can all be explained in terms of variable mixing of a small number of independent major element components, which are common to them. Later, the composition and distribution of these components may be used to infer their origin, and hence the origin of the sediments themselves.

Linear trends on two element variation diagrams may be interpreted on the basis of the Lever rule as mixing trends between phases which contain the relevant elements. The chemical components described below are end members identified from variation diagrams, and are those chemical entities which behave independently of each other, causing variations in the bulk composition. Physically they represent either individual minerals, for example calcite, or groups of minerals which co-vary.

Silica

The existence of a silica component is inferred from the presence of radiolaria in the sediments. However, abundances are very low and have no detectable effect upon the silica content of the rocks. Those rocks containing secondary silica as a result of hydrothermal alteration are not included in this discussion.

Analcite

Analcite is observed in X-ray diffraction traces in most of the sediments found in the A lava unit. Sediments from the C/D lava unit are largely analcite free. The effect of this upon the chemistry of the sediments is clearly illustrated in Figs. 4.2A, B. The compositions fall in a triangular field, with analcite at the apex. That the triangular field is full, indicates that preferential loss of the original Mg and Al has not occurred. Simple mixing of analcite with the variable Mg/Al aluminosilicate perfectly explains the range of composition, thus it is proposed that analcite has been quantitatively added to the rock. This is observable in some places in the form of veins or vugs of euhedral analcite but more frequently the analcite is too fine grained. The compositions can be

Fig. 4.2

Major element chemical variations in the interlava metalliferous sediments. All axes are wt % element.

a,b) Illustrate the influence of analcite on the composition of the sediment. The distribution can be best explained in terms of simple mixing of analcite with the rock.

c) A triangular plot of Si-Al-Mg, except that Si and Al have been corrected for analcite, assuming that all Na is in analcite. The distribution of compositions is different from that of the lavas, which are less variable. The pattern instead resembles that of the lava alteration smectites.

d) Al-Fe-Mg with Al corrected for analcite. The distribution again resembles that of the lava smectites, but there is enrichment in Fe from the metalliferous component of the rock.

e) Al-Fe-Mn shows mixing between three compositions. Al-rich Mn depleted aluminosilicate. Fe rich but Mn bearing component, and Mn component.

f) Mn-Fe. Though many of the rocks are relatively Mn depleted, there is a clearly defined minimum Mn/Fe ratio. This probably corresponds with Mn directly associated with the iron oxides.

Fig. 4.2

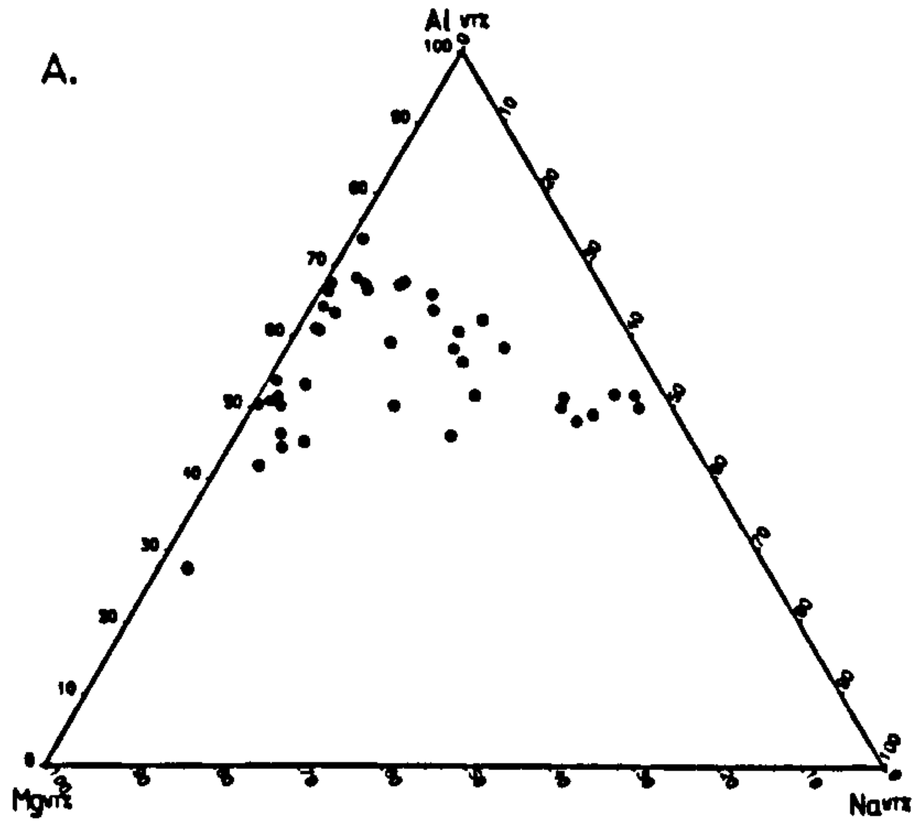
A.
Al wt%
Mg wt%
Na wt%

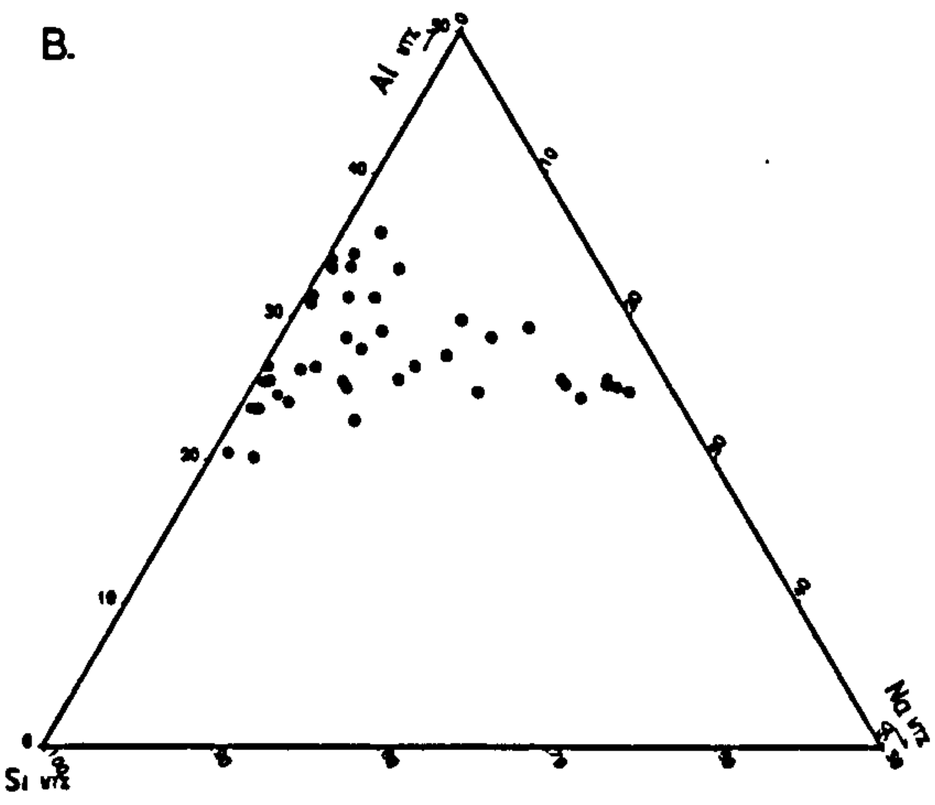
B.
Al wt%
Na wt%
Si wt%

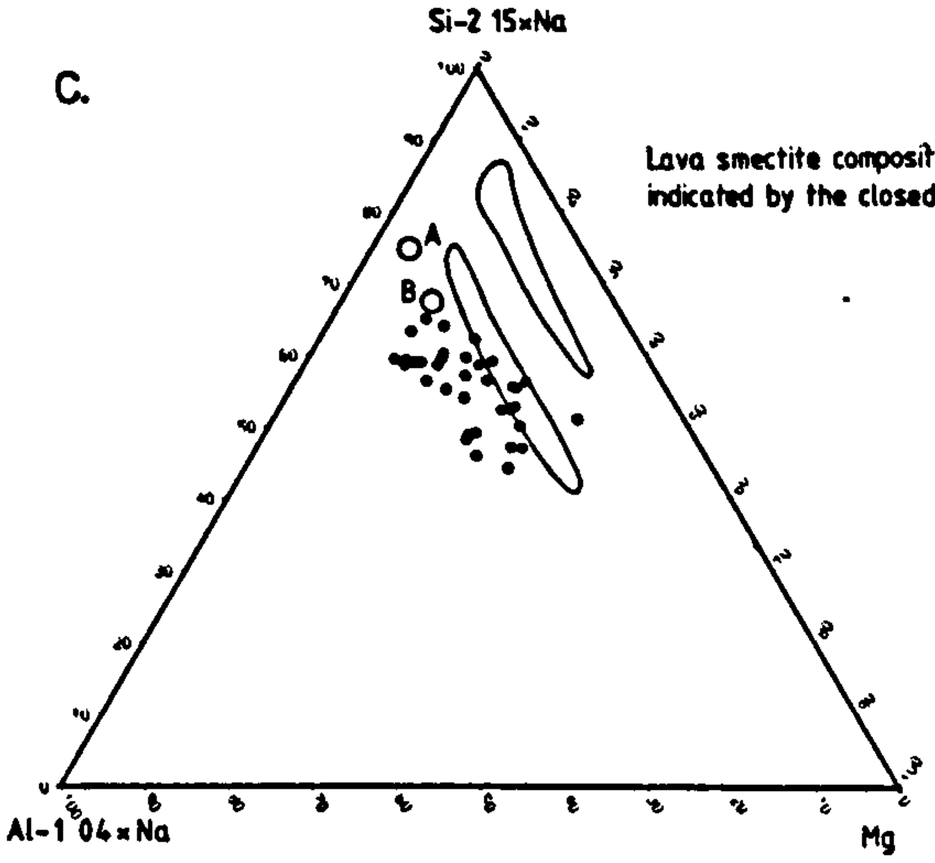
C.
Si-2 15×Na
Lava smectite composition
indicated by the closed fields
A
B
Al-1·04×Na
Mg

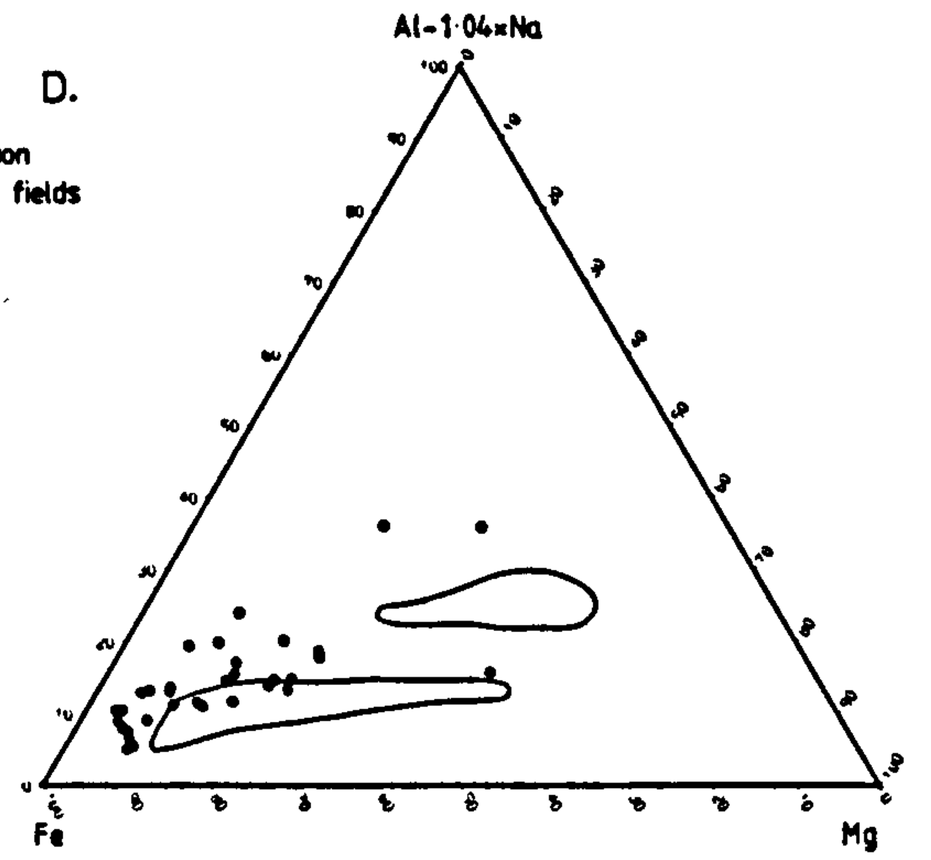
D.
Al-1·04×Na
Fe
Mg

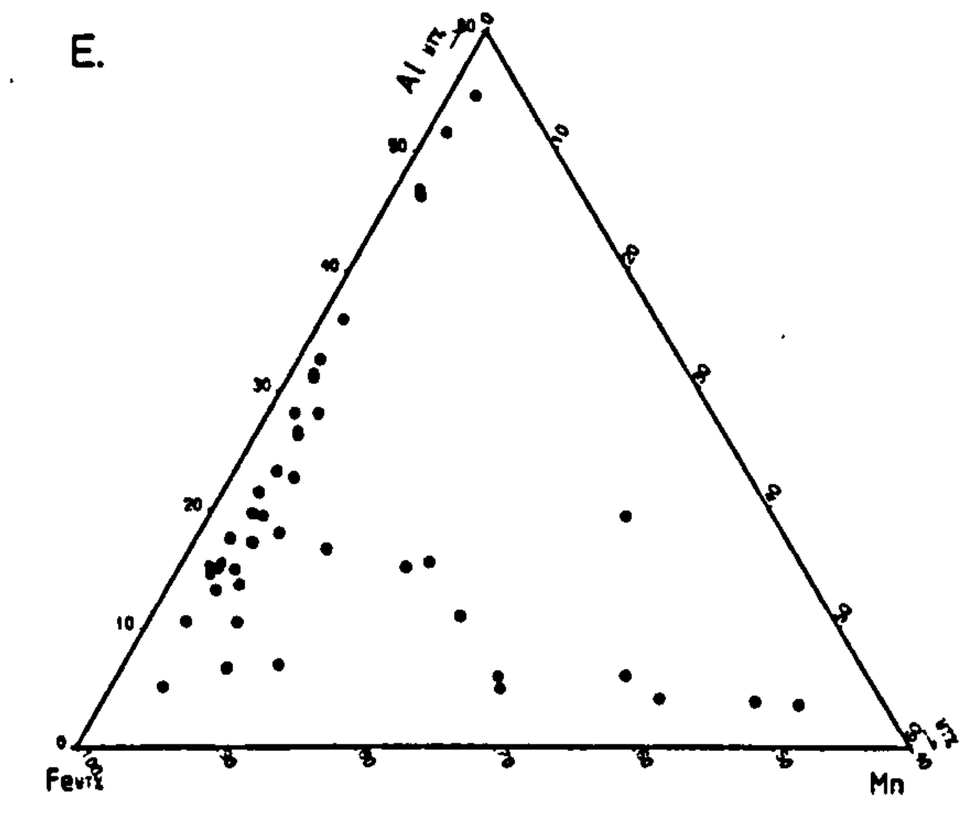
E.
Al wt%
Fe wt%
Mn

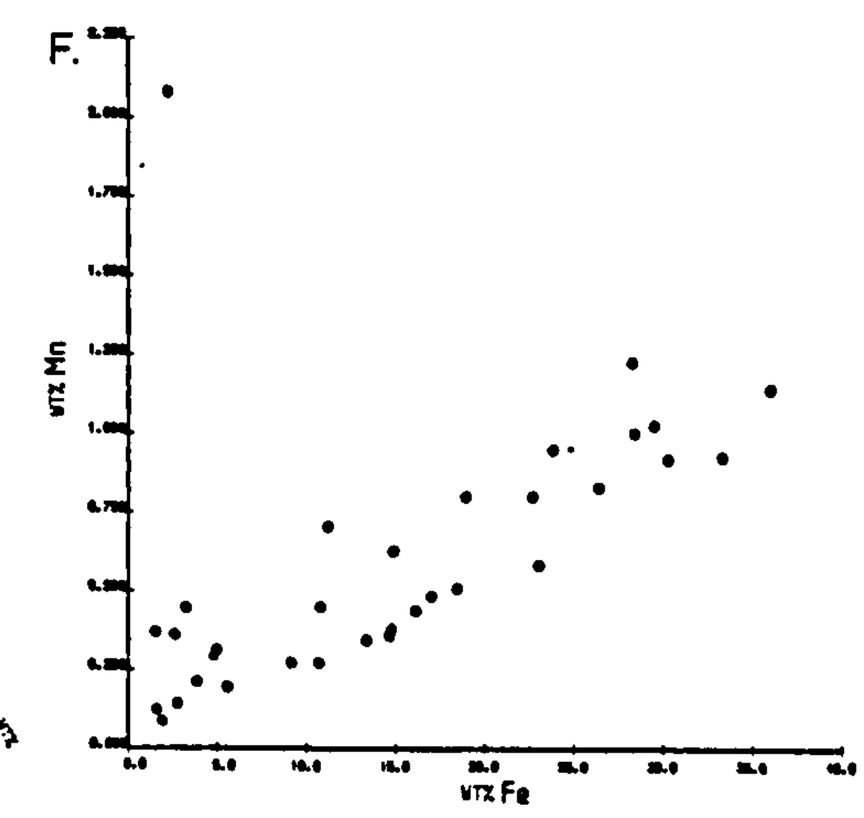
F.
wt% Mn
wt% Fe

recalculated on an analcite-free basis, affording more reasonable comparison of the sediments throughout the succession. For this a composition for the analcite is required. From Fig. 4.2A the Na:Al ratio is 49:51. On Fig. 4.2B the maximum silica limit intersects this Na:Al ratio at Si : Al : Na = 51.3 : 24.8 : 23.9. This is very similar to the ideal ratio of 52.9 : 25.4 : 21.7.

•

Calcite

Carbonate is present in many of the sediments from the C/D unit lavas. Calculation of the quantity of carbonate present strictly requires knowledge both of the composition of the carbonate, and the Ca content of the other phases, neither of which is known accurately. A correction can be applied for the Ca in apatite, but Ca in the aluminosilicates is variable, and any correction would be unreliable. Non-apatite, non-carbonate Ca values are however less than 1.5%, and so recalculation on a Ca-free basis is not a serious over-simplification.

Direct measurements of Mg content were not made. However there is no significant change in Mg/(corrected Al) over the range of carbonate contents suggesting that Mg contents could be no more than 1%.

Apatite

Ca/P ratios are all in excess of those expected for apatite (by the ratio given by probe data from phosphatised cuticle, and XRF from the Mangalene phosphatic concretion). None however fall below this line, and all excess can be explained by the other aluminosilicates and/or carbonate. Carbonate corrected data shows no correlation with Fe. It is thus considered likely that P is not present as ferriphosphate. Where phosphate concentrations are high (> 1%) apatite is detectable on XRD. A correction for Ca and calculation of the abundance of apatite is based upon the assumption that all P is in apatite with Ca/P = 2.65

Aluminosilicate

The non-analcite aluminosilicate of the interlava oxide is mostly smectite (XRD). Quartz is absent from all but one sample,

distinguishing the aluminosilicate from that in the supralava sediments. Quartz in the one sample may have been derived as fragments from a hydrothermal vent; the ochre, proximal to the vents, can be quite rich in quartz. The interlava umbers are complicated by containing small but significant amounts of feldspar and other volcanic silicate minerals.

Fe in the clays is masked by the goethite, so variations in Si Al and Mg are more useful. These can be looked at for both naturally analcite-free sediments, and recalculated analyses. (This is necessary owing to the Si and Al enrichment accompanying formation of the analcite).

In Table 4.8 elemental ratios in the lavas and in the interpillow oxides are compared. The ratios for those sediments corrected for analcite are similar to those which are naturally analcite-free. The Mg/Al and Ti/Al ratio are similar for all the interpillow sediments. They are close to the ratios for the C/D unit lavas, but distinctly different from those of the A unit lavas. Consequently even for those sediments contained deep within the A unit lavas, the lithogenous component seems to have been derived from the C/D unit lavas.

The interlava umbers have on average lower Mg/Al and greater Ti/Al ratios than have the interpillow oxides, more closely resembling the A unit lavas. This is in keeping with their location directly on top of the A unit lavas, and the presence of fine epiclastic detritus derived by erosion of this.

Fig. 4.2C shows a plot of Si-Al-Mg on which the interpillow oxide sediments are compared with the lava compositions. The sediments lie closest to the C/D unit lavas, but exhibit a much greater variation in composition. Shown also in the diagram are the fields in which probe determinations of lava alteration smectites fall. The distribution of the interpillow oxides resembles that of smectites from the upper lava units, but with slightly greater Al contents. The Al contents of lava alteration smectites vary with location, so although the fields do not quite coincide, it is proposed that the aluminosilicate component of the interpillow oxides was derived by transport of smectites from the uppermost lava exposed adjacent to the area in which the host pillow lavas were

accumulating. This proposal is supported by evidence given in Chapter 3, Section 3.2.1. that the upper lava units were erupted on the rift flank highs.

It is important to calculate the Fe content of the aluminosilicate component of the sediment, in order to estimate the abundance of hydrothermal Fe. Unfortunately owing to the variable Fe content of the smectites, no really satisfactory method has been determined. An approximation has been obtained using the observation that smectite compositions fall in elongate fields perpendicular to the Al apex of the Al-Fe-Mg plot (Fig. 4.2D). A line at 35% Al has been chosen as this encompasses all the data. This gives the solution:

$$Fe = 1.9\ Al - Mg$$

Iron oxide

Goethite is detectable on XRD traces in all samples other than jaspers. On an Al-Fe-Mn triangular diagram (Fig. 4.2E) two trends are observed: A mixing line between Mn-poor and Al-rich aluminosilicate and an Fe-rich component, and a mixing line between Fe-rich and Mn-rich components. Importantly, the Fe-rich component contains a proportion of Mn. This is illustrated more clearly in Fig. 4.2F, where a well defined minimum Mn/Fe ratio is observed. The abundance of free iron is determined by subtracting from the total an estimate of the Fe content of the aluminosilicate (see above).

Thus free Fe is given by: Total -(1.9 Al-Mg).

Manganese oxides

As has been discussed above, no primary manganese phases have been detected. However, the high concentration of manganese in some of the samples cannot be accounted for without a manganese phase, and for the reasons given above δ-MnO_2 is a likely candidate. Excess manganese over the amount related to the iron component (above) is treated here as a separate phase.

Thus free manganese is given by

$$Mn_{free} = Mn_{total} - 0.263Fe$$

4.2.6 Vertical and horizontal distribution of chemical components

The relative abundances of major element components, not including analcite which is regarded as entirely of secondary origin, are shown in the columns on Fig. 4.3. The abundance of carbonate is shown separately from the other components, to avoid confusion caused by the variability of this component. Any upward change in the relative abundance of iron and aluminosilicate is much smaller than the intersample variance. A general vertical increase in both carbonate and manganese oxide is apparent. The peak in manganese oxide at the interlava umber horizon is distinctive. Some tendency for the apatite to co-vary with the manganese oxide is also observed.

The mean proportion of the iron component shows a steady decrease from Mathiati, through Yialias to Margi, a distance of 5km, but variances are great, and the only significant difference is between Mathiati at the one end, and Margi at the other.

4.2.7 Factor analysis and multiple regression

The chemical components described in the preceding section were identified by examination of graphically displayed data. The same end may be achieved using factor analysis, and this method is employed in the following discussion of trace element associations with major element components.

The principles of factor analysis are thoroughly discussed by Davies (1973), and only a brief account of the nature of pertinent assumptions is given here. The R-mode factor analysis is based on a vector analysis of an inter-element correlation coefficient matrix. For an NxN element correlation matrix, the data can be regarded as defining the surface of an N-dimensional ellipsoid for which N axis vectors fully account for the shape, and hence variation in the data. In practice a small number of these axes account for most of the variance, the majority being of low significance. In the factor model, it is assumed that a small number of axes, along with a small contribution from independent unique sources, will fully account for the variance. This being the case, all but a few of the axes may be discarded, and the remaining ones rigidly rotated to fit the data in a more easily interpreted fashion. Strictly, if the factor model is

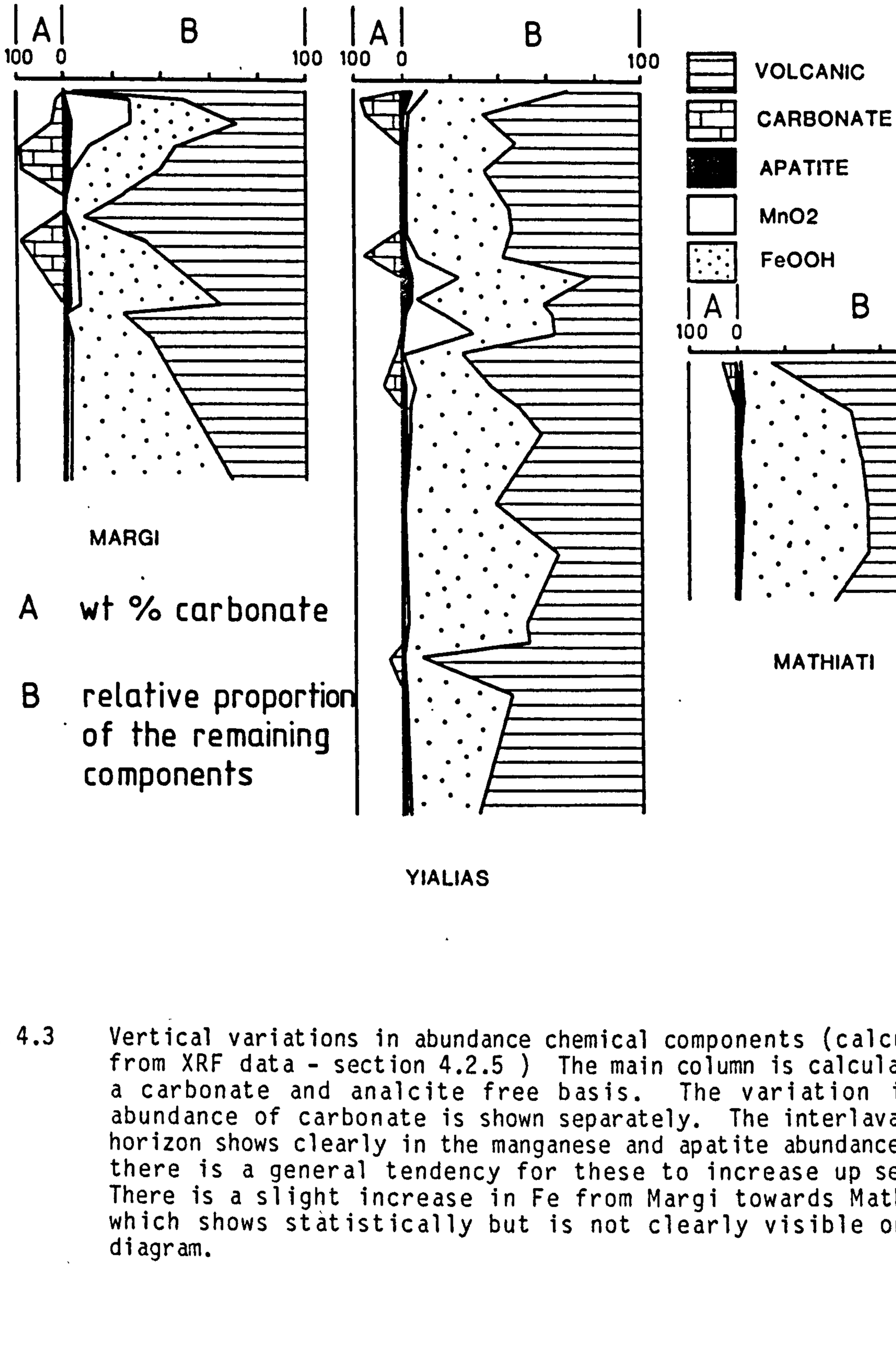

Fig. 4.3 Vertical variations in abundance chemical components (calculated from XRF data - section 4.2.5) The main column is calculated on a carbonate and analcite free basis. The variation in the abundance of carbonate is shown separately. The interlava umber horizon shows clearly in the manganese and apatite abundances, and there is a general tendency for these to increase up section. There is a slight increase in Fe from Margi towards Mathiati, which shows statistically but is not clearly visible on this diagram.

Fig. 4.4

MARGI-MATHIATI INTER-PILLOW OXIDE SEDIMENTS

R-MODE FACTOR ANALYSIS - varimax rotated factor loadings

A - eigenvalue B - percent contribution

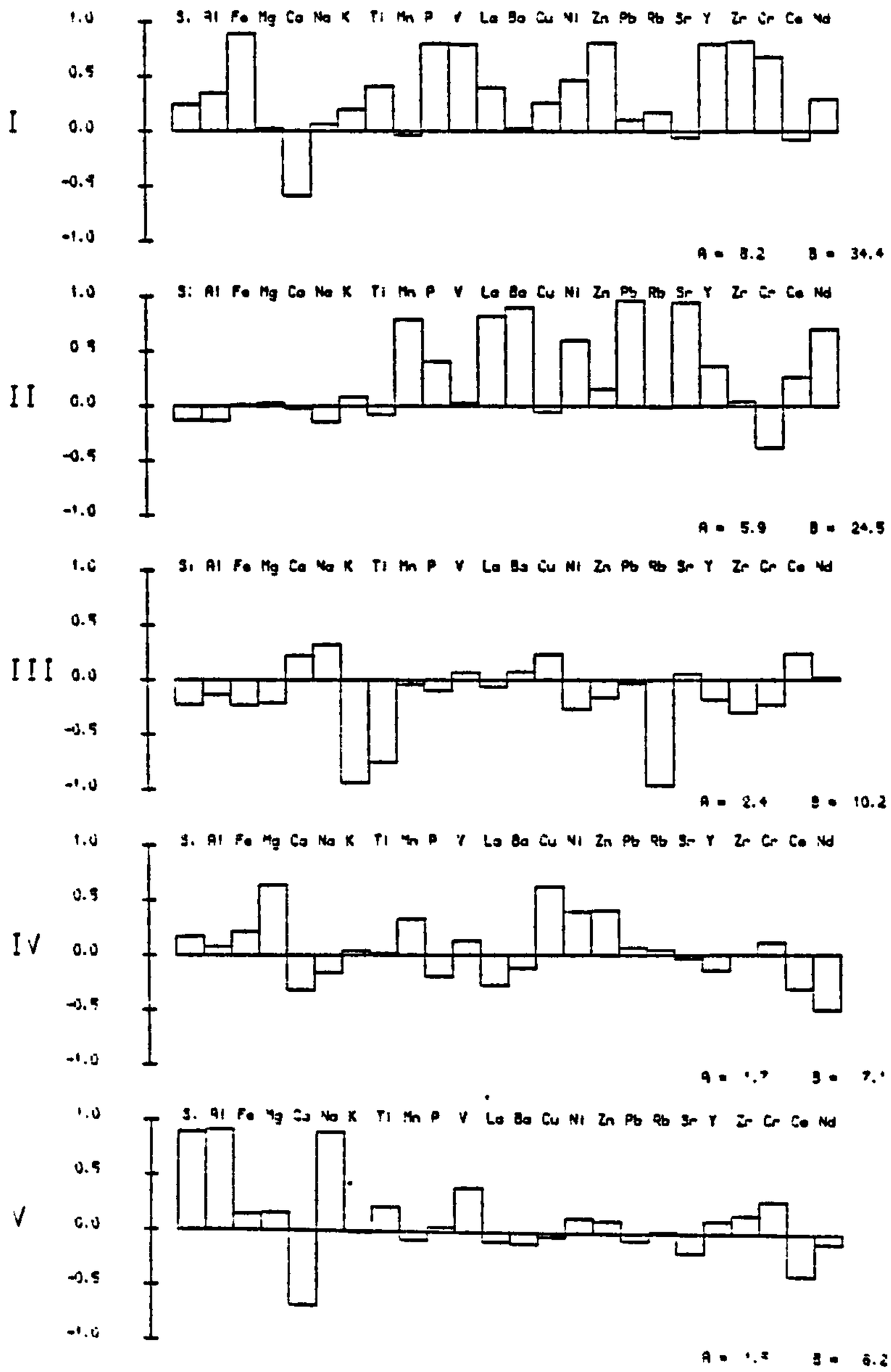

Fig. 4.5

MARGI-MATHIATI INTER-LAVA UMBERS

R-MODE FACTOR ANALYSIS - varimax rotated factor loadings

A - eigenvalue B - percent contribution

FACTOR

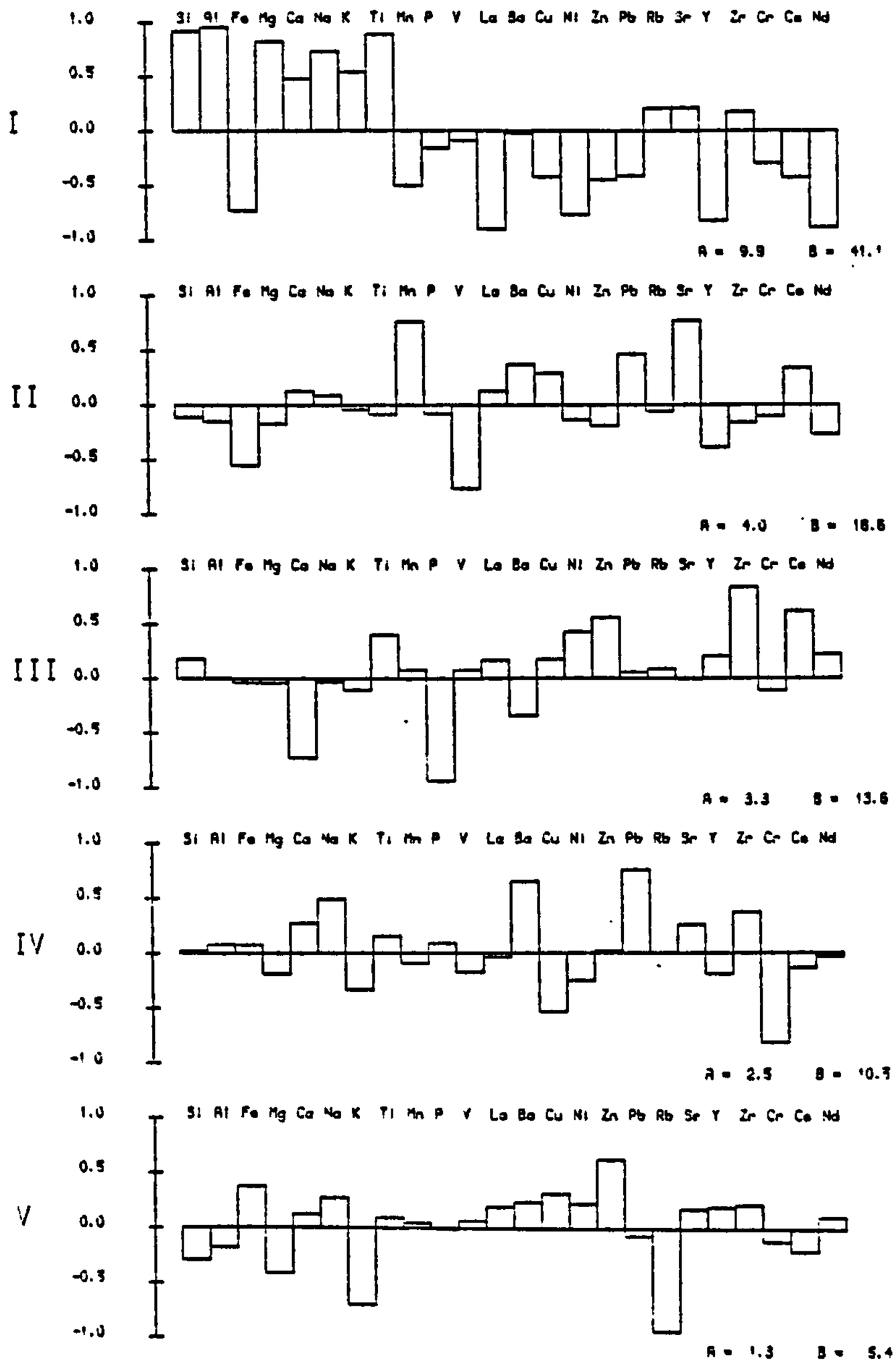

to be valid, the number of independent composition controlling factors must be known exactly. In practice this is impossible to achieve. Most geologists have adopted a process of trial and error concerning the number of chosen factors. There is no theoretical support for this approach but the useful results obtained, to some extent justify the use of this method. The factor rotation scheme adopted here is the varimax of Kaiser. In this the chosen factors are rigidly rotated such that factor loading approach either one or zero. This has the result of making individual factors more easily interpretable. The computer program used here is that of Davies (1973).

The factor analysis illustrates the strong association of some of the trace elements with certain major elements. If the assumption is made that the trace element abundances are dependent upon certain major elements, then the relationships can be quantified using regression analysis. If there is more than one independent controlling major element, then a multiple regression calculation may be used to determine partial regression coefficients. The best fit solutions calculated for the trace elements are those which yield the highest F statistic values. The computer program used is that of Davies (1973).

4.2.8 Trace element distribution

Some of the trace elements are strongly associated with particular major element components. For those which show such associations, factor analysis and multiple regression may be used to assess the significance and to quantify the relationships. The regression analysis assumes that trace elements are dependent upon independent major elements, and further that trace element/major element ratios do not vary systematically. Consequently, before applying these mathematical techniques it is necessary to examine the data manually. In the following account, the data is considered graphically prior to applying factor analysis or multiple regression.

Fig. 4.6

Trace element variation diagrams for the interlava sediments. Crosses = interpillow oxide sediments from Margi - Yialias River. M = Mn-rich interpillow sediments. Closed circles = interpillow oxide sediments from Mathiati mine. Squares = interlava umber Margi-Mathiati. Triangles = interlava umber from Kalavasos. Open circle = mean ochre.

a) Cu/Fe Very great scatter showing variable ratios. Mean ochre falls in the range of values. The Mathiati sediments are more Cu rich than those from Margi.

b) Zn/Fe Very good positive correlation for all sediments including the ochre, arguing that Fe is the dominant controlling factor.

c) Ni/Fe Similar trend to Zn, but with lower values in the ochre, and locally high values in the manganiferous sediments.

d) Ba/Fe Good correlation of Ba with Fe. Locally extreme Ba values occur, deviating from this trend.

e) V/Fe Good general correlation with Fe, but interlava umbers, and the mean ochre, are low. Some extreme values occur.

f) Zr/Fe Positive correlation with some scatter. An association with iron is implied.

Fig. 4.6

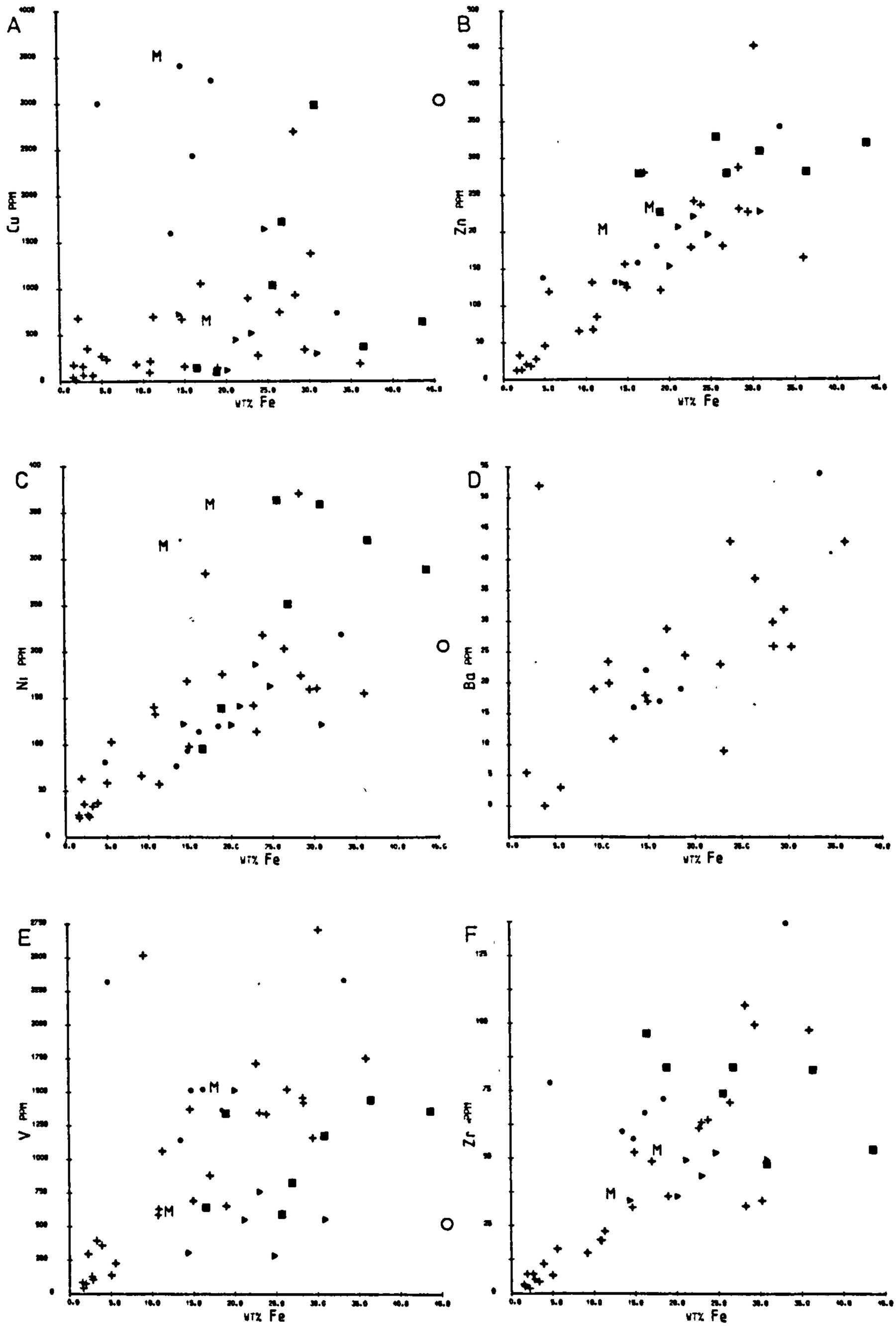
A
Cu PPM
WT% Fe
B
Zn PPM
WT% Fe
C
Ni PPM
WT% Fe
D
Ba PPM
WT% Fe
E
V PPM
WT% Fe
F
Zr PPM
WT% Fe

Fig. 4.7

Trace element variation diagrams for the interlava sediments. Crosses = interpillow oxide sediments from Margi-Yialias River. M = Mn-rich interpillow sediments. Closed circles = interpillow oxide sediments from Mathiati mine. Squares = interlava umber from Margi-Mathiati. Triangles = interlava umbers from Kalavasos. Open circle = mean ochre.

a,b) In the interpillow oxides, where Pb is low, there is a general correlation with Fe. In the interlava umber, Pb is strongly enriched and a weak correlation with Mn is observed.

c) Ni is enriched slightly in some of the interlava umbers, but a correlation with Mn is not good.

d) Ba is enriched in the interlava umbers, but does not show a good correlation with Mn.

e) Sr is enriched in the interlava umbers, and a weak correlation with Mn is observed.

f) A good correlation of Rb with K is observed. The ratios have the same range of values as have the altered lavas.

Fig. 4.7

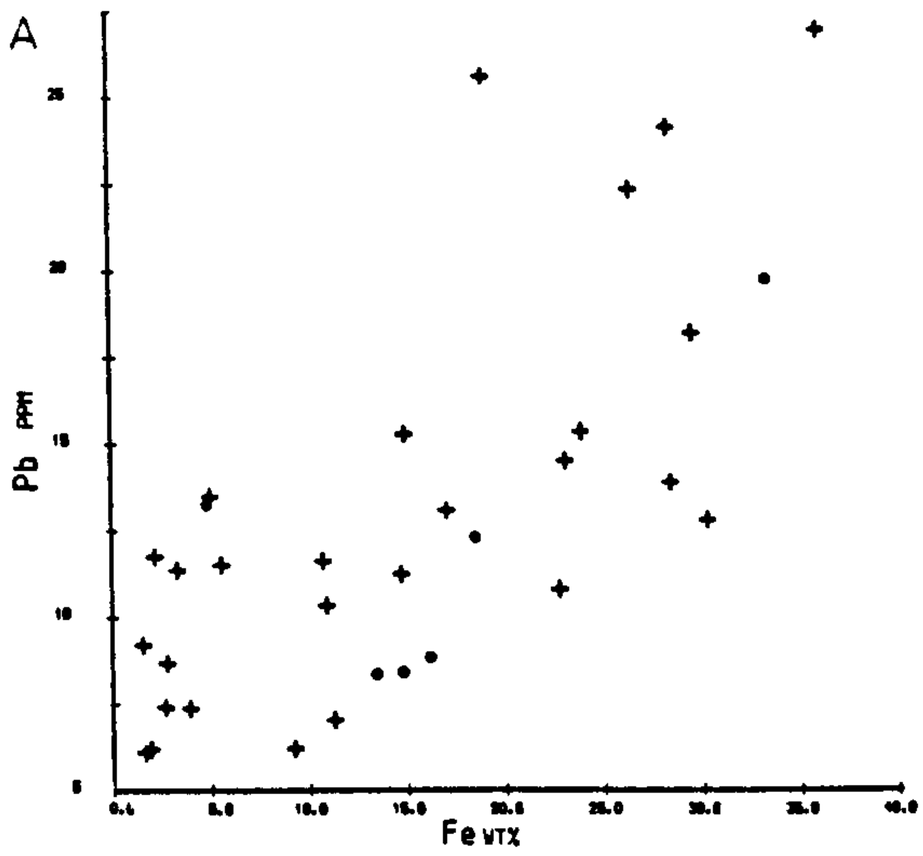
A
Pb PPM
Fe WTX

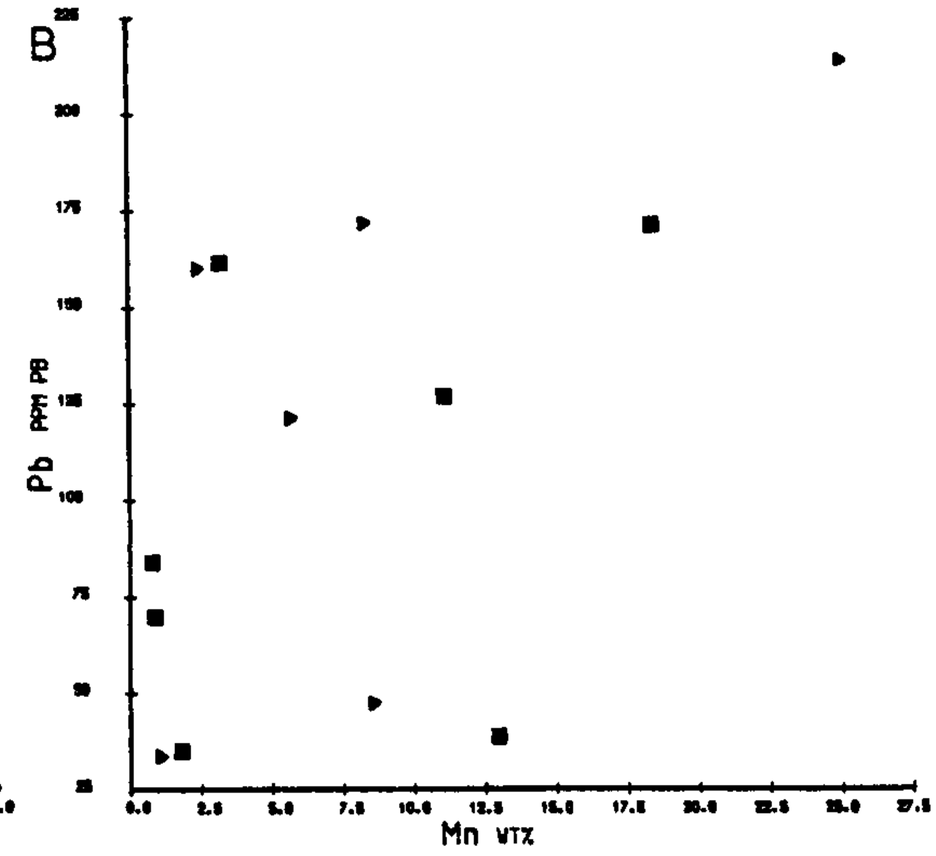
B
Pb PPM PB
Mn WTX

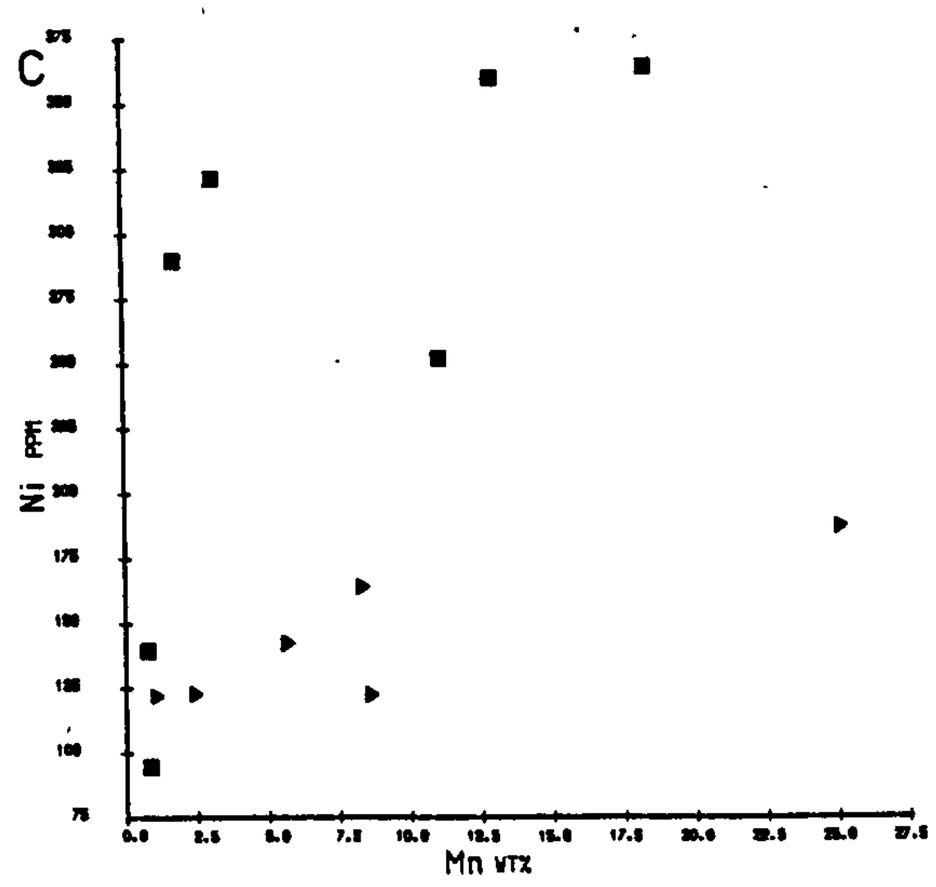
C
Ni PPM
Mn WTX

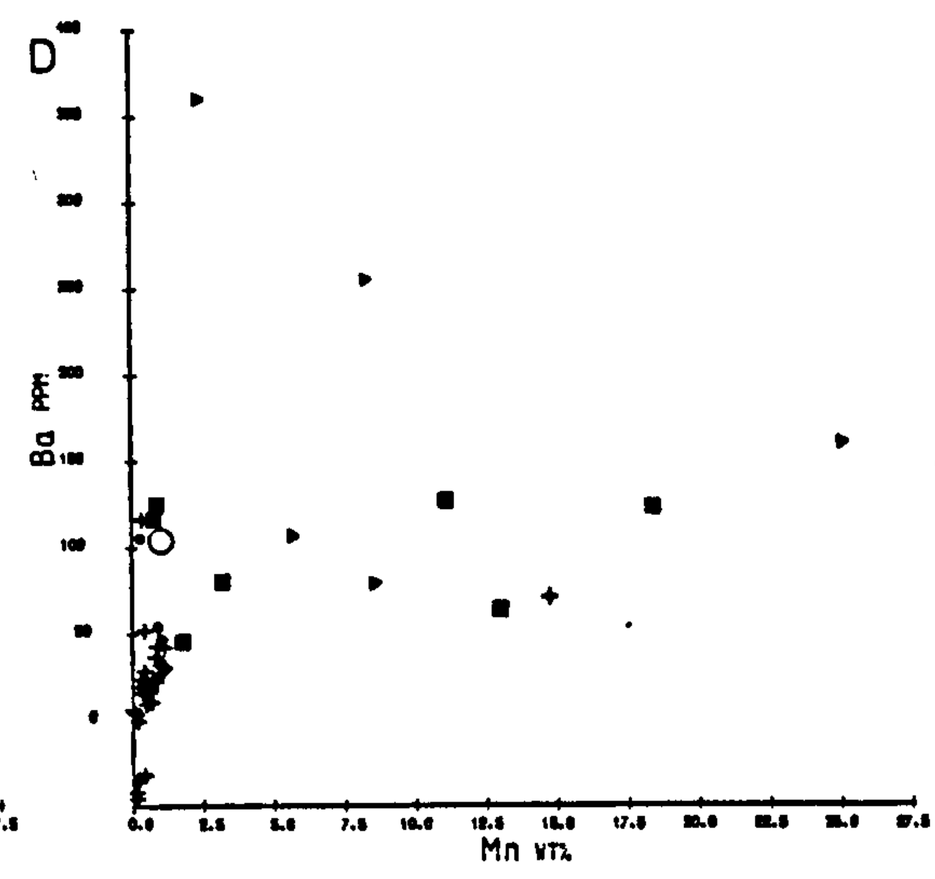
D
Ba PPM
Mn WTX

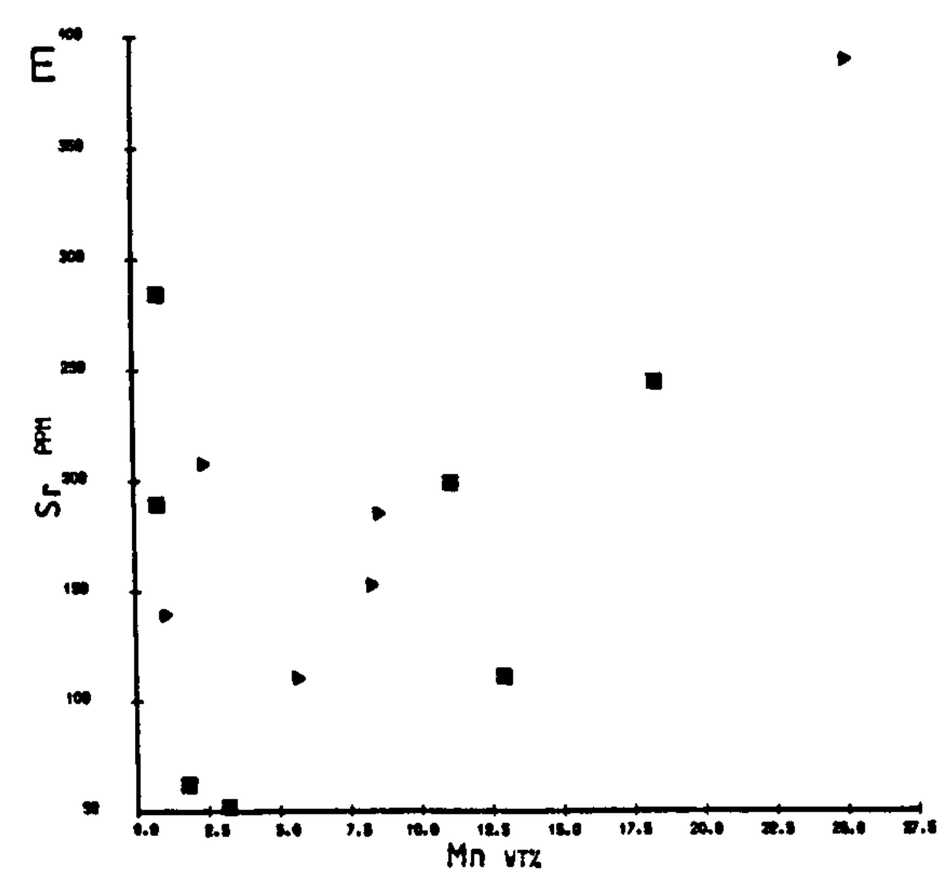
E
Sr PPM
Mn WTX

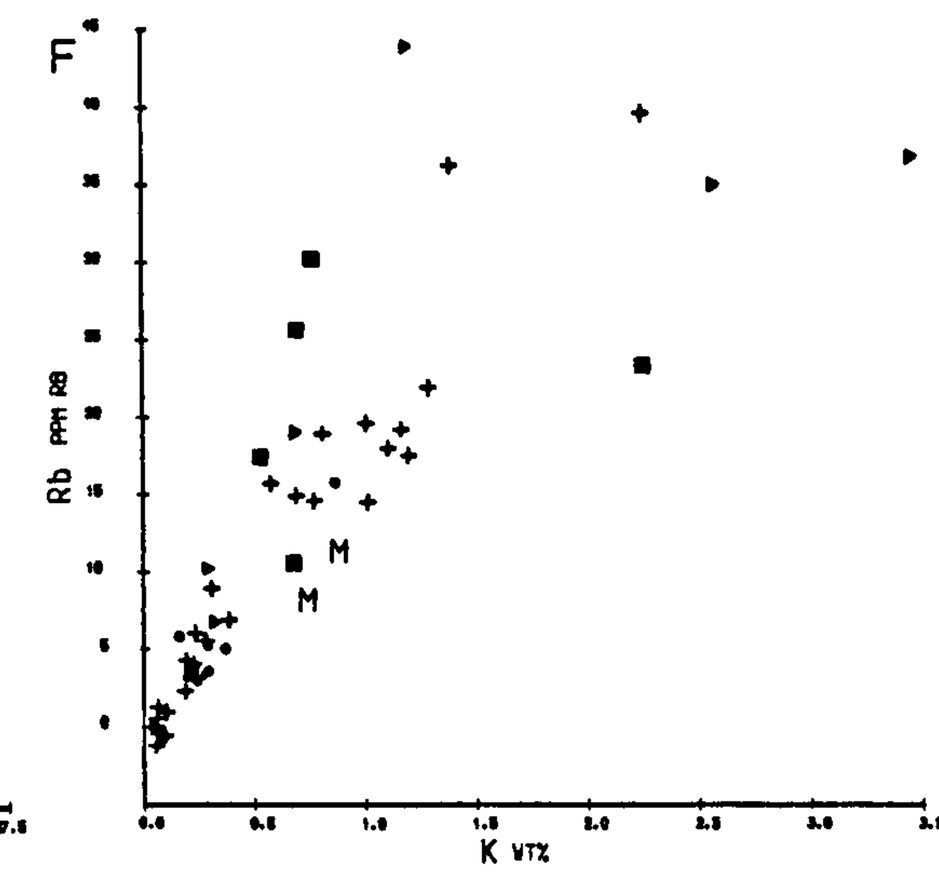
F
Rb PPM RB
M
M
K WTX

Fig. 4.8

Trace element variation diagrams for the interlava sediments. Crosses = interpillow oxide sediments from Margi-Yialias River. M = Mn-rich interpillow sediments. Closed circles = interpillow oxide sediments from Mathiati mine. Squares = interlava umber from Margi-Mathiati. Triangles = interlava umber from Kalavasos. Open circle = mean ochre.

a) A positive correlation of Ca with P is observed for the sediments other than limestones. The ratio is close to that of the supralava umbers which contain francolite. The extreme Ca enrichments are due to carbonate.

b) The carbonates are not excessively enriched in Sr over the mudstones, but a slight association is observed.

c,d,e) La Nd and Y are all correlated with Fe. In contrast, in the supralava umber these elements are associated with phosphate.

Fig. 4.8

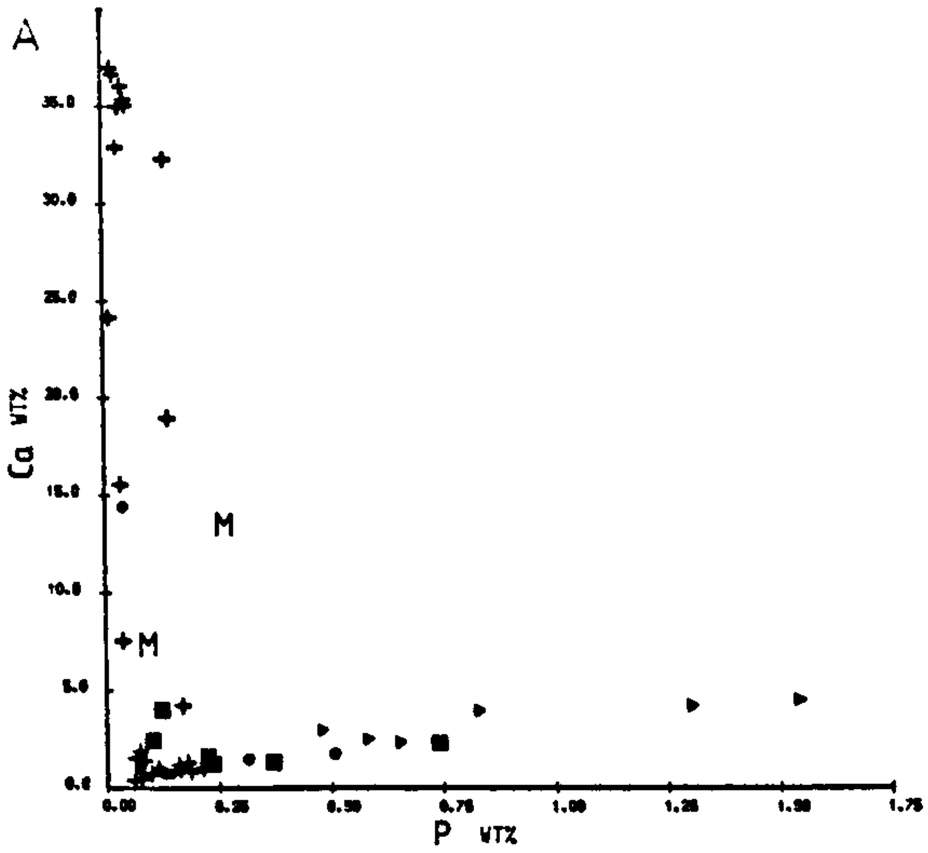

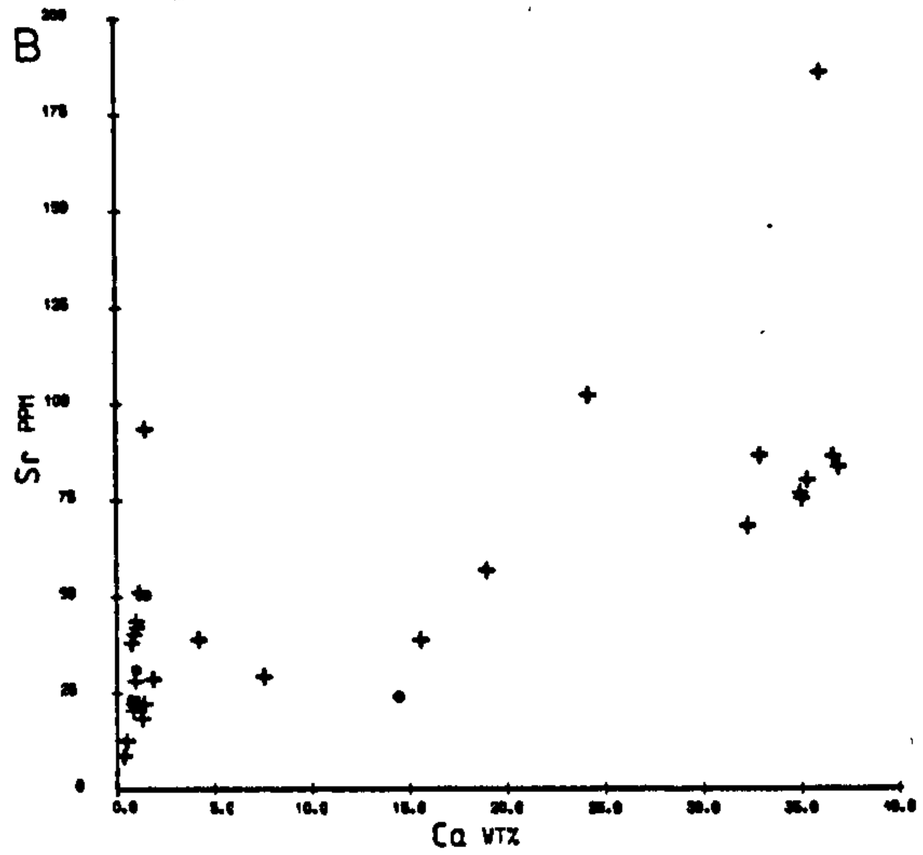

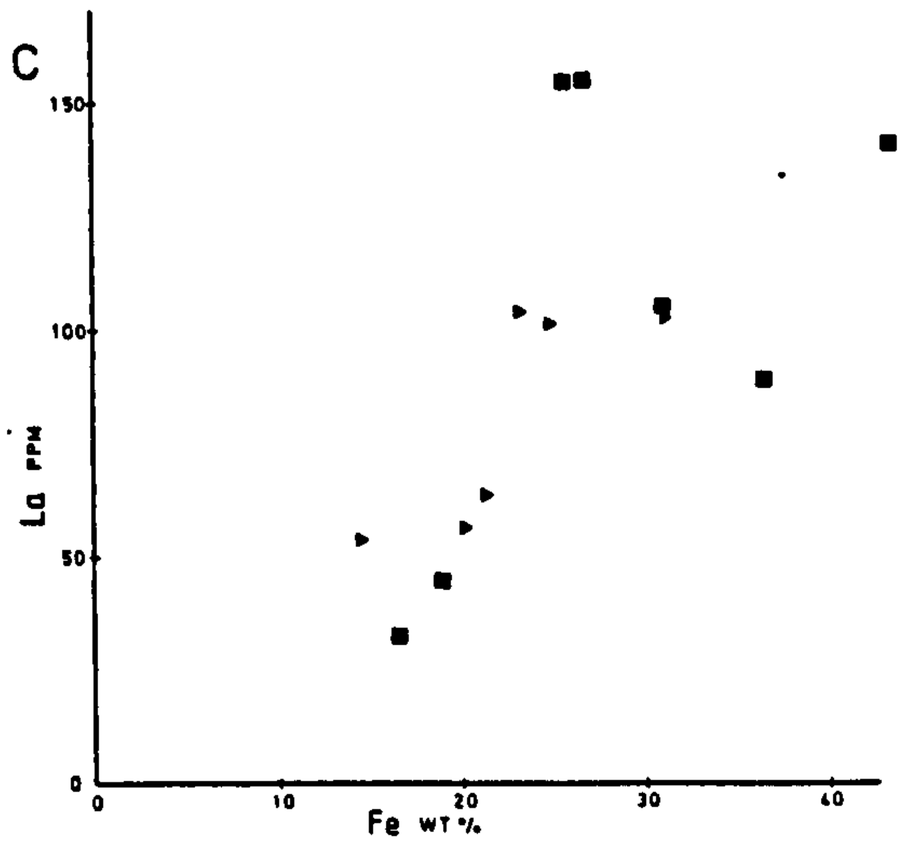

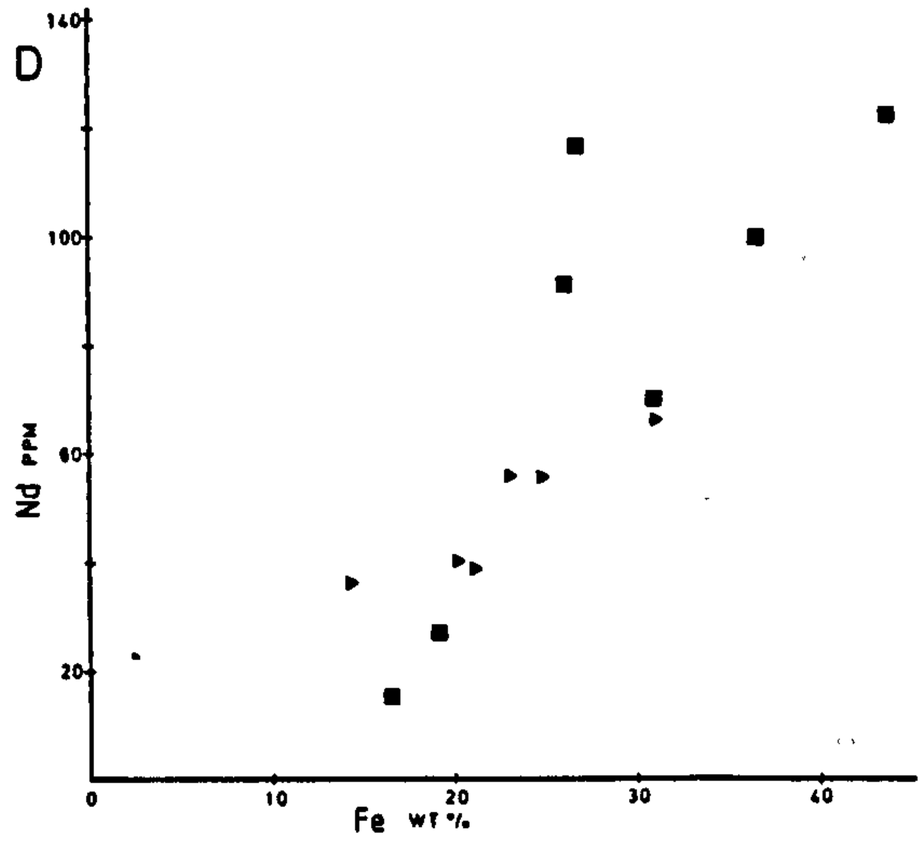

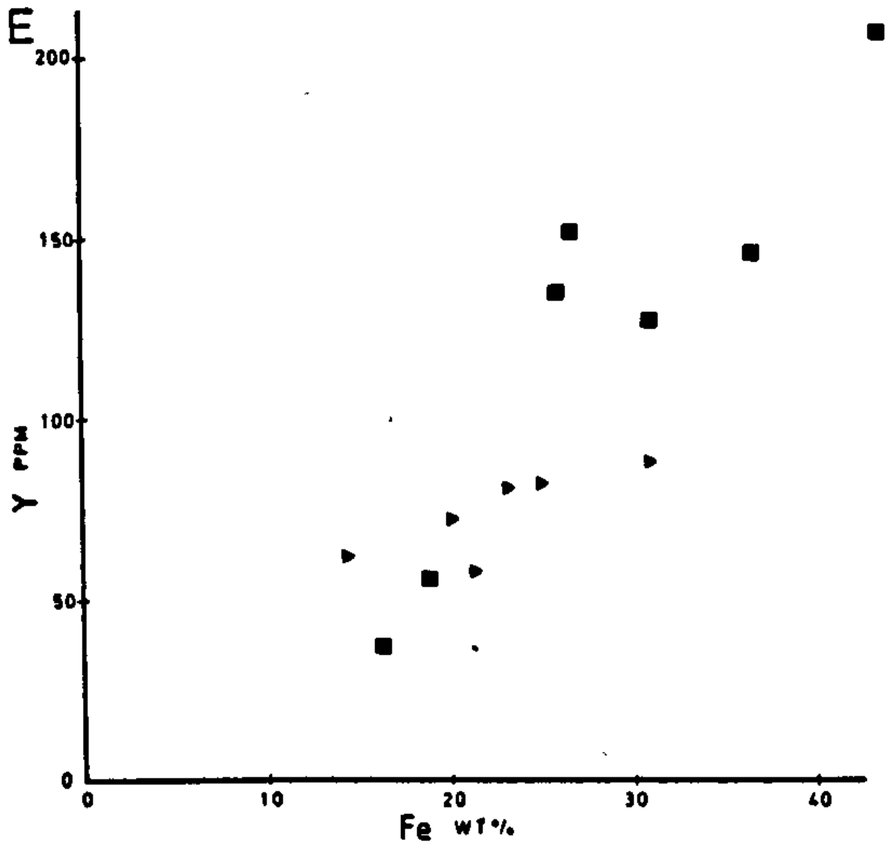

4.2.8.1 Inter-element relationships

Barium. Barium has a mean concentration in the interlava umber of 120ppm, in the interpillow oxide sediments (Manganese free) of 28ppm, and in the ochre of 105ppm. These values are in excess of that predicted by mixing with a C/D unit lava source (mean 30ppm). The particularly high values in the interlava umbers suggest an association of barium with manganese, and this is supported by the high barium concentrations in the manganiferous interpillow sediments.

A plot of Ba/Fe (Fig. 4.6D) illustrates an association of barium with the iron component in the manganese poor interpillow sediments. As Mn and Fe co-vary in the Mn-poor sediments, Ba also correlates with Mn, but the significance of the regression is much lower. The manganiferous sediments have much greater concentrations of barium, but the Ba/Mn ratio is variable (Fig. 4.7D).

The association of barium with manganese shows up very clearly in the interpillow oxide sediments, using factor analysis, owing to the barium enrichment in the manganiferous varieties (Fig. 4.4). The association is not present in the interlava umbers (Fig. 4.5). This result is caused by the variable Ba/Mn ratios. A multiple regression analysis does not yield a significant solution.

The high barium concentration in the ochre is not due to manganese, and its great variability suggests that it is independent of the major element components. A possible cause might be barite, as this mineral is ubiquitous at the known modern oceanic sulphide deposits (Hekinian et al., 1980; Haymon and Kastner, 1981; Normark et al., 1983).

Cerium. Cerium has a mean concentration of 16ppm in the interlava umber, but is below the detection limit in both the interpillow oxide and the lavas. An association with the manganese component is implied, but the values are erratic and nothing more definite may be said.

Cobalt. Cobalt was determined by atomic absorption spectroscopy for 6 samples of interpillow oxide sediments, and one sample of interlava umber. The mean concentration in the interpillow oxides

(37ppm) is lower than the value in the interlava umber (50ppm). However the former is reduced because of the low concentration in the carbonate-rich sediments. if the carbonates are not included, the new mean (49±10) is very close to the interlava umber value. This implies that there is no particular association of Co with manganese. The mean Co content in ochre is 110ppm which is high but the Co/Fe ratio is similar to the other sediment types.

Chromium. Chromium has a mean concentration of 30ppm in the interlava umbers, 25ppm in the interlava oxide sediments and 20pm in the ochre. If chromium is supplied by the aluminosilicate component, then this must have a Cr/Al ratio of 6.4×10^{-4} (the same value for all the interlava sediments). The C/D lava unit of the Margi-Mathiati area has, however, a Cr/Al ratio of 30×10^{-4}. The discrepancy could be accounted for if the alteration smectites contained less Cr than their source lavas. Electron microprobe determination of chromium in the smectites (mean of 18 analyses 165ppm) is close to the detection limit (c. 120ppm) but nevertheless suggests that there is not a deficiency. The source area for the aluminosilicte component, which was not the lavas in which the sediment occurs, may have had a lower Cr content. Upper unit lavas containing sufficiently low Cr (c. 60ppm) are known (Pearce, 1975; Schmincke et al., 1983), but are apparently not common. Thus the Cr content of the sediment poses an objection, though not an insuperable one, to the view that the aluminosilicate was derived from upper unit lavas.

Copper. The mean copper content of the interlava umber is 827ppm and for the interpillow oxides 923ppm. A plot of Cu against Fe (Fig. 4.6A) shows the considerable scatter of values. As a result of this, any association of copper with either Fe or Mn is concealed. However as multiple regression of Copper on Fe and Mn gives a weakly significant fit for the interlava umbers. The ochre Cu/Fe ratio lies within the field of the more Cu-rich sediments. The high variability is interesting, suggesting a degree of independence in the supply of copper.

Lanthanum. The mean lanthanum content of the interlava umber is 92ppm and in the interpillow sediments 14ppm. Both are greatly in excess of that in the lavas. No association of lanthanum with major elements is observed in the interpillow sediments, except an inverse relationship to carbonate. However the manganese-rich varieties have elevated values. In the interlava umber the high La concentrations might thus be attributed to the manganese component, however as is clear both from the La/Fe plot (Fig. 4.8C) and factor analysis (Fig. 4.5) a strong association of La with Fe exists. A multiple regression gives a best fit line if both Fe and Mn are regarded as controlling independent variables.

Neodymium. The mean concentration of neodymium in the interlava umbers is 64ppm and in the interpillow sediments 12ppm. The behaviour is identical to that of lanthanum, in the interlava umber correlating most strongly with Fe (Fig. 4.8D), but yielding the most significant multiple regression on both Fe and Mn. Again this contrasts with the supralava umber where apatite is the predominant control.

Nickel. The mean nickel content of the interlava umber is 206ppm and in the interpillow sediment 132ppm, contrasting with 56ppm in the C/D unit lava. For the majority of samples, a good correlation of nickel with iron is observed (Fig. 4.6C). Some of the interlava umbers and manganiferous interpillow sediments fall on the nickel rich side of the group, suggesting that manganese can have a significant effect upon upon nickel. The association of nickel with Fe and Mn shows up clearly in the factor loadings (Fig 4.5). A multiple regression of Ni on Fe and Mn yields a highly significant solution. In the ochre the Ni/Fe ratio is low compared with the other interlava sediments, but the difference is small.

Strontium. The mean strontium content of the interlava umbers is 179ppm, in the interpillow oxide sediments 83ppm and in ochre is 38ppm. In the interpillow oxide sediments there is considerable difference between the carbonate free mudstones (31ppm) and the carbonates (82ppm), however, the most striking enrichments are in

the manganese rich varieties with values ranging as high as 945ppm. These relationships are illustrated in a plot of Ca v. Sr (Fig. 4.8B) for the manganese free interlava sediments. A correlation of Ca/Sr in the carbonates is observed. However relatively high Sr contents are found in the non-carbonate sediments, and these may be explained simply by mixing with a C/D unit lava source (C/D unit lava 111ppm). The strong association of Sr with Mn is illustrated in a Mn/Sr plot (Fig. 4.7E). The points which fall off the line to the Sr rich side are those which contain most aluminosilicate. In the factor loadings, for both the sediment types, the association with manganese is so great as to conceal any other associations. In the interlava umbers a multiple regression gives a best fit for strontium on Ti, Ca and Mn with Mn most important. The Ca content represents largely apatite, showing that it contains a significant proportion of Sr. This is in keeping with direct observations on phosphates from the supralava umbers.

Lead. The mean lead content of the interlava umbers is 110ppm, in the interpillow sediments 20ppm and in the ochre 180ppm. The manganese-rich interpillow sediments also are particularly enriched in lead. The association of lead with manganese shows clearly in the factor loadings. However, lead - manganese ratios are variable (Fig. 4.7B) and a multiple regression yields a solution of low significance. The high Pb content of the mean ochre is strongly biased by the Skouriotissa samples. The other ochres have Pb/Fe ratios similar to the manganese-poor interpillow oxide sediments. The high Pb values at Skouriotissa are also observed in the basal manganese poor umbers (Robertson, 1976a). An alternative source for this enrichment is required.

Rubidium. The mean rubidium content of the interlava umber is 20ppm and in the interpillow oxide sediments 10ppm. The strong association of Rb with K shows clearly in both the factor loadings and the K/Rb plot (Fig. 4.7F). A wide range of K/Rb ratios is observed, the range being coincident with that of the altered lavas.

Vanadium. The mean vanadium content of the interlava umbers is 873ppm, of the interpillow sediments is 1048ppm, and of the ochre 491ppm. Within the interpillow sediments there is a good correlation of V with Fe, but this is not the case with the interlava umbers (Fig. 4.6E). The latter have a much lower V/Fe ratio. The association of vanadium with Fe in the interpillow oxides shows clearly in the factor loadings. This is less clear but still true of the interlava umber. A multiple regression of V on Fe and Ti yields a weakly significant solution. All the ochre is depleted in V compared with the interlava sediments, even though the vanadium-iron association is otherwise so good. This implies some difference in the Fe component in the proximal ochre.

Yttrium. The mean yttrium content of the interlava umbers is 100ppm and of the interpillow sediments 39ppm. In the interlava umbers, as with the La and Nd, Y shows a good correlation with Fe (Fig. 4.8E), but in this case the association is also true for the interpillow sediments. The associations show up clearly on the factor loadings. A multiple regression of Y on Fe on Mn gives a highly significant result.

Zinc. The mean zinc content of the interlava umber is 242ppm, in the interpillow sediment 141ppm and in the ochre 535ppm. A good correlation for both types of Zn with Fe is observed (Fig. 4.6B). This shows up very clearly in the factor loadings. In the interlava umber the most significant multiple regression for Zn is on Fe, Ti and Mn (Table 4.9). The Zn/Fe ratio for the ochre is very close to that of the other interlava sediments.

Zirconium. The mean zirconium content of the interlava umber is 60ppm and in the interpillow sediment 42ppm. These are thus significantly enriched with respect to a potential C/D lava source. A plot of Zr/Fe (Fig. 4.6F) shows a weak correlation for the interpillow sediments, but considerable scatter for the interlava umber. The factor analysis shows this clearly: for the interpillow sediments a high degree of association, but none in the umber. A multiple regression of Zr on Fe and Ti for the interlava umbers does

however yield a significant solution, with the Zr/Ti ratio being close to that for the mean C/D unit lava. The Zr content of the ochre is variable, but is high, lending support to the Fe-Zr association.

4.2.8.2. Trace element composition of major element components.

Aluminosilicate

A full major element analysis for the aluminosilicate cannot be calculated owing to the unknown iron content. However certain elemental ratios can be determined. Further, for a few trace elements - zinc, strontium, vanadium and zirconium, trace element/titanium ratios are obtained from multiple regression solutions. These elemental ratios are presented in Table 4.8, where they are compared with those in the C/D unit lavas and lava smectites.

Iron oxide

The iron oxide component contains a significant proportion of manganese (Mn/Fe = 0.028) but cannot be shown to contain any other major elements. In the supralava umbers, a small proportion of Si, Ti and Mg are associated with the iron component (Chapter 5, Section 5.4.6). The greater variation in composition of the interlava sediments may be concealing a similar association, but this cannot be demonstrated.

Trace element/Fe ratios for the interpillow sediments, obtained by simple linear regression, and for the interlava umbers, obtained by solution of multiple regression are presented in Table 4.10. The results are very similar. These differ from the ratios in the mean ochre principally in having greater V/Fe and lower Zn/Fe and Pb/Fe ratios.

Manganese oxide

The composition of the manganese oxide component has been obtained from multiple regression solution for the interlava umbers. (Except Ba for which the scatter is too great. The quoted value is an estimated mean.) The results are presented on Table 4.10.

TABLE 4.8

Absolute range taken from graphs		Interpillow sediments	Mean C/D unit Lava N=26	Smectite N=27	Bentonite
	Si/Al	1.78 - 3.50	2.82 ± 0.41	2.87 ± 0.65	3.97 ± 0.17
	Fe/Al				
	Mg/Al	0.37 - 1.22	0.50 ± 0.15	1.73 ± 0.43	0.42 ± 0.03
	K/Al	0.064 - 0.430	0.216 ± 0.247	0.18 ± 0.30	0.22 ± 0.01
	Ti/Al	0.010 - 0.044	0.046 ± 0.010	0.005 *	0.049 ± 0.003
Multiple regression solutions					
Values $\times 10^4$	Zn/Ti	234	184 ± 51		471 ± 42
	Sr/Ti	227	302 ± 113		
	V/Ti	830	616 ± 168		323 ± 24
	Zr/Ti	81	94 ± 21		291 ± 27

* Large standard deviation

Comparison of elemental ratios for the interlava oxide sediments with the supralava sediments, lavas and lava derived smectites.

Table 4.9

Interlava umber multiple regression solutions

Elements	Partial Regression Coefficients	R	F
Cu/Fe	27.1	0.51	1.7
/Mn	50.5		
La/Fe	3.4	0.85	12.9
/Mn	3.0		
Nd/Fe	3.6	0.88	16.4
/Mn	1.2		
Pb/Fe	0.79	0.54	2.1
/Mn	4.45		
Sr/Ti	227.0	0.93	19.6
/Mn	11.2		
/Ca	40.1		
V/Fe	36.0	0.55	2.2
/Ti	830.0		
Y/Fe	5.3	0.90	22.1
/Mn	1.2		
Zn/Fe	8.7	0.86	8.1
/Ti	234.0		
/Mn	5.1		
Zr/Fe	1.3	0.71	5.2
/Ti	80.5		

Coefficients are $x10^4$

Apatite.

In contrast to the supralava umbers, the apatites in the supralava sediments are not Y and REE enriched. Only Sr is demonstrably associated with apatite

$$Sr/Ce = 4.01 \times 10^{-3}$$

Calcite

The only element which is demonstrably associated with calcite is Sr. A regression of Sr and Ca in the carbonates gives a

$$Sr/Ca \text{ ratio of } 3.96 \times 10^{-4}$$

4.3 DISCUSSION: INTER-RELATIONSHIPS AND ORIGIN OF THE INTERLAVA SEDIMENTS

In the following sections arguments concerning the origin of the interlava sediments, and the relationship between the various types are discussed.

4.3.1 Sources for compositional components

The compositional components described above occur throughout the interlava sediments in varying proportions. There are two possible approaches to determining their origins. Firstly, comparison of the component composition, either with potential local sources, or with known modern equivalents. Secondly, by considering spatial variations in abundance of the components, particularly with respect to potential sources such as the ore bodies.

The iron component

Hydrothermal metalliferous sediments rich in hydrated iron oxides are common in the modern oceans. The great majority of these are found on spreading axis crests, or as basal sediments where they are inferred to have accumulated at ridge crests in the past (Boström and Peterson, 1969; Cronan, 1976) These are inferred to have precipitated from high temperature hydrothermal effluent released from hot springs at the ridge axes (Edmond et al., 1982). Partition studies (Cronan, 1976) indicate that copper and zinc and to a lesser extent lead, are most strongly associated with the iron component in these sediments which is precisely what is observed for

the Cyprus interlava sediments (Section 4.2.8.2).

A possible local source for the iron component is the sulphide ore. The abundance of iron in the interpillow sediments, and interlava umbers in the Margi-Mathiati area shows a tendency to increase in the direction of the Mathiati ore body, attaining a maximum in the proximal ochre. Constantinou and Govett (1972) discuss in detail evidence for the origin of ochre through oxidative weathering and erosion of the sulphide. Key points of evidence are:-

1) Ochre is always located above, and seldom outside the area of the ore.
2) An upward increasing proportion of ochre, containing corroded fragments of pyrite, occurs interbedded with the sulphide.
3) The chemical peculiarities of the different ochre bodies are matched by those of the associated ore.
4) The degree of variability, and absolute range of copper concentrations in the ochre is similar to that in the ore.

Constantinou and Govett (1972) propose that the process by which the ochre was derived from the ore was <u>in situ</u> submarine oxidative attack, followed locally by mechanical reworking of the resulting "gossan". Gradations from pure ore through increasingly oxidised zones into pure ochre, in some places, testify to <u>in situ</u> oxidation. The presence elsewhere of interbedded ochre and sulphide, in which adjacent blocks of sulphide have different chemical compositions, indicates mechanical reworking. Robertson (1976a) emphasises the importance of sedimentary processes, noting the existence at Skouriotissa of erosional channels. Thus a proportion of the iron oxide, probably most of that in the ochre, was derived directly from sedimentary sulphide ore. However Robertson (1976a) observing a chemical gradation from the proximal ochre, through finely bedded ochre, into the overlying umbers, proposed that there was an alternative source of iron; primary precipitation in the water column near the vent.

The composition of the iron component in the interlava umber and the interpillow sediments is not identical to the ochre. The ochre is more variable and exhibits significantly different V/Fe and

TABLE 4.10

Trace element composition of the iron component.

$X10^4$	Ferruginous interpillow sediments	Iron component interlava umber	Whole rock ratios ochre	EPR crestal	ERR basal
Mn/Fe	277	-	205	3333	3019
Ba/Fe	1.20 - 2.0	-	2.3	-	310
Ca/Fe	5 - 79	27.05	67	41	39
Ni/Fe	4.6 --6.3	8.27	4.5	23.9	22.9
Pb/Fe	0.4 - 0.6	0.79	3.9	8.44	5.o
V/Fe	43 - 62	36	10.7	25	-
Zn/Fe	7.5 - 9.5	8.7	11.7	21.1	23.4
Zr/Fe	2.4 - 3.3	1.3			
Y/Fe		5.3			
La/Fe		3.4			
Nd/Fe		3.6			

Trace element composition of the Mn oxide component.

$x10^4$	Inter lava umber	Mean Hydrothermal crust	Mean hydrogenous crust
Ba/Mn	4	13.1 $\pm$ 12.9	139 $\pm$ 58
Cu/Mn	50.5	6.6 $\pm$ 8.6	72 $\pm$ 50
Ni/Mn	5.9	13.4 $\pm$ 15.78	152 $\pm$ 42
Pb/Mn	4.5	0.21 $\pm$ 0.26	60 $\pm$ 87
Sr/Mn	11.2		
Zn/Mn	5.1	20.8 $\pm$ 30.1	60 $\pm$ 30
Y/Mn	1.2	-	
La/Mn	3.0	0.105 $\pm$ 0.081	25 $\pm$ 15
Nd/Mn	1.2	-	

These ratios are calculated either graphically, or through multiple regression, and are the trace element enrichments in chemical components within the rock types.

Pb/Fe ratios. However the ratios Ni/Fe, Zn/Fe, Co/Fe and Cu/Fe are very close, and the range and variability of Cu is very similar. From this a related source is suggested. The ochre contains corroded sulphide fragments and quartz, both of which are absent from the other interlava sediments. It is therefore proposed that they were not derived by erosion of the sulphide in the way that the ochres were. At the East Pacific Rise vents, large amounts of particulate sulphide are supplied to the water column (Spiess et al., 1980); Edmond et al., 1982), a proportion of which settles as sulphide in the immediate vicinity of the vent. Much however settles more slowly and becomes widely dispersed in the water column, where it is oxidised prior to accumulation. In Cyprus accumulation of oxidized vent sulphide, to form the distal interlava sediments, would account for their chemical similarity to the ochre, but allow also for the differences observed. The alternative that much of the vented iron oxidised directly from solution requires that this attained the same trace element/iron ratios as the oxidized sulphide. The constancy of the elemental ratios, favours a single source for the iron, and the similarity with the ochre favours derivation from iron sulphide. The majority of the widely dispersed iron sulphide must have been oxidized prior to accumulation, because in many of the sediments, carbonate, apatite and manganese oxide, which would have been unstable in the presence of oxidising pyrite, are preserved.

Manganese oxide

The composition of the manganese component is compared with modern hydrothermal crusts in Table 4.10. The degree of enrichment of the elements is closest to that of the hydrothermal crusts, though the relative importance of the elements differ. The implications is that the manganese was deposited rapidly from solutions enriched in manganese.

The geographical distribution of the manganiferous sediments is the same as that for the interlava metalliferous sediments as a whole, but more detailed vertical and lateral variations are the result of post depositional mobilisation and are thus of no help. The broad spatial association with the other metalliferous sediments

implies a source closely related to that of the iron.

Aluminosilicate

Potential sources for the aluminosilicate component fall into two categories: externally supplied bentonitic clays as seen in the supralava umbers (Chapter 5, Section 5.5.6); and the local lavas. The chemical composition of the component is quite unlike that of the bentonites (Table 4.8). Further the bentonite contains quartz and detrital illite, both of which are absent from the interlava sediments. The composition of the aluminosilicate component is very close to that of the C/D unit lavas but could this result from diagenetic modification of the bentonitic clay? If so then major chemical changes must have taken place including a significant alteration of the Zr/Ti ratio. Furthermore such a dramatic modification must affect only interlava sediments and not even the most basal of the supralava sediments. Though the interpillow sediments may have been subjected to higher temperatures during incorporation into the lava flows, this is not the case with the interlava umbers, which are also similar to the lavas.

On balance it seems more likely that the differences in composition are primary and not secondary.

Apatite

Phosphatised cuticle accounts for a part of the observed apatite, but is not abundant enough to be the sole contributor. Phosphate enrichment in oceanic metalliferous sediments has been described by Berner (1973), who attributes this to the adsorption of phosphorus onto hydrated iron oxides, possible resulting in the formation of a ferric phosphate. If this has been the case in the interlava sediments, then diagenetic alteration of this to apatite has occurred.

In contrast to the supralava umbers, the apatite in the interlava sediments is not enriched in Y, La or Nd. This may be the result of differing accumulation rates influencing the amount of time during which diagenetic enrichment may take place.

Carbonate

The primary origin of a proportion of the calcite is attested to by the presence of carbonate microfossils. The distribution of carbonate in these sediments poses a problem, as none occurs in either the interlava umber, or the first-formed supralava sediments. A plausible solution is obtained if the Troodos spreading axis was close to but just below the carbonate compensation depth, such that final dissolution of carbonate skeletal material occurred at the sediment surface. Sediment which was overridden rapidly by lava flows might then retain the carbonate, protected from dissolution by trapped pore waters. In sediments which were exposed, dissolution would proceed to completion.

4.3.2 Relative accumulation rates

It is not possible to calculate absolute accumulation rates, but there are several points to note concerning relative rates. The externally supplied bentonitic clay which form an important component in all the supralava sediments (Chapter 5, section 5.5.6) are seemingly masked. Unless a coincidence of cessation of volcanism at the spreading axis and a change in supply of bentonitic clays occurred, the absence of detectable bentonitic clay in the interlava sediments suggests that the sedimentation rate of locally-derived material was substantially greater than this external supply. The proportion of the iron component in the interlava sediments is less than that in the supralava umber, but if the sedimentation rate was relatively higher in the interlava sediments, then the absolute rate of accumulation of iron will have been greater. The chief importance of this point concerns the origin of the iron component in the supralava umber, and will be further discussed in the next chapter. However it is also important with respect to the character of a hydrogenous component. In the supralava umber the phosphate is enriched in La Nd and Y, and the manganese component is more trace metal enriched than that in the interlava sediment. The processes by which the manganese and phosphate components become enriched are time dependent, (Toth, 1980; Arrhenius et al., 1957) and the relative enrichments in supra- and inter-lava umber may be accounted for by a difference in

accumulation rate.

4.3.3 Secondary modification of mineralogy and chemistry

Post-depositional modification of the sediments is of two principal types: first, widespread mostly low temperature alteration resulting in recrystallisation of the hydrated ferric oxides, precipitation of carbonate and analcite, and removal of manganese; secondly, localized high temperature alteration related to hydrothermal feeder zones, leading to the formation of jasper.

Goethite

All the iron oxide is present as goethite, but by analogy with modern oceanic metalliferous sediments (Boström and Peterson, 1969) this is secondary after non-crystalline hydrated ferric oxides. This process has not apparently resulted in chemical modification. The goethite in the interlava sediments is of higher crystallinity than that in the umber (Constantinou and Govett, 1972). This suggests that the recrystallisation was affected by the temperature distribution in the *in situ* ophiolite.

Manganese oxide

Field evidence suggests that manganese oxide has been leached from the interpillow sediments. Where the interpillow sediment pockets are large this has not gone to completion. That the interlava umbers, occurring as a horizon right across the area, do not show any signs of this leaching, suggests that it was not the result of large-scale movement of fluid. Instead a more local process is called for, affecting only the interpillow sediments. The process of incorporation of sediment into pillow fractures and interstices would result in it being subjected to elevated temperatures before ultimate cooling of the lava flows. Basalt leaching experiments indicate that some reactions of seawater with hot basalt proceed very rapidly. Bischoff and Dickson (1975), found that both the pH and the oxidation potential of the fluid were extensively modified after only 72 hours at 200°C. Given that the lavas had an initial Fe^{2+}/total Fe ratio comparable to modern tholeiitic basalts, then three parts by volume of lava would be

needed to reduce the manganese in one part of interlava umber. H^+ ions released during interaction would also further aid dissolution. Thus it is possible that the manganese in the interlava sediments was lost due to interaction with the hot lavas. However, the supralava umbers locally have lost manganese (Robertson, 1975) which cannot be explained by interaction with hot lava, so a further mechanism, possibly related to slower cold interaction with lava is required.

Analcite

In the modern oceans analcite is very abundant in volcaniclastic sediments (Kastner, 1981), where it is believed to have been formed through the diagenetic alteration of basaltic glass. The occurrence of analcite in the Cyprus interlava sediments is accompanied not only by enrichment in sodium, but also in aluminium and silicon, and thus may not be analogous to those described in the modern oceans. The increasing abundance with depth, complementary to a decrease in smectite abundance suggests temperature control. The temperatures are not well constrained, but the persistence of goethite suggests that temperatures were considerably less than 115°C (Bischoff, 1969).

Carbonate

In the upper part of the section, carbonate becomes increasingly abundant. Much of this is in the form of veins which cut both the sediment and lava. Locally the sediment is indurated by carbonate in the vicinity of these veins. The relative importance of secondary carbonate is difficult to estimate owing to the degree of recrystallisation.

Localized high-temperature alteration

In the vicinity of mineralised normal faults and in stockwork regions below ore bodies, siliceous jaspers are common. Textural evidence (Section 4.2.2.3) demonstrates that these are altered interlava sediments. The zones in which jaspers occur are commonly narrow, generally less than 50m across. High temperatures in these zones indicated by fluid inclusion studies and isotope equilibrium

temperatures (Heaton and Sheppard, 1977; Spooner and Bray, 1975) imply high temperature gradients laterally to the faults, testifying to the efficiency of fluid transport through faults, versus that in the surrounding lavas. A more detailed examination of this problem is being undertaken by Hugh Richards, and Colin Richardson (Newcastle University).

4.3.4 Inter-relationship of sediment types

From the preceding description it can be seen that there are close spatial and chemical associations between the diverse metalliferous sediment types within the lava pile. Of particular importance is their concentration in limited areas in which occur massive sulphide orebodies. The direct derivation of the ochres from sulphide by erosion and oxidation is unquestionable. The chemical similarity of the iron component of the more distal interlava sediment to that in the ochre, and the spatial relationship of the two indicates a related source. Whereas the ochres seem to have been derived by erosion of deposited sedimentary sulphide, accumulation of vented sulphide particles, oxidized in the water column, seems more probable as a source for the distal sediments, as this will account for both the similarities and dissimilarities. The chemical and mineralogical diversity of the distal oxide interlava sediments may be accounted for largely by variations in post depositional modification, though to a small extent also by variation in supply of other primary sediment types, notably carbonate. The component most subject to secondary alteration has been manganese dioxide. Although it remains in doubt as to the original extent of manganese enrichment, it is clear that some of the interpillow oxides were originally manganiferous, but lost this at an early stage. It is probable that originally all the oxide facies sediments, with the exception of the ochres which contained significant sulphide, were ferromanganiferous, and that the interlava umbers are typical of the primary unaltered oxide facies sediment.

All other variations may be accounted for by widespread but variable enrichment in Na and Si at depth, and localized high temperature alteration in the vicinity of hydrothermal outlets.

4.3.5 Distribution of metalliferous sediments in the Troodos Massif

The concentrations of interlava sediments occur in five regions about the Troodos massif (Constantinou and Govett, 1973). Spooner (1977) on the basis of the theoretical modelling of hydrothermal cells has suggested that fixed thermal anomalies are required to impose spatial stability. He suggests that magma chambers would make suitable candidates for these thermal anomalies. Also on the basis of theoretical modelling Strens and Cann (1982) have demonstrated that to produce significant sulphides on the ocean floor it is necessary to freeze magma, lending support to Spooner's ideas. On the basis of this evidence it is reasonable to suppose that each of the hydrothermal centres on Cyprus is located above a deepseated igneous intrusion.

4.3.6 Dispersal of hydrothermal effluent

In the modern Pacific ocean hydrothermal iron and manganese are transported hundreds and even thousands of kilometres from the mid ocean ridges (Dymond et al., 1973; Heath and Dymond, 1977; Edmond et al., 1982). The reason for this is that buoyant hydrothermal fluids become entrained in the mid depth circulation system. In the Troodos massif, the non-uniform cover of metalliferous sediments suggests that hydrothermal produces were not transported through great distances. These differences are discussed more fully in the next chapter.

4.4 CONCLUSIONS

1) The sulphide ore bodies were produced by 'black smoker' type vents aligned with ridge-parallel normal faults. These were not uniformly distributed, but instead occurred in clusters separated by areas of lower activity.

2) The oxide sediments are spatially and genetically related to the sulphide-producing vents. In contrast to the proximal ochre, which was derived by oxidative erosion of the sulphide sediments, the interpillow oxide sediments and interlava umber were probably supplied by particulate sulphide released by the vents and subsequently oxidised in the water column.

3) The major element compositional variation of the interlava sediments can be described in terms of variable mixing of iron oxide-, manganese oxide-, aluminosilicate-, carbonate-, apatite-, and analcite- chemical components. Variations are due either to inhomogeneous supply of primary sediment components, or to secondary modification; particularly leaching of manganese oxides, and addition of analcite.

4) Trace elements were also partly controlled by major element compositional components. However Ba, Sr, Pb, Ni and REE are also influenced by hydrogenous enrichment, and are elevated in those sediments which accumulated most slowly. Zn, is in nearly constant proportion in the iron component throughout the sediment types. Cu is extremely variable probably due to primary variations in the Cu content of the sulphide ore. V and Zr are both enriched in the iron oxide components, but show systematic differences between the ochre and other interlava oxide sediments, suggesting some differences in the origin of the latter.

5) The interlava umber probably represents the unaltered sediment type; the interpillow oxide having lost manganese oxide through reduction in contact with the lavas. The ochre on the other hand, rich in sulphide detritus, may never have contained significant manganese oxide.

6) The interlava umber differs from the supralava umber in two respects: first, in showing far less hydrogenous trace element enrichment, probably due to higher accumulation rates; secondly, in containing a different aluminosilicate component, derived entirely from locally exposed lavas. The supralava umbers contain externally derived bentonitic clay.

7) The interlava sediments have been subjected to both low and high temperature hydrothermal alteration. The low temperature alteration resulted in formation of analcite and rarely natrolite. The high temperature alteration occurred near hydrothermal conduits, and caused transformation of goethite to haematite, and silicification, to produce jaspers. That jaspers are not the general sediment type observed, even at the base of the lava pile, suggests that temperatures did not exceed 100°C.

Plate 4.1

Interpillow oxide sediments from the Margi area of the north eastern Troodos. a) oxide-sediment occupying an interstitial pocket, containing abundant fragments of spalled glass. b) Sub-radial cooling fractures filled by oxide-sediment. c) Bedded oxide-sediment with truncated upper surface. Host lavas are mostly oblate pillows.

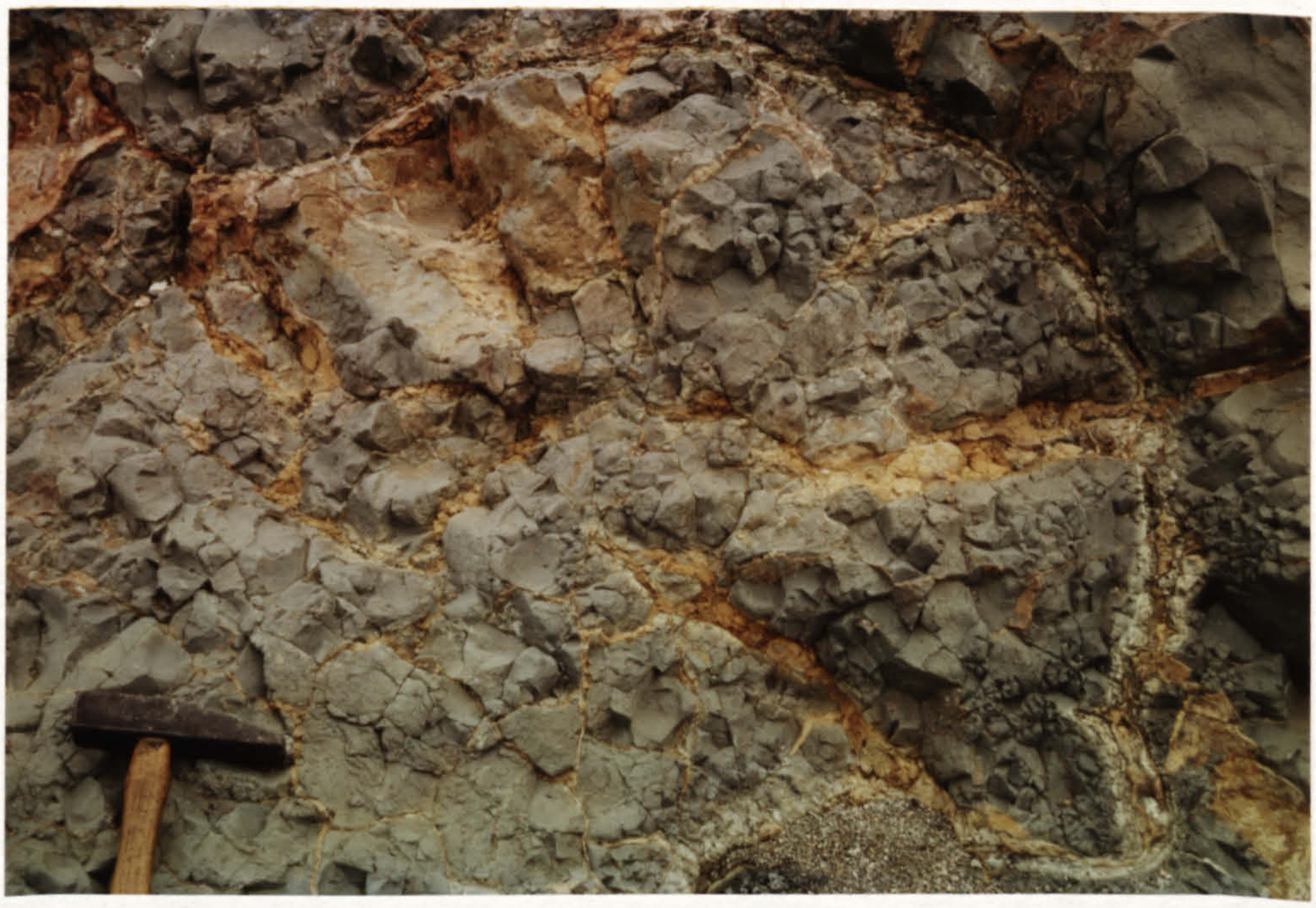


1

Plate 4.2

Interlava umbers a) Margi area, looking NW from the Margi-Kataliondas road. The dark shaley umber 60 cm thick, is overlain by olivine basaltic sheet flows. b) Kalavasos, in the banks of the Vasilikos river. A 30 cm thick umber layer is underlain by aphyric lavas, and overlain by limburgites. Samples 81-205, and 81-206 were collected from this outcrop.

Plate 4.3

Photomicrographs of interlava sediments.

a,b,) Typical texture of ferruginous mudstone. Sample 82-B5 and 82-11 (sample localities shown in Fig. A1). Characteristically isotropic in texture: flattening has been prevented by the rigid pillow lava framework.

c) Interlava ferruginous limestone (sample 81-39). Texture is similar to the mudstone but has an overgrowth of crystalline carbonate.

d) Bedded jasper, from near the Analiondas-Mathiati road, showing the contact between a quartz-epidote rich and a haematite rich layer. Pale regions in the haematite rich area are filled by quartz and epidote.

e) Massive, sulphide-bearing jasper from the Kokkinopezoula open cast mine. The rock is a deep red colour and rich in mosaic quartz, but still retains the same texture as the ferruginous mudstones shown above.

f) Interlava umber (sample 82-67) showing pyrolusite overgrowths and veins.

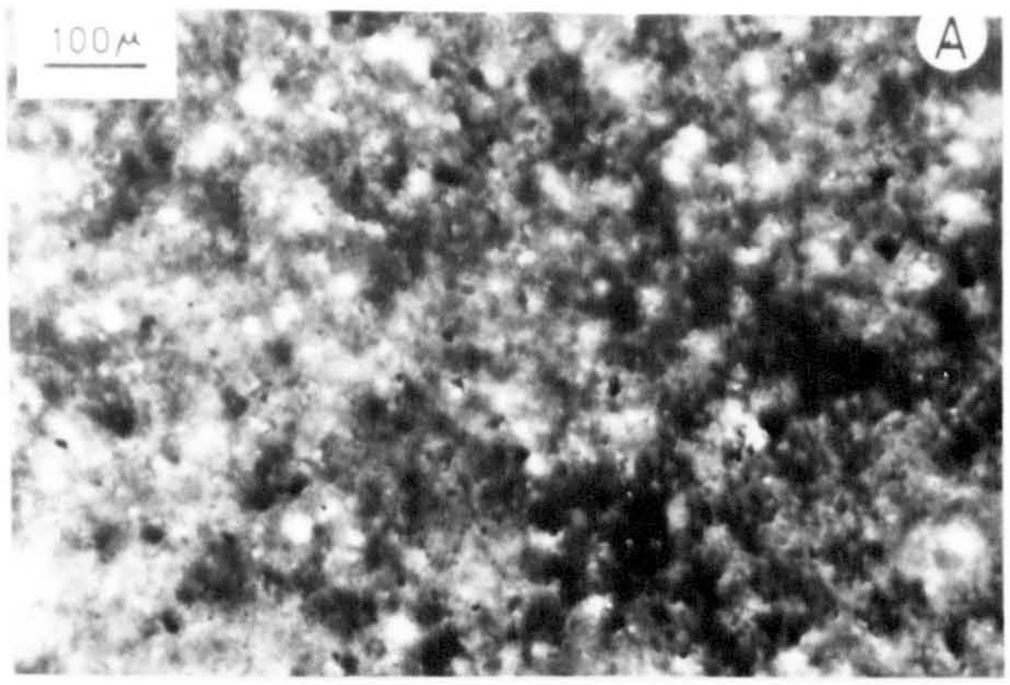
100μ
A

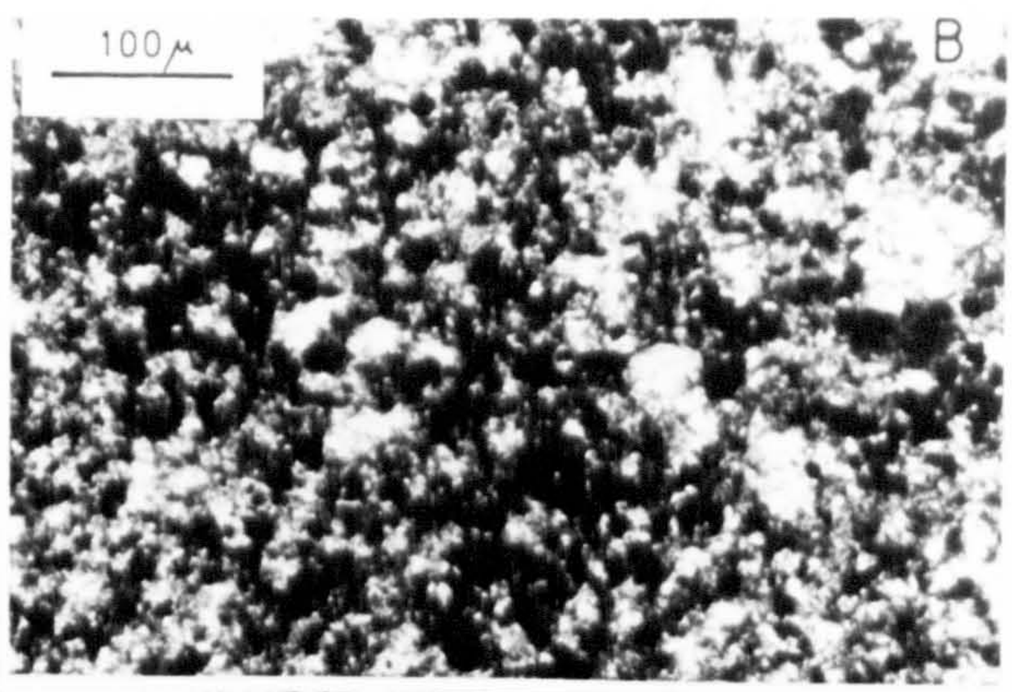
100μ
B

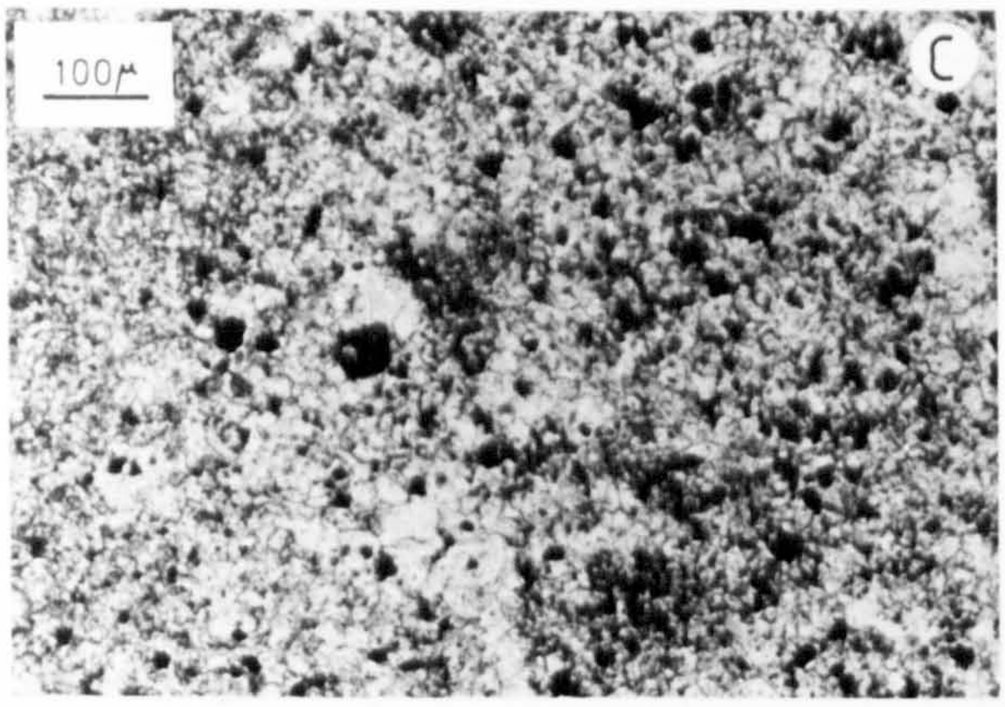
100μ
C

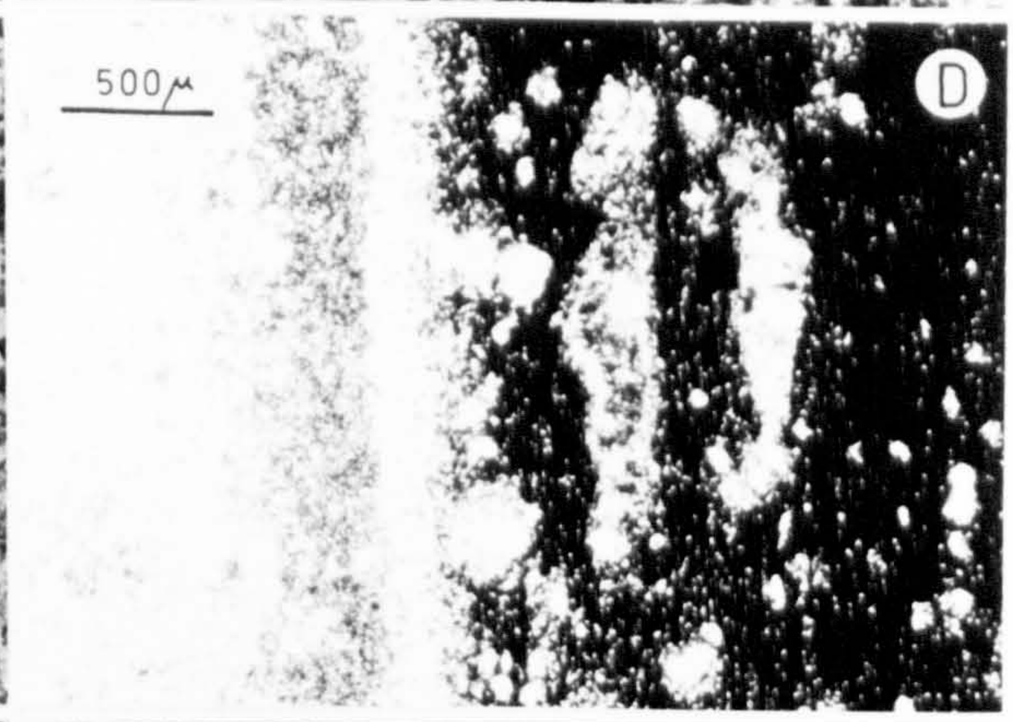
500μ
D

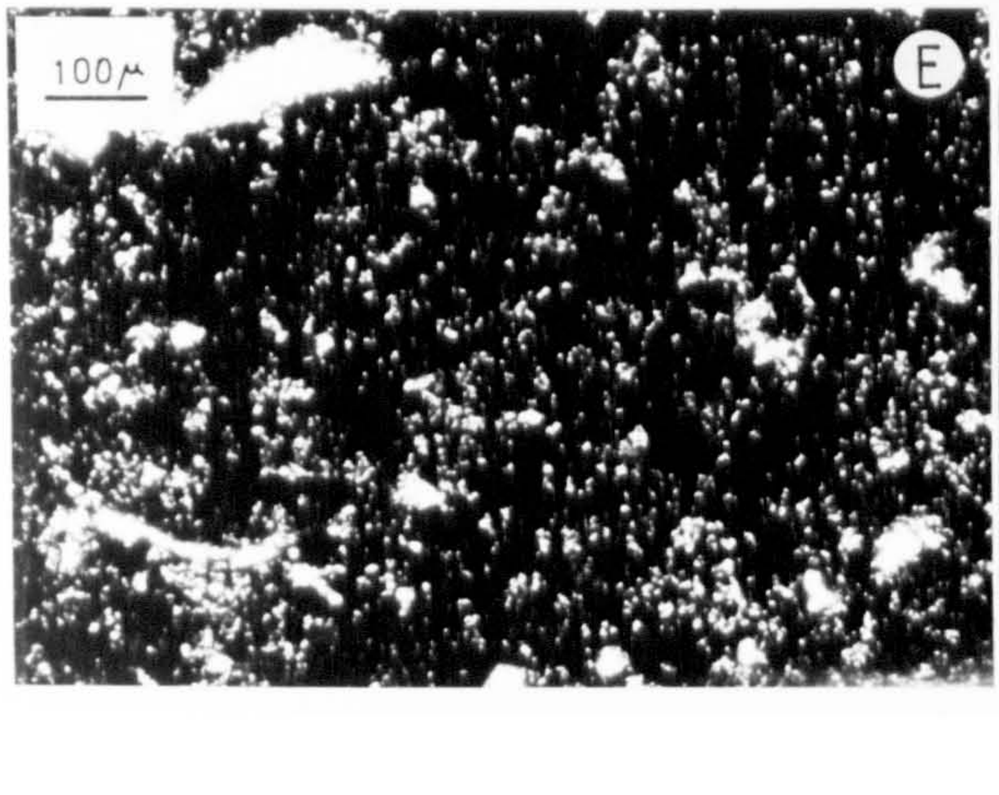
100μ
E

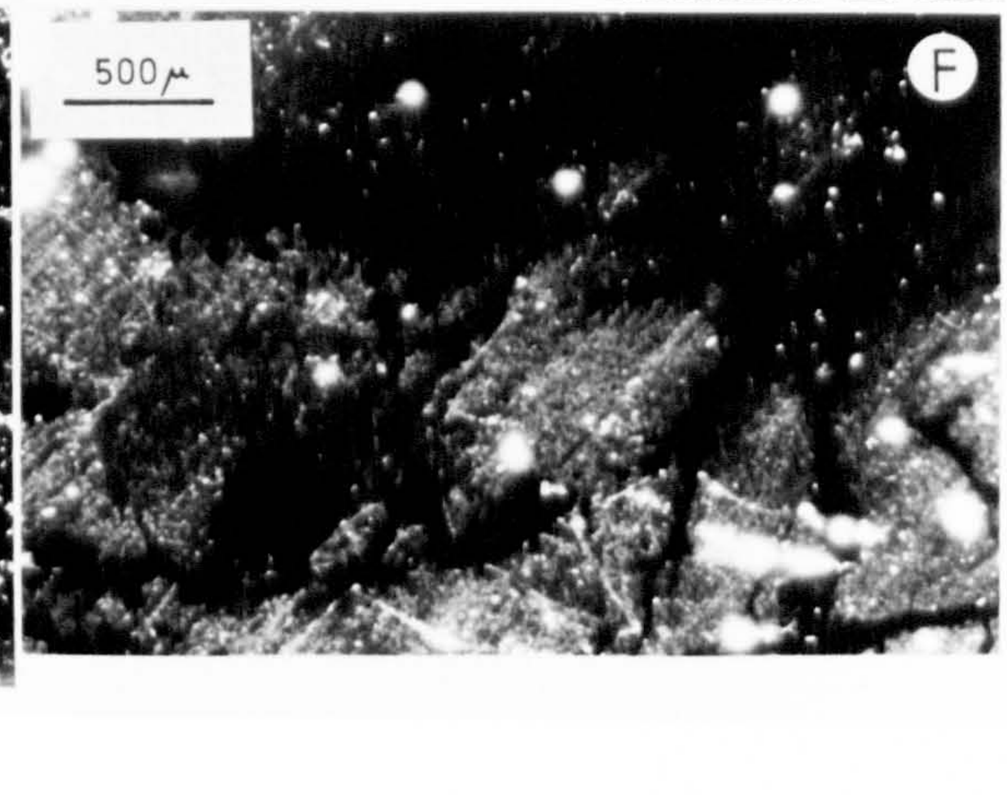
500μ
F

Plate 4.4

Photomicrographs of interlava sediment.

a,b) Partially recrystallised vermiform structures within interpillow ferruginous limestone. Sample 81-38.

c) Groundmass, and pyrolusite overgrowths in an interlava umber (sample 82-67; location given in Fig. A1), 2 km SSE of Margi.

d) Angular fragments of lava, in crude beds (bedding vertical in photograph) in interlava umber from the Kalavasos area (sample 81-207).

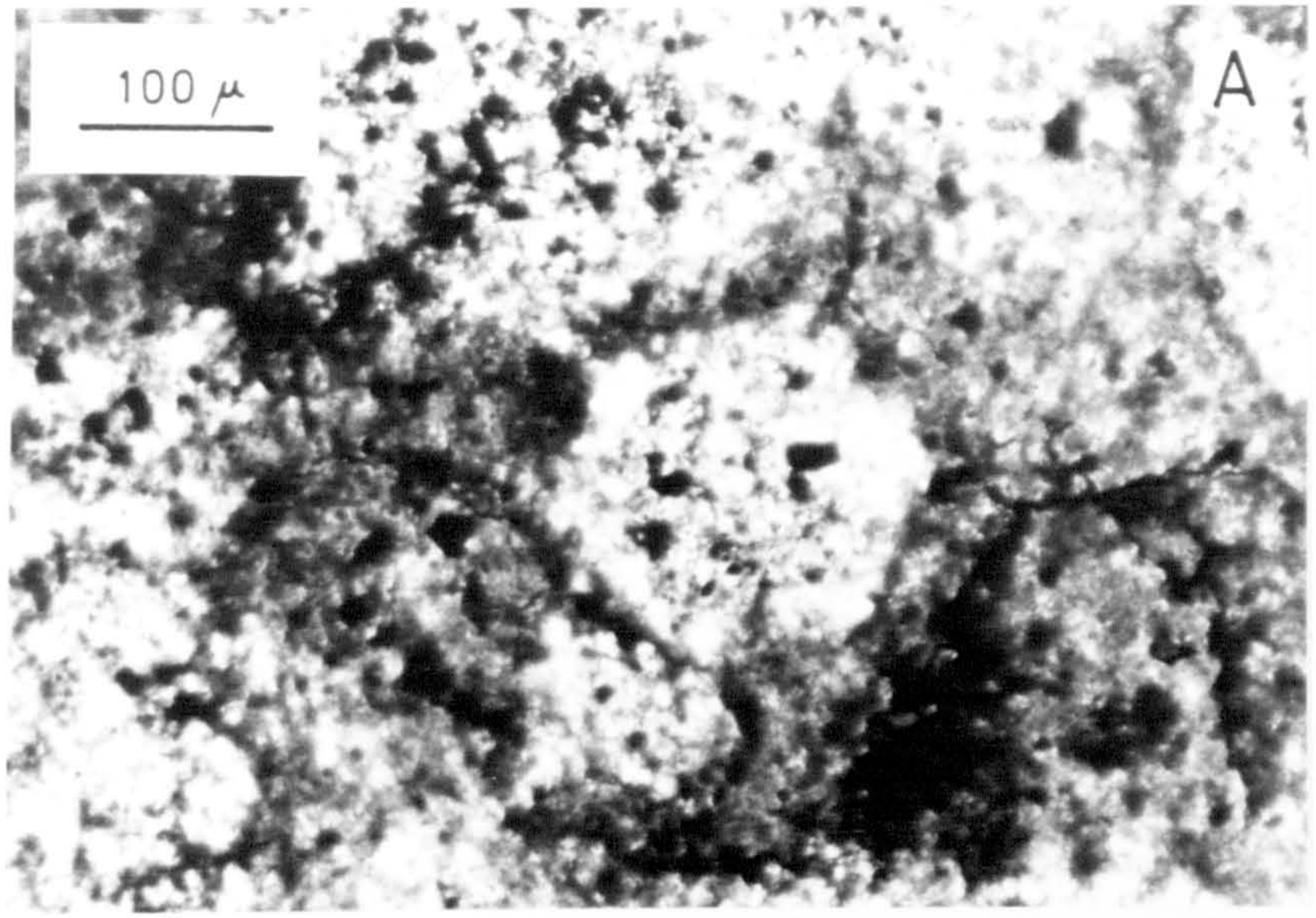
100 μ
A

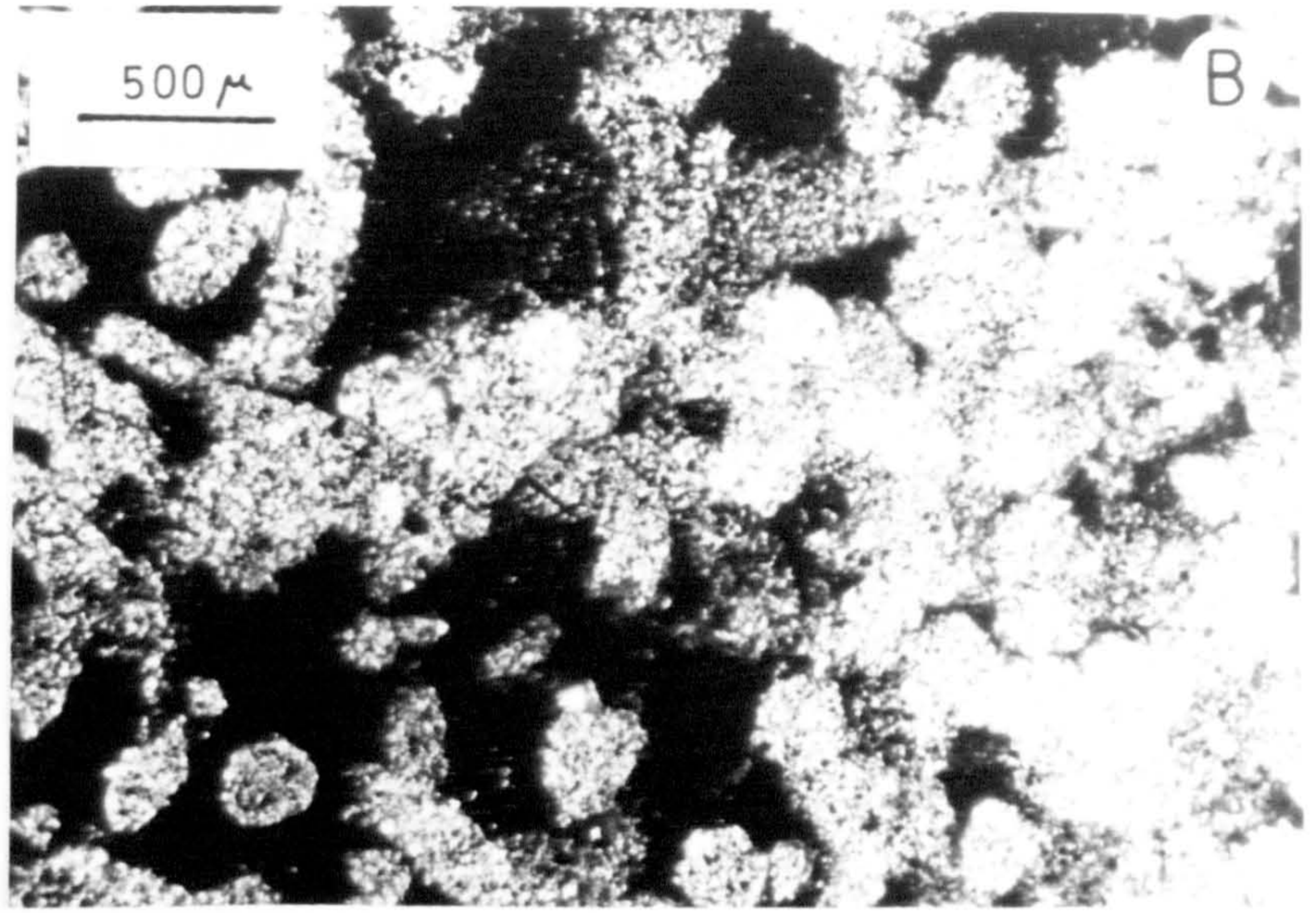
500 μ
B

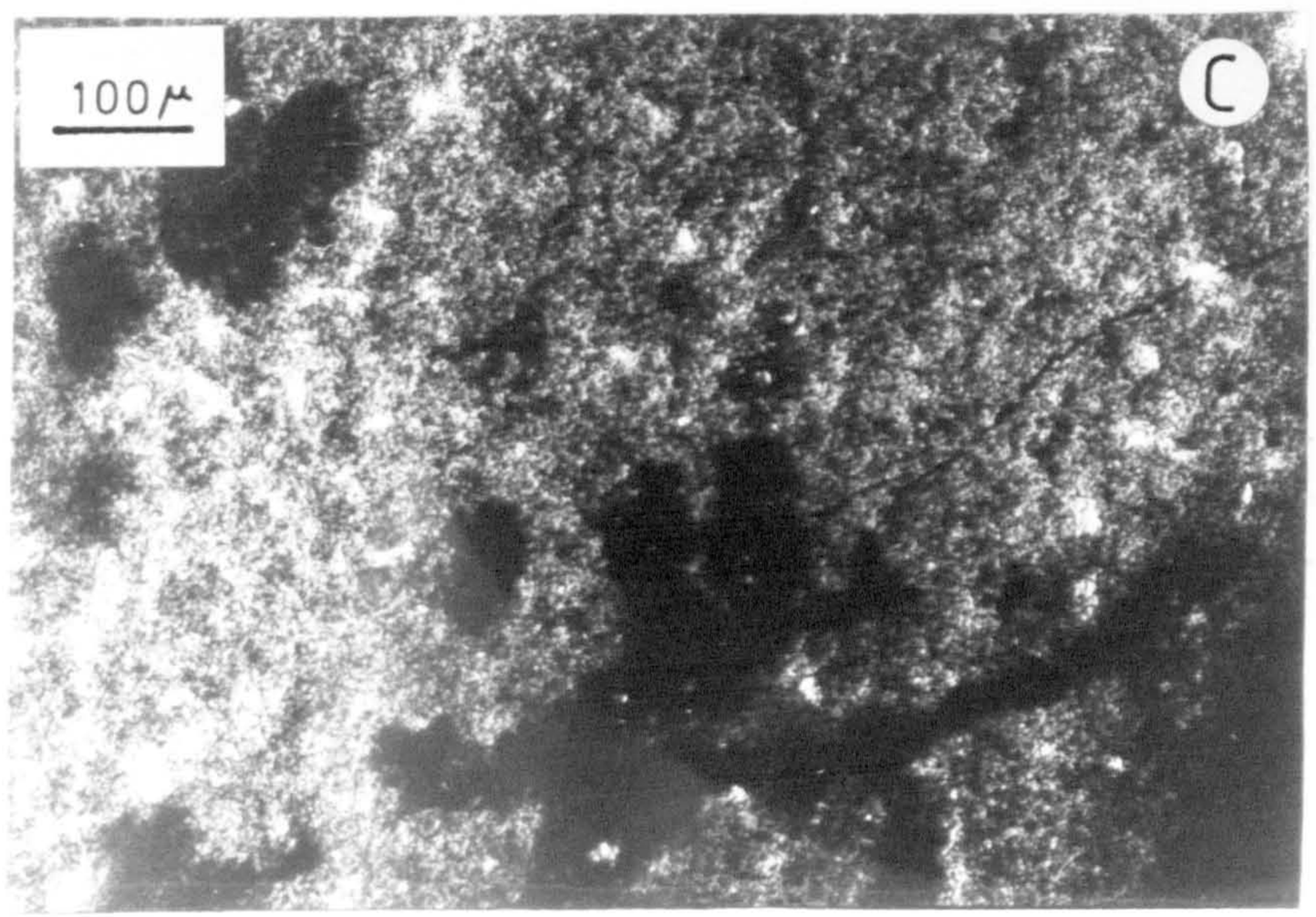
100 μ
C

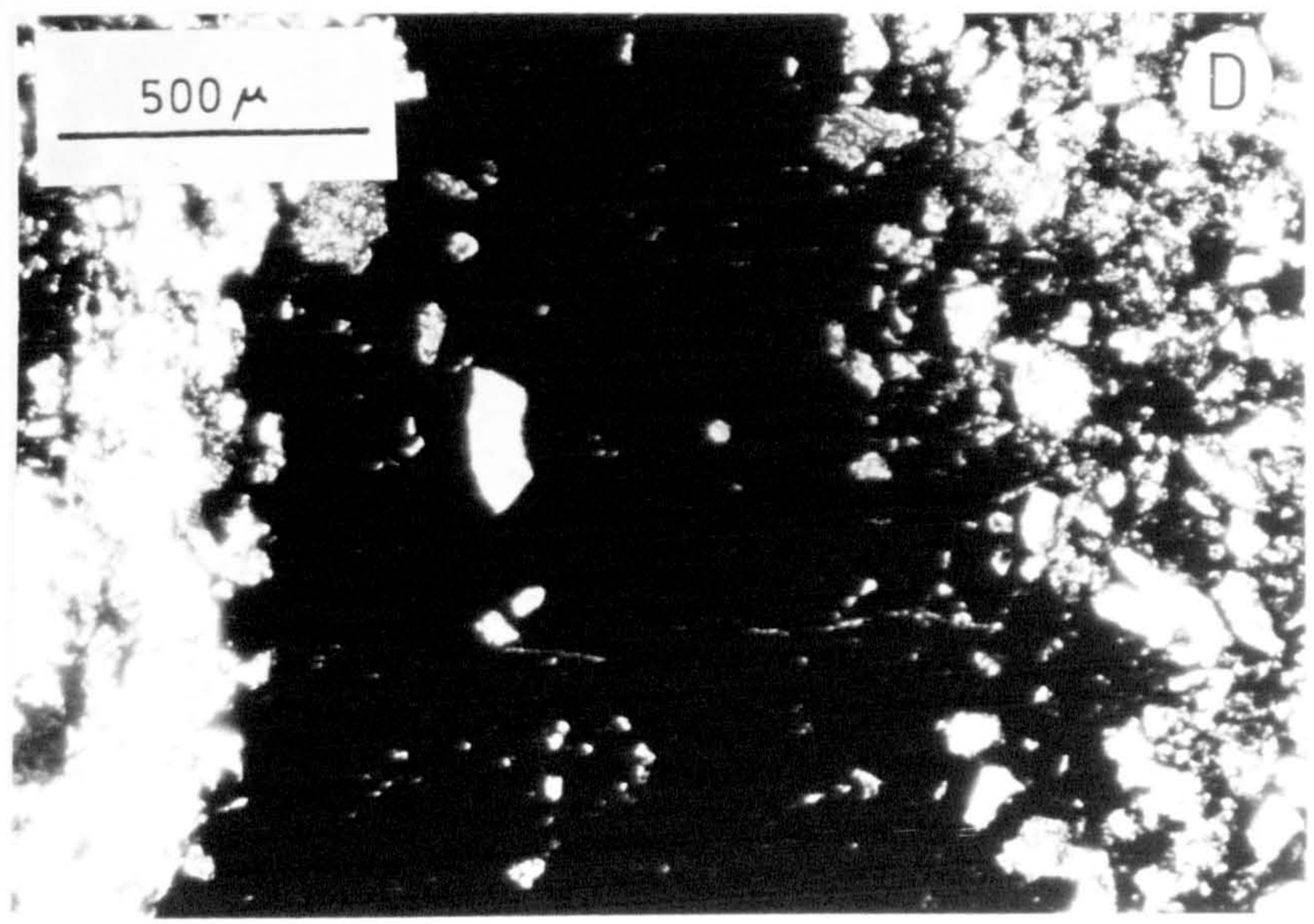
500 μ
D

Plate 4.5

Faunal remains in interlava sediments of the Margi area. Sample localities are shown in Fig. A1.

a,b) Ostracod shells in ferruginous limestone. Sample 82-52B)

c,d) Faecal pellets, possibly attributable to Favreina. Sample 81-33.

e) In addition to faecal pellets, occur poorly preserved Foraminifera. A vestige of surficial ornamentation is preserved.

f) Coccolith, unidentified, from a ferruginous limestone. Sample 81-53.

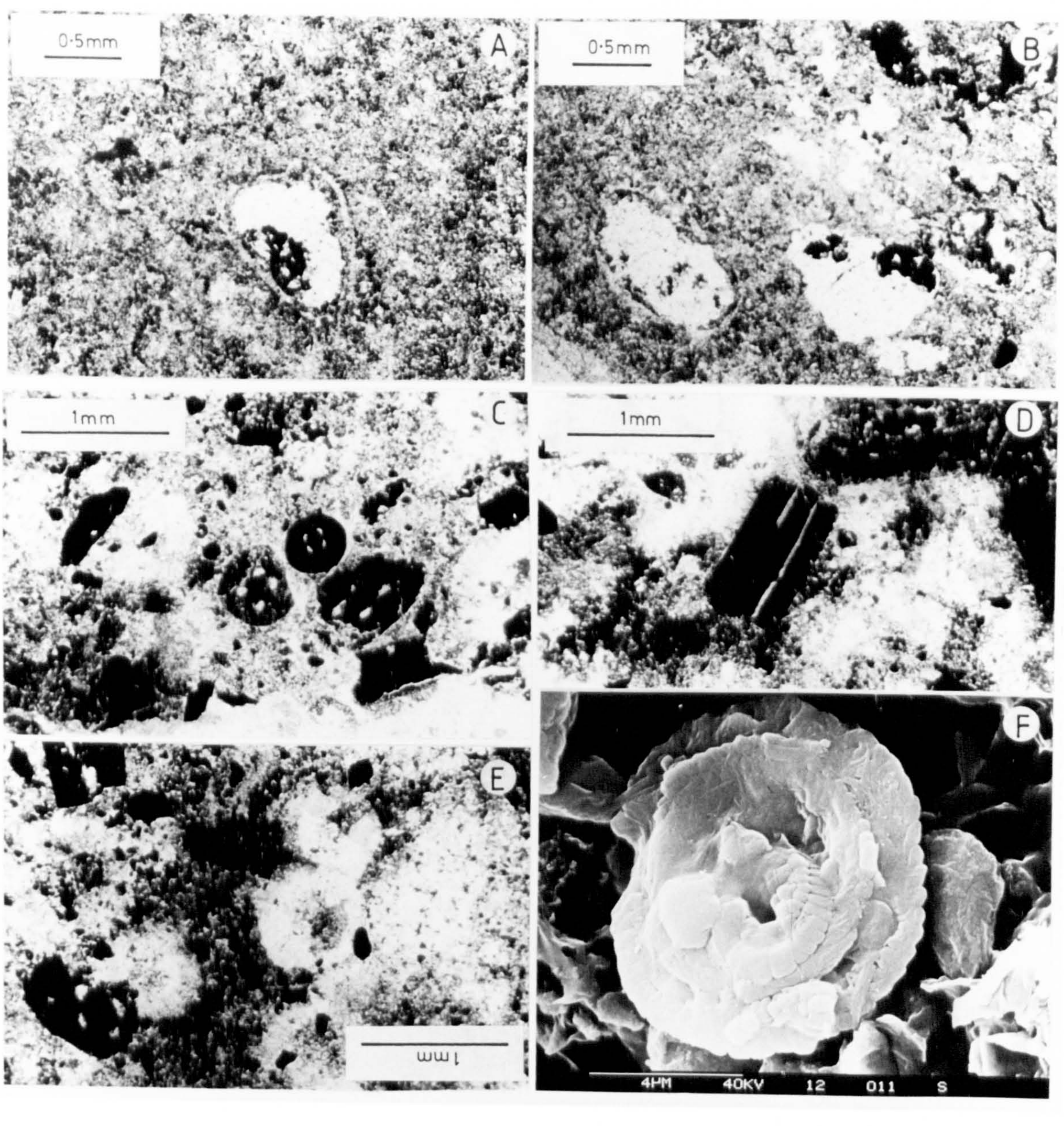
0·5mm
A
0·5mm
B
1mm
C
1mm
D
E
1mm
F
4HM 40KV 12 011 S

CHAPTER 5

SUPRA-LAVA METALLIFEROUS SEDIMENTS

5.1 INTRODUCTION

Recent interpretations of the Cyprus umber have fallen into four categories. First, that they are weathering and erosion products of the lavas (Constantinou and Govett, 1972). Secondly, that they are related to the sulphide mineralisation (Hutchinson, 1975; Corliss et al., 1972; Searle, 1973; Williams, 1973; Pantazis, 1973). Thirdly, that they precipitated from solutions produced by the interaction of sea water with hot basalts (Elderfield et al., 1972). Fourthly, that they accumulated from low temperature hydrothermal solutions at slightly off-axis vents (Robertson, 1975, 1976a; Soler et al., 1982).

The slow weathering interpretation is dismissed by Robertson (1975) on the basis that umber accumulation was rapid, and occurred throughout eruption of the uppermost lavas. The abundance and uniformity of the umbers also argues against formation through direct interaction of sea water with basalt. Evidence presented in this chapter, concerning the composition of constituent materials, and the continuity of metalliferous sediment accumulation, strongly favours an origin through distal accumulation around axial sulphide-producing vents.

The following account is divided into two principal sections. The first comprises a description and discussion of the field and petrographic evidence. The second comprises description of the mineralogy and chemistry of the metalliferous sediments, followed by a discussion of the data as a whole.

5.2 SUCCESSION AND PHYSICAL CHARACTERISTICS OF THE SUPRALAVA METALLIFEROUS SEDIMENTS

5.2.1 Succession

Three geological formations, the Perapedhi, the Kannaviou and the Lower Lefkara, ranging in age from Campanian to Eocene lie on the upper surface of the Troodos Pillow Lavas. This results from the irregular topography of the lava surface, leading to progressive infilling of hollows. Lava was thus locally bare of sediment until sometime during the Eocene. The Perapedhi Formation, comprising the umbers, and overlying bentonitic clays and radiolarites, is exposed only in depressions in the lava surface. The succeeding Kannaviou Formation, comprising bentonitic clays, volcanogenic sandstones and radiolarites is also discontinuous, and is itself overlapped by the marls of the Lower Lefkara Formation.

The basal sediments comprising the umbers, clay-rich umbers, bentonitic clays and radiolarites were assigned to the Perapedhi Formation (Wilson, 1959). Owing to the irregularity of the lava surface, the thickness of these is greatly variable. In the majority of exposures the umber has a mean thickness of 2.5m (Robertson, 1975), but in some localities, such as Dhrapia, thicknesses are as great as 35m. The overlying clay-rich umbers have a mean thickness of 2.7m (op. cit.), but are not invariably present. The overlying bentonitic clays and radiolarites are also variable. In the north of the massif, a thickness in the order of 10m is common, but in the southwest the Perapedhi Formation continues upwards into the volcaniclastic sediments of the Kannaviou Formation, which is up to several hundred metres thick. A problem exists concerning the distinction of the Perapedhi and Kannaviou Formations. The bentonitic clays and radiolarites assigned by Wilson (1959) to the Perapedhi Formation are mineralogically identical to the bentonitic clays of the Kannaviou Formation. The latter was defined by Lapierre (1968) who distinguished it from the Perapedhi Formation on account of the abundance of volcaniclastic sandstones. Further the clay component of the pure umber is essentially the same as the bentonites (section 5.5.6) and at one locality (Cyprus bore hole CY1) interlava sediment is also of

this type. Although the thick Kannaviou volcanogenic sandstones (confined to the SW), postdate the umber, it is clear that volcanogenic material related to this was accumulating during eruption of the lavas, and throughout deposition of the umbers. A fuller discussion of this problem is deferred to chapter 6, section 6.1.2.

Assigning ages to the lower part of the sedimentary cover has proved problematic. A definite Maastrichtian age for the Lower Lefkara Formation has been obtained from foraminifera (Henson et al., 1949; Mantis, 1970). However, radiolaria extracted from the Perapedhi Formation, are an incongruous assemblage of mid- and Upper-Cretaceous forms (Irwin et al., 1980; Empson-Morrin, Pers. Comm. 1982). Irwin et al. (1980) favour a Mid-Cretaceous age. The presence of the Campanian markers, Patulibracchium californiaensis, P. delvallensis and Neosciadiocapia diabloensis (Empson-Morrin) argue strongly for a younger age, but uncertainty does exist. Isotopic age dating of the lavas gives a range of 110-80 Ma (Delaloye et al., 1980) which does not discriminate between the two possibilities.

Unfortunately this uncertainty makes it impossible to realistically estimate the accumulation rate of the sediments.

5.2.2 Lithological Types

The predominant lithology is a fine-grained brown sediment termed umber. The pure umber is characteristically non-fissile. Contained within it are varying abundances of bedded cherts, irregular vitreous cherts, and manganese concretions or veins. Basal umber may contain large amounts of coarse basaltic debris, locally grading downwards into clast-supported talus deposits.

The other principal lithology is a dark, grey or brown, fissile mudstone, here termed clay-rich umber. This never occurs beneath the pure umber, but may be the basal lithology where the latter is absent.

The clay-rich umber grades upward into pink or white fissile mudstones, radiolarian mudstones or radiolarites, and with which it may be interbedded. Where the former is absent, pure umber is in normal contact with the clays and radiolarites.

5.2.2.1 Umber.

The pure umber is fine grained rich-brown massive-textured rock. Its density ranges between 1.3 - 1.4gcm^{-3} owing to the extremely high porosity. When struck it is brittle, breaking with conchoidal fracture, but it is only weakly consolidated. In contact with water it becomes soft and clayey, partly as a result of swelling clays that are component minerals. Most deposits exhibit no sign of bedding, though fine continuous or discontinuous lamination is common. The thick umber deposits of the south west of the massif are unusual in containing discontinuous beds of pale-brown umber, 10-30cm thick. Slump structures are observed in many of the umbers (Robertson, 1975).

Small scale sedimentary structures. Characteristic sedimentary structures are illustrated in Plates 5.8 &5.9. Extensive post-depositional disruption bears witness to instability of the sediment during accumulation.

Large scale slump structures are described by Robertson (1975): slumping on the small scale is equally abundant. At Margi the texture varies from completely homogeneous through continuous lamination (Plates 5.9A, 5.9E, 5.8D) and discontinuous lamination (Plate 5.9B) to chaotic irregular lamination (Plate 5.9C,D). Contortion of the laminae is common (Plate 5.8A, 5.9C). Microfaulting is locally important, leading to a very disjointed appearance (Plate 5.8A, 5.9A). In Plate 5.9a some of the faults pass right through the sample but others which have displacements of c. 1cm at the base have progressively smaller displacements upwards, and fail to cut the uppermost laminations. Clearly faulting was occurring within the uppermost 1-3cm of the sediment. Burrowing is visible in some samples and probably contributed to the irregular appearance of much of the sediment. Well preserved laminations elsewhere indicate that

burrowing was not pervasive.

Accumulation of the sediments upon a steeply sloped basement is the probable cause of this deformation. Creep of the sediment mass towards the centre of the trough resulting in the early step-faulting and contortion.

Petrography. In thin section pure umber is very homogeneous. It is pseudo-isotropic as a result of abundant fine-grained goethite. In plane-polarized light the material is inhomogeneous on a scale of c. 100μm, resulting in an irregular mottled appearance (Plate 5.1A,B). The paler patches are enriched in aluminosilicates. Abundant sub-elliptical diffuse, dark to opaque, objects characteristically occur in the umber, as in the interlava sediments (Chapter 4, Section 4.2.2.3). These are in the order of 20μm in long axis. Electron microprobe analyses demonstrate that these dark zones are strongly enriched in manganese and barium (section 5.4.4).

Contained within the fine-grained matrix are dispersed fragments. locally, where epiclastic material has washed into the umber, coarse fragments of altered lava, and lava-derived minerals are abundant. However throughout most of the umber fragments of this type are absent. Radiolaria are locally abundant, occurring as flattened ellipsoids of goethite with long axes 100-200μm. Rarely tridentate spicules occur (Elderfield et al., 1972). Small fragments of phosphatised cuticle are common, though seldom abundant. These are usually in the form of short broken sheets in which some internal structure is visible (Plate 5.1E), but small circular cross-sections also occur. The forms are characteristic of arthropoda and the size suggests Ostracods to be a likely source (E.N.K. Clarkson, pers. comm., 1983). This possibility is supported by the presence of more complete ostracod remains in the interlava sediments (Chapter 4, Section 4.2.2.3).

Basal pale umber. The lowermost parts of the umber may be ochreous in colour, contrasting strongly with the brown above. The contact between the pale and dark regions is sharp and generally cross-cuts

bedding. Fractures passing through the umber are sometimes bounded by similar pale zones. Rarely, as at Skouriotissa, a transition from basal pale- to dark-umber is concordant with bedding and may be a primary phenomenon.

Cherts. Cherts contained within the umber are of two types. Firstly, in umber deposits occurring in the south of the massif, notably at Dhrapia and Mangalene (near Parekklisha), thin laterally continuous beds of radiolarian chert are found. Secondly, and more commonly, occur bulbous masses, varying from vein-like forms 2-10cm across to equant bodies several metres across, of dark-brown chertified umber (Plate 5.3B). Good examples are seen at Asgata, and in the umbers between Margi and Mathiati. Umber laminations pass through these, and there is no doubt that they were formed by secondary silicification.

Veins. The basal parts of umber deposits are commonly cut by subvertical veins of palygorskite, and manganese oxides. These are ptygmatically folded attesting to their early origin. They are more fully described below (section 5.2.5).

Concretions. Black pyrolusite concretions varying from pea size to continuous irregular sheets tens of centimetres across occur in many of the umbers.

Phosphatic concretions are rare, but in the Mangalene Umber are relatively abundant. They are generally ellipsoidal and 4-6cm in long axis. In thin section they are mottled, and composed predominantly of cryptocrystalline phosphate (identified as francolite - see section 5.3.2). A proportion of host umber is included within them.

5.2.2.2 Clay-rich umber

The clay-rich umber is a grey to brown fissile mudstone. It is considerably more compact than the underlying pure umber, having a density of 1.6-1.7gcm^{-3}. Fresh samples break into slabs because of the fissile character, and the absence of conchoidal fracture further

distinguishes it from the pure umber. Weathered surfaces are rubbly: in contact with water it sensibly swells and cracks, a characteristic shared with the overlying pink clays. This is seen well at Margi (Plate 5.4D) where massive pure umber is capped by formless clay-rich umber, and partially buried by degraded debris from the clays.

Fine-scale continuous parallel lamination is the dominant feature in hand specimen. The contortion and microfaulting common in the umbers are not present.. Small ptygmatically folded white veins of palygorskite occur, but these are only centimetres long, in contrast to the umbers. There is evidence of burrowing in the form of 0.5-1.0cm across flattened cylinders in the rock which are composed of pale pink clay. The extremely sharp boundaries to these suggest that the infill may have descended from the overlying pink clay.

In thin section the clay-rich umber is more finely laminated than the pure umber (Plate 5.2A-D). Many of the interlaminae contacts are sharpened due to bedding-slip (Plate5.2 A,C). In the absence of these, irregular normal contacts are seen (Plate 5.2D).

In common with the umber diffuse dark objects c.10μm across are present, though they are less abundant. In crossed nicols the matrix is strongly anisotropic due to alignment of clay minerals.

Small plagioclase crystals (<50μm) are common in the matrix, but rare large (up to 2mm) euhedral andesines also occur.

Phosphatised cuticle is far more abundant than in the pure umber (Plate 5.2B) but is identical in form and composition.

At Margi, the contact with the overlying bentonitic clay is well exposed. In the field the contact is demonstrably concordant with bedding, suggesting that it does not simply reflect a diagenetic change. However in thin-section, localised evidence of small-scale manganese remobilisation can be seen (Plate 5.2E). It is notable that the contact is sharp, being transitional over a distance of less

than 50μm.

5.2.3 Sites of metalliferous sediment accumulation

The majority of the umbers occur in small pockets in the lava surface, though locally umbers are abundant within the lava pile. Robertson (1975) subdivided the umbers into five categories according to field relations. These are briefly summarised below.

Small hollow umbers. Small lensoid occurrences 10-50m across containing in their thickest parts 0.5-7m of pure umber, and 0.5-4.5m of clay-rich umber. The umber is generally undisturbed and finely laminated.

Fault-bounded umbers. Thicker and of larger plan area than the small hollow umber (for example Lymbia is 130m long, 20m wide and 15m thick), these are so named for their situation in faulted grabens or half grabens. Talus is abundant in the lowermost parts, and slumping of the umber is common.

Interlava umber. Interlava umbers, discussed in Chapter 4 Section 4.2.2.2, are rare in comparison with supralava umbers, but are locally abundant in the vicinity of the Mathiati and Kalavasos Mines.

Umbers associated with thick lava breccias. Thick and extensive volcanic breccias outcrop between Vavla and Ayios Mamas south of the Arakapas Fault Zone. At several localities, particularly in the vicinity of the Kalavasos mining district, these are overlain by the thickest umber deposits to be found in Cyprus. These umbers are peculiar in containing radiolarian cherts, and discontinuous (less than 25m wide) trough-shaped lenses of umber.

Sulphide-related umber deposits. At Mathiati and Skouriotissa, there is a close spatial relationship between sulphide ore bodies and overlying umber. At Mathiati, the umber is separated from the sulphide by unmineralised lavas. At Skouriotissa the umber lies directly upon the sulphide ore. Most commonly the ore is covered by ochre, and umber occurs separately (section 4.2.2.1).

Similarity of umber types. The umber deposits have been categorised above according to differences in their relationships to the other lithological types. However it is important to appreciate the continuity that exists between these types, and the high degree of similarity of most deposits. Many occurences described as small hollow umbers may be related to normal faults not exposed. For example the umber at Pyrga is underlain by coarse lava breccia resembling the talus in the fault-bounded umbers. No fault is observed but the geometry of the deposit would permit one to remain hidden. The close spatial relationship of umbers with sulphide ore bodies at Mathiati and Skouriotissa has been noted (Robertson, 1975). However, the spatial relationship of umbers with sulphides in general is variable. Umbers such as at Pyrga, and at Perapedhi, are not near known mineralisation, and elsewhere, for example at Agrokypia, sulphides occur without known umber deposits. Considering the limited areal extent of the occurrences, and the variable exposure: at Agrokypia the upper lava surface is mostly concealed beneath a late Tertiary unconformity, it is not possible to arrive at any definite conclusions as to the relationship. It is noteworthy however, that the important sulphide mining areas of Skouriotissa, Kambia, Mathiati, Kalavasos, and Limni, all have extensive umber deposits within a few kilometres.

5.2.4 Modification of umber deposits through loading compaction

Most umber deposits are located in hollows of varying shape and steepness, and as a consequence their present form has been greatly modified by loading compaction. This is manifested most notably in the saucer or trough shaped forms in which dips are orientated towards the centre or axis of the hollows. Compaction of the umbers has also modified the overlying clays and chalks. For example, 0.5km west of Margi, chalks are seen folded into a syncline above a north-south orientated trough (Fig. 5.1). Veins cutting the umber have become ptygmatically folded, and radiolaria are strongly flattened, permitting estimation of the minimum degrees of compaction involved. The compaction is further evidenced by the presence of steeply dipping slickensides which are most common close to the

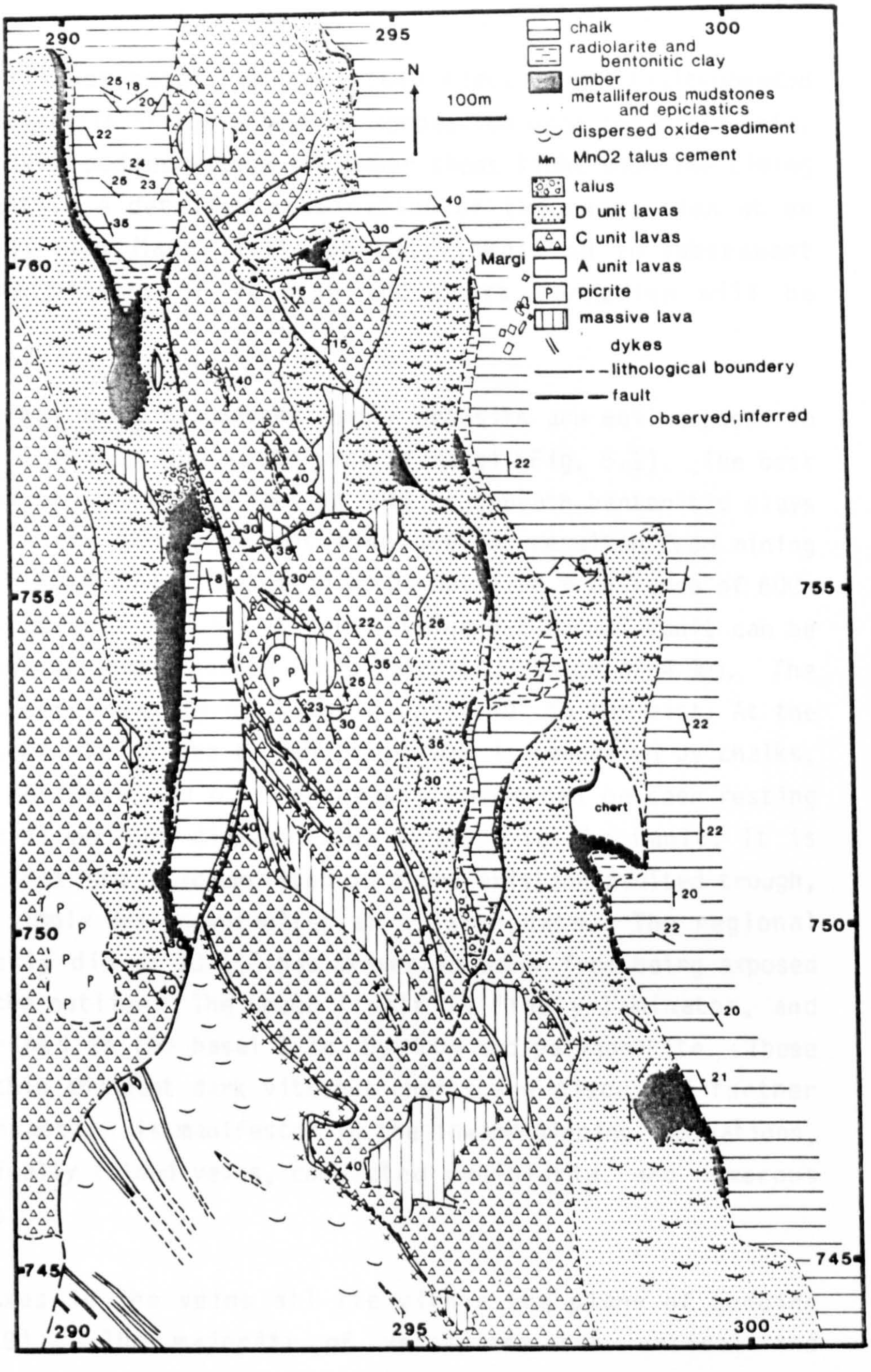

Fig. 5.1 The upper part of the lava pile is well exposed near the village of Margi. Supralava sediments, generally diping north-easterly, are preserved in faulted hollows in the lava surface (see Figure 3.3 for cross-sections). The inliers formed by accumulation in hollows, rather than by downfaulting of a previously continuous sediment cover. Compaction of the sediment into the pre-existing depressions is evident from the inwardly directed dips in the trough at the NW corner of the map.

irregular pillowed bases, or the steep sides of the fault-bounded umbers. An analysis of the effect of compaction upon the radiolaria, veins and chert bodies within the umber sheds light upon the timing of these events. A detailed examination of the compaction at an umber deposit near Margi will be described, and in subsequent sections the history of veining and chert formation will be discussed.

The Margi umber deposit. Several umber deposits are well exposed in the area to the west and south-west of Margi (Fig. 5.1). The best exposed of these occurs in a faulted outlier beneath bentonitic clays and chalks, where the excellent exposure has resulted from mining activities (Plate 5.3A). The umber crops out over a distance of 600m in a half-graben of which the controlling N-S normal fault can be traced southwards down sequence for a lateral distance of 4 km. The umber rests concordantly on lavas dipping 40° to the east. At the faulted eastern edge of the trough, the umber is concealed by chalks, but at the northern end of the deposit umber can be seen resting concordantly on westward-dipping talus adjacent to the fault. It is thus clear that umber accumulated in a pre-existing faulted trough, and has not simply been downfaulted at a later date. The regional north-easterly dip of 10-15° has prevented umber from being exposed all around the outlier. The umber itself is finely laminated, and strongly veined in the basal 1-2m, by MnO_2 and palygorskite. These veins, and thin abundant dark vitreous cherts are discussed further below. Compaction is manifested in the inward dipping laminations, the ptygmatically folded veins, compacted radiolaria, and numerous slickensides.

Fold axes in the veins all lie within the plane of bedding (Plate 5.6B). The majority of veins are sub-vertical and perpendicular to the bedding, but others may be concordant with bedding or oblique. Calculation of shortening on 15 veins yields a bedding perpendicular component of shortening of 0.54 ± 0.07. The values are not influenced by the orientation of oblique veins indicating that shear was predominantly pure. A shape fabric analysis of flattened radiolaria in three samples gives the same

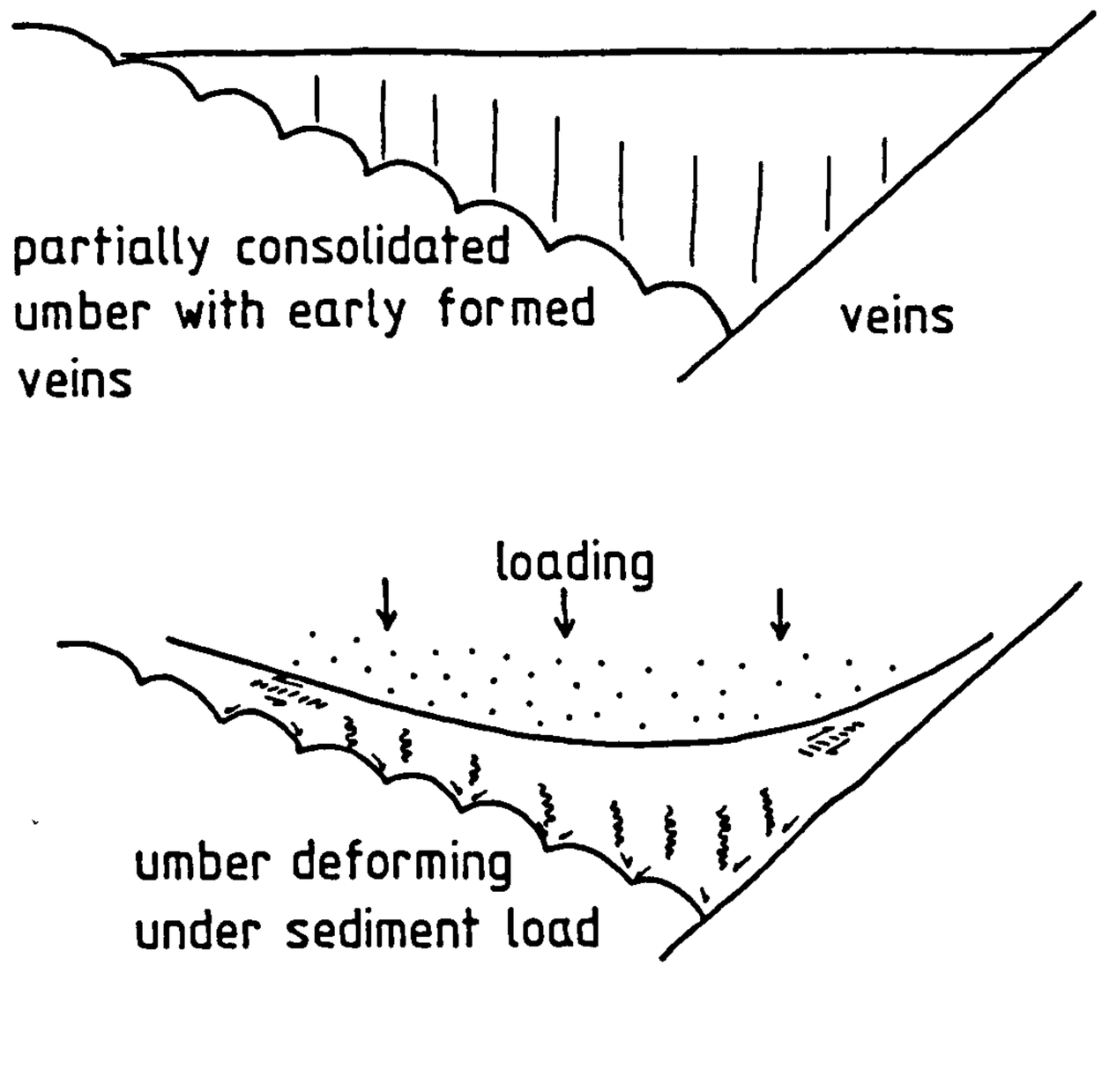

Fig. 5.2

Differential compaction of umber into hollows in the lava surface. Early formed veins become ptygmatically folded. Slip surfaces develop about irregularities. Simple shear is taken up in shear zones containing early formed tension gashes.

result: predominantly pure shear and shortening of 0.52 ± 0.11, 0.51 ± 0.14 and 0.36 ± 0.13. Though compaction resulted mostly in pure shear, near the edges of the umber pit where slopes are greatest, bed parallel zones 2-10cm thick contain sets of sigmoidal palygorskite veins spaced from a few to a few tens of millimetres apart. These zones, spaced 10-30cm apart, indicate simple shear up slope.

In addition to pervasive compaction and zones of simple shear, discrete sub-vertical fractures are common near the base of the deposit or close to the fault. Surfaces of the fractures are polished and gently curved with sub-vertical striations (Plate 5.6C). It is not possible to estimate displacement. Where the underlying lavas are exposed, the fractures occur concentrically dispersed about up-standing pillows, and may thus be attributed to differential compaction onto the irregular surface. This is seen more clearly in the steep-sided fault-bounded umbers, where slickensides are concentrated near the edges to the deposits. There is no textural evidence of later movement of these faults in the Margi area.

The various deformational features can all be explained by compaction of the umber into the faulted-hollows. The relationships between the structures are illustrated on Fig. 5.2. The V-shaped trough would be filled by a wedge of umber, and after partial consolidation, veined by MnO_2 and palygorskite (see below). Upon loading by overlying sediments, the umber would be compressed into a trough shape. The compaction would involve predominantly pure shear, deforming the radiolaria and ptygmatically folding the veins. Slip surfaces would develop about irregularities on the lower surface. Compaction into this V-shape has for space reasons to involve simple shear up-slope in both directions away from the axis of the trough. This shear has not been distributed homogeneously, but instead by flexural slip of bed-parallel units, with zones of simple shear in between, in which form tension gashes. The formation of slickensides and tension gashes in muddy sediments which are only partially consolidated has been observed in DSDP cores (Lunberg and Moore, 1979; Cowan, 1979).

5.2.5 Origin of the MnO_2-Palygorskite veins

Umbers are commonly, though not ubiquitously, veined by MnO_2 and Palygorskite. Particularly good examples are at Ayia Marina and, as described above, at Margi. The veins generally comprise an outer part of fibrous palygorskite, which appears micaceous in hand specimen, and an inner part of intergrown MnO_2 and palygorskite, but the latter part may be absent. They are largely confined to the lower 1-2m of the deposits and vary in thickness from less than 1mm to 10mm. The majority are near vertical, but others occur parallel to bedding or are oblique. As described above, their ptygmatically folded form has resulted from compaction of the sediment. Originally they were near planar, as can be seen where they are preserved in early formed cherts (see below). The degree of compaction which they have suffered is the same as that calculated for deformed radiolaria in the umber (see previous section). It is thus apparent that the veining occurred as soon as the umber was competent enough to permit deformation of the radiolaria. The radiolaria have been replaced by goethite, and are likely to have deformed passively from an early stage. Identical veins are found commonly in the uppermost parts of the lava sequence, and are of probable low-temperature hydrothermal origin. Thus it seems likely that the umber veining occurred soon after accumulation as a response to this hydrothermal activity. The absence of veins in the upper parts of the umber might be related either to increasing sediment load opposing veining, or cessation of the hydrothermal activity.

5.2.6 Origin of secondary cherts in the umbers

Cherts in the umbers are of two varieties. Firstly, occurring only in the umbers of the southern margin of the Troodos massif, are laterally continuous bands of radiolarite. Secondly, irregular often bulbous masses of vitreous dark chert may occur. The latter, in which ghosts of the original umber laminations are visible, are of clear secondary origin. They vary from equant masses a few centimetres across, to laterally continuous masses concordant with bedding, for example at Asgata (Robertson, 1975). The secondary cherts at Margi, are generally flattened, up to 2-3m across and 0.1-1m thick. Most are disposed sub-vertically though rarely they

may be concordant with bedding. The surfaces are always rounded, smoothly bulging in sharp contact with the surrounding umber (Plate 5.3B). The density of veins within the chert is the same as in the adjacent umber, but the veins are entirely unfolded. Silicification has thus occurred prior to significant compaction of the umber. The flattened nature suggests that silica may have been introduced along fractures within the early formed plastic sediment. This view is in agreement with observations at the Asgata umber, where silicification is seen to be related to early slumping of the partially consolidated sediment (Robertson, 1975).

5.2.7 Manganese-depleted umber

Pale coloured manganese-depleted umber occurs in association with more normal umber at several localities. At Kambia and Ayia Marina the basal few centimetres are of this type. The sharp contact with the overlying normal umber cross-cuts sedimentary laminations, indicating the secondary character of this depletion. At the Arsos umber pit, situated in the Trouli inlier, alternating bands of normal- and paler orange-umber occur, with sinuous contacts also cross-cutting bedding. Manganese depletion may also be related to faulting, for example in the umber deposit 0.5km west of the Mathiati mine. There, a zone of manganese depletion 20-30cm thick occurs adjacent to a faulted contact (Plate 5.6D). The cause of this depletion is uncertain, but as argued above (Chapter 4, section 4.3.3) the lavas represent an important reservoir of reduced species, having not been fully oxidized to this day. Downward percolation of oxidizing seawater has resulted in the partial oxidation of lavas even at the bottom of the lava pile (Spooner, 1977). If circulation were restricted by the presence of an impervious body of sediment, depletion of oxygen by interaction with lava might reduce the water sufficiently to take manganese into solution. Hence umber in contact with lava might be susceptible to manganese depletion. This proposed mechanism is unsatisfactory in not explaining more fully why some umbers have suffered depletion and others not, but does make some progress towards accounting for the phenomenon.

5.2.8 Sub-umber bleaching of lavas

A common feature of umber deposits is the white bleached character of the lavas beneath them. This bleaching, which can be seen clearly in the photograph of the umber at Margi (Plate 5.3A), is generally fairly superficial affecting only the outer centimetre or of the lava. In lava fragments floating within the umber, this weathering is more extreme.

This surficial weathering must be distinguished from the more penetrative smectitic alteration which occurs along some faults in the upper lavas. This results in a greater degree of decomposition, and produces a soft greenish friable rock.

The white colour is imparted by a greater abundance of pale smectite, resulting from enhanced weathering. Apart from enrichment in potassium, rubidium and magnesium associated with the formation of the smectite, no major chemical changes have occurred.

Robertson (1975) proposed that this alteration might have resulted from hydrothermal activity related to the formation of the umber. However the uniformity of the phenomenon wherever umber is in contact with lava, and its absence from fault zones where hydrothermal alteration should be more extreme, argues against this. The field evidence instead points to an enhancement of alteration where lava is in contact with umber. Possibly, pore waters associated with the umber have catalysed the decomposition of the lava.

5.2.9 Sediment Inter-relationships

The generalised sequence of sediments beneath the Lefkara marls is basal umber, overlain by clay-rich umber, then by bentonitic clays, radiolarian mudstones, and/or radiolarites. However any or all of these sediment types may be absent. The inter-relationships of these sheds light upon their origin.

The umber, where present, is always the basal unit. It is thus closely related temporally to the lavas, an observation borne out by

the common occurrence of chemically related interpillow metalliferous sediments in the lavas beneath umber deposits. In many areas however, pure umber and interpillow oxide sediments are absent, and suitable hollows in the lava surface are filled by clay-rich umbers or non-metalliferous sediments. Thus umber sediment sources had limited range, being unable to produce a uniform distribution. The umbers are succeeded either sharply, or gradationally by the later sediments, but are not intercalated with them. Where gradations occur, these are over distances of a few tens of centimetres at most.

The clay-rich umber where it occurs, is either basal or on top of the pure umber, and thus also shows a spatial and hence temporal relationship with the lavas. The contact with the overlying non-metalliferous sediments is again not gradational, but may be intercalated as at Layia. There occurs a 10m thick deposit of rhythmically interbedded dark clay-rich umber and pink radiolarian clays.

That these inter-relationships are common throughout the Troodos massif, suggests that the upward change in composition is due to variation in the metalliferous component, rather than variation in supply rate of the clay. If the latter were true, regional variations in the clay content of the umber should be observed.

5.3 MINERALOGY OF THE UMBER

Mineralogical data for the umbers have been presented by Elderfield et al. (1972), Robertson and Hudson (1973), Constantinou and Govett (1972), Desprairies and Lapierre (1973) and Guillemot and Nesteroff (1980). Owing to the fine grained character of the sediment, the most useful tool is X-ray diffraction (XRD). In addition scanning electron microscope, electron microprobe, whole rock chemistry, and thermogravimetric studies have been employed. New data are presented from a detailed examination of the umber at Margi, supplemented by samples from other selected localities. The regional distribution of mineral phases are discussed using previously published data, and new data from a general survey.

5.3.1 Techniques

X-ray Diffraction. The XRD analysis of samples was undertaken at the Grant Institute of Geology. CuKα radiation (40kV 20ma) 1° divergence slit, 1° scatter slit. Phillips PW 1050 goniometer PW1965 proportional counter. Diffracted beam graphite monochromator. Standard scanning rate 1°2θ/minute, but slow scans used for accurate measurement. Sample preparation: back filled 11 x 20 mm aluminium sample holders.

Electron micro-probe analysis Analyses were carried out at the Grant Institute of Geology using a Cambridge Instruments microscan 5. Operating conditions: Gun potential 20KeV.

Probe current (measured using Faraday cage)

Crystal spectrometers : 30nA

Energy dispersive spectrometer : 6nA.

The energy dispersive analysis was performed using a Link Systems spectrometer. ZAF correction were performed using the method of Sweatman and Long (1969).

Scanning electron microscope. Analyses were carried out at the Department of Botany, Edinburgh University using a Cambridge Stereoscan 250.

Thermogravimetry Analyses were performed at the Department of Chemistry, Edinburgh University, using a Stanton Redcroft TG-770 thermogravimetric balance. Samples were heated in air at a rate of $8^1/2$°/minute up to 850°C.

Mn^{4+} determination. Analyses were performed at the Grant Institute of Geology, using the available oxygen method of Wilson (1964). In principal the sample is digested and reacted with vanadyl sulphate. The Mn^{4+} can be calculated from the amount of vanadate formed, which is determined titrametrically using standardised ferrous ammonium sulphate. The method assumes that no Fe^{2+} occurs in the sample, which in the absence of stable mafic minerals is justifiable.

5.3.2 Mineral characteristics

Goethite. All samples of pure umber contain goethite in sufficient abundance to be detected in whole rock samples using XRD. The diffraction peaks are broad owing to the fineness of grain size (half height width of the (110) peak is 0.8 ± 0.1°2θ using CuKα radiation). Peak broadening due to fine grain size causes displacement of the peak positions (Shulze, 1984). After correction for this effect the 110, 130 and 111 peaks are observed to be 4.19, 2.69 and 2.450Å respectively. These are sufficiently close to pure goethite to preclude significant substitution of Al or Mn for Fe. Reference is made by Robertson and Hudson (1973) and Guillemot and Nesteroff (1980) to the amorphous character of the X-ray diffraction patterns. A thermogravimetric analysis was used to determine the abundance of FeOOH, by the dehydration reaction $2FeOOH \rightarrow Fe_2O_3 + H_2O$. A dehydration step attributable to FeOOH begins at ca 200°C. Coarsely crystalline goethites achieve a dehydration maximum at 385-405°C (Mackensie, 1957), but this temperature decreases with grain size. Synthetic goethites achieve a maximum dehydration rate at 293°C, very close to that observed in the umber. The size of the step indicates that all non-aluminosilicate iron is FeOOH. That the step is smooth, suggests that this is a single phase, argu ing against the existence of any amorphous FeOOH. The single smooth step, and the size of the step indicates that it accounts for all the non-alumino-silicate iron.

Sample	%Wt loss	Calculated FeOOH Wt%	XRF total Fe FeOOH
81 144	3.90	38.4	46.23
81 142	4.85	47.8	51.69
81 151	4.75	46.8	50.54

The clay-rich umber does not contain sufficient goethite to show XRD peaks for this mineral. However, the thermogravimetric trace for 81-135 shows a step of 0.4 wt% at 300°C, corresponding to an FeOOH content of 4.4 wt%. This value is extremely approximate, because of the low sensitivity of the method. With such low values, and the broadness of the diffraction peaks, failure to detect

goethite in the clay-rich umber is expected.

Manganese minerals. The most commonly identifiable manganese mineral is pyrolusite, which occurs in veins and as concretions. Elderfield et al., (1972) describe in two of their seven samples a mineral with an X-ray diffraction pattern (10.80, 4.84, 2.65, 1.41Å) which they interpret as a mixture of 10Å-manganite and δ-MnO_2. In this study no crystalline manganese phases were identified in the umber, though 10Å manganite and another crystalline manganese mineral were found in veins (described below).

The abundance of manganese in both the pure- and clay-rich-umber requires that some manganese phase is present. Further, Varnavas (1980) found that 73% of the manganese is concentrated in the hydroxylamine - soluble fractions, along with 74% of the cobalt, 75% of the lead and 77% of the barium. Poorly crystalline δ-MnO_2 yields broad X-ray diffraction peaks at 2.40 and 1.40Å. In these positions, they will tend to be masked by goethite. δ-MnO_2 is commonly selectively enriched in Co and Pb because of its high specific surface area, which further argues in favour of this being the predominant manganese mineral in the umber. Enrichment of Na and Ca with the manganese, indicated by the micro-probe study (section 5.4.4) is also in keeping with this conclusion. The Mn^4 /total Mn ratio for the samples of umber from Margi is 0.907, which is compatible with published data for δ-MnO_2 (Burns and Burns, 1979). A thermogravimetric analysis of umber samples failed to identify any thermal decomposition reactions for manganese phases. However there are no data available concerning the decomposition of the poorly crystalline δ-MnO_2. Manganites on the otherhand have characteristic thermogravimetric curves (MacKensie, 1957)

The same problems are true of the clay-rich umber. The Mn^{4+}/-total Mn ratio for one sample from Margi is 0.840, which is distinctly different from that of the umbers. A less completely oxidised manganese phase is indicated.

TABLE 5.1

X-ray diffraction data for manganese oxides from Margi

81 58 vein passing through uppermost lavas
81 158m vein in umber

	81 58		81 158mn	
dÅ	I/Io		dÅ	I/Io
9.52	86		6.95	25
6.97	8		4.92	17
4.73	100		3.11	100
2.43	17		2.40	21
2.41	34		2.15	24
2.34	20		1.83	10
2.23	3		1.54	14
1.978	3		1.425	5
1.623	1			
1.419	2			

Chemical compositions of manganese oxide samples.

a) 81 - 58 Comprises todorokite, calcite and barite.
b) 81 - 158mn Comprises Mn oxide and palygorskite.
c) 81 - 111m Bentonitic clay containing todorokite
d) 81 - 88 Pyrolusite nodule from the Margi umber

	a)	b)	c)	d)
Mn^{4+}	30.96	11.61)	15.52	50.17
Mn^{2+}	4.14	1.19)		-
Si	3.56	21.32	19.29	6.66
Al	2.70	4.03	4.93	1.27
Fe	0.53	2.34	3.00	1.03
Mg	3.63	5.39	2.34	0.57
Ca	5.22	0.16	1.22	0.56
Na	0.65	0.18	1.39	0.24
K	0.56	0.93	1.31	0.37
Ti	0.04	0.02	0.30	0.09
P	-	0.62	0.19	0.05
Ba	8577	2960	10055	19539
Co	1082	103	334	111
Cu	940	56	709	492
Ni	1361	58	367	210
Pb	-	129	507	-
Sr	1739	3324	1820	3718
V	801	195	1286	1012
Y	17	-	33	24
Zn	104	31	121	85
Zr	13	53	69	22

- = Not detected

Passing through the lavas, and occuring in the umber, are veins and concretions of manganese minerals. The subspherical or irregular flattened sheets (see section 5.2.2.1) are composed of pyrolusite. These overgrow the sediment (for example in the interlava umber, Plate 4.3F) and are clearly of secondary origin. The composition of one of these is presented in Table 5.1. Veins in the lavas and umber are composed of less crystalline manganese phases, and may be unaltered.

In the lavas manganese oxides occur as veins, and as cements in sedimentary breccias. Much of this material is pyrolusite, but locally, less well crystalline phases are observed. The X-ray diffraction pattern of sample 81-58, collected from the lavas at Margi, 5m below the sediment cover, is presented in Table 5.1. The pattern is very close to that of todorokite, differing only in the absence of a ca. 4.5Å reflection. The chemical composition is similar to published data for todorokites (Burns and Burns, 1979), except for Ca which is high due to the presence of carbonate.

The manganese mineral occurring as veins in the umber also gives a strong XRD pattern (sample 81-158mn, Table 5.1). However the pattern does not resemble any of the common manganese phases observed in deep-sea manganese deposits. Instead it is identical to a mineral described by Mikheev (1957) termed vernadite. It is unfortunate that this should be the name commonly adopted for the δ-MnO_2 found in the oceans, but from which it is quite distinct. Its chemical composition reflects an intimate intergrowth with palygorskite which also occurs in the veins, accounting for the high Si, Al, Fe and Mg content.

Quartz. Quartz is commonly present in the umber. This is not visible in thin section or using SEM, except where veins related to cherts are present. Radiolarian remains are replaced by goethite. At Margi, quartz is in far greater abundance than can be explained by the presence of radiolaria. In an attempt to determine the abundance of quartz, a standard addition analysis was performed on one sample using powdered vein quartz as a standard. Samples were packed in

powder cases. Four subsamples were run. One with no added quartz, and the remainder with 1, 2 and 4% of quartz added respectively. Intensity was determined by measuring peak area. A very good linear solution yielded a result of 2.55 + 0.40% quartz.

In the clay-rich umber quartz is far more abundant. A similar standard addition method for a sample from Margi gave a quartz concentration of 11.2 + 1.1%. Again, quartz is not visible in thin section or using SEM.

Apatite. Apatite is commonly sufficiently abundant to be detectable in whole rock powders using XRD. A small proportion of it is present as discrete fragments of phosphatised arthropod cuticle (Plate 5.1E); electron microprobe analyses of this material are discussed below. Locally phosphatic concretions 2-8cm across are observed in the umber. A sample of a phosphatic concretion obtained from the Mangalene umber pit, near Parekklisha, has been analysed chemically by XRF. In the pure umber apatite is also concentrated in pale coloured beds. In thin section these contain irregular angular fragments which are composed of small crystals of a colourless low-birefringent material. The origin of these fragments is uncertain, but their shapes are suggestive of lava fragments, and some sort of diagenetic replacement by phosphate is a possibility.

Both the pure umber and clay-rich umber are enriched in phosphorus (At Margi, pure umber: 0.84 wt%P., clay-rich umber 0.31 wt%P.). A highly significant correlation of Ca with P suggests that this is all apatite (Fig. 5.11B). The slope of the regression line indicates that the apatite is phosphorus-poor with respect to stoichiometric hydroxy- or fluorapatite. Electron micro-probe analysis of the phosphatised cuticle and XRF analysis of the phosphatic concretion sample also give high Ca/P ratios (Table 5.2). The electron micro-probe analyses give very poor totals even when F, CO_2 and OH are taken into account, a phenomenon resulting from the poor polish obtainable upon this soft material, and its fine fibrous character. If the assumption is made that the only important cations are Ca, Mg and Na, the structural formulae show a deficiency

TABLE 5.2

APATITE CHEMICAL AND MINERALOGICAL COMPOSITION

WDS Electron micro-probe determinations of phosphatic cuticle. Samples from Margi.

	115 P1	115 P3	115 P4	115 P5	110 P2	110 P9	160 P1	160 P2
SiO_2	0.68	0.08	0.09	0.30	0.64	1.57	*	0.35
Al_2O_3	0.14	0.02	0.01	0.08	*	0.09	*	*
FeO**	0.12	0.01	0.07	0.14	0.12	0.25	0.44	1.02
MgO	0.21	0.17	0.18	0.23	0.21	0.24	0.16	0.28
CaO	40.84	42.10	41.40	43.43	43.18	45.79	40.57	40.15
Na_2O	*	*	*	*	*	0.14	1.29	0.60
K_2O	0.06	0.02	0.03	0.07	0.03	0.08	*	*
TiO_2	0.02	0.02	0.01	*	0.01	0.03	*	*
MnO	0.06	0.01	0.03	0.13	*	*	*	*
P_2O_5	29.03	29.39	29.11	29.47	28.79	31.48	27.78	25.85
Total	71.16	71.80	70.94	73.86	72.98	79.67	70.23	68.25

Number of ions on the basis of Ca + Na + Mg = 10

P	5.59	5.48	5.52	5.34	5.24	5.39	5.10	4.90
Mg	0.07	0.06	0.06	0.07	0.07	0.07	0.05	0.09
Ca	9.93	9.94	9.94	9.93	9.93	9.93	9.41	9.65
Na	*	*	*	*	*	*	0.54	0.26

XRF whole rock analysis of phosphatic concretion From Mangalene 80-6

			(ppm)
	6.22	Cr	93
	1.06	Cu	93
	4.72	Ni	42
	0.60	Sr	848
	41.28	Zn	165
	1.01	V	97
	0.08	La	1232
	0.03	Ce	237
	3.07	Nd	927
	30.77	Y	898
CO_2	2.75		
	88.84		

	5.54	
C	0.79	6.33
	0.19	
	9.40	10
	0.41	

X-ray diffraction data for phosphatic concretion (80-6)

d Å	I/Io	HKL	d Å	I/Io	HKL
4.07	4	200	2.144	11	311
3.88	4	111	2.060	4	113
3.441	27	002	2.04	3	400
3.169	6	102	1.998	3	203
3.074	14	210	1.940	26	222
2.807	100	211	1.887	12	312
2.778	55	112	1.838	29	213
2.712	61	300	1.802	14	321
2.626	19	202	1.7759	12	410
2.523	4	301	1.7507	10	402
2.286	7	212	1.7204	14	004
2.257	24	310			

Lattice parameters

a (Å) = 9.393
c (Å) = 6.881
c/a = 0.733

Based upon the empirically derived equations:-

$a(Å) = 9.4436 - 0.03362 \times F - 0.0899 \times CO_3 + 0.0238 [F \times CO_3]$

$c(Å) = 6.8755 + 0.0074 \times F$

F = 0.743
C = 0.313

* Not detected
** Total iron expressed as FeO

of P. (Table 5.2). Qualitative EDS electron micro-probe studies, and whole rock XRF analysis of the phosphate concretion indicate the Sr Y and REE's are important, possible comprising 1 wt% of the rock. If these are included in the structural formulae, the phosphorus deficiency becomes greater. In the phosphatic concretion the CO_2 content of the rock can account for the deficit, through substitution of carbonate for phosphate, suggesting that the apatite is a francolite. A problem arises however, from the XRD analysis of the phosphatic concretion. The d spacings, presented in Table 5.2 are intermediate between hydroxyapatite and fluorapatite but quite distinct from carbonate fluorapatite (francolite) (data from Brindley and Brown,). Using an empirically derived equation relating lattice parameters to composition (McClellen et al., 1969), the abundance of both F and CO_2 can be calculated (see Table 5.2). Both values are low for francolite, and the CO_2 estimate is only 1/3 of that measured chemically. Significantly, if the Ca content is recalculated assuming that the CO_2 is present in calcite, the new structural formulas contain sufficient phosphorus for the apatite to be a stoichiometric hydroxy- or fluorapatite. On the basis of a thermodynamic analysis of francolites, it has been deduced that CO_2-rich varieties are metastable with respect to CO_2-poor (Chien and Black, 1976). Various geological processes, such as diagenesis, weathering or metamorphism can effect a systematic alteration of francolite to fluorapatite (McClellan, 1980). Further, it has been proposed that OH may substitute for F during diagenesis (Price and Calvert, 1978; Burnett, 1977). Thus it seems that the apatite observed in the supralava sediments is a partially degraded francolite, in which the OH/F ratio is unusually high. It is interesting that the Ca/P ratio is constant and high, even though the XRD data indicate that some of the Ca must now be present as carbonate. Some kind of exsolution process may be implied

A defocused beam electron micro-probe study of sample 160 (pure umber) shows that except where phosphatic cuticle occurs, the phosphate is evenly enriched through the sediment. A mechanism of adsorption of phosphate upon amorphous iron oxide has been proposed

by Berner (1973) to account for the high abundance of phosphorus in the East Pacific Rise metalliferous sediments, and the correlation of P with Fe. In the electron micro-probe traverse of the clay-rich umber (Fig 5.9) a weak correspondence of P with Fe is observed. Possibly a similar mechanism can account for the phosphate enrichment, which has subsequently been diagenetically modified to apatite.

Trace element enrichments in the phosphatic concretion are high. Notably Sr-848 ppm, La-1232 ppm, Nd-927 ppm, Y-898 ppm. No quantitative probe determinations of these elements were obtained but on EDS scans La and Nd were detectable. The whole rock chemistry (section 5.4.7.3) further illustrates the strong association of La, Nd, Y and Sr with the phosphate. This trace element enrichment is far greater than is observed in normal marine phosphates (Manheim and Gulbrandsen, 1979). However deep-sea apatites may contain 1 or more per cent of Rare earth elements (Arrhenius et al., 1957; Arrhenius and Bonatti, 1965), adsorbed from sea water during early diagenesis.

Smectite. In the pure umber two varieties of smectite are observed; montmorillonite and a trioctahedral form, probably saponite. No nontronite has been identified, in contrast to many modern metalliferous sediments.

Montmorillonite is the most abundant smectite, commonly being the only type present. In the clay-rich umber only montmorillonite is found. It is characterised in the XRD trace in having a (06) peak at 1.504Å. Care must be taken if palygorskite is abundant as this has a significant peak at 1.508Å, but the trioctahedral clay is distinct with an 06 peak at 1.522Å. Desprairies and Lapierre (1973) extracted smectites from the umber and the Kannaviou Formation, for chemical analysis. Structural formulae are given in Table 5.3. One sample yielded a ferromagnesian saponite.

The trioctahedral clay is a saponite and occurs only locally, in the basal parts of umber deposits. Compositionally it falls very close to the trend defined by the lava alteration saponites.

		SiO_2	Al_2O_3	Fe_2O_3		Mn_3O_4	MgO	CaO	Na_2O	K_2O	TiO_2	% PF	CO_2	H_2O^+ 200-1 050	H_2O^- 40-200	Total %
				structural	libre											
Analyses Chimiques	O 1	20,08	2,97	18,14	33,41	1,25	3,83	2,33	0,17	–	0,16	16,44	1,26	9,26	5,92	98,78
	5923	51,28	9,94	9,09	3,88	6,38	5,34	1,69	0.41	1,66	0,38	11,25	0,15	5,82	5,28	101,30
	5925 a	52,66	15,82	8,02	3,09	0,67	3,66	0,38	0,50	2,89	0,79	12,33	0,68	5,62	6,03	100,81
	5925 b	52,68	10,98	9,61	3,08	4,57	4,84	1,45	0,77	1,93	0,44	10,99	0,03	6,05	4,91	101,34
	5922	50,33	14,35	7,99	3,63	1,00	3,92	0,35	0,28	1,82	0,80	16,80	3,63	3,87	9,30	101,27
Formules Structurales	O 1	$(Si_{3.04}\ Al_{0.54}\ Fe^{+3}_{0.42})(Fe^{+3}_{1.64}\ Mg_{0.54})\ Mg_{0.32}\ Na_{0.04}\ Ca_{0.11}\ O_{10}\ (OH)_2$														
	5923	$(Si_{3.97}\ Al_{0.03})(Al_{0.89}\ Fe^{+3}_{0.53}\ Mg_{0.62})\ Ca_{0.13}\ Na_{0.66}\ K_{0.17}\ O_{10}\ (OH)_2$														
	5925 a	$(Si_{3.87}\ Al_{0.13})(Al_{1.24}\ Fe^{+3}_{0.44}\ Mg_{0.36})\ Na_{0.08}\ K_{0.27}\ O_{10}\ (OH)_2$														
	5925 bb	$(Si_{3.96}\ Al_{0.04})(Al_{0.92}\ Fe^{+3}_{0.54}\ Mg_{0.54})\ Ca_{0.12}\ Na_{0.12}\ K_{0.18}\ O_{10}\ (OH)_2$														
	5922	$(Si_{3.88}\ Al_{0.12})(Al_{1.20}\ Fe^{+3}_{0.46}\ Mg_{0.45})\ Na_{0.04}\ K_{0.16}\ O_{10}\ (OH)_2$														
Pourcentage des principaux oxydes	O1	43	6	39			8									
	5923 25 a et b 5922	64-65	13-19	10-12			4-7									

TABLE 5.3

Analyses and structural formulae of smectites extracted from the umber and overlying clay-rich umber. O1 is from the region of Konni, near the Nata-Anarita road, and the remainder are from Kinousa. The data are from Desprairies and Lapierre(1973)

Derivation from the weathering volcanic basement seems highly likely.

Quantitative determination of the goethite in the umber using thermogravimetry, and the general absence of a 1.52Å 06 reflection indicates that none of the iron in the umber occurs as nontronite. Nontronite is found in various low-temperature hydrothermal deposits (Hoffert et al., 1978; Corliss et al., 1978; Cann et al., 1977), at the hydrothermal sulphide chimneys (Hekinian et al., 1980), and in the Bauer Deep (Sayles and Bischoff, 1973). In the latter it is believed to have formed by diagenetic reaction of iron oxide with biogenic silica (Heath and Dymond, 1977). At the EPR crest, nontronite is absent (Dymond et al., 1973).

Illite. In agreement with the findings of Desprairies and Lapierre (1973), the sheet silicate component of the pure umber and clay-rich umber contains 15-20% dioctahedral illite (06 = 1.503Å). This proportion is the same as is observed in the sandstones and mudstones of the Kannaviou Formation (op. cit.).

Kaolinite. Kaolinite does not occur in sufficient abundance to be detected using XRD, even on size separated fractions. However plates of well crystallised kaolinite are occasionally observed using SEM (Plate 5.2D).

Clinoptilolite. Clinoptilolite - a silica rich heulandite - is common in the bentonitic clays, but has been found only in one umber locality (the Mangalene umber pit, Parekklisha) where it occurs most abundantly in the ochre coloured silty beds. Identification is by XRD, the mineral not being large enough to be visible in thin section or using SEM. The origin of the clinoptilolite, probably formed during diagenesis, is discussed in Chapter 6, section 6.5.6.

Feldspar. In both the pure umber and clay-rich umber occur crystals of feldspar, generally less than 50μm across. These show up clearly as blue luminescent grains using a luminoscope. Rarely feldspar crystals may be up to 2 mm across (Plate 5.2A). Locally these may be

sufficiently abundant to be detectable in whole rock samples using XRD, as at Margi. Electron micro-probe analysis of the large feldspar clast in sample 81 133 (Plate 5.2A) shows it to be a calcic andesine. Intermediate composition plagioclases have been introduced with the bentonitic material.

Palygorskite. Palygorskite occurs in two forms in both the pure- and clay-rich umber; either as veins or as discrete fibres homogeneously dispersed through the sediment.

The veins, which appear micaceous in hand specimen, are composed of densely packed fibres (Plate 5.7C). An electron micro-probe analysis of this material is presented in Table 5.4. The totals are high for palygorskite owing to rapid volatilisation of the sample under the beam.

Palygorskite is ubiquitous in all the supralava sediments in the form of small fibres 1-20μm in length (Plate 5.7A,B). A centrifuge separate of nominal size less than 0.5μm comprises entirely palygorskite in all sediment samples from Margi. The sparse fibres are too small for electron microprobe analysis. At Skouriotissa, some beds are particularly enriched in palygorskite (Robertson, 1976a).

Concerning the origin of palygorskite there is much debate. Most occurrences in deep-sea sediments are in Tertiary and Mesozoic material (Hathaway et al., 1970; von Rad and Rösch, 1972; Weaver and Beck, 1977; Couture, 1977; Church and Velde, 1979). Weaver and Beck (1977) argue in favour of formation in coastal lagoons suggesting that deep-sea occurrences are all of detrital origin. Couture (1977) and Church and Velde (1979) argue in favour of an authigenic origin through alteration of smectites, phillipsite or volcanic glass, in the presence of high silica and magnesium activities. Silica could be supplied either by diagenetic breakdown of silica-rich volcanic material or from dissolution of opaline organisms. The oxygen isotope composition of the palygorskite from the Pacific sediments

TABLE 5.4

Palygorskite chemical composition

Electron micro-probe analysis (using crystal spectrometres) of vein palygorskite from sample 81-160 (Margi).

	160-3	160-4
SiO_2	63.31	59.73
Al_2O_3	7.94	7.84
Fe_2O_3	8.89	8.86
MgO	10.64	9.96
CaO	0.19	0.20
Na_2O	0.23	0.24
K_2O	0.20	0.18
TiO_2	0.03	0.01
MnO	0.11	0.11
Total	91.61	87.13

suggests an elevated temperature (not greater than 50°C) (Church and Velde, 1979).

In Cyprus, it is clear that the vein palygorskite formed in situ. Veins of palygorskite are common also in the lavas, and were probably precipitated from low-temperature hydrothermal fluids. The ubiquitous fibres in the supralava sediments are probably of authigenic origin. The terrigenous component in these sediments is silica-rich bentonitic material (section 5.5.6) providing a ready source for silica. Whether or not elevated temperatures were required is not possible to determine. The palygorskite-rich beds at Skouriotissa, may have formed through alteration of volcanic detritus.

5.3.3 Lateral variation of mineral abundance

Some minerals are common to all umber deposits, but others occur more rarely or even uniquely.

Pure umber

Ubiquitous Minerals. Goethite is present in all pure umber samples analysed. Manganese phases are absent only from basal leached umber and the Skouriotissa basal umber. In the latter case this may be a primary absence (Robertson, 1976a). Palygorskite, apatite, montmorillonite and quartz occur in all the samples investigated during this study, but are not reported in all samples by previous workers (Elderfield et al., 1972; Robertson and Hudson, 1973; Guillemot and Nesteroff, 1980). Montmorillonite, illite, palygorskite and quartz, are reported ubiquitously by Desprairies and Lapierre (1973) but apatite is not. A re-investigation of some of this material (Dhrapia) shows that these minerals do occur but in small amounts. Apatite in particular is seldom in sufficient abundance to be detected using XRD, but its presence is indicated by the constant Ca/P ratio (section 5.4.6). It is thus considered that montmorillonite, illite, quartz, palygorskite and apatite do occur ubiquitously.

Non-ubiquitous minerals

The most important mineral which occurs only locally is saponite. The bulk of the aluminosilicate material in the umber is identical to that of the Kannaviou Formation, but locally erosion products from the volcanic basement, mostly in the form of saponite, occur in the supralava umber. This is in contrast to the interlava sediments where the reverse is true (Chapter 4, section 4.3.1).

Clinoptilolite has been detected only in one umber deposit, the Mangalene umber pit near Parekklisha. This mineral is abundant in the basal non-metalliferous clays, where it probably formed diagenetically from acid or intermediate volcanic material, or smectites.(Chapter 6, section 6.5.6). Its absence from most of the umber, which contains the same volcanic detritus as the Kannaviou Formation, requires explanation. The presence of palygorskite indicates that activities of both silica and magnesium were high. High magnesium activity does not favour the formation of clinoptilolite (Hay, 1977).

Clay-rich umber. Data on the mineralogy of the clay-rich umber are scarcer. Neither iron nor manganese phases are identifiable using XRD, but the presence of a manganese mineral is required from the abundance of the element, and the presence of goethite is proven using thermogravimetry. The analysed samples contain an aluminosilicate assemblage identical to that of the overlying Kannaviou Formation: predominantly montmorillonite, quartz and illite. Clinoptilolite has not been observed in any of the samples. At Margi the transition between the clay-rich umber and the overlying bentonitic clay occurs over less than one millimetre. Immediately above the contact clinoptilolite becomes abundant. The appearance of silica-rich clinoptilolite in the bentonite is complemented by a decrease in the abundance of quartz, thus preserving the Si/Al ratio. The significance of this is discussed in Chapter 6, Section 6.5.6.

5.4 GEOCHEMISTRY OF THE SUPRALAVA METALLIFEROUS SEDIMENTS

The following account falls into three parts. First, the mean composition of the sediments, and the spatial variation in composition are described. Secondly, the chemical composition of components within the sediments is described. Thirdly, the sources of the components and the manner of their accumulation and diagenesis are discussed. The discussion includes a comparison with modern analogues.

Chemical analysis. The methods are described in the appendix.

5.4.1 Bulk composition of the sediments

In Table 5.5 are presented the mean chemical compositions of the pure umber, clay-rich umber, and bentonitic clay (radiolarian-free). The values are the means of the mean compositions from the different localities.

Both the pure-and clay-rich-umber are enriched in Fe, Mn, P, Ba, Co, Cu, La, Nd, Ni, Pb, Sr, V, Y, Zn and Zr with respect to the bentonitic clay. Si, Al, Ca, Na, Ti and Cr are all greater in the bentonite. The clay-rich umber generally falls intermediate between the bentonite and the umber in terms of absolute abundances. Some elements are different, such as K, Mg and Ce being greatest in the clay-rich umber.

However, the clay-rich umber cannot be regarded as simply a mixture of umber and bentonite. The Fe/Mn ratio of the umber is 0.23, but in the clay-rich umber is 0.34. As approximately half the Fe in the clay-rich umber is contained in the bentonitic component, the Mn/Fe ratio of the metalliferous component is greater still. The absolute trace metal enrichments in the clay rich umber are lower than those in the pure umber, but represent a much greater relative enrichment owing to the lower abundance of Fe and Mn.

TABLE 5.5

Mean chemical composition of the metalliferous sediments.

	Mean supra-lava umber	Mean clay-rich umber	Mean bentonitic clay	Divided by mean bentonitic clay	
				Pure clay-rich	
Si	9.03	24.89	28.47	0.32	0.87
Al	2.15	6.33	6.85	0.31	0.92
Fe	30.89	8.82	5.15	6.00	1.71
Mg	1.02	2.24	2.16	0.47	1.04
Ca	1.76	1.25	1.84	0.96	0.67
Na	0.30	0.69	1.27	0.24	0.54
K	0.63	2.19	1.54	0.41	1.42
Ti	0.11	0.33	0.36	0.30	0.92
Mn	7.03	3.01	0.24	29.29	12.54
P	0.60	0.22	0.17	3.53	1.29
Ba	1071	502	140	7.65	3.59
Ce	31	122	68	0.46	1.79
Co	125	78	27	4.63	2.89
Cr	42	39	110	0.38	0.35
Cu	846	299	144	5.88	2.08
La	138	102	47	2.94	2.17
Nd	91	92	44	2.07	2.09
Ni	254	139	98	2.59	1.42
Pb	265	156	19	13.95	8.22
Rb	22	91	69	0.32	1.32
Sr	1044	268	302	3.46	0.89
V	1106	205	88	12.57	2.35
Y	92	92	55	1.05	1.05
Zn	361	278	231	4.10	3.16
Zr	183	98	75	2.44	1.31
$Mn/_{Fe}$	0.23	0.34	0.047		

5.4.2 Inter-deposit variation

Pure Umber. The compositions of umber from 9 localities are shown in Table 5.6. The localities are indicated on the map (Fig. 5.3). Variations are due to differing abundances of aluminosilicate elements (Al, Si, Mg, Na, K, Ti), iron, manganese and trace element abundances.

The principal major element variation can be illustrated using an Al-Fe-Mn triangular diagram (Fig. 5.5). All the umbers plot in the Fe rich corner of the triangle. The supralava umbers contain very little Al and fall in elongate fields sub-parallel to the Fe-Mn axis, showing that change in the relative abundance of Fe and Mn is the most important variation. The umber from Analiondas and Margi shows increasing Al with increasing Mn, a phenomenon which is discussed more fully below. Of the localities sampled, Dhrapia is the most depleted in Al, and Margi, the most enriched. Dhrapia is also the deposit with the least Mn. Skouriotissa shows the greatest variation in Mn/Fe, owing to the high Mn content in the upper parts, and Mn depletion in the base (Robertson, 1976a). The interlava umbers show a wide range of compositions. The higher Al contents are due to admixing with locally derived epiclastic debris.

The trace elements show considerable variation, but may be divided into three classes according to the manner of their variation. Firstly, Rb and Cr vary with the aluminosilicate minerals (section 5.4.7.3.). Secondly, Zn, Cu, Co, Ni and V show relatively small total variation and broadly covary. Thirdly Pb, Sr and Ba show large total variation, particularly depletion in some of the deposits. The trace elements are all presented plotted against Zn in Fig. 5.4. In general the Dhrapia deposit and the interlava umbers contain the lowest abundance of trace elements, depletion in Ba, Sr and Pb being most marked. The Margi umber, here subdivided into a lower and upper part, shows the greatest enrichment in most elements. The abundance of copper deviates from the general trend, being exceptionally enriched in the Skouriotissa deposit (which has only intermediate abundances of the other trace elements), and locally enriched in the interlava umbers.

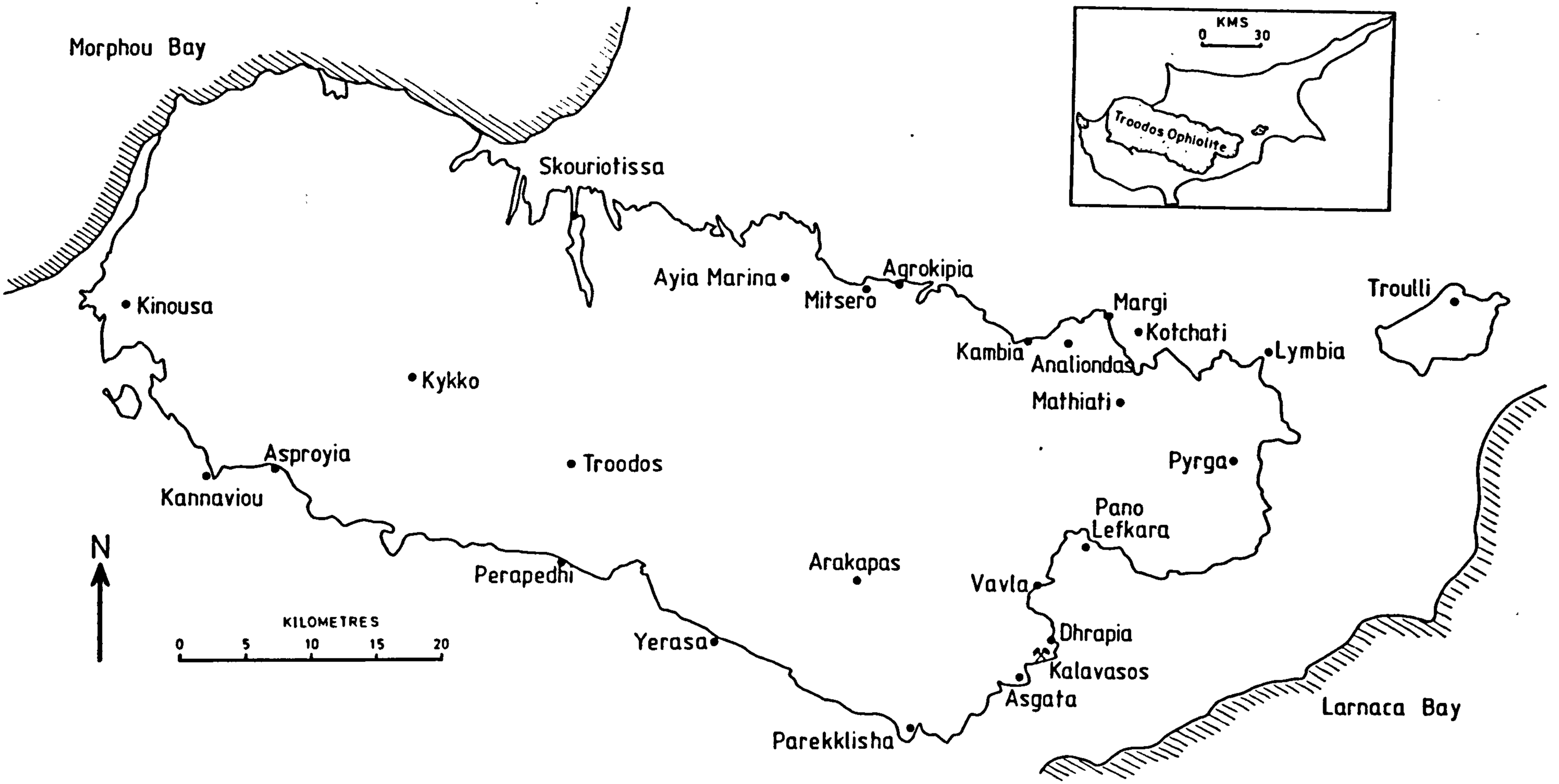

Fig. 5.3 Troodos ophiolite complex. Localities referred to in the text.

TABLE 5.6

MEAN CHEMICAL COMPOSITION OF THE SUPRALAVA UMBERS.

Locality	Skouriotissa		Kambia (east)	Margi upper	Margi lower	Mathiati 1km W. of mine		Analiondas	Dhrapia	Mangelene	Mean/ mean
Source	R Pale N=2	R Dark N=5	B N=1	B N=17	B N=13	B 82-37	B 82-38	V N=13	R N=9	B N=3	
Si	7.95 ± 1.32	6.08 ± 1.53	10.92	9.84 ± 1.10	7.93 ± 1.27	5.81	8.19		5.79 ± 1.06	17.20 ± 2.80	9.03
Al	2.25 ± 0.26	1.62 ± 0.39	3.05	2.83 ± 0.27	1.91 ± 0.36	1.12	2.74	1.47 ± 0.16	1.15 ± 0.15	3.29 ± 0.76	2.15
Fe	39.87 ± 5.94	25.08 ± 6.91	24.43	29.96 ± 2.64	33.54 ± 3.33	36.18	28.06	37.14 ± 2.58	33.20 ± 5.32	26.74 ± 3.76	30.89
Mg	0.60 ± 0.08	0.39 ± 0.18	1.30	1.29 ± 0.11	1.31 ± 0.28	0.97	1.07	1.11 ± 0.15	0.51 ± 0.19	1.16 ± 0.09	1.02
Ca	0.32 ± 0.16	5.65 ± 8.19	1.03	1.23 ± 0.19	2.49 ± 2.51	1.18	1.04	0.66 ± 0.22	2.51 ± 3.41	1.40 ± 0.39	1.76
Na			0.32	0.38 ± 0.24	0.14 ± 0.04	0.28	0.26			0.39 ± 0.15	0.30
K	0.65 ± 0.11	0.59 ± 0.18	0.85	0.95 ± 0.16	0.51 ± 0.12	0.23	0.89		0.30 ± 0.13	0.66 ± 0.09	0.63
Ti	0.13 ± 0.00	0.11 ± 0.03	0.14	0.14 ± 0.01	0.09 ± 0.02	0.05	0.13		0.09 ± 0.03	0.11 ± 0.00	0.11
Mn	0.95 ± 0.95	8.29 ± 4.66	9.43	7.22 ± 0.87	5.55 ± 0.50	7.39	11.64	8.57 ± 0.72	5.57 ± 4.34	1.48 ± 1.06	7.03
P	0.31 ± 0.06	1.78 ± 2.45	0.34	0.34 ± 0.07	0.84 ± 0.91	0.22	0.22		1.20 ± 1.35	0.23 ± 0.08	0.60
Ba	33 ± 17	1064 ± 198	334	1382 ± 325	1001 ± 115	3330	708	1905 ± 244(N=5)	121 ± 229	48 ± 4	1071
Ce			36	44 ± 8	27 ± 9	*	43				31
Co	120 ± 13	109 ± 20		95 ± 3(N=5)	158 ± 25(N=6)		100	189 ± 21	96 ± 23		125
Cr	35 ± 38	11 ± 3	19	14 ± 3	3 ± 6	55	40		41 ± 17	148 ± 62	42
Cu	2150 ± 493	1215 ± 127	748	832 ± 49	721 ± 88	919	801	826 ± 127	774 ± 331	542 ± 298	846
La			153	160 ± 16	156 ± 56	118	169			71 ± 38	138
Mo	79 ± 44	124 ± 62							34 ± 16		
Nd			101	107 ± 10	108 ± 37	62	108			60 ± 24	91
Ni	204 ± 187	312 ± 65	285	399 ± 58	231 ± 23	281	215	291 ± 56	133 ± 19	170 ± 25	254
Pb	165 ± 21	203 ± 38	476	524 ± 49	382 ± 85	123	205	166 ± 33	94 ± 19	218 ± 77	265
Rb			31	28 ± 4	15 ± 4	*	32			22 ± 1	22
Sr	55 ± 1	1152 ± 167	108	1702 ± 119	1572 ± 157	3407	201		236 ± 161	250 ± 139	1044
V	1193 ± 434	568 ± 154	664	1201 ± 60	1527 ± 230	2078	643		1091 ± 419	918 ± 70	1106
Y			109	110 ± 15	106 ± 39	56	97			72 ± 18	92
Zn	474 ± 9	330 ± 84	346	483 ± 40	381 ± 71	377	356	342 ± 81	279 ± 60	319 ± 35	361
Zr	776 ± 461	499 ± 199	103	106 ± 10	90 ± 18	79	108		331 ± 75	74 ± 13	183

* Not detected.

TABLE 5.7

Average compositions of the clay-rich umber

	N=4 Skouriotissa	N=17 Margi	N=2 Kalavasos	N=23 Mean mean	Mean bentonite
Si	23.26 ± 0.39	24.75 ± 0.81	26.65 ± 0.93	24.89	28.47
Al	6.43 ± 0.13	6.59 ± 0.25	6.06 ± 0.50	6.33	6.85
Fe	10.89 ± 0.82	8.43 ± 0.70	7.13 ± 0.42	8.82	5.18
Mg	2.02 ± 0.24	2.28 ± 0.11	2.41 ± 0.54	2.24	2.16
Ca	1.32 ± 0.11	1.26 ± 0.24	1.18 ± 0.18	1.25	1.84
Na	- -	0.69 ± 0.06	- -	0.69	1.27
K	1.99 ± 0.06	2.70 ± 0.17	1.87 ± 0.12	2.19	0.54
Ti	0.35 ± 0.02	0.32 ± 0.02	0.32 ± 0.01	0.33	0.36
Mn	3.54 ± 0.50	2.90 ± 0.47	2.59 ± 0.89	3.01	0.24
P	0.18 ± 0.03	0.31 ± 0.09	0.18 ± 0.00	0.22	0.17
Ba	266 ± 32	1117 ± 256	123 ± 43	502	140
Ce	-	122 ± 12	-	122	68
Co	62 ± 7	110(N=1)	63 ± 2	78	27
Cr	34 ± 5	54 ± 8	30 ± 2	39	110
Cu	367 ± 60	261 ± 58	270 ± 72	299	144
La	-	102 ± 23	-	102	47
Mo	13 ± 3	-	-	13	-
Nd	- -	92 ± 19	-	92	44
Ni	119 ± 20	181 ± 30	118 ± 22	139	98
Pb	168 ± 9	175 ± 22	125 ± 11	156	19
Rb	-	91 ± 16	-	91	69
Sr	115 ± 10	483 ± 208	205 ± 99	268	302
V	164 ± 40	303 ± 170	147 ± 32	205	88
Y	-	92 ± 19	-	92	55
Zn	358 ± 39	175 ± 21	302 ± 9	278	231
Zr	84 ± 12	120 ± 12	89 ± 5	98	75

- = Not determined

Fig. 5.4

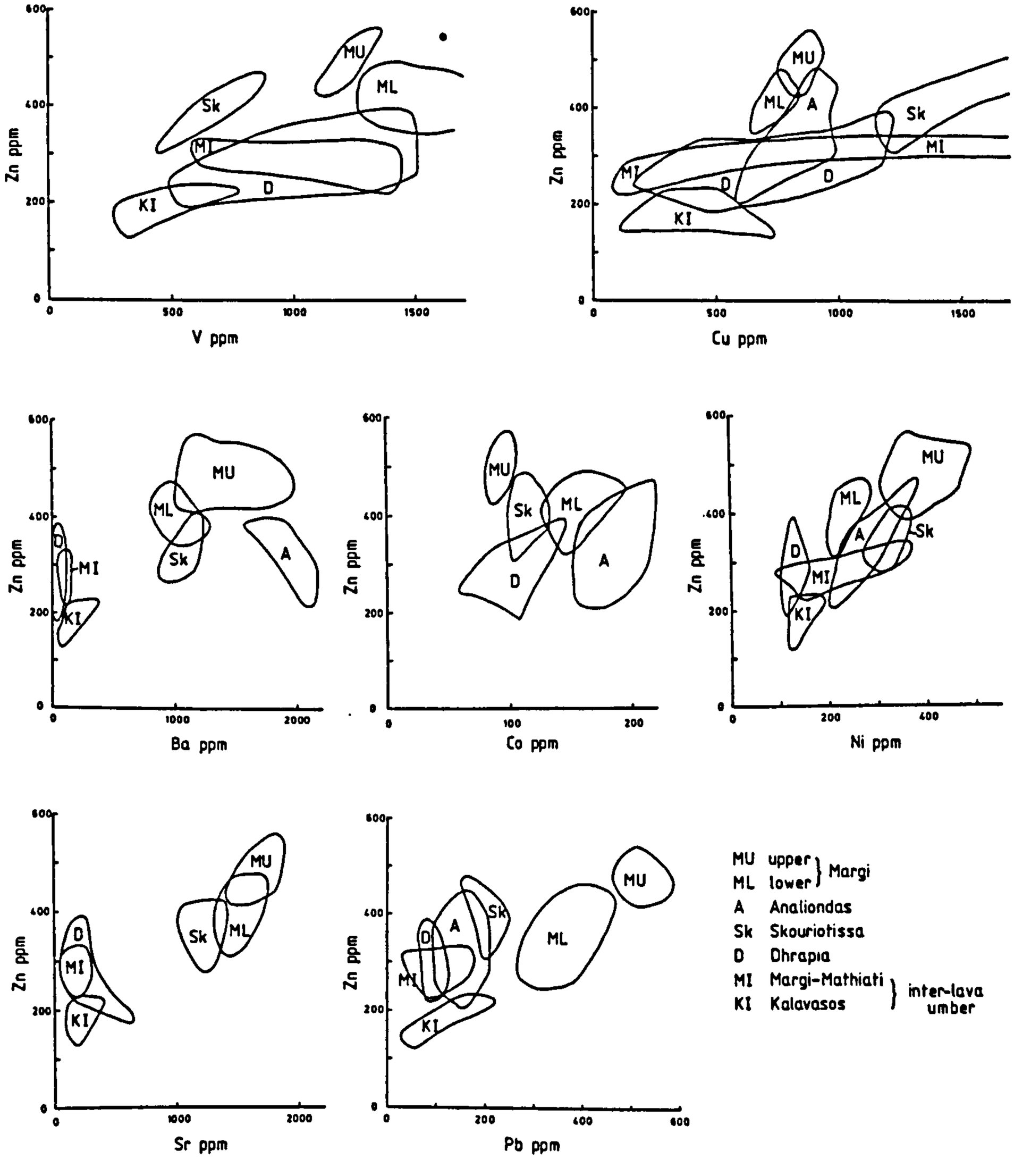

Trace element compositional field for the different analysed umber localities. In general, the interlava umbers and Dhrapia are most depleted and Margi most enriched. Skouriotissa differs in the abundance of Cu.

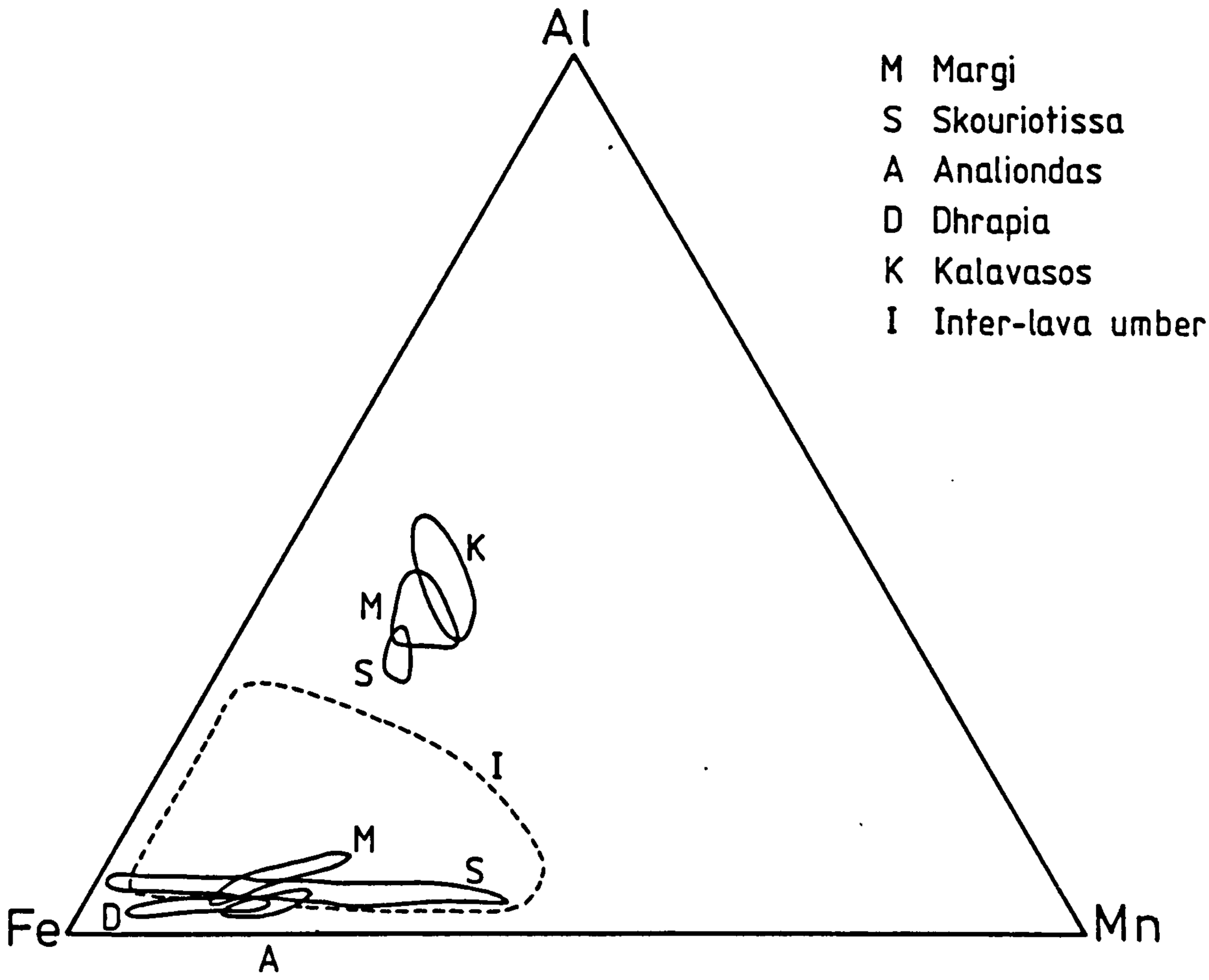

Fig. 5.5 Major element compositional fields of different umber localities

Fig. 5.6 Trace element composition comparison of different clay-rich umbers. The Skouriotissa and Kalavasos samples are richer in Cu and Zn, but depleted in all other elements, with respect to the Margi samples.

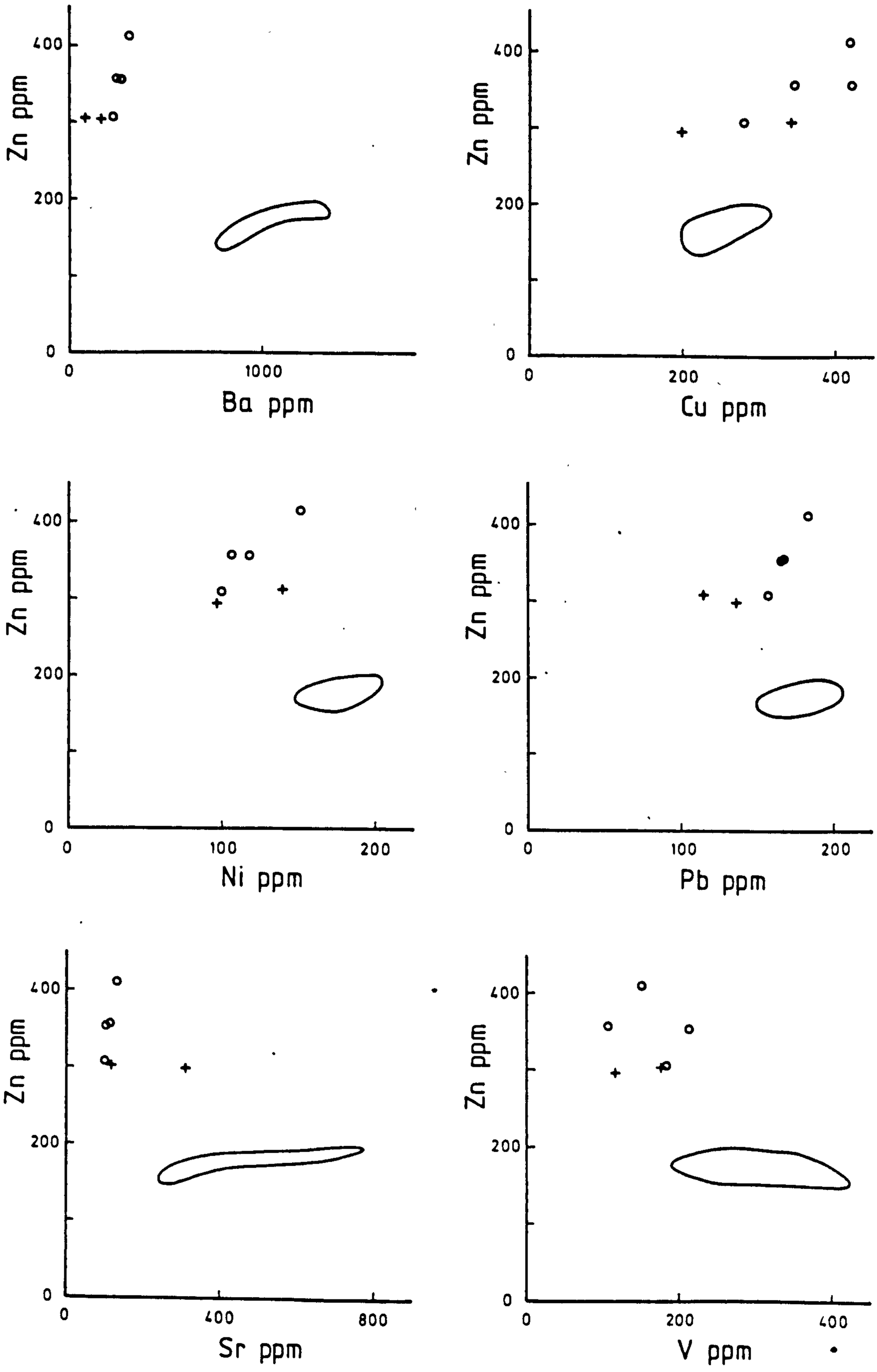

Clay-rich umber. The compositions of the clay-rich umber from three localities are presented in Table 5.7. The major element compositions are extremely similar, differing only slightly in the relative abundances of Fe, Mn and Al (Fig. 5.5). The trace elements are plotted against Zn in Fig. 5.6. The samples from Skouriotissa and Kalavasos are richer in Zn and Cu than the Margi samples, but relatively are depleted in all the other. At Margi, for which there are 17 analyses it can be seen that Zn shows only a small variation, and all the elements except Ba and Sr show less variation than is seen in the pure umber. Ba and Sr however are like the pure umber in having a wide spread of values.

5.4.3 Intra-locality variations

Measured sections for which analytical data exist are at Margi and Skouriotissa. At Margi, 67 analyses of umber, clay-rich umber and overlying non-metalliferous sediments, from a 13 metre section, form the basis of a detailed examination of the sediment geochemistry (see following sections).

Skouriotissa. 14 analyses from a 32 foot section of umber, clay-rich umber and bentonitic clay were presented by Robertson (1976a). Chemical variation with depth is displayed on Fig. 5.7.

Abrupt changes occur at the boundaries of the lithological units, though gradations exist within each type.

Vertical changes in the major element abundances are characterised by an up section decrease in the Fe and Mn, both within the pure- and clay-rich-umber, and also between these. Mn is however depleted in the basal parts of the pure-umber. A complementary increase in Si and Al accompanies the decrease in Fe and Mn. Ca shows little variation except for extreme maxima attributable to enrichment in P which occur in the pure umber. These maxima are accompanied by complementary dilution of the other elements.

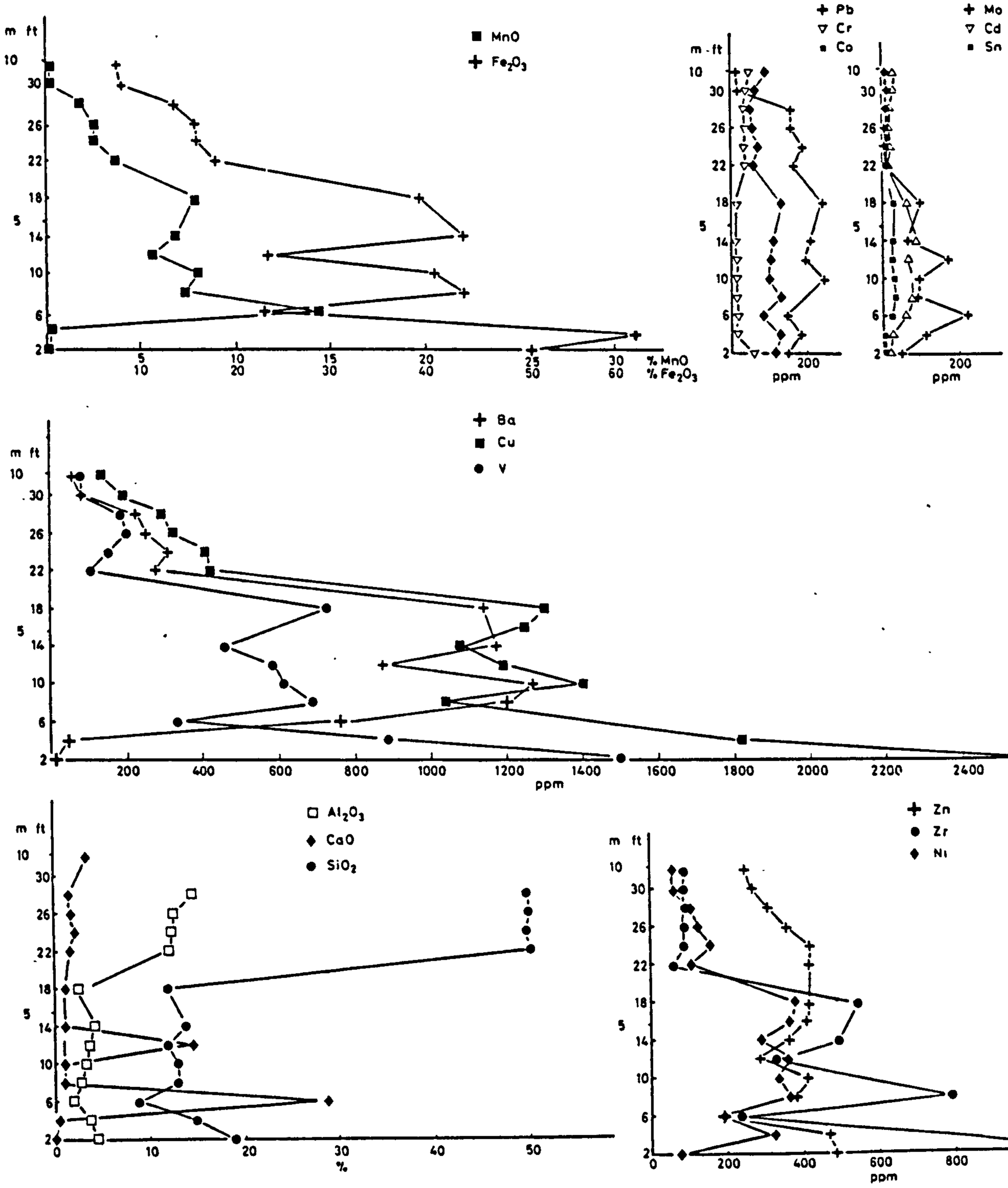

Fig. 5.7 Chemical composition plotted against height in section from the Skouriotissa umber. Data from Robertson, 1976a.

Of the trace elements, only Cr follows the trend of the Al and Si, all the others show greater or lesser enrichment in the umber. Zn-Cu-V-Zr are all enriched in the pure umber, and are strongly enriched along with Fe in the basal Mn-depleted umber. Zn differs somewhat in showing a more gradual decline through the clay-rich umber and bentonite. Ba and to a lesser extent Ni are depleted in the basal Mn-poor umber, but are otherwise also strongly enriched with respect to the overlying bentonite. Pb and Co are only slightly enriched in the pure- as opposed to clay-rich-umber, and Co is depleted in the clay-rich umber with respect to the bentonite.

Margi area. The main umber pit at Margi (section 5.2.4) has been sampled closely over a 13m section, of which the lower 3.5m, sampled with a mean spacing of 7cm, comprises pure umber and clay-rich umber. The data are presented in Fig. 5.8. The analytical data are tabulated in the appendix.

The stepped character of the composition is even more marked than in the Skouriotissa deposit. The transition between the pure- and clay-rich umber is less than 5cm thick, and between the clay-rich umber and the bentonite less than 1mm.

The vertical changes in major element abundance can be viewed in terms of the mineralogy. The covariance of Si-Al-Mg-Na-K-Ti is due to the aluminosilicate component. Si is locally enriched due to biogenic opal. The Ca maxima at the base of the section in the umber coincide with P maxima and are due to apatite as at Skouriotissa. The Ca enrichment at the top of the section is due to the incoming of calcite (in the non-metalliferous sediments). Fe and Mn are strongly enriched in the umber. Fe shows a upward decline in the pure umber but is fairly constant in the clay-rich umber. Mn increases upwards in the pure-umber, showing clear separation from the Fe. In the clay-rich umber Mn follows Fe.

The trace elements fall into three categories. Cr-Rb are enriched in the bentonite, following the aluminosilicate trend. Rb

Fig. 5.8

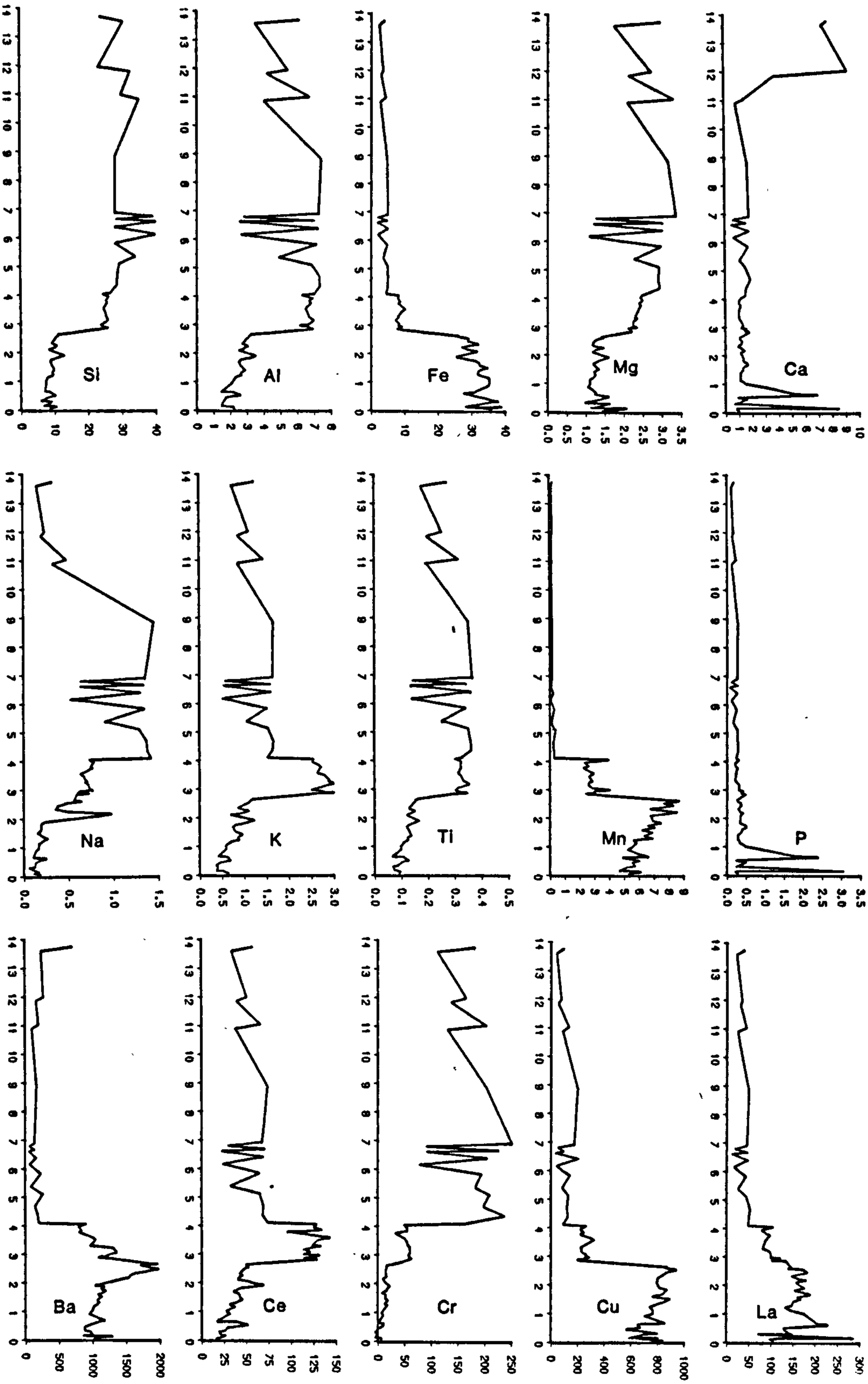

Wt % element concentrations plotted against height in metres through the umber at Margi. Data are given in the Appendix.

Fig. 5.8 continued

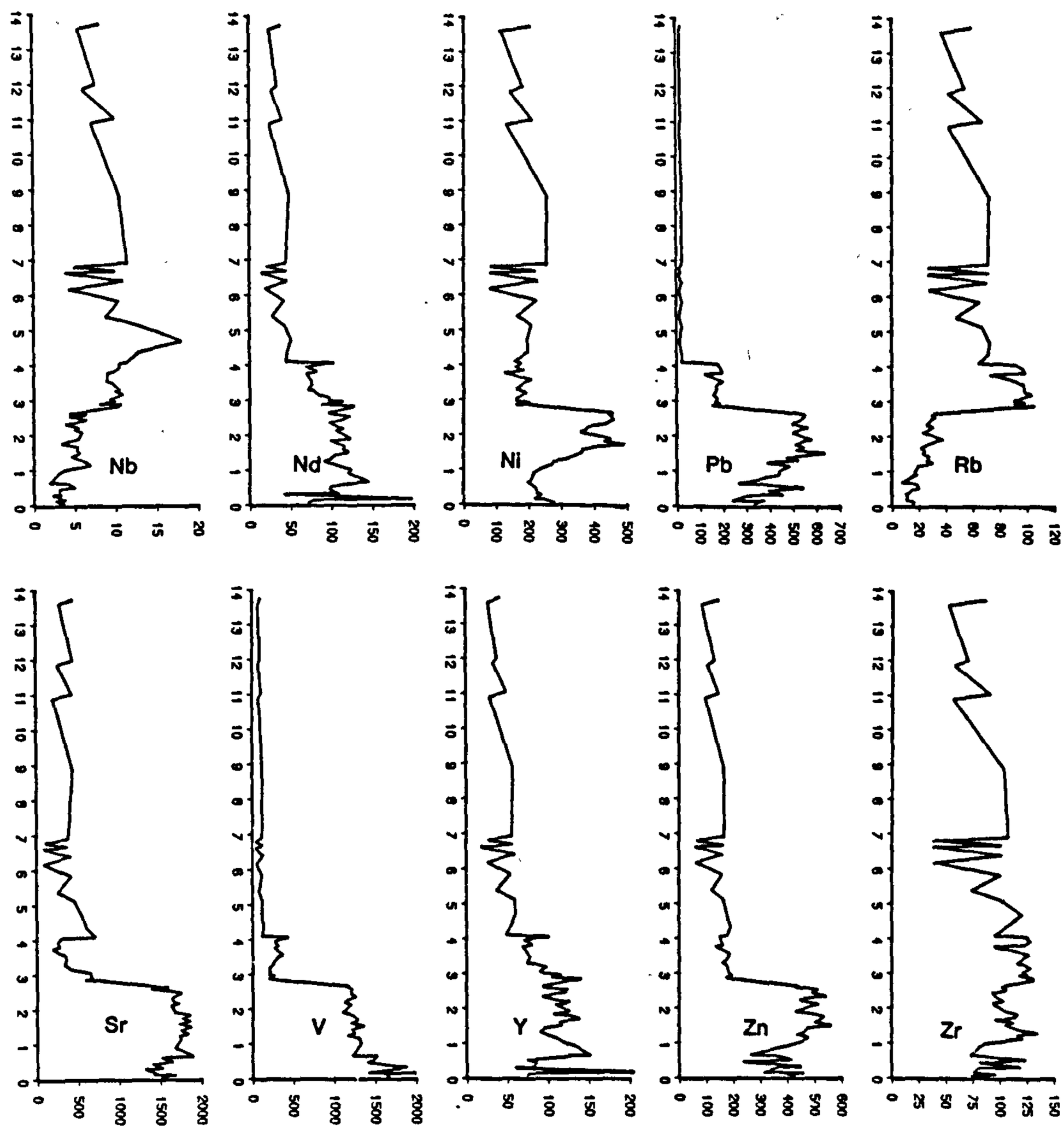

clearly reflects most closely the K content of the samples. Ba-Cu-Ni-Pb-Zn are strongly enriched in the umber with respect to the bentonitic clays, and like Mn increase upwards in the pure umber. Ni is slightly different in that it is higher in the bentonite than in the clay-rich umber. Sr-V-Y-La-Nd are all enriched in the umber, but show upward decreases in the pure umber. The sharp maxima in the La-Nd-Y contents coincide with maxima in the P. Two elements behave somewhat differently. Zr is fairly constant throughout, indicating that the Zr content of the Fe component is similar to that in the aluminosilicate. Ce is strongly enriched in the clay-rich umber, but is not markedly enriched in the pure-umber.

Comparison of the Skouriotissa and Margi umber sections

In general terms the two sections are similar. Basal enrichment in iron, manganese and trace elements, decreasing in two steps upwards to the non-metalliferous bentonitic clays (The manganese depletion at the lowermost parts of the Skouriotissa deposit excepted). However in detail there are differences. Most importantly, the manganese content of the pure umber increases upwards at Margi, along with most of the trace elements, and the reverse is true at Skouriotissa. An upward increase in accumulation rate of the clay could account for the trend at Skouriotissa, a possibility which cannot be entirely ruled out. However, the similarity in basal sequences about the island, where umber compositions do not vary greatly (section 5.2.9) argues against large changes in clay accumulation rate.

5.4.4 Defocused beam electron micro-probe study

The range in composition of the Margi umber is small because of the near homogeneous mixing of the components. The scale of this homogeneity, and to some extent the composition of the components, may be further examined by analysing small areas using a defocused electron beam on the micro-probe. The beam was defocused to ca. 20μm diameter, so analyses represent average compositions over approximately 300μm^2. Inhomogeneity may be examined down to this scale.

TABLE 5.8

ELECTRON MICRO-PROBE DEFOCUSED BEAM SCAN.

	Sample XRF whole rock	81-155(pure umber) 21 points probed	% standard deviation observed	calculated instrumental
Si/Al	3.42	3.32 ± 0.37	11.1	1.6
Fe/Al	15.35	18.54 ± 5.44	29.3	1.3
Mg/Al	0.49	0.47 ± 0.12	24.7	2.4
Ca/Al	0.48	0.48 ± 0.20	41.6	3.2
K/Al	0.30	0.28 ± 0.10	36.2	5.4
Na/Al	0.070	0.102 ± 0.045	44.7	12.3
Ti/Al	0.048	0.051 ± 0.029	56.6	13.7
P/Al	0.140	0.111 ± 0.059	53.2	40.4
Mn/Fe	0.165	0.191 ± 0.108	56.3	1.1
Ba/Mn	0.017	0.018 ± 0.003	18.5	25.0

Chemical data. Probe data recast to 90% total as oxides.

	XRF	Micro-probe 155-8	155-15		
Si	7.84	5.85	5.75	155 - 8	Dark zone
Al	2.29	1.68	1.90	155 - 15	Intermediate
Fe	35.17	34.38	50.58		region
Mg	1.11	1.13	0.84		
Ca	1.11	1.43	0.72		
Na	0.16	0.30	0.09		
K	0.68	0.57	0.46		
Ti	0.11	0.11	0.11		
Mn	5.80	18.63	3.96		
P	0.32	0.20	0.30		
Ba	0.10	0.38	-		

Fig. 5.9

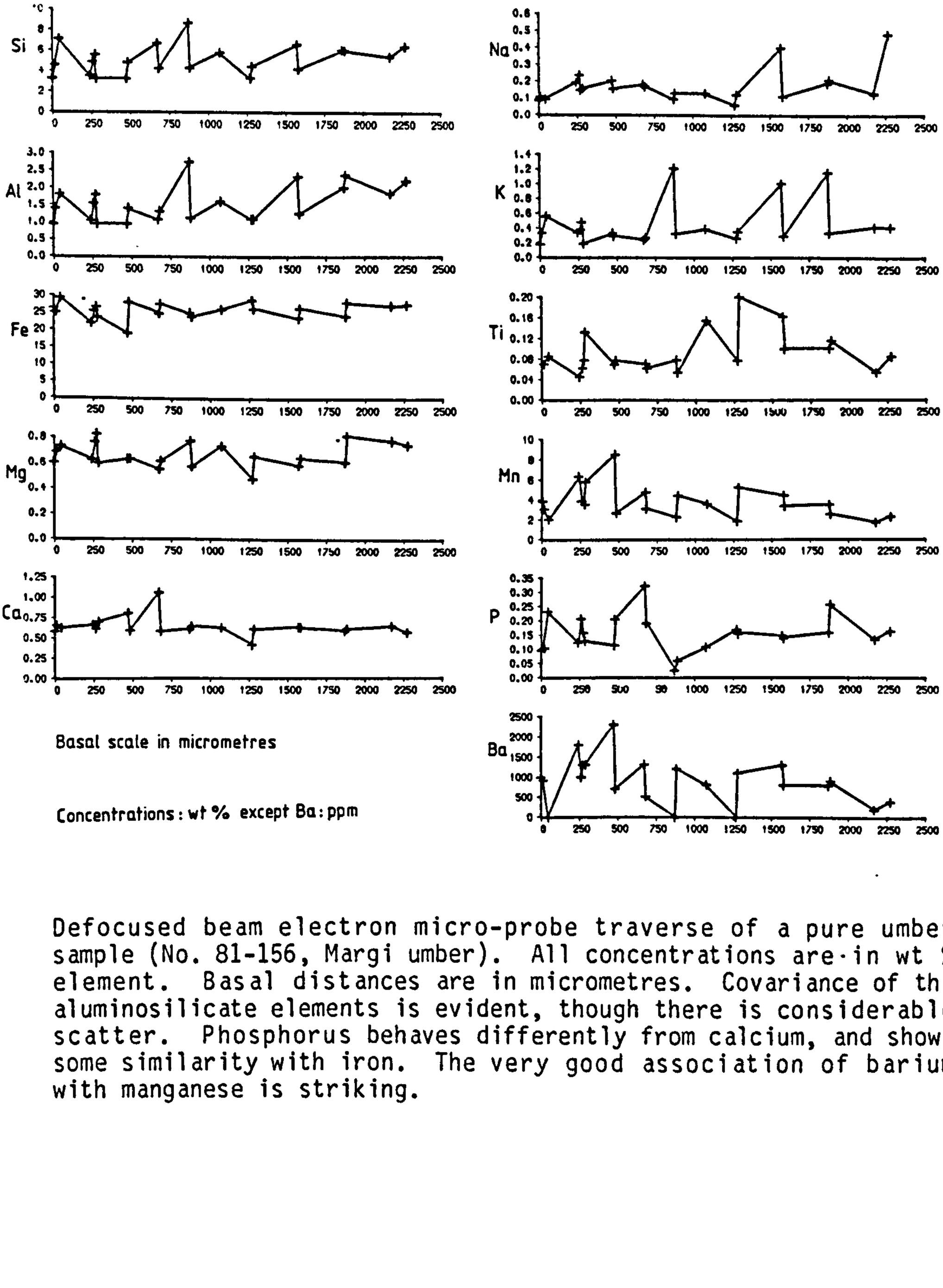

Defocused beam electron micro-probe traverse of a pure umber sample (No. 81-156, Margi umber). All concentrations are in wt % element. Basal distances are in micrometres. Covariance of the aluminosilicate elements is evident, though there is considerable scatter. Phosphorus behaves differently from calcium, and shows some similarity with iron. The very good association of barium with manganese is striking.

Method. The analyses were performed using crystal spectrometers, reading four peaks and two backgrounds (of ten seconds each). Apart from defocusing of the beam conditions were identical to that described in section 5.3.1

Results. Twenty one points were analysed along a 2.2mm linear traverse perpendicular to bedding in sample 81-155 (pure umber, margi). Because of the extremely poor totals, resulting from the highly porous character of the sediment, elemental ratios are presented rather than absolute values, in Table 5.8. Also on the Table two of the analyses are presented with totals recalculated to 90% in order to permit easy comparison with the whole rock analysis. In addition, the values are plotted against distance along traverse, in Fig. 5.9.

Comparison with XRF whole rock analysis. In Table 5.8 the XRF whole rock analysis ratios are compared with the mean of the twenty one probed points. The extremely close similarity both justifies the technique and indicates near homogeneity on the millimetre scale. This is not so on a smaller scale; the standard deviations for all the ratios but Ba/Al and P/Al, are greatly in excess of the calculated analytical error. Thus considerable inhomogeneity is indicated on the sub-millimetre scale.

Small scale chemical inhomogeneity.

The variation of composition with space are shown in Fig. 5.9. Si, Al, K, Mg show broadly similar variations indicating that the aluminosilicate fraction is fairly evenly dispersed. Considerable scatter indicates local small scale inhomogeneity in distribution of the various clay minerals. Ti behaves slightly more independently, though still mirroring the trend of Al but this may be an artifact of the low abundance of Ti in the sample. Mn and Fe behave independently of each other, clearly residing in different mineral phases. Surprisingly considering the constancy of the whole rock Ca/P ratio, P and Ca behave independently. A peak coincident to both Ca and P is due to impingement on apatite fragment in the sediment. P

does not covary well with any of the other elements; there are similarities to both the Fe and Al trends. The covariance of Ba with Mn is striking, giving the best correlation of any two elements.

Two aspects of the inhomogeneity are particularly important; the variation in the aluminosilicate elements, and the presence of ellipsoidal manganese-rich regions (see section 5.2.2.1).

Aluminosilicate variation: On the scale of the analyses there are real variations in the relative proportions of Si-Al-Mg-K-Ti, contrasting with the constancy of these in the scale of whole rock analyses. Local variations in the mixture of the aluminosilicate minerals is evident.

Manganese-rich regions: These are enriched in Mn, Ba, Na and Ca and depleted in Fe with respect to the remainder of the rock. The composition of one of these areas is given in Table 5.8. There is a resemblance of these regions, in composition and scale, to micro-manganese nodules. However, their diffuse boundaries (section 5.2.2.1) suggest that they may be secondary rather than primary in origin.

5.4.5 Chemical variation of the Margi umber deposit. Inter-element correlations

The variation in the major element composition of the Margi umber can be described in terms of mixing of a small number of well defined chemical components. The knowledge thus obtained is useful in interpreting other localities where less complete sampling makes such a study impossible. A similar treatment of trace elements is presented in the following section.

The Margi Umber. The vertical variation in the Margi umber is described in section 5.4.3. Over a 3.5m section of umber and clay-rich umber, 47 samples were collected. In the following discussion this is divided into three parts: upper and lower

divisions of the pure umber, overlain by clay-rich umber. The pure umber subdivision is based entirely on differences in trace element abundances, there being no textural evidence for this.

Methodology. If the chemical variation of a system is caused by variable mixing of components of constant composition, then both the composition and relative abundance of the components can be determined. Variation diagrams form the basis of the analysis here, but a factor analysis is also used. A comparison of the two methods is given at the end of the section. Simple two-element plots may be used where dilution by unrepresented elements is not a problem. Three-element diagrams have been found most useful as a means of avoiding such dilution effects.

Two-element variation diagrams. Good positive correlations are observed between Si-Al and Ti-Al (Fig. 5.10A,B), yielding trends onto which both the umber and clay-rich umber fall. The samples of pure umber which are slightly silica-enriched are those with abundant veins of palygorskite. Clearly the greater part of the Si, Al and Ti reside in a relatively invariant aluminosilicate component.

Fe shows a good negative correlation with Al, showing that most of the Fe is independent of the aluminosilicate (Fig. 5.10C). Mn however behaves differently in the pure umber than in the clay-rich umber. In the pure umber it correlates positively with Al contrasting with the Fe (Fig. 5.10D). In the clay-rich umber the correlation is negative. The contrasting behaviour is further illustrated in a plots of Mn-Fe (Fig. 5.10E). In the pure umber there is a negative correlation of Mn with Fe demonstrating the separation of the two elements. In the clay-rich umber Mn correlates positively with Fe showing that the two are not clearly separated.

P does not correlate with Fe (Fig. 10F) a point worth noting because of the observed Fe-P correlation in a possible modern analogue from the East Pacific Rise (Berner, 1973). P instead correlates strongly with Ca, suggesting that it is entirely contained

Fig. 5.10

Major element variation diagrams for the Margi pure and clay-rich umbers.

a,b) Good positive correlations of Si and Ti with Al, indicate constancy of composition of the aluminosilicate. The elevated Si value in the most Al-Si depleted umber (a) are due to palygorskite veins.

c) The antipathetic relationship of Fe with Al, is due to the two comprising the greater part of the rock.

d) Mn differs strongly from Fe and show a sympathetic relationship with Al in the pure umber. An antipathetic relationship is however observed in the clay-rich umber.

e) The separation in behaviour of Fe and Mn is brought out in the plot of Mn against Fe. In the pure umber a negative slope is observed. In the clay-rich umber the separation is absent.

f) There is apparently no correlation of P with Fe. However, that the P values are as great in the pure as opposed to clay-rich umber, indicates that an association with iron exists.

Fig. 5.10

a = clay-rich b = pure

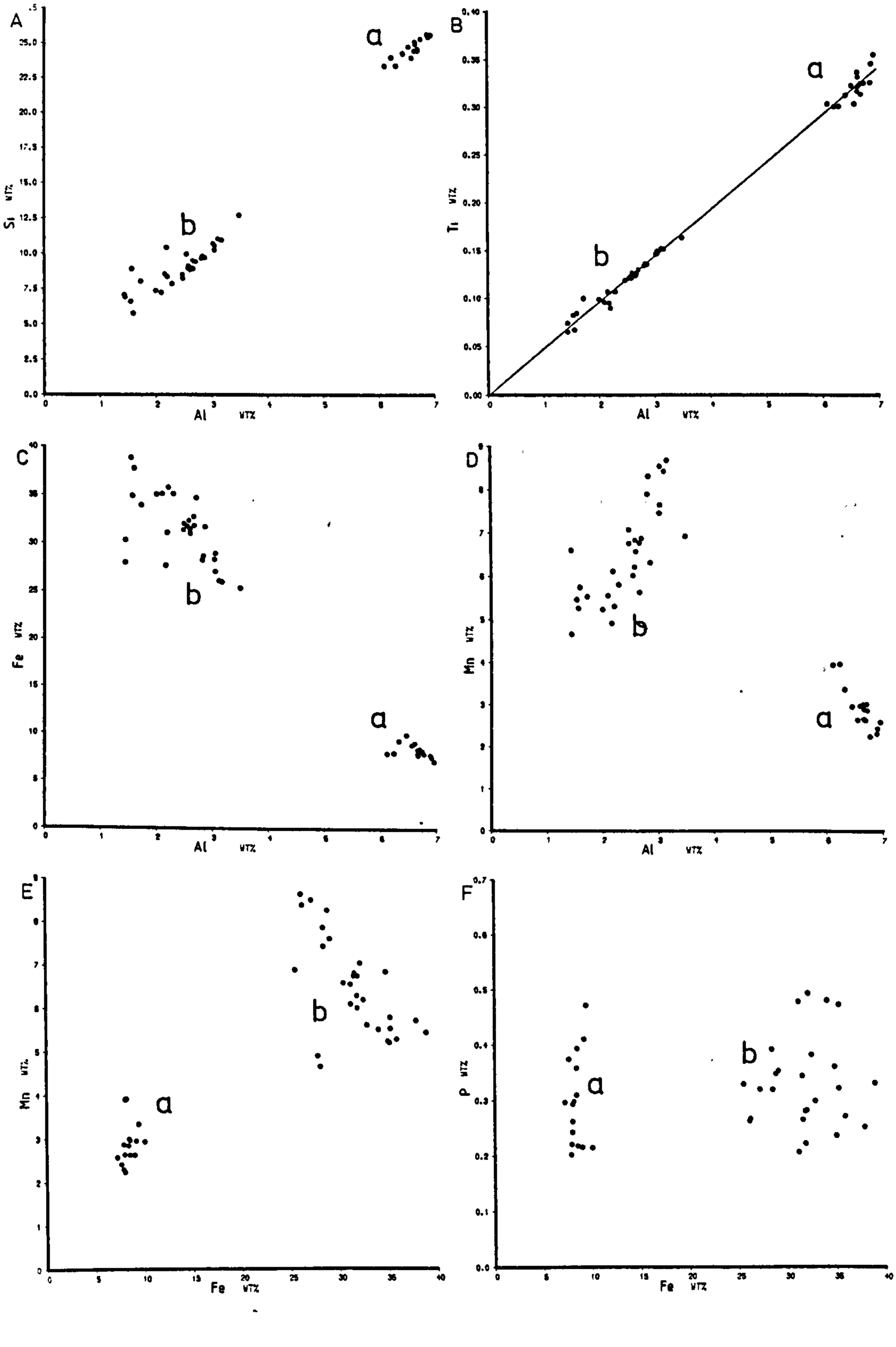

Fig. 5.11

Major and trace element variations in the Margi pure and clay-rich umbers.

Crosses = upper pure umber. Squares = lower pure umber. X = clay-rich umber.

a) A very good correlation of Rb with K is observed.

b) The strong Ca-P association indicates that the two are chemically controlled by apatite.

c) Sr is influenced strongly by manganese and does not show an association with Ca.

d,e,f.) Y, La and Nd are are associated with P. For Y the ratios are similar in the pure and clay-rich umber. However, for La and Nd, the enrichment is greater in the pure umber, than in the clay-rich umber.

Fig. 5.11

a = clay-rich b = pure

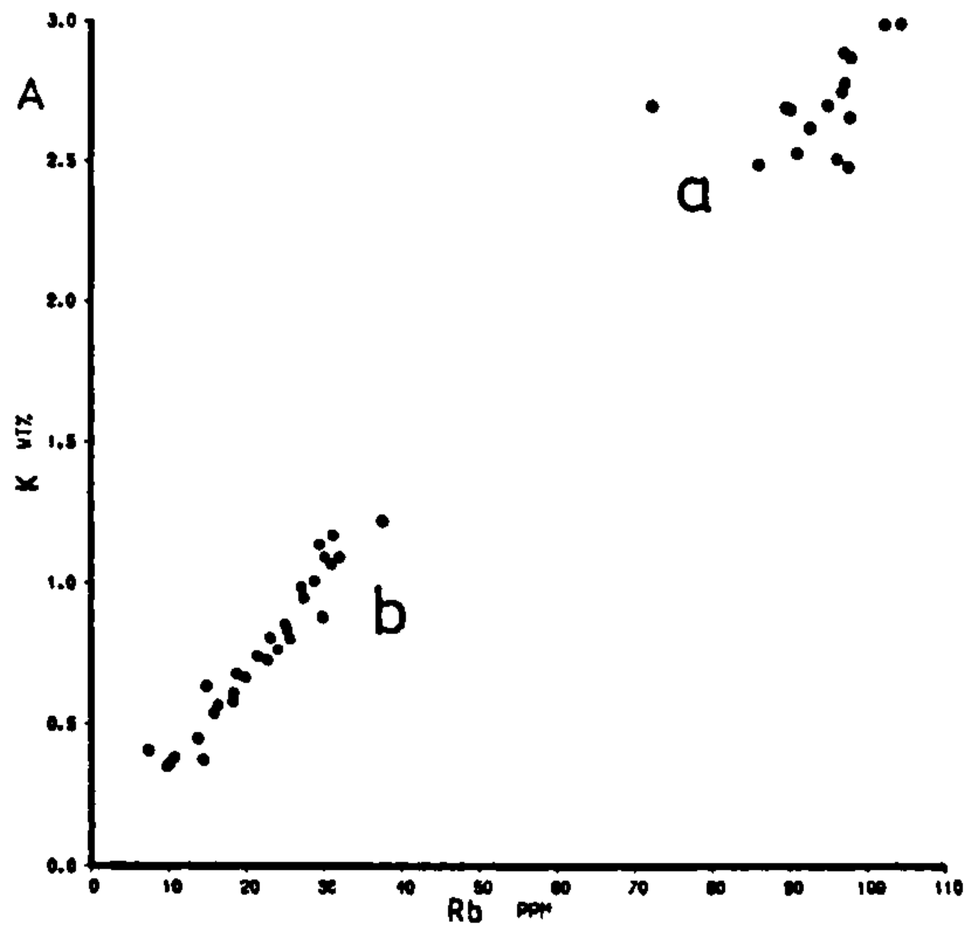

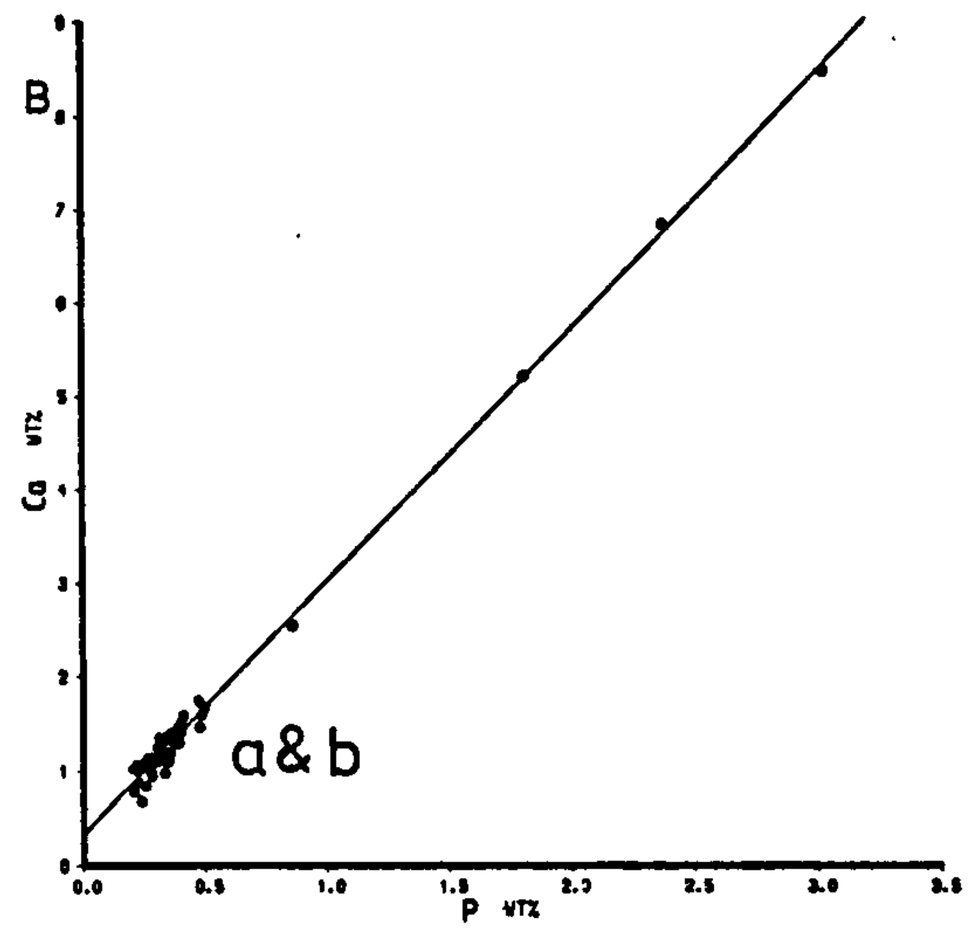

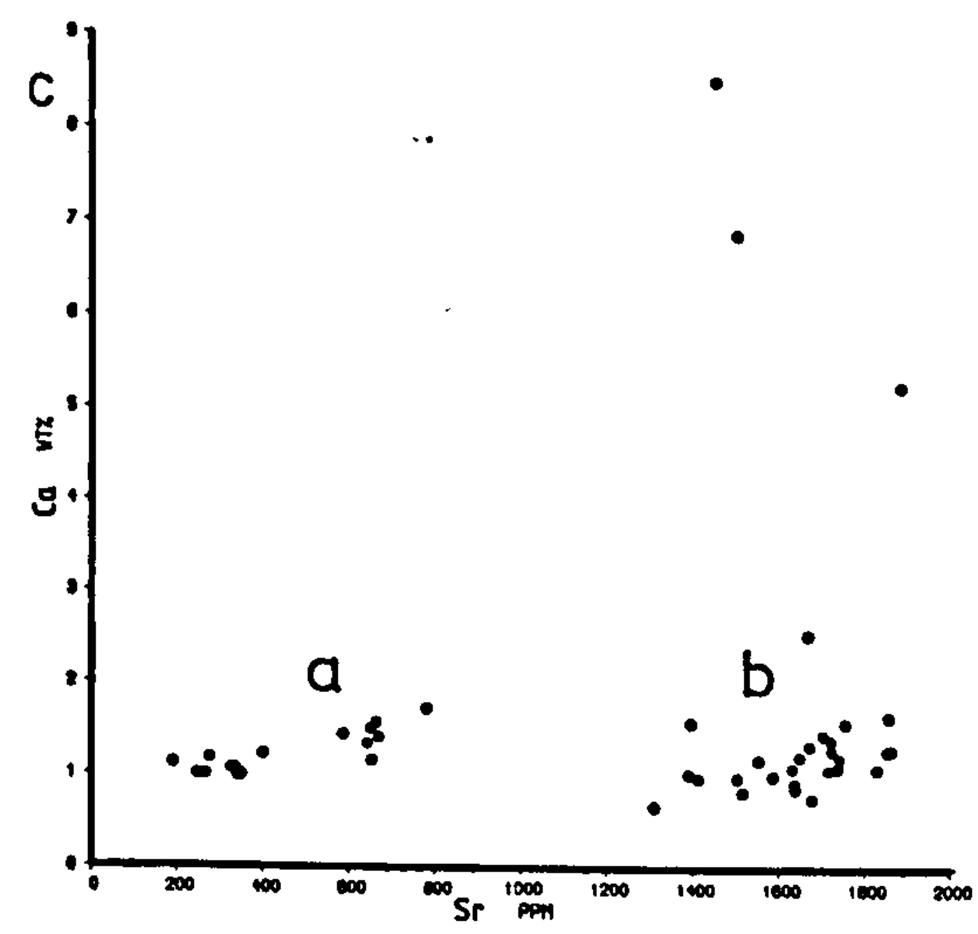

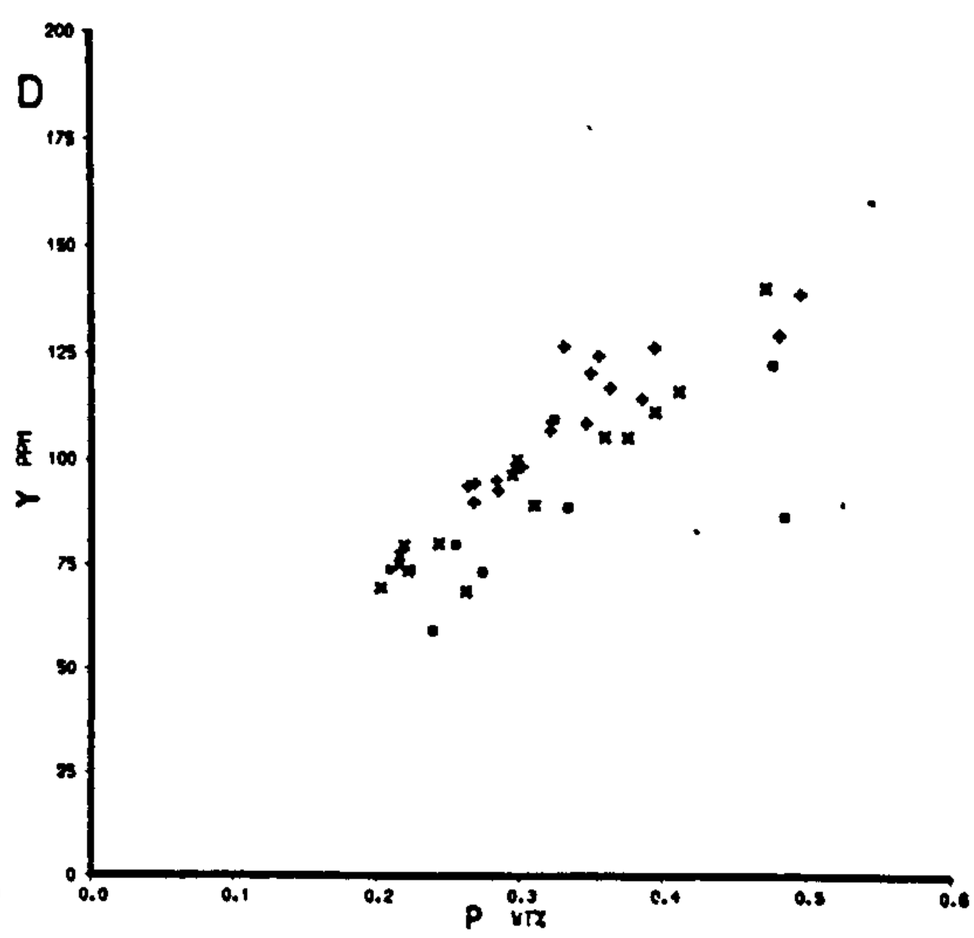

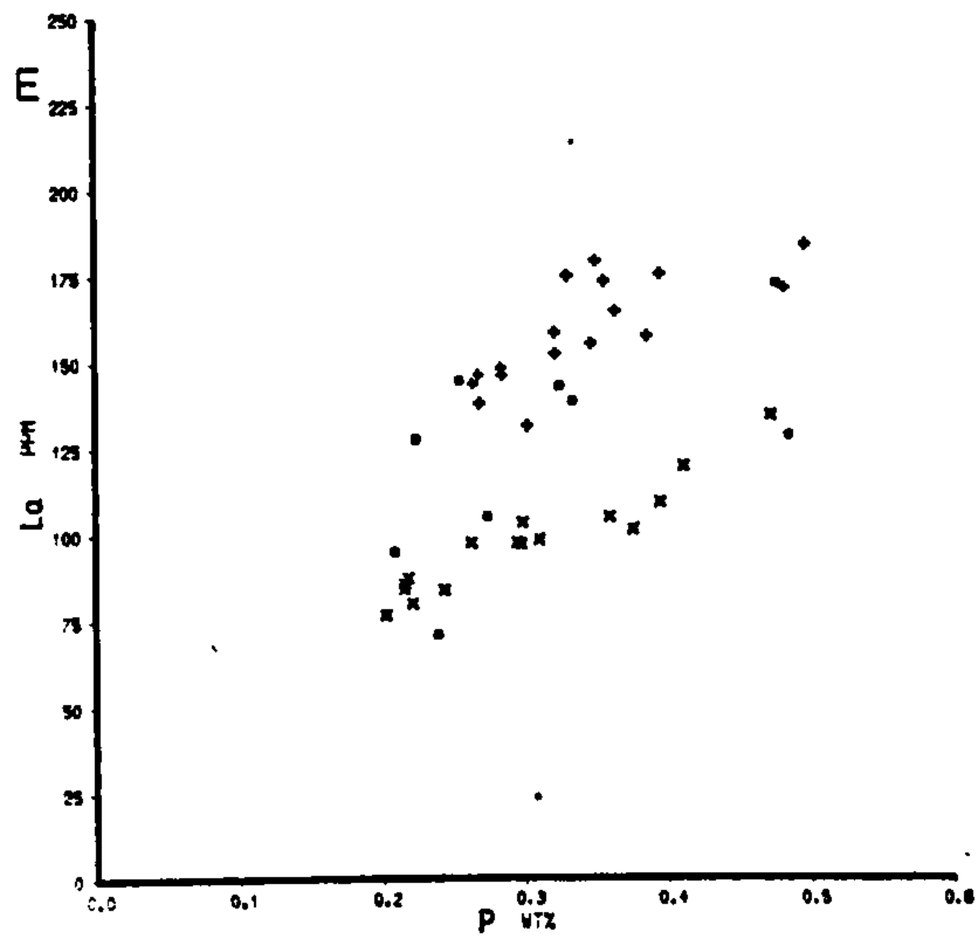

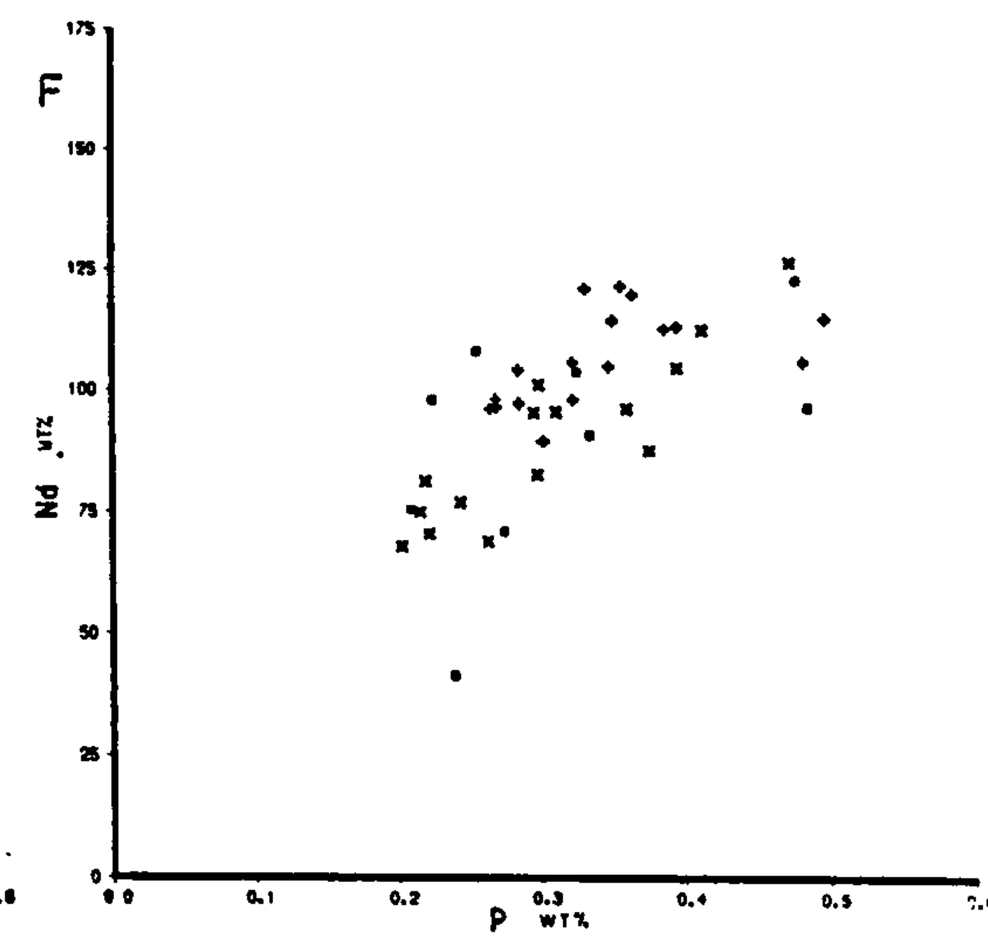

in an apatite (Fig. 5.11B).

In the preceding qualitative examination, five chemical components have been identified. 1) Aluminosilicate; 2) Iron; 3) Manganese; 4) Palygorskite; 5) Apatite. Using triangular diagrams the composition of these components can be further studied.

Three-element variation diagrams. Triangular diagrams are presented in Fig. 5.12. The extremely low scatter observed in these supports the view that the major element components are of nearly constant composition throughout the deposit.

In a Mg-Al-Si plot (Fig. 5.12F) the clay-rich umber falls in a small field. The pure umber has a greater spread and has a higher relative abundance of Mg. The tail on the umber field extends towards the composition of the palygorskite veins, and is thus to be expected. The difference in composition between the main cluster of points and the clay-rich umber cannot however be explained this way. The difference is not due to the aluminosilicate compositions as might be expected, but stems instead from Mg-Al-Si-Ti, associated with the Fe component. This is clear from the triangular plots Figs. 5.12A-E. The extremely low scatter trends represent mixing lines between two components of constant composition. Notably, the Fe-rich component contains small but significant concentrations of Si, Al, Mg and Ti. The regression lines all meet the element-Fe axis, giving a ratio for the elements where K has diminished to zero. It is possible that the Fe component contains K as well as the other elements, in which case element/Fe ratios in the component are higher. However, for the sake of simplification it is assumed that the K is all in the aluminosilicate, and element/Fe ratios for the Fe component are taken where K is zero. These ratios are presented in Table 5.9. They have been calculated both using the clay-rich umber and pure umber together, and with the uppermost umber (free of palygorskite veins) alone. The ratios are not significantly different. Element-K ratios can be determined for the aluminosilicate component. Element/Ti ratios calculated from these are shown in Table 5.9, where they can

Fig. 5.12

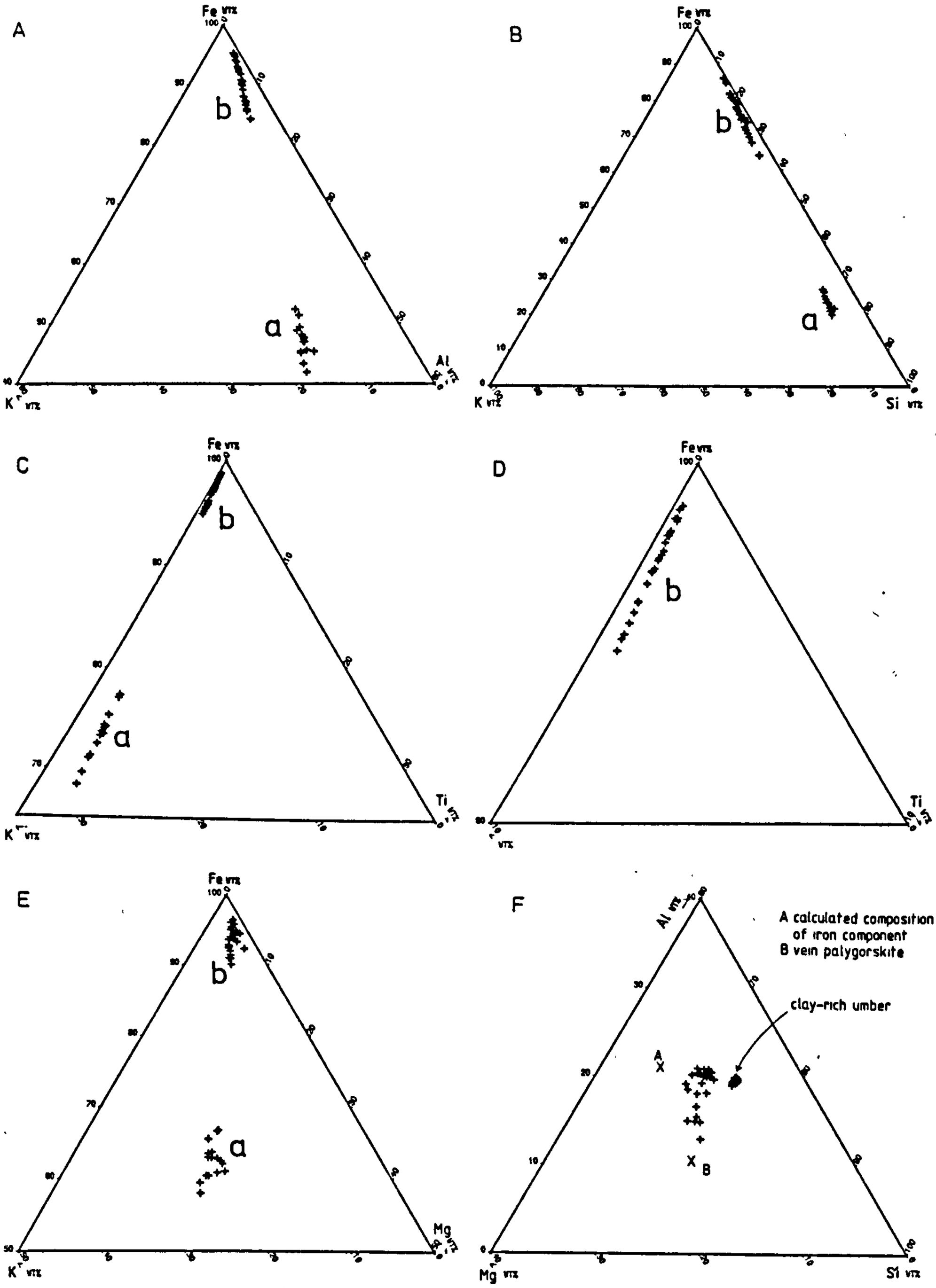

a = clay-rich b = pure

Triangular plots of the Margi pure- and clay-rich umber. Plots a-e all represent mixing between an aluminosilicate of near constant composition, with an Fe rich end member, in which there are small but significant amounts of Si, Al, Mg and Ti. The difference in composition of the pure and the clay-rich umber (f) can be explained through this and the presence of palygorskite veins in some of the pure umber samples.

be compared with the overlying bentonites. The ratios are the same for the pure- and clay-rich-umber, but differ from the bentonite.

5.4.6 Major element component compositions

From the chemical variation observed in the data, five major element components have been identified. In essence what this means is that with only five independently varying components, the compositions of which can be obtained either by assumption (i.e all Mn occurs in a single phase) or by mixing lines on the variation diagrams (giving for example the Si, Al, Mg, Ti content of the iron component), the chemical variation of the data set can be explained. Thus the procedure is one of simplification. A summary of the composition of these components is given below.

Iron oxide. The iron oxide component is composed of FeOOH (section 5.3.2) but has Si, Al, Mg and Ti associated with it. The element/Fe ratios are given in Table 5.9. In the interlava ferruginous sediments, there is a small proportion of manganese associated with the iron. Chemical leaching studies on the umber yield the same result (section 5.4.7.1). In the major element variation diagrams, the abundant independent manganese component conceals this effect.

Manganese oxide. The manganese oxide is composed of $MnO_{1.8}$. The interelement variations do not show an association with other major elements, but the chemical leaching study suggests an association of Ca with Mn, and the micro-probe analyses shows an association with Ca and Na.

Aluminosilicate. The aluminosilicate component is similar in composition to the average bentonite, but differs from that immediately overlying. Element/Ti ratios are given in Table 5.9.

Palygorskite. Veins of palygorskite occur in sufficient abundance to significantly enrich the rock in Mg and Si. The composition is given by probe data on vein samples (Table 5.4).

TABLE 5.9

ELEMENTAL RATIOS OBTAINED FROM TRIANGULAR DIAGRAMS

The iron-rich component

	Clay-rich- and pure -umber		Pure umber	
		%error 1 SD		%error 1 SD
Si/Fe	0.043	24	0.069	53
Al/Fe	0.020	23	0.026	29
Mg/Fe	0.018	22	0.013	62
Ti/Fe	0.00099	23	0.0012	25

The aluminosilicate component.

	K/Ti	Si/Ti	Al/Ti	Na/Ti	Mg/Ti	K/Rb	Cr/Ti
Bentonite	4.54 ± 0.24	80.9 ± 2.28	20.44 ± 0.61	3.11 ± 0.64	8.64 ± 0.70	227 ± 10	607 ± 72
Clay-rich umber	8.99 ± 0.19	67.0 ± 9.16	17.8 ± 1.8	2.41 ± 0.39	5.71 ± 1.49	294 ± 52	173 ± 25
Pure umber	9.13 ± 0.12	70.8 ± 11.8	21.2 ± 1.0	7.21 ± 1.61	8.93 ± 2.33	333 ± 67	130 ± 30

Apatite. A Ca/P ratio of 2.69 is observed in the umber, with a very good correlation(r = 0.997). A ratio this high indicates that there is considerable substitution of CO_2 for P_2O_5, indicating that the apatite phase is a francolite (section 5.3.2)

Factor analysis: Problems of interpretation.

An R-mode factor analysis .was performed on the lower pure umber, the upper pure umber and the clay-rich umber. Interpretation of these is not simple, demonstrating that the method can only be used in cooperation with other techniques. A description of the technique is given in Chapter 4, section 4.2.7.

Lower umber. The factor loadings are shown in Fig. 5.14. Factor I contains iron as positive, and Ca,Na and P as negative, representing a complementary association of iron and apatite. Factor II contains Si, Al, Na, K and Ti and seems thus to represent the aluminosilicate component. Factor III contains again Fe as positive, but contains Si and Mg as negative. The latter two probably represent the palygorskite component. Factor IV contains only manganese. Factor V contains no significant major elements.

Upper Umber. The factor loadings are shown in Fig. 5.13. Factor I contains Si, Al, Mg, K and Ti as strong positive with Mn weakly associated. In opposition to this is Fe and less strongly P as negative. Factor II contains strongly positive Ca and P representing apatite. Factor III contains Mn and Na suggesting that Na is indeed associated with the manganese phase. Palygorskite veins do not occur in abundance in the upper umber, and there is no sign of such a phase in the factor loadings.

Clay-rich umber. The clay-rich umber is more difficult to interpret. Factor loadings are shown in Fig. 5.15. Factor I contains Si, Mg and Na as positive, and, Ca and P as strongly negative. Factor II contains Si, Al, K and Ti as negatives, probably representing the

Fig. 5.13

MARGI UPPER PURE UMBER

R-MODE FACTOR ANALYSIS - varimax rotated factor loadings

A - eigenvalue B - percent contribution

FACTOR

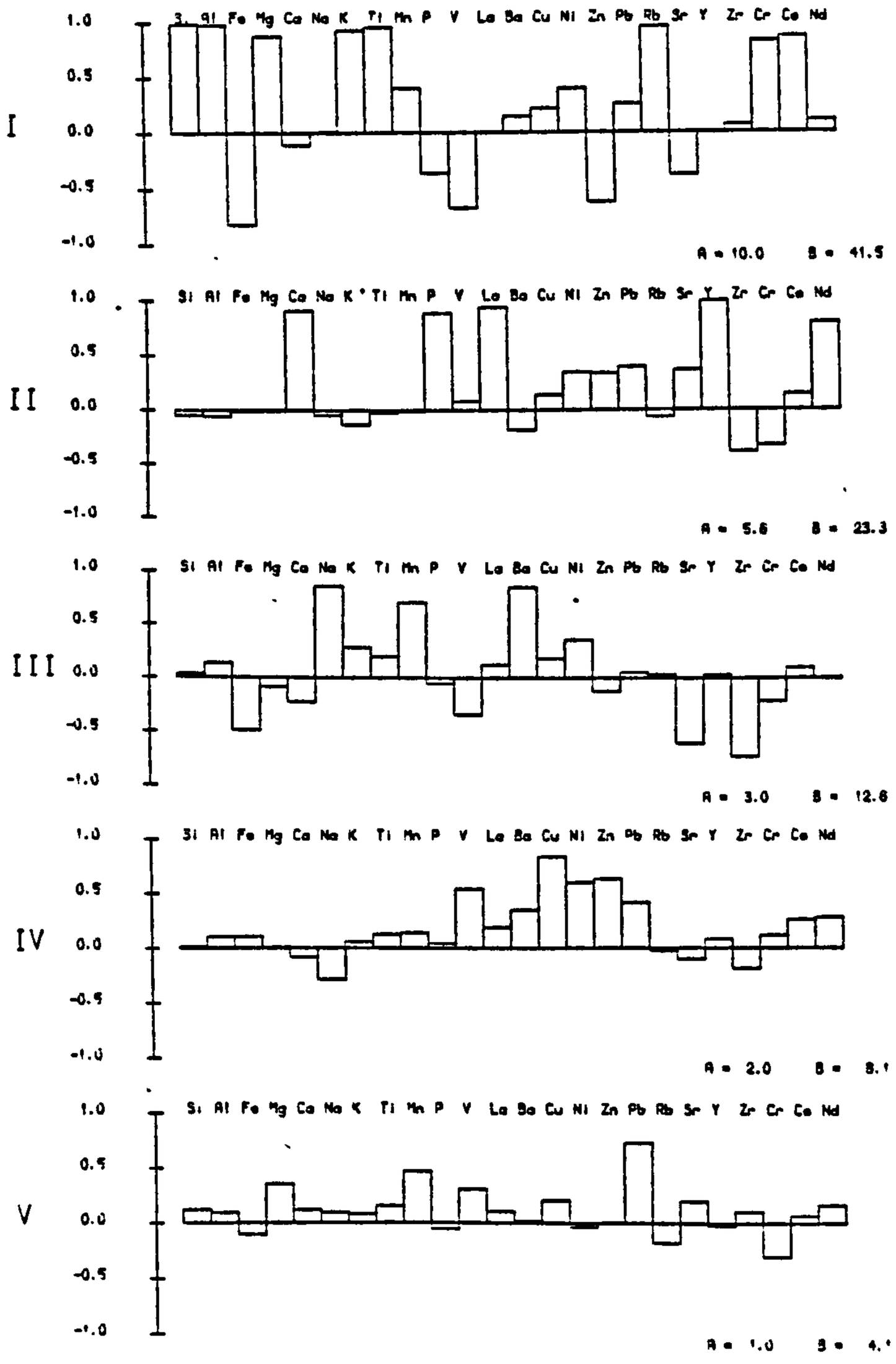

Fig. 5.14

MARGI LOWER PURE UMBER

R-MODE FACTOR ANALYSIS - varimax rotated factor loadings

A - eigenvalue B - percent contribution

FACTOR

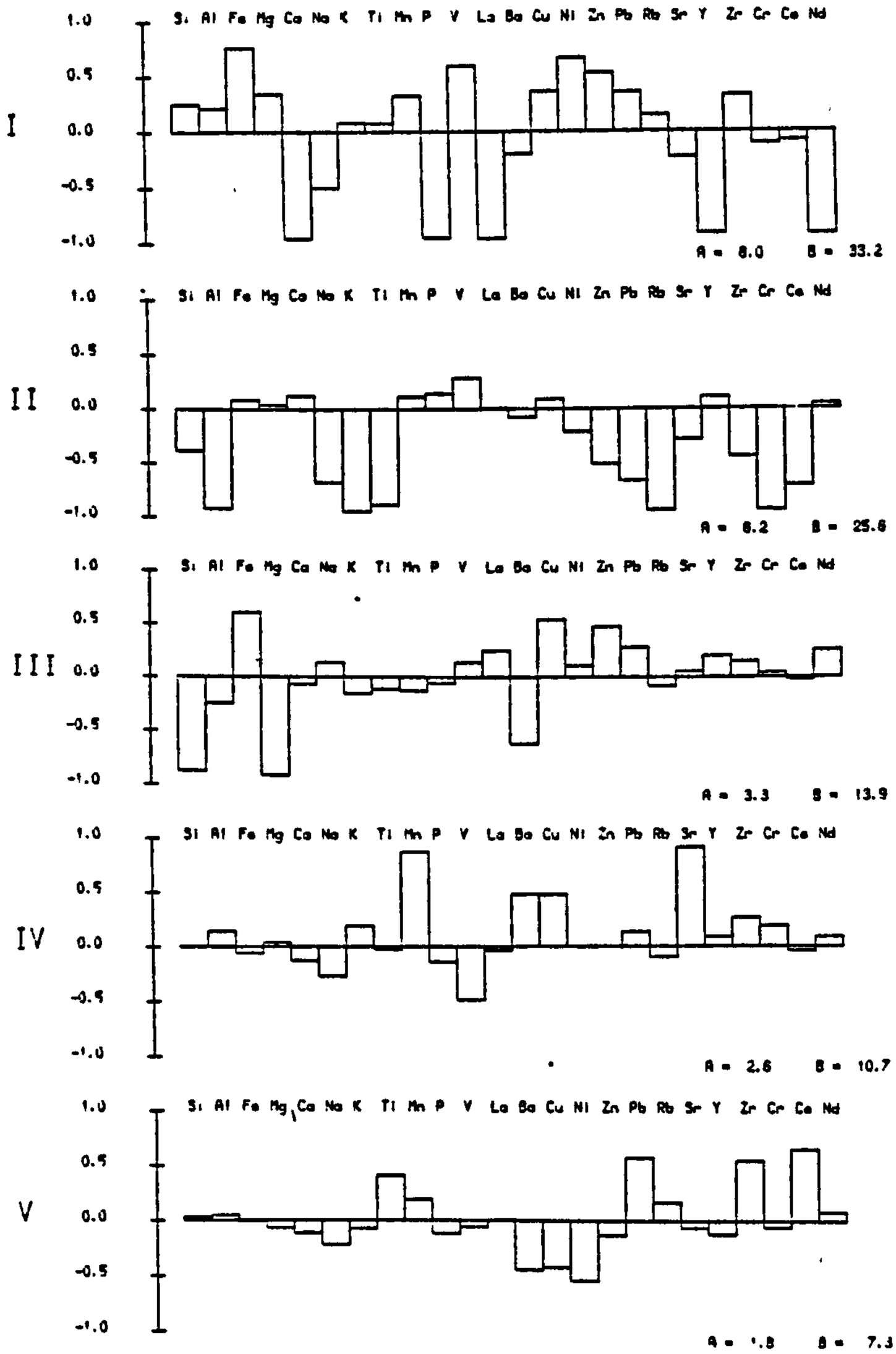

Fig. 5.15

MARGI CLAY-RICH UMBER

R-MODE FACTOR ANALYSIS - varimax rotated factor loadings.

A - eigenvalue B - percent contribution

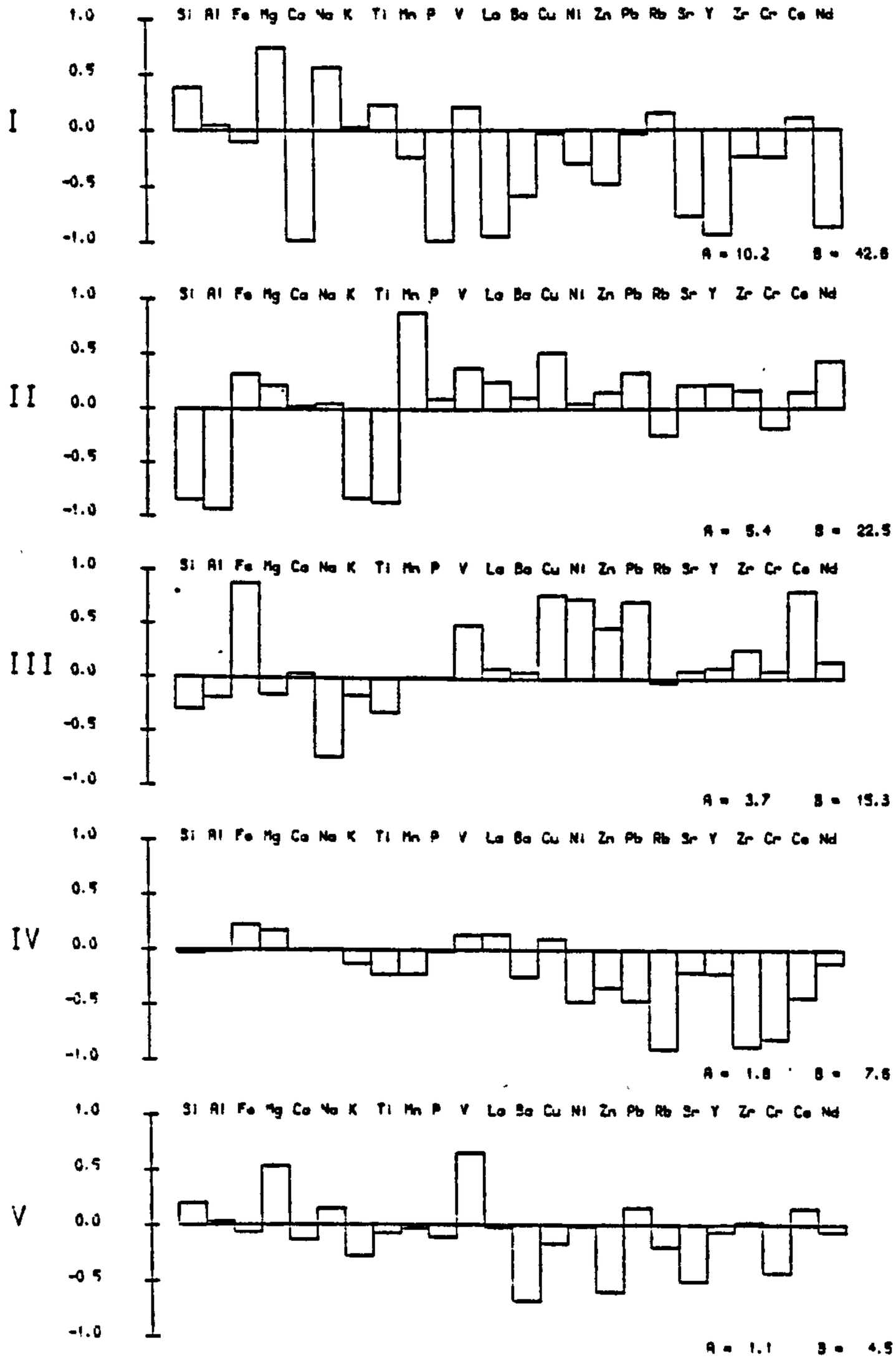

dominant aluminosilicate phase. In opposition to this as positive is manganese. Factor III contains Fe as positive and Na as negative, the latter possibly representing plagioclase. Factor IV contains no major elements.

Discussion. The principal difficulty in interpretation stems from the number of Factors which clearly represent two components which behave antipathetically. In the lower umber for example the iron component and the apatite both occur in Factor I. Together they behave independently with respect to the rest of the rock, covarying in a complementary fashion. This behaviour is to be expected if closure is approached (i.e. if two elements comprise the entire composition, they must vary antipathetically) which can account for the presence of both the iron and aluminosilicate components in Factor I in the upper umber. In other cases, where closure has not occurred, the association in one factor implies some kind of genetic relationship. For example, in factor I of the clay rich umber, Mg with Si and Na vary antipathetically with phosphate. The total abundance of the Mg-rich part of the component, which may be either palygorskite or smectite, and the phosphate, are independent of the remainder, but have a complementary relationship with each other. What controls this, whether diagenetic or primary, is not clear.

5.4.7 Trace element geochemistry

Studies from Skouriotissa, Analiondas and Margi

In fine grained sediments, where mechanical separation of minerals cannot be achieved, there are two approaches to determining the distribution of trace elements. First, interelement correlations may be examined using a combination of graphical and computer numerical methods. Interpretation of such interelement relationships may be difficult, if for example mineral compositions vary significantly through the samples considered, or if different mineral phases correlate positively. Secondly, selective chemical leaching may be used to separate phases. Here, problems result from uncertainties concerning the selectivity of the leaches. In this section, the

results of a leaching experiment reported by Varnavas (1980), and a comprehensive interelement correlation study undertaken as part of this project, are compared. The two methods complement each other and are most easily interpreted when taken together.

First, the results of the leaching experiment, on samples from Skouriotissa and Aliondas, are summarised. Secondly the interelement correlation study results are described and discussed.

5.4.7.1 Selective leaching studies

A direct approach to trace element partitioning is to selectively leach out mineral phases. Results can be difficult to interpret owing to uncertainty over the selectivity of the leaches, and the method has been criticised recently (Wakefield, 1980). Nevertheless constraints on element distribution can be obtained, and a comparison with the interelement correlation method is instructive and in this case lends support to both. A leaching experiment was carried out on pure umber samples from Skouriotissa and Aliondas by Varnavas (1980). Three leaches were analysed along with the residue. The leaching solutions were in order of application: acetic acid, a mixture of acetic acid and hydroxylamine HCl, and hydrochloric acid, after the method described by Cronan (1976). The acetic acid leach is used to remove carbonate and adsorbed ions, the hydroxylamine HCl to remove reduceable manganese and ferro-manganese oxides, the HCl to remove iron oxides and partial attack silicates. The residue was analysed after digestion in $HF/HNO_3/HClO_4$.

Iron was found to be chiefly in the HCl-soluble fraction, and in small amounts in the residue, the latter attributed to detrital clays.

Manganese was found predominantly in the hydroxylamine HCl fraction (73% at Aliondas and 76% in the Manganese-rich umber at Skouriotissa). At Aliondas the remainder was largely divided between the HCl-soluble, and residual, fractions. In the Skouriotissa manganese-poor umber, the manganese was mostly contained

in the HCl-soluble fraction along with the iron. This supports the observation from the interlava sediment (Chapter 4, section 4.2.5) that manganese in small quantities is contained in the iron phase.

Nickel was found mostly in the HCl-soluble and hydroxylamine HCl-soluble fractions, particularly in the former, while significant amounts are also found in the residual fraction.

Cobalt and lead were found to behave similarly. At Analiondas, and in the Mn-rich umber at Skouriotissa, they are richest in the hydroxylamine fraction, however significant amounts are also found in the HCl-soluble fraction.

Zinc and copper also behave similarly, being concentrated predominantly in the HCl-soluble fraction. At Skouriotissa, significant amounts occur also in the hydroxylamine HCl fraction.

Barium in the Mn-rich umbers was found predominantly in the hydroxylamine HCl fraction. Only small amounts occur in the HCl-soluble and residual fractions. In the Skouriotissa Mn-poor umber, the barium was observed chiefly in the residual fraction.

Aluminium was found chiefly in the HCl-soluble fraction, but also abundantly in the residual.

Calcium was found predominantly in the acetic acid-soluble fraction. Varnavas interprets this as calcite, but in view of the absence of calcite (section 5.3.2) it seems more probable that it resides in apatite. Significant, but small amounts of calcium occur in the hydroxylamine HCl-soluble fraction, and thus may be associated with the manganese phase.

Magnesium was found chiefly in the HCl-soluble and residual fractions.

These results are discussed in relation to the interelement

correlations in the following section.

5.4.7.2 Inter-element correlations - The Margi umber

The data from 47 samples of umber and clay-rich umber, are plotted on variation diagrams (Figs. 5.16, 5.17) and were submitted to a factor analysis.

Methodology

Variation diagrams. The majority of the trace elements are strongly enriched in the metalliferous sediments, and thus an association with the manganese and iron phases was assumed. Exceptions include the REE and a few others with are associated with the apatite phase. To examine the relationship of the trace elements which might be present in both the manganese and iron phases, three-element plots are used. These are in effect triangular diagrams with the vertical (trace element) axis greatly stretched. The result is a rectangular field (the base of a triangle with the basal internal angles tending to 90°), in which dilution effects are eliminated. In all cases iron is at the lower left hand, and manganese at the lower right hand, corner, with the trace element on the vertical axis. The iron has been corrected for aluminosilicate iron, (the value of which is taken from the overlying non-metalliferous bentonite (0.66 x Al). In cases where the trace element is important in the aluminosilicate fraction, a correction has also been applied.

Interpretation of variation diagrams : hazards. On the variation diagrams a linear trend might be interpreted as indicating mixing (Lever rule) between an iron phase and a manganese phase, with the slope of the line indicating the relative enrichment of the trace element in the respective phases. For example the good positive trend observed for the copper (Fig. 5.17A) might be taken to indicate the presence of a copper-enriched manganese phase, and a relatively copper-poor iron phase. However, a complication is introduced because of the positive correlation of aluminium with manganese (Fig. 5.10D). The copper plot then might be interpreted in terms of copper increasing with aluminium. This need not mean that copper is located

Fig. 5.16

a = clay-rich b = pure

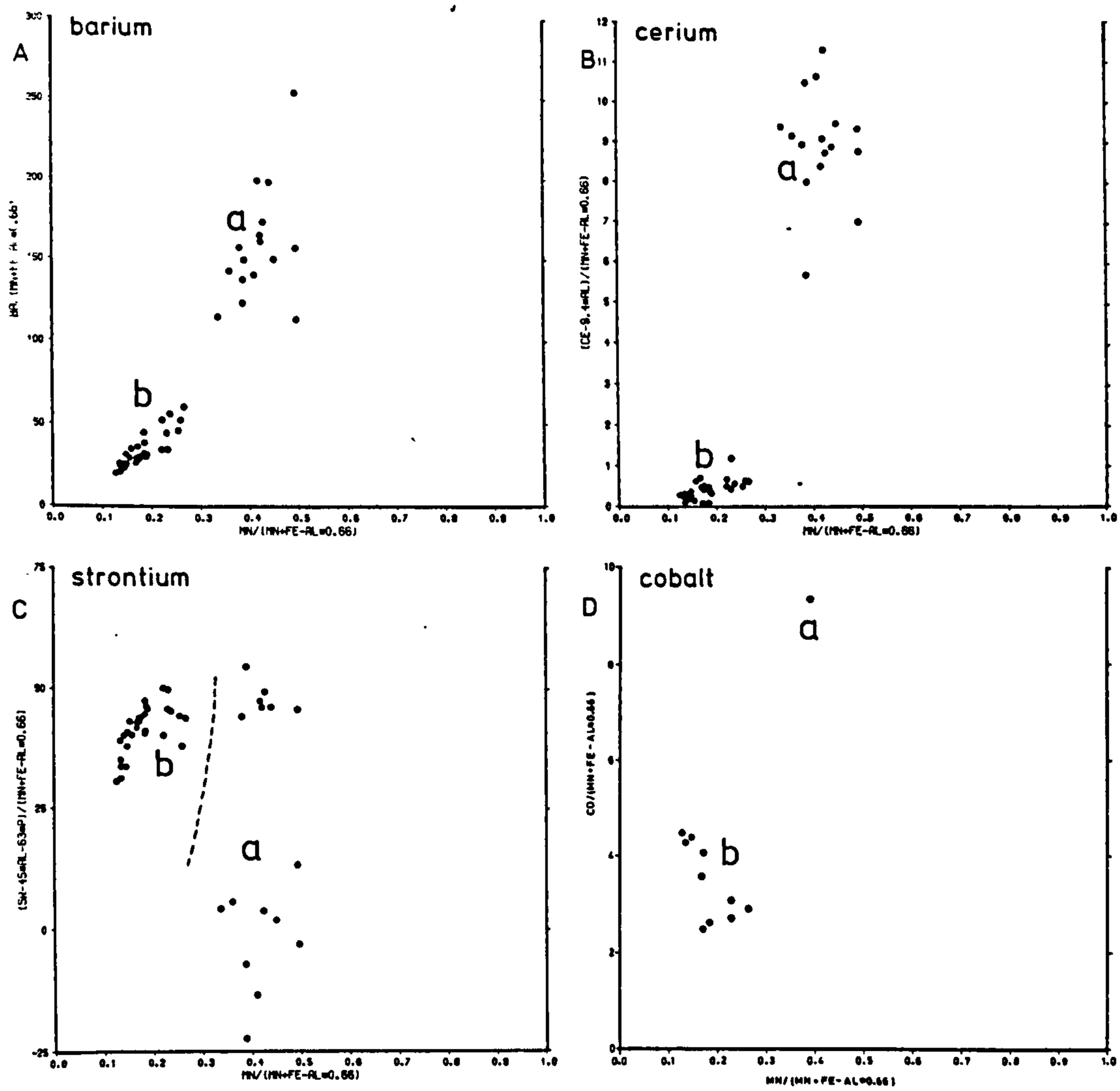

Trace element enrichment diagrams for the Margi pure and clay-rich umber. For Ba, Co and Ce, there is a greater enrichment in the clay-rich as opposed to pure umber (the clay-rich is the more manganese rich). The Sr is more variable, with some of the clay-rich umber samples depleted.

Fig. 5.17

a = clay-rich b = pure

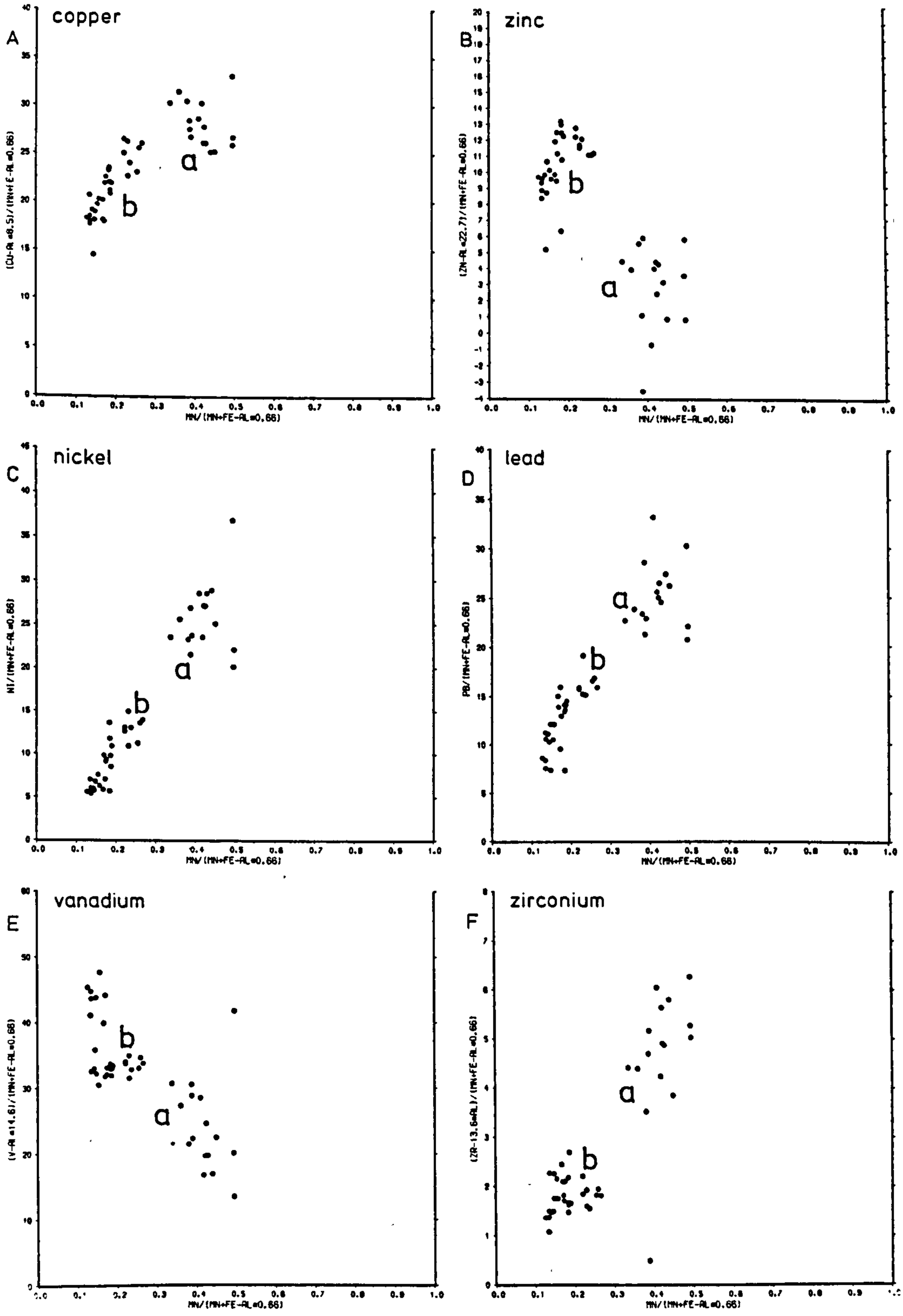

Trace element enrichment diagrams for the Margi pure and clay-rich umber. For Cu, Ni, Pb and Zr, there is increasing trace metal enrichment with increasing relative Mn, hence the clay-rich umbers are the most enriched. V and Zn show the opposite trend, though Zn shows a position gradient in the pure umber.

in an aluminosiliate phase but rather that as the accumulation rate of the sediment decreased, marked by an increasing proportion of background aluminosilicate, greater authigenic enrichment of the sediment in copper occurred. Thus the variation diagrams must be treated with caution, balancing what is observed with the leaching experiment results.

Numerical methods. Discrimination of the various factors influencing the trace element abundances is limited using graphical techniques, owing to the impracticability of handling more than three elements at a time. Computer numerical techniques in which any number of dimensions may be handled are thus useful. A factor analysis has been used to illustrate associations.

Results. The variation diagrams are presented in Figs. 5.16, 5.17. The factor loadings are presented in graphical form in Figs. 5.13, 5.14, 5.15.

Barium

	ppm
Bentonite	179 ± 40
Clay-rich umber	1117 ± 256
Upper pure umber	1382 ± 325
Lower pure umber	1001 ± 115

Ba is strongly enriched in the metalliferous sediments. In the leaching experiment study it was found to be almost entirely associated with Mn. In Fig. 5.16A Ba is plotted against corrected Fe and Mn. The strong positive correlation is in agreement with the leaching experiment. The factor analysis also shows a strong correlation of Ba with Mn in the pure umber, particularly the upper division (Figs. 5.13, 5.14, 5.15). In the lower umber Ba is also associated with the Si-Mg (palygorskite) factor. This is because of the association of very Ba rich MnO_2 with palygorskite in the veins (section 5.3.2). The clay-rich umber samples fall on the Ba rich side of the trend passing through the pure-umber (Fig. 5.16A). The

greater relative Ba enrichment may be due to an association of Ba with apatite, as indicated in the factor analysis. Probe data indicate that the discrete apatite fragments are not enriched in Ba, and the phosphatic nodule from Mangalene, likewise. Thus the Ba may still be contained in the Mn minerals, but may have its abundance controlled by the same process as for the apatite.

Cobalt

	ppm	N
Bentonite	34	1
Clay-rich umber	111	1
Upper pure umber	95 ± 3	5
Lower pure umber	158 ± 28	5

Co was determined for only twelve of the samples so a factor analysis was not attempted. In the leaching experiment Co was found to be predominantly associated with the Mn fraction, but also significantly with Fe. In Fig. 5.16D Co is plotted against corrected Fe, and Mn. In the pure umber it is most enriched in the lower unit. It is however also strongly enriched in the clay-rich umber.

Hydrogenous enrichment of Co is necessary to explain the abundance in the clay-rich umber, but in the pure umber this is apparently not the case. A hydrothermal origin is implied by the higher abundance in the basal umber, and the concentrations are similar to those in the sulphide and the ochre..

Chromium

	ppm	
Bentonite	208 ± 24	(110 ppm mean of all Bentonite)
Clay-rich umber	54 ± 8	
Upper pure umber	14 ± 3	
Lower pure umber	3 ± 6	

Cr is more abundant in the bentonite than in the metalliferous sediments. The Cr content of the lithogenous component in the umber is far lower than that in the bentonite. This is due to a Cr-Ni-Mg-rich component which appears in the bentonite. For the pure umber the factor analysis supports an association of Cr with the aluminosilicate. In the clay-rich umber the Cr is associated with factor IV along with Ce, Rb and Zr, which is interpreted as being of lithogenous origin.

The above results preclude significant hydrogenous enrichment of Cr.

Copper

	ppm
Bentonite	140 ± 37
Clay-rich umber	262 ± 59
Upper pure umber	832 ± 49
Lower pure umber	721 ± 88

Cu is strongly enriched in the metalliferous sediments. The leaching experiment identified a strong association of Cu with the Fe component, and a somewhat weaker one with the Mn. A plot of Cu (bentonite corrected) against corrected Fe and Mn (Fig. 5.17A), shows a strong positive correlation, indicating either association of Cu with Mn, or with Al. A significant association with Fe is also observed, and although this is weaker than for Mn, the greater abundance of Fe would make it the dominant carrier of Cu. The factor analysis shows an association of Cu with both Fe and Mn in the lower pure umber and the clay-rich umber, but not in the upper pure umber. There are also associations with factors containing only trace elements.

The results from the leaching and the interelement correlations are compatible if Cu is located dominantly in the Fe component, but in variable abundance, correlating with Mn, suggesting a possible accumulation rate control. A minimum abundance of Cu associated with

the Fe, found by extrapolation of the trend in Fig. 5.17A to the Fe-Cu axis, may be a measure of the original hydrothermal Cu enrichment.

Nickel

	ppm	
Bentonite	212 ± 27	(98 mean of all bentonite)
Clay-rich umber	181 ± 30	
Upper pure umber	399 ± 58	
Lower pure umber	231 ± 23	

The pure umber is only slightly enriched in Ni with respect to the bentonite, and the clay-rich umber is slightly depleted. This is because of a change in composition of the bentonite - as with the Cr- caused by the incoming of a Cr-Ni-Mg component. The bentonite elsewhere contains far less Ni.

The leaching experiment identified a strong association of Ni with Fe, and a lesser one with Mn. However the Mn phase is richer in Ni than is the Fe phase. A plot of Ni against corrected Fe and Mn (Fig.5.17C) shows a strong positive gradient, indicating the association of Ni with Mn or Al. The factor analysis does not show a strong association with either Mg or Cr. In the lower umber the strongest association is with Fe and with Cu, in the upper pure umber with Cu, and in the clay-rich umber with Fe.

Taken together with the leaching experiment data, hydrogenous enrichment of Ni, becoming incorporated into both Mn and Fe phases satisfies the observations. The strong association with Mn and with Al indicates accumulation rate control.

Lead

	ppm
Bentonite	21 ± 3
Clay-rich umber	175 ± 22
Upper pure umber	525 ± 49
Lower pure umber	382 ± 85

Pb is very strongly enriched in the metalliferous sediments, particularly the upper umber, with respect to the bentonite. The leaching experiment found that most of the Pb occurred in the Mn phase. The plot of Pb against corrected Fe and Mn shows a good positive gradient, supporting the association of Pb with Mn (Fig. 5.17D). The factor analysis shows for the lower pure umber a close association of Pb with Al and with Ce, for the upper pure umber, fairly independent, but weakly with other trace elements, and in the clay-rich umber with iron.

Incorporation of the majority of Pb in the Mn phase is probable. The factor analysis suggests that the abundance of Pb is controlled by some hydrogenous processes. The overall trend observed in Fig. 5.17D shows that the absolute enrichment of the Mn mineral is similar in both the pure and clay rich umbers.

Rubidium

	ppm	K/Rb
Bentonite	69 ± 3	228
Clay-rich umber	91 ± 16	297
Upper pure umber	28 ± 4	342
Lower pure umber	15 ± 4	350

Rb is depleted in the pure umber with respect to the overlying sediments, but it is richer in the clay-rich umber than in the bentonite. This follows very closely the behaviour of K. K/Rb ratios are not constant throughout, but decrease up section, stepping down somewhat at the contact between the pure umber and clay-rich umber. In the pure umber, the factor analysis shows the association of Rb

with K (Fig. 5.11A) however in the clay rich umber it is in a trace element factor associated with Cr, Ce, Zr. It is however quite clear that the Rb content is controlled dominantly by the abundance of K-rich minerals. Variations in the K/Rb ratio may stem from changes in the relative importance of minerals such as illite, feldspar and clinoptilolite.

Strontium

	ppm
Bentonite	475 ± 105
Clay-rich umber	483 ± 200
Upper pure umber	1702 ± 119
Lower pure umber	1572 ± 157

Sr is very strongly enriched in the pure umber relative to the bentonite and clay-rich umber. A plot of Sr (bentonite corrected) against corrected Fe and Mn (Fig. 5.16C) shows the enrichment in the pure umber but depletion in the clay-rich umber. A broad positive gradient indicate an association with Mn or Al. In the lower umber, the Sr-Mn association is apparent in the factor analysis. However, in the upper pure umber Sr is instead associated with Fe, and weakly with apatite. In the clay-rich umber, a strong association of Sr with apatite is clear. This is supported by the XRF analysis of the phosphatic nodule from Mangalene which is Sr enriched (Table 5.2). Sr association with Mn is also true of analysed Mn veins (Table 5.1), so partitioning of Sr between Mn and Phosphate phases seems plausible. This does not explain the high relative enrichment in the pure umber.

Vanadium

	ppm
Bentonite	113 ± 5
Clay-rich umber	304 ± 170
Upper pure umber	1202 ± 60
Lower pure umber	1527 ± 230

V is strongly enriched in the metalliferous sediments, particularly in the pure umber. In Fig. 5.17E, V (bentonite corrected) is plotted against corrected Fe, and Mn. There is considerable scatter, but taken as a whole there is a negative gradient, suggesting that V is associated with Fe, and is not subjected to varying degrees of hydrogenous enrichment. The factor analysis shows a strong association of V with Fe in the pure umber. In the upper pure umber it is also associated with Pb, Cu and Zn. In the clay-rich umber the association with Fe is weaker, and an association with Mg is observed.

The association with Fe is beyond question, and is the same as is observed in the interlava ferruginous sediments and the ochre (Chapter 4 section 4.2.8.2). The association with trace elements rather than Fe, in the factor analysis of the clay-rich umber, suggests that it may have been subject in part to the same enrichment processes as the other trace elements.

Zinc

	ppm
Bentonite	165 ± 11
Clay-rich umber	175 ± 21
Upper pure umber	483 ± 40
Lower pure umber	381 ± 71

Zn is strongly enriched in the pure umber, particularly in the upper part, but is not greatly enriched in the clay-rich umber. The leaching experiment found that most of the Zn was associated with the Fe fraction, but with a significant amount in the Mn component. In Fig. 5.17B Zn (bentonite corrected) is plotted against corrected Fe and Mn. Within the pure umber there is a positive gradient, but overall with the clay-rich umber there is a negative gradient. The negative gradient agrees with the leaching experiment results indicating an association with Fe. The factor analysis shows an association of Zn with Fe and with Al in the lower umber, with Fe,

Cu, Pb, Ni and V in the upper pure umber, and with Fe, and Ba, Sr and P in the clay-rich umber. This association with the other trace elements, and the positive gradient for the pure umber on the variation diagrams, suggests that hydrogenous enrichment may be important.

Zirconium

	ppm
Bentonite	102 ± 7
Clay-rich umber	120 ± 12
Upper pure umber	106 ± 10
Lower pure umber	90 ± 18

Zr is not enriched in the metalliferous sediments, with respect to the bentonite, but must however be associated with the metalliferous component. In Fig. 5.17F Zr (bentonite corrected) is plotted against corrected Fe and Mn. The positive gradient suggests an association with Mn or Al. The factor analysis shows, for the lower pure umber an association with Al, Fe, Ce and Pb, for the upper pure umber with Fe, and for the clay-rich umber with Ce, Cr, Rb. An association with Fe is also indicated by the enrichment in the Fe-rich interlava sediments. The positive gradient in the variation diagram suggests that some sort of hydrogenous enrichment is involved.

Rare-earth elements and yttrium

Lanthanum, cerium, neodymium and yttrium were analysed for all the samples. Because of the similarity of behaviour of lanthanum, neodymium and yttrium, they are discussed together. Cerium behaves quite differently and is discussed later.

	Lanthanum	Neodymium	Yttrium
Bentonite	47 ± 3	44 ± 3	55 ± 4
Clay-rich umber	102 ± 23	92 ± 19	92 ± 19
Upper pure umber	160 ± 16	107 ± 10	110 ± 15
Lower pure umber	156 ± 56	108 ± 37	106 ± 39

The La, Nd and Y are enriched in the metalliferous sediments. However unlike the other trace elements, they are strongly associated with P. Fig. 5.11D, E, F show plots against P. The correlation is best for Y but is good also for the others. Notably, the enrichment is greater for the clay-rich umbers, in La and Nd. The associations show very strongly in the factor analysis (Figs. 5.13, 5.14, 5.15).

This is in contrast with the interlava umbers from Margi-Mathiati and Kalavasos, where La, Nd and Y are associated with iron. Enrichment with P is however observed in the phosphatic nodule from Mangalene (section,5.3.2).

Cerium

	ppm
Bentonite	68 ± 3
Clay-rich umber	122 ± 12
Upper pure umber	44 ± 8
Lower pure umber	28 ± 9

Ce is significantly enriched in the clay-rich umber with respect to the bentonite. In the pure umber most but not all of the Ce can be accounted for in the lithogenous component. A plot of Ce (bentonite corrected) against corrected Fe and Mn (Fig. 5.16B) shows the small excess in the pure umber, and greater enrichment in the clay-rich umber.

The factor analysis supports the association of Ce with the aluminosilicate in the pure umber (Figs. 5.13, 5.14). In the lower pure umber Ce also occurs weakly in a factor dominated by Pb, suggesting that the weak excess over lithogenous abundances may be due to hydrogenous enrichment. In the clay-rich umber the Ce occurs

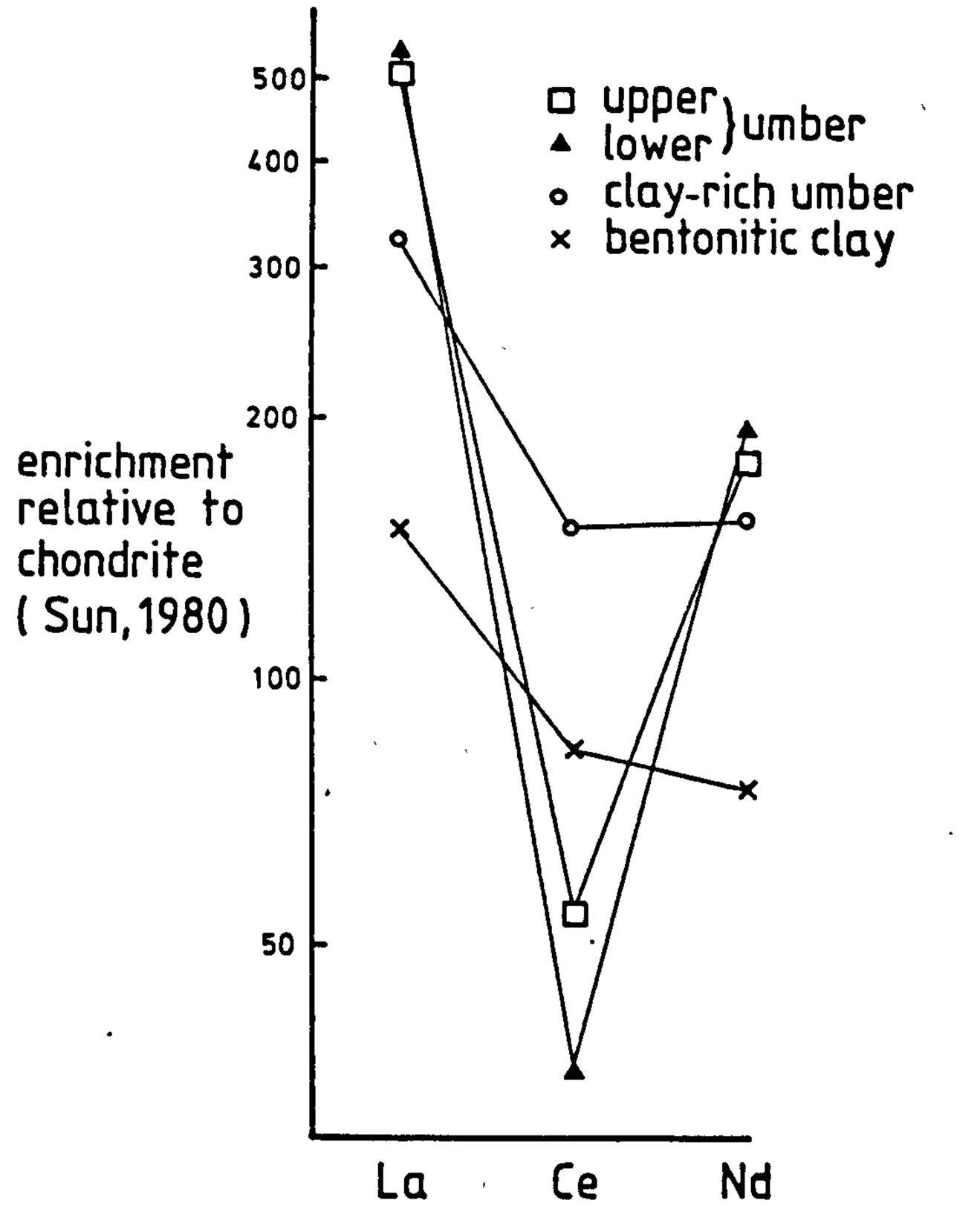

Fig. 5.18

Mean compositions of the different sediments from the Margi area, normalised to chondrite. The negative cerium anomaly, which is observed in the pure umber is characteristic of hydrothermal sediments. Slower accumulation of the clay-rich umber has resulted in greater hydrogenous enrichment, and the characteristic negative cerium anomaly, is not observed.

dominantly in a factor containing Fe. This testifies to the greater importance of hydrogenous enrichment in the clay-rich umber.

REE Discussion The contrasting behaviour of Ce is illustrated in the REE profile, normalised to chondrite (Fig. 5.18). In the pure umber there is a strong negative Ce anomaly. In the clay-rich umber the profile is also enriched but does not show a Ce anomaly. The negative Ce anomaly is characteristic of hydrothermal sediments, owing to the rapid accumulation; hydrogenous enrichment in Ce is slow. Hydrogenous metalliferous sediments have positive Ce anomalies. The clay-rich umber falls in an intermediate position, in keeping with a distal hydrothermal origin.

The results are identical to those found by Robertson and Fleet (1976) in a study of eleven light and heavy REE's. However some additional information has emerged. First, an association of REE with phosphate rather than with iron or manganese oxides is deduced, from the interelement correlations. Secondly, Robertson and Fleet (1976) observe that the abundance of Ce in the umber is controlled by the proportion of aluminosilicate present. This work supports that view, but shows in addition, for the clay-rich umber, an enrichment of Ce above that predicted from the aluminosilicate abundance. Clearly in the more slowly deposited clay-rich umbers, adsorption of Ce has occurred.

5.4.7.3 Trace elements in relation to the major element phases

In the umber at Margi, Fe increases towards the base, whereas both Mn and Al increase upwards. The covariance of Mn and Al implies that their accumulation rates were similar. If the accumulation rate of Al is considered to have been constant, then that of Mn also approximated to this, and that of Fe waned with time. The abrupt upward appearance of the clay-rich umber is accompanied by a large change in the Mn/Fe ratio, but no significant changes in Mg, Si, K,

Ti and Cr to Al ratios in the lithogenous component. On the strength of this and field evidence discussed in section 5.2.9 it is considered most likely that the appearance of the clay-rich umber resulted from a catastrophic change in hydrothermal supply, rather than a significant change in Al accumulation rates. This is not true for the termination of the clay-rich umber. In the overlying bentonite there is no sign of the hydrothermal component, and the composition of the lithogenous components is very different. Swamping of the hydrothermal component by a large increase in lithogenous supply seems to be required.

The behaviour of the trace elements in the metalliferous sediment can be considered in the framework of varying accumulation rates. Some of the trace elements increase up section. If the elements are contained in the Mn phase then an upward increase is expected (Mn increases up-section). However waning total accumulation rates may permit greater authigenic enrichment of the sediment, independent of the relative proportion of the metalliferous components. Discrimination between the two possibilities can, to some extent, be achieved by reference to the chemical partitioning observed in the leaching experiments.

The trace elements can be divided into groups according to their behaviour.

Cr, Rb. These show no enrichment in the metalliferous components. Rb is greater in the clay-rich umber than in the bentonite owing to the difference in the K content of the lithogenous component.

Cu, Zn, V. These all show an association with the Fe component. Zn and V are strongly enriched in the pure umber with respect to the clay-rich umber. Zn shows a tendency to be hydrogenously enriched in the pure umber being greater in the upper part. Cu is included with these in spite of its upward increasing abundance and its enrichment in the clay-rich umber, because extrapolation of the enrichment trend (Fig. 5.17A) shows a significant initial Cu/Fe ratio.

The significance of this association with the Fe phases is discussed in section 5.5.5.

Cu, Ni, Pb, Zr. These all give trends in the variation diagrams indicating similar relative enrichment in both the pure- and clay-rich-umbers. The positive gradients indicate association either with the Mn component or the Al (accumulation rate control)

Ba, Ce, Co. These elements have variable behaviour in the pure umber. Ba gives positive gradient, Co a negative, and cerium is depleted. They all however show much greater relative enrichment in the clay-rich umber than in the pure umber.

La, Nd, Y. These elements are all enriched in both the pure- and clay-rich umber, but are associated with the phosphate phase.

Sr behaves anomalously. The trend is similar to Zn, but the factor analysis shows that an association with Fe is unlikely.

5.4.8 Isotope geochemistry

The isotopic compositions of oxygen, strontium and lead have been determined by various workers. Conclusions which can be drawn from this work are discussed below. Hydrogen isotopes have also been examined, but were found to be very unstable, rapidly re-equilibrating under experimental conditions (Heaton, 1977).

Oxygen isotopes. The oxygen isotopic composition of interlava sediments, ochres and umbers were determined by Heaton (1977). They are all found to lie on a mixing line between smectite and hydrogenous ferromanganese nodule abundances. It was concluded that all, had equilibrated with cold Cretaceous sea water. This is compatible with either direct precipitation of iron oxide from dissolved hydrothermal ferrous iron, or oxidation of particulate

sulphide.

A $\delta^{18}O$ determination for one of the Margi umbers (sample 81-158 $\delta^{18}O$ = 10.4, analysed by Dr. H. Friedrichson, Tübingen) falls on the same trend.

Strontium. The initial strontium isotope ratio for the umbers of 0.7079 ± 0.0013 is indistinguishable from Cretaceous ocean water (0.7076 ± 0.0006) Gale et al., (1980). Thus the strontium in the metalliferous sediments has been derived from seawater.

Pb isotopes. The lead isotopic ratio falls between the Troodos lavas (similar or slightly less radiogenic than MORB. Spooner and Gale, 1982) and modern hydrogenous ferromanganese nodules (Gale et al., 1980). Of the analysed samples Skouriotissa gave the least radiogenic values (most similar to the lavas) and Dhrapia the most (falling in the field of modern manganese nodules). Gale et al. (1980), conclude that primary adsorption from mixed hydrothermal solutions and seawater account for this range,and that diagenetic modification has not occurred. The argument in support of this veiw is that there is a negative correlation of Pb/Fe with radiogenic enrichment. However, in view of the stronger association of Pb with manganese than with iron (section 5.4.7.2) the argument is invalid. Unfortunately neither manganese nor aluminium values are quoted, so it is not possible to test directly the alternative hypothesis. The general inverse correlation of manganese and aluminium, with iron, does however suggest that a correlation between these and the degree of radiogenic enrichment may exist. If this is the case then the radiogenic character of the Dhrapia deposit, which is rich in iron and contains little lead, contrasting with the unradiogenic Skouriotissa samples, suggest that the isotopic composition of the iron component is variable. This would support one of the conclusions of Gale et al. (1980) that variable mixing of sea water and basalt derived lead had occurred in the hydrothermal vents.

5.5 DISCUSSION

In the following section various models for the origin of the umbers are discussed. Before proceeding to this, a brief review of possible modern analogues is given.

5.5.1 Modern oceanic metalliferous sediments

Cronan (1980), in a review of mid-ocean ridge metalliferous sediments, subdivides them into two general varieties. These are the widespread dispersed background deposits accumulating over large areas of the mid-ocean ridges, and anomalous deposits superimposed upon them in certain small areas.

Widespread mid-ocean ridge metalliferous sediment

Most mid-ocean ridge sediments, and basal sediments (presumably formed at past mid-ocean ridges) are characteristically dark-brown fine-grained seemingly amorphous sediments. The deposits are usually mixed or interbedded with calcium carbonate, having accumulated above the carbonate compensation depth. They contain anomalous abundances of cobalt, copper, lead, molybdenum, nickel, silver and zinc. Their mineral constituents include grains and globules of iron oxides a few tens of microns in diameter, together with micro-manganese nodules, biogenic remains, fragments of submarine volcanic rocks and their alteration products such as palagonites and zeolites, and clay minerals. The older, basal, sediments contain goethite rather than amorphous iron oxide, but are otherwise very similar to their younger counterparts.

Both in terms of the mineral constituents, and chemical composition, there are striking similarities with the umbers (section 5.5.8). Absence of calcium carbonate in the Cyprus umbers is the most important difference, resulting probably from a difference in the carbonate compensation depth (section 2.2).

The metalliferous sediments are both most abundant, and richest on the East Pacific Rise, though they occur elsewhere, for example on

the Mid Atlantic Ridge (Cronàn, 1972). This variation in abundance between different ridges has been attributed to differences in spreading rate Boström et al. (1976). Using data from the Pacific, Atlantic and Indian oceans, Boström et al. (op. cit.) obtained a good correlation between spreading rate and (Fe + Mn)/Al, the latter being an index of metalliferous enrichment.

The similarity in Fe/Mn ratio of the East pacific Rise 21°N high temperature hot springs fluids to that of the widespread crestal sediments argues for a genetic relationship (Edmond et al., 1982).

Anomalous metalliferous sediments

Superimposed upon the more normal metalliferous sediments are sometimes found very localised variations in composition. Information accumulated to date indicates that these deposits are scarce and of very localised extent. Among these deposits are the iron-rich deposits from Amph. 2D (Bonatti and Joensuu, 1966), manganese-rich sediments from the the crest of the Mid-Atlantic Ridge at 26°N (Scott et al., 1974; Rona, 1976), the nontronite-manganese oxide associations from the axial valley of the Gulf of Aden, the FAMOUS area, and the Galapagos Mounds (Cann et al., 1977; Hoffert et al., 1978; Corliss et al., 1978) and the sulphide deposits in the Gulf of California (Lonsdale, 1978), on the East Pacific Rise (Francheteau et al., 1979) and at the Juan de Fuca Ridge (Normark et al., 1983).

These all involve extreme fractionation of iron and manganese, and the oxides are characterised by extremely low trace metal abundances. There are similarities between the manganese deposits, and manganese veins found in the upper lavas of the Troodos ophiolite (section 5.5.3), but they are completely different from the umbers.

Affinities of the umber

The umber is very similar in composition to the East Pacific Rise crestal and basal sediments (Section 5.5.8) if the latter are calculated on a carbonate-free basis. They also occupy an identical position in the stratigraphy. However there are some important

differences: the umbers are not homogeneously distributed and show sharp upper contacts with less metal enriched sediments (section 5.2.9). The localised occurrence of the umbers has led to their interpretation as "anomalous" deposits accumulated close to small lower temperature hydrothermal vents (Robertson, 1975; Soler et al., 1982). However, their chemical composition clearly allies them with the dispersed, more slowly accumulated, crestal type sediments. Any interpretation of their origin must account for the differences in the spatial associations.

5.5.2 Models for the origin of the umber

A number of distinctly different interpretations have previously been suggested to explain the occurrence of the umber. Before discussing their relative merits, some constraints issuing from field relations and chemical characteristics are summarised.

1) In areas of metalliferous sediment enrichment there is a complete continuity of occurrence of such sediments through the extrusive sequence. Further, there is continuity also in the composition of constituents within the sediment (section 5.5.5). Several of the earlier models were influenced by the erroneous belief of a separation in time and space of eruption of the Upper Pillow Lavas from the remainder of the complex.

2) The individual umbers, though differing in some details, show only small chemical variations, and within each deposit are likewise nearly homogeneous. There is no evidence of extreme chemical fractionation. The abundance of lithogenous material within the umbers, also shows little variation, suggesting that accumulation occurred steadily. The proportion of this component, generally comprising 20-30% of the rock suggests that accumulation was not only steady but also quite slow (only 3-5 times faster than the background pelagic sediment).

3) There is a close similarity in chemical composition with the widely dispersed East Pacific Rise crestal sediments.

Suggestions that the umbers originated by slow weathering of the lavas (Constantinou and Govett, 1972; Lapierre, 1972) are incompatible with both the composition of the umber and continuity of occurrence through the lava pile.

Formation through direct interaction of sea-water with hot basalt (Elderfield et al., 1972), is compatible neither with the duration of steady accumulation which is observed, nor the localisation of the sediments in areas of peculiarly high enrichment. It is also probably an inadequate mechanism to account for the abundance of metalliferous sediment.

Models involving local accumulation from low temperature hot springs, are compatible with the distribution of the sediments, and can be reconciled with the continuity of occurrence through the lava pile. However, it is difficult to explain the duration of steady accumulation, and the absence of extreme chemical fractionation, which is characteristic of modern low-temperature deposits (Section 5.5.1).

The various attempts to relate the umbers to formation of the sulphides at axial high temperature hot springs (Corliss et al., 1972; Pantazis, 1973; Searle, 1973; Williams, 1973; Hutchinson, 1975), were based on trace element composition, analogy with other mining areas and on theoretical grounds. There was no attempt to explain fully the spatial association of the umbers with the sulphide ores.

The conclusion from this work is that the latter hypothesis is correct, and a model for the origin is proposed, after discussion of various aspects of the composition and origin of the constituents of the umber.

5.5.3 Variations in trace element enrichment in the manganese phase:- The origin of the manganese

From the study of interelement ratios in the Margi umber and the chemical partitioning (Varnavas, 1980), elements which have been enriched by hydrogenous processes have been identified. These include Ba, Ce, Co, Cu, Ni, Pb, La, Nd and Y. Variations in the abundances of these elements should yield information concerning rates of accumulation. La, Nd and Y, which are associated with the phosphate mineral are discussed in the next section.

Composition of the Manganese Phases - Skouriotissa and Analiondas

The trace element composition of the manganese phase can be calculated directly from chemical partitioning data of Varnavas (1980). The compositions are presented in Table 5.10. where they are compared with average compositions of hydrothermal and hydrogenous iron and manganese crusts from the modern oceans. The difference from hydrothermal crusts is striking: the Cyprus manganese phase being far more enriched in lead, cobalt and barium. They are not so trace element enriched as the mean hydrogenous crusts, but they do fall into the range of enrichment of these more slowly accumulated deposits. Thus for the manganese fraction of the Skouriotissa and Analiondas deposits, a considerable degree of hydrogenous enrichment has occurred. How does this compare with other umber deposits in Cyprus?

Inter-deposit variations in enrichment

Of the trace elements which are influenced by hydrogenous processes, barium, nickel and lead are those which from the Margi data, seem least variable, and are least influenced by initial enrichment in the iron component (section 5.4.7.3). The relative enrichment of these elements, for which the trace element/(corrected iron + manganese) ratio is taken as a measure, is shown in Table 5.11. It can be seen that of the three elements barium is the most variable, though the overall trend is similar to that of nickel and

TABLE 5.10

COMPOSITION OF THE MANGANESE COMPONENT OF THE SKOURIOTISSA AND ANALIONDAS UMBERS.

The umber data have been arbitrarily scaled to Fe+Mn = 40 to make them visually comparable with the modern examples.

			---------- Modern ocean data ----------			
	Analiondas	Skouriotissa Mn-rich	Hydrothermal-crust* Mn-rich	Fe-rich	Hydrogenous* crusts	Hydrogenous* nodules
Fe	7.72	10.93	0.18	25.04	21.65	17.81
Mn	32.28	29.07	46.01	9.54	10.80	22.04
Al	0.19	0.38	0.13	0.38	2.16	1.31
Ca	0.50	0.32				
Mg	0.80	0.31				
Ni	343	452	642	214	1695	6248
Co	697	378	19	81	1214	3732
Pb	643	718	10.0	24	525	1141
Zn	161	154	1030	154	565	1173
Cu	187	651	321	190	711	3463
Ba	7855	3124	382	343	1395	2243

Lead/Manganese ratios for different metalliferous sediments.

Margi	Clay-rich umber	0.0060
Skouriotissa	Clay-rich umber	0.0048
Kalavasos	Clay-rich umber	0.0048
Margi	upper umber	0.0073
Margi	lower umber	0.0069
Kambia		0.0051
Skouriotissa		0.0024
Analiondas		0.0019
Mathiati		0.0017
Dhrapia		0.0017
Kalavasos Interlava umber		0.0015
Margi-Mathiati Interlava umber		0.0014
Average hydrogenous nodule*		0.0052
Average hydrogenous crust*		0.0049
Average Hydrothermal crust*		0.00002

Ce/(Fe + Mn)

Margi clay-rich umber	0.0008
Mean hydrogenous nodule*	0.0019
Mean hydrogenous crust*	0.0017
Mean hydrothermal crust*	0.000004

*Data from Toth,(1980)

Table 5.11

RELATIVE ENRICHMENT OF UMBERS IN BARIUM, LEAD AND NICKEL.

Clay-rich umbers	Fe + Mn	Traces x 10^4 Ba / Fe + Mn	Ni / Fe + Mn	Pb / Fe + Mn	Al wt%
Margi	6.98	160.1	19.5	25.1	6.59
Skouriotissa	10.19	26.1	7.9	16.5	6.43
Kalavasos	5.72	21.5	13.8	21.9	6.06
Pure umbers					
Margi upper	37.18	37.2	10.7	14.1	2.83
Margi lower	39.09	25.6	5.91	9.77	1.91
Kambia	33.86	9.9	8.42	14.1	3.05
Skouriotissa	33.37	31.9	9.35	6.08	2.25
Analiondas	45.71	41.7	6.37	3.63	1.47
Mathiati 1	43.57	76.4	6.45	2.82	1.12
Mathiati 2	39.70	17.8	5.42	5.16	2.74
Dhrapia	38.77	3.12	3.43	2.42	1.15
Interlava umbers					
Margi-Mathiati	35.42	2.77	7.34	2.77	3.66
Kalavasos	30.85	5.45	4.67	4.05	4.21

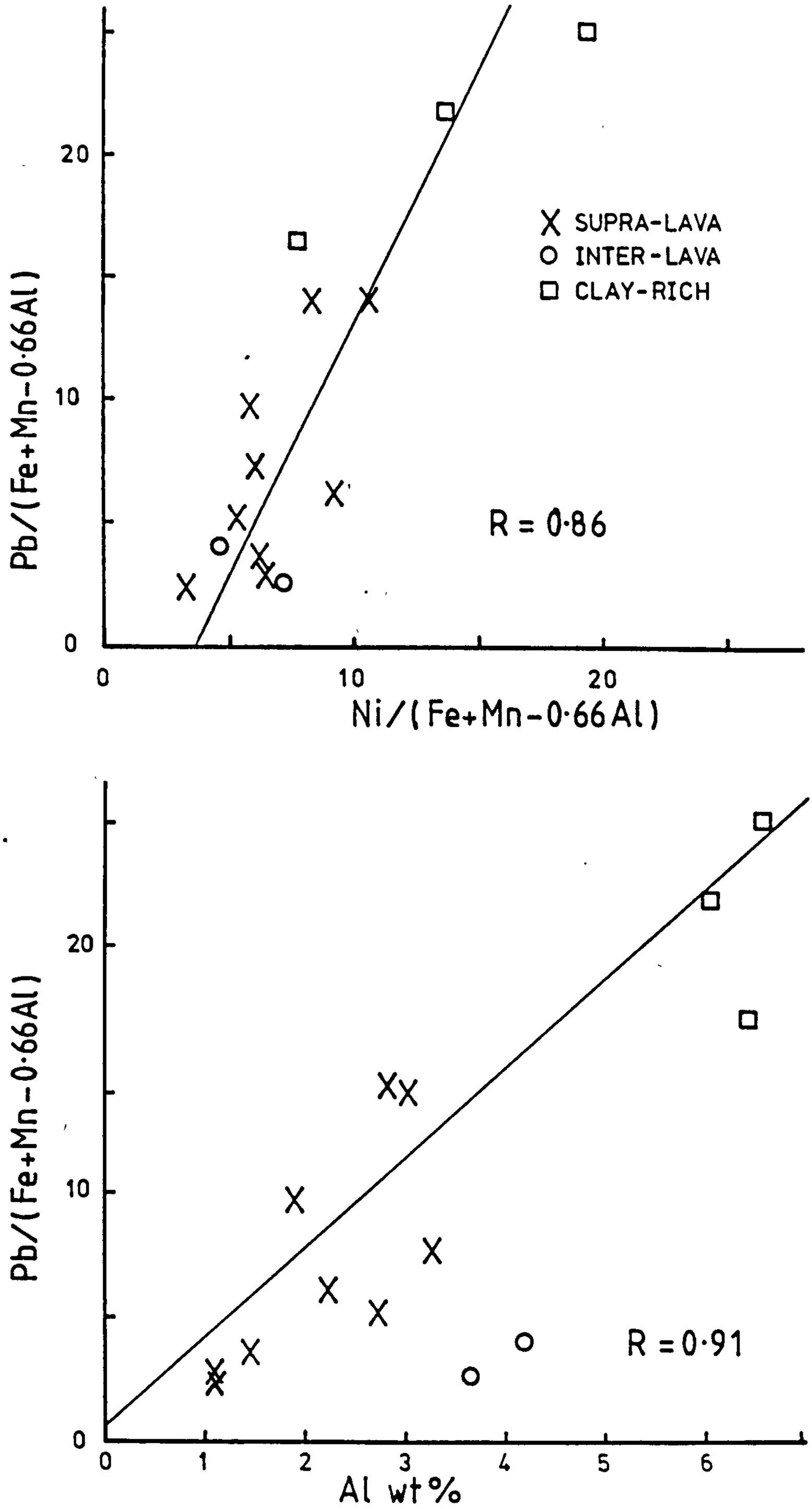

Fig. 5.19

Symbols indicate the mean composition of different pure and clay-rich umber localities. a) Shows the correlation of lead and nickel enrichments. b) Shows the correlation of lead enrichment with total aluminium concentration.

lead. A plot of nickel enrichment against lead enrichment for the different localities gives a good correlation (Fig. 5.19). (R = 0.86) for all the locality means. A common and consistent enrichment process is implied. If the rate of accumulation of aluminium approximates to a constant, and the lead enrichment is inversely proportional to accumulation rate, then a positive correlation of total aluminium and lead enrichment is expected. This is indeed the case (Fig. 5.19), with the exception of the interlava sediments in which the lithogenous supply is quite different and probably more rapid (Chapter 4, section 4.3.2). The extremely good correlation (R = 0.91) lends support to the above contentions. Even allowing for some variation in the accumulation rates, a hierarchy can be proposed in which the interlava umbers are most rapidly accumulated and the clay-rich umbers most slowly. Of the pure umber deposits, using these criteria, Dhrapia would be the most rapidly deposited, followed by Analiondas and Mathiati, then by Skouriotissa, Mangalene and the lower part of the Margi umber, with the upper Margi umber and Kambia most slowly deposited.

5.5.4 Trace element enrichment of the phosphate

The phosphate present in the umber at Margi, and in the phosphate concretion from the Mangalene deposit, is a francolite (section 5.3.2). This is strongly enriched in La, Nd, Y and Sr. The enrichment in these elements is not however constant. From the Margi whole rock chemical data, element/phosphorous ratios can be calculated, and compared with those from the Mangalene phosphatic nodule (Table 5.12). It can be seen that the phosphate in the clay-rich umber is significantly more enriched than that in the pure umber, which is again enriched over that in the Mangalene nodule. Further, the interlava umbers from Margi-Mathiati, and Kalavasos, failed to show an association of these elements with the phosphate; Y, La and Nd abundances in the deposits were lower than would be predicted from the above ratios. Thus, although less data are available, what exists does show the same hierarchy of enrichment as

TABLE 5.12

YTTRIUM- AND REE- PHOSPHATE RATIOS

	Y/P	La/P	Nd/P
Mangalene*	0.0067	0.0092	0.0069
Margi pure umber**	0.0192 ± 0.0053	0.0179 ± 0.0077	0.0080 ± 0.0062
Margi clay-rich umber	0.0163 ± 0.0074	0.0232 ± 0.0061	0.0206 ± 0.0045

* Phosphatic nodule. Ratios taken directly from XRF data
** Derived from whole rock data by classical linear regression treating the trace elements as variables dependent on phosphorus.

is observed for the manganese related trace elements. This argues in favour of an accumulation rate influenced authigenic enrichment process. This has been argued as the cause of REE enrichment of phosphatic remains in deep-oceanic sediments (Arrhenius and Bonatti, 1965).

5.5.5 The iron-rich component : composition and origin

The evidence against a local low-temperature vent origin for the umber is outlined in section 5.5.2. There are two compelling observations. First, the iron profile at the Margi umber shows a steady decline of iron over a distance of 2.5 m. This intervals comprises approximately one third lithogenous component. Even allowing lithogenous accumulation rate an order of magnitude greater than normal pelagic, a duration in the order of 10000 years is obtained. During this period there is very little local variation in concentration; the iron source was clearly quite stable. Modern oceanic low temperature hot springs are characterised by variable, and extreme fractionation of, iron and manganese. In contrast the basal EPR metalliferous sediments, comprising material transported from the ridge, are more constant. Secondly, the composition of the iron component is very similar to that in the interlava sediments, which are themselves gradational with those ochres which were undoubtedly derived by oxidative erosion of sulphide ore (section 4.3.1). The arguments concerning the composition are expanded below.

Composition of iron component

Whereas the manganese phases and the phosphate are extremely variably enriched in trace elements, showing systematic trends up section, the iron component is fairly constant. Of the compositions shown in Table 5.13, the most variable elements, are barium and copper. Some diagenetic enrichment in barium of the iron cannot be ruled out, and may account for the variation. Variability of copper content is a characteristic of the pure ochre, and is attributed to primary variations in the source sulphides (Constantinou and Govett, 1972). The copper content of the interpillow oxide sediments is also

TABLE 5.13

COMPOSITION OF THE IRON COMPONENT

	Chemical partitioning study Varnavas (1980)			Inter-element correlation study		Mean Ochre
	Analiondas	Skouriotissa Mn-rich	Skouriotissa Mn-poor	Margi pure umber	Mean interlava oxide	
Fe	32.16	31.57	43.46	35.00*	35.00*	45.82
Mn	1.07	2.03	1.29	-	0.97	0.94
Si	-	-	-	2.42	-	-
Al	1.05	1.21	1.45	0.91	-	2.62
Ca	0.05	0.08	0.03	-	-	-
Mg	0.73	0.44	0.48	0.46	-	-
Ti	-	-	-	0.042	-	-
Ni	166	182	249	-	161- 221	207
Co	26	33	99	-	-	110
Pb	18	34	139	-	14- 21	180
Zn	261	263	354	385	263- 333	535
Cu	759	1265	5334	350	175-2765	3077
Ba	258	995	15	-	42-70	105

* Arbitrary iron value from which to calculate abundances given trace element ratios.
- Not determined

extremely variable, with a range covering that of the ochres. The Skouriotissa umber has particularly high copper contents and this is matched by both the ochre and sulphide (Constantinou and Govett, 1972; Robertson, 1976a). The similar trace element assemblage of the ochre and the iron components of the other sediments argues in favour of a common source.

The significant association of silica, aluminium, magnesium and titanium, in remarkably constant proportions, with the iron component in the Margi umber is important. A similar association is also observed in the Analiondas and Skouriotissa deposits. In these, as in the interlava oxide sediments (including the ochres) a small but significant proportion of manganese is found associated with the iron phase. The agreement between the chemical leaching, and the interelement correlation data suggests that the elements are incorporated in the iron oxide phase. Possibly selective adsorption of sea water has occurred.

Origin of the Iron component

A hydrothermal origin for the iron component is indisputable, however the exact form of this source is uncertain. Ferrous iron emerging from the vents undoubtedly formed sulphides, and this locally oxidised to produce the ochre. However it is possible that iron escaped fixing into sulphides and was released into the water column where direct oxidation could occur. This question has been addressed concerning the modern Pacific hot springs. In high temperature hot springs, there is a considerable excess of H_2S over Fe^{2+}, and it seems that vented iron is all in the form of fine particulate sulphide (Edmond et al., 1982). In Cyprus all that can be said is that the constancy in trace element composition of the iron component argue for a single source. As some of this, in the erosive ochres, is directly derived from sulphide, it seems probable that all the remainder is as well.

5.5.6 Origin of the Lithogenous component

For the bulk of the supralava sediment, the major element ratios

and the mineralogy indicate that the lithogenous component resembles the bentonitic clay found overlying the umbers (sections 5.3.2, 5.4.6). Only the interlava umbers and the basal parts of some of the supralava umbers contain locally derived basaltic detritus. The origin of the bentonitic component is discussed in Chapter 6, section 6.5.1).

5.5.7 Diagenesis

The metalliferous sediments have not been deeply buried. Along the northern margin several hundred metres at most are required to explain the observed compaction (section 5.2.6). In the south west, beneath the Kannaviou Formation, thicknesses nearer 1 km are possible (Robertson, 1977c). Diagenetic alteration of the sediment is restricted to accumulation of francolite, transformation of amorphous hydrated iron oxide to goethite, formation of palygorskite, and locally clinoptilolite, and silicification to produce chertified umber.

Formation of Goethite

The modern oceanic metalliferous sediments of the East Pacific Rise crestal type are predominantly amorphous (Dymond et al., 1973; Cronan, 1976). Small quantities of goethite are present in the Bauer Deep sediments, but most of the iron is amorphous (Ekland, 1974). On the other hand, in the basal metalliferous sediments from the Pacific, goethite is more abundant (Dymond et al., 1973). The Cyprus metalliferous sediments contain goethite as the sole iron phase. Although there is no direct evidence that this was originally amorphous, it is probable that this was the case, and that goethite formed with ageing. There is no evidence that this transformation resulted in alteration of the trace element abundances.

Iron-smectite

In the Bauer Deep sediments iron-smectite, an Al poor nontronite, is abundant (Bischoff, 1973; Dymond et al., 1973). It has been argued that the smectite forms through reaction of amorphous

iron oxide with biogenic silica (Heath and Dymond, 1977). Nontronite has not been detected in any of the Cyprus metalliferous sediments - in all cases considered the iron is completely accounted for by goethite and lithogenous material (section 5.3.2).

Francolite

Fragments of ostracod cuticle, and sharks teeth in the sediments are composed of francolite, but cannot account for the total phosphate enrichment. Locally, nodular concretions are observed, and more abundantly, layers occur within the umber which are strongly enriched in phosphate (P up to 10%). Clearly diagenetic mobilisation of phosphorus has occurred. A mechanism for original enrichment is suggested from the observation by Berner (1973) that the East Pacific Rise metalliferous sediments are enriched in phosphorus. There, the phosphorus correlates with iron, and adsorption of phosphorus by amorphous iron oxides is postulated as a mechanism. In the umbers a correlation of phosphorus with iron is not observed, but instead the good correlation of the former with calcium suggests that it is all in the form of apatite (variety, francolite). Possibly, phosphorus was originally enriched through adsorption onto iron oxides, but during diagenesis this was remobilised and accumulated locally as francolite. The form of the apatite bearing fragments in the phosphate rich layers, suggests that lava fragments rich in calcium may have constituted sites of secondary francolite formation. The high yttrium and REE content of the francolite (section 5.4.7.3) suggests that diagenesis was sufficiently early to permit incorporation of sea water elements into the phosphate. Increasing trace element enrichment with decreasing accumulation rate (section 5.5.3) also supports an early diagenetic origin; the phosphate in the more slowly accumulated sediment having access to seawater for longer periods.

Palygorskite and Clinoptilolite

In addition to veins of palygorskite which occur in the umber and the uppermost lavas fine needles of this are found throughout the umber and overlying sediments. A discussion of the possible origin

of this mineral is given in section 5.3.2. It was concluded that an early diagenetic origin is most likely, owing to the silica-rich character of the sediments, and the readily available source of magnesium. It is not clear whether elevated temperatures are required.

Clinoptilolite has only been found in one umber deposit; the Mangalene umber near Parekklisha. A diagenetic origin for this mineral is probable (Chapter 6, section 6.5.6). The necessary conditions for the formation are not dissimilar to those for the palygorskite, but it is favoured by lower Mg^{2+} activities. Its presence in only the one locality, and its abundance in the overlying non-metalliferous sediments indicates that conditions were generally unsuitable. Possibly higher Mg^{2+} activities existed favouring the formation of smectite and palygorskite (Chapter 6, section 6.5.6).

Silicified Umber

Textural evidence suggests that the nodular siliceous umber was formed very early (section 5.2.6). The chemical composition of two examples from the Margi umber are compared with unsilicified umber from the same locality (Table 5.14). Chemically they are strongly enriched in silica, and depleted in all other elements. Some fractionation has occurred as the depletions have not been uniform. The depletions are illustrated in Fig. 5.20, showing the two samples normalised to the mean umber. Sample 81-93 is clearly enriched in phosphate compared with the mean, which is probably primary variation. The higher strontium in this sample may also be related to this. Lead and nickel are particularly low and the REE and yttrium are high.

The oxygen isotope composition of the sample 81-93 is $\delta\,^{18}O$ = 30.5 $\pm$ 0.15°/•• (Analysed by Dr. H. Friedrichson, Tübingen). The problems with obtaining temperature values from low temperature silica minerals using oxygen isotopes are discussed by Knauth and Epstein (1975). They consider that extrapolation of experimental curves to temperatures as low as 0-30°C is unreasonable, and instead

TABLE 5.14

CHEMICAL COMPOSITION OF SILICIFIED UMBER

	81-93	91-171	Mean lower umber	Divided by mean umber 81-93	81-171
Si	36.77	35.99	7.93	4.64	4.54
Al	0.24	0.44	1.91	0.126	0.230
Fe	6.91	9.33	33.54	0.206	0.278
Mg	0.16	0.51	1.31	0.122	0.389
Ca	1.96	0.57	2.49	0.787	0.229
Na	0.07	0.02	0.14	0.411	0.118
K	0.06	0.10	0.51	0.118	0.196
Ti	0.02	0.02	0.09	0.222	0.222
Mn	1.73	1.29	5.55	0.312	0.232
P	0.69	0.20	0.84	0.821	0.238
Ba	433	199	1001	0.433	0.199
Ca	160	200	721	0.222	0.277
La	59	51	156	0.378	0.327
Nd	39	37	108	0.361	0.343
Ni	61	39	231	0.264	0.169
Pb	38	40	382	0.099	0.105
Sr	510	349	1572	0.324	0.222
V	293	363	1527	0.192	0.237
Y	46	44	106	0.434	0.415
Zn	82	101	381	0.215	0.265
Zr	12	19	90	0.133	0.211

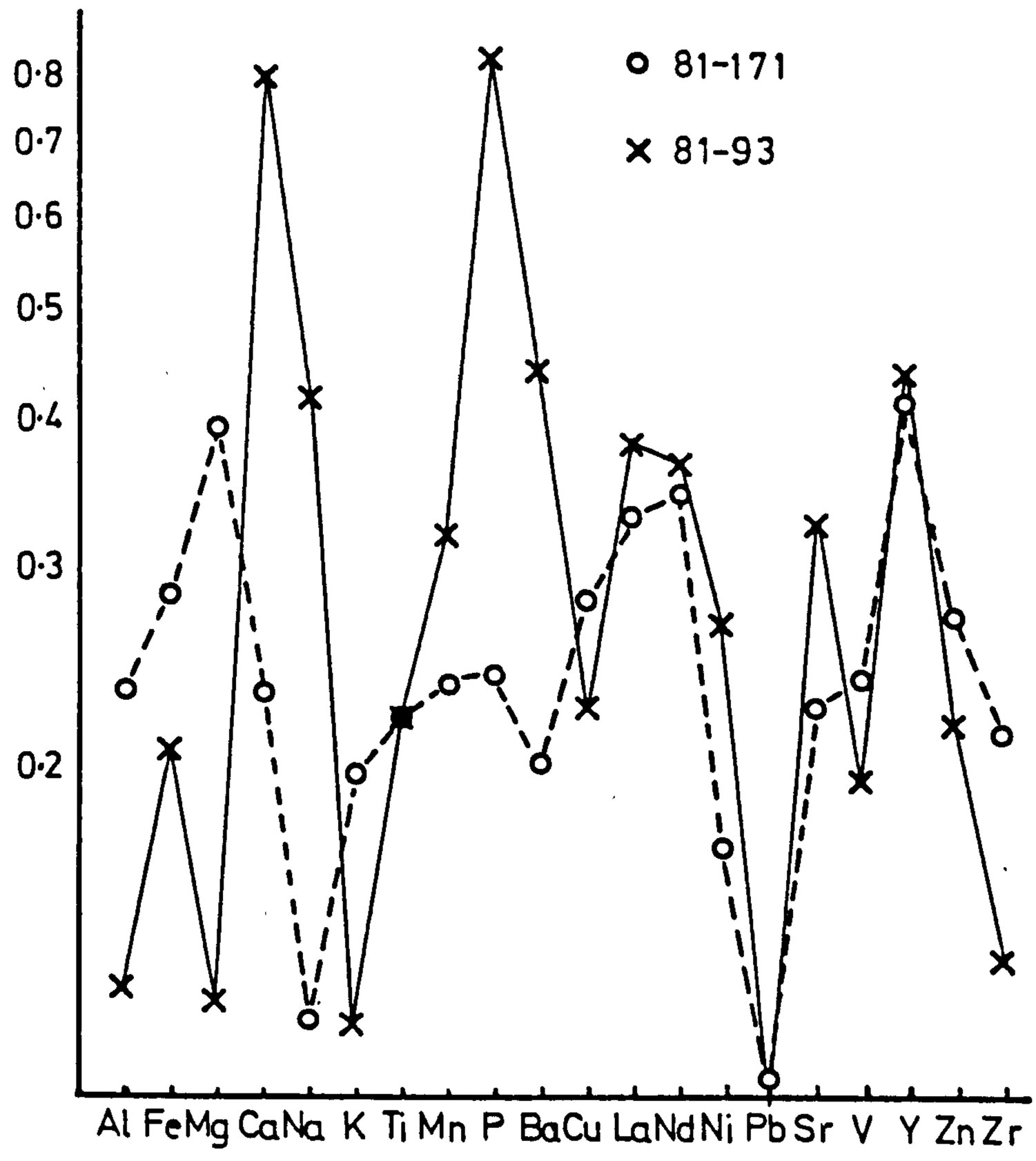

Fig. 5.20

Two analyses of silicified umber from Margi, are normalised to mean non-silicified Margi umber. The phosphate enrichment in 81-93 is probably a primary variation. However the other differences are likely to represent differential alteration upon silicification.

selected their most enriched sample and arbitrarily chose a temperature of 0°C for this. By using this $\delta^{18}O$ value of 39.0 °/•• as zero, assuming that $\ln\alpha \propto 10^6T^{-2}$, and assuming $\delta^{18}O$ = -1°/•• for Cretaceous sea water (Heaton and Sheppard, 1977), temperatures may be obtained. Firstly, though, the $\delta^{18}O$ value of the quartz must be estimated. The sample 81-93 contains 78% quartz and 22% residual umber (based on XRF analysis). Unsilicified umber has a $\delta^{18}O$ value of 10.2°/••. Correcting using this value gives a $\delta^{18}O$ for quartz of 36.2°/•• corresponding to a temperature of 6 $\pm$ 0.6°C.

From the textural and isotope data a low-temperature, shallow burial depth origin for the chert is most probable. Where the silica came from, and why it should now be present in massive nodules, is a matter for conjecture. The small amount of radiolaria, and the silica-rich lithogenous component may answer the first question.

5.5.8 Comparison with modern metalliferous sediments

The East Pacific Rise metalliferous sediments comprise grains or globules of iron oxide, micromanganese nodules, biogenic remains, including fish debris, fragments of submarine volcanic rocks and their alteration products, and clay minerals (Dymond et al., 1973; Cronan, 1976). The older basal metalliferous sediments, formed at the spreading centre in the past, are similar but contain goethite rather than amorphous iron oxides (Dymond et al., 1973). The Cyprus umbers are strikingly similar to these both in terms of mineralogy and chemical composition (Robertson and Hudson, 1973). There is no doubt that the sediments share a closely similar origin. There are however differences both in composition and distribution. Various aspects of the similarities and dissimilarities are discussed below.

Metalliferous component composition

Work on interelement correlations and trace element partition studies in EPR sediments show that although on the broad scale Fe and Mn are closely associated, they occur in separate phases (Cronan, 1976). Trace elements are variably partitioned between the phases. For example Ni and Co are strongly associated with the manganese

TABLE 5.15

COMPOSITION OF UMBERS COMPARED WITH EASTERN PACIFIC SEDIMENTS

	EPR *	Pure Umber	Clay-rich umber	Normalised to EPR: Pure umber	Normalised to EPR: Clay-rich umber
Fe	18.0	30.89	8.82	1.72	0.49
Mn	6.0	7.03	3.01	1.17	0.50
Ba	ND	1071	502		
Cu	730	846	299	1.16	0.41
Ni	430	254	139	0.59	0.32
Zn	380	361	278	0.95	0.73
Pb	152	265	156	1.74	1.03

* Data from Boström and Peterson (1969)
ND Not determined

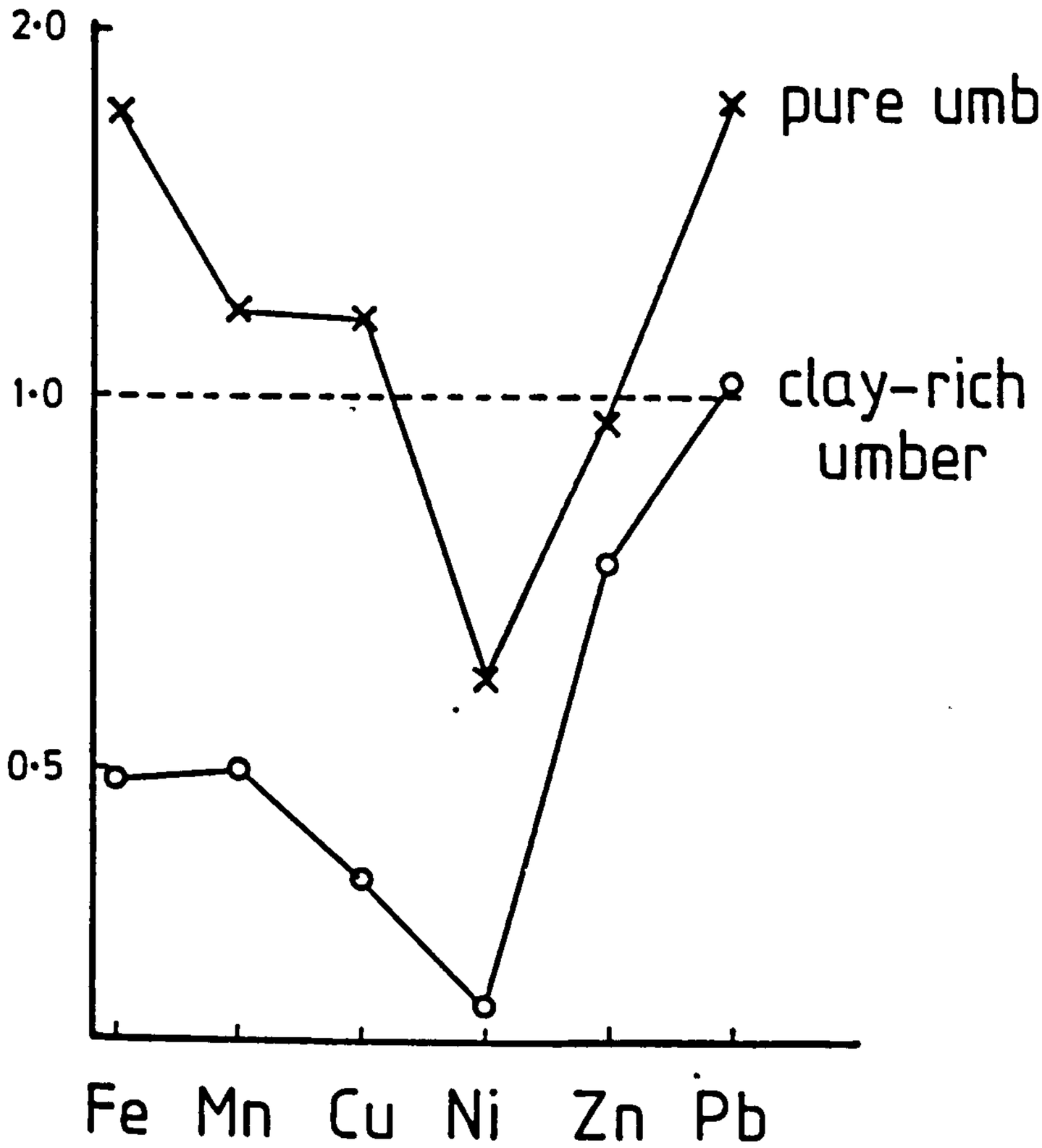

Fig. 5.21

Mean compositions of all pure umber and all clay-rich umber (mean of means, rather than mean of all samples), normalised to mean East Pacific Rise crestal sediment. (Boström and Peterson, 1969). Relative nickel depletion and lead enrichment of the Cyprus sediments are the most important differences.

phase, Cu and Sn with the iron phase, and Pb more evenly distributed. This is very similar to the Troodos sediments (section 5.4.7.3) although Pb is in Cyprus more strongly associated with manganese. The relative enrichment in trace elements is different though. In Fig. 5.21, mean umber and mean clay-rich umber are normalised to average East Pacific Rise sediments (Boström and Peterson, 1969). The Cyprus sediments are similar but are depleted in Ni and enriched in Pb. Ni depletion with respect to MORB is a characteristic of the lavas. Pb is less certain - of two analyses of sheeted dykes one is lower and one higher than East Pacific Rise lavas (Hamelin et al., 1984), but this leaves the mean composition unknown. The strong association of Pb with Ni and with Al argues for their incorporation by absorption from sea water (section 5.5.3). If this argument is correct the Troodos ocean water must have been depleted in Ni and enriched in Pb relative to the present day Pacific. Whereas it is clear that East Pacific Rise vents supply trace elements (Edmond et al., 1982) it is still not clear what proportion of the total oceanic supply they represent. Estimates for Pb based on isotopic evidence vary from 100% to only 0.5% (Turekian, 1983). The Pb and Ni anomalies shared by both the Cyprus lavas and sediments, provides evidence for a strong influence of the basement on the local oceanic Pb and Ni contents.

Concentration of hydrothermal iron in basal sediments

Using data from metalliferous sediments from the Pacific, Atlantic and Indian Oceans, Boström et al., (1976) identified a strong correlation of the degree of hydrothermal enrichment with spreading rate.

$$(Fe + Mn)/Al = 0.59 \exp(0.53 \times SR) \quad R = 0.96$$

SR = Total spreading rate

This correlation implies both that Al accumulation rates world wide are fairly constant, and that the total amount of iron released is closely related to the spreading rate. If the equation is applied

to Cyprus sediments the following spreading rate estimates are obtained.

	SR
Margi umber	5.63 - 6.60
Inter lava umber	5.05 - 6.93

The values are that of an intermediate rate spreading axis. They are sensitive to the accumulation of Al, which cannot be estimated. It is probable that accumulation rates were higher than modern deep-oceanic sediments, because of their volcaniclastic character, which would lead to an underestimation of the rate. However another possible difference between the Troodos and modern spreading centres concerns the dispersal of hydrothermal effluent (see below). Lower transport distances for the hydrothermal component would cause greater local enrichment in iron and manganese, making the estimate high. These two effects, one reducing and the other increasing the estimated rate, can only be discussed qualitatively so no reasonable value can be obtained.

Dispersal of hydrothermal effluent

At modern spreading centres, hydrothermal products released to the water column, are caught up in the mid-depth circulation system and transported great distances (Edmond et al., 1982). For example the ^{3}He plume can be detected over 1000 km west of the East Pacific Rise, and the zone of iron enrichment also extends over 1000 km away from the spreading axis. This transport mechanism has resulted in relatively smooth gradational decrease in hydrothermal enrichment away from the axis.

In Cyprus, the metalliferous sediments differ in two respects. First, they are not ubiquitous. Although it is not possible to relate all umber occurrences to sulphide vents, it is clear that the umber distribution was never uniform (section 5.2.9). Secondly, the up section decrease in iron abundance is characterised by steps (section 5.4.3) rather than being gradational as in the Pacific. This latter point is particularly important, because it is not affected by

the preservation potential. The stepped decreases indicate that local effects have not been masked by any homogenisation process.

If a dispersal mechanism, such as mid-depth circulation, is assumed absent, then the observed characteristics of the Cyprus sediments can be explained. Both iron and manganese would be concentrated in the vicinity of the vents, and without the homogenising influence of transportation, local effects such as the death of a vent system would leave their imprint in the sedimentary record.

5.5.9 Relationship of umber with sulphide

If the bulk of the umber material derives from high temperature hot springs, then an association with the sulphide mineralisation is expected. It is not however necessary that umber shows a relationship to sulphide ore deposits; indeed this cannot be true of some cases. For example, at Mathiati, an umber deposit lies on unmineralised supra-ore lavas; the sulphide-producing vents must have been buried prior to accumulation of the umber, so an alternative source must be found. Near Mathiati, extensive mineralised dyke-parallel normal faults (section 3.1.6) might have supplied the iron. The interlava umbers on Mathiati, Kambia and Kalavasos mining districts, do however provide evidence of an association of umber with hydrothermal centres which produced sulphide ore bodies.

5.5.10 Depositional model for the umber

A depositional model which is compatible with all the observations described in the previous sections is presented below. The model is based upon the assumptions which are listed below, and though inevitably hypothetical is internally consistent, and offers an explanation of the variation and distribution of the metalliferous sediment types.

1) There is a spatial association of the different metalliferous sediment types (section 5.2.9).

2) The iron component of the different metalliferous sediment types is of similar trace element composition (section 5.5.5).

3) Relative enrichment in manganese and in trace elements varies laterally, and tends to increase upwards in the sequence (section 5.5.3).

4) There is an upward decrease in the abundance of the iron component, which includes large steps (section 5.4.3).

The variation in composition and size of umber deposits is seen as resulting from variable interplay of five sediment sources.

1) Externally-derived lithogenous and biogenous sediment.

Smectite, illite and quartz in fairly constant proportions are derived from an external source and accumulate at a fairly constant rate over the entire area. Biogenic silica, comprising radiolaria are periodically supplied in abundance resulting in laterally continuous radiolarian-rich beds. Carbonate fossils: foraminifera; coccoliths; and ostracods, are produced in the overlying water column, but are only preserved in sediments which are rapidly buried by lava flows. Carbonate dissolution proceeds to completion in sediments exposed for long periods at the sea-floor.

2) Locally derived volcanic detritus.

Macroscopic volcanic detritus is locally present in the sediments accumulating in the volcanically active zone. Microscopic detritus in the form of lava-derived smectites accumulate rapidly in the axial zone, where they are abundant enough to mask the externally derived lithogenous material. Basal parts of some of the supralava sediments also contain locally derived volcanic detritus, but this is volumetrically insignificant.

The close confinement of local volcanic detritus to the axial zone implies a geographical constraint, supporting the existence of a well defined median valley (see Chapter 3, section 3.2.1).

3) Iron component

This differs from the lithogenous or biogenous sediments in being localised. Source locations are initiated in the axial volcanic zone, but continue activity when they have spread beyond it. Debouched iron accumulates in the axial volcanic zone and also on the faulted upper surface of volcanics outside the median valley. Sediment accumulating progressively further from the source contains decreasing amounts of iron (increasing dilution by pelagic sediment). Through time the abundance of devolved iron gradually decreases up to cessation of activity which is abrupt. Locally areas of influence of different iron sources, possibly of different ages, overlap so accumulation continues, albeit at lower rates, when the local source dies.

The greater concentration of iron rich sediments above the lavas, rather than within them implies that the axial region was narrow.

4) Manganese Component

The manganese component has two sources. The most volumetrically important is coincident with the iron source. The general increase in Mn/Fe ratios of deposits accumulating further from the axis indicates that manganese was dispersed more widely than the iron.

Manganese is also supplied from low temperature fluids passing through the last erupted lavas. Locally at least, these lavas are erupted at the walls to the median valley (Chapter 3, section 3.2.1), indicating that low-temperature manganese vents can occur slightly off axis.

5) Hydrogenous Component

Hydrogenous enrichment of the sediment in trace metals is

inversely proportional to the accumulation rate, which as the aluminosilicate supply is assumed constant, is controlled dominantly by the accumulation rate of iron. This has the consequence that in general the degree of hydrogenous enrichment of the sediment increases from the axis outwards to the most off axis of the metalliferous sediments.

Of the assumptions on which this model is based, that of constant lithogenous supply rate is the most questionable. It is based largely on the observed correlation of Pb enrichment with Al concentration which is predicted if Pb enrichment is inversely proportional to accumulation rate, and if the Al accumulation rate is constant. It is apparent that locally changes in accumulation rate did occur; between the clay-rich umber and bentonitic clay at Margi, the lithogenous component changes composition, and the degree of hydrogenous enrichment decreases. Yet the small variation in Al abundances of umber, and the similarity of umber sequences about the Troodos massif (section 5.2.9) are in support of the assumption.

5.6 CONCLUSIONS

1. The umbers accumulated at the ridge crest, supplied by iron derived from axial high temperature vents. They are not the local products of low temperature vents as has recently been supposed. The source of the iron may have been particulate sulphide which became oxidised in the water column. Manganese was supplied by the same vents, but accumulated more widely.

2. The major element chemical composition can be described in terms of variable mixing of iron oxide-, manganese oxide-, apatite-, opal-, and aluminosilicate- chemical components.

3. The trace elements are in part controlled by the major element chemical components, but are strongly modified by hydrogenous processes. Variations in this enrichment, which generally increases away from the spreading axis, are compatible with control by sediment accumulation rate. The effect adequately accounts for chemical variation in the umbers, including the interlava varieties.

4. Stepped upward decrease in iron of the metalliferous sediments, indicates that homogenisation of vent effluent had not occurred. This is one of the most significant differences between the Troodos, and the East Pacific Rise, where mid-depth circulation transports and mixes the hydrothermal effluent.

5. The chemical and mineralogical similarity with the East Pacific Rise crestal sediments is notable, and similar controlling processes are implied. There are however some compositional differences; the Cyprus sediments are enriched in Pb and depleted Ni with respect to the East Pacific Rise sediments. This may reflect basement control over sediment composition, as the same features are observed of the Troodos igneous with respect to MORB.

6. Low temperature hydrothermal activity was confined to formation of veins and talus cements composed of manganese oxides. In some of these todorokite is still preserved.

7. Burial resulted only in transformation of amorphous iron oxide to goethite, formation of palygorskite and rarely clinoptilolite possibly after a smectite precursor, and early formation of nodular vitreous cherts. During very early diagenesis francolite formed in the sediment, strongly enriched in REE and yttrium.

Plate 5.1

Photomicrographs of pure umber - all samples from Margi.

a,b) Sample 81-155 mottled groundmass texture resulting from irregular distribution of clay-rich areas (pale) and c. 20 μm diameter manganese-rich ellipsoids. The latter are possibly micro-manganese nodules. The larger pale ellipsoidal shapes in (a) are flattened radiolaria.

c,d) MnO_2-palygorskite veins, ptygmatically folded, in samples 81-155 and 81-160 respectively. Shortening on the veins is similar to that indicated by flattening of radiolaria.

e) Fragment of phosphatised arthropod cuticle in sample 81-160. Parallel structure is faintly visible.

f) Flattened radiolarian test, now replaced by well crystalline goethite.

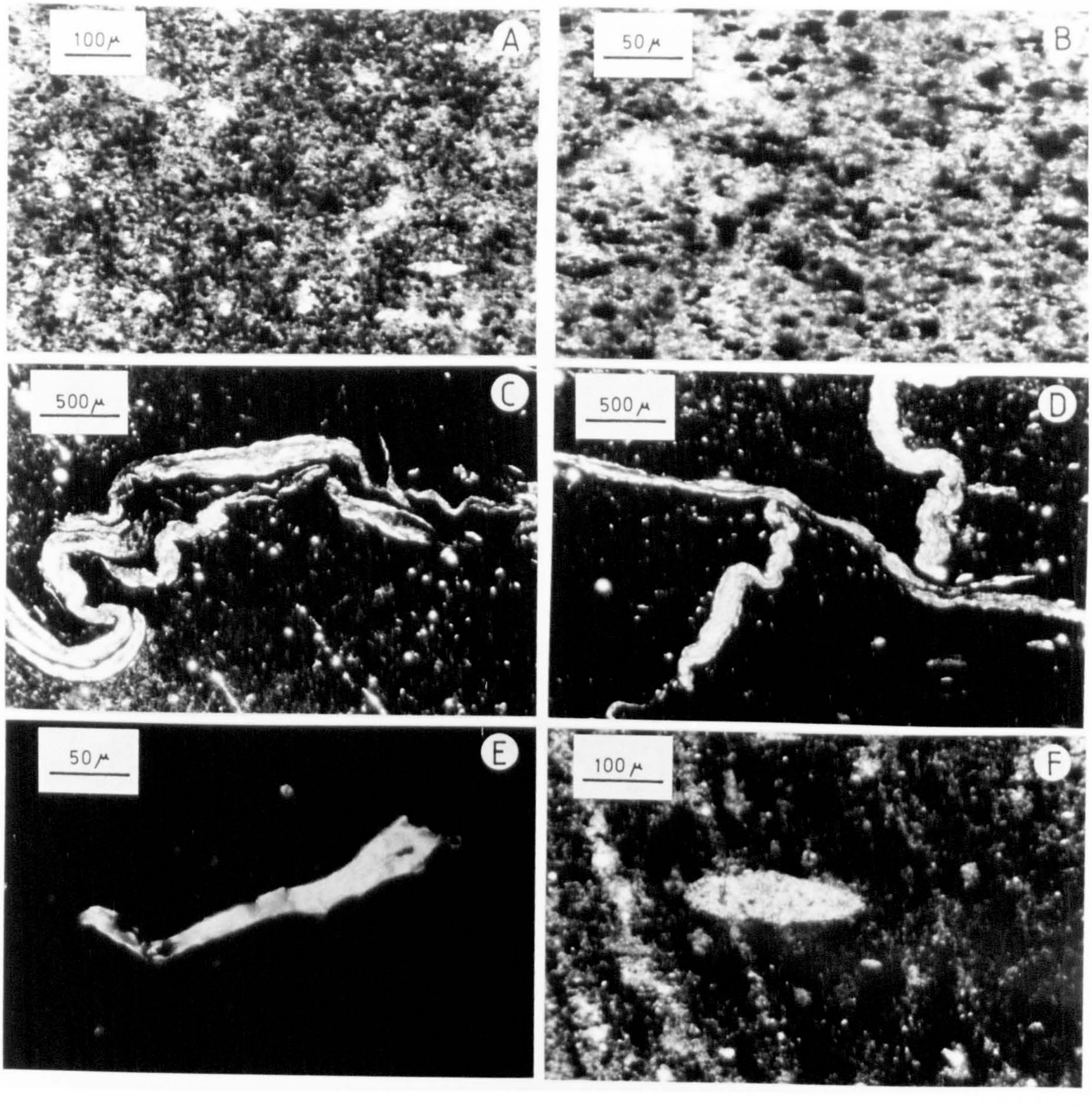
100 μ
A
50 μ
B
500 μ
C
500 μ
D
50 μ
E
100 μ
F

Plate 5.2

Photomicrographs of clay-rich umber samples from Margi.

a) Large euhedral andesine in parallel laminated clay-rich umber.

b) Detail of lamination showing the importance of slip surfaces. Small fragments of phosphatised cuticle are abundant.

c) Detail of slip surfaces.

d) Normal, unfaulted gradation between pale and dark laminae.

e) Contact between clay-rich umber and overlying bentonitic clay. Remobilisation of manganese is evident at the contact.

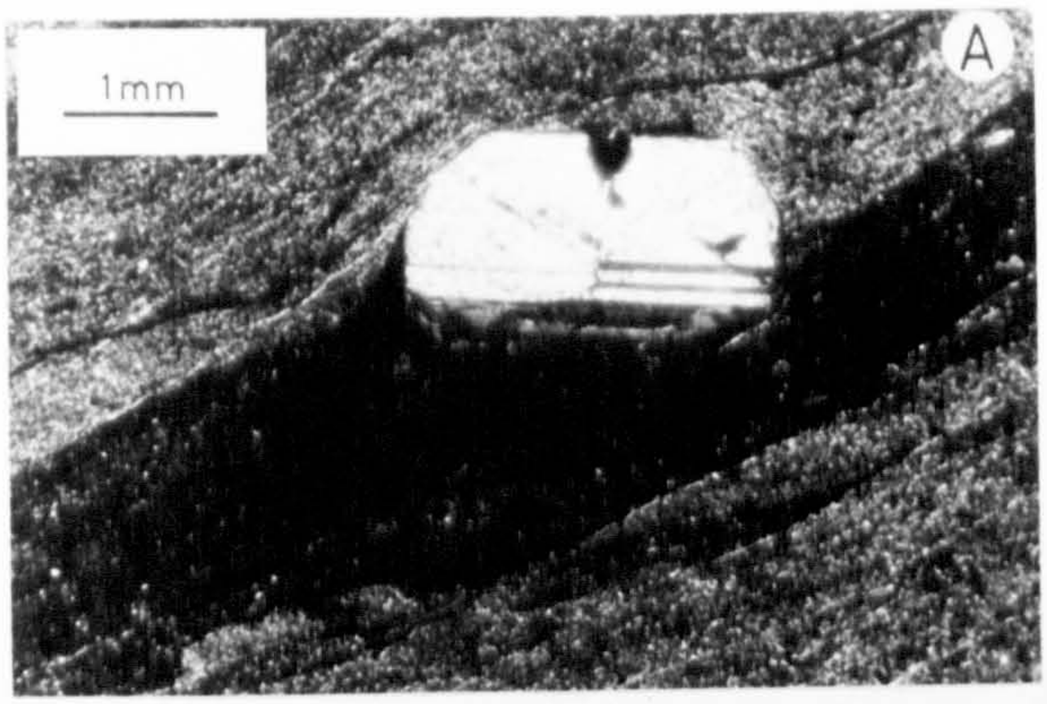
1mm
A

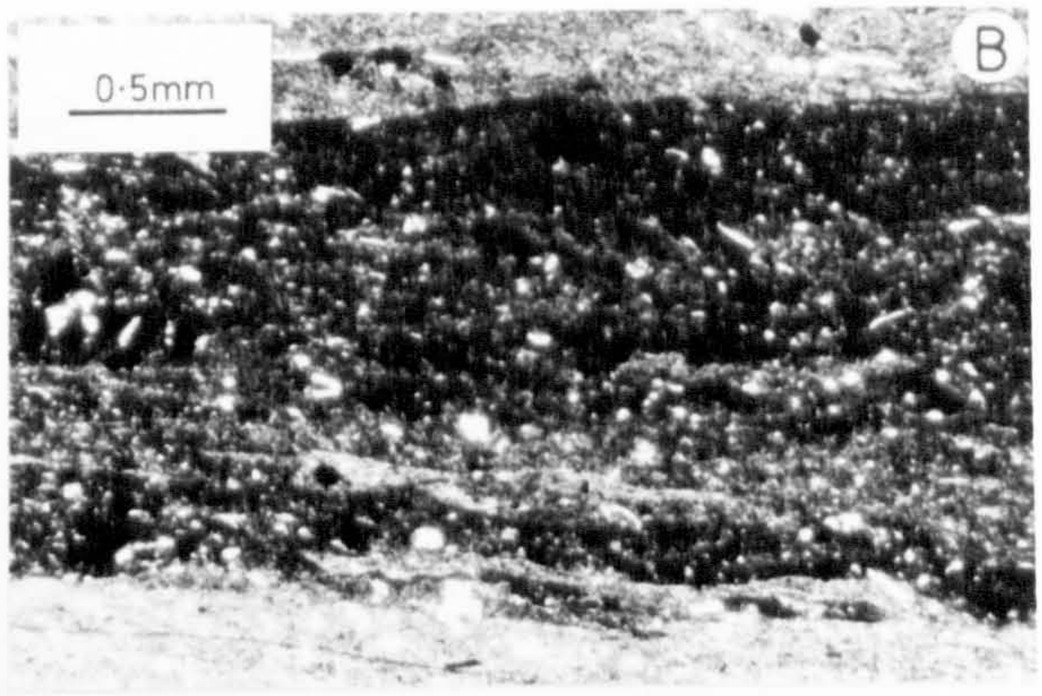
0·5mm
B

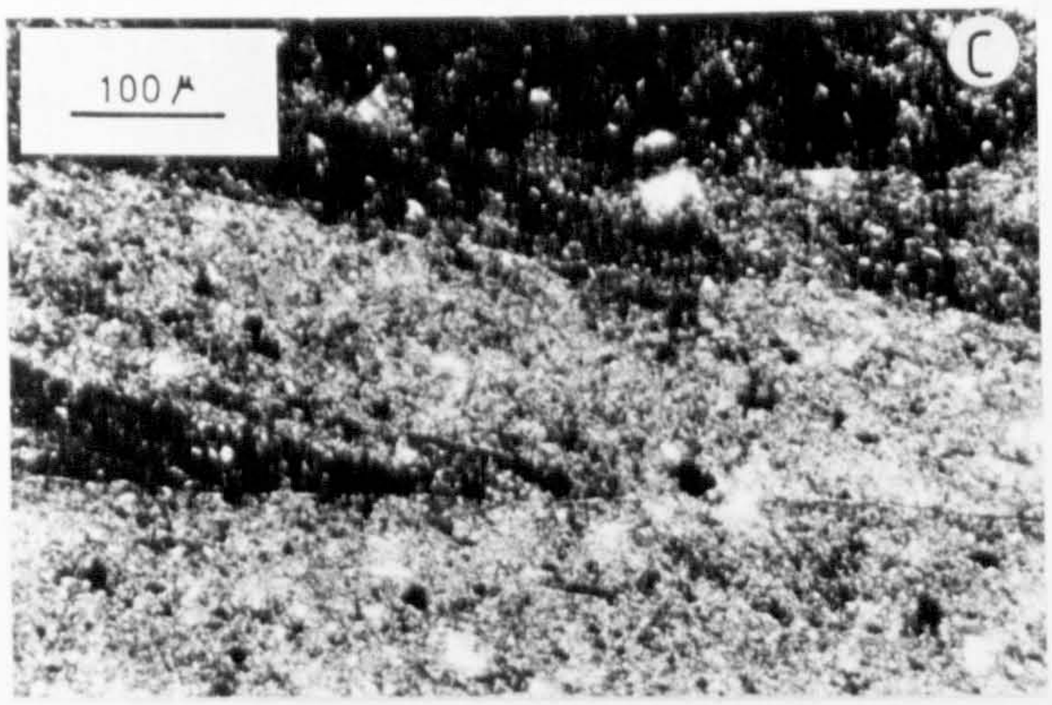
100 μ
C

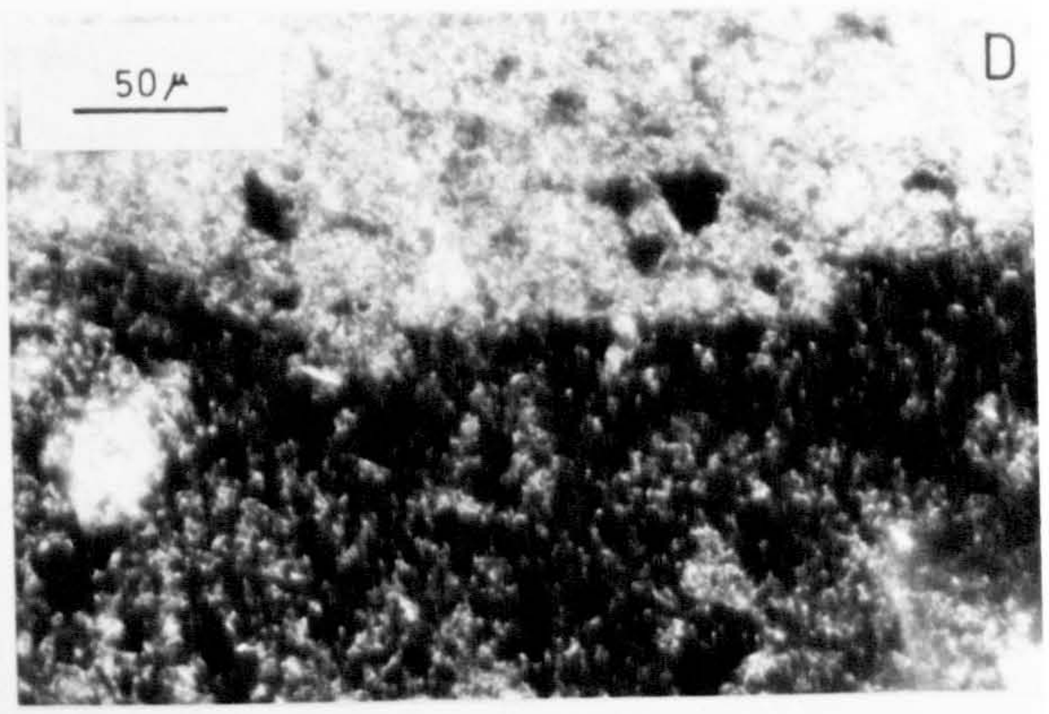
50 μ
D

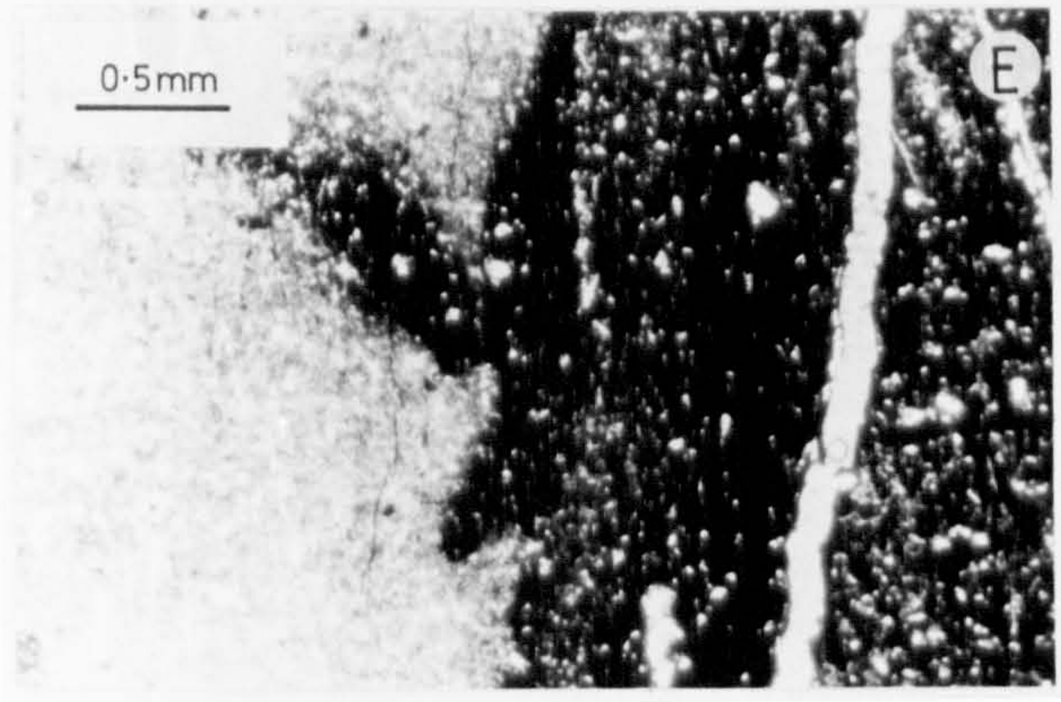
0·5mm
E

Plate 5.3

a) The principal umber pit near Margi. The lavas and overlying sediments dip easterly (to the right). The pale bleached sub-umber lavas are clearly visible. The overlying pink bentonitic clays and radiolarites, and chalks are exposed to the right. The bounding fault to this half graben runs parallel to the strike, but is just out of sight to the right of the photograph.

b) Nodular chertified umber from the Margi umber pit. MnO_2-palygorskite veins are clearly visible passing through both the silicified and un-silicified umber.

Plate 5.4

Supralava sediments in the Margi area.

a) View to the east from a chalk outlier, to another fault bounded elongate outlier of supralava sediments.

b) View to the NW back to the outlier in which is the principal umber pit near Margi. The elongate character of the outlier, with the near edge fault bounded, is evident. The small dark hill to the right of the photograph is a lensoid body of picrite.

c) The principal umber pit. Grey lavas (bottom) are overlain by dark pure umber and clay-rich umber, rubbly pink bentonitic clays and by white chalks. Up thrown lavas are visible in the back right of the photograph.

d) Pure umber overlain by almost completely disaggregated clay-rich umber and by rubble derived from the bentonitic clays. This disruption results from the presence of smectites which swell and break up the rock during wet weather.

A

B

Plate 5.5

Fault-bounded umber from 1 km west of the Mathiati mine.

a,b) NW-SE orientated graben 2-3m deep infilled by horizontally laminated umber. (b) Shows detail of the edge of this. Slip surfaces parallel to the bounding faults are common.

c) An en echelon continuation of the graben system. Here the structure is deeper, and is mostly filled by crudely bedded talus. The structure runs up to the right of the photograph. Solid sheet flows are visible to the left and right, with talus breccia in between.

d) A horizontally laminated umber pocket within the coarse talus shown in (c).


A


B


C


D

Plate 5.6

Details of supralava umber.

a) Grey weathered pillow draped with pure umber. Palygorskite veins are visible in the lava.

b) Clearly visible fold hinges to a ptygmatically folded MnO_2-palygorskite vein in the pure umber at Margi. The fold axes lie within the plane of the bedding.

c) Striated slip surface in the pure umber at Margi.

d) Leaching of the umber in contact with lava breccia (1km west of Mathiati mine).

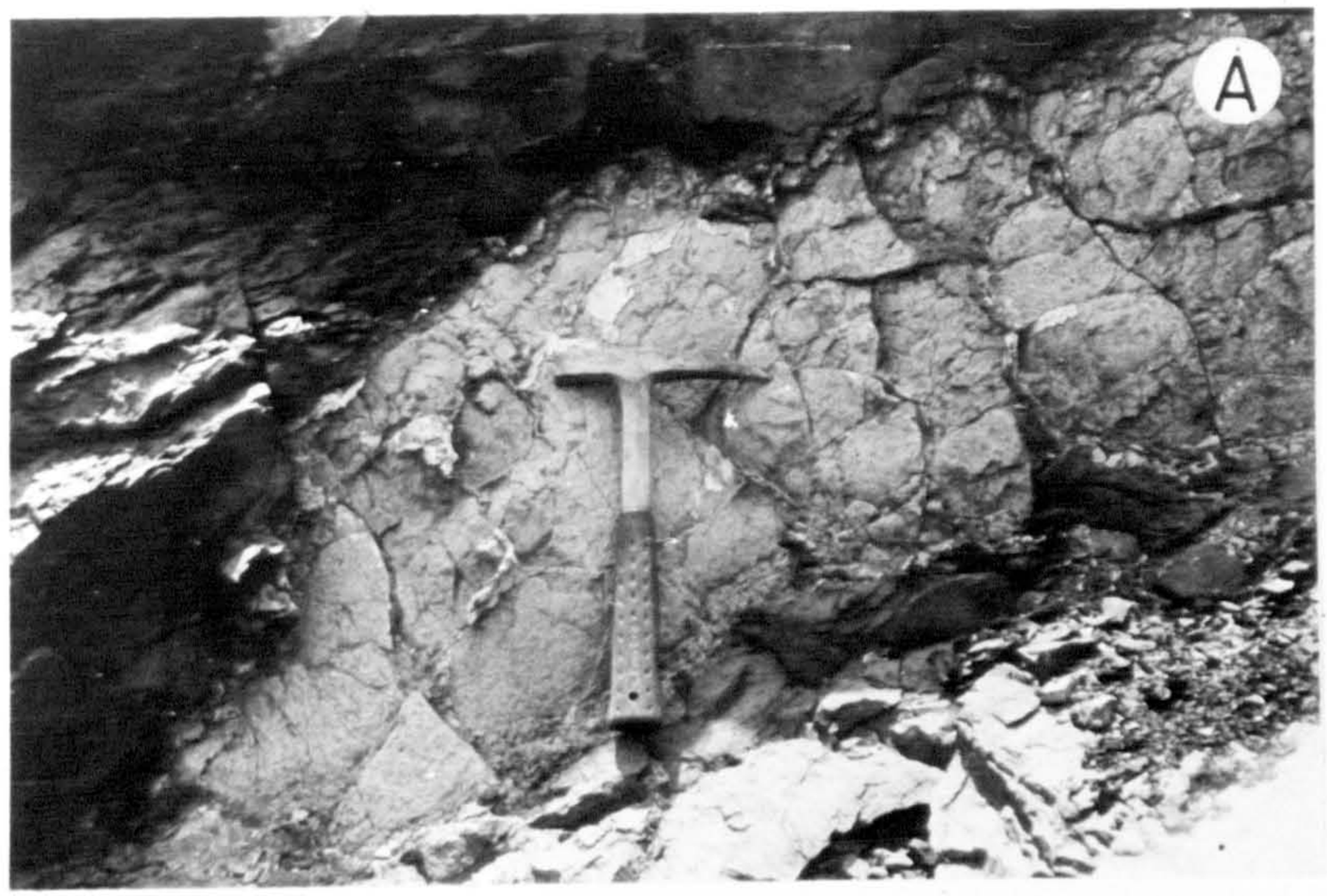
A

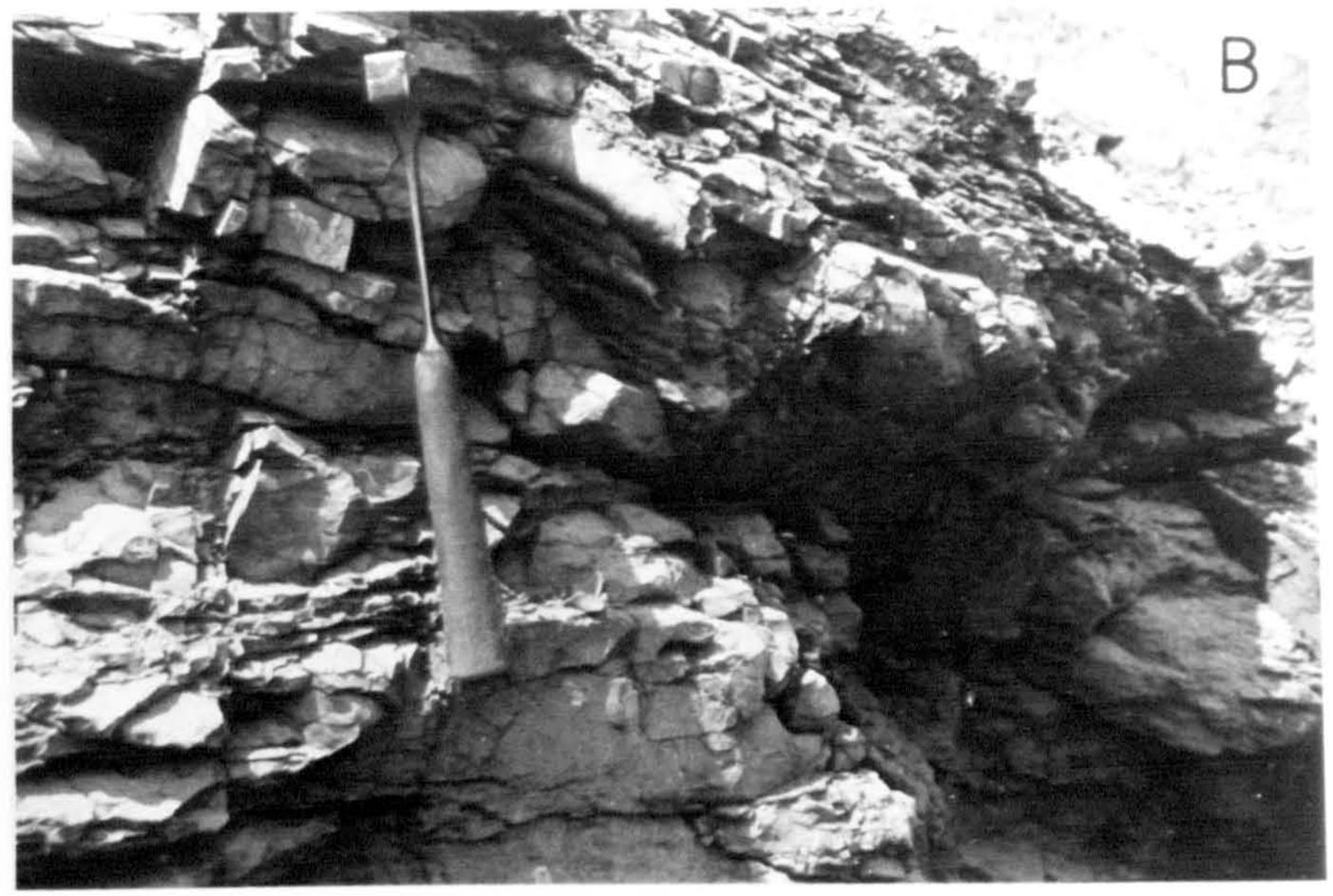
B

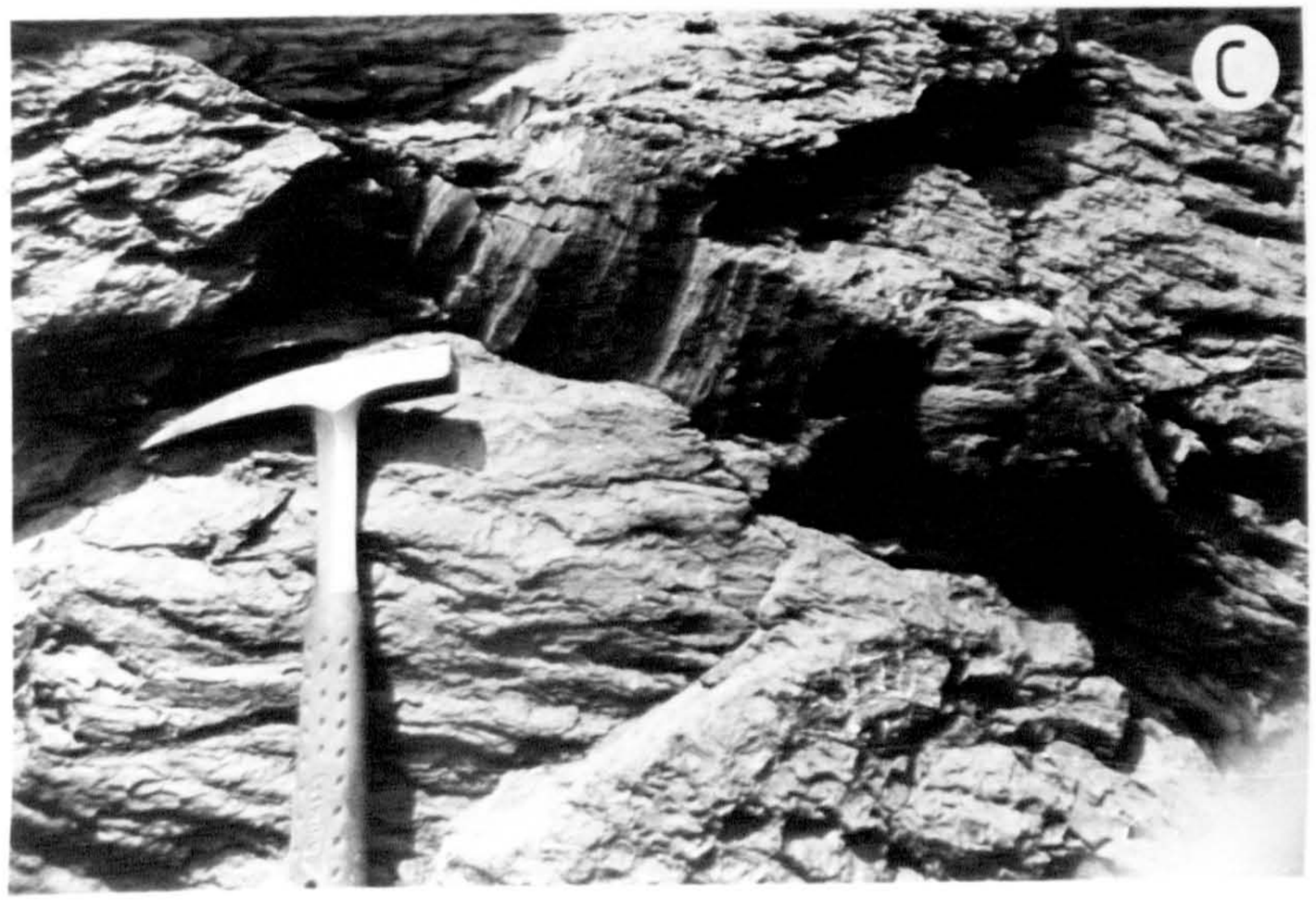
C


D

Plate 5.7

Scanning electron microscope images of the umber.

a,b) Fibres of palygorskite and leaves of illite-montmorillonite occur throughout the umber. The granular material is probably iron oxide.

c) Densely packed fibres of palygorskite in a palygorskite-MnO_2 vein.

d) Well crystalline kaolinite.

e,f) Clay-rich umber. The dominance of flaky illite-montmorillonite is evident. Granular masses, probably of iron oxide, also occur.

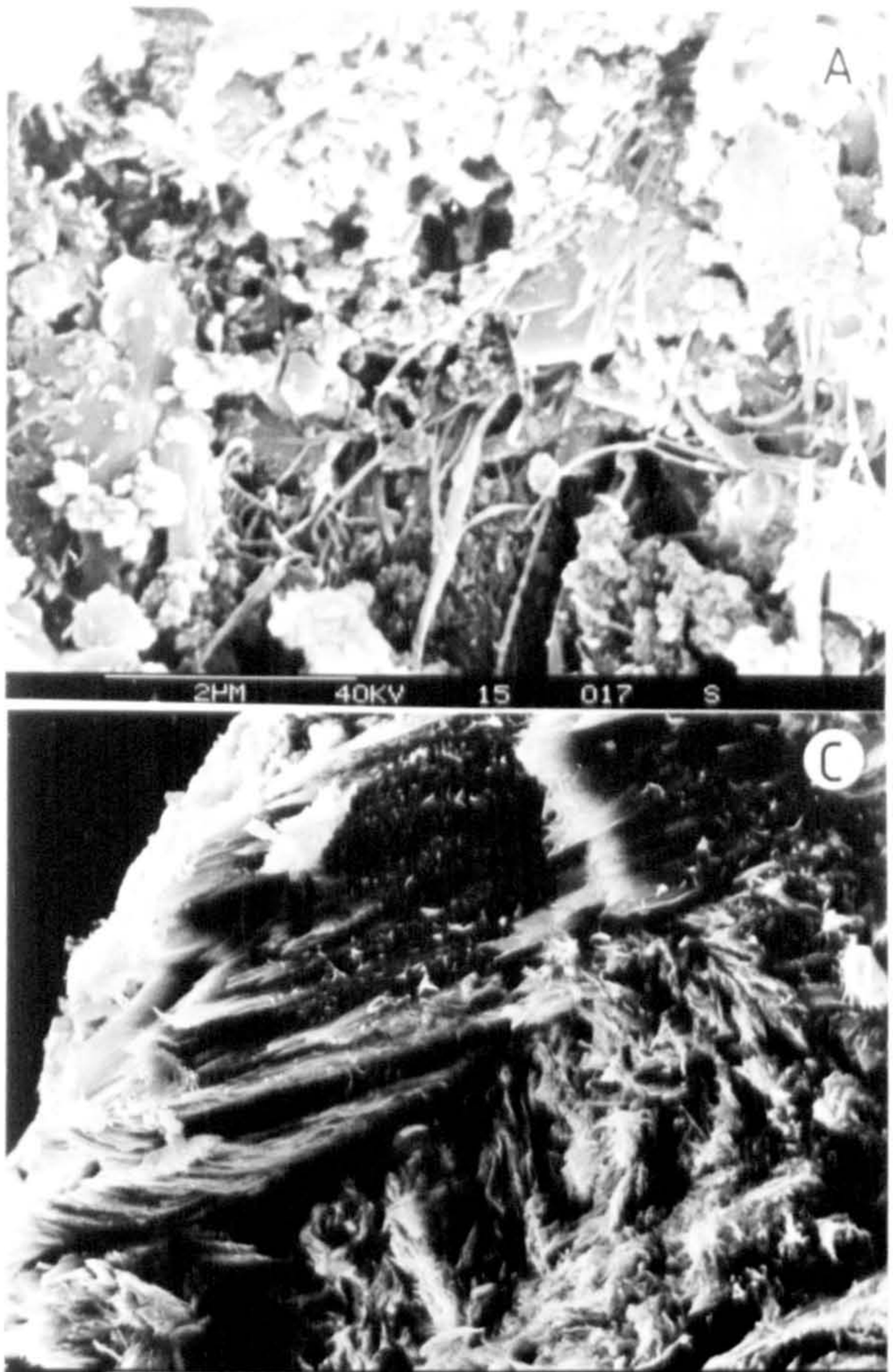
A
2μM 40KV 15 017 S

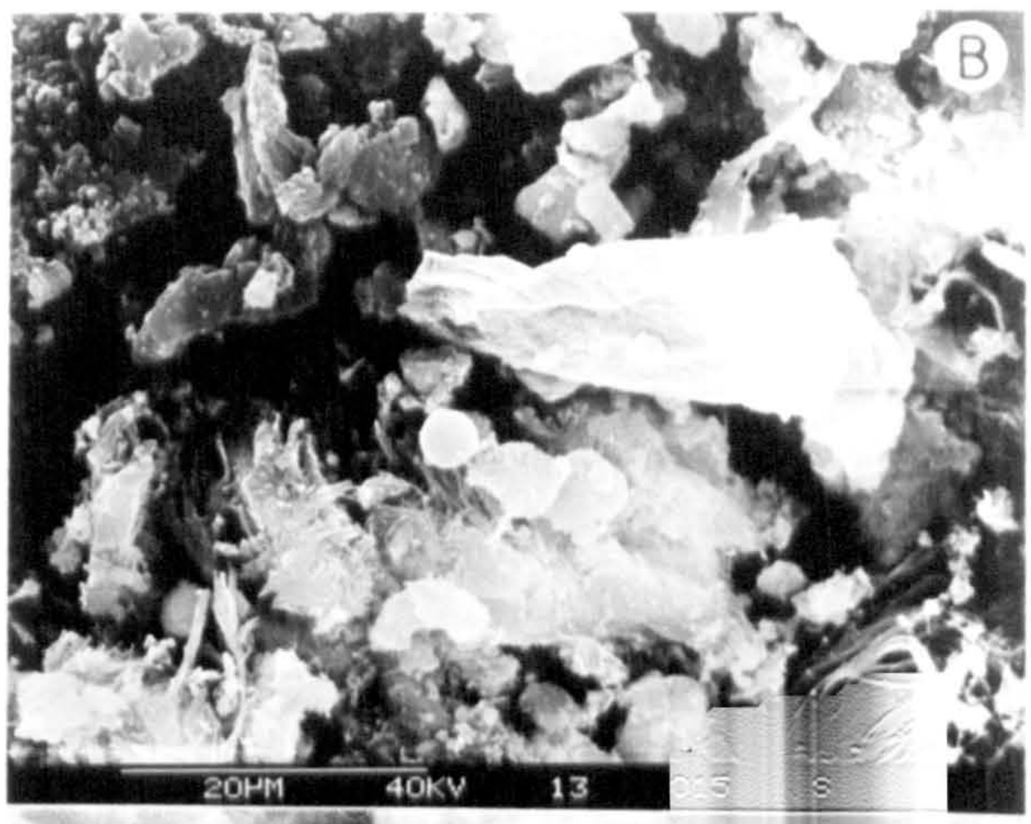
B
20μM 40KV 13 015 S

C
100μM 40KV 11 013 S

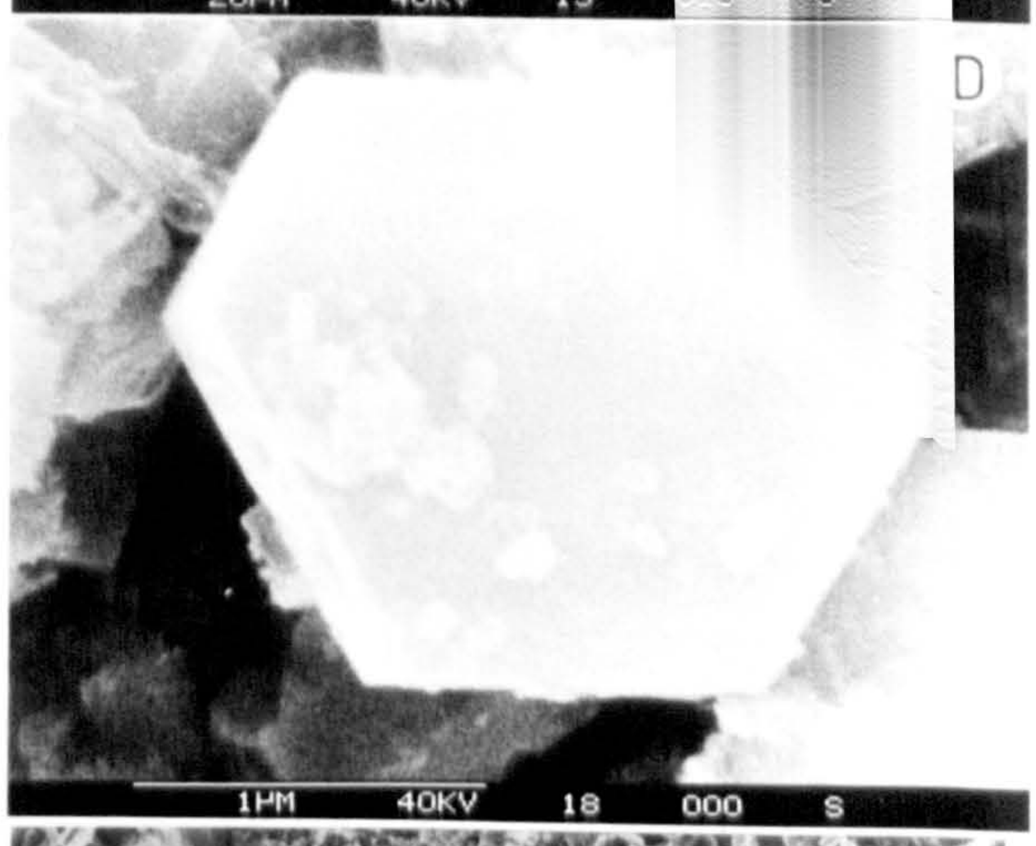
D
1μM 40KV 18 000 S

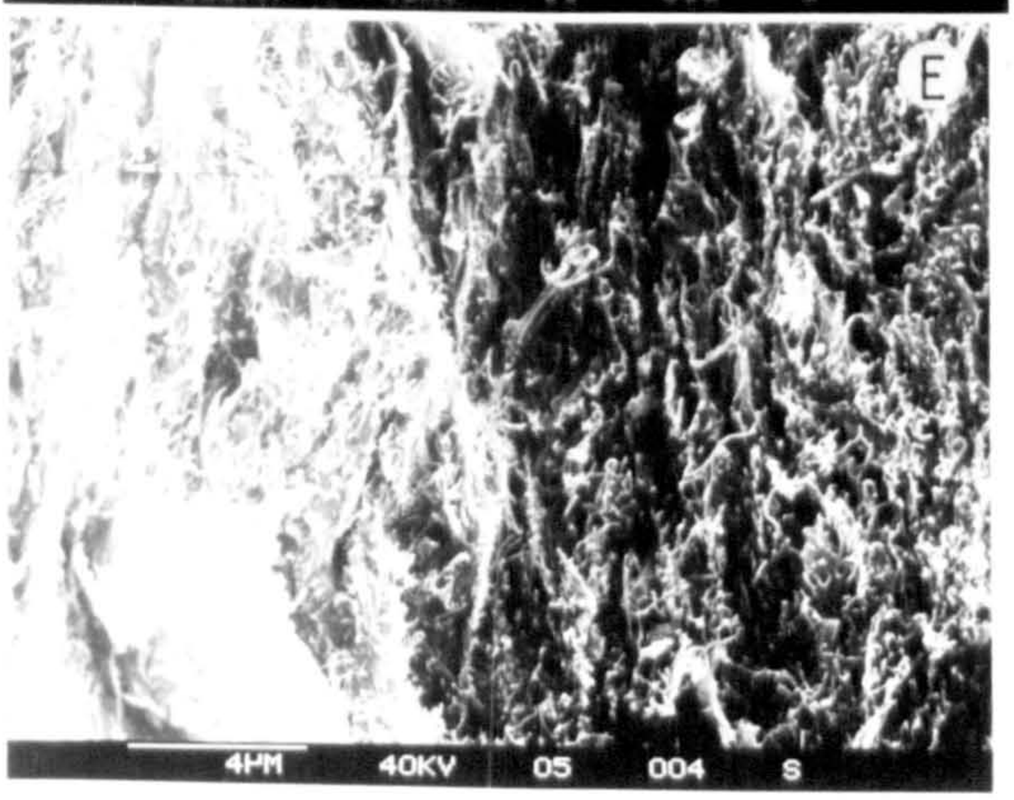
E
4μM 40KV 05 004 S

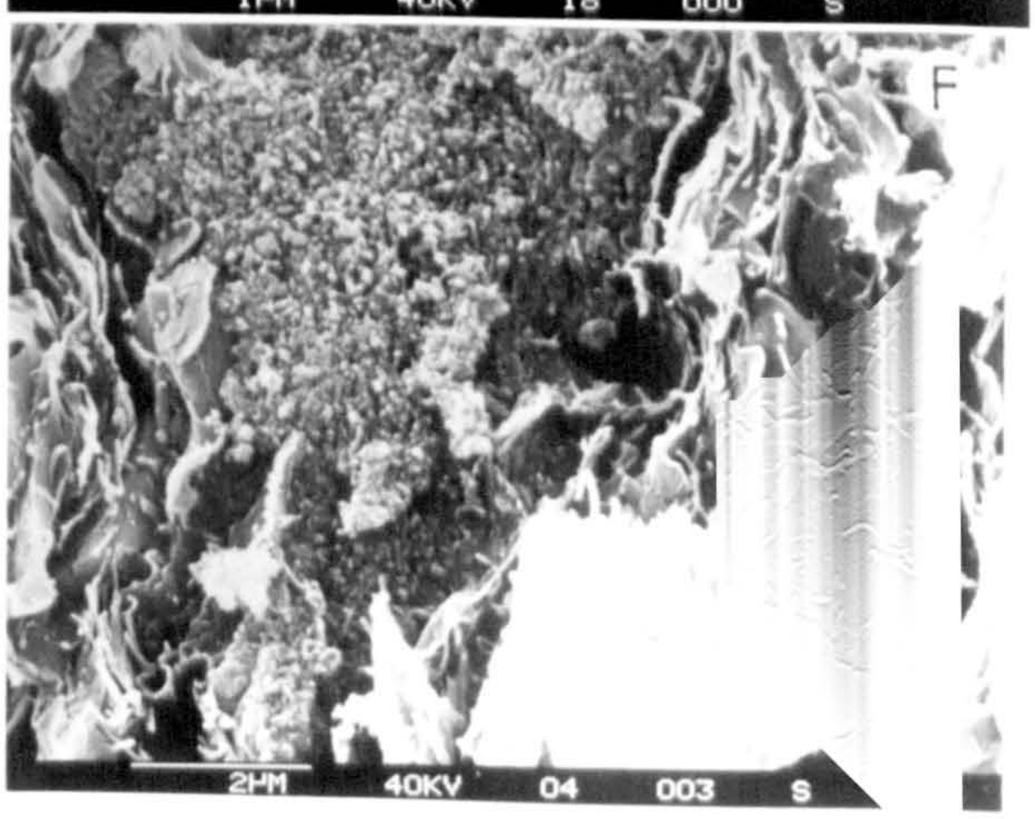
F
2μM 40KV 04 003 S

Plate 5.8

Texture of umber and clay-rich umber from Margi. Scale arrow is 5 mm long.

a) Slight contortions of parallel laminae.

b) Contact between clay-rich umber and overlying bentonitic clay. Remobilisation of manganese is indicted by the irregular overgrowth near the contact. On the broader scale the contact is entirely concordant.

c) Soft-sediment faults passing through slightly contorted parallel laminae.

d) Continuous parallel laminae.

A

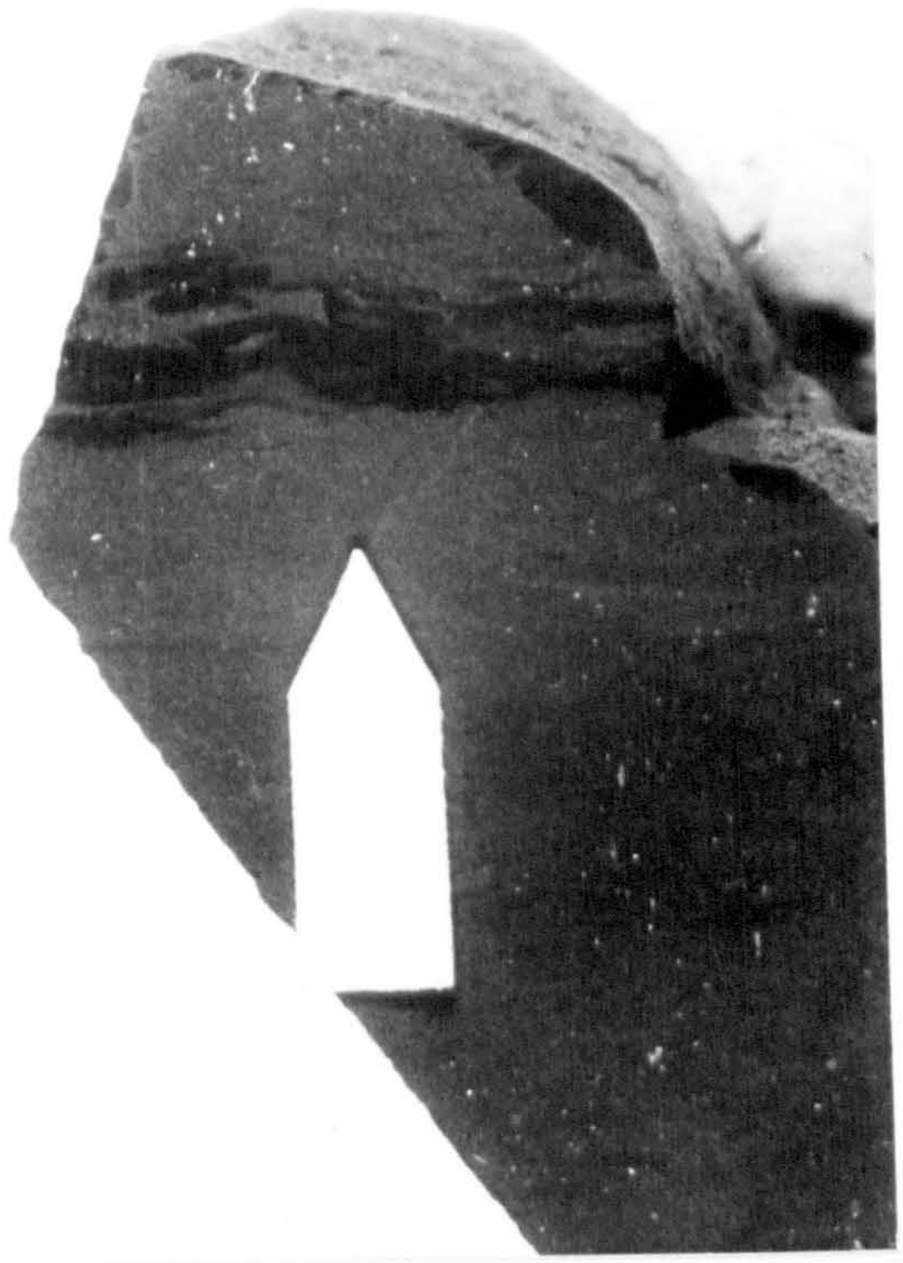

B

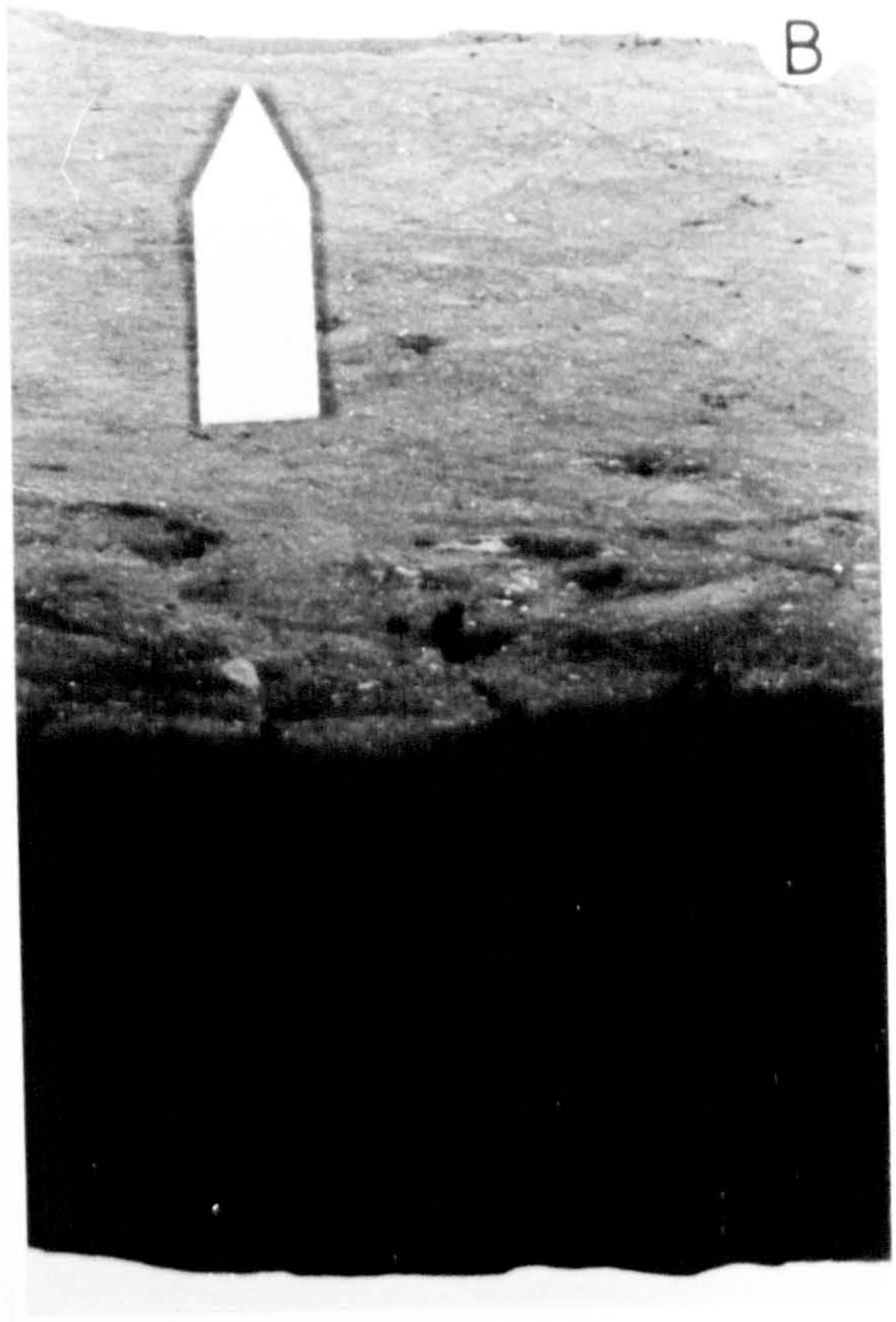

C

D

Plate 5.9

Texture of umber from Margi. Scale arrow is 5 mm long.

a) Soft-sediment faults passing through continuous parallel laminae. Some faults traverse the specimens, but others progressively die out upwards, and do not cut the uppermost laminae.

b) Discontinuous parallel laminae. This results in part from low angle soft sediment faulting.

c,d) Irregular lamination, due in part to faulting and slumping, but also possibly to bioturbation.

e) Ptygmatically folded palygorskite veins passing through parallel laminated umber.


A


B

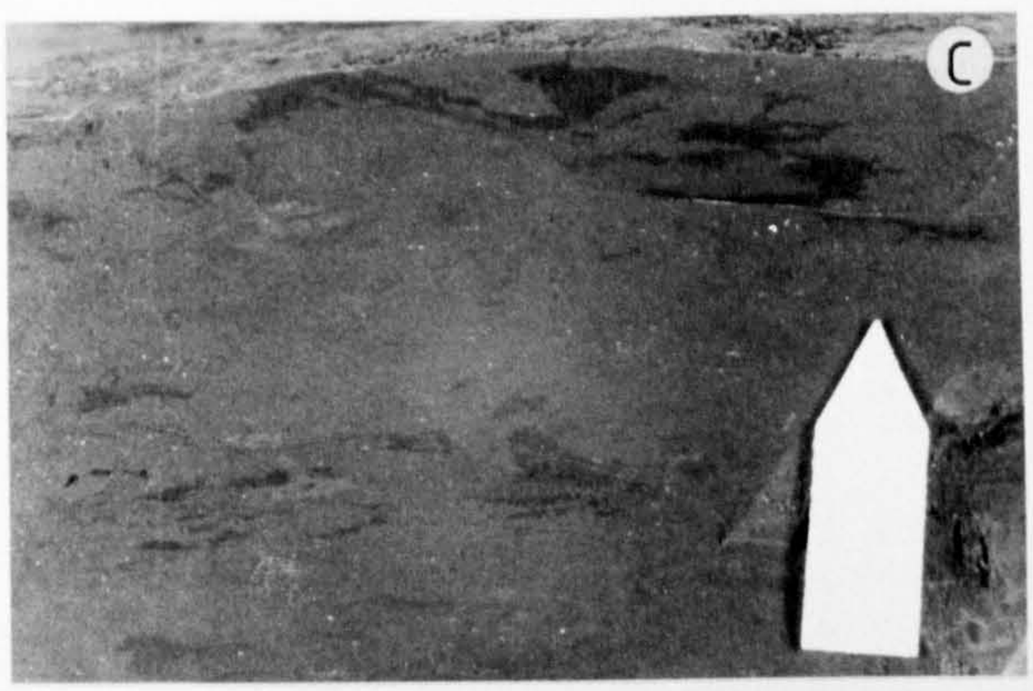
C

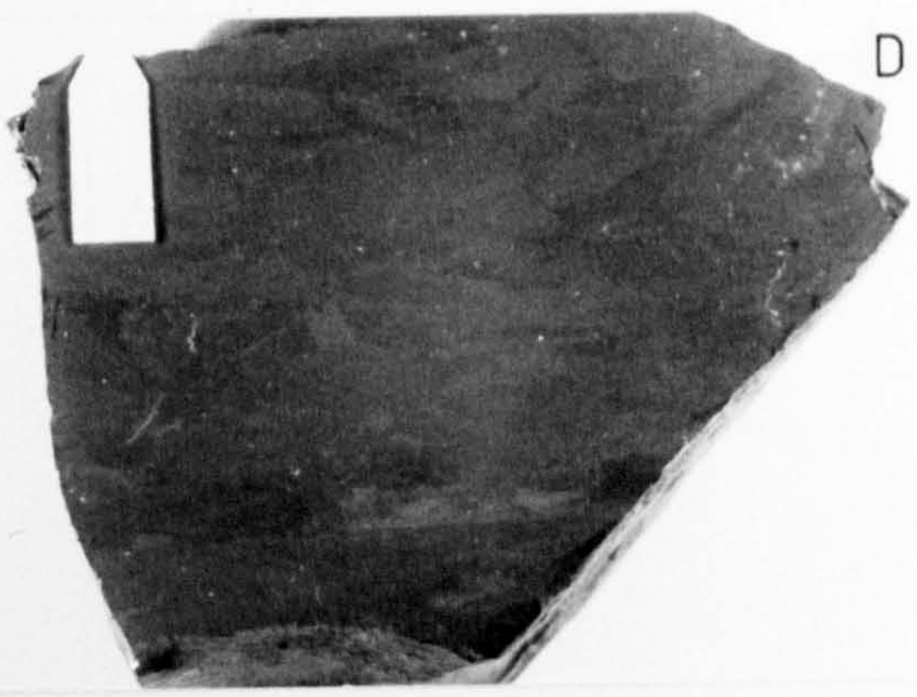
D

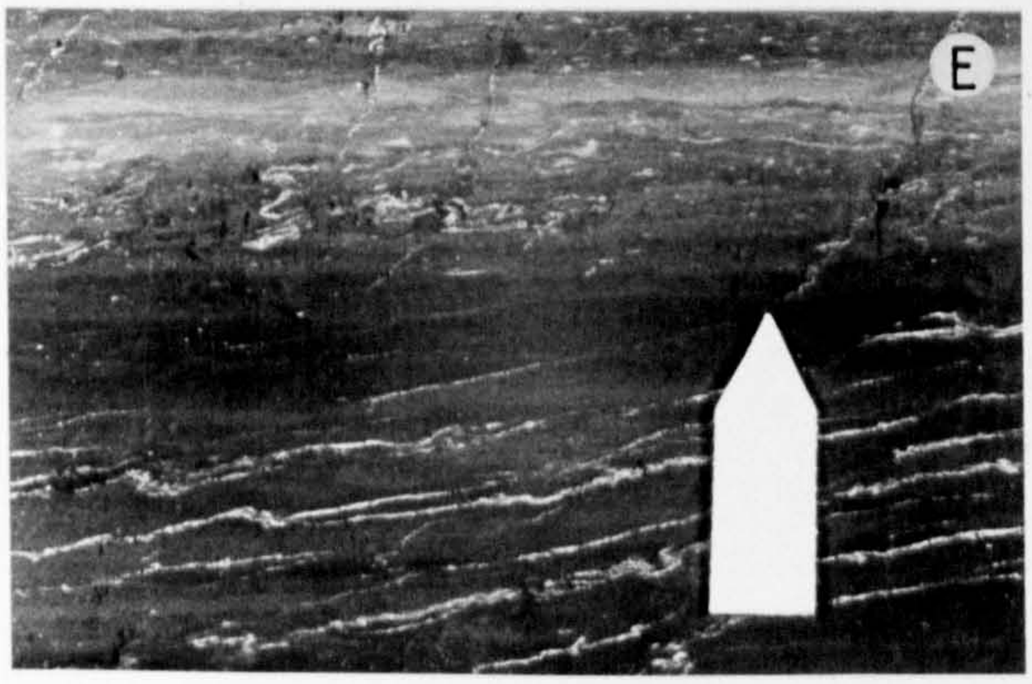
E

CHAPTER 6

GEOCHEMISTRY AND MINERALOGY OF THE NON-METALLIFEROUS COVER SEDIMENTS

6.1.1 Introduction

The Upper Cretaceous non-metalliferous sediments which overlie the Troodos lavas and metalliferous sediments have been described by Lapierre (1972), Desprairies and Lapierre (1973), Robertson and Hudson (1974) and Robertson (1977c). A comprehensive study of these sediments has not been undertaken, but their potential importance as contributors to the metalliferous sediments has prompted a brief survey of their mineralogy and geochemistry.

The lithological types fall into three groups which are variably intermixed. First, volcaniclastic sediments varying from sandstones to fine clays. These comprise the lithogenous component of the metalliferous sediments, and are thus of particular interest. Secondly, radiolarian cherts, occurring locally as thin beds within the other lithological types most abundantly towards the base of the succession. Thirdly, chalks which are absent from the lowermost sediments and appear up section exhibiting signs of partial dissolution. These sediment types form a continuous series, varying in age from Campanian to Maastrichtian, but have been subdivided into different geological formations. The volcaniclastic sediments occur in the Perapedhi and Kannaviou Formations, and the Moni clays, and are even found as interlava sediments within the Troodos massif. The appearance of carbonate upsection defines the base of the Lefkara Formation.

In the following account, nomenclature and distribution are first discussed, followed by descriptions of the mineralogy and chemistry. The chapter is completed by a discussion of the origins and conditions of accumulation of the sediments.

6.1.2 Nomenclature of the cover sediments

The umbers are in all places overlain by bentonitic clay and associated radiolarites (Robertson and Hudson, 1974). These

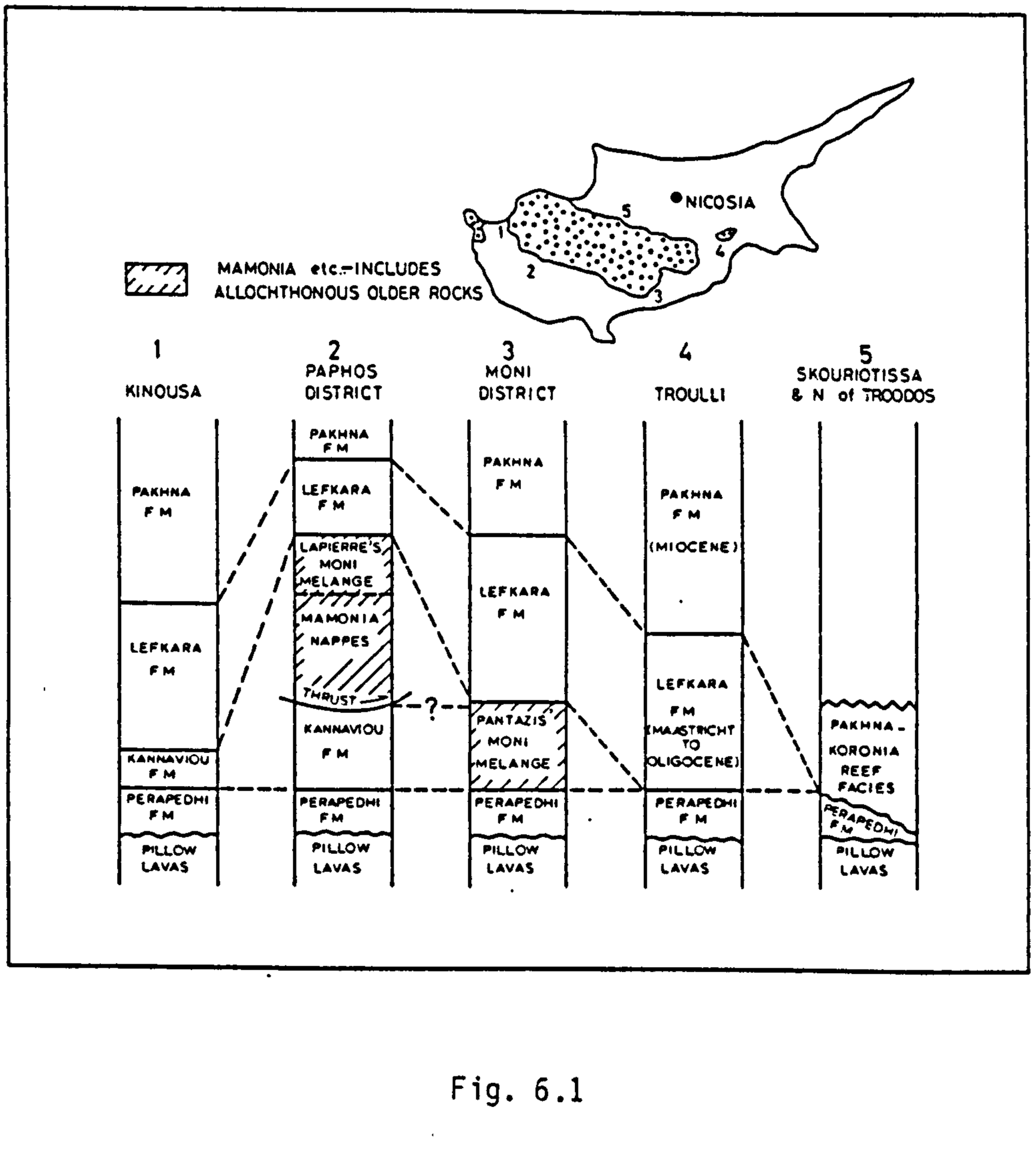

Fig. 6.1

Regional variations in thickness of the supralava sediments. After Robertson, 1976c.

sediments which are thin and discontinuous in the north and east, thicken westwards on the southern margin, reaching their greatest thickness (ca. 600m) in the Paphos District, where they contain immature volcaniclastic sandstones and siltstones. In the Nicosia, Limassol and Larnaca Districts,the umbers, radiolarites and radiolarian mudstones have been termed the Perapedhi Formation, (Wilson, 1959) and the bentonitic clays have been distinguished by the term Moni Formation (Pantazis, 1967). In the Paphos District, the sediment types have all been included in the Kannaviou Formation (Lapierre, 1968, 1972). Robertson and Hudson (1974) proposed that restriction of the term Perapedhi Formation to the umbers and radiolarian rocks, and application of the term Kannaviou Formation to the overlying volcanogenic sediments, would resolve the contradictions. However, the problem remains because the Kannaviou-type bentonitic clays form the lithogenous component to the radiolarites (Desprairies and Lapierre, 1973; This work - section 6.3.3), and to the umbers (Chapter, 5 section 5.5.6). In view of the volumetric dominance of the volcaniclastic sediments, the term Kannaviou Formation might best be extended to all the basal sediments, with umbers comprising the lowermost member of this.

6.2 SEDIMENTARY COVER SUCCESSION AND LATERAL VARIATIONS

The pelagic sedimentary cover of the Troodos massif has been described by Robertson and Hudson (1974). A brief summary of the succession and its lateral variations are described before going on to discuss the mineralogy and chemistry of these sediments.

In all places, except where Tertiary unconformities conceal the upper surface, the umbers are succeeded first by volcaniclastic sediments (most commonly bentonitic clays) and radiolarites, and then by marls mostly of Maastrichtian age (see Plate 6.1 A,B).

6.2.1 Volcaniclastic sediments

The variations in thickness of the volcaniclastic sediments are summarised in Fig. 6.1 (Robertson, 1977c). In the southwest the sediments reach their greatest thickness, where they comprise over 600m of loosely consolidated fine and medium grained sandstones interbedded with bentonitic clays. The upper parts are frequently

disturbed and are intercalated with the overlying allochthonous units. The basal parts in some localities such as Akamas and Kinousa are gradational with the umbers. Individual sandstone beds are up to 30m in thickness and are lenticular. In Akamas and at Kinousa, sandstones appear within a few tens of metres of the base of the succession, but further southeast, several hundreds of metres of bentonitic clays precede the first sandstones. To the south east, in the Limassol District, sandstones are absent, and the bentonitic clays are thinner. In the Nicosia District the bentonitic clays are thinner still - less than 10m thick. Further west, along the northern margin, the sediment tends to be concealed by unconformable Miocene sediments, but are locally exposed as at Ayia Maria and Skouriotissa.

6.2.2 Radiolarites and radiolarian mudstones

The basal parts of the volcaniclastic succession contain abundant beds of radiolarian chert (Plate 6.1A). South of the Arakapas fault zone, such chert beds are also found in the umbers (notably at Dhrapia and Mangalene). The radiolarian-rich beds are characteristically thin and concentrated in umber hollows, though at some localities, such as Kambia, and Vavla, thick sequences are found (c.35 m). At Vavla, the umbers are absent, and the radiolarian-rich clay rests directly on the lavas.

The radiolarite beds are typically 5-30cm thick and are laterally continuous on the scale of the exposures (50m at Margi). Inter-beds may be either radiolarian-rich clays, or as at Margi, may be completely devoid of siliceous microfossils.

6.2.3 Upper Cretaceous chalks

The umbers and the basal volcaniclastic sediments, though locally rich in radiolaria, are invariably carbonate-free. The lowermost beds of the overlying chalks show evidence of selective dissolution of carbonate microfossils. Planktonic foraminifera are poorly preserved, and the relatively high abundance of coccoliths is characteristic of extensive carbonate dissolution (Berger and von Rad, 1972).

6.3 MINERALOGY AND PETROGRAPHY

Mineralogical studies have centred on X-ray diffraction, owing to the importance of the clay mineral assemblage. However, in the coarser volcaniclastic sediment petrographic examination is possible, and in the radiolarian sediment, scanning electron microscope techniques have been employed (Robertson and Hudson, 1974).

6.3.1. Sandstones of the Paphos District

Petrographic descriptions of the volcaniclastic sandstones are presented by Robertson (1977c), and Desprairies and Lapierre (1973). There is evidence of bimodal volcanism. The lowermost sandstones contain abundant fragments of undevitrified acid volcanic glass, as well as volcanic quartz, alkali feldspar and plagioclase. Foraminifera and radiolaria also occur and the whole is cemented by a sparry calcite. Higher in the succession, pumice is generally lacking, and fragments of polycrystalline mica-bearing quartzite phyllite and chert appear. The beds are non-turbiditic, but apparently originated in slumping and bottom transport by currents. Structureless pumice beds may be most easily interpreted as ash-fall deposits.

In addition to the fragments of acid volcanic origin, numerous fragments of basalt, basaltic glass and dolerite occur. Altered plagioclase and pyroxenes associated with these are also found.

6.3.2 Bentonitic clays

The mineralogy of the bentonitic clays has been investigated by Desprairies and Lapierre (1973). In addition the clays from the Margi area, the subject of a geochemical analysis presented below, are described.

Phyllosilicates

The bentonitic interbeds in the Paphos area contain 60-100% sodic smectite, 0-20% illite, and 0-25% chlorite. Locally a regularly interstratified illite-montmorillonite may comprise 60%. These values, however, represent the total range - the greater part of the material contains close to 80% smectite, 20% illite and a trace of chlorite.

The Moni Formation, in the Limassol District has a distinctly different mineral assemblage. The phyllosilicates comprise 25% smectite, 15% illite, 15% chlorite, and 45% kaolinite (Desprairies and Lapierre, 1973). The latter mineral is not found in abundance in any of the other sediments, though individual plates are observed in the umber at Margi (Chapter 5, section 5.3.2).

The basal bentonitic clays overlying the umbers in the east and north of the massif, have the same phyllosilicate assemblage as the Paphos District clays, comprising smectite with subordinate illite and a trace of chlorite.

The smectite and illite are both dioctahedral, and are commonly sodic. The sodium enrichment distinguishes them from the clays in the umbers but is probably the result of differing partial neomorphism (Desprairies and Lapierre, 1973).

Silica minerals Quartz in small abundances is ubiquitous. A discussion of the variation in quartz content is given below. In addition to quartz, Opal-ct is locally abundant, though not ubiquitous. Alteration after diatom and radiolarian remains is the origin (Robertson, 1977a).

Clinoptilolite

Clinoptilolite is abundant in the lowermost bentonitic clays in all places studied (Kinousa and Limassol District, Desprairies and Lapierre (1973); Kalavasos and Pano Lefkara, Guillemot and Nesterof (1980); Margi and Dhrapia this work) clinoptilolite is abundant. It is also present in pink clays in the upper 10m of the CY1 bore hole (Akaki River). It does not however occur in the higher parts of the thick volcanogenic succession in the Paphos District, nor in the Moni Formation in the Limassol District. In a well exposed section of Margi the clays and radiolarites were sampled from a 10m section conformable on the clay-rich umber. These sediments are rich in clinoptilolite. In Fig. 6.2 an X-ray diffraction determination of quartz, clinoptilolite and clays are plotted against height up section. No attempt has been made to calibrate this. However a trend of decreasing clinoptilolite, is observed, the abundance at the top being less than half that of the bottom. There is some

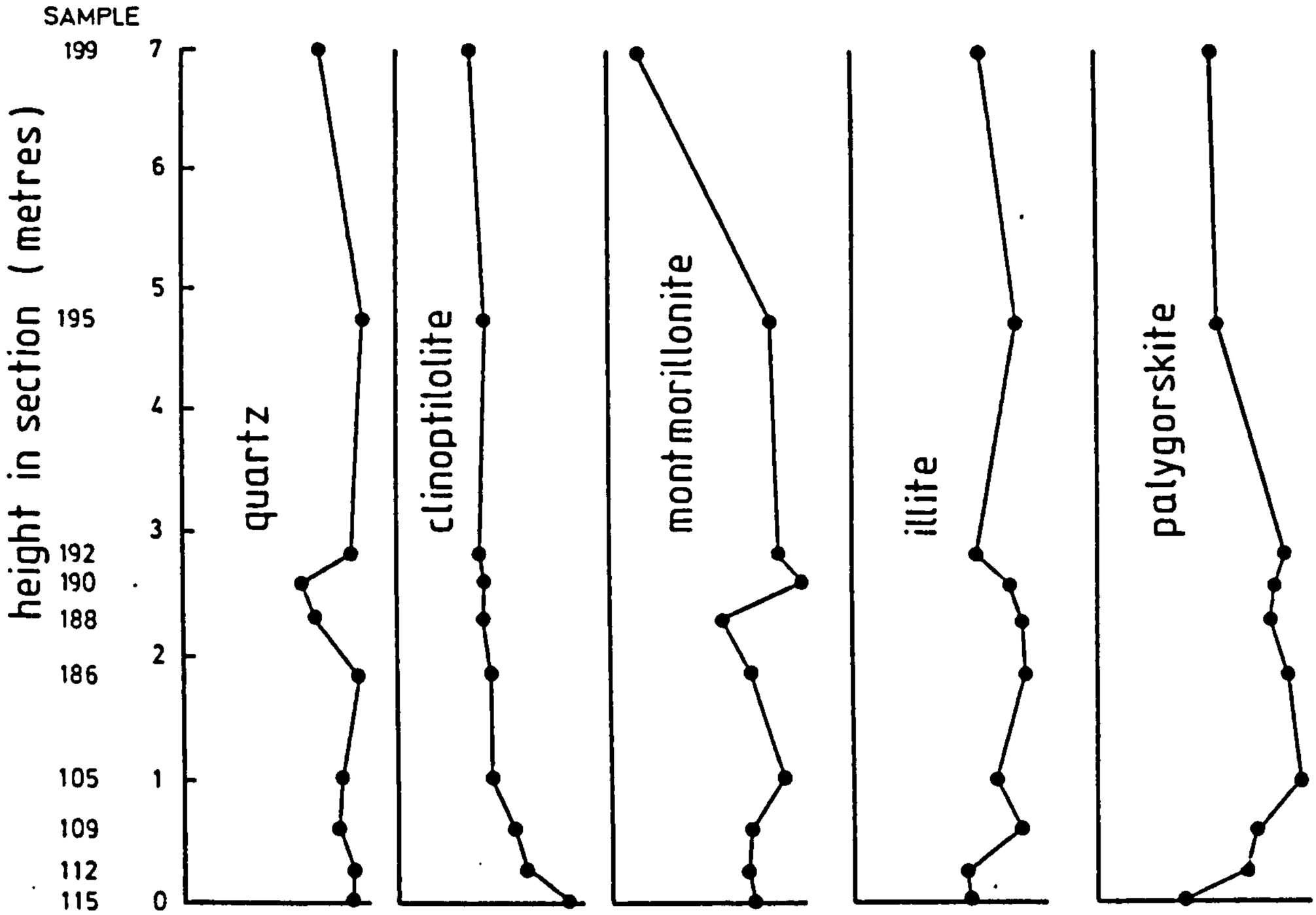

Fig. 6.2

Variation in abundance of aluminosilicate minerals and quartz in the bentonites at Margi. The base of the section is the contact with the clay-rich umber. Abundances are only relative, and were determined using X-ray diffraction. Mass attenuation coefficients for correction of the data were calculated using XRF whole rock chemical analyses.

evidence that clay varies antipathetically with respect to clinoptilolite. This behaviour, as well as the general observation that clinoptilolite is absent in higher sections, supports a diagenetic origin. This is expanded upon below (section 6.5.6).

Manganese minerals

The bentonitic clays are generally depleted in manganese but near the base small regions of enrichment occur. These regions have diffuse boundaries (Plate 6.2D) and seem thus to be of diagenetic origin. X-ray diffraction peaks to 9.6, 4.8, 2.4, 1.42 and 1.40 Å are characteristic of todorokite. In Table 6.1 the chemical composition of one of these concretions is presented, and the composition of the manganese component calculated by comparison with the mean composition of the bentonite. The composition is comparable with published data for todorokites (Burns and Burns, 1979).

Other minerals

Low abundance of small feldspar crystals are commonly observed in the bentonite clays. These may be perfectly euhedral (Plate 6.2E).

Palygorskite is observed using SEM, occuring in the form of small needles. A size fraction nominally less than 0.5μm comprises entirely palygorskite. The origin of this is almost certainly diagenetic as is discussed in Chapter 5, section 5.3.2.

Apatite is present in the form of ostracod fragments and fish teeth (Plate 6.2B). These however form only a small part of the rock and do not have a strong influence on the whole rock phosphorus abundances. Electron micro-probe studies show that the ostracod cuticle is significantly enriched in REE, though quantitative determination was not attempted. Again the abundances are too low to strongly influence the whole rock composition.

Contained within the bentonitic clays at Margi are opaque iron minerals, 10-30μm across. Probe totals are low even if all the iron is assumed to be Fe_2O_3, owing to the poor polish that this mineral takes. Silica and alumina are very low, but titanium oxide is between 6.5-11.5 wt%. Without knowledge of the totals it is not possible to identify the mineral, which might be any combination of

TABLE 6.1

COMPOSITION OF MANGANESE-RICH CONCRETION

	111Mn	Mean Margi bentonite	Ratio	Calculated composition of the manganese component*	Compositional range of modern todorokites**
Si	19.29	28.18	0.685	2.9	0.17 - 0.70
Al	4.93	7.10	0.694	0.9	0.01 - 0.19
Fe	3.00	4.69	0.640	-	0 - 1.15
Mg	2.34	2.99	0.783	1.1	0.61 - 1.36
Ca	1.22	1.62	0.753	0.5	0.86 - 2.34
Na	1.39	1.27	1.194	1.6	0.16 - 1.07
K	1.31	1.57	0.834	0.8	0.29 - 1.29
Ti	0.30	0.35	0.857	0.2	-
Mn	15.52	0.21	73.9	43.6	46.20 - 51.39
P	0.19	0.25	0.760	-	ND
Ba	10055	179	56.2	28000	1700 - 39,000
Ce	89	68	1.309	127	
Co	334	34	9.82	884	80 - 1400
Cr	114	208	0.548	-	
Cu	709	140	5.064	1751	80 - 120,000
La	31	47	0.660	-	
Nd	30	44	0.682	-	
Ni	367	212	1.731	651	400 - 50,000
Pb	507	21	24.14	1397	
Rb	33	69	0.478	-	
Sr	1820	475	3.83	4286	90 - 1100
V	1286	113	11.38	3436	
Y	33	55	0.600	-	
Zn	121	165	0.733	40	300 - 79,000
Zr	69	102	0.676	-	

* Calculated by assuming that none of the La,Nd,Y, or Zr occur in the Mn phase, subtracting the aluminosilicate fraction of each element according to this, and recasting the major elements to give 100% total oxides.
** Data from Burns and Burns (1979)

Comparison with the umber manganese phase

	Analiondas***	Skouriotissa***	Calculated bentonite concretion
Fe	7.72	10.93	-
Mn	32.28	27.07	43.6
Al	0.19	0.38	0.9
Ca	0.50	0.32	0.5
Mg	0.80	0.31	1.1
Ni	343	452	651
Co	697	378	884
Pb	643	718	1397
Zn	161	154	40
Cu	187	651	1751
Ba	7855	3124	28000

*** Data from Chapter 5, section 5.5.3

haematite, illmenite or magnetite.

6.3.3 Radiolarian chert

The radiolarian cherts are described by Robertson (1977a). Thinly bedded non-calcareous radiolarites and radiolarian mudstones form granular cherts in the basal parts of the bentonitic clays. X-ray diffraction reveals abundant Opal-ct and quartz with some smectite and clinoptilolite. In thin section, numerous radiolarians are seen in a matrix of brown optically translucent, almost isotropic, silica, with some finely disseminated clay and rare grains of divitrified glass. Preservation of radiolarian shells varies; they are normally filled by brown isotropic silica, and may be partially or totally replaced by chalcedonic quartz.

The radiolarian cherts in the Margi area contain the same clay mineral assemblage as the host bentonitic clays, and are chemically identical other than the enrichment in silica (section 6.5.4). In the upper parts of the section, both the radiolarites and the bentonitic clays contain increasing abundances of calcite, marking a gradual transition to the overlying Lefkara chalks.

6.3.4 Basal chalks

The basal chalks contain dominantly calcite, and are generally free of biogenic silica. In the Margi area there is a transition to the chalks from the underlying bentonitic clays with gradually increasing carbonate content. In this region the lithogenous component of the chalks is identical to the bentonites. How far upsection in the chalks the bentonitic material is important is not clear.

6.4 GEOCHEMISTRY OF THE SEDIMENTS

In the following section the mean composition and regional variations are considered before examining the inter-element relationships in detail.

6.4.1 Chemical composition of the sediments

On Table 6.2, the mean compositions of the bentonitic clays, radiolarites, and the carbonate-rich Margi bentonite is shown. In general the radiolarite is depleted in all elements except silica, with respect to the bentonitic clay. In the Kalavasos samples the higher abundances of lead is related to manganese enrichment. At Margi, both manganese and lead are depleted in the radiolarites. The carbonate-rich samples are depleted in most elements, but are markedly enriched in calcium, barium, and strontium. The slightly higher relative abundance of silica is due to the presence of biogenic opal. The higher magnesium, chromium and nickel are related to an ultramafic phase which increases in abundance up-section (section 6.5.1).

6.4.2 Regional variations in composition

Sampling is insufficiently complete to allow a full assessment of regional variations, but some notable features emerge from the existing data.

Bentonitic Clays.

The Margi samples are relatively enriched in magnesium, chromium and nickel, which are concentrated in an ultramafic phase (section 6.5.1). The Skouriotissa and Dhrapia samples contain greater amounts of iron and zinc. Copper is higher at Skouriotissa, as it is in all sediment types from there (Table 6.3).

Radiolarites

The relative enrichment in silica is variable. The Margi sediments are again characterised by higher magnesium (relative to Al), chromium and nickel. Manganese is richer at Kalavasos, and this is accompanied by a greater relative abundance of barium, lead and strontium (Table 6.4).

TABLE 6.2

MEAN COMPOSITIONS OF THE NON-METALLIFEROUS SEDIMENTS

	Bentonitic clays	Radiolarites	Carbonate bearing clays (Margi)
Si	28.47	38.67	27.42
Al	6.85	3.83	4.78
Fe	5.18	2.75	3.11
Mg	2.16	1.24	2.37
Ca	1.84	0.80	6.99
Na	1.27	0.60	0.23
K	1.54	0.80	0.98
Ti	0.36	0.22	0.22
Mn	0.24	0.34	0.12
P	0.17	0.12	0.14
Ba	140	62	341
Ce	68	29	45
Co	27	22	-
Cr	110	73	148
Cu	144	86	63
La	47	19	30
Nd	44	21	30
Ni	98	63	159
Pb	19	27	17
Rb	69	34	48
Sr	302	235	356
V	88	48	75
Y	55	27	34
Zn	231	149	115
Zr	75	51	66

Data from this work and A.H.F. Robertson (unpublished data)

TABLE 6.3

MEAN COMPOSITIONS OF BENTONITIC CLAYS

	N=1 SKOURIOTISSA	N=10 MARGI	N=1 DHRAPIA	Mean Mean
Si	28.70	28.18 ± 0.81	28.52	28.47
Al	6.67	7.10 ± 0.22	6.77	6.85
Fe	5.32	4.69 ± 0.23	5.53	5.18
Mg	1.63	2.99 ± 0.21	1.87	2.16
Ca	1.57	1.62 ± 0.15	2.34	1.84
Na	ND	1.27 ± 0.27	ND	1.27
K	1.74	1.57 ± 0.07	1.32	1.54
Ti	0.37	0.35 ± 0.02	0.35	0.36
Mn	0.40	0.21 ± 0.08	0.10	0.24
P	0.12	0.25 ± 0.02	0.15	0.17
Ba	84	179 ± 40	156	140
Ce	ND	68 ± 3	ND	68
Co	22	34(N=1)	25	27
Cr	64	208 ± 24	59	110
Cu	177	140 ± 37	116	144
La	ND	47 ± 3	ND	47
Nd	ND	44 ± 3	ND	44
Ni	57	212 ± 27	26	98
Pb	26	21 ± 3	9	19
Rb	ND	69 ± 3	ND	69
Sr	237	475 ± 105	193	302
V	76	113 ± 5	76	88
Y	ND	55 ± 4	ND	55
Zn	268	165 ± 11	261	231
Zr	82	102 ± 7	40	75

ND = Not determined

TABLE 6.4

MEAN COMPOSITIONS OF RADIOLARITES AND MARLS

	Radiolarites				Carbonate bearing
	MARGI	KALAVASOS		MEAN	MARGI
		1	2		
Si	37.47 ± 2.56	34.83	43.71	38.67	27.42 ± 4.04
Al	3.39 ± 0.91	6.24	1.85	3.83	4.78 ± 1.02
Fe	2.34 ± 0.65	4.09	1.82	2.75	3.11 ± 0.57
Mg	1.58 ± 0.49	1.69	0.45	1.24	2.37 ± 0.47
Ca	0.71 ± 0.22	1.25	0.43	0.80	6.99 ± 2.01
Na	0.60 ± 0.19	ND	ND	0.60	0.23 ± 0.06
K	0.70 ± 0.21	1.25	0.46	0.80	0.98 ± 0.19
Ti	0.17 ± 0.05	0.35	0.15	0.22	0.22 ± 0.04
Mn	0.07 ± 0.02	0.25	0.69	0.34	0.12 ± 0.04
P	0.11 ± 0.03	0.22	0.04	0.12	0.14 ± 0.02
Ba	68 ± 17	77	41	62	341 ± 209
Ce	29 ± 6	ND	ND	29	45 ± 9
Co	ND	19	25	22	ND
Cr	113 ± 39	67	38	73	148 ± 26
Cu	58 ± 23	126	73	86	63 ± 18
La	19 ± 5	ND	ND	19	30 ± 6
Nd	21 ± 4	ND	ND	21	30 ± 5
Ni	108 ± 34	34	46	63	159 ± 34
Pb	12 ± 2	32	36	27	17 ± 2
Rb	34 ± 9	ND	ND	34	48 ± 9
Sr	146 ± 67	447	112	235	356 ± 86
V	53 ± 15	36	56	48	75 ± 13
Y	27 ± 6	ND	ND	27	34 ± 6
Zn	79 ± 24	225	143	149	115 ± 23
Zr	48 ± 15	63	42	51	66 ± 13

ND = Not determined

6.4.3 Inter-element correlations study - Margi sediments

Introduction

From a 10m section above the Margi umber, 10 samples of bentonitic clays, 5 samples of radiolarite and 4 samples of calcite-bearing clay were collected. An inter-element correlation study was performed using both variation diagrams and factor analysis. The details of the factor analysis technique are given in Chapter 4 section 4.2.7.

6.4.3.1 Major element components

Variation diagrams

The major elements are shown plotted against Al in Fig. 6.3 and 6.4. The gross trends are apparent from these. The Si/Al plot (Fig. 6.3A) shows most of the bentonitic clays clustering close to the trend of the umber and clay-rich umber. The radiolarites and some of the bentonitic clays lie on a mixing line towards pure silica. The calcite bearing samples have variable silica contents, but fall below the mixing line between aluminosilicate and silica because of dilution. The Fe/Al, K/Al and Ti/Al ratios are all constant throughout the section regardless of sediment type. Ca/Al is constant in all but the calcite-bearing samples. Na/Al is constant for most of the samples, but Na is strongly depleted in the calcite-bearing samples, and in one of the bentonitic clays and one radiolarite. This change appears to be stratigraphic, the Na content showing marked depletion in the upper part of the section. The Mg/Al ratio is constant except for the lowermost of the bentonitic clays which are depleted. The Mn/Al ratios are more scattered. Manganese is, however, richest in the lowermost bentonitic clays which is the major cause of the variation. The P/Al ratio also shows a small variation, and is greatest in the lowermost bentonitic clays. That this results from a phosphate enrichment is supported by the La, Nd and Y ratios which are also greater in the lowermost sediments.

From these variation diagrams five chemical components are identified: aluminosilicate, apatite, biogenic silica, carbonate and MnO_2. However, it is clear that the aluminosilicate is not of constant composition, and further subdivision may be possible.

Fig. 6.3

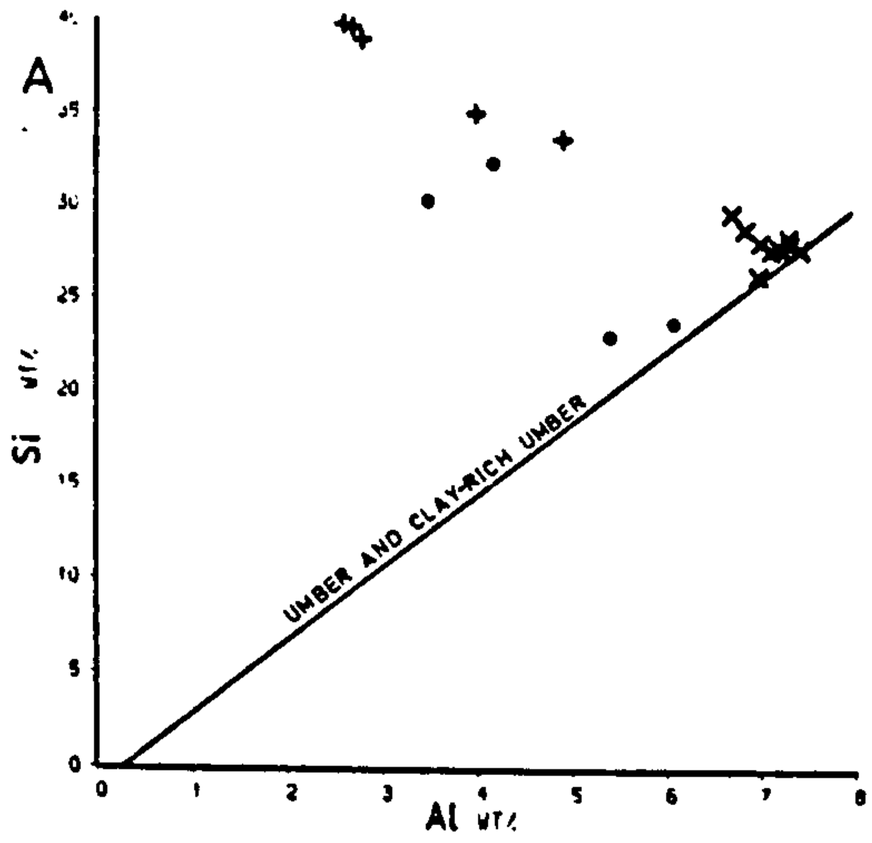

Element variation diagrams for the Margi bentonitic clays, radiolarites and marls. X = bentonitic clay + = radiolarites. O = marls. The observed trends all reflect mixing of silica, carbonate and aluminosilicate. Na depletion, relative to Al, is observed in the uppermost sediments in the section.

Fig. 6.4

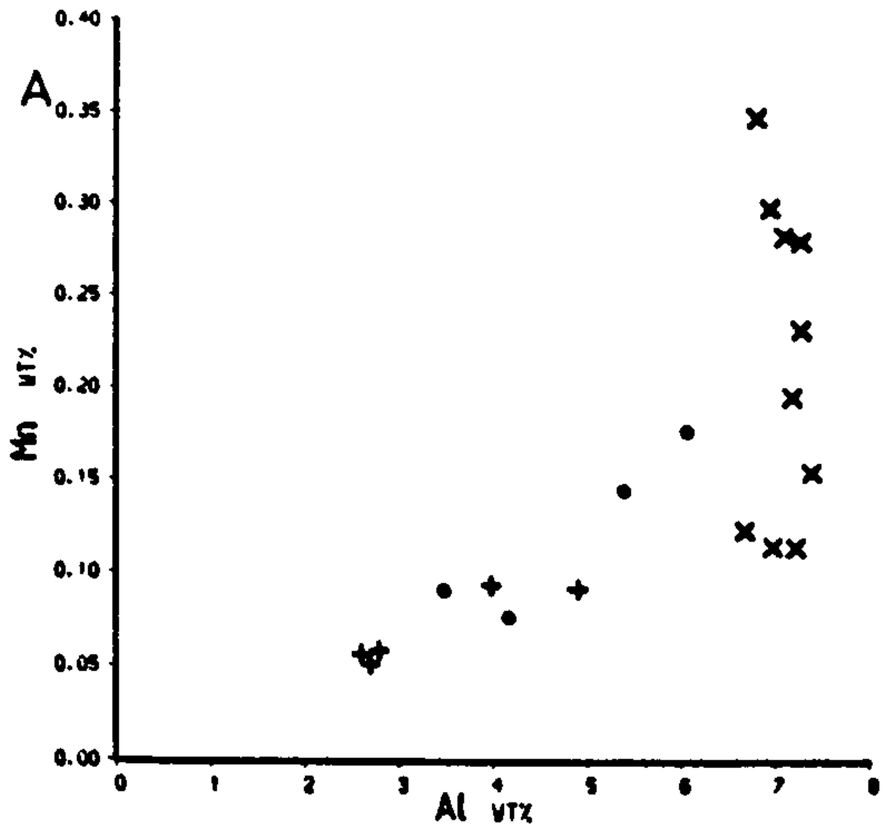

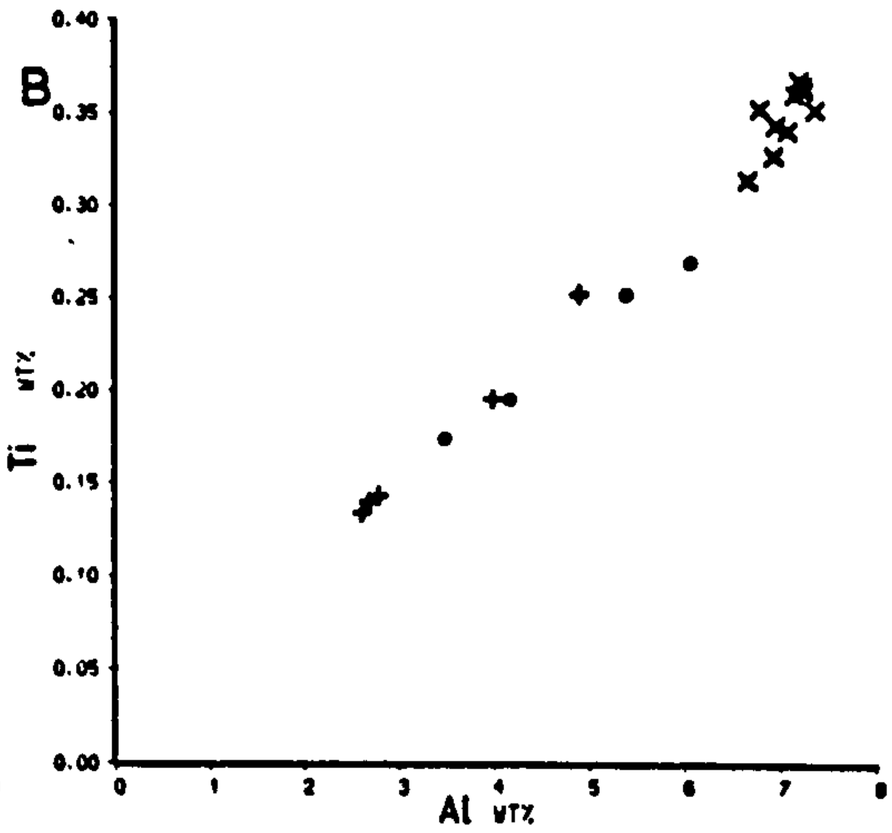

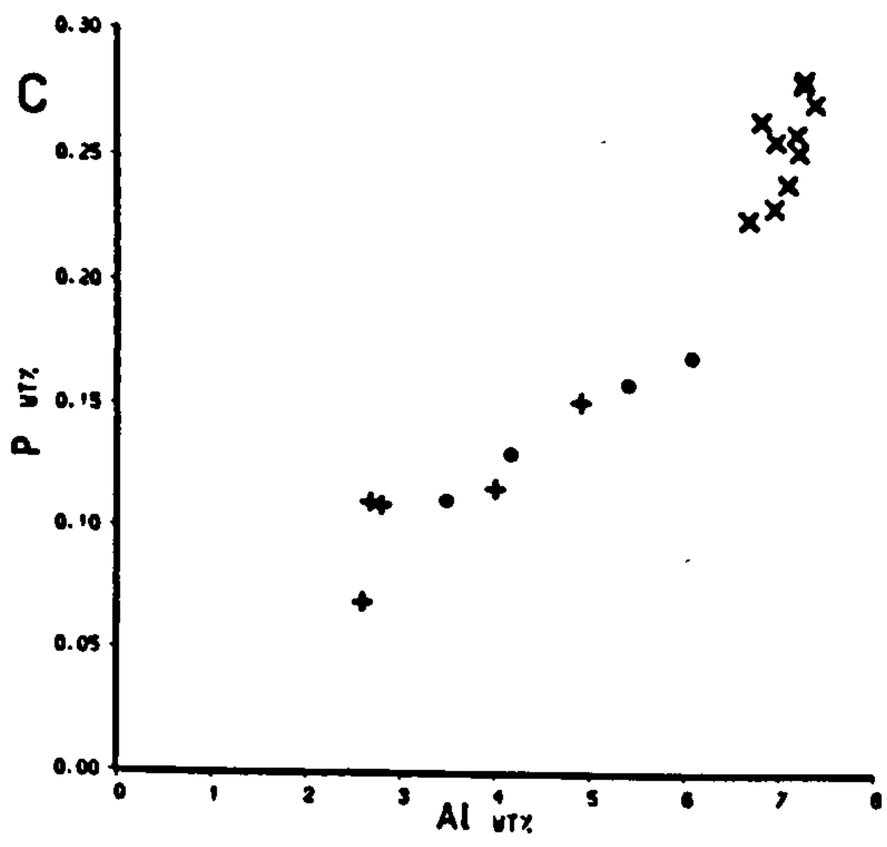

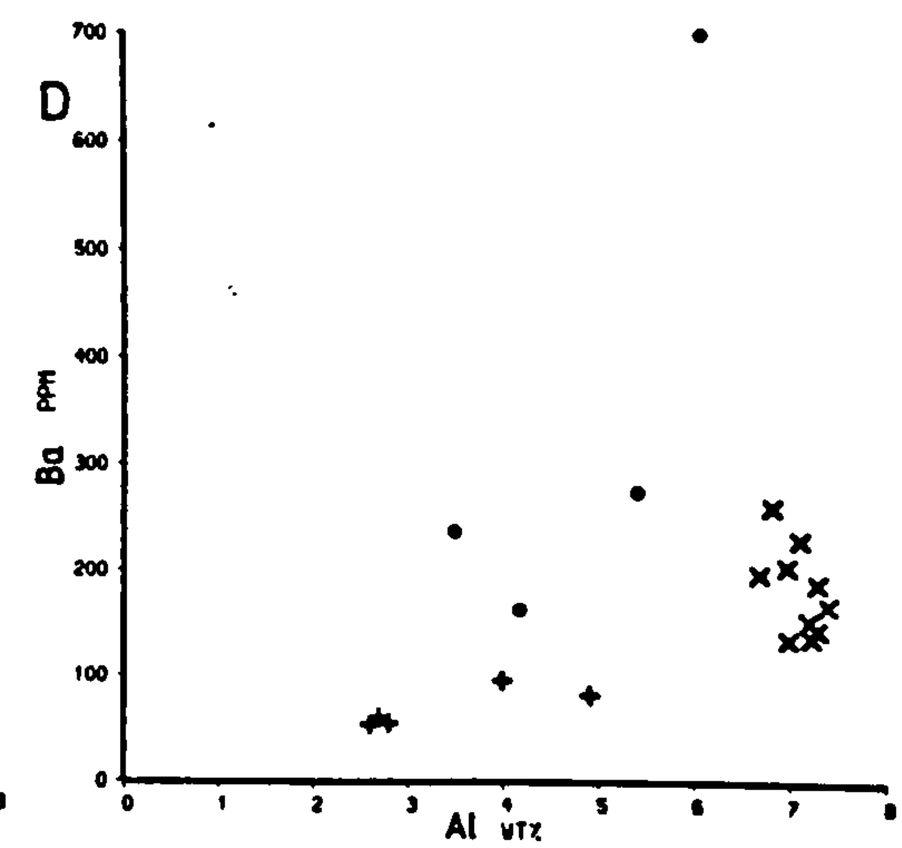

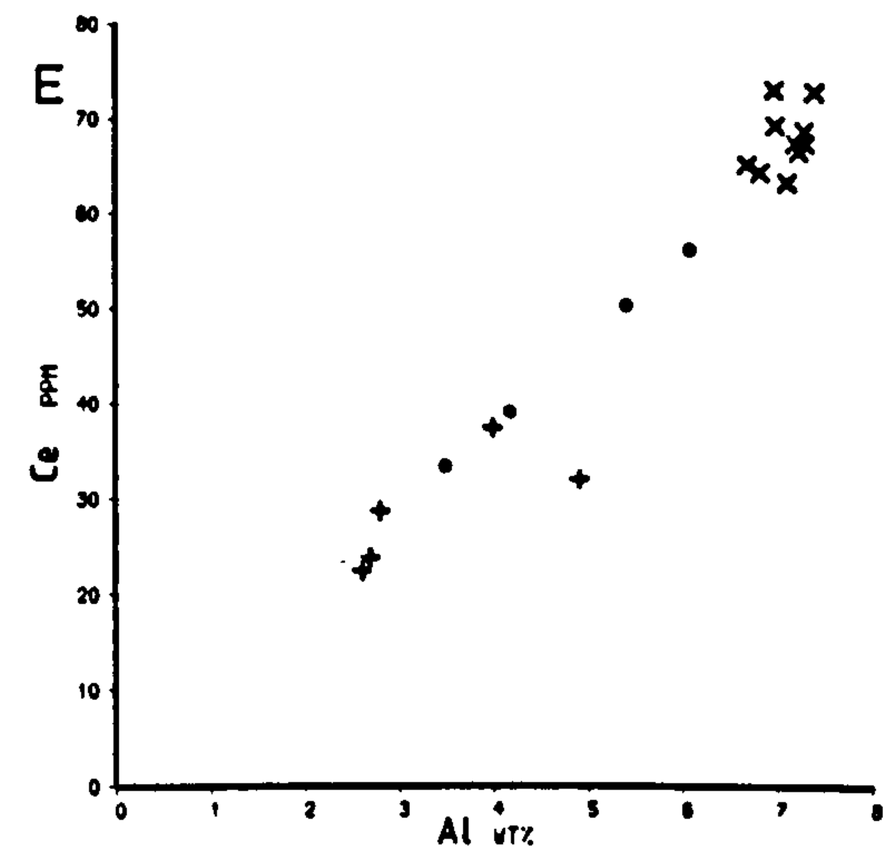

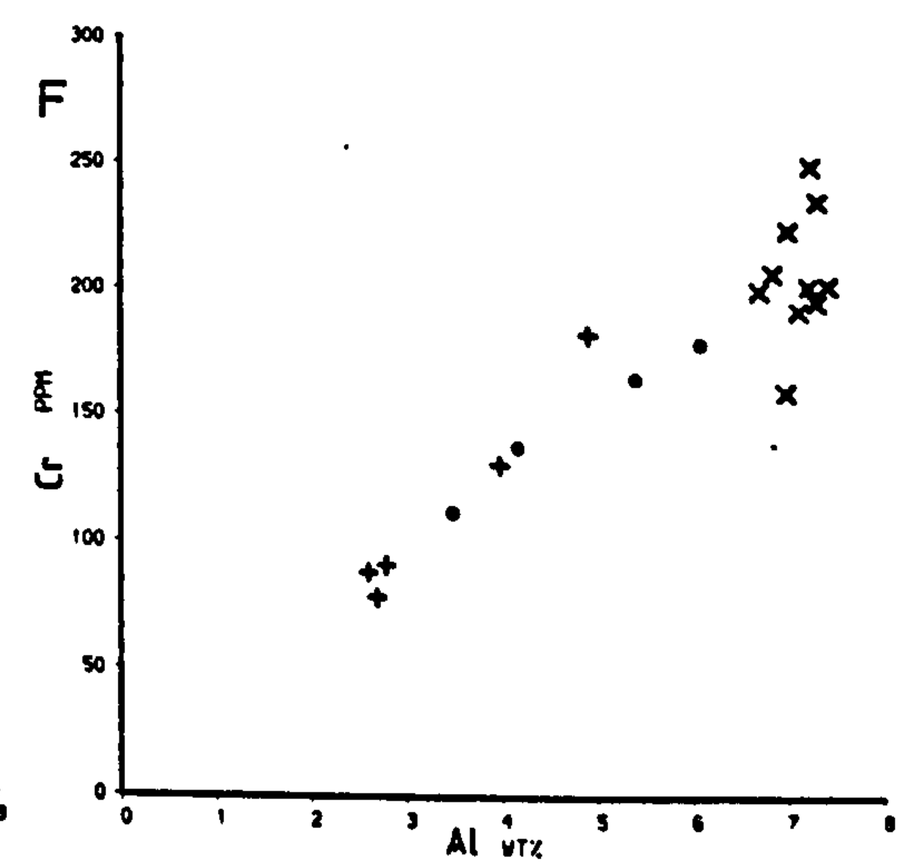

Element variation diagrams for the Margi bentonitic clays, radiolarites and marls. X = bentonitic clay + = radiolarites. O = marls. The importance of an Mn component in the sediment is apparent from (a). Ba follows the Mn trend in the bentonitic clays, but is significantly enriched in the marls. Cr is associated with the aluminosilicate.

Fig. 6.5

MARGI BENTONITIC CLAYS

R-MODE FACTOR ANALYSIS - varimax rotated factor loadings

A - eigenvalue B - percent contribution

FACTOR

6.4.3.2 Factor Analysis

The factor analysis was applied to the 10 bentonitic clay samples, with a view to identifying systematic variations in the aluminosilicate (Fig. 6.5). Factor I contains Al-Fe-Ca-Na-K-Ti-P suggesting that both Si, Mg and Mn are independent of the principal aluminosilicate phase. Factor II contains dominantly Mg and Ca. Factor III contains Si and Mg in opposition to Al and Na. Factor IV contains Mn. Factor V does not contain significant major elements.

The clay is therfore a complex mixture, as would be expected considering its mineralogy (smectite + illite + quartz + MnO_2 + plagioclase + palygorskite). Interpretation of the result is necessarily tentative. In addition to a dominant aluminosilicate component (Factor I), there is separate Mg factor with associated trace elements (tentatively identified as an ultra-mafic phase). The elements in factor II may be interpreted as plagioclase (sodic) opposing an association of Si and Mg which might represent palygorskite. A manganese component is clearly distinguishable.

6.4.3.3 Trace element associations - Margi sediments

The distribution of trace elements is illustrated in Figs. 6.6, 6.7, 6.8 where various two element, mostly Element/Al, plots are shown. A factor analysis was also performed on the bentonitic clays alone. The results of this are discussed below.

Barium

	ppm
Calcite-bearing clay	341
Radiolarite	68
Bentonite clay	179
Mn-rich sample	10055
Clay-rich umber	1117

As can be seen from the values above, Ba is very strongly enriched in the Mn-rich concretions. This shows up on plot 6.4d, where there is a basal enrichment in Ba coinciding with such an enrichment in Mn. The situation is modified however by the

Fig. 6.6

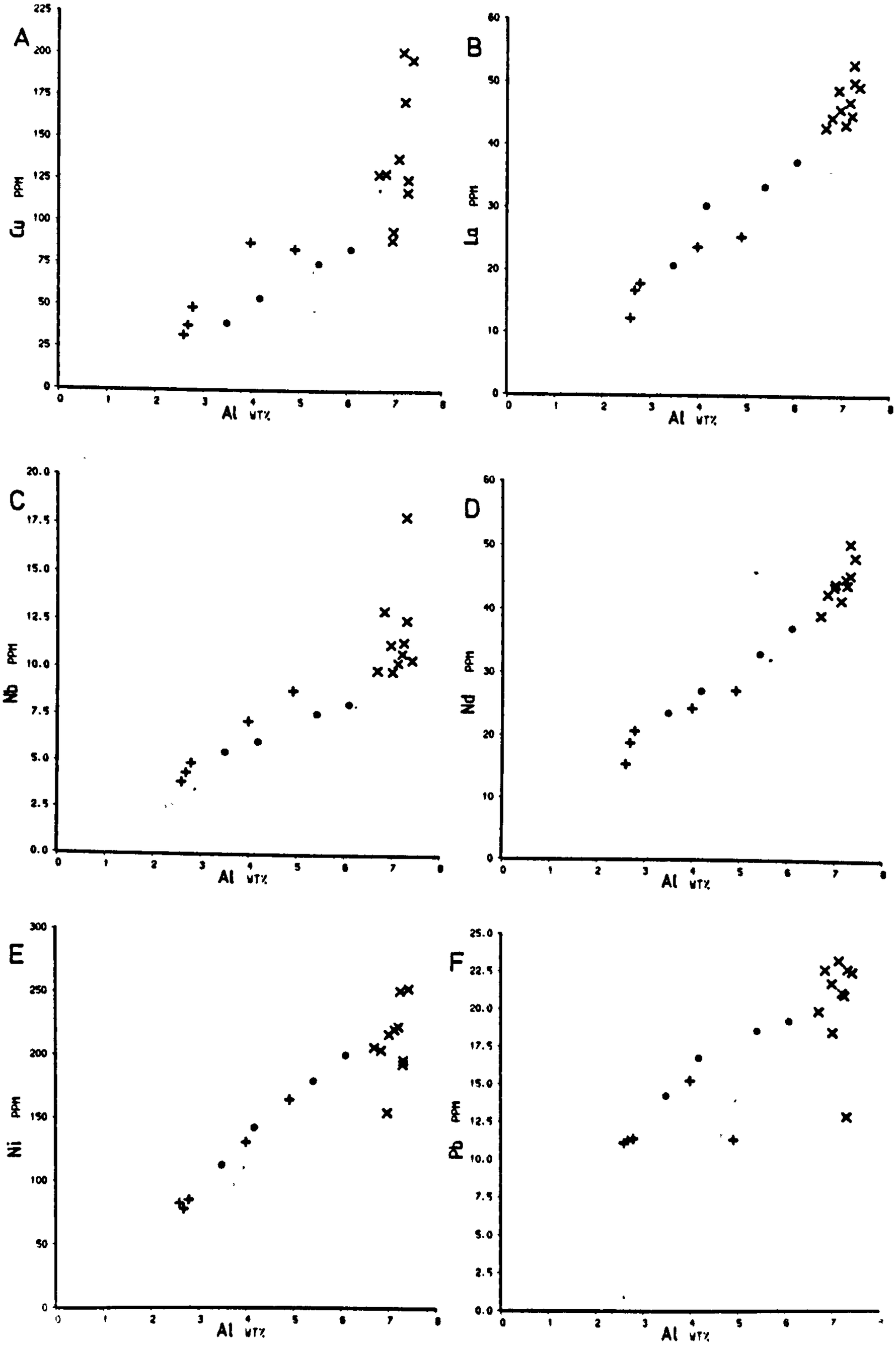

Element variation diagrams for the Margi bentonitic clays, radiolarites and marls. X = bentonitic clay + = radiolarites. O = marls. Cu follows the trend of Mn. The others show more nearly constant ratios with Al.

Fig. 6.7

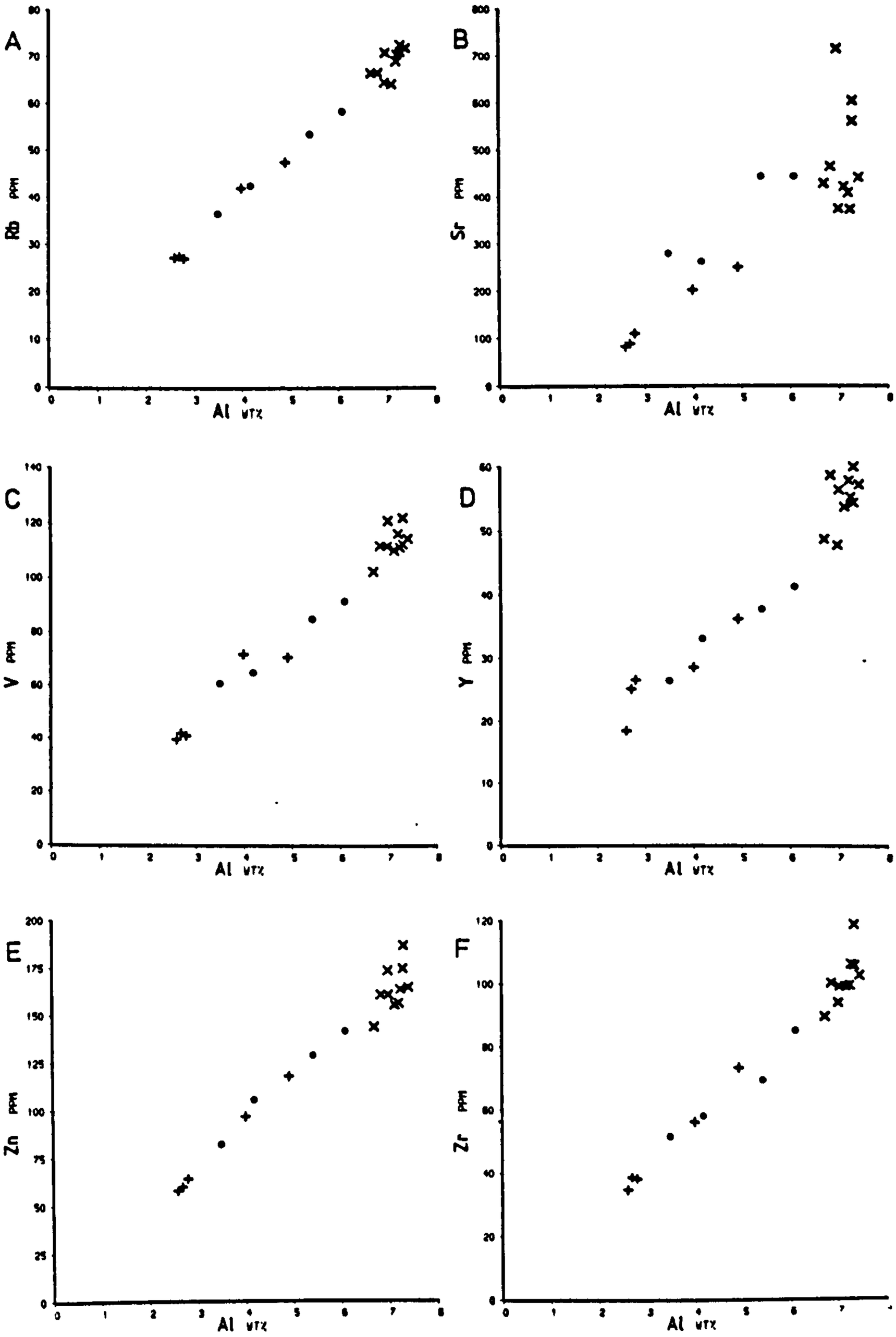

Element variation diagrams for the Margi bentonitic clays, radiolarites and marls. X = bentonitic clay + = radiolarites. O = marls. Sr follows Mn, though is also weakly enriched in the marls. The others show near constant ratios to Al.

Fig. 6.8

Element variation diagrams for the Margi bentonitic clays, radiolarites and marls. X = bentonitic clay + = radiolarites. O = marls.

a) The Ca-P correlation observed, other than in the marls, is not due to apatite, but to the composition of the aluminosilicate.

b) Sr shows only a weak association with excess Ca. The carbonate must be depleted in strontium.

c) The Rb/K ratio is very constant, and is distinctly different from that in the Troodos lavas.

d,e) For both Ba and Pb, there is a positive correlation of relative enrichment with relative Mn abundance. In the case of Ba, this is not so of the marls, and in the case of Pb, is true only of the bentonitic clays.

Fig. 6.8

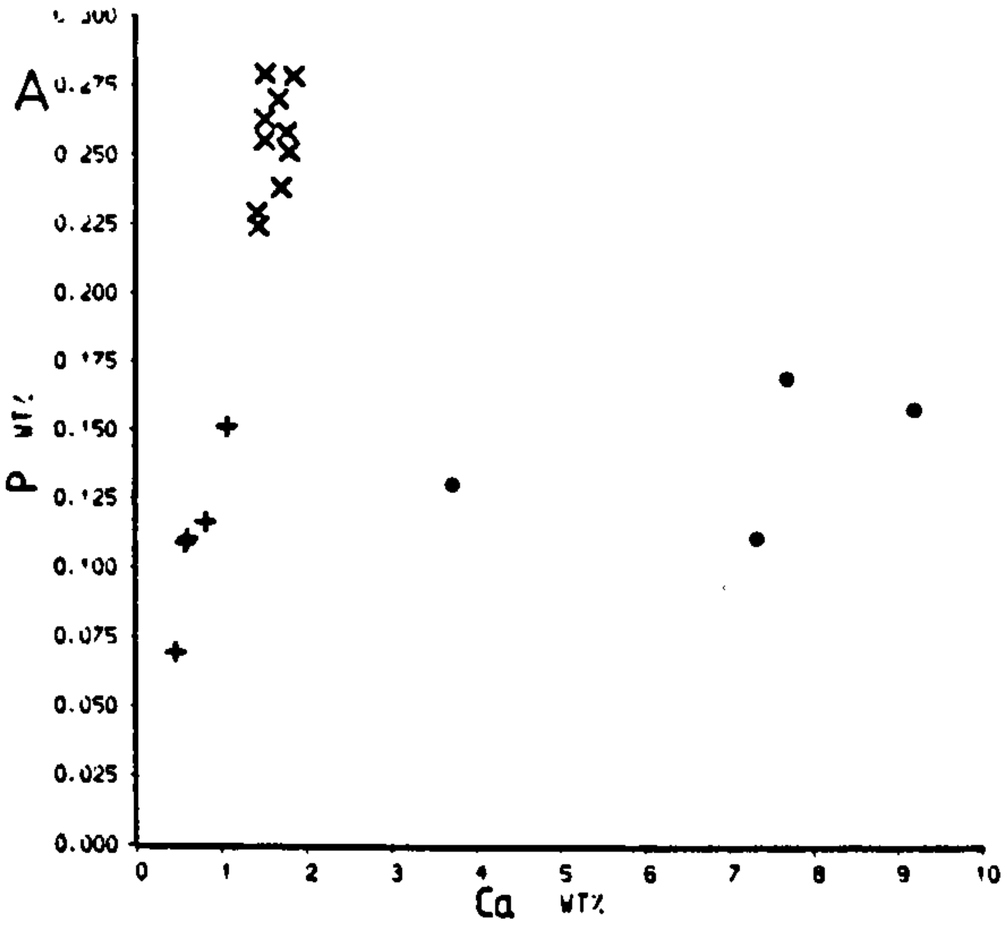
A
P WT%
0.300
0.275
0.250
0.225
0.200
0.175
0.150
0.125
0.100
0.075
0.050
0.025
0.000
0 1 2 3 4 5 6 7 8 9 10
Ca WT%

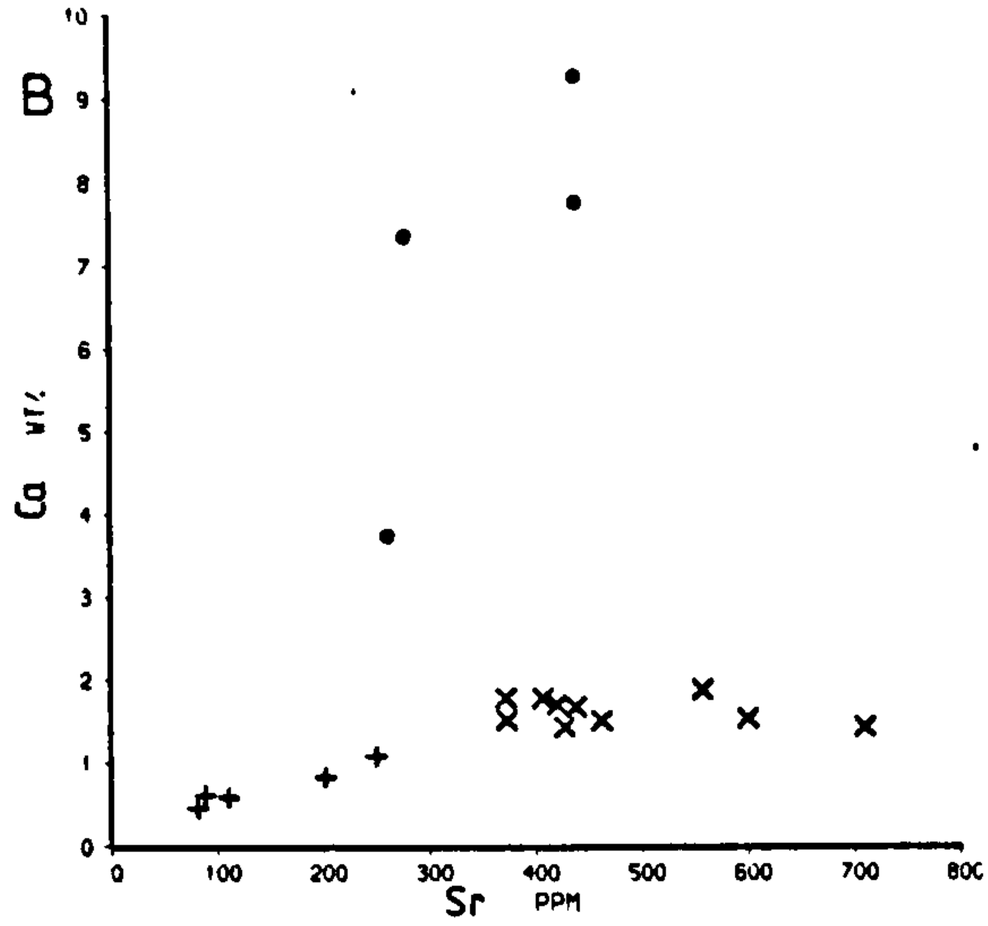
B
Ca WT%
10
9
8
7
6
5
4
3
2
1
0
0 100 200 300 400 500 600 700 800
Sr PPM

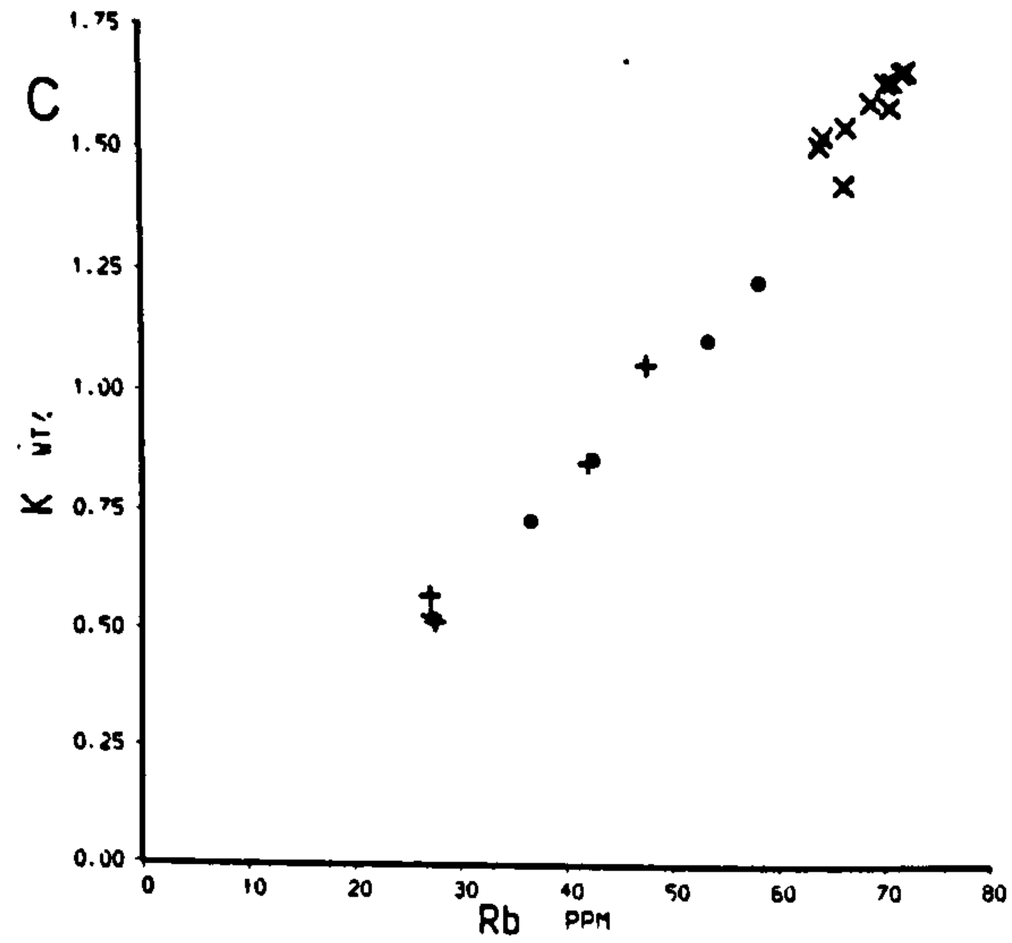
C
K WT%
1.75
1.50
1.25
1.00
0.75
0.50
0.25
0.00
0 10 20 30 40 50 60 70 80
Rb PPM

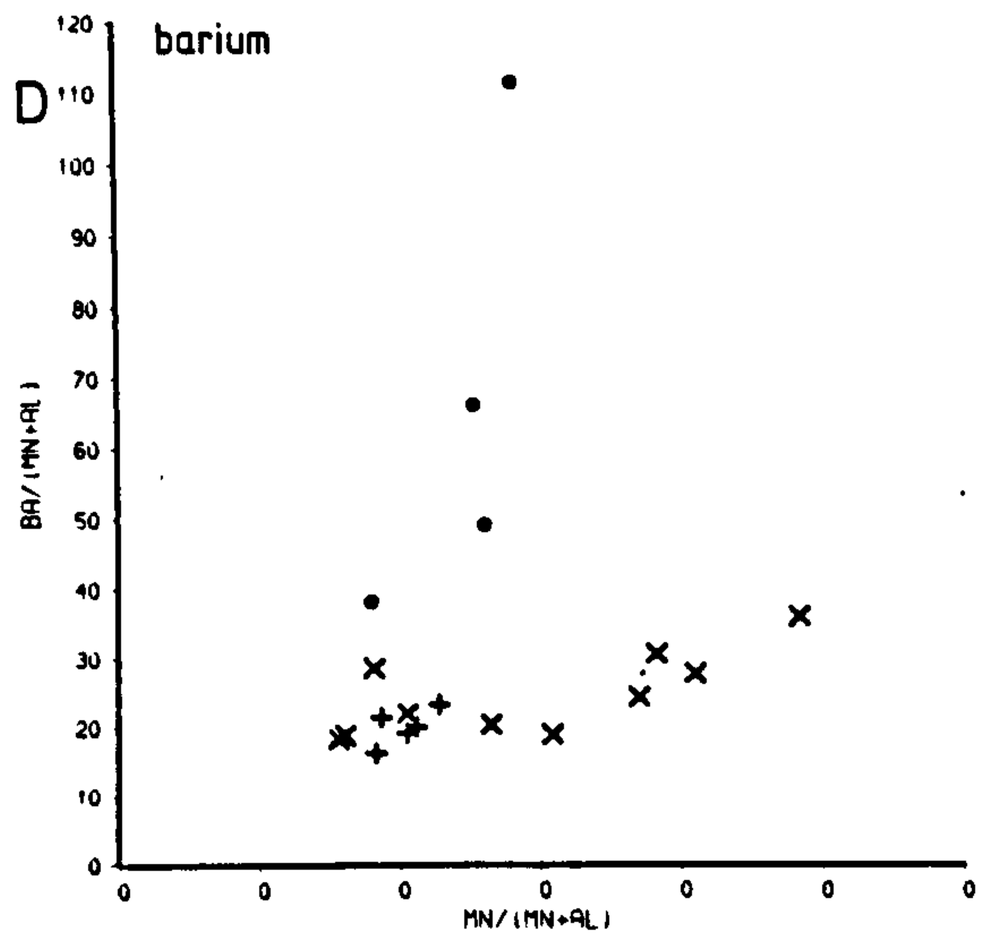
D
barium
BA/(MN+AL)
120
110
100
90
80
70
60
50
40
30
20
10
0
0 0 0 0 0 0 0
MN/(MN+AL)

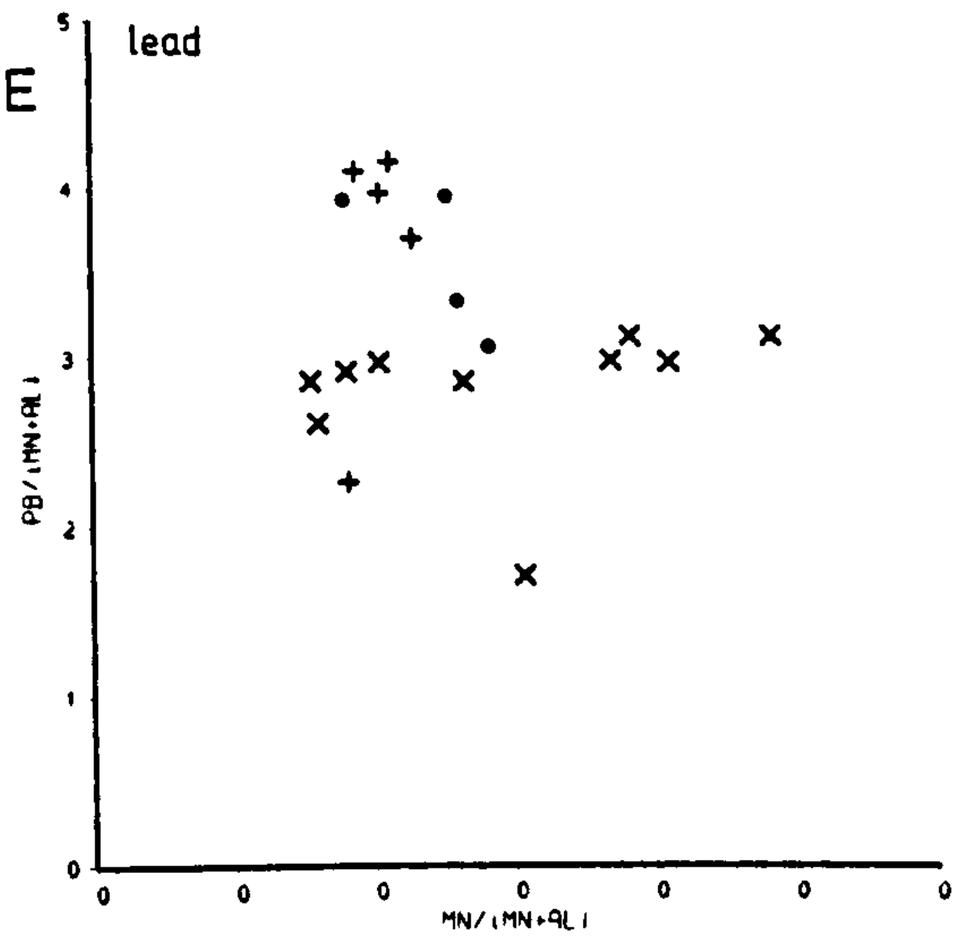
E
lead
PB/(MN+AL)
5
4
3
2
1
0
0 0 0 0 0 0 0
MN/(MN+AL)

enrichment of Ba in the carbonate-bearing samples. An association of Ba with calcite has been described from the modern oceans, in addition to an association with hydrogenous ferromanganese oxide. The former is believed to relate to productivity rather than to direct replacement of calcium by barium (Arrhenius and Bonatti, 1965; Boström, et al., 1973).

The factor analysis of the bentonitic clays also shows the nearly exclusive association of Ba with Mn. It is clear that if Mn-related Ba is removed, very little remains.

Cerium

	ppm
Calcite-bearing clay	45
Radiolarite	29
Bentonitic clay	68
Mn-rich sample	89
Clay-rich umber	122

Ce is most strongly enriched in the clay rich umber, but is also slightly so in the Mn-rich sample. The abundances in the radiolarite and carbonate bearing samples can be explained by dilution of the clay alone. In the factor analysis, Ce correlated with Na and Al in factor III. It is seperate from the main alumino-silicate and is not associated with Mn.

Cobalt

	ppm
Bentonitic clay	34
Mn-rich sample	334
Clay-rich umber	110

Just three analyses exist for the above sediments from the Margi area, but close agreement is found with data obtained elsewhere (see Tables 6.3, 6.4). The strong enrichment in the Mn-bearing material indicates hydrogenous enrichment of Co in the ferromanganese phase. As with Ba, very little Co remains in the rock if if this component is removed.

Chromium

	ppm
Carbonate-bearing clay	148
Radiolarite	113
Bentonitic Clay	208
Mn-rich sample	114
Clay-rich umber	54

Cr is enriched in all the supra-umber sediments, even in the radiolarites which are strongly diluted by silica. This marked change is illustrated in Fig. 5.8. where the increase in Cr is seen to correspond exactly with the change from clay-rich umber to bentonitic clay. This change is accompanied by a change in K, Mg, Ni to Al ratios, though the other elements remain nearly constant. In Fig. 6.4F the variability of the Cr/Al ratio is illustrated, and the similarity to the Mg/Al distribution is worth noting.

Clearly a mafic source is required to explain the abundance of the Cr. Yet, the most obvious source - the Troodos Lavas -must be dismissed, because of essentially acidic volcanic composition of the bentonitic clay (section 6.5.1). The Cr content of the upper lavas is little more than that of the bentonites, requiring very large amounts to be admixed - this material is just not there. The only way to supply enough Cr without altering the major element chemistry is have a highly enriched phase. No chromite has been observed, but the presence of traces of chlorite in the X-ray diffractograms may offer an explanation. Weathering of ultramafics can produce chlorite with nearly 10% chromium (Deer, Howie and Zussman*). The association of Cr with Ni and Mg (Fig. 6.5) is also in support of this view, though the stronger association with Fe and V may indicate that another mafic phase is important.

* Vol 3, page 146

Copper

	ppm
Calcite-bearing clay	63
Radiolarite	58
Bentonitic clay	140
Mn-rich sample	709
Clay-rich umber	261

Cu is strongly enriched in the Mn-bearing samples. It also shows a decrease relative to Al up section, possibly reflecting the upward decrease in Mn. The enrichment in the bentonitic clay is very variable, but does not closely follow the Mn as its distribution might suggest. The factor analysis shows a strong association of Cu with Ni and Mg, suggesting that some kind of mafic source may also exert an influence.

Nickel

	ppm
Calcite-bearing clay	159
Radiolarite	108
Bentonitic clay	212
Mn-rich sample	367
Clay-rich umber	181

There is an enrichment of Ni in the supra-umber sediments. This argues for an increase in the terrigenous supply of Ni. However an association of Ni with Mn is also observed, in the Mn-rich sample. The very strong association of Ni with Cu and Mg is apparent in the factor analysis.

Lead

	ppm
Calcite-bearing clay	17
Radiolarite	12
Bentonitic clay	26
Mn-rich sample	507
Clay-rich umber	175

Pb is very strongly enriched in the Mn-bearing samples - much more so in the Mn-rich bentonitic clay than in the clay-rich umber. The enrichment is illustrated in Fig. 6.6F, where a slight enrichment of Pb in the basal bentonitic clay is observed. This is further illustrated in a vertically stretched triangular diagram (Fig. 6.8E), which for the bentonites shows a linear relationship with a high Pb/Mn intercept. The slight relative enrichment of the Pb in the carbonate rich clays may reflect a biogenic input, but this is far from certain. The strong association of Pb with Mn is also illustrated in the factor analysis (Fig. 6.5).

Rubidium

	ppm
Calcite-bearing clay	48
Radiolarite	34
Bentonitic clay	69
Mn-rich sample	33
Clay-rich umber	91

Rb is enriched in the clay rich umber with respect to the overlying sediments. This is in part due to the higher K content, but also to a higher Rb/K ratio. With the exception of the Mn-rich sample, the K/Rb ratios are constant (227 $\pm$ 10). A comparison with the underlying sediments is given in Table 5.9 . The excellent Rb/Al and Rb/K correlations are shown in Figs. 6.7A, 6.8C. respectively.

Strontium

	ppm
Calcite-bearing clay	356
Radiolarite	146
Bentonitic clay	475
Mn-rich sample	1820
Clay-rich umber	483

Sr is very strongly enriched in the Mn-rich sample of bentonite, but is comparable in the clay-rich umber to the bentonitic clay and carbonate-bearing clay. In Fig. 6.7B, the Sr/Al plot shows not only the variable Sr enrichment in the bentonite, reflecting the associations with Mn, but also the slight enrichment in the carbonate-rich samples. In Fig. 6.8B, the Ca/Sr plot shows this weak association, indicating a very high Ca/Sr ratio. The factor analysis indicates an association of Sr with Zn (Fig. 6.5).

Vanadium

	ppm
Calcite-bearing clay	75
Radiolarite	53
Bentonitic clay	113
Mn-rich sample	1286
Clay-rich umber	304

The V is strongly enriched in the metalliferous sediments but is low and of constant proportion to Al in the other types in Fig. 6.7C. However the factor analysis indicates that V correlates best with Cr, and thus may be related to an independent mafic component.

Zinc

	ppm
Calcite-bearing clay	115
Radiolarite	79
Bentonitic clay	165
Mn-rich sample	121
Clay-rich umber	175

There is a slightly greater Zn/Al ratio in the clay rich umber than in the overlying sediments, arguing for for some kind of enrichment. However there is not a significant difference between any of the supra umber sediment types, including the Mn-rich sample. The Zn/Al plot (Fig. 6.7E) shows this constant ratio, but also shows some variation in the bentonitic clays. The factor analysis shows that Zn is not exclusively associated with Al, but correlates also with Sr.

Zirconium

	ppm
Calcite-bearing clay	66
Radiolarite	48
Bentonitic clay	102
Mn-rich sample	69
Clay-rich umber	120

There is a slightly greater Zr/Al ratio in the clay-rich umber than in the overlying sediments, but as with Zn there is no significant difference between the supra-umber sediment types (Fig. 6.7F) The factor analysis also shows a very strong association of Zr with the Al.

Lanthanum, Neodymium and Yttrium

These three elements are discussed together owing to the similarity of their behaviour.

	ppm	La/Al	ppm	Nd/Al	ppm	Y/Al
Calcite-bearing clay	30	6.3	30	6.3	34	7.1
Radiolarite	19	5.6	21	6.2	27	8.0
Bentonitic clay	47	6.6	44	6.2	55	7.7
Mn-rich sample	31	6.3	30	6.1	33	6.7
Clay-rich umber	102	15.5	92	14.0	92	14.0

All three elements are strongly enriched in the clay-rich umber, as they are in the pure umber, but element/Al ratios vary little through the different supra-umber samples (Fig. 6.6B, D, 6.7D). They do however show slight enrichment in some of the bentonitic clay samples, similar to the trend of phosphate.

The factor analysis shows a strong association with Al.

6.4.3.4 Trace element associations - a summary

The trace elements fall into three principal categories. First, Rb-Zn-Y-Zr-La-Ce-Nd show little or no variation through the sediment types and correlate well with Al. Some Y-La-Nd is associated with phosphate, but this component is not abundant.

Secondly, Ni-Cr-Cu-V behave differently and show independence from Al and an association with Mg or Fe. Ni and Cu are also influenced by the Mn enrichment.

Thirdly, Ba-Co-Cu-Ni-Pb-Sr-V are all more or less strongly enriched in the Mn component. The association of Ba, Sr and Pb with Mn is clearly observed in the bentonitic clay samples, indicating that ratios with Mn are fairly constant. For the other elements, variations caused by the Mn component are either irregular, or insignificant.

The above observations apply to the sediments from the Margi area. However there is strong chemical similarity between the different sites which have been examined (section 6.4.2). The most important differences concern the Mg-Ni-Cr contents which are very

much enriched at Margi.. Clearly the component containing these elements was more abundant at Margi. Other small differences in enrichment, for example of Fe and Zn, are probably related to proximity and activity of the hydrothermal source.

6.5 DISCUSSION

In the preceding sections, the mineralogy and chemistry of the non-metalliferous cover sediments has been described. Below, the chemical and mineralogical data are discussed in terms of the origins and diagenesis of the sediments.

6.5.1 Chemical composition of the lithogenous component- possible terrigenous sources

The chemical composition of the Margi bentonitic clay is shown in Table 6.5. Using the composition of the manganese-rich sample, the trace element composition of the sediment is corrected for manganese-related hydrogenous elements. In contrast to modern deep sea clays this makes relatively little difference. The resulting composition is unusual, resembling acid-intermediate volcanic compositions in most respects, but containing high abundances of copper, nickel, chromium and magnesium. The strong association of Cr-Ni-Mg and the relatively great abundances of the Cr-Ni, are suggestive of ultramafic material - a mafic component would contain insufficient of these two elements to have such an effect without greatly influencing the other elements.

If the assumption is made that all the Cr is present in an ultramafic component, and a composition for this is assumed (from Turekian and Wedepohl, 1961), then a recalculated composition can be obtained (Table 6.5). This new composition resembles a rhyo-dacitic composition both in respect to the trace and major elements. The composition does however show a deficiency in alkalis and an enrichment in iron. Of the trace elements, barium is very low, and both zinc and copper are high. The latter two may result from the proximity of the Troodos spreading axis.

In summary, the rather odd composition of the bentonitic clay can be explained if it is assumed to comprise a mixture of a minor ultramafic component and a major intermediate-acid volcanic component. Such an interpretation of an argillaceous rock, comprising a number of discrete minerals, must be regarded with caution. However, from the character of the Kannaviou volcaniclastic sandstones, there is no doubt that an important volcanic source existed. In the Eastern Mediterranean at this time, intrusions of serpentinites

TABLE 6.5

RECALCULATION OF THE BENTONITIC CLAY COMPOSITION

Subtraction of the manganese component assuming all manganese occurs as free oxide.Subtraction of an ultramafic component assuming all Cr is in this.

	Mean bentonitic clay	Bentonite minus Mn component (see table 6.1)	Mean ultramafic rock (Turekian & Wedepohl,1961)	Bentonite minus ultramafic rock (recalc. to oxide total 100%)	Mean high-Ca granite (Turekian & Wedepohl 1961)
Si	28.18	28.18	20.5	32.1	31.4
Al	7.10	7.10	2.0	8.6	8.2
Fe	4.69	4.69	9.43	4.4	2.96
Mg	2.99	2.99	20.4	0.4	0.94
Ca	1.62	1.62	2.5	1.6	2.53
Na	1.27	1.27	0.42	1.5	2.84
K	1.57	1.57	n	2.0	2.52
Ti	0.35	0.35	0.03	0.43	0.34
Mn	0.21		0.16	n	0.05
P	0.25	0.25	0.022	0.3	0.09
Ba	179	44	0.4	55	420
Ce	68	68	n	86	81
Co	34	30	150	13	7
Cr	208	208	1600	n	22
Cu	140	132	10	165	30
La	47	47	n	59	45
Nd	44	44	n	55	33
Ni	212	209	2000	n	15
Pb	21	15	1	19	15
Rb	69	69	0.2	87	110
SR	475	454	1.0	571	440
V	113	96	40	114	88
Y	55	55	n	69	35
Zn	165	165	50	199	60
Zr	102	102	45	121	140

n = negligible

along various strike slip zones, such as the Mamonia and Antalya Margin, provides a ready source for an ultramafic component.

The origins of the Kannaviou volcanic rocks remains enigmatic, and is beyond the scope of this work. At present a study is in progress of the character of these sandstones, and the similar but slightly younger volcanics from the Kyrenia Range (A.H.F. Robertson, pers. com.)

6.5.2 Vertical changes in accumulation rate

At the Margi locality it appears that the aluminosilicate accumulation rate increased dramatically, bringing about termination of the clay-rich umber (section 5.4.7.3) and accompanied by the appearance of the Mg-Cr-Ni-rich ultramafic source. How general is this upward increase accumulation rate? The contrast in composition between the interlava- and supralava-sediment aluminosilicate composition might be seen as reflecting a vertical increase in bentonitic clay abundance, but it is most easily explained in terms of a high local sediment production in the axial zone. In the Paphos area, there is an upward increase in abundance of volcaniclastic sandstones in the succession, which might reflect increasing proximity of the source area, which is consistent with sedimentological evidence. Higher in the succession, carbonate becomes important, and data concerning the character of the non-carbonate fraction are lacking. However, prior to the onset of carbonate accumulation, in the Paphos area, the volcanic sandstones become less abundant. It seems that the supply increased up into the Maastrichtian, but waned before the Lower Tertiary.

6.5.3 The composition of the manganese component - Accumulation rates of the bentonitic clays

The composition of the manganese component in the bentonitic clay has been calculated from the analysis of a manganese-rich sample (Table 6.1). The X-ray diffraction pattern of this mineral closely resembles that of todorkite (section 6.3.2). In Table 6.1 the range of composition of modern todorkites is indicated, and on the whole, a close similarity with the Cyprus sample is observed. Also on Table 6.1, the manganese component is compared with that in

TABLE 6.6

Partitioning of trace elements between lithogenous and hydrogenous phases: A comparison of a North pacific clay core, and the Margi bentonitic clay.

North Pacific core*

Element	Total	Lithogenous	%	Nodule Associated hydrogenous	%	Non-nodule associated hydrogenous	%
Fe	5.37	5.18	96	0.14	3	0.06	1
Mn	0.51	0.08	15	0.40	79	0.03	6
Cu	314	213	67	45	14	56	18
Ni	191	46	24	88	46	59	30
Co	88	15	17	71	80	2	2
Pb	28	23	82	4	14	c.1	4
Cr	97	92	95	3	3	2	2
V	141	119	84	8	6	1	10

* Data from Chester and Hughes (1969)
% The percentages are of the total composition

Margi bentonitic clay

		Lithogenous	%	Manganese associated	%
Fe	4.69	4.69	100	-	0
Mn	0.21	- **	0	0.21	100
Cu	140	138	99	8	1
Ni	212	209	99	3	1
Co	34	30	88	4	12
Pb	21	14	67	7	33
Cr	208	208	100	-	0
V	113	96	85	17	15

** Manganese is assumed solely in the manganese phase

Comparison of Atlantic and Pacific deep-sea clay with Margi bentonitic clay.

	Pacific***	Atlantic "	Cyprus
Fe	65000	82000	46900
Mn	12500	4000	2100
Cu	570	130	140
Ni	293	79	212
Co	116	38	34
Pb	162	45	21
Cr	77	86	202
V	130	140	113

*** Data from Goldberg and Arrhenius (1958), El Wakeel and Riley, (1961), and Landergren (1964).

" Data from Wedepohl (1960) and Turekian and Imbrie (1966)

the underlying umber. Greater enrichments are seen in all elements except the zinc, which is particularly low. The high cobalt, but low zinc, is characteristic of hydrogenous as opposed to hydrothermal manganese oxides (Toth, 1980).

The composition of the manganese phase resembles that in modern sediments, but its abundance is quite different. In Table 6.6 the chemical partitioning between lithogenous and hydrogenous fractions are given for a North Pacific sediment core, and for the Margi bentonitic clays. In terms of total abundances, the Cyprus clay is depleted strongly in manganese, copper and cobalt, and enriched in nickel and chromium. As is discussed above (section 6.5.1) the latter two are influenced by an unusual lithogenous component. The partitioning shows the striking difference. In the Pacific sediment, a significant proportion of the manganese, copper, cobalt, nickel and lead are in the manganese nodule component. In the Cyprus sediments the manganese-related enrichment is negligible except for cobalt and lead.

One of the characteristics of deep-sea clays is the relatively slow rate of accumulation of their non-biogenous components. In these sediments, micromanganese nodules are abundant, and play an important role in controlling some elements, notably Mn, Cu, Ni, Co, Pb (Chester and Hughes, 1969). The general inverse correlation of trace element enrichment with accumulation rate led Wedepohl (1960) to propose the "trace element veil" theory. In essence this states that the "excess" trace elements in the deep sea clays are removed homogeneously, and are superimposed upon deep sea clays of varying accumulation rates. It is now clear that this is an over simplification; there are differences in accumulation rate of "excess" trace elements between the Pacific and the Atlantic (Chester and Aston, 1976) and there is local modification through surface water organic productivity and mid-ocean ridge hydrothermal activity (Boström et al., 1973b). The Troodos bentonitic clay is strongly manganese and trace element depleted when compared with Pacific deep-sea clay (Table 6.6). This is less apparent with the Atlantic deep-sea clay, because of the ultramafic source of nickel in Cyprus, but it remains that there is a lower hydrogenous enrichment in the Cyprus clay. In view of the proximity of the spreading axis, this

low metal content implies an aluminosilicate accumulation rate greater than that of normal deep-sea clay.

6.5.4 Siliceous sediments - compositions and origin

Compositionally the radiolarian-rich clays differ only in silica abundance from the bentonitic clays. The mean composition is shown normalised to mean bentonitic clay in Table 6.7. Of elements other than silica, Mn-Ba-Sr show a real depletion, but this is within the between-sample variation observed in the bentonitic clays. Clearly the biogenic silica has not brought in significant amounts of any other elements.

The silica enrichment can be explained either by short periods of low clay accumulation rates, or short periods of high silica production and preservation. The extreme rarity of radiolarians in the inter-chert clay would suggest a very great accumulation rate contrast if the former explanation is true. The cherts accumulation would have to represent the greatest part in time. However the sharks teeth, abundant in the clays, are rare in the cherts, suggesting that the chert accumulated at a greater rate than the clay. Thus periodic high radiolarian productivity in the overlying surface water is favoured. In the modern oceans, radiolarian productivity is related to upwelling of nutrient rich deepwaters either near continental margins, or along the equator. In view of the subsequent events, gradual uplift and rotation of the ophiolites from the Maastrichtian onwards, the proximity to a continental margin seems likely.

The diagenesis of the radiolarian sediments has been discussed by Robertson (1977a). The good preservation of the radiolarian shells was tentatively attributed to local hydrothermal silica enrichment - owing to the proximity of the umbers. In view of the non-local origin of the umbers this is now considered unlikely. The highly siliceous character of the host clay, in contrast to the overlying carbonates, is probably adequate to explain the phenomenon.

TABLE 6.7

MARGI RADIOLARIAN AND CARBONATE-RICH SEDIMENTS

Normalised to Margi bentonitic clay

	Radiolarian	Carbonate
Si	1.33	0.97
Al	0.48	0.67
Fe	0.50	0.66
Mg	0.53	0.79
Ca	0.44	4.31
Ne	0.47	0.18
K	0.45	0.62
Ti	0.49	0.63
Mn	0.33	0.57
P	0.44	0.56
Ba	0.38	1.91
Ce	0.43	0.66
Cr	0.54	0.71
Cu	0.41	0.45
La	0.40	0.64
Nd	0.47	0.68
Ni	0.51	0.75
Pb	0.57	0.81
Rb	0.50	0.71
Sr	0.31	0.75
V	0.47	0.66
Y	0.49	0.62
Zn	0.48	0.70
Zr	0.47	0.65

6.5.5 Carbonate-bearing sediments

The mean composition of the Margi carbonate-bearing sediments, from the top of the section, is compared with the mean bentonitic clay in Table 6.7. A sight silica-enrichment results from the inclusion of carbonate-rich radiolarian chert bands. Along with calcium, barium is strongly enriched. There are possible weak enrichments of magnesium, strontium, lead and nickel. These might reflect a greater input of biogenic material in general, causing slight enrichment of these in the sediment.

Of particular interest with respect to the carbonate component is its absence from the basal sediments. The umbers are always completely free of carbonate, which first appears in the overlying non-metalliferous sediments, where its lowermost part is characterised by a dissolution assemblage (Robertson and Hudson, 1974). Primary carbonate is found also in interlava sediments (Chapter 4, section 4.2.3). It seems thus likely that carbonate was supplied throughout, but that dissolution proceeded to completion in the basal sediments. In the volcanic succession, rapid burial by overriding lava flows may have preserved the sediment from dissolution. Thus during formation, the ophiolite lay close to, but just below, the carbonate compensation depth - a value of 2.5 km inferred from fluid inclusion studies (Spooner, 1980). The gradual upward appearance of carbonate might reflect either the subsequent uplift history of the massif (Robertson, 1977b) or a fall in the carbonate compensation depth.

6.5.6 Diagenesis

Diagenetic reactions fall into two classes. Firstly there are the early diagenetic reactions involving MnO_2 and small amounts of phosphatic debris. Secondly there are the somewhat later reactions resulting in the formation of clinoptilolite and palygorskite.

The formation of the manganese oxide concretions and the trace metal enrichment of these and the phosphate are discussed in sections 5.5.3 and 5.5.4 respectively. These reactions probably occurred close to the sediment-water interface, where chemical exchange with the water column was possible.

Clinoptilolite and Palygorskite

The enrichment of the sediment in clinoptilolite at the base of the succession, and its upward decrease in abundance, suggests primarily temperature control, as no major change in sediment composition occurs over the same range. The sharpness of the fall off (reduction to one half over a distance of 4m), argues for formation at a depth of only a few metres, influenced by a steep thermal gradient.

There is no direct textural evidence for mineral precursors to clinoptilolites (Boles, 1977). The very common association with smectites argues for a genetic association. This may suggest the former presence of volcanic glass which has been suggested as a precursor (Kastner and Stonecipher, 1977).

Very similar arguments are presented for the formation of palygorskite through the diagenetic reaction of smectite, volcanic glass or phillipsite with silica and magnesium.

By assuming a smectite precursor to both these mineral phases the chemical reactions which might have occurred in the sediment can be considered. To do this compositions for the mineral phases need to be known. For the smectite the composition determined by Desprairies and Lapierre (1973) for the umber montmorillonites has been used. For the palygorskite, the electron microprobe composition of umber palygorskite veins is used: it is not possible to analyse the fibres of palygorskite in the clay matrix directly. Clinoptilolite compositions are unknown, and for the sake of calculation a mean value of deep sea clinoptilolites was used (Boles, 1977).

The results (Table 6.8) indicate that formation of palygorskite would require the addition of silicon, magnesium and iron, and would release a little potassium. On the contrary, formation of clinoptilolite would require addition of silicon, sodium and potassium and would release magnesium and iron. Naturally the actual abundances of these elements involved are very dependent upon the precise composition of the phase - the concentrations of calcium, potassium and sodium are particularly variable. However the principal elements involved, iron, magnesium and silicon, are less sensitive to this variation. Depending upon the relative importance of the

TABLE 6.8

MINERAL REACTIONS IN THE BENTONITIC CLAY ASSUMING A SMECTITE PRECURSOR AND CONSERVATION OF ALUMINIUM.

Unit cell composition

	Smectite(1)	Palygorskite(2)	Clinoptilolite(3)
O	22	22	72
Si	7.75	7.74	29.48
Al	2.37	1.16	6.56
Fe	0.95	0.91	0.03
Mg	0.97	1.94	0.33
Ca	0.13	0.04	0.47
Na	0.11	0.06	1.74
K	0.41	0.04	2.93

(1) From Desprairies and Lapierre (1973)
(2) From Chapter 5 section 5.3.2
(3) From Boles (1977)

Reactions assuming conservation of aluminium

Smectite + 8 Si + 3 Mg + Fe -> Palygorskite + 0.33 K

Smectite + 3 Si + 0.5 Na + 0.7 K -> Clinoptilolite + Fe + Mg

two reactions, different amounts of non-mineral material are required. If magnesium is assumed conserved, then clinoptilolite is the dominant product (as is observed). Silica would have to be consumed, and iron would be expelled. Uncertainties concerning the alkali element content of the clinoptilolite and smectite, means that changes in these elements cannot be reliably calculated. However the changes are small and it is probable that the net reaction is near isochemical. The fate of any iron released is uncertain, but formation of goethite is probable, which may be important with respect to the stability of magnetic remnance.

6.5.7 CONCLUSIONS

From the preceding discussion a number of important points emerge.

First, the mineral assemblages observed in the volcanogenic clays are relatively constant around the Troodos massif. Only the Moni clay of the Limassol District differs, being rich in kaolinite which is virtually absent elsewhere. However the upper part of the Moni clay includes the Kathikas melange (Swarbrick and Naylor, 1980) which is related to the Mamonia rocks rather than the Troodos. The normal volcanogenic clay assemblage continues both down into the umbers and locally the interpillow sediments, and also up into the lowermost marls of the Lefkara Formation. Essentially, the Kannaviou sediments form the background sedimentation to which is variously added locally derived detritus, hydrothermal precipitates and biogenic components, to form all the lithological types of the Pre-Tertiary sediments. A case can be made for incorporating the Perapedhi Formation in the Kannaviou Formation, distinguishing umber, clay-rich umber, radiolarite etc. as lithologies within the formation.

Secondly, the presence of clinoptilolite only within the lowermost volcanogenic clays, and the rapid upward decrease in abundance, argue for diagenesis in response to a steep thermal gradient.

Thirdly, the paucity of hydrogenous manganese and trace elements in the sediment suggests a relatively rapid accumulation rate. The major and trace element assemblage are controlled domin-

antly by the mixing of two terrigenous components: one of acid-intermediate volcanic origin, and the other, ultramafic.

Fourthly, the sediments accumulated initially just beneath the carbonate compensation depth, probably around 2.5km.

Fifthly, periodic bursts of radiolarian productivity resulted in the formation of thin chert bands, mostly near the base of the succession.

Plate 6.1

Dark clay-rich umber overlain by pink bentonitic clay at Margi.

a) Continuous thin beds of radiolarite are visible in the upper part of the section.

b) Sharp contact of the clay-rich umber and the bentonitic clay.

Plate 6.2)

Bentonitic clay at Margi.

a,b) Compact texture with strong alignment of clay minerals. Zones of manganese enrichment, and phosphatised cuticle are visible. In (b) a sharks tooth has been intersected.

c) Contact with the underlying clay-rich umber. Remobilisation of manganese has locally occurred along the contact.

d) Manganese-rich region in the bentonite clay. These, composed of todorokite, are clearly of secondary origin, but may have formed very early.

e) Euhedral plagioclase surrounded by flaky illite-montmorillonite.

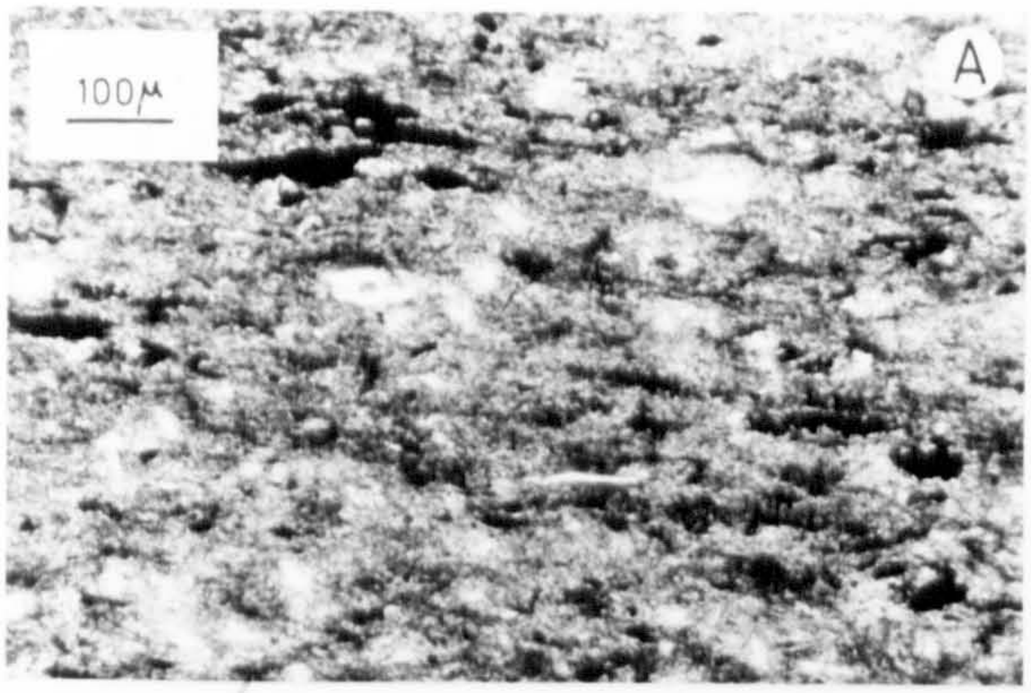
100μ
A

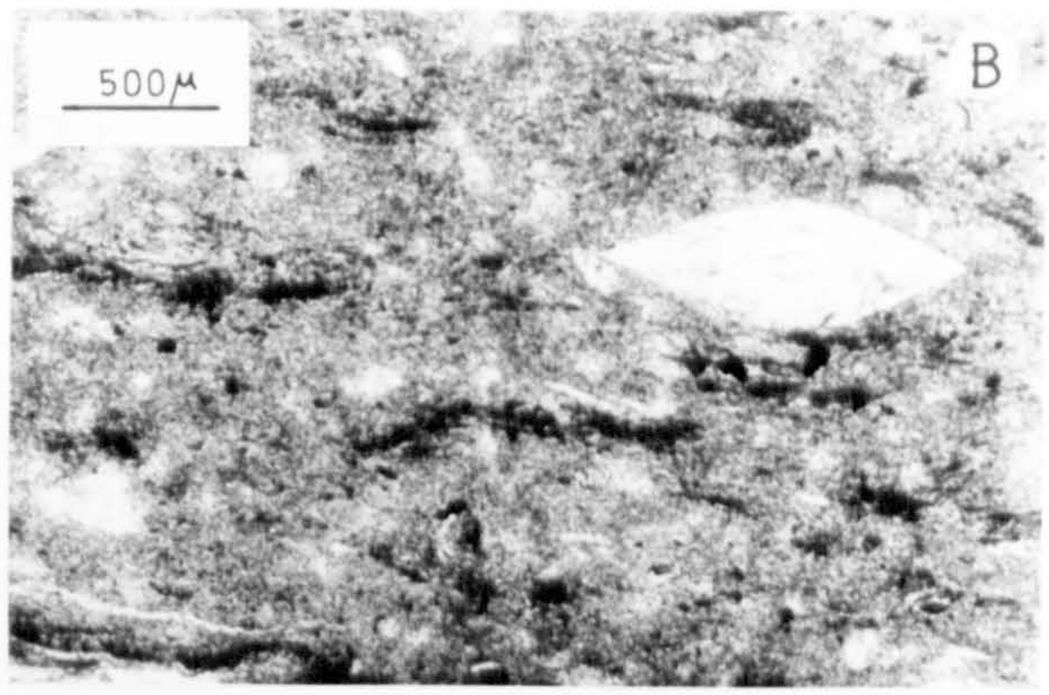
500μ
B

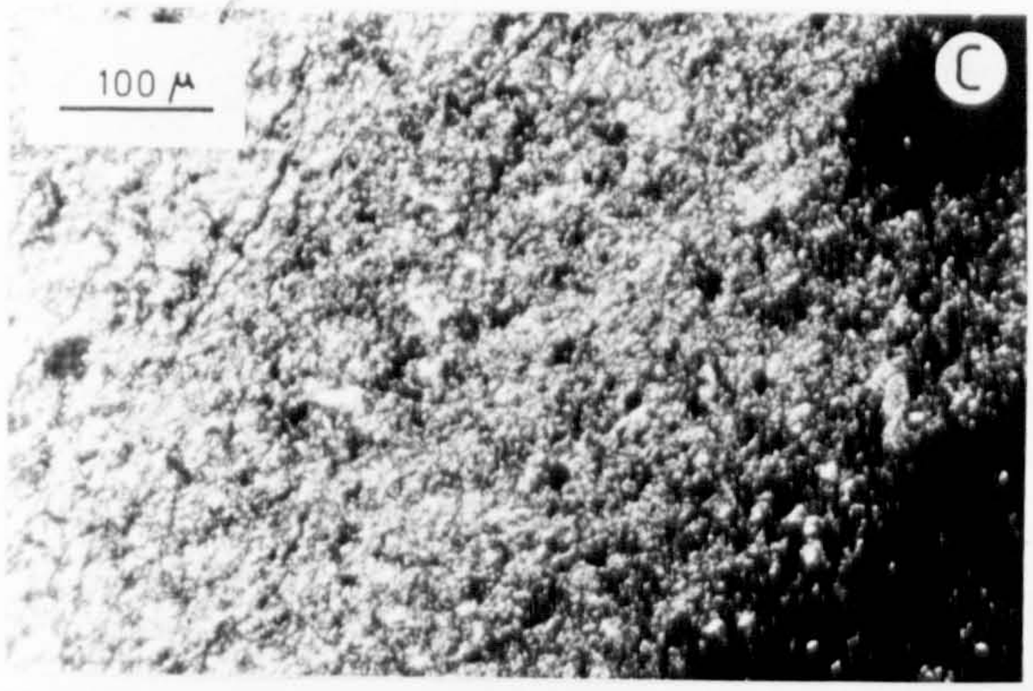
100 μ
C

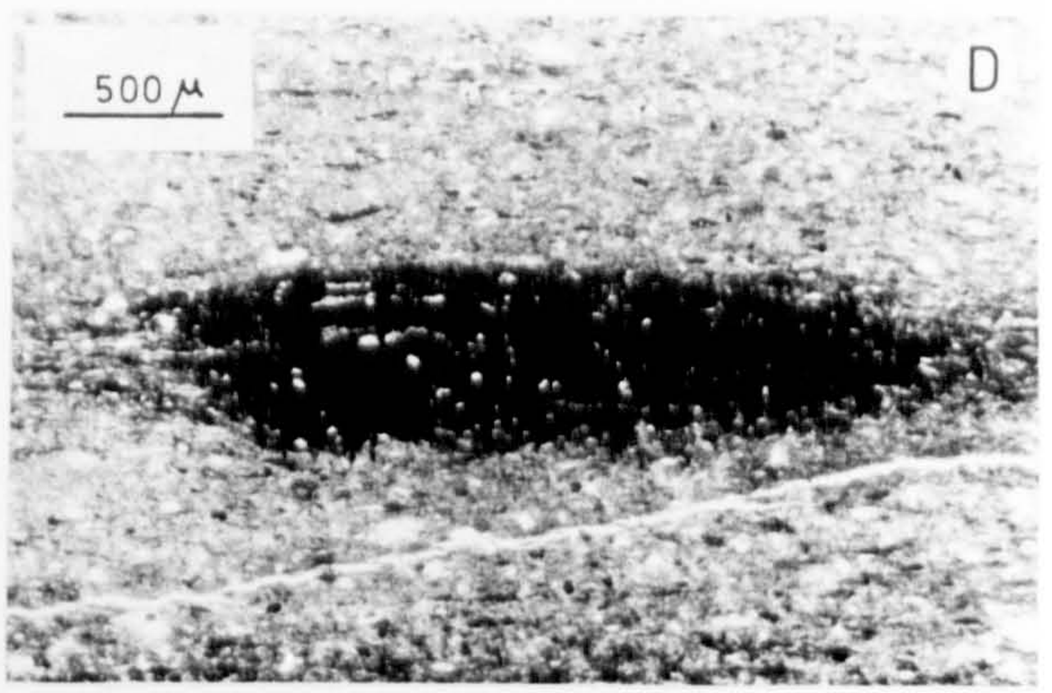
500 μ
D

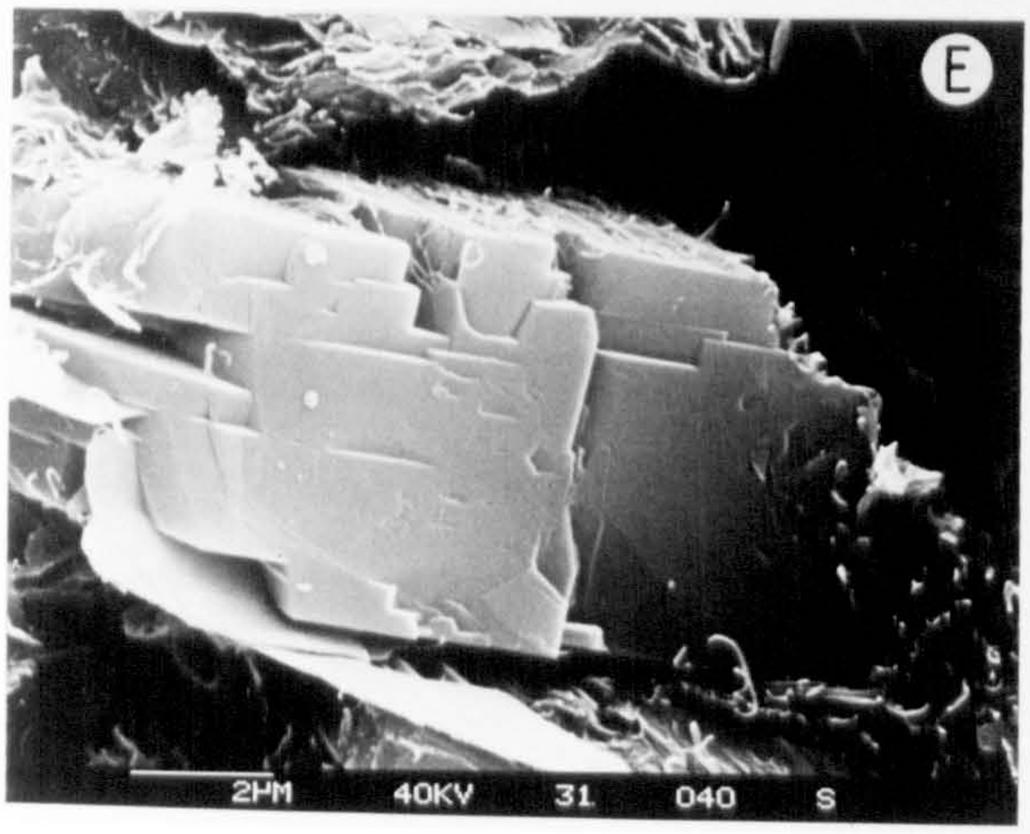
E
2μM 40KV 31 040 S

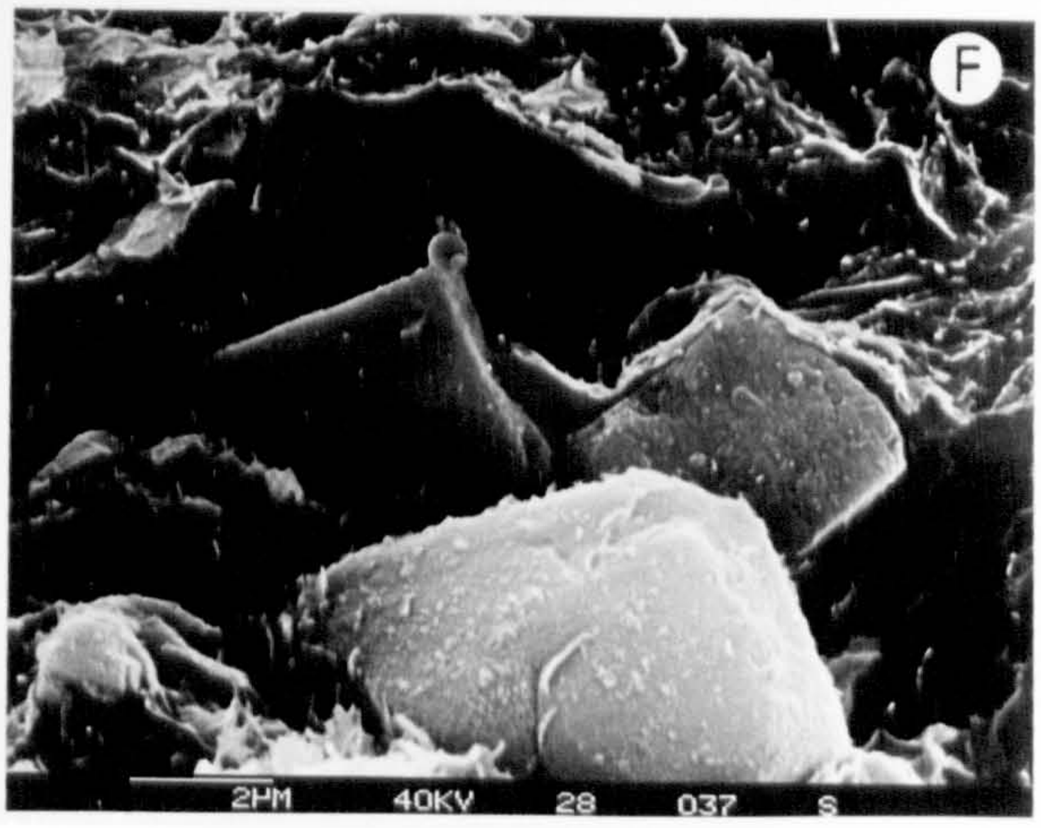
F
2μM 40KV 28 037 S

THE SEDIMENTARY GEOCHEMISTRY OF THE TROODOS OCEAN

The following account is essentially a compilation of the results described in the previous chapters. The purpose is to present a unified discussion of the sedimentary processes operating in the Troodos ocean, and how these have influenced the chemical composition of the sediments. The discussion is divided into two parts: In the first, the various sediment sources are discussed in a geographical framework. Secondly, starting with the major elements, there follows a discussion of factors influencing the sediment composition.

7.1 PALAEO-GEOGRAPHICAL ASPECTS OF THE TROODOS OCEAN

In Fig. 7.1 are shown the small scale morphological details inferred from studies of the Troodos massif, (section 3.2.1) and the regional tectonic setting based on a synthesis of Eastern Mediterranean geology (Robertson and Woodcock, 1980; Robertson and Dixon, 1984). These interpretations are necessarily speculative. Following is a discussion of the critical observations on which these are based.

Water depth. During formation the ophiolite lay near the carbonate compensation depth (Chapter 6, section 6.5.5). However owing to the variability of Cretaceous carbonate compensation depths, and the proximity of continental margins, this does not help in determining the water depths (Robertson and Hudson, 1974). Fluid inclusion studies in hydrothermal stockwork zones (Spooner and Bray, 1977; Spooner, 1980) demonstrate that a near normal oceanic water depth is required to account for the high temperatures but lack of evidence for boiling. A water depth of 2.5km is proposed. The high vesicularity of the lavas, which has led people to suggest a shallow origin, probably resulted from the unusually high volatile content of the lavas (Schmincke, 1984 conference report).

Palaeogeography of the Troodos ocean

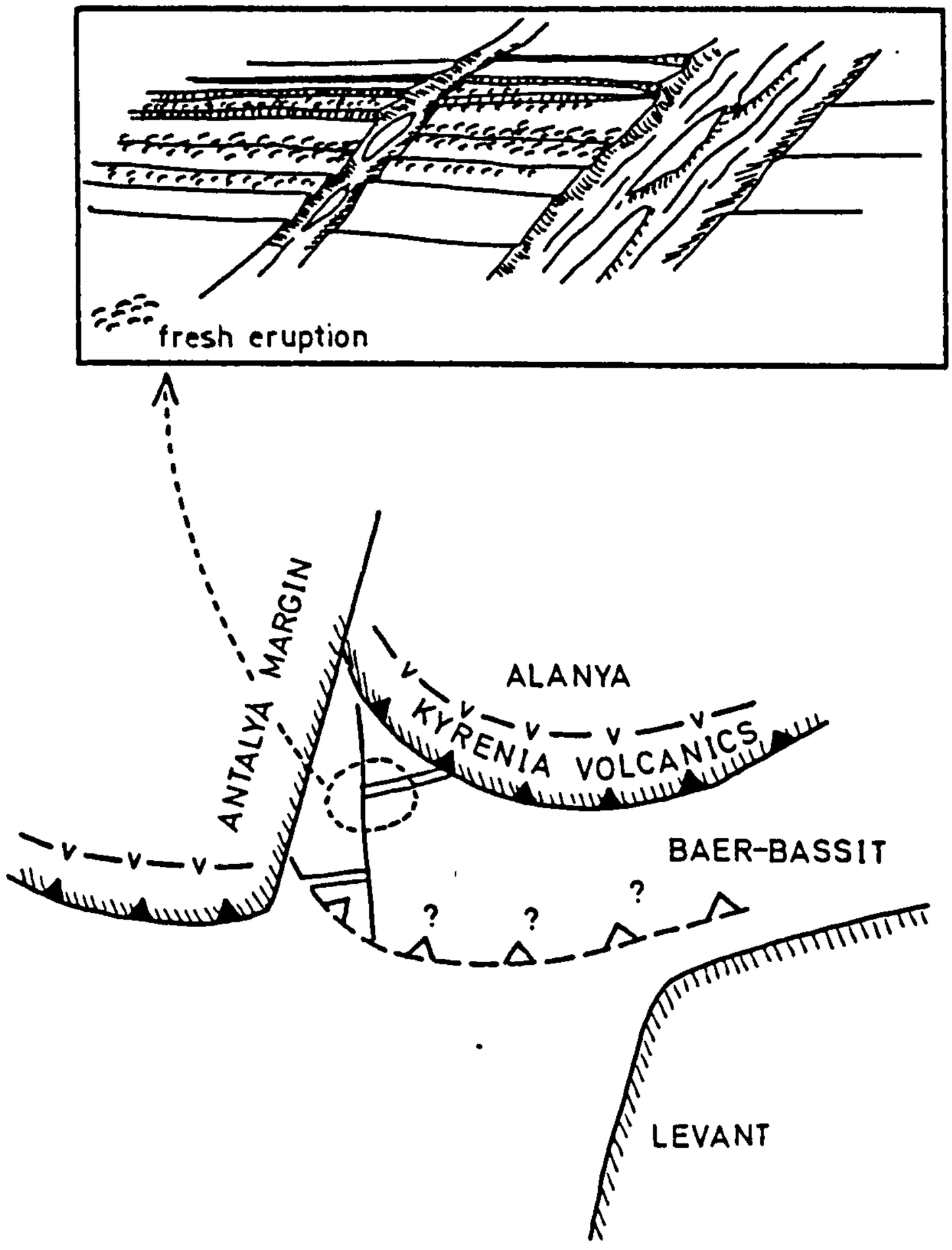

Fig. 7.1

Morphology and regional setting of the Troodos spreading axis. The morphology is deduced from studies of the sediments and structure of the extrusion sequence (Chapter 3, section 3.2.1). The regional setting is modified after Robertson and Woodcock (1980), incorporating information from Robertson and Dixon (1984).

Size. The size of the Troodos Ocean remains uncertain. The fragment that remains is approximately 100 x 70km, but the regional setting (Fig. 7.1) would permit an area at least an order of magnitude greater than this.

Ridge geometry. The relationship of the volcanic sequence to the structure of the ophiolite indicates the importance of slightly off-axis ridge-parallel normal faulting (Chapter 3 section 3.1.6). The near total confinement of axially-derived volcanic detritus to the interlava sediments argues for a well defined median valley (Chapter 4 section 4.3.1). The presence of most of the oxide sediment on top rather than within the volcanics, points to the axial volcanic zone, and median valley, being narrow.

Ridge-parallel fracture systems dominate the brittle structure and in mineralised zones have acted as channels for hydrothermal fluids.

Regional setting. The question of the regional setting is less easy to answer. There is no doubt that the Mamonia continental margin lay broadly to the west, and that the Kyrenia margin lay to the north (Robertson and Woodcock, 1980). However detrital sediments on the ophiolite show no sign of these other than olistoliths within the autochthonous Moni clays. Instead an important but enigmatic Upper Cretaceous bi-modal volcanic event supplied most of the detritus (Chapter 6, section 6.5.1). A locally important ultramafic component in the sediments may relate to serpentinite occurrences along the Mamonia complex or Antalya continental margins or in the Moni melange. Geochemical data from the lavas suggest that some form of subduction zone, probably northward dipping, lay beneath the spreading axis (Pearce, 1975, 1980), but the position and character of this is uncertain.

7.2 SEDIMENT SOURCES

The sedimentary materials on the Troodos ophiolite were derived from three distinct sources illustrated on Fig. 7.2. First a general source of pelagic or hemipelagic character, with material derived from the overlying water column either by sedimentation or

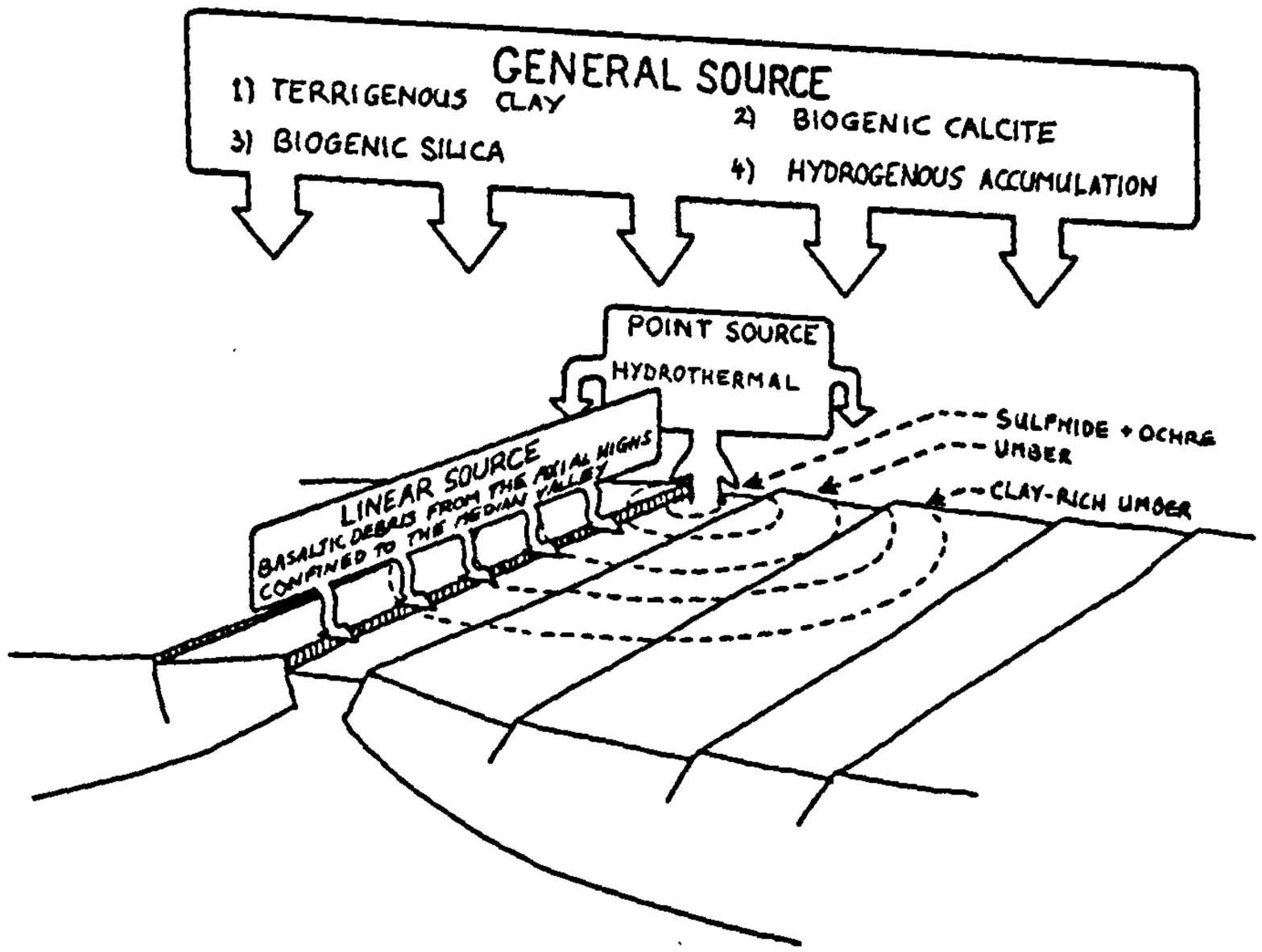

Fig. 7.2

Schematic model of sedimentary sources. The general source comprises quasi-pelagic aluminosilicate, biogenic carbonate and opal, and hydrogenous enrichment. Accumulation is close to the carbonate compensation depth, and dissolution goes to completion in the earlier sediments. The linear source, is so called because of its association with the ridge axis. It comprises fine volcanogenic detritus derived from the axial highs. The point source comprises hydrothermal vent areas. These are not uniformly distributed along the length of the ridge, hence the designation. The range of influence is limited, so hydrothermal sediments are not uniformly distributed

hydrogenous accumulation. Secondly, a linear source of basaltic detritus derived from the walls of the axial valley. Thirdly, point sources of hydrothermal precipitates.

General source

The general source can be subdivided into four categories.

Biogenic Carbonate. Rare recrystallised foraminifera and coccoliths are found in the axial interlava sediments, indicating that biogenic carbonate was reaching the sea-floor (section 4.2.2.3). In exposed sediments, dissolution seems to have proceeded to completion so that basal sediments are carbonate-free. A fall in the relative position of the carbonate compensation depth occurred during the Maastrichtian, possibly related to uplift of the massif, and carbonate preservation is characteristic of these and later sediments.

Biogenic silica. Radiolaria are found in almost all sediments in the massif, but are generally of low abundance. However thin beds of radiolarian cherts occur showing that in addition to the low background contributions, there were periodic bursts of radiolarian productivity.

Terrigenous components. A fine grained bentonitic clay (montmorillonite-illite-quartz) accumulated in most areas throughout formation of the ophiolite, and continued at least until the Maastrichtian. To the west this sediment is accompanied by coarse volcaniclastic sandstones. The geochemistry indicates that this volcanogenic material had a source of acid-intermediate volcanic character. In addition to this, a minor amount of an ultramafic terrigenous material is detectable, possibly derived from serpentinites in the continental margins to the west and south (Chapter 6, section 6.5.1) with respect to present Cyprus position.

Most of this terrigenous sediment accumulated relatively slowly from the overlying water column. However the interbedded coarse volcanogenic sandstones indicate proximity to a sediment source, and suggest the sedimentation was nowhere truly pelagic in character.

Hydrogenous material Hydrogenous enrichment in manganese, phosphate and related trace metals is important. The manganese and

phosphate enrichment, relative to aluminium, generally increases towards the axial zone. In the former case this is due to hydrothermal precipitation, but for the latter, adsorption of phosphate onto hydrated iron oxides is more likely (section 5.5.7). The trace metal enrichment of the manganese and phosphate components follows the reverse trend, increasing with distance from the axis. Decreasing iron accumulation rate, and hence total rate, away from the axis permited greater hydrogenous and early diagenetic enrichment of the sediment.

Linear Source

In addition to the general quasi-pelagic background, there is an important local source of lithogenous material in the walls to the median valley (Fig. 7.2). In all sediments found in the axial volcanic zone, the lithogenous component is dominated by smectites derived from the weathering lavas. In all but a very few samples the accumulation rate of this locally-derived material so far exceeded that of the background as to conceal it. Importantly, the faulted median valley walls acted as a barrier to outward transport of the basaltic detritus, and such material is rare in sediments outside the axial valley.

Point source

Superimposed upon the other more general sediment sources, are more localised sources of hydrothermal precipitates centred at the ridge axis (Fig. 7.2). Strictly the vent areas are probably elongate, comprising clusters of hot springs aligned with ridge parallel fractures (Chapter 3, section 3.1.4), but compared with their range of influence (c. 5km) they approximate to point sources. It is interesting to note that the bulk of the precipitates from the vents accumulated proximally, in contrast to the situation in the modern East Pacific Rise, where similar materials are transported up to 1000 km by mid-depth circulation (Chapter 5, section 5.5.8).

7.3 GEOCHEMISTRY OF THE OCEANIC SEDIMENTS

The chemical composition of the sediment reflects the interplay of the sediment sources described above. In the following section controls on the distribution of each element in turn will be discussed, based on evidence presented in the three previous chapters. In addition comparison will be made with modern deep-oceanic sediments.

Diagramatic representation

A series of diagrams (Fig. 7.4) have been prepared to illustrate the partitioning of elements between the different sources. For simplification these include only supralava sediments, with no locally derived basaltic material, and are based on a single continuously sampled 13m section (from the Margi area, section 5.4.3). The variation in abundance of independent chemical components within the sediment is plotted against depth in Fig. 7.3. The abundance of chemical components was calculated on the basis of a number of assumptions which are presented in Table 7.1. The coefficients used, for example, the Fe/Al ratio of the alumino-silicate, were obtained either from graphical data indicating ratios (section 5.4.5) or from the composition of the non-metalliferous clays. For the following discussion, sources have been grouped into three categories: hydrothermal, lithogenous and excess. The latter is the remainder after subtraction of the other two, and comprises both biogenic and hydrogenous components. It must be clearly understood that these are model values, and are intended only to illustrate gross trends. By making no attempt to distinguish a biogenic source from a hydrogenous source, as has been attempted in modern sediments (Heath and Dymond, 1977), the model remains one step less removed from reality. Its principal value here is in permitting comparison with similar work in the modern Pacific sediments.

The hydrothermal component is taken as the iron component of the interlava sediments (Table 7.2). This does not take all the hydrothermal manganese into account - only that which is incorporated in the irón component (section 4.2.5). The reason for this is that the bulk of the manganese is independent of the hydrothermal

TABLE 7.1

CHEMICAL COMPONENT DEFINITIONS

Fe(excess)=Fe(total)-Fe(Al)

(Fe-0.6416*Al-0.125)*1.8214

Mn(excess)=Mn(total)-Mn(Al)

Mn*1.5527

Si(excess)=Si(total)-Si(Al)-Si(palygorskite)

(Si-2.1985*Al-4.64*Mg+3.013)*2.143

Carbonate=Ca(total)-Ca(apatite)-Ca(Al)

(Ca-2.6905*P-0.038*Al-0.308)*2.5

Apatite=P(total)-P(Al)

(P-0.038*Al+0.021)*6.079

TABLE 7.2

ASSUMED COMPOSITIONS FOR LITHOGENOUS AND HYDROTHERMAL COMPONENTS.

Lithogenous (L) = a (AL-b(Fe-cAl))

Hydrothermal (H) = d (Fe-cAl)

Excess (E) = total - L - H

where a = element/Al in lithogenous component
b = Al/Fe in hydrothermal component
c = Fe/Al in lithogenous component
d = element/Fe in hydrothermal component

	a.	b.	
Si	3.80	0.0729	b = 0.0202
Al	1.00	0.0202	
Fe	0.62	1.0	c = 0.622
Mg	0.42	0.0226	
Ca	0.23	0	
Na	0.18	0	
K	0.22	0	
Ti	0.049	0.00099	
Mn	0.008*	0.0237	* assumed from intermediate volcanic abundance (Turekian & Wedepohl,1961)
P	0.033	0	
Ba	4	1	
Ce	9.4	0	
Cr	8.5	0	
Cu	8.5	8.5	
La	6.0	0	
Nb	1.35	0	
Nd	6.20	0	
Ni	4.20	5.01	
Pb	2.7	0.6	
Rb	9.8	0	
Sr	45	0	
V	14.6	40	
Y	7.5	0	
Zn	22.7	7.1	
Zr	13.6	1.7	

The values are taken from graphical data presented in Chapters 4 and 6. The element/Al ratios for the bentonite are derived from the Margi data after correction for manganese-related trace elements. Exceptions are nickel, chromium and magnesium which for the umber are derived from other localities because of the ultramafic component in the bentonites. The element/Fe ratio is derived from the interlava sediment data for average of minimum element/Fe ratios.

MAJOR CHEMICAL COMPONENTS

RELATIVE ABUNDANCE v. POSITION IN SECTION

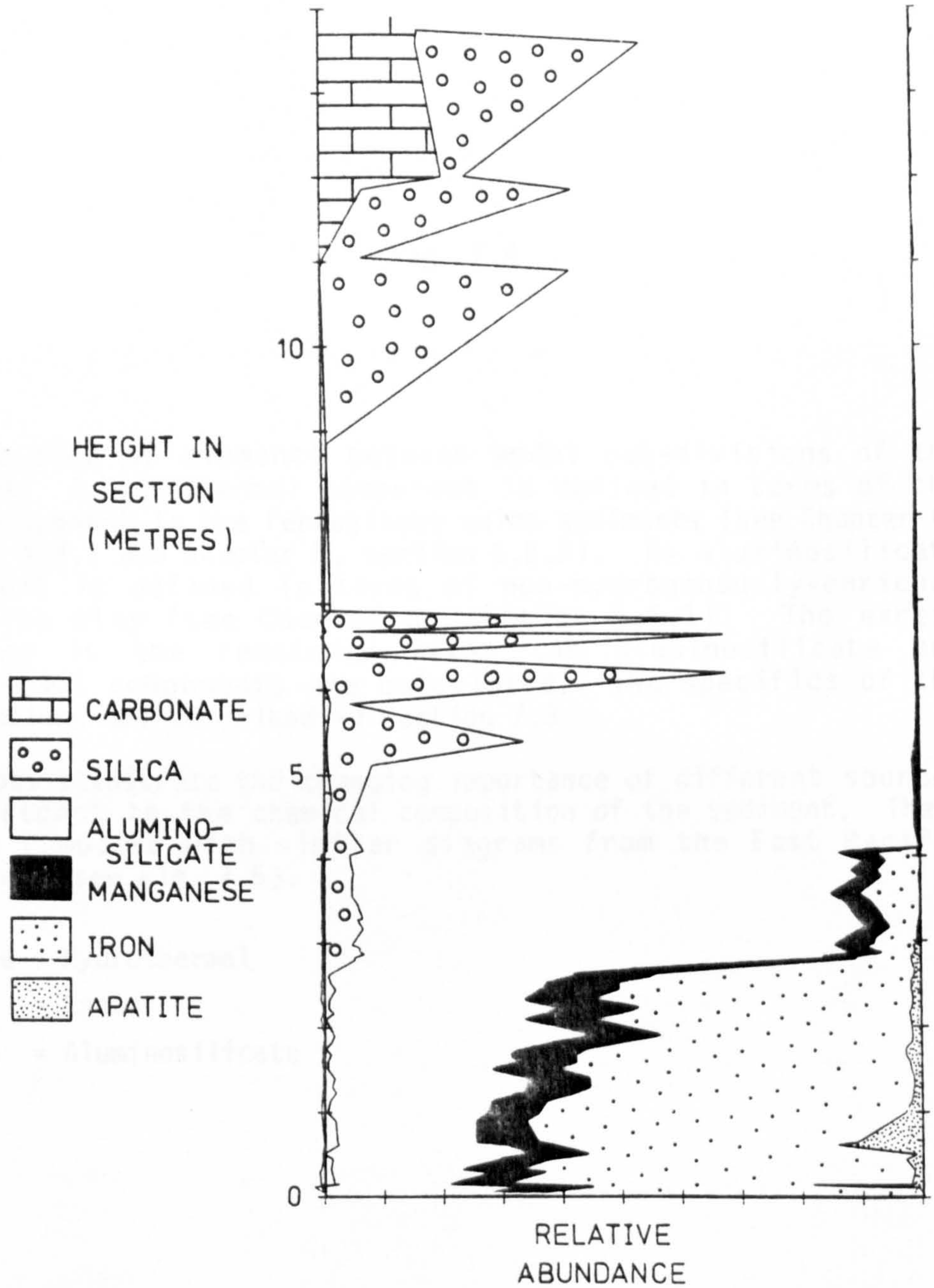

Fig. 7.3

Variations in major element component abundances up section at the Margi principal umber deposit. The components are calculated from the XRF whole rock chemical data, using criteria described in Chapter 5, section 5.4.6. The upward decrease in iron and manganese, in two steps, is evident. Peaks of opal enrichment occur in the upper part of the section, and at the top carbonate appears in, marking a transition to the Lefkara chalks.

Fig. 7.4

Distribution of elements between model sub-divisions of the sediment. A hydrothermal component is defined in terms of the iron component in the ferruginous oxide sediments (see Chapter 4, section 4.3.1 and Chapter 5, section 5.5.5). An aluminosilicate component is defined in terms of non-hydrogenously-enriched bentonite clay (see Chapter 6, section 6.5.1). The excess category is the remainder after the aluminosilicate and hydrothermal components are calculated. The specifics of the calculations are described in section 7.3

The plots illustrate the changing importance of different sources with respect to the chemical composition of the sediment. These can be compared with similar diagrams from the East Pacific sediments (see Fig. 7.5).

Stipple = Hydrothermal

Plain = Excess

Stripe = Aluminosilicate

Fig. 7.4

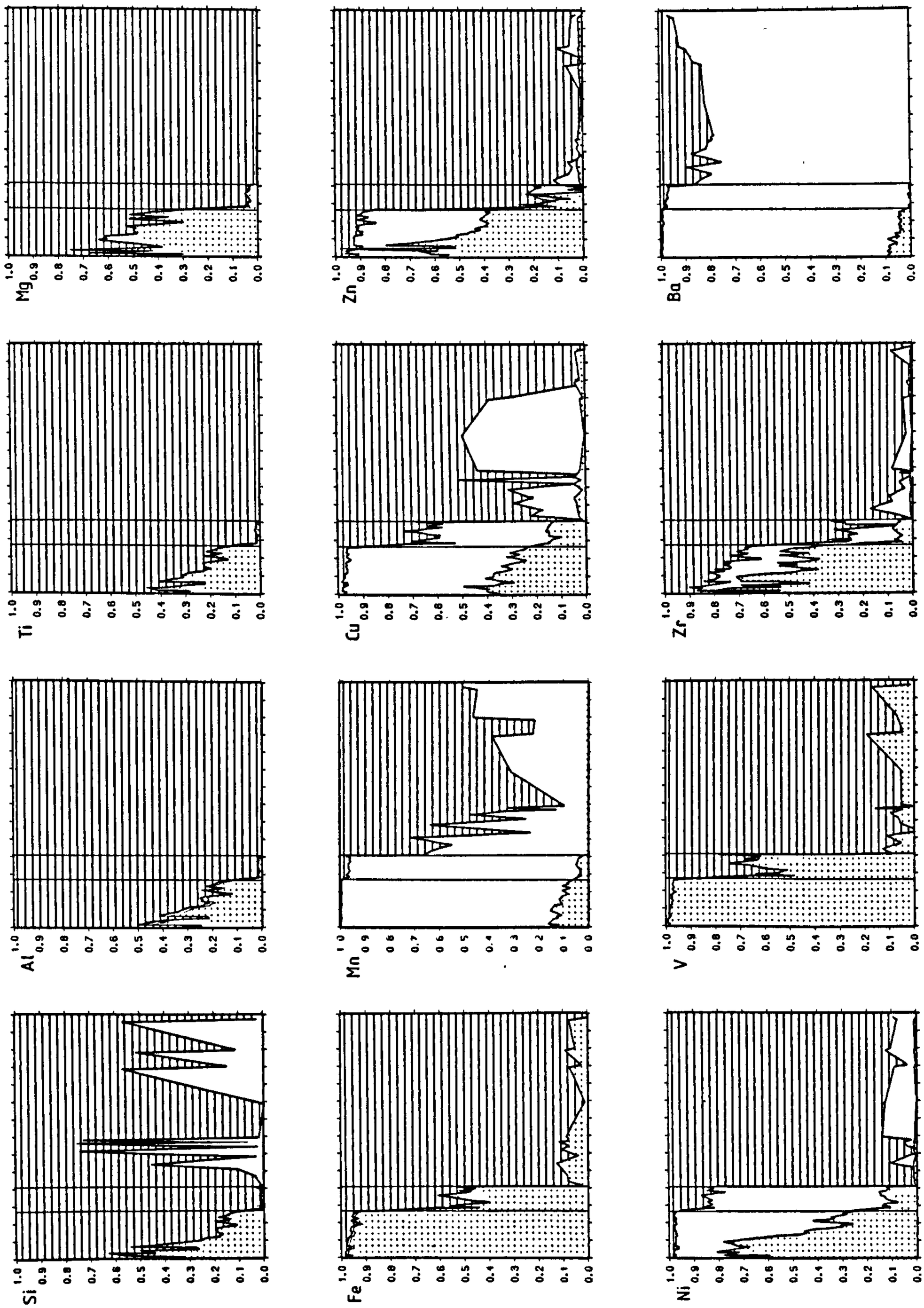

Vertical continuous lines indicate the contacts between the pure umber(left), the clay-rich umber(centre) and overlying non-metalliferous sediments.

Vertical continuous lines indicate the contacts between the pure umber(left), the clay-rich umber(centre) and the overlying non-metalliferous sediments

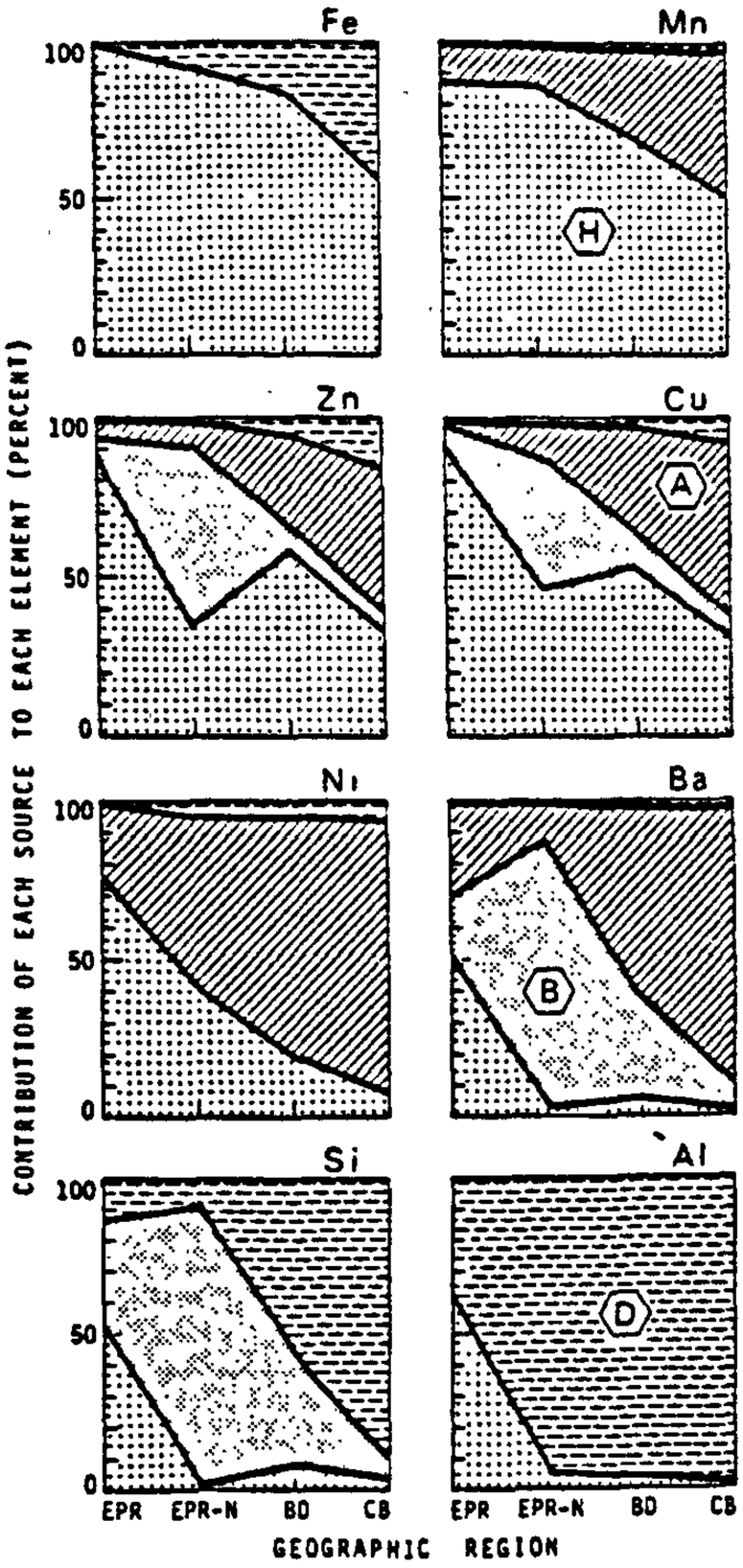

Partitioning of East Pacific Rise (EPR), Bauer Deep (BD), and Central Basin (CB) sediments between hydrothermal (*H*), detrital (*D*), biogenous (*B*), and hydrogenous (*A*) sources.

Fig. 7.5

Distribution of elements between model lithogenous, biogenous, hydrothermal, and hydrogenous components, in sediments from the Eastern Pacific. Diagram is from Heath and Dymond (1977). In most respects a striking similarity with the diagrams from Cyprus is observed, bearing in mind that for the Cyprus example, the hydrogenous and biogenous components have not been subdivided.

iron, and the trace element enrichment shows a continuum from hydrothermal to hydrogenous character. In this overview manganese is thus treated as an excess, "hydrogenous", element, though its increase in abundance towards the base of the section leaves no doubt that most is ultimately of hydrothermal origin.

The lithogenous component is taken as the composition of the bentonite after allowance has been made for themade for the associated manganese component. The only complication is the necessity to have different values for the non-metalliferous clay, owing to a greater proportion of ultramafic material present, influencing particularly chromium and nickel. The compositions used are shown in Table 7.2.

Silicon, aluminium, magnesium and titanium

These elements are strongly partitioned to the aluminosilicate-rich lithogenous component. However they have also an important proportion associated with the hydrothermal component. Of the silicon, titanium and aluminium, up to 50%, and the magnesium, 70%, is contained in the hydrothermal component in the axial sediment. This phenomenon has been observed for the East Pacific Rise crestal sediments for silicon and aluminium (Fig. 7.5), but data concerning titanium and magnesium are not available. Either adsorption of the elements, from seawater or hydrothermal fluids, onto the precipitating iron, or physical expulsion of aluminosilicate fragments with the vent fluids, are required to explain this. The constancy of element/Fe ratios in the component (section 5.4.5) suggests that the former is more probable -saturation adsorption would permit a constant ratio. Silicon differs slightly in that it is strongly enriched (up to 75%) in the "excess" component in radiolarian rich beds. Thus a biogenic source for silicon can be very important.

Iron

The iron is divided exclusively between hydrothermal and lithogenous components. Greater than 95% is hydrothermal in the most axial sediments, but this proportion drops in two steps to to 0-10% in the overlying bentonitic clay. This stepped increase contrasts with the situation in the Pacific (Fig. 7.5). The first

step decrease is due to sudden cessation of activity of a nearby hydrothermal vent - the continued, but lower, iron enrichment relating to a more distant vent area (section 5.5.10). At the East Pacific Rise, the mid-depth circulation transports and homogenises the hydrothermal precipitates, thus concealing local effects as seen in Cyprus. The second step decrease relates instead to an increase in local aluminosilicate accumulation rate (Section 5.4.7.3).

Manganese

Manganese is dominantly contained in the "excess" category, being of low abundance in both the hydrothermal iron and lithogenous components. However, this excess represents manganese of hydrothermal origin. This decreases in abundance away from the axis, and accumulates progressively more slowly, resulting in progressively greater trace metal enrichments. Thus a continuum is observed between manganese of hydrothermal character, and that of hydrogenous. None of the sediments have positive cerium anomalies, though the magnitude of the negative anomalies decrease away from the axis.

The difference from the Pacific is striking (Fig. 7.5). This is partly due to the greater proportion of lithogenous manganese in Cyprus (due to lesser hydrogenous components), and also due to the different definition of the hydrothermal component used by Heath and Dymond (1977).

Vanadium and Zirconium

Both vanadium and zirconium follow closely the behaviour of iron, the former particularly so. They are both contained dominantly in the hydrothermal and lithogenous components. Vanadium shows no significant "excess" so this part has been ignored. The zirconium does however show a small "excess" which might be explained in terms of some kind of hydrogenous enrichment, as has been described in marine manganese nodules (Calvert et al., 1978).

The strong association of vanadium and zirconium with iron is particularly interesting in that it has not been described from modern mid-ocean ridge sediments.

Copper, Zinc and Nickel

These elements are partitioned between all three components. In the axial sediments an important part (40-80%) is of hydrothermal origin, and only a very small part is lithogenous. However away from the axis, the lithogenous component becomes more important, particularly for nickel and zinc. The "excess" which is probably entirely attributable to hydrogenous enrichment, is greatest in the axial sediments, where the large proportion of iron and manganese in them makes the sediments particularly receptive to this. Zinc differs slightly, it shows lesser hydrogenous enrichment, in the axial sediments, and none at all in the non-metalliferous sediments.

Differences with the Pacific (Fig. 7.5) are due to the more important lithogenous component in Cyprus. The recognition of a biogenic component for zinc and copper in the Pacific samples, has not been tested in Cyprus.

Lead and Cerium

Both lead and cerium are strongly enriched in the excess component -probably attributable to hydrogenous enrichment. None of the cerium and only a very little of the lead occurs in the hydrothermal component. Again the very great hydrogenous enrichment in the axial sediments reflects the highly adsorbant character of these, rather than an association with a possible hydrothermal source.

Cerium shows a relatively greater excess in the most distal iron-rich sediments, because of the stronger hydrogenous enrichment of cerium in these more slowly deposited sediments.

Barium

Barium is contained very dominantly in the "excess" component, a finding identical in the Pacific (Fig. 7.5). The hydrothermal barium component is far smaller in Cyprus.

Phosphorus, Yttrium, Lanthanum, Neodymium and Strontium

Phosphorus shows a very strong enrichment in the excess component in the axial sediments. In the non-metalliferous sediments however it is dominantly in the lithogenous component. The behaviour is mirrored very closely by that of yttrium, lanthanum and neodymium, which are all contained within the phosphate phase

(section 5.5.4). The behaviour of strontium is similar, but the match is less good. Association with phosphate and with the manganese component accounts for this trend (section 5.5.3).

Phosphate enrichment in spreading axis metalliferous sediments has been described from the Pacific (Berner, 1973), where it has been attributed to adsorption of phosphate onto hydrated iron oxides. A similar process seems to have operated in the Troodos Ocean.

Enrichment of REE and yttrium in deep-sea phosphates has been described in the Pacific (Arrhenius and Bonatti, 1965). Incorporation from sea water during very early diagenesis is the suggested mechanism. The hydrogenous enrichment of these elements is strong evidence in favour of relatively low rates of accumulation,

7.4 DISCUSSION

7.4.1 Major elements

The primary major element variations in the Troodos pelagic sediments were controlled by proximity to local sediment sources, and the variable productivity and preservation of biogenic detritus.

The locally derived sediments comprise hydrothermal precipitates from vents distributed along the ridge axis and volcanic detritus from elevated parts of the ridge. The former had very limited ranges of influence, with the result that not all the axial sediments are metalliferous. However in areas close to hydrothermal vents, the sediments can be composed almost entirely of iron and manganese. The manganese is distributed more widely than the iron, so there is an overall trend of increasing Mn/Fe ratios with distance from the vents. However in detail there is a great deal of variability, and the ratios are extremely susceptible to secondary modification. In contrast to the along axis variations in the metalliferous sediment abundance, the other local source, the volcanic detritus, is more uniformly distributed. Spatially it is confined to the axial zone, but within this it is unconstrained. The composition of the axial sediment is strongly influenced by this local source, which generally completely conceals the pelagic clays.

The observed supralava basal metalliferous sediments are carbonate-free, having accumulated below the carbonate compensation depth (CCD). Rare foraminifera and coccoliths are found preserved in basal sediments which were rapidly buried by lavas, indicating that a proportion of the dissolution occurred at the sediment surface. In the non-metalliferous sediments overlying these, which accumulated later as the crust was cooling, an upward transition through a dissolution facies, to well preserved pelagic chalks, documents the changing relative position of the CCD, probably due uplift of the crust. If the spreading axis was still operative during this time (elsewhere), then presumably the basal metalliferous sediments would also be carbonate-rich. Thus the reversal of the normal oceanic sedimentation pattern, where carbonate rich basal sediments pass upwards into carbonate free facies, can be seen in terms of a slightly elevated CCD (with respect to ocean floor), and an interruption of the normal subsidence history by an uplift event.

Siliceous biogenic detritus is less affected by dissolution and its distribution seems controlled instead by variations in surface water productivity. A low concentration background radiolarian production was supplemented by periodic bursts of activity leading to thin beds of radiolarian cherts separated by layers of sediment with sparse radiolarian tests.

The variation in phosphorus content (mirrored also by calcium) of the sediment differs from that of the other elements. It is very strongly enriched in the axial metalliferous sediments, not because of common source, but through adsorption onto the iron component. This behaviour - the fixing of the sea water elements into the metalliferous sediments - is more important with the trace elements. Table 7.3 shows the enrichment of the elements with respect to lithogenous aluminium, which may be taken as a measure of relative accumulation rate. The phosphorus accumulation rate is increased four fold in the axial metalliferous sediments with respect to the clay. Thus locally the axis sediments are an important sink for phosphorus, but on the ocean scale the effect is negligible.

TABLE 7.3

RELATIVE ACCUMULATION RATE

	Pure umber	Attributable to Hydrothermal source
Si	1.11	0.25
Al	1.27	0.27
Fe	20.49	19.48
Mg	1.38	0.72
Ca	3.92	-
Na	0.95	-
K	1.00	-
Ti	1.28	0.17
Mn	110.00	?
P	4.33	-
Ba	24.60	0.60
Ce	2.06	-
Co	8.92	6.75
Cu	19.00	5.82
La	10.9	-
Nd	7.71	-
Ni	31.8	12.0
Pb	80.9	2.78
Sr	11.4	-
V	33.9	33.8
Y	6.35	-
Zn	9.37	4.13
Zr	3.32	1.59

These values are calculated assuming constant Al accumulation rate, and are relative to the overlying bentonitic clay. The hydrothermal value is that part of the total which can be attributed to the iron component (see section 5.5.5).

7.4.2 Trace elements

Most of the trace elements are strongly enriched in the axial metalliferous sediments, partly through direct hydrothermal contribution but largely because of the highly adsorbant character of the sediments. In Table 7.3 the relative enrichment in the axial metalliferous sediments is shown, along with the proportion of this which might be of direct hydrothermal origin (section 7.4.3).

Only chromium and rubidium do not show any enrichment in the metalliferous sediments. Cerium and zirconium show only small enrichments. All of the vanadium, and significant proportions of the cobalt, copper, nickel and zinc, can be attributed to a direct hydrothermal origin (drawing a distinction between direct precipitation of metals from hydrothermal fluids, and any contribution to sea water concentrations from these fluids). A proportion of the cobalt, copper, nickel and zinc, and the greater part of the lead, strontium, yttrium and REE were preferentially fixed into the axial metalliferous sediments. For lead in particular, with an estimated axial accumulation rate two orders of magnitude greater than elsewhere, the axial sediments must have had a profound influence on the total budget.

7.4.3 Hydrothermal contribution

Estimating the hydrothermal contribution in the modern oceans has proved difficult (Turekian, 1983). Studies of the composition of hydrothermal waters, and of isotope variations offer the best hope (op. cit.). In ancient oceanic sediments the isotopic data may also be used, but direct knowledge of hydrothermal fluid compositions is lacking. Including the isotopes, there are four lines of reasoning relevant to this question.

Firstly, isotopic data for lead and strontium suggest a dominantly basement source for the former (hydrothermal) and sea water source for the latter. These findings are in agreement with studies in the modern oceans, except for a slightly greater influence of sea water derived lead. However these results do not help in determining the source of other elements.

Secondly, the sulphide deposits, which are believed to precipitate directly and rapidly from hydrothermal solutions, are enriched in copper, zinc, nickel, cobalt and to a lesser extent, lead. There is thus no doubt that these elements were being contributed, but in what abundance is not known.

Thirdly, although most of the oxide metalliferous sediments are enriched in trace metals through hydrogenous processes, and thus absolute enrichments mostly decrease towards the source vents, some element show the reverse trend. Importantly copper, zinc and vanadium are all greatest in the proximal metalliferous sediments. It is using the minimum trace element enrichment in the proximal oxide sediments, that estimates for the possible hydrothermal contributions have been calculated (Table 7.3).

Fourthly, one can consider the absolute trace metal abundances in the sediments, and compare these with what is observed in other mid-ocean ridge sediments. In the Troodos ophiolite, the metalliferous sediments are very similar in composition to those at the East Pacific Rise, except for an enrichment in lead, and depletion in nickel (section 5.5.8). That these elements are similarly depleted or enriched in the Troodos igneous rocks, when compared with Pacific ocean crust, argues for a basement, and thus hydrothermal, influence on the composition. This is very interesting when in the light of inter-element studies, both nickel and lead are concentrated in the slowly accumulated hydrogenous fraction. These two observations can be reconciled only if the nickel and lead budgets of the Troodos ocean were strongly influenced by the spreading axis.

7.5 CONCLUSIONS

1) The variations in chemical composition of the sediments can, to the first approximation, be explained in terms of inter-mixing of three categories of sediment source. A background quasi pelagic source has superimposed upon it locally derived volcanic detritus from a linear source comprising the rift flank highs, and hydrothermal precipitates originating from axial hot springs (point sources).

The on-axis localised sediment sources result in atypical compositions, most importantly localised basal metalliferous enrichment.

2) The types of sediment sources, and their chemical composition are similar to those observed at modern oceanic spreading axes. The most important difference lies in the localised character of the hydrothermal sediments, resulting from the absence of a dispersal mechanism such as is prominant at the modern axes.

3) Trace elements are strongly enriched in the axial metalliferous sediments; the ochres, interpillow oxides, and umbers, partly as a result of the local hydrothermal source, and partly due to the propensity of the iron and manganese oxides to adsorb dissolved elements. Of the twenty five elements analysed only sodium, potassium, rubidium and chromium were not enriched. Zirconium and vanadium, commonly regarded as inert are both enriched, the latter strongly so.

For some of these elements, notably lead, barium, copper and nickel, the axial metalliferous sediments comprise a significant sink.

4) The hydrothermal vents exhale significant amounts of iron, manganese, copper, zinc, nickel, lead and vanadium.

THE ORIGINS AND GEOCHEMISTRY OF THE TROODOS METALLIFEROUS SEDIMENTS: A CONCLUSION

Previous interpretations of the metalliferous sediments of the Troodos massif are diverse. In most recent models umber formation is seen as separate from the sulphide event, and is attributed to slightly off axis low temperature hydrothermal activity. This study of the field relations, mineralogy and chemistry provides new constraints, which are in conflict with the currently accepted interpretations. A new interpretation, involving derivation and subsequent transport of iron and manganese, from axial high temperature vents is proposed. A model has been developed to explain the chemical variations not only of the hydrothermal sediments, but also of the related non-metalliferous sediments. The origin of the sediments is viewed within the framework of processes at a spreading axis, an assumption which requires justification in the light of geochemical evidence for the "non-oceanic" character of the lavas.

The character of the Troodos spreading axis

The presence of a sheeted dyke complex some 80 km across, requiring 100% extension over this distance, remains the most powerful argument for a spreading axis origin. Various geological and geochemical arguments may be used to refine this interpretation. Low relief on the palaeo-ridge is indicated by the scale of the dyke-parallel normal faulting. A well defined median valley is indicated by the confinement of locally derived volcanic detritus to the interlava sediments. These observations are all in keeping with intermediate rate spreading. A normal mid-ocean ridge water depth is indicated by fluid inclusion studies of stockwork quartz (through estimation of confining pressure), and the metamorphic assemblages within the igneous complex indicate that geothermal gradients were similar to those of modern spreading axes. The processes of hydrothermal activity are identical within the resolution of the available tests. Differences are however observed in the sedimentary cover: the aluminosilicate accumulation rate seems to have been relatively high, and the basal sediments are carbonate free, in contrast to modern ridge crests.

Observed compositional peculiarities of the lavas have led to speculation concerning the original tectonic setting. However it is clear that if it were not for the lava chemistry, there would be no reason to suspect that the Troodos ophiolite was not formed in a normal mid-ocean ridge setting.

Metalliferous sedimentation at the Troodos spreading axis

Compositional variations in the basal sediments can be explained by interplay of a number of independent sediment sources. These fall into three broad categories: general background; local detrital and axial hydrothermal. The general background sediment source comprised quasi-pelagic aluminosilicates, biogenic carbonate and/or silica, and hydrogenous material. The local detrital sediment was derived from rift flank highs, and was closely confined to the median valley. The axial hydrothermal material was derived from high temperature hotsprings, and comprises dominantly iron and manganese. The hydrothermal sources had limited range and thus proximity to a vent, exerted a strong influence on the resulting sediment composition.

In the immediately vicinity of the vents, sulphide sediment accumulated with negligible admixed non-hydrothermal sediment. Oxidative erosion of these led to formation of iron-rich manganese poor sediments, rich in sulphide fragments (the ochre). Though sulphide accumulated at the vent, all of the manganese and much of the iron was dispersed into the water column, the latter probably in the form of fine particulate sulphides. Subsequent to oxidation this material accumulated both within the volcanically active zone (to form interpillow oxide sediment, or interlava umbers) or on the flank of the rift beyond this region where it became concentrated in faulted hollows in the lava surface (the supralava umbers). That most of the sediments fell outside the volcanically active zone argues for this being narrow.

Hydrothermal alteration and diagenesis of the sediment

Secondary modification of the sediment is variable and it is useful to separate discussion of the interlava - from the supralava sediment, which were affected quite differently.

Interlava: Where sediment was permitted to accumulate without disruption by volcanic activity, diagenetic enrichment in phosphorus occurred leading ultimately to the formation of REE and Y enriched francolites. Where, however, sediments were rapidly engulfed by pillow lava flows, this enrichment either did not occur or was eliminated. Carbonate detritus, which dissolved completely in the exposed sediment, was preserved by the engulfing process, though some recrystallisation occurred in contact with the hot lavas. The engulfed sediments further interacted with the host lavas, resulting in reduction and loss of the manganese oxides. Where buried deeply by later lavas, elevated temperatures resulted in enrichment of the oxide sediment in Na, Al and Si, with the formation of analcite and rarely natrolite. Similarly, buried interpillow sediment close to high temperature hydrothermal conduits, were altered and silicified to form jaspers.

Supralava: The supralava metalliferous sediments were not subjected to this alteration, though locally manganese oxides were reduced where in contact with the underlying lavas. Unlike the interlava sediments, which were protected by a rigid framework of lavas, the supralava sediments suffered compaction upon burial. Early formed veins were ptygmatically folded, and radiolaria flattened. Differential compaction of the basal sediments, into irregular hollows has resulted in their present basin- or trough-like form. Diagenesis, apart from early francolite enrichment, consisted of transformation of the original amorphous hydrated iron oxide into goethite, formation of palygorskite and/or clinoptilolite, probably at the expense of smectite, and formation of nodular vitreous cherts in the lowermost sediments.

Controls on chemical composition

The composition of the sediments are controlled both by primary variations in source, and secondary modifications. Thus the chemical and mineralogical diversity of the sediment can be considered in terms of the depositional model described above, if due allowance is made for chemical alteration. The major element variations are simpler than those of the trace elements, and the two groups are discussed separately.

Major elements: The major element composition of the sediment is controlled by the relative importance of a number of sediment sources. These are 1) externally derived clay 2) locally derived volcanic detritus 3) hydrothermal iron, 4) hydrothermal manganese 5) biogenic/diagenetic apatite 6) biogenic carbonate 7) biogenic silica. In addition, alteration may introduce carbonate, silica or analcite, and can remove manganese oxide. Of the primary controls, proximity to a source of hydrothermal iron or manganese has the greatest effect upon the sediment composition. Biogenic silica is found locally in beds of radiolarite, and thus can locally have a great influence. Carbonate has mostly been lost through dissolution, but can be abundant in the interlava sediments, preserved by rapid burial, and appears in the upper parts of the basal section because of a change in relative position of the carbonate compensation depth. Phosphate was probably adsorbed onto iron oxides, but became altered to francolite during early diagenesis.

Trace elements: The trace elements are only in part controlled by primary source variations. Elements such as Cr and Rb are entirely controlled by aluminosilicate source, and in the non-metalliferous sediments, the aluminosilicate source is the dominant control on most trace element abundances. However even in these, hydrogenous manganese exerts a significant influence at least on Sr, Ba and Pb. In the metalliferous sediment, the hydrothermal iron component brings in with it significant amounts of V, Cu, Zn, Zr and lesser amounts of Mn, Co, Ni, Pb and Ba. Hydrothermal manganese occurs in a separate phase, and behaves independently of iron, though it has a similar overall distribution. The manganese and iron-oxides both scavenged trace elements from sea water, adding to the Cu and Zn enrichment, and largely controlling the Ni, Pb, Sr and Ba abundances. Rare earth elements and Y are also associated with the ferromanganese oxides, but dominantly occur in the francolite. In the umbers, the Pb enrichment correlates positively with the total Al concentration, as would be expected if Al accumulation rates were constant (with the result that total accumulation rate was controlled by hydrothermal iron), and Pb enrichment was inversely proportional to total accumulation rate. Although Pb shows this affect particularly well, partly because it is not significantly

contained in phases other than the ferromanganese oxides, this process probably strongly influences other element abundances.

The result of these hydrogenous processes is that relative trace metal enrichment of the phosphate and ferromanganese oxides increase up section (away from ridge axis) due to a fall off in total sediment accumulation rates. However, as the abundance of the phosphate and ferromanganese oxides decrease up section, the absolute enrichment declines. The presence at the ridge axis of sediments which have great propensity to scavenge trace elements, results in the axial sediments being an important sink for some trace elements, notably Pb and Ba.

Modern comparisons

In terms of both mineralogy and chemistry, the umbers are extremely similar to the East Pacific Rise crestal sediments. Differences are limited to the relative enrichment of a few elements, and to the inhomogeneous distribution of the metalliferous sediment at the ridge crest. In Cyprus, slightly greater enrichment in Pb and lesser in Ni, may well be related to the peculiar composition of the Troodos igneous rocks which are Ni depleted with respect to MORB. The more significant difference concerns the inhomogeneous distribution of the metalliferous sediments: umbers do not occur in all places, and show sharp upward changes in composition, implying local control on sediment supply. In contrast, at the East Pacific Rise, the vented hydrothermal effluent is caught up in the mid-depth circulation, mixed and transported up to 1000 km, and local effects thus smoothed out. The Troodos ocean by implication, lacked similar mid-depth circulation.

APPENDIX

Sediment analytical data

Below, after description of the different analytical methods employed, chemical data for the umbers, clay-rich umbers, and non-metalliferous bentonitic clays and radiolarites are tabulated. For all the data, sample localities are given as precisely as possible, either using grid references (always referring to Cyprus K17 series, 1: 50,000 topographical maps) or locality maps. The area localities are shown in Fig. 5.3

Analytical techniques

Analyses undertaken for this study

Edinburgh X-ray fluorescence analysis.

Major element analyses were performed on fused glass discs after the method of Norrish and Hutton (1969). Trace elements were analysed using pressed powder discs. A Phillips PW1450 sequential automatic X-ray spectrometer was used, applying corrections for inter-element mass absorption effects. USGS and CRPG rock standards (Abbey, 1980) were used to calibrate the data. For a full outline of the procedures of sample preparation, analysis and data processing see Fitton et al. (1984) and Thirlwall (1979).

Atomic absorption - Edinburgh

Atomic absorption analysis for Co, Cu and Mn were performed using a Varian Techtron atomic absorption spectrophotometer 4/5 using an air/acetylene mixture, under the supervision of M.J. Saunders. Samples were digested in PTFE crucibles using an $HF-HNO_3-HClO_3$ attack. MnO_2 precipitates which formed in the manganese-rich solutions were dissolved in a mutual reduction reaction involving hydrogen peroxide.

Colorimetry

Iron was determined colorimetrically using a Perkin-Elmer 550 spectrophotometer and a thioglycollic acid colorimetric agent.

TABLE A1

Cobalt data, and comparison of atomic absorption and colorimetric data with XRF

Sample No	Iron(Wt%) Colorimetric	Iron(Wt%) XRF	Manganese(Wt%) AA	Manganese(Wt%) XRF	Copper(ppm) AA	Copper(ppm) XRF	Cobalt(ppm) AA
81 115B							34
81 135	9.39	9.39			332	281	110 ± 3 N=6
81 136							124 (128)*
81 138					1051	875	95 (96)*
81 142							96
81 144			7.84	7.88			93
81 146							92
81 151	31.77	34.74	6.36	6.86			99
81 156	34.91	35.18	5.59	5.54			193
81 160	31.33	31.83	5.88	6.02	803	674	129
81 161					937	797	182
81 162	38.71	38.88	5.39	5.45			193
81 164	30.43	31.13	5.95	6.11	789	658	145
81 165							139
81 88			50.17	49.99	534	492	111
81 158mn			12.80	13.58	65	56	103
81 58			35.09	36.24			1082
82 B6							48
82 20							57
82 21							55
82 38							100
82 52A							18
82 52B							34
82 67							50

* Bracketed value from standard addition method.

Copper	XRF = 0.83 x AA + 12.6 (ppm)	R = 0.998
Iron	XRF = 1.02 x COL + 0.12	R = 0.995
Manganese	XRF = 1.004 x AA + 0.24	R = 0.9997

Comparison of wet chemistry with XRF for iron, manganese and copper

The results for a small data set are shown in Table A1, along with the cobalt data. Also given is the equation relating the results of the compared techniques. For manganese and iron the slopes are not significantly different from one, and the intercepts are very small. Thus there is extremely good agreement. For copper, an extremely good correlation is again observed and the intercept is also very small. However the slope of the line is 0.83; the XRF values being consistently low. This situation results from the uncertainty of published standard values for copper, and it is probable that the atomic absorption values are more reasonable. Nevertheless no correction has been applied to the XRF data for copper in this work. Analytical precision is more important than accuracy for the inter-element correlation study, and without greater confidence as to the absolute copper concentrations, a correction was considered unjustifiable.

Data analysed by A.H.F. Robertson

Samples for major element analyses were fused with lanthanum oxide and lithium borate, ground and pressed into discs after a method described by Rose et al (1963). Samples were analysed in batches of four with an internal standard to correct for machine drift, using a PW1212 automatic X-ray fluorescent spectrometer.

Trace elements were analysed using optical emission spectroscopy, with accuracy checked using international standards.

The chemical data

Interlava sediments

All samples were analysed using XRF at Edinburgh. 6 cobalt determinations are quoted in Table A1. Sample localities in the Mathiati-Margi area are shown in Fig. A1. The six samples from the Kalavasos area were collected from exposures on the north-east bank of the Vasilikos River, and tributaries in the vicinity (near GR 246 510, sheet 20) except sample 81 204 which came from an exploratory trench close to the mine office (ca GR 243 513).

Umber

Margi. 66 samples of umber, clay-rich umber, radiolarite and bentonitic clay were collected from a 13 m bedding perpendicular section in the principal umber pit at Margi, in May, 1981. Recent mining activities have destroyed this section. The height in the section at which samples were collected, and their field identifications are shown in Table A.2

Other localities are east of Kambia (ca. GR 245 744, sheet 12), Mathiati 82-38 (GR 312 712, sheet 20) 82-37 (GR 310 731, sheet 20) and at Mangalene (1 km northwest of Parekklisha). The samples from Dhrapia and Skouriotissa were collected and analysed by A.H.F. Robertson.

Clay-Rich umber

Among the samples collected from Margi are 17 clay-rich umbers. The locations in the sample traverse are shown in Table A2. Other clay-rich umbers were collected and analysed by A.H.F. Robertson, from above the Skouriotissa umber, and below the sediment cover south of the Mavridhia mine, Kalavasos.

Bentonitic clays, radiolarites and marls

A total of 19 non-metalliferous sediments occur in the section collected from Margi (Table A2). Of these, 7 are radiolarian-rich, and 4 are carbonate-rich. Other samples of non-metalliferous clay were collected and analysed by A.H.F. Robertson, from Skouriotissa, Kalavasos, and Dhrapia. In all cases these were sampled from close to underlying umber or clay-rich umber.

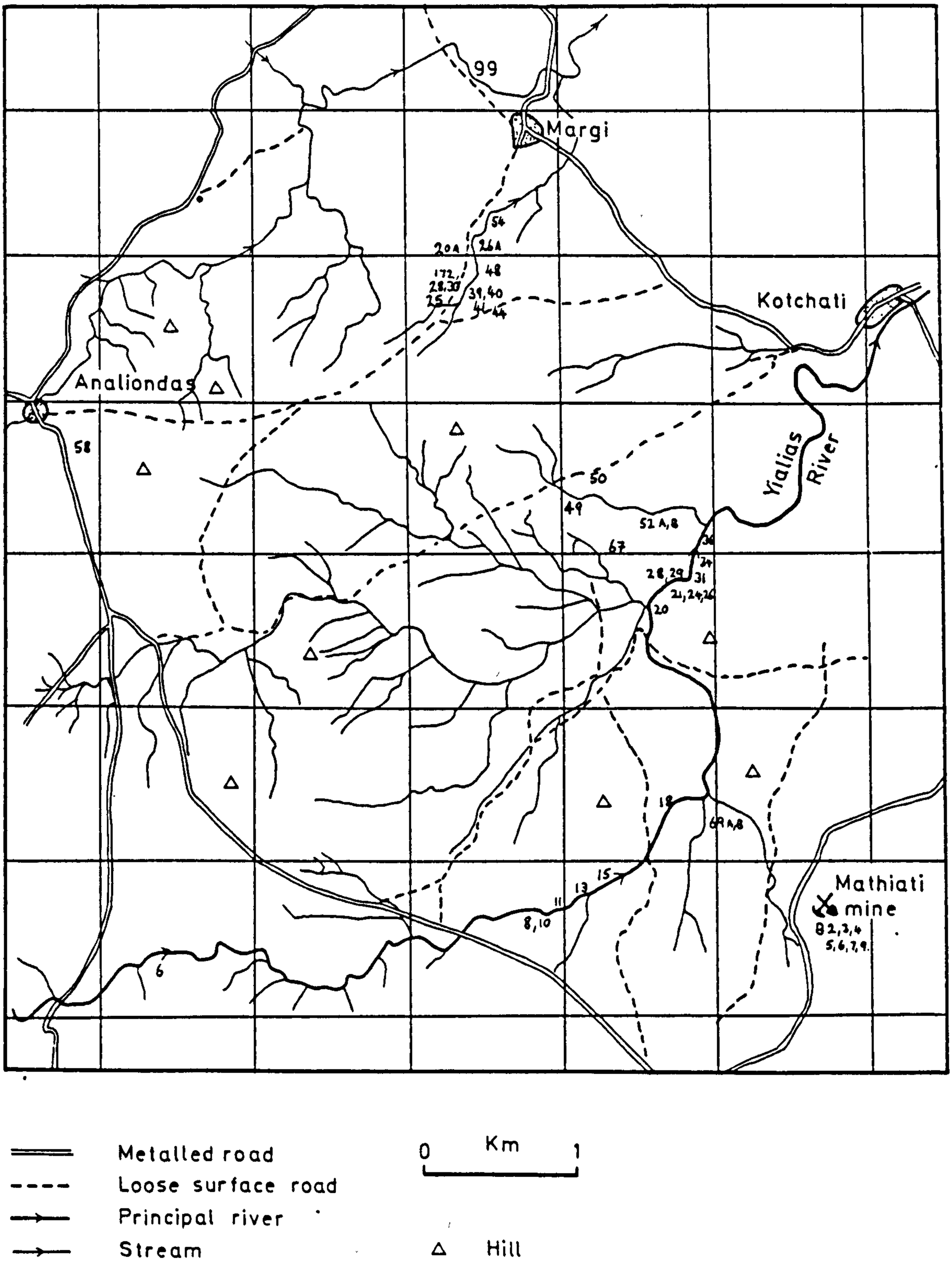

Fig. A.1

Margi-Mathiati area. Sample localities for the interlava sediments. The map is drawn after Cyprus, series K717 1:50,000 sheet Nos. 12 and 20.

TABLE A2

ANALYTICAL DATA FOR THE MARGI UMBER

66 samples were collected from a 14m section through umber, clay-rich umber, bentonitic clay and radiolarites. Locality is shown in Fig.5.1.

Lithology	Sample No.	Height in section (m)	Lithology	Sample No.	Height in section (m)
B	203	13.75	C	133	2.89
R	202	13.60	C	132	2.87
B	201	12.01	C	135	2.83
R	200	11.86	U	138	2.63
B	199	11.05	U	139	2.60
R	198	10.90	U	140	2.53
B	195	8.86	U	141	2.45
B	192	6.92	U	142	2.33
R	191	6.80	U	143	2.23
B	190	6.68	U	144	2.17
R	189	6.62	U	145	2.10
B	188	6.41	U	146	1.90
R	187	6.17	U	147	1.83
B	186	5.84	U	148	1.75
R	185	5.39	U	149	1.68
B	105	5.12	U	150	1.59
B	109	4.70	U	151	1.51
B	112	4.37	U	152	1.40
B	115B	4.10	U	153	1.30
C	115A	4.05	U	154	1.14
C	116	3.95	U	156	1.00
C	117	3.83	U	157	0.90
C	118	3.77	U	168	0.65
C	119	3.56	U	159	0.62
C	121	3.47	B	160	0.51
C	124	3.29	U	167	0.45
C	122	3.28	U	161	0.32
C	123	3.17	U	166	0.30
C	127	3.05	U	165	0.15
C	129	2.98	U	162	0.15
C	130	2.95	U	164	0.12
C	131	2.90	U	163	0.06

B = Bentonitic clay R = Radiolarite C = Clay-rich umber U = Umber

Inter-pillow sediment Margi-Mathiati (Edinburgh XRF)

	JB20A@1	JB26A@1	25@1	39@1	40@1	41@1	44@1	48@1	54@1	99@1
SI	7.63	16.52	15.37	0.80	1.16	0.68	4.01	7.73	19.18	2.56
AL	2.39	6.84	5.98	0.38	0.51	0.34	1.86	4.15	5.02	0.84
FE	1.90	17.00	18.96	1.62	2.76	1.55	17.66	12.01	10.70	4.99
MG	2.21	6.97	3.92	0.68	0.98	0.25	0.92	3.69	12.61	0.88
CA	24.10	1.16	4.19	36.61	35.30	36.92	13.65	7.43	1.46	32.26
NA	0.08	1.28	1.99	*	*	*	0.03	0.18	0.63	0.09
K	1.01	0.69	0.31	0.06	0.03	0.05	0.74	0.88	0.29	0.20
TI	0.08	0.12	0.06	0.02	0.01	0.02	0.06	0.05	0.03	0.02
MN	0.09	0.48	0.80	0.12	0.14	0.37	11.28	14.73	0.27	0.31
P	0.01	0.16	0.17	0.02	0.05	0.02	0.27	0.09	0.06	0.14
BA	5	29	24	*	*	*	2609	71	23	*
CE	4	6	8	*	6	1	11	3	*	4
CR	71	3	5	4	3	2	*	4	0	6
CU	13	1055	139	172	65	36	683	3543	91	269
LA	1	12	44	7	7	9	87	5	7	11
NB	0	2	2	1	1	1	3	3	1	0
ND	4	13	43	7	11	10	61	1	5	14
NI	63	285	176	21	22	23	363	317	140	59
PB	6	13	26	6	9	9	197	78	12	13
RB	14	15	9	1	0	0	8	11	5	4
SR	102	51	39	86	79	83	964	245	93	68
V	74	879	653	39	105	77	1561	626	585	137
Y	10	48	87	21	28	22	82	33	27	22
ZN	33	280	120	13	20	12	236	206	131	45
ZR	7	49	36	3	5	3	55	38	20	7

	82-6@16	82-8@16	82-10@16	82-11@16	82-13@16	82-15@16	82-18@16	82-20@16	82-21@16	82-24@16
SI	18.03	12.22	14.55	21.20	20.50	10.22	11.34	11.31	10.70	8.28
AL	7.25	4.51	5.06	10.02	9.72	5.31	4.27	5.62	5.20	3.50
FE	14.66	28.30	5.55	9.15	10.84	30.28	23.05	29.46	28.38	11.24
MG	4.45	3.56	3.05	0.78	0.67	2.32	5.44	1.48	1.84	1.19
CA	1.24	1.84	15.56	0.33	0.44	1.07	1.35	0.86	0.97	18.93
NA	4.01	0.40	0.17	9.12	8.35	2.62	0.50	1.92	0.70	0.48
K	0.39	0.58	2.24	0.10	0.24	0.19	0.23	1.01	1.29	1.20
TI	0.07	0.12	0.22	0.02	0.05	0.04	0.09	0.10	0.12	0.06
MN	0.36	1.22	0.19	0.27	0.45	0.92	0.58	1.02	1.00	0.70
P	0.18	0.07	0.03	0.06	0.08	0.16	0.08	0.16	0.21	0.14
BA	18	30	3	19	20	26	9	32	26	11
CE	*	*	*	*	*	*	*	*	*	*
CR	38	40	59	58	18	88	43	37	45	34
CU	667	2710	235	176	212	1383	14616	337	933	694
LA	11	12	5	1	20	9	10	18	27	15
NB	3	4	2	1	2	4	4	7	5	2
ND	13	2	7	2	13	*	2	10	25	13
NI	169	372	103	66	133	161	115	161	175	57
PB	11	24	12	6	10	13	15	18	14	7
RB	7	16	39	1	6	2	4	20	22	17
SR	18	29	39	9	12	22	22	40	42	57
V	1371	1457	224	2517	627	2707	1345	1160	1422	1063
Y	44	50	25	25	36	44	48	60	74	47
ZN	156	286	118	65	67	451	240	225	230	85
ZR	32	32	16	15	20	34	63	99	106	23

	82-26@16	82-28@17	82-29@17	82-31@17	82-34@17	82-36@17	82-50@17	82-52A@17	82-52B@17
SI	15.51	1.16	13.06	14.63	13.41	2.27	8.70	0.32	0.48
AL	5.63	0.60	5.82	6.42	6.07	0.85	4.42	0.17	0.28
FE	14.93	2.67	26.41	22.72	23.83	3.87	36.02	2.18	3.29
MG	2.65	0.59	2.85	2.47	5.11	1.22	1.49	0.19	0.26
CA	7.53	34.96	0.90	0.70	0.95	32.90	0.81	36.01	35.03
NA	0.06	0.00	1.17	2.48	0.12	*	0.08	0.02	0.02
K	1.38	0.10	0.81	0.77	1.11	0.07	1.16	0.06	0.07
TI	0.19	0.02	0.06	0.07	0.10	0.02	0.12	0.01	0.01
MN	0.63	0.36	0.83	0.80	0.95	0.21	1.14	2.08	0.45
P	0.04	0.03	0.12	0.10	0.12	0.03	0.19	0.04	0.05
BA	17	116	37	23	43	*	43	744	52
CE	*	1	*	*	*	*	*	4	34
CR	25	6	54	50	39	11	54	6	9
CU	158	156	746	892	274	61	189	680	352
LA	8	7	18	10	19	10	15	7	8
NB	3	1	4	3	5	1	6	0	2
ND	3	8	8	1	9	11	*	9	16
NI	98	23	204	143	219	37	156	35	33
PB	15	7	22	11	15	7	27	12	11
RB	36	*	19	15	18	1	19	*	*
SR	29	76	28	38	44	86	20	185	75
V	690	124	1521	1714	1338	357	1752	295	391
Y	29	11	31	51	42	19	54	10	13
ZN	124	20	180	178	236	27	163	13	18
ZR	52	7	70	61	64	11	97	2	4

	B2@22	B3@22	B4@22	B5@22	B6@22	B7@22
SI	19.12	15.95	17.61	16.36	15.16	12.60
AL	8.63	7.52	8.50	7.49	6.66	5.99
FE	13.42	16.19	14.77	18.49	4.80	33.31
MG	2.24	1.51	0.96	1.76	1.69	2.52
CA	0.95	0.67	0.69	0.91	14.37	1.46
NA	6.32	6.25	6.87	5.27	5.44	0.50
K	0.24	0.29	0.29	0.37	0.16	0.87
TI	0.11	0.12	0.08	0.11	0.03	0.19
MN	0.34	0.44	0.38	0.51	0.29	0.92
P	0.07	0.13	0.14	0.12	0.04	0.31
BA	16	17	22	19	105	54
CE	*	*	*	*	*	4
CR	33	40	39	38	67	64
CU	1602	2442	3418	3262	3004	733
LA	5	13	11	10	27	33
NB	3	3	3	3	4	7
ND	4	15	11	13	32	39
NI	77	114	94	120	81	220
PB	8	9	8	12	13	20
RB	3	4	5	5	6	16
SR	31	22	23	31	24	51
V	1141	1519	1514	1367	2319	2331
Y	34	47	36	47	37	106
ZN	131	157	129	180	137	341
ZR	60	67	57	72	78	137

Inter-lava umber Margi-Mathiati (Edinburgh XRF)

	30@10	28@10	172@10	82-49@19	82-67@19	82-69A@21	82-69B@21
SI	8.72	19.48	20.74	9.14	5.94	4.80	4.54
AL	2.89	7.04	6.78	2.39	1.86	2.44	2.27
FE	36.47	18.88	16.47	26.88	25.68	43.59	30.86
MG	1.22	2.38	2.25	1.43	0.78	1.05	0.94
CA	1.26	2.39	3.93	1.21	1.43	2.22	1.68
NA	*	1.62	2.15	0.10	0.09	*	*
K	0.76	2.25	0.68	0.70	0.53	0.22	0.27
TI	0.12	0.70	0.69	0.12	0.10	0.05	0.06
MN	3.21	0.82	0.88	11,09	18.35	1.80	12.97
P	0.37	0.10	0.12	0.23	0.22	0.74	0.50
BA	80	116	125	127	124	46	65
CE	9	4	4	80	70	4	6
CR	11	3	13	40	30	46	39
CU	370	94	141	1726	1031	634	3000
LA	89	43	32	155	155	141	105
NB	7	2	3	6	5	6	5
ND	100	27	16	117	91	122	70
NI	321	139	95	252	365	289	360
PB	161	84	70	127	171	35	39
RB	30	23	11	26	17	3	3
SR	51	189	284	199	244	62	110
V	1442	1345	641	824	591	1359	1179
Y	146	55	37	151	135	206	127
ZN	279	226	279	278	329	318	308
ZR	82	83	96	83	74	52	48

Inter-lava umber Kalavasos (Edinburgh XRF)

	204@7	205@7	206@7	207@7	208@7	210@7
SI	13.30	8.08	9.89	14.80	16.45	3.46
AL	4.90	3.92	4.07	5.09	5.50	1.79
FE	21.14	30.90	24.74	20.08	14.34	23.02
MG	1.54	1.06	1.53	2.73	2.27	0.95
CA	3.00	4.57	2.35	4.28	2.51	4.02
NA	1.00	1.72	1.39	0.11	0.40	0.09
K	1.19	0.33	0.69	2.57	3.46	0.29
TI	0.21	0.07	0.17	0.17	0.21	0.06
MN	5.64	2.40	8.27	1.03	8.54	25.04
P	0.48	1.55	0.66	1.31	0.58	0.83
BA	106	360	255	46	79	161
CE	*	*	10	1	19	*
CR	16	16	21	41	45	5
CU	444	297	1651	121	721	522
LA	64	103	102	57	54	105
NB	3	4	3	2	2	3
ND	38	67	56	40	36	56
NI	143	123	164	122	123	187
PB	121	160	172	34	47	213
RB	44	7	19	35	37	10
SR	110	208	153	139	185	390
V	550	554	285	1516	303	759
Y	58	87	82	72	61	81
ZN	206	226	195	153	131	220
ZR	49	49	52	36	34	43

Pure umber Dhrapia (A.H.F. Robertson)

	7040@8	7060@8	7100@8	7120@8	7140@8	7170@8	7190@8	7210@8	7220@8
SI	7.95	4.68	6.08	4.91	5.14	4.68	6.08	7.01	5.61
AL	1.32	0.95	1.27	0.95	1.06	1.06	1.38	1.11	1.22
FE	22.10	37.77	33.57	32.52	26.30	37.77	33.22	37.77	37.77
MG	0.84	0.42	0.54	0.42	0.30	0.30	0.42	0.84	0.48
CA	3.07	0.43	0.79	0.71	11.86	2.43	1.14	1.14	1.00
K	0.66	0.31	0.29	0.22	0.22	0.17	0.31	0.32	0.22
TI	0.10	0.05	0.67	0.06	0.08	0.08	0.13	0.12	0.09
MN	16.34	2.02	3.25	2.48	5.26	7.90	7.51	2.94	2.40
P	2.18	0.21	0.26	0.28	4.36	2.18	0.38	0.43	0.53
BA	18	14	28	58	66	63	768	32	45
CO	107	86	112	76	60	103	85	87	145
CR	13	56	51	38	41	49	42	14	69
CU	457	173	1051	1180	717	857	851	482	1200
MO	39	20	12	28	71	40	31	23	43
NI	111	141	149	163	113	135	104	149	130
PB	70	75	111	122	94	97	121	75	77
SR	651	87	184	261	227	196	296	106	117
V	561	511	915	1493	586	1273	1493	1493	1493
ZN	186	250	344	289	246	225	255	332	386
ZR	288	409	315	427	156	373	330	321	363

Pure umber Skouriotissa (A.H.F.Robertson)

	239@1	331@1	332@1	333@1	334@1	335@1	336@1	337@1
SI	8.88	7.01	4.21	6.08	6.08	5.61	8.88	5.61
AL	2.43	2.06	1.06	1.53	1.69	1.43	2.22	1.80
FE	35.67	44.07	16.16	30.77	28.68	16.44	30.77	27.63
MG	0.66	0.54	0.30	0.42	0.54	0.18	0.24	0.66
CA	0.21	0.43	20.37	1.43	0.79	10.43	0.09	0.79
K	0.73	0.57	0.36	0.57	0.62	0.56	0.91	0.56
TI	0.13	0.13	0.07	0.10	0.12	0.10	0.15	0.10
MN	0.28	1.62	4.34	11.23	12.48	8.52	1.07	12.08
P	0.35	0.26	5.45	0.22	0.18	4.36	0.18	0.27
BA	21	45	756	1190	1190	870	1190	1190
CO	110	129	78	133	104	102	107	130
CR	62	8	16	9	9	12	8	11
CU	2500	1803	1080	1400	1180	1080	1250	1300
MO	48	110	227	85	92	172	68	98
NI	72	336	198	368	335	327	277	365
PB	150	179	145	190	246	189	206	243
SR	56	54	966	1050	1400	1300	1150	1050
V	1500	886	331	689	613	578	452	746
ZN	480	467	194	381	404	282	313	407
ZR	450	1102	233	798	591	332	497	545

Pure umber Margi (Edinburgh XRF)

	138@5	139@5	140@5	141@5	142@5	143@5	144@5	145@5	146@5	147@5
SI	11.00	11.05	10.30	9.83	8.97	10.65	9.72	8.23	12.74	10.72
AL	3.16	3.11	3.04	2.84	2.67	3.05	2.81	2.48	3.49	3.03
FE	26.09	26.22	29.04	28.76	31.87	27.16	28.35	31.46	25.48	28.42
MG	1.40	1.45	1.27	1.19	1.17	1.41	1.23	1.16	1.57	1.39
CA	1.01	1.03	1.19	1.21	0.94	1.23	1.40	1.10	1.35	1.29
NA	0.55	0.64	0.45	0.37	0.35	0.49	0.97	0.83	0.24	0.19
K	1.17	1.14	1.09	1.01	0.85	1.10	0.99	0.72	1.22	1.06
TI	0.15	0.15	0.15	0.14	0.13	0.15	0.14	0.12	0.16	0.15
MN	8.67	8.41	7.63	8.29	6.76	8.53	7.88	6.75	6.90	7.44
P	0.26	0.27	0.36	0.35	0.29	0.32	0.39	0.35	0.33	0.32
BA	1962	1700	1804	1970	1645	1547	1524	1402	1036	1169
CE	49	50	51	46	42	45	41	40	68	45
CR	16	15	16	14	15	16	10	10	21	17
CU	875	856	940	864	832	799	799	791	814	870
LA	144	139	175	180	146	159	177	156	176	153
NB	4	6	4	6	4	5	5	6	5	4
ND	96	97	122	115	98	106	114	105	121	98
NI	456	442	453	460	433	377	374	358	449	428
PB	521	550	548	533	496	559	525	498	576	537
RB	31	29	32	29	25	30	27	23	38	31
SR	1588	1392	1554	1742	1638	1649	1722	1631	1673	1855
V	1149	1171	1219	1193	1248	1156	1121	1201	1099	1185
Y	94	94	124	120	92	109	126	108	126	106
ZN	439	432	513	490	539	443	461	512	432	483
ZR	102	105	105	93	96	103	93	95	105	116

	148@5	149@5	150@5	151@5	152@5	153@5	154@5	155@6	156@6	157@6
SI	8.89	8.51	8.96	9.43	9.77	9.12	9.48	7.84	7.20	7.35
AL	2.60	2.48	2.57	2.70	2.86	2.59	2.66	2.29	2.10	2.00
FE	31.13	32.08	32.40	34.74	31.77	31.55	32.81	35.17	35.18	35.10
MG	1.28	1.17	1.26	1.32	1.21	1.24	1.20	1.11	1.10	1.06
CA	1.59	1.67	1.29	1.30	1.12	1.10	1.09	1.11	1.46	2.55
NA	0.18	0.19	0.18	0.15	0.20	0.26	0.20	0.16	0.16	0.13
K	0.80	0.74	0.76	0.80	0.95	0.83	0.88	0.68	0.57	0.58
TI	0.13	0.12	0.12	0.13	0.14	0.12	0.12	0.11	0.10	0.10
MN	6.56	7.06	6.20	6.86	6.30	6.82	5.62	5.80	5.54	5.23
P	0.48	0.50	0.39	0.36	0.28	0.27	0.30	0.32	0.48	0.86
BA	1119	1185	1073	1134	1061	1099	1061	1002	979	946
CE	40	35	42	42	45	38	30	37	27	31
CR	13	7	14	12	16	11	17	12	7	9
CU	855	840	762	891	836	780	742	764	767	704
LA	173	186	158	166	149	147	132	144	174	183
NB	3	5	5	6	5	6	6	7	4	3
ND	107	115	113	120	104	98	90	104	123	120
NI	490	409	362	363	337	311	276	268	234	217
PB	509	544	514	634	470	516	387	479	438	438
RB	26	21	24	23	27	25	30	19	16	18
SR	1755	1857	1724	1862	1737	1831	1718	1740	1703	1669
V	1248	1287	1207	1354	1202	1245	1155	1302	1326	1296
Y	128	138	114	116	95	90	98	109	121	133
ZN	534	519	500	560	470	455	433	474	436	392
ZR	114	96	112	105	115	134	115	120	87	81

	159@6	160@6	161@6	162@6	163@6	164@6	165@6	166@6	167@6	168@6
SI	8.53	9.98	5.76	6.63	8.35	10.45	7.05	8.93	8.03	6.97
AL	2.16	2.54	1.59	1.54	2.21	2.19	1.44	1.56	1.72	1.44
FE	27.77	31.83	37.81	38.88	35.82	31.13	28.05	34.95	33.97	30.40
MG	1.22	1.58	0.98	1.11	1.43	2.00	1.21	1.63	1.40	1.25
CA	6.83	0.88	0.83	0.98	0.99	0.77	8.46	0.68	1.59	5.22
NA	0.25	0.14	0.12	0.12	0.18	0.11	0.17	0.05	0.12	0.10
K	0.61	0.66	0.36	0.37	0.63	0.54	0.35	0.38	0.45	0.40
TI	0.11	0.12	0.08	0.08	0.09	0.10	0.07	0.07	0.10	0.06
MN	4.90	6.02	5.73	5.45	5.30	6.11	4.65	5.26	5.52	6.59
P	2.38	0.22	0.25	0.33	0.27	0.21	3.05	0.24	0.49	1.81
BA	1082	943	884	859	1025	1290	998	965	880	1157
CE	39	49	25	27	15	24	22	19	28	17
CR	10	7	*	*	6	4	0	*	1	1
CU	648	674	797	803	835	658	586	714	568	852
LA	228	128	145	139	106	95	286	71	129	205
NB	4	5	3	4	4	3	4	2	3	2
ND	133	98	108	91	71	76	197	41	97	144
NI	196	211	228	242	277	251	214	237	221	203
PB	379	544	452	373	333	343	235	297	395	265
RB	18	20	10	14	15	16	10	11	14	7
SR	1507	1640	1518	1414	1506	1679	1459	1311	1396	1889
V	1519	1479	1875	1984	1662	1611	1411	1773	1398	1219
Y	122	74	80	88	73	74	204	59	86	151
ZN	350	415	445	456	421	390	310	365	238	262
ZR	84	123	118	80	73	95	75	80	81	73

Clay-rich umber Margi (Edinburgh XRF)

	115A@4	116@4	117@4	118@4	119@4	121@4	122@4	123@4	124@4	127@4
SI	24.18	25.84	25.19	25.52	24.48	24.94	25.24	25.82	25.30	24.74
AL	6.24	6.89	6.67	6.77	6.45	6.55	6.66	6.95	6.66	6.72
FE	8.11	7.85	8.55	8.00	10.05	8.99	7.98	7.21	7.91	8.39
MG	2.42	2.48	2.38	2.43	2.36	2.32	2.33	2.22	2.27	2.24
CA	1.18	1.01	1.00	1.12	1.00	0.99	1.06	1.22	1.07	1.34
NA	0.73	0.77	0.74	0.76	0.64	0.67	0.69	0.72	0.71	0.73
K	2.54	2.52	2.66	2.71	2.63	2.79	2.88	2.99	2.90	2.70
TI	0.30	0.32	0.32	0.32	0.31	0.32	0.33	0.35	0.33	0.31
MN	3.93	2.29	2.61	2.23	2.93	2.61	2.63	2.56	2.86	2.84
P	0.30	0.20	0.22	0.26	0.22	0.22	0.24	0.30	0.22	0.31
BA	898	785	830	790	999	1036	998	1312	957	1349
CE	128	125	134	96	143	128	133	114	123	120
CR	48	55	53	33	51	54	59	60	57	60
CU	264	218	248	215	318	283	228	230	217	262
LA	104	77	88	98	86	84	84	97	80	99
NB	10	10	10	9	9	10	10	11	10	9
ND	101	68	81	69	75	75	77	83	71	96
NI	175	160	182	124	206	187	168	191	160	160
PB	176	186	194	123	198	174	165	157	167	174
RB	91	96	98	73	93	97	98	103	97	90
SR	277	248	266	191	342	350	339	401	326	644
V	422	260	304	265	361	295	250	205	240	211
Y	100	70	80	68	75	77	80	98	73	89
ZN	149	153	159	133	186	178	167	177	157	180
ZR	125	127	122	95	126	121	121	127	115	120

	1290A	1300A	1310A	1320A	1330A	1350A
SI	23.55	24.16	24.81	25.68	24.64	23.59
AL	6.12	6.60	6.71	6.91	6.65	6.32
FE	8.03	9.15	8.43	7.62	8.48	9.39
MG	2.31	2.11	2.18	2.19	2.15	2.20
CA	1.15	1.57	1.41	1.44	1.50	1.73
NA	0.77	0.62	0.60	0.72	0.66	0.58
K	2.49	2.69	2.76	3.00	2.71	2.49
TI	0.30	0.30	0.32	0.34	0.31	0.30
MN	3.91	2.94	2.99	2.41	2.97	3.33
P	0.30	0.41	0.36	0.38	0.39	0.47
BA	1240	1215	1207	1080	1160	1277
CE	113	131	124	114	127	128
CR	57	57	59	61	58	55
CU	256	291	238	196	240	281
LA	98	120	105	102	110	135
NB	10	9	10	11	8	10
ND	96	113	97	88	105	127
NI	159	180	199	158	192	203
PB	164	181	172	150	177	196
RB	98	90	97	105	95	86
SR	655	665	669	587	650	781
V	195	262	235	193	235	282
Y	96	116	105	105	111	140
ZN	185	193	182	174	182	195
ZR	125	117	125	126	130	130

Clay-rich umber (A.H.F. Robertson)

Skouriotissa-------| Kalavasos

	338@2	339@2	340@2	341@2	573@4	575@4
SI	23.84	22.91	23.37	22.91	25.71	27.58
AL	6.45	6.24	6.40	6.61	5.56	6.56
FE	11.82	11.05	11.12	9.58	7.55	6.72
MG	1.75	2.29	2.23	1.81	2.96	1.87
CA	1.29	1.50	1.29	1.22	1.00	1.36
K	1.99	1.91	2.07	1.99	1.74	1.99
TI	0.34	0.34	0.38	0.35	0.31	0.34
MN	4.34	3.41	3.48	2.94	3.48	1.71
P	0.18	0.22	0.18	0.13	0.18	0.18
BA	279	310	251	225	80	165
CO	57	74	58	57	65	61
CR	27	41	34	35	28	32
CU	423	421	346	280	342	198
MO	10	17	14	12	0	2
NI	106	152	120	100	139	96
PB	168	183	164	158	114	136
SR	114	131	105	112	106	303
V	105	152	212	186	179	115
ZN	356	414	356	306	308	296
ZR	65	89	85	96	93	84

Bentonitic clay and radiolarite Margi (Edinburgh XRF)

	105@3	109@3	112@3	115B@3	185@11	186@3	187@11	188@3	189@11	190@3
SI	28.97	28.54	28.23	26.49	33.71	27.81	39.67	27.94	39.86	28.24
AL	6.82	7.29	7.29	6.96	4.90	7.11	2.68	7.19	2.59	6.98
FE	4.75	4.93	4.91	4.41	3.47	4.58	1.86	4.82	1.82	4.72
MG	2.91	2.88	2.93	2.45	2.26	2.96	1.09	3.04	1.20	2.99
CA	1.51	1.86	1.52	1.42	1.07	1.70	0.61	1.77	0.45	1.51
NA	1.28	1.36	1.37	1.41	0.90	1.34	0.52	1.29	0.63	1.33
K	1.54	1.65	1.63	1.52	1.05	1.50	0.52	1.59	0.52	1.58
TI	0.35	0.36	0.36	0.33	0.25	0.34	0.14	0.36	0.13	0.34
MN	0.35	0.23	0.28	0.30	0.09	0.28	0.05	0.19	0.06	0.11
P	0.26	0.28	0.28	0.23	0.15	0.24	0.11	0.26	0.07	0.25
BA	258	142	184	201	80	226	58	150	53	133
CE	65	69	68	74	32	64	24	68	23	70
CR	208	197	237	161	182	193	78	203	87	225
CU	130	119	126	90	84	139	38	203	32	95
LA	44	52	50	48	25	43	17	47	12	45
NB	13	18	13	11	9	10	4	11	4	10
ND	42	50	45	44	27	41	19	45	15	44
NI	205	193	196	155	165	221	78	223	82	218
PB	23	13	23	22	11	23	11	21	11	19
RB	67	73	71	65	48	64	27	69	27	71
SR	461	556	599	708	249	418	87	406	81	372
V	111	112	122	111	70	110	42	116	40	121
Y	59	60	54	48	36	54	25	58	18	56
ZN	161	175	187	174	118	156	60	157	58	161
ZR	101	119	106	94	73	100	38	100	35	100

	191@11	192@3	195@3	198@11	199@3	200@12	201@12	202@12	203@12
SI	39.02	27.86	27.91	35.10	29.78	32.43	23.10	30.34	23.82
AL	2.78	7.23	7.40	3.99	6.69	4.16	5.40	3.48	6.07
FE	1.87	4.89	4.64	2.67	4.25	2.84	3.52	2.32	3.78
MG	1.27	3.34	3.14	2.10	3.28	2.12	2.70	1.74	2.93
CA	0.58	1.79	1.67	0.82	1.43	3.73	9.21	7.33	7.70
NA	0.63	1.35	1.44	0.32	0.47	0.20	0.24	0.15	0.32
K	0.57	1.62	1.65	0.85	1.42	0.86	1.10	0.73	1.22
TI	0.14	0.37	0.35	0.20	0.31	0.20	0.25	0.17	0.27
MN	0.06	0.11	0.15	0.09	0.12	0.08	0.14	0.09	0.18
P	0.11	0.25	0.27	0.12	0.22	0.13	0.16	0.11	0.17
BA	54	135	165	94	194	161	272	236	697
CE	29	67	74	38	66	39	51	34	57
CR	90	251	203	130	201	137	165	111	179
CU	49	173	198	88	129	55	75	39	84
LA	18	44	49	24	43	30	33	21	37
NB	5	11	10	7	10	6	8	5	8
ND	21	44	48	24	39	27	33	24	37
NI	85	252	254	131	207	142	180	112	201
PB	11	21	23	15	20	17	19	14	19
RB	27	71	72	42	67	43	53	37	58
SR	109	371	437	201	426	261	441	279	441
V	41	111	114	72	102	65	85	61	91
Y	26	55	57	28	49	33	38	26	41
ZN	64	164	165	97	144	105	129	82	142
ZR	38	107	103	56	90	58	70	52	85

Bentonitic clay and radiolarite (A H F Robertson)

	Skouriotissa	Kalavasos			Dhrapia
	34203	57705	57805	58206	58306	72309
SI	28.70	43.48	43.94	35.06	34.59	28.52
AL	6.67	2.38	1.32	5.93	6.56	6.77
FE	5.32	2.24	1.40	4.13	4.06	5.53
MG	1.63	0.66	0.24	1.63	1.75	1.87
CA	1.57	0.50	0.36	1.22	1.29	2.34
K	1.74	0.58	0.33	1.40	1.11	1.32
TI	0.37	0.22	0.08	0.34	0.36	0.35
MN	0.40	0.66	0.71	0.13	0.37	0.10
P	0.12	0.03	0.05	0.18	0.25	0.15
BA	84	41	40	82	71	156
CO	22	34	16	17	20	25
CR	64	51	24	63	71	59
CU	177	79	67	68	183	116
NI	57	67	24	35	33	26
PB	26	14	57	22	41	9
SR	237	154	70	603	291	193
V	76	74	38	33	39	76
ZN	268	153	134	221	230	261
ZR	82	52	31	79	46	40

BIBLIOGRAPHY

Abbey, S. 1980. Studies in "Standard Samples" for use in the general analysis of silicate rocks and minerals. Part 6 : 1979 Edition of "Usable Values" Geol. Surv. of Can., Paper 80-14.

Adamides, N.G. 1975. Geological history of the Limni concession, Cyprus, in the light of the plate tectonic hypothesis, Trans. Inst. Min. Metall., 84, B17-23.

_____ 1980. The form and environment of formation of the Kalavasos ore deposits - Cyprus, In: A. Panayiotou (ed.). "Ophiolites", Proc. Int. Ophiolite Symp., Cyprus, 117-127.

Arrhenius, G.O.S. and Bonatti, E. 1965. Neptunism and Vulcanism in the ocean. In "Progress in Oceanography" M. Sears (ed.) Amer. Assoc. Advanc. Sci. Washington. Vol 3 pp 7-22.

_____, Bramlette, M.N. and Picciotto, E . 1957. Localisation of radioactive and stable heavy nuclides in ocean sediments, Nature, 180, 85-86.

Ballard, R.D. and van Andel, Tj. H., 1977. Morphology and tectonics of the inner rift valley at lat. 37°50'N on the Mid-Atlantic Ridge, Bull. Geol. Soc. Am., 88, 507-530.

_____ and Moore, J.G., 1977. Photographic Atlas of the Mid-Atlantic Ridge Rift Valley, Springer-Verlag, New York.

_____ , van Andel, Tj. H. and Holcomb, R.T., 1982. The Galapagos rift at 86°W. Variations in volcanism, structure and hydrothermal activity along a 30-kilometer segment of the rift valley, J. Geophys. Res., 87, 1149-1161.

_____, Francheteau, J., Juteau, T., Rangan, C. and Normark, W., 1981. East Pacific Rise at 21°N: the volcanic, tectonic and hydrothermal processes of the central axis, Earth Planet. Sci. Lett., 55, 1-10.

Baragar, W.R.A., Plant, A.G., Pringle, G.J. and Schau, M. 1977. Petrology and alteration of selected units of Mid-Atlantic Ridge basalts sampled from sites 332 and 335, Deep Sea Drilling Project, Can. J. Earth Sci., 14, 837-874.

Bear, L.M., 1960. The geology and mineral resources of the Akaki-Lythrodonda area, Cyprus Geol. Surv. Dept. Mem., 3, 60pp.

Berger, W.H. and von Rad, U. 1972. Cretaceous and Cenozoic Sediments from the Atlantic Ocean, Leg 14, DSDP. In: Hayes et al. (eds.). Initial Reports of the Deep Sea Drilling Project, 14, 787-954.

Berner, R.A. 1973. Phosphate removal from sea water by adsorption on volcanogenic ferric oxides, Earth Planet. Sci. Lett., 18, 77-86.

Bischoff, J.L. 1969. Goethite-Hematite stability relations with relevance to sea water and the Red Sea Brine System. In: Hot brines and recent heavy metal deposits in the Red Sea" E.T. Degens and D.A. Ross (eds.). Springer Verlag, p.402-406.

_____ and Dickson, F.W. 1975. Sea water-basalt interaction at 200°C and 500 bars. Implications for origin of sea-floor heavy-metal deposits and regulation of sea water chemistry, Earth Planet. Sci. Lett., 25, 385-397.

Boles, J.R. 1977. Zeolites in deep-sea sediments. In: F.A. Mumpton (ed.) Mineralogy and geology of natural zeolites. Min. Soc. Am., Reviews in Mineralogy, Vol. 4, 137-160.

Bonatti, E. and Joensuu, O. 1968. Palygorskite from Atlantic deep-sea sediments, Am. Min., 53, 975-983.

Boström, K. and Peterson, M.N.A., 1969. The origin of aluminium-poor ferromanganoan sediments in areas of high heat flow on the East Pacific Rise, Marine Geol., 7, 427-447.

_____, Joensuu, O., Moore, C., Boström, B., Dalziel, M. and Horowitz, A. 1973a. Geochemistry of Barium in pelagic sediments, Lithos, 6, 159-174.

_____, Joensuu, O., Valdes, S., Charm, W. and Glaccum, R. 1976. 'Geochemistry and origin of East Pacific Sediments sampled during DSDP Leg 34. Initial Report of the Deep Sea Drilling Project, 34, 559-574.

_____, Kraemer, T. and Gartner, S. 1973b. Provenance and accumulation rates of opaline silica, Al, Ti, Fe, Mn, Cu, Ni and Co in Pacific pelagic sediments, Chem. Geol., 11, 123-148.

Bryan, W.B. and Moore, J.G., 1977. Compositional variations of young basalts in the Mid-Atlantic Ridge rift valley near lat. 36°49'N, Bull. Geol. Soc. Am., 88, 556-570.

Burnett, W.C. 1977. Geochemistry and origin of phosphorite deposits from off Peru and Chile, Bull. Geol. Soc. Am., 88, 813-823.

Burns, R.G. and Burns, V.M. 1979. Manganese Oxides. In: R.G. Burns (ed.) Marine minerals, Min. Soc. Am., Reviews in Mineralogy, Vol. 6, 1-40.

Calvert, S.E., Price, N.B., Heath, G.R. and Moore, T.C. Jr. 1978. Relationship between ferromanganese nodule compositions and sedimentation in a small survey area of the equatorial Pacific, Mar. Res., 36, 161-183.

Cameron, W.E., Nisbet, E.G. and Dietrich, V.J. 1980. Petrographic dissimilarities between ophiolitic and ocean-floor basalts. In: A. Panayiotou (ed.) "Ophiolites", Proc. Int. Ophiolite Symp. Cyprus, 182-192.

Cann, J.R. 1969. Spilites from the Carlsberg Ridge, Indian Ocean, J. Petrol., 10, 1-19.

_____ 1971. Petrology of basement rocks from Palmer Ridge, NE Atlantic, Phil. Trans. R. Soc. Lond., A268, 605-618.

_____ 1974. A model for oceanic crustal structure developed, Geophys. J. R. Astr. Soc., 39, 169-187.

_____ 1979. Metamorphism in the ocean crust, American Geophysical Union, Washington, Geodynamics Project: Scientific Report, 48, 230-238.

_____, Winter, C.K. and Pritchard, R.G. 1977. A hydrothermal deposit from the floor of the Gulf of Aden, Min. Mag. Lond., 41, 193-199.

Chester, R. and Aston, S.R. 1976. The geochemistry of deep-sea sediments. In: "Chemical Oceanography" J.P. Riley and R. Chester (eds.). Academic press, London, New York, San Francisco, Vol 6, edition 2, 360-383.

_____ and Hughes, M.J. 1969. The trace element geochemistry of a North Pacific pelagic clay core, Deep-Sea Res., 16, 639-654.

Chien, S.H. and Black, C.A. 1976. Free energy of formation of carbonate apatites in some phosphate rocks, J. Soil Sci. Soc. Am., 40, 234-239.

Church, T. and Velde, B. 1979. Geochemistry and origin of a deep-sea Pacific palygorskite deposit, Chem. Geol., 25, 31-39.

Constantinou, G., 1972. The geology and genesis of the sulphide ores of Cyprus. Ph.D. Thesis, University of London.

_____ and Govett, G.J.S., 1972. Genesis of sulphide deposits, ochre and umber of Cyprus, Trans. Inst. Min. metall., 81, B34-46.

_____ and Govett, G.J.S., 1973. Geology, geochemistry and genesis of Cyprus sulphide deposits, Econ. Geol., 68: 843-858.

_____ 1976. Genesis of conglomerate structure, porosity and collomorphic textures of the massive sulphide ores of Cyprus. In: Plate tectonics and metallogeny, D.F. Strong (ed.). Geol. Assoc. Cas. Spec. publ., 14.

_____ 1980. Metallogenesis associated with Troodos Ophiolite. In: A. Panayiotou (ed.) "Ophiolites", Proc.Int. Ophiolite Symp., Cyprus, pp 663-674.

Corliss, J.B. 1971. The Origin of metal-bearing submarine hydrothermal solutions, J. Geophys. Res., 76, 8128-8138.

_____, Graf, J.L., Skinner, B.J. and Hutchinson, R.W. 1972. Rare earth data for iron and manganese sediments associated with the sulphide ore bodies of the Troodos Massif, Cyprus, Prog. Abstr. geol. soc. Am., 4 (7).

_____, Lyle, M., Dymond, J. and Crane, K., 1978. The chemistry of hydrothermal mounds near the Galapagos Rift, Earth Planet. Sci. Lett., 40, 12-24.

Couture, R.A. 1977. Composition and origin of palygorskite-rich and montmorillonite-rich zeolite-containing sediments from the Pacific Ocean, Chem. Geol., 19, 113-130.

Cowan, D.S. 1979. Origin of "vein structure" in slope sediments on the inner slope of the middle America Trench off Guatemala. Initial Results Deep Sea Drilling Project, 67, 645-649.

Cronan, D.S. 1972. The Mid-Atlantic Ridge near 45°N XVII: Al, As, Hg and Mn in Ferruginous sediments from the Median valley, Can. J. Earth Sci., 9, 319-323.

_____ 1976. Basal metalliferous sediments from the Eastern Pacific. Bull. Geol. Soc. Am., 87, 928-934.

_____ 1980. Underwater Minerals, Academic press. p 194-213.

Cullis, C.G. and Edge, A.B. 1922. Report on the cupriferous deposits of Cyprus, Crown agents for Overseas Governments and Administration, London.

Davies, J.C. 1973. Statistics and data analysis in Geology, Wiley, pp 473-536.

Desprairies, A. and Lapierre, H. 1973. Les Argiles liées au Volcanisme du massif du Troodos (Chypre) et leur Remanienment dans sa couverture, Revue de Géographie Physique et de géologie Dynamique, 15, 499-510.

Delaloye, M., de Souza, H., Wagner, J.-J. and Hedley, I. 1980. Isotopic ages on ophiolites from the estern Mediterranean. In: A. Panayiotou, (ed.). "Ophiolites", Proc. Int. Ophiolite Symp. Cyprus, 292-295.

Dymond, J., Corliss, J.B., Heath, G.R., Field, C.W., Dasch, E.J. and Veeh, H.H. 1973. Origin of metalliferous sediments from the Pacific Ocean, Bull. Geol. Soc. Am., 84, 3355-3372.

Edmond, J.M., Measurer, C., Mangum, B., Grant, B., Sclater, F.R., Collier, R. and Hudson, A. 1979. On the formation of metal-rich sediments at ridge crests, Earth Planet. Sci. Lett., 46, 19-30.

_____, Von Damm, K.L., McDuff, R.E. and Measures, C.I., 1982. Chemistry of hot springs on the East Pacific Rise and there effluent dispersal, Nature, 297, 187-191.

Eklund, W.A. 1974. A microprobe study of metalliferous sediment components, Unpublished MSc Thesis, Oregon State University, 77pp.

El Wakeel, S.K. and Riley, J.P. 1961. Chemical and mineralogical studies of deep-sea sediments, Geochim. Cosmochim. Acta., 25, 110-146.

Elderfield, H., Gass, I.G. and Hamond, A. 1972. The origin of ferromanganese sediments associated with the Troodos Massif of Cyprus, Sedimentology, 19, 1-19.

Fitton, J.G., James, D.E. and Thirlwall, M.F. 1984. "A users' guide to X-ray fluorescence analysis of rock samples, 2nd ed,*

Fleet, A.J. and Robertson, A.H.F., 1980. Ocean ridge metalliferous and pelagic sediments of the Semail Nappe, Oman, J. Geol. Soc. Lond., 137, 403-422.

Francheteau, J., Needham, H.D., Choukroune, P., Juteau, T., Seguret, M., Ballard, R.D., Fox, P.J., Normark, W., Carranza, A., Cordoba, D., Guerrero, J., Rangin, C., Bougault, H., Cambon, P. and Hekinian, R., 1979, Massive deep-sea sulphide ore deposits discovered on the East Pacific Rise, Nature, 277, 523-528.

Gale, N.H., Spooner, E.T.C., and Potts, P.J. 1981. The Pb and Sr isotope geochemistry of metalliferous sediments associated with Upper Cretaceous ophiolitic rocks in Cyprus, Syria, and the Sultanate of Oman, Can. Jour. Earth Sci., 18, 1290-1302.

Garrison, R.E. 1972. Inter and intrapillow limestones of the Olympic Peninsula, Washington. Jour. of Geol., 80, 310-322.

Gass, I.G., 1960. The geology and mineral resources of the Dhali area, Cyprus Geol. Survey Dept. Mem., 4, 116pp.

_____ and Masson-Smith, D. 1963. The geology and gravity anomalies of the Troodos massif, Cyprus, Phil. Trans. R. Soc. Lond., A255, 417-467.

_____, 1968. Is the Troodos Massif of Cyprus a fragment of Mesozoic ocean floor, Nature, 220, 39-42.

_____ and Smewing, J.D. 1973. Intrusion, extrusion and metamorphism at constructive margins: Evidence from the Troodos Massif, Cyprus, Nature, 242, 26-29.

_____, Neary, C.R., Plant, J., Robertson, A.H.F., Simonian, K.O., Smewing, J.D., Spooner, E.T.C. and Wilson, R.A.M. 1975. Comments on 'The Troodos ophiolitic complex was probably formed in an island arc' by A. Miyashiro, Earth Planet. Sci. Lett., 25, 236-238.

_____ 1980. The Troodos Massif: its role in the unravelling of the ophiolite problem and its significance in the understanding of constructive plate margin processes, in, A. Panayiotou (ed.) "Ophiolites", Proc. Int. Ophiolite Symp., Cyprus, pp 23-35.

Goldberg, E.D. and Arrhenius, G.O.S. 1968. Chemistry of Pacific Pelagic clays, Geochim. Cosmochim. Acta., 13, 153-212.

* Unpublished report, Grant Inst. Geol., Univ. Edinburgh

Green, D.H. 1971. Composition of basaltic magmas as indicators of conditions of origin : applications to oceanic volcanism, Phil. Trans. R. Soc., Lond. A268, 707-722.

Guillemot, D. and Nesteroff, W.D. 1980. Les dépôts métallifères Crétacés de Chypre: Comparison avec leurs homologues actuels du Pacifique, In: A. Panayiotou, (ed.). "Ophiolites", Proc. Int. Ophiolite Symp. Cyprus, 139-146.

Hamelin, B., Dupré, B. and Allègre, C.J. 1984. The lead isotope systematics of ophiolite complexes, Earth Planet. Sci. Lett., 67, 351-366.

Hathaway, J.C., McFarlin, P.F. and Ross, D.A. 1970. Mineralogy and origin of sediments from drill holes on the continental margin off Florida. United States Geological Survey, Prof. Paper, 581-E, E1-E26.

Hay, R.L. 1977. Geology of zeolites in sedimentary rocks. In: F.A. Mumpton (ed.). "Mineralogy and geology of natural zeolites", Min. Soc. Am, Reviews in Mineralogy, Vol. 4, p.53-63.

Haymon, R.M., and Kastner, M. 1981. Hot spring deposits on the East Pacific Rise at 21°N preliminary description of mineralogy and genesis, Earth Planet. Sci. Lett., 53, 363-381.

Heath, G.R. and Dymond, J. 1977. Genesis and transformation of metalliferous sediments from the East Pacific Rise, Bauer Deep, and Central basin, northwest Nazca Plate, Bull. Geol. Soc. Am., 88, 723-733.

Heaton, T.H.E. 1977. A hydrogen and oxygen isotope study of the metamorphism and mineralisation of the Troodos complex, Cyprus, Unpublished PhD. Thesis, University of Edinburgh, pp.35 and pp.77.

_____ and Sheppard, S.M.F., 1977. Hydrogen and oxygen isotope evidence of sea-water-hydrothermal alteration and ore deposition, Troodos complex, Cyprus, Geol. Soc. London Spec. Publ., 7, 42-57.

Hekinian, R., Feurier, M., Bischoff, J.L., Picot, P. and Shanks, W.C. 1980. Sulfide deposits from the East Pacific Rise near 21°N, Science, 207, 1433-1444.

Henson, F.R.S., Browne, R.V. and McGinty, J. 1949. A synopsis of the stratigraphy and geological history of Cyprus, Q. J. geol. Soc. Lond., 105, 1-41.

Hoffert, M., Perseil, A., Hekinian, R., Choukroune, P., Needham, H.D., Francheteau, J. and Le Pichon, X., 1978. Hydrothermal deposits sampled by diving saucer in Transform Fault "A" near 37°N on the Mid-Atlantic Ridge, FAMOUS area, Oceanol. Acta., 1, 73-86.

Hutchinson, R.W. 1965. Genesis of Canadian massive sulphides reconsidered by comparison to Cyprus deposits, Can. Min. Metall. Bull., 58, 972-986.

Irwin, W.P., Murchey, D.L., Jones, D.L. and Kling, S.A. 1980. Mid-Cretaceous radiolarians in Perapedhi Formation, Cyprus, Ophioliti, 5, 265.

Jarrel, O.W. 1947. Geology of pyrite deposits from Petra tou Limniti to Lefkara, Cyprus, Unpubl. Rep. Cyprus Mines Co-orporation.

Kastner, M. 1981. Authigenic silicates in deep-sea sediments: Formation and diagenesis. In: "The Sea", Vol. 7, 915-980.

_____ and Stonecipher, S.A. 1978. Zeolites in pelagic sediments of the Atlantic, Pacific and Indian Oceans. In: L.B. Sand and F.A. Mumpton, (eds.). "Natural zeolites, occurrence, properties, use". Pergamon Press, p.199-220.

Kidd, R.D.W. and Cann, J.R., 1974. Chilling statistics indicate an ocean floor spreading origin for the Troodos complex, Cyprus, Earth Planet. Sci. Lett., 24, 151-155.

_____ 1977. A model for the process of formation of the upper oceanic crust, Geophysics J. R. Astr. Soc., 50, 149-183.

Knauth, L.P. and Epstein, S. 1975. Hydrogen and oxygen isotope ratios in silica from the JOIDES Deep Sea Drilling Project, Earth Planet. Sci. Lett., 25, 1-10.

Landergren, S. 1964. Rep. Swed. Deep Sea Exped. 10.

Lapierre, H. 1968. Découverte d'une serie volcano-sédimentaire probablement d'age Crétacé supérieure au S.W. de l'Île de Chypre, C.r hebd. seanc. Acad. Sci., Paris, D.266, 1817-1820.

_____ 1972. Les Formations sédimentaires et éruptive des nappes de Mamonia et leurs rélations avec le massif de Troodos (Chypre), Doctoral Thesis, University of Nancy, 420pp.

Lister, C.R.B. 1972. On the thermal balance of a Mid-Ocean ridge, Geophys. J. R. Astr. Soc., 26, 515-535.

Lonsdale, P., 1977a. Deep-tow observations at the mounds abyssal hydrothermal field, Galapagos Rift, Earth Planet. Sci. Lett., 36, 92-110.

_____ 1977b. Structural geomorphology of a fast-spreading rise crest: the East Pacific Rise near 3°25'S, Mar. Geophys. Res., 3, 251-293.

_____ 1978. Submersible exploration of Guaymas Basin: S.I.O. Report 78-1 Scripps Instn. Of Oceanography, University of California.

Lunberg, N. and Moore, J.C. 1979. Structural features of the middle America Trench slope off southern Mexico, DSDP leg 66, Initial Reports of the Deep Sea Drilling Project, Vol.66, 793-805.

McClellan, G.H. 1980. Mineralogy of carbonate fluorapatites, J. Geol. Soc. Lond., 137, 675-681.

_____ and Lehr, J.R. 1969. Crystal chemical investigation of natural apatites, Amer. Min. 54, 1379-91.

Macdonald, K.C. and Luyendyk, B.P., 1977. Deep-tow studies of the structure of the Mid-Atlantic Ridge crest near lat. 37°N, Bull. Geol. Soc. Am., 88, 621-636.

MacKensie, R.C. 1957. The oxides of iron, aluminium and manganese. In: R.C. MacKensie (ed.). "The differential thermal investigation of clays". Min. Soc. Lond., pp.299.

Malahoff, A., Cronan, D.S., Skirrow, R. and Embley, R.W. 1983. The geological setting and chemistry of hydrothermal sulphides and associated deposits from the Galapagos Rift at 86°W, Marine Mining, 4, 122-137.

Manheim, F.T. and Gulbrandsen, R.A. 1979. Marine phosphorites. In: R.G. Burns (ed.). "Marine Minerals", Min. Soc. Am. Reviews in Mineralogy, Vol. 6, 151-173.

Mantis, M. 1970. Upper Cretaceous-Tertiary foraminiferal zones in Cyprus, Cyprus Res. Centre, 111, 227-241.

Mikheev, V.I. 1957. "X-ray Determination of Minerals" 414. Cited in the Powder Diffraction File No. 15-604.

Miyashiro, A. 1973. The Troodos ophiolitic complex was probably formed in an island arc, Earth Planet. Sci. Lett., 19, 218-224.

_____, Shido, F. and Ewing, M. 1971. Metamorphism in the Mid-Atlantic Ridge near 24° and 30°N, Phil. Trans. R. Soc. Lond., A268, 589-603.

Moores, E.M. and Vine, F.J., 1971. The Troodos massif, Cyprus and other ophiolites as oceanic crust: evaluation and implicaitons, Phil. Trans. R. Soc., A268, 433-466.

Moussoulos, L. 1957. Contribution a l'étude de Gisements de Pyrite Cuivreuse de l'Île de Chypre. Recherches Géologiques et Minieres dans la Region de Kalavasos, Ann. Géol. des Pays Hell., ser 1, T. VIII, Athens, 269-320 (in Greek with French summary).

Muehlenbachs, K. and Clayton R.N. 1972. Oxygen isotope composition of the oceanic crust and its bearing on seawater, J. Geophys. Res.,81, 4365-4369.

Normark, W.R., Morton, J.L., Koski, R.A. and Claque, D.A. 1983. Active hydrothermal vents and sulphide deposits on the southern Juan de Fuca ridge, Geology, 11, 158-163.

Norrish, K. and Hutton J.T. 1969. An accurate X-ray spectrographic method for the analysis of a wide range of geological samples, Geochim. Cosmochim. Acta., 33, 431-453.

Oudin, E. and Constantinou, G. 1984. Black smoker chimney fragments in Cyprus sulphide deposits, Nature, 308, 349-352.

Pantazis, Th.M. 1973. Contribution to discussion, Trans. Inst. Min. Metall., 82, B128-129.

Pearce, J.A., 1975 Basalt geochemistry used to investigate past tectonic environments on Cyprus, Tectonophysics, 25, 41-67.

_____ 1980. Geochemical evidence for the genesis and eruptive setting of lavas from Tethyan ophiolites. In: A. Panayiotou (ed.) "Ophiolites", Proc. Int. Ophiolite Symp., Cyprus, 261-272.

_____ and Cann, J.R. 1973. Tectonic settings of basic volcanic rocks determined using trace element analyses, Earth Planet. Sci. Lett., 19, 290-300.

Price, N.B. and Calvert, S.E. 1978. The geochemistry of phosphorites from the Namibian Shelf, Chem. Geol., 23, 151-170.

Pritchard, G.R., Cann, J.R. and Wood, D.A. 1979. Low-temperature alteration of oceanic basalts. DSDP Leg 49, Initial Report of the Deep See Drilling Project, 49, 709-714.

Robertson, A.H.F. and Hudson, J.D. 1973. Cyprus umbers: Chemical precipitates on a Tethyan ocean ridge, Earth Planet. Sci. Lett., 18, 93-101.

_____ and Hudson, J.D., 1974. Pelagic sediments in the Cretaceous and Tertiary history of the Troodos Massif, Cyprus, Spec. Publ. Int. Assoc. Sedimentol., 1, 403-436.

_____ 1975. Cyprus umbers: basalt-sediment relationships on a Mesozoic ocean ridge, J. Geol. Soc. Lond., 131, 511-531.

_____ 1976a. Origin of ochres and umbers: evidence from Skouriotissa, Troodos Massif, Cyprus, Trans. Inst. Min. Metall., 85, B245-251.

_____ 1976b. Pelagic chalks and calciturbidites from the lower Tertiary of the Troodos Massif, Jour. Sed. Pet., 46, 1007-1016.

_____ and Fleet, A.J., 1976. The origins of rare earths in metalliferous sediments of the Troodos Massif, Cyprus, Earth Planet. Sci. Lett., 28, 385-394.

_____ 1977a. The origin and diagenesis of cherts from Cyprus, Sedimentology, 24, 11-30.

_____ 1977b. Tertiary uplift history of the Troodos Massif, Cyprus, Bull. Geol. Soc. Am., 88, 1763-1772.

_____ 1977c. The Kannaviou Formation, Cyprus: volcaniclastic sedimentation of a probable Late Cretaceous volcanic arc, J. Geol. Soc. Lond., 134, 269-292.

_____ 1978 Metallogenesis along a fossil oceanic fracture zone: Arakapas fault belt, Troodos Massif, Cyprus, Earth Planet. Sci. Lett., 41, 317-329.

_____ and Woodcock, N.H., 1979. The Mamonia Complex, southwest Cyprus: the evolution and emplacement of a Mesozoic continental margin, Geol. Soc. Am. Bull., 90, 651-665.

_____ and Woodcock, N.H., 1980. Tectonic setting of the Troodos Massif in the east Mediterranean, In: A. Panayiotou (Ed.) "Ophiolites", Proc. Int. Ophiolite Symp., Cyprus, 36-49.

_____ and Dixon, J.E. 1984. Aspects of the geological evolution of the Eastern Mediterranean, Introduction to Spec. Publ. Geol. Soc. Lond. No 14. J.E. Dixon and A.H.F. Robertson (eds.). "The geological evolution of the Eastern Mediterranean", in press.

Robinson, P.T. and Gibson, I.L., 1973, Cyprus Crustal Study Project Hole CY-1, Lithological unit summaries, unpublished report, University of Waterloo, Waterloo, Ontario, Canada.

Robinson, P.T., Flower, M.F.J., Schmincke, H.-U. and Ohnmacht, W. 1977. Low temperature alteration of oceanic basalts, DSDP leg 37. In: F. Aumento, and E.G. Melson, et al., Initial Report of the Deep Sea Drilling Project, Vol. 37, 775-794.

_____, Melson, W.G., O'Hearn, T. and Schmincke, H.-U. 1983. Volcanic glass compositions of the Troodos Ophiolite, Cyprus, Geology, 11, 400-404.

Rona, R.A., Harbison, R.N., Bassinger, B.G., Scott, R.B. and Nalwalk, A.J., 1976. Tectonic fabric and hydrothermal activity of Mid-Atlantic Ridge, Lat. 26°N, Bull. Geol. Soc. Am., 87, 661-674.

Rose, H.J., Alder, J., Flanagan, F.J. 1963. X.R.F.A. of light elements in rocks and minerals, Applied Spectroscopy, 17, 81.

Sayles, F.L. and Bischoff, J.L. 1973. Ferromanganoan sediments in the Equatorial East Pacific, Earth. Planet. Sci. Lett., 19, 330-336.

Scarfe, C.M. and Smith, D.G.W. 1977. Secondary minerals in some basaltic rocks from DSDP Leg 37, Can. J. Earth. Sci., 14, 903-910.

Schmincke, H.-U. and Rautenschlein, M. 1982. Volcanology along the Kamara Potamos, unpublished report.

_____ and Rautenschlein, M., Robinson, P.T. and Mehegan, J.M. 1983. Troodos extrusive series of Cyprus: A comparison with oceanic crust, Geology, 11, 405-409.

Sclater, J.G., Anderson, R.N. and Bell, M.L. 1971. Elevation of ridges and evolution of the central Eastern Pacific, J. Geophys. Res., 76, 7888-7915.

Scott, M.R., Scott, R.B., Rona, P.A., Butler, L.W., and Nalwalk, A.J. 1974. Rapidly accumulating manganese deposit from the median valley of the Mid-Atlantic Ridge, Geophys. Res. letters, 1, 355-358.

Searle, D.L. 1973. Contribution to discussion, Trans. Inst. Min. metall., 82, B129-130.

Shulze, D.G. 1984. The influence of aluminium on iron oxides. VIII. Unit-cell dimensions of Al-substituted goethites and estimation of Al from them, Clays and Clay Minerals, 32, 36-44.

Simonian, K.O. and Gass, I.G., 1978. Arakapas fault belt Cyprus: A fossil transform fault, Bull. Geol. Soc. Am., 89, 1220-1230.

Skirrow, R. and Coleman, M.L., 1982. Origin of sulphur and geothermometry of hydrothermal sulphides from the Galapagos rift, 86°W, Nature, 229, 142-144.

Smewing, J.D., Simonian, K.O. and Gass, I.G., 1975. Metabasalts from the Troodos Massif, Cyprus: genetic implications deduced from petrology and trace element composition, Contrib. Min. Pet., 51, 49-64.

Soler, E., Bernard, A.J. and Nesteroff, W.D. 1982. Sulphidic hydrothermal activity on marine ridges: a comparison between Modern (East Pacific Rise, 21°N) and ancient (Cyprus) deposits, Oceanol. Acta., 5, 105-120.

Spiess, F.N., Macdonald, K.C., Atwater, T., Ballard, R., Carranza, A., Cordoba, D., Cox, C., Diaz Garcia, V.M., Francheteau, J., Guerrero, J., Hawkins, J., Hayman, R., Hessler, R., Juteau, T., Kastner, M., Larson, R., Luyendyk, B., Macdougall, J.D., Miller, S., Normark, W., Orcutt, J., and Rangin, C. 1980. East Pacific Rise : hot springs and geophysical experiments, Science, 207, 1421-1433.

Spooner, E.T.C., Beckensdale, R.D., Fyfe, W.S. and Smewing, J.D. 1973. ^{18}O enriched ophiolitic metabasaltic rocks from E. Ligur ia (Italy), Pindos (Greece) and Troodos (Cyprus), Contrib. Min. Pet., 47, 41-62.

_____ and Bray, C.J. 1975. Hydrothermal fluids of sea water salinity in ophiolite sulphide ore deposits in Cyprus, Nature, 266, 808-812.

_____, 1977. Hydrothermal model for the origin of the ophiolitic cupriferous pyrite ore deposits of Cyprus, Geol. Soc. London Spec. Publ., 7, 58-71.

_____, 1980. Cu-pyrite mineralisation and seawater convection in oceanic crust - the ophiolitic ore deposits of Cyprus. In: D.W. Strangeway (ed.), Geol. Assoc. Canada. Spec. Paper, 20, 685-704.

_____ and Gale N.H. 1982. Pb isotopic composition of ophiolitic volcanogenic sulphide deposits, Troodos Complex, Cyprus. Nature, 296, 239-242.

Strens, M.R. and Cann, J.R., 1982. A model of hydrothermal circulation in fault zones at mid-ocean ridge crests, Geophys. J. R. astr. Soc., 71, 225-240.

Swarbrick, R.E. and Naylor, M.A. 1980. The Kathikas melange, S.W. Cyprus: Late Cretaceous submarine debris flows, Sedimentology, 27, 63-78.

Sweatman, T.R. and Long, J.V.P. 1969. Quantitative electron-probe microanalysis of rock-forming minerals, J. Petrol., 10, 332-379.

Thirlwall, M.F. 1979. The Petrochemistry of the British Old Red Sandstone Volcanic Province, Unpublished Ph.D. Thesis, University of Edinburgh.

Toth, J.R. 1980. Deposition of submarine crusts rich in manganese and iron, Bull. Geol. Soc. Am., 91, 44-54.

Turekian, K.K. and Wedepohl, K.H. 1961. Distribution of the elements in some major units of the Earth's crust, Bull. Geol. Soc. Am., 72, 175-192.

_____ and Imbrie, J. 1966. The distribution of trace elements in deep-sea sediments of the Atlantic Ocean, Earth Planet. Sci. Lett., 1, 161-168.

_____ 1983. Geochemical mass balances and cycles of the elements. In: "Hydrothermal processes at seafloor spreading centres". P.A. Rona, K. Boström and L. Laubier (eds.), Nato Conference Series IV.

Varnavas, S.P. 1980. Partition geochemical investigation of ferromanganese deposits from the Troodos Massif, Cyprus. In: "UNESCO" Int. Symp. on Metall. of Mafic and Ultramafic complexes. (IGCP Project No. 169), Vol. 2 p.391-410.

Vine, F.J., Poster, C.K. and Gass, I.G. 1973. Aeromagnetic survey of the Troodos igneous massif, Cyprus, Nature, Phys. Sci., 244, 34-38.

von Rad, U. and Rösch, H. 1972. Mineralogy and origin of clay minerals, silica and authigenic silicates in Leg 14 sediments. In: D.E. Hayes et al., (eds.), Initial Deep Sea Drilling Project, 14, 727-739.

Wakefield, S.J. 1980. Geochemical studies on the leaching of metalliferous sediment from the East Pacific, J. Geol. Soc. Lond., 137, 379-380.

Weaver, C.E. and Beck, R.C. 1977. Miocene of the SE United States, a model for chemical sedimentation in a peri-marine environment, Developments in sedimentology 22, Elsevier, Amsterdam 234p.

Wedepohl, K.H. 1960. Spurenanalytische Untersuchungen an Tiefseetonen aus dem Atlantik, Geochim. Cosmochim. Acta., 18, 200-231.

Williams, D. 1973. Contribution to disscussion, Trans. Inst. Min metall., 82, 171-72.

Wilson, A.D. 1964. The titrimetric and spectrophotometric determination of the oxidising capacity of manganese compounds, Analyst, 89, 571-578.

Wilson, R.A.M. 1959. The geology of the Xeros-Troodos area, Cyprus, Geol. Surv. Dept. Mem., 1, 73pp.

Reproduced from

OPHIOLITES AND OCEANIC LITHOSPHERE

Edited by
I. G. Gass, S. J. Lippard & A. W. Shelton

Published for The Geological Society
by Blackwell Scientific Publications

Evolving metallogenesis at the Troodos spreading axis

J. F. Boyle & A. H. F. Robertson

SUMMARY: An area of the eastern Troodos Massif has been mapped in detail to identify stages of volcanism, faulting and metallogenesis which could be related to the evolution of the late Cretaceous Troodos spreading axis. The field relations and comparisons with modern spreading ridges suggest the following succession of events. Pillowed and massive flows making up most of the lava volume were erupted on a relatively flat sea floor at the axis of a well-defined median valley. Volcaniclastic sediments accumulated during a hiatus in volcanism. The Mathiati massive sulphide formed in the vicinity of ridge-parallel fractures towards the margins of the rift valley, whilst ferromanganiferous oxide-sediments were deposited in the surrounding area. Normal faulting, at first parallel to the rift axis, then at 30–40° to it, accompanied formation of the rift-valley walls, together with renewed eruption of lavas, equivalent to the Upper Pillow Lavas. Small grabens and half-grabens, which formed during this stage, were fringed with lava talus, then gradually filled, first with ferromanganiferous umbers precipitated from local hydrothermal vents, then, as the spreading axis migrated away, by more hydrogenous metal-oxide sediments and later deep-sea deposits. In Cyprus, metallogenesis persisted from the median valley to the flanks of particular regions of crust. Also the inferred site of formation of the Mathiati sulphide towards the margin of the rift valley differs from that of the known 'smokers' which are active closer to the spreading axis.

It is now firmly established that the various metalliferous sulphide- and oxide-deposits of the Troodos Massif were formed by hydrothermal processes at a late-Cretaceous oceanic spreading axis (Constantinou & Govett 1972, 1973; Robertson 1976; Spooner 1977; Heaton & Sheppard 1977). An important remaining question is how exactly the oxide- and sulphide-sediments can be related to the stages of construction of a spreading axis. The approach here has been to map the lava succession of a selected area in sufficient detail to identify the main phases of metalliferous accumulation, and to relate these to the structural and volcanic development of the ridge. This is timely in view of the recent upsurge of interest in the Troodos ophiolite, stimulated by the work of the International Deep Crustal Research Group (IDCRG).

Over the last few years, new deep-ocean exploration techniques have immeasurably increased knowledge of hydrothermal processes at spreading ocean ridges (e.g. Ballard & van Andel 1977; Lonsdale 1977a, b). The extremely close parallels which can now be drawn with ophiolites like the Troodos facilitate interpretation of the latter; conversely, detailed mapping of ophiolites can add a depth dimension not readily available in the oceans.

Geological setting of the Mathiati–Margi area

The Troodos Massif has long been recognized as an intact ophiolite succession created at some form of Upper-Cretaceous spreading axis (Gass 1968; Moores & Vine 1971), although the exact tectonic setting remains controversial (e.g. Pearce 1980; Robertson & Woodcock 1980). The sheeted dykes, which constitute the key evidence of a spreading genesis, are orientated overall N–S in the Troodos (Kidd & Cann 1974), but complications exist, particularly in the east where the present study is located.

The extrusive succession has been subdivided into the Lower Pillow Lavas and the Upper Pillow Lavas (Wilson 1959), the former being largely basaltic andesites and the latter mostly olivine basalts. The boundary between these two units is uncomformable in some areas, but transitional in others (Wilson 1959; Bear 1960; Gass 1960), leading to uncertainty over the location and significance of this subdivision. More recent attempts to divide the lavas have been based upon other criteria, e.g. metamorphic grade (Gass & Smewing 1973; Smewing *et al.* 1975) and petrochemistry (current work by the International Deep Crustal Research Group). In the absence of a generally accepted definition of the Upper and Lower Pillow Lava units, we have simply mapped the lavas as local units and assigned letters to them.

An area on the eastern margin of the Troodos Massif in the vicinity of the well-known Mathiati mine (Fig. 1) was chosen for mapping because both sulphide- and oxide-metalliferous sediments are abundant and because regionally low dips and fault repetitions allow the individual units to be traced substantial distances laterally. In this area the dyke trend is consistently NW–SE deviating from the regional N–S direction. The sedimentary cover dips at 10–20° to the NE defining the mean dip of the lavas, but locally within the lavas dips range up to 30–40°, where rotation on normal faults has taken place. The distinctive ferromanganiferous oxide-sediments, the umbers, occur in small hollows along the contact between the

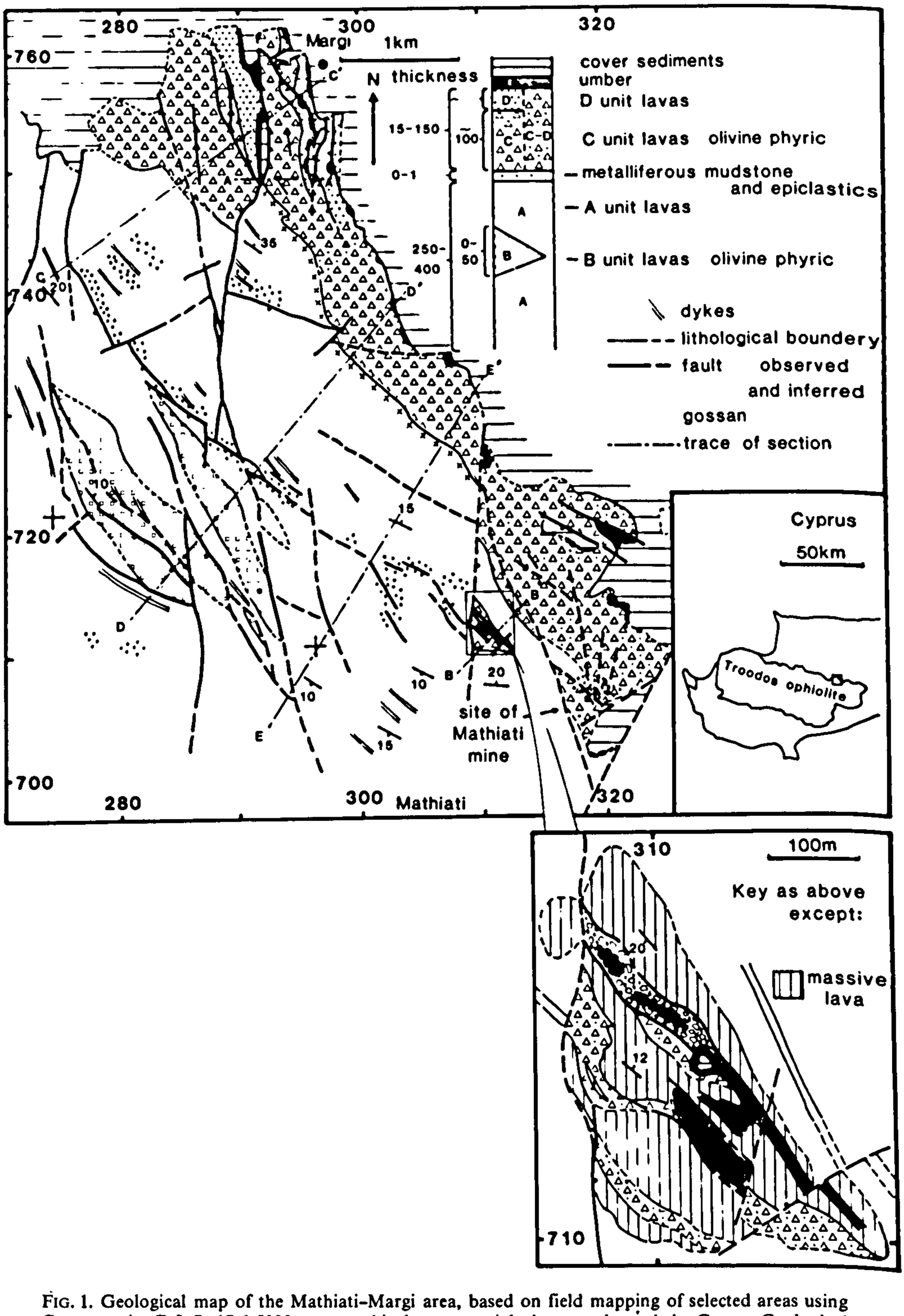

FIG. 1. Geological map of the Mathiati–Margi area, based on field mapping of selected areas using Cyprus series D.L.S. 17 1:5000 topographical maps, aerial photographs and the Cyprus Geological Survey Department 1:31,680 map (Gass, 1960). Inset: detail of an area 0.8 km NW of Mathiati mine.

stratigraphically highest lavas and the overlying sedimentary cover. Mostly ferruginous metal-oxide sediments are disseminated throughout the lava pile, largely in pillow interstices. The Mathiati massive sulphide orebody (Constantinou & Govett 1973) is located within the lava pile towards the southern end of the area mapped (Fig. 1).

The Mathiati–Margi area contains a higher proportion of both sulphide- and oxide-sediments (at all levels of the lava succession) than adjacent areas except the SE where there is the Sha mining area (1 km SE of Map, Fig. 1).

Lithostratigraphy

In the Mathiati–Margi area, Gass (1960) recognized a Lower Pillow Lava unit composed of pyroxene andesites, with subordinate basaltic, dacitic and keratophyric lavas, separated by a thin layer of metalliferous mudstones and volcaniclastic sediments from an Upper Pillow Lava unit composed of basalts, olivine basalts, limburgites and picrites. Both extrusives and high-level intrusives were identified. As our mapping was intended mainly to shed light on the metallogenesis in the area, we found it convenient to subdivide the succession along the laterally continuous interlava sediment horizon and then according to the presence or absence of olivine phenocrysts. A unit of olivine basalts was identified in the lower part of the succession in a region previously mapped as Lower Pillow Lavas (Gass 1960). Phenocrysts of pyroxene were found to be too variable in distribution to use in mapping. The stratigraphic distribution and relative abundance of each of the units mapped is shown in Fig. 1.

Lava morphology

The area mapped consists of *c.* 60–70% pillow lavas and 30–40% massive lavas. This is comparable with the proportions drilled in CY-I of the IDCRG (69.9% pillow lava, 28.4% massive lavas; Robinson & Gibson 1983). In both the area mapped and in CY-I, hyaloclastite is very subordinate, although in some exposures, e.g. the Akaki River section of North Troodos, hyaloclastite is relatively more abundant. In the Mathiati–Margi area dykes first appear in the lower part of the succession locally as swarms comprising >50% of the outcrop.

The original eruptive morphology of the extrusives in the area can be interpreted in the light of observations from modern spreading axes (Ballard *et al.* 1981, 1982; Ballard & Moore 1977). Steep-sided pillowed flows form topographic highs around eruptive centres which are located along fissures at the ridge axis. The early flows of each eruptive cycle tend to be sheet-like, travelling further than the pillowed flows (*c.* 1 km), pouring down slope and ponding in fault hollows. All except the most recent lavas are dissected by minor ridge-parallel fractures.

In the mapped area in Cyprus, differential erosion has tended to reverse the original sea-floor topography; the more resistant high-level intrusions and the massive flows form the high ground while the pillow lavas and the fragmented extrusives now form depressions (relief 20–50 m). The original relationships can however still be observed, e.g. near Mathiati (Fig. 1, inset; Fig. 3, Section B-B′), where massive flows of the C-D lava units dip in opposite directions on either sides of a valley. Older A-unit pillow lavas on the floor of the intervening valley are cut by a 4 m thick dyke which could have fed a pillow volcano originally located between the oppositely dipping massive flow units.

In outcrop most of the lava pillows are relatively uniform in size and shape (~1 m across), but locally throughout the succession some of the lava pillows are conspicuously elongated as 'bolsters', or larger still as 'mega-pillows'. The 'mega-pillows', which range up to 10 m across, commonly possess pillow-lobed lateral and upper contacts and are thought to represent sites of lava transport and extrusion (Schmincke & Rautenschlein 1982). The 'mega-pillows' often occur in groups capping small hills of more normal pillow lavas. Although hard to measure, the apparently radiating dips of these lavas suggest that they originated as small pillow-lava volcanoes.

Two types of fragmental extrusive rocks are recognized, hyaloclastites and pillow breccias. Small elongate lenses of hyaloclastite up to 5 m thick are present, associated with both massive and pillowed extrusives, throughout the lava pile and are best exposed in stream sections. The hyaloclastites are typically green to brown, weakly bedded to massive, consisting of poorly sorted glassy fragments and small intact pillows ~10 cm in diameter. In the oceans hyaloclastite is seen to form particularly on steep flow fronts (Ballard & Moore 1977), and a similar origin is favoured in Cyprus.

The pillow breccias are concentrated in the upper parts of the D lava unit. The breccias range from totally disorganized pillow segments, to some cases where the outlines of original pillows can still be recognized (Robertson 1975). These breccias contain little true hyaloclastite material and are interpreted as the result of collapse of pillow lavas along small submarine fault scarps (see below).

Interlava sediments

Excluding the fragmental extrusives mentioned above, three types of interlava sediments are present: (i) dispersed metal-oxide sediments; (ii) a horizon of ferromanganiferous mudstones and epiclastics; and (iii) massive sulphide and ochres.

Orange iron-rich oxide-sediments are dispersed throughout the volcanic succession but are concentrated in lava unit D and the upper part of lava unit A (Fig. 2). The oxide-sediment fills spaces between individual lava pillows and is often seen as small veins penetrating cooling fractures in the lavas. These field relations result from disruption of accumulating sediments by overriding laval flows. Compositionally, the oxide-sediments are largely ferruginous with variable amounts of ferromanganiferous oxides, clays, carbonates and spalled volcanic glass. Faecal pellets, coccolith guards and poorly preserved radiolaria are also present. It is unclear as to what extent the sediments were originally ferromanganiferous but were leached to leave a ferruginous residue during the later stages of hydrothermal activity. The dispersed metal-oxide sediment has previously been interpreted regionally as a hydrothermal precipitate ponded in the pillow lavas during the later stages of lava eruption (Robertson 1976; Robertson & Fleet 1976). The present work now shows that in the Margi area the dispersed sediment is more widespread within the lava pile, defining broad horizons extending several kilometres around Margi and to the SE (Fig. 2). A possible source for this oxide-material would be oxidation of sulphide precipitates drifting away from more axial vents, and this would adequately explain their widespread dispersed character. This process has been observed at Pacific spreading axes (Edmond *et al.* 1982). The downward decrease in abundance of dispersed oxide-sediment within the lava pile could result either from reduced sedimentation rates, or more probably from more rapid eruption of the earlier pillow lavas.

At the contact between the A and C lava units there is a laterally continuous horizon of ferromanganiferous mudstones underlain by epiclastic sediments. The epiclastics are fine to medium grained, poorly bedded, generally massive and contain altered lava fragments in a muddy matrix which is commonly iron- and manganese-rich. Thickness varies from 0 to 1 m. The ferromanganiferous horizon above is 0–1 m thick, very fine grained, either massive or finely laminated and generally resembles the umbers above the highest lavas. This sediment is interpreted as a mixture of background pelagic and hydrothermal oxide-sediment which accumulated above the epiclastics, during a pause in lava eruption. The laterally continuous, unponded character of these sediments indicates that the sea floor was relatively flat and had not undergone significant tilting at this stage.

The formerly economic Mathiati sulphide orebody and stockwork mineralization in the S of the area mapped (Fig. 1) now exists as a tilted horst overlain by unmineralized lavas (Constantinou & Govett, 1972). Until recent quarrying the massive ore was seen to be overlain by ferruginous ochres. These formed by a combination of submarine oxidation of massive sulphide (submarine gossans) and as hydrothermally precipitated ferruginous metal-oxide sediment; ochre of erosive origin is minimal (Robertson 1976). Constantinou (1980) reports that the sulphide occurs at the contact between the Lower and Upper Pillow Lavas, which places it at the same stratigraphic level as the ferromanganiferous mudstone horizon described above. Later faulting has obscured the sea-floor topography in the vicinity of the mineralization, but a stratigraphic association with the sediment horizon would indicate that it formed prior to the major faulting. The inferred depositional geometry of the orebody suggests it was probably formed in a fault-controlled bathymetric depression (Constantinou 1980).

Supra-lava sediments

In the area mapped, the stratigraphically highest lavas are overlain by ferromanganiferous oxide-sediments (umbers), metal-enriched clays, radiolarites and mudstones of the Perapedhi Formation, dated as Campanian. In turn these are overlain by Maastrichtian pelagic chalks of the Lefkara Formation (Robertson & Hudson 1973, 1974). The umbers commonly occur in faulted depressions on the original lava surface where underlying lavas have locally undergone extensive low-temperature hydrous alteration indicating a local source for the hydrothermal fluids. Robertson (1976) interpreted the umbers as hydrothermal precipitates ponded in hollows during and after the waning stages of volcanism. The pelagic chalk cover accumulated later in gradually shallowing seas up to a Mid-Tertiary emergence.

Fault stages

A major objective of this work has been to determine the relationships of metalliferous sediment accumulation to faulting of the extrusive sequence and to use this as a basis for comparisons with modern spreading axes.

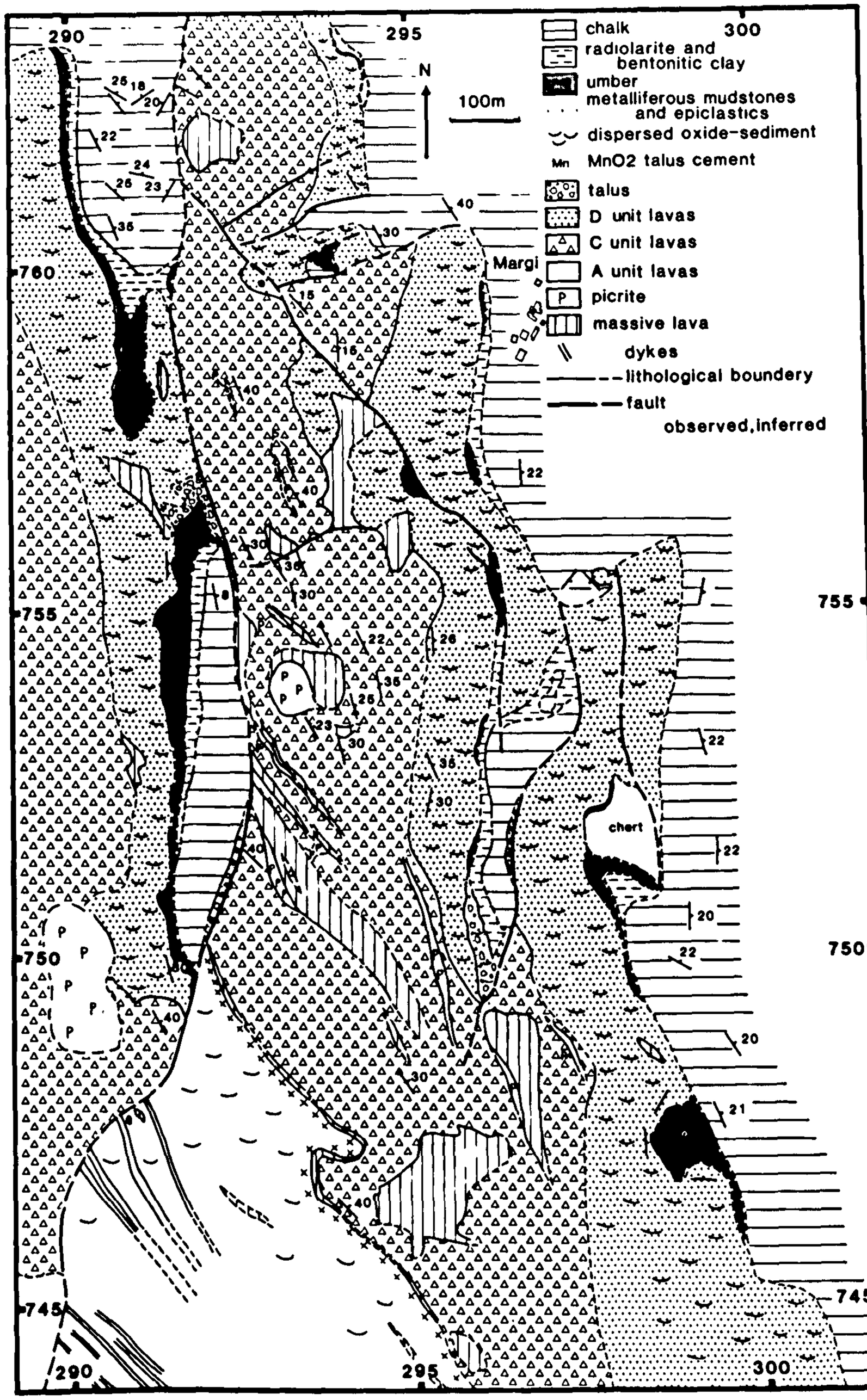

FIG. 2. Geological map of an area south of Margi village to show the relationships of the metalliferous sediments to the lava units and faults. See Fig. 1 for location (grid) and details of the volcanic succession. Base map: 1:5000 topographical series D.L.S. 17 sheets 39/V, 30/XXXIX.

In the mapped area, a major transverse fault and two generations of normal faults predate pelagic sediments above the umbers. The transverse fault is at the SE end of the area and trends NE–SW, perpendicular to the dykes (Fig. 1). An earlier generation of normal faults trends parallel to the dykes (NW–SE) and a later one trends both N–S and NW–SE (Fig. 1). The earliest sediments, the umbers, are found ponded in grabens and half-grabens created by this faulting. The umbers, after allowing for differential compaction, have the same dip as the overlying chalks, showing that faulting and tilting was mostly before umber accumulation.

The transverse fault

The most prominent fault in the area runs close to the southern edge of the Mathiati opencast at a high angle to both generations of normal faults and is also perpendicular to the orientation of dykes in the area mapped. None of the normal faults can be traced across this fault. To the S outside the area mapped, the dykes swing round to parallel this NE–SW-trending fault suggesting that it may have been active early. Since this fault is at right angles to the local dyke trends, we suggest it may have operated as a minor transform fault.

The normal faults

The normal faults are of two generations here termed *type 1* and *type 2*. The type 1 faults displace only the A and B lava units. The type-2 faults displace the type-1 faults and were coeval with eruption of the C and D lava units.

Type 1: earlier normal faults

The earlier normal faults, which cut the A and B lava units, are parallel to the NW–SE dyke trend (Fig. 1). The maximum observed vertical-fault offset is *c.* 160 m, determined by displacement of the B lava unit (Fig. 3, Section D-D'), but offsets could possibly have been as great as 400 m. These earlier faults are parallel to those which bound the Mathiati sulphide body and have often been extensively gossanized. Shearing, which has taken place along these fault planes, is compatible with post-mineralization movement. The field relations discussed above show that the laterally continuous horizon of ferromanganiferous and epiclastic sediment above the A lava unit accumulated on an almost flat sea floor, thus the type-1 faulting cannot have involved significant differential vertical motion prior to this stage. Although the type-1 faults may have existed as fractures from a very early stage, major movement on them is constrained to an interval following the deposition of the sediment blanket, and prior to eruption of the C and D unit lavas.

Type 2: later normal faulting

The C lavas and the type-1 faults are displaced by later faults, mostly trending N–S, but some, particularly in the S of the area, follow the pre-existing NW–SE trend. Several lines of evidence suggest that the N–S faulting took place over a short time interval during eruption of the C and D lava units. Firstly, there is a marked upward decrease in dip and change in direction of strike through the C and D lava units (Fig. 2). Secondly, thin sheet and pillowed flows of the lower part of the *c.* 150 m thick succession give way upward to disrupted pillow lavas intercalated with lava breccia and hyaloclastite, indicating a steeper palaeoslope. Thirdly, upfaulted C unit lavas are locally overlain by the D unit with an unfaulted extrusive contact (Fig. 3). The D lavas did not entirely fill the half-grabens, leaving fault hollows which subsequently became sites of umber accumulation.

There are also the type-2 faults which cut the C–D lava units but are parallel to the NW–SE trend of the earlier type-1 faults. These are best exposed in an outlier of C–D unit lavas, umbers and cover sediments located in the S of the area mapped, 1 km N of Mathiati (Fig. 1, inset; Fig. 3). These faults form small grabens in the C–D unit lavas which also later became sites of umber accumulation. No cross-cutting relations with the N–S trending type-2 faults have been observed.

It is important to note that, although there is a clear relative age difference between the type-1 and the type-2 normal faults, this need not imply a large time separation. The volcaniclastic and metal-oxide blanket beneath the C unit lavas could well record a significant time interval, followed by the normal faulting and extrusion of the C and D lava units.

Stages of spreading-axis construction

The field relations of the Mathiati–Margi area can now be considered in the context of new crust forming and moving away from a spreading axis. The following stages are recognized:

(i) Most of the lava volume was rapidly extruded as pillowed and massive flows very close to the spreading axis. The rapidity of this earlier eruption restricted interlava sediment to minor dispersed oxide-sediment. During a subsequent hiatus, volcaniclastic material was eroded, presumably by sea-floor currents, and accumulated on a more or less flat sea floor.

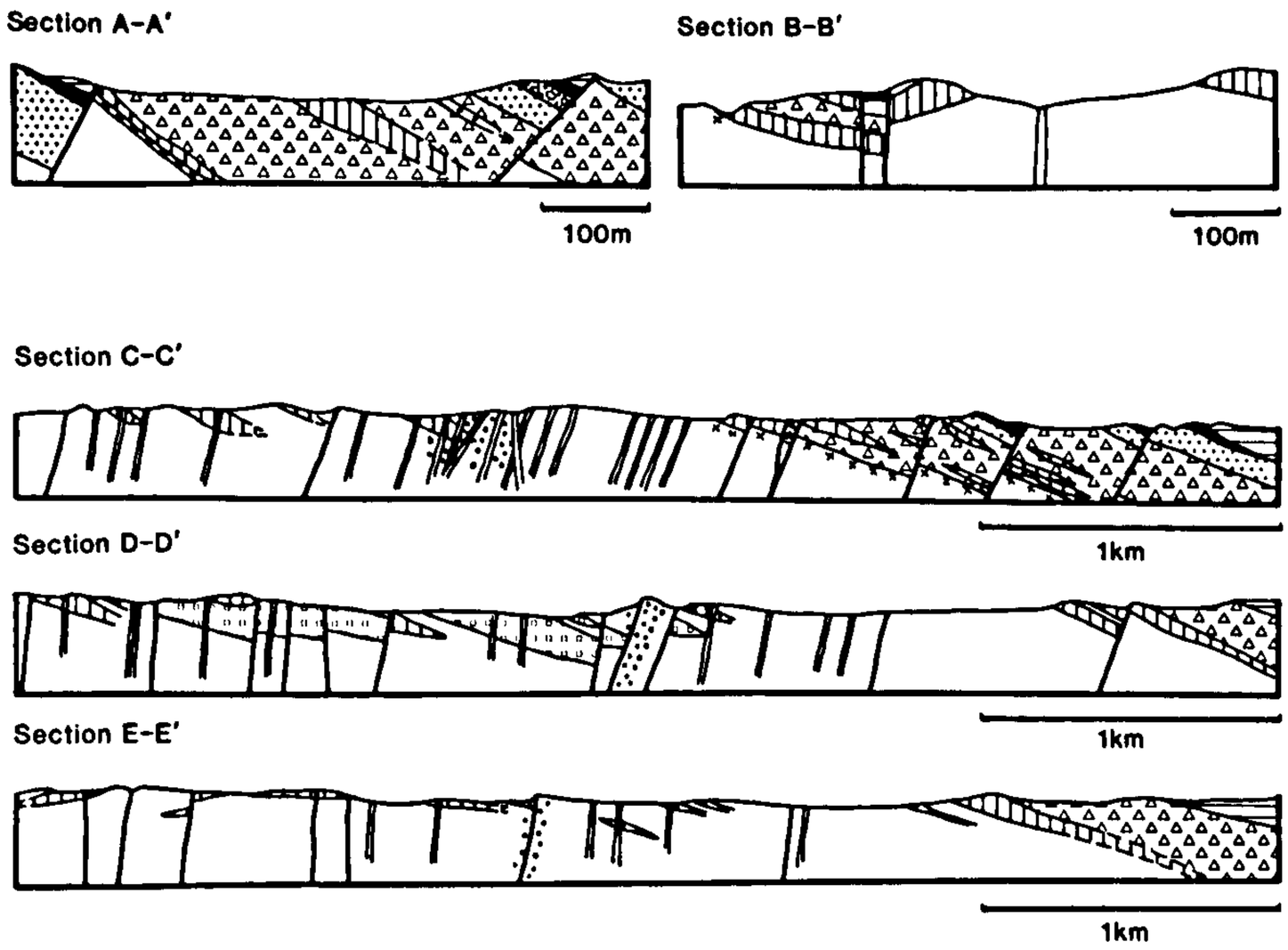

FIG. 3. Geological cross-section to show the relationships of faults to the lava succession. See Fig. 1 for lines of section and the key to symbols. Vertical scale = horizontal scale.

(ii) The sulphide sediments and a halo of metal-oxide sediments were then deposited in an area close to the minor transform fault. Numerous fractures parallel to the spreading axis were mineralized, and the sulphide probably formed in a related shallow graben.

(iii) Blocks of lava 0.5–3 km wide were rapidly rotated parallel to the spreading axis, with vertical throws in the order of 160 m. The sulphide orebody was also dissected and rotated at this stage.

(iv) Basaltic eruptions resumed partially smoothing the topography. At the same time N–S faults became active and blocks up to 0.5 km across were rotated up to 30°. Metal-oxide sediments accumulated during eruption and were dispersed throughout the upper part of the lava succession. Restricted to the south of the area mapped, the later faulting continued after the end of volcanism forming a series of grabens.

(v) The newly formed grabens, and the half-grabens of the north of the area which were not completely filled by the later lavas, were flanked by lava talus and then progressively filled by umber. The solutions from which the umbers were precipitated caused extensive hydrous alteration of the subjacent lavas. During the waning stages of hydrothermal discharge the umbers and the associated lavas were veined by palygorskite and poorly crystalline MnO_2.

(vi) Later, after the spreading axis had migrated away, metalliferous clays accumulated with a greater hydrogenous component (unpublished chemical data), then the remaining hollows were progressively filled with radiolarites, mudstones and pelagic carbonates, although the basement remained exposed in places for up to 20 Ma.

The question which then arises is how typical these stages are of the Troodos Massif as a whole. This excludes the Arakapas fault zone, which is interpreted as a fossil transform fault (Simonian & Gass 1978), with its own distinctive hydrothermal metalliferous oxide-sediments (Robertson 1978). The gross lava succession, the position of the sulphide orebodies and the style of faulting in the Mathiati–Margi area are very similar to many other parts of the Troodos Massif. There is often an abrupt upward change to more mafic compositions in the lavas (Gass 1980). The major sulphide orebodies are mostly, if not all, located beneath these more mafic lavas (Constantinou & Govett 1973). Also Adamides (1980) has demonstrated that the major sulphide mineralization of Kalavasos was controlled by early faulting, although this area is complicated by the close proximity to the Arakapas fault zone. The Mathiati–Margi area is peculiar in its richness of mineralization and metalliferous sediments

throughout the lava succession. Away from mining districts hydrothermal sediments are generally scarce and are completely absent from some areas, e.g. the Akaki river section on the northern margin of the Troodos Massif. The implication of the tendency of interlava metalliferous sediments, umbers and sulphides to form at different levels in the lava stratigraphy, but in the same general area, is that zones of elevated hydrothermal activity must have persisted on particular segments of the crust throughout and for some time after lava eruption.

One remaining puzzle is why some of the later (type-2) faults were orientated *c.* 40° clockwise from the trend of the earlier (type-1) faults which had paralleled the inferred spreading axis. This change took place during the later stages of the principal tectonic event, which corresponds to the construction of the rift-valley walls, and was coincident with eruption of the later more mafic lavas.

Metallogenesis at modern spreading axes

We now review the main morphological, structural and metallogenic features of the Atlantic and Pacific spreading axes, which are relevant to interpretation of the Troodos ophiolite.

Atlantic

The Mid-Atlantic Ridge in the TAG area (26°N) is topographically rugged with a median valley *c.* 20–30 km across and 1–2 km deep. Normal faults along the walls of the median valley are inferred to possess throws up to 1 km, locally exposing gabbros (Rona *et al.* 1976). The TAG hydrothermal field comprising manganese deposits, is situated on the inner wall of the rift, 10–12 km from the axis.

In the FAMOUS area (37°N) the axial graben is still 20–30 km across, but shallower (1 km relief). The topography of the inner rift-valley floor is subdued and is controlled by eruption with relatively little faulting. The walls of the median valley are dissected by normal faults spaced 0.5 to 8 km apart with inferred displacements up to 500 m (Ballard & van Andel 1977). Only in transform fault 'A' have hydrothermal deposits been found, these comprising nontronite and manganese oxides (Hoffert *et al.* 1978).

Pacific

At the Galapagos rift, which has an intermediate spreading rate (60 mm yr^{-1} total), there is a narrow median valley 3–8 km across with a total relief of 100–250 m (Lonsdale 1977a; Ballard *et al.* 1982). Normal faults spaced 1–6 km apart, with inferred throws of *c.* 100 m, are formed in a tectonically active zone at the margin of the median valley (*c.* 4 km from the axis). Inactive sulphide deposits are located as 85° 49–50'W along a fault associated with the southern boundary of the north rift valley (Skirrow & Coleman 1982) and at 86° 0–15'W located along both the northern and southern scarps of the rift valley. Active hydrothermal fields, none of high-temperature type, are located immediately on the axis. The hydrothermal mounds, composed of MnO_2 and nontronite, are situated on the sedimentary cover above basement fractures, 20–30 km south of the axis.

The Juan de Fuca ridge, which is also an intermediate-rate spreading axis (60 mm yr^{-1} total), is morphologically similar to the Galapagos rift, with a well-defined median valley *c.* 3 km across and *c.* 100 m deep (Normark *et al.* 1983). The inner walls are composed of low terraces bounded by steep normal faults (throws *c.* 30 m) and define an axial volcanic floor about 1 km across. Along the centre of the valley, which is largely flat and unfaulted, there is a nearly continuous depression 50–200 m across and about 25 m deep. Four of the known sulphides occur in this median depression, and one is located against the scarp at the foot of the eastern inner wall. Low-temperature active vents occur along the median depression.

The much faster-spreading East Pacific Rise at 3°25'S (150 mm yr^{-1} total) differs from the Galapagos by the absence of a well-defined axial graben. Most of the faulting takes place in a zone of extension 1–15 km from the ridge axis (Lonsdale 1977b). In contrast to the Atlantic and the Galapagos spreading axes, the fault blocks are symmetrical horsts and grabens rather than asymmetrical half-grabens (Lonsdale 1977b). Numerous sulphide deposits of high-temperature origin (*c.* 370°C) have been discovered on the EPR at 21°N. The active vents are located in a linear zone 200–300 m wide right on the spreading axis. The sulphides sampled by Francheteau *et al.* (1979) were found in small faulted depressions about 700 m from the axis, with notional ages of 10–20,000 years.

Discussion

Profiles of basement topography on the rift flanks are compared in Fig. 4. The slow-spreading TAG area, with huge fault throws and exposed plutonic rocks, and the fast-spreading EPR, with symmetrical block-faulting are not compatible with the area mapped. The FAMOUS area, and the intermediate spreading axes of the Galapagos

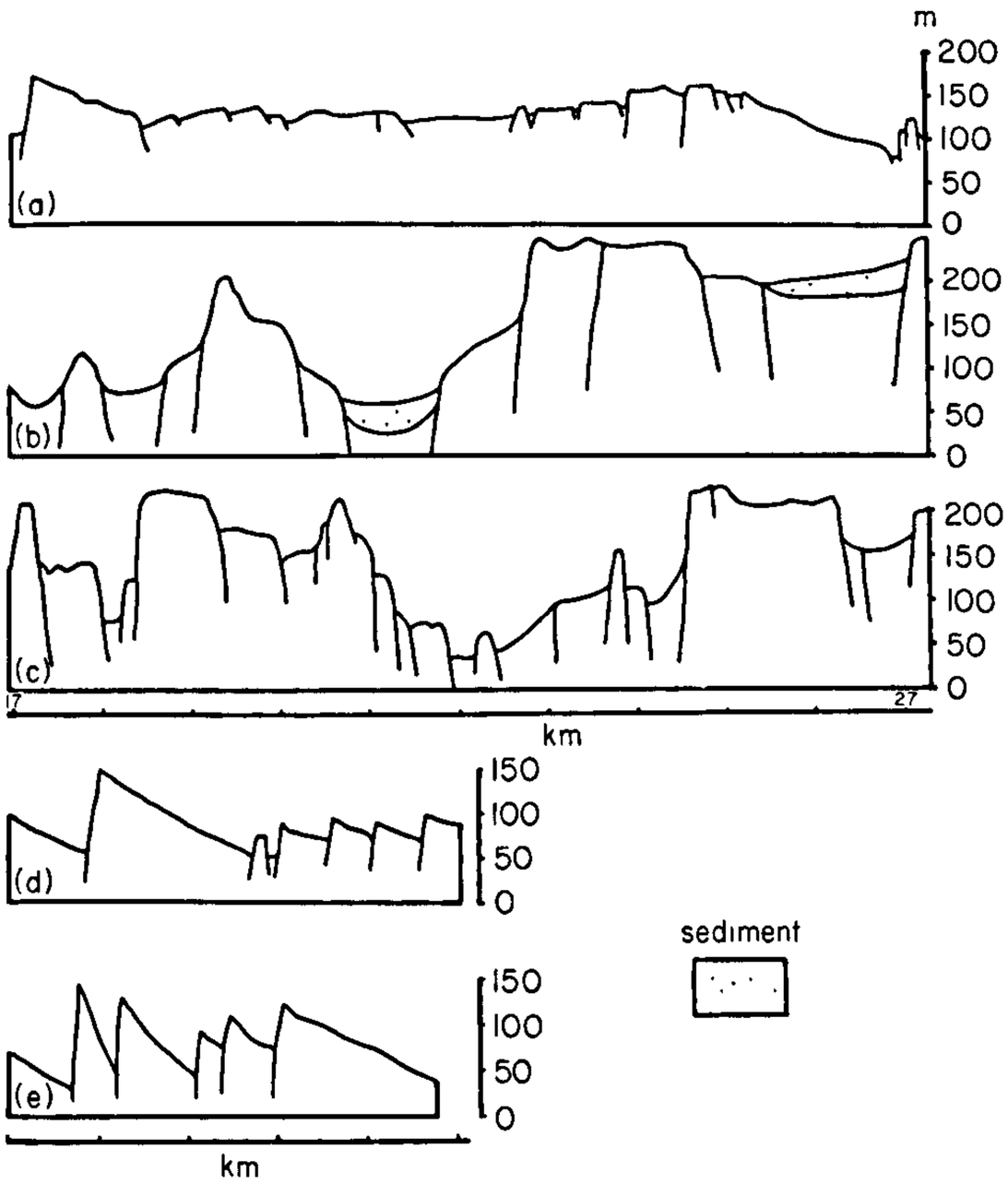

FIG. 4. Comparisons of the topography of modern spreading axes with those inferred from the Mathiati–Margi area of Cyprus. (a) Galapagos (Lonsdale 1977a); (b) FAMOUS area (Macdonald & Luyendyk 1977); (c) East Pacific Rise (Lonsdale 1977b). A–C are shown for 17–27 km from the spreading axis on the ridge flanks. D–E style of basement topography inferred for Cyprus at an equivalent distance from the axis. In each case the ridge is to the left.

and Juan de Fuca ridges which have asymmetrical block-faulting and lower relief compare more closely. The maximum estimated fault-controlled relief of *c.* 160 m for the mapped area compares with 500 m for the FAMOUS area, *c.* 100 m for the Galapagos and 30 m for the Juan de Fuca spreading axes. In modern spreading axes the median-valley walls are uplifted on ridge-parallel faults, apparently in contrast with the two directions of faulting in the Mathiati–Margi area. It is however clear that the area mapped is not large enough to allow a more confident comparison with modern-ridge morphology to be made.

On modern spreading axes the bulk of the lava pile is produced in a narrow relatively unfaulted volcanically active zone around 2 km across where topography is largely controlled by volcanism (Lonsdale 1977a, b; Ballard & van Andel 1977; Ballard *et al.* 1981, 1982). Consistent with earlier interpretations (Smewing *et al.* 1975; Robertson & Fleet, 1976) we envisage the A and B lava units of the Mathiati–Margi area (Lower Pillow Lavas) as having been erupted in a similar narrow, volcanically controlled, axial zone. The massive and pillowed flows were erupted from fissures with little vertical relief. Eruption rates were high enough to preclude much accumulation of pelagic sediments, in contrast, for example, with the higher levels of the extrusive succession of the Semail ophiolite, Oman, which contain pelagic chalks in addition to metalliferous oxide-sediments (Fleet & Robertson 1980). The dispersed sediments in Cyprus consist of mixed-background pelagic sediment and metalliferous oxide-sediment which was hydrothermally precipitated from vents, possibly originating as fine sulphide particles. Volcanism ceased and, as the area moved off the axis still within the axial valley, currents were sufficiently active to erode lava to form a laterally continuous thin blanket of volcaniclastic sediment over a wide area of relatively flat sea floor.

Massive sulphides in the ocean have to date

only been discovered on the Pacific spreading axes. All of the high-temperature vents (*c.* 370°C) are located on the youngest lavas on the spreading axis. Some inactive sulphides are found near major scarps at the edges of the median valley as in the Galapagos rift (Skirrow & Coleman 1982) and the Juan de Fuca ridge (Normark *et al.* 1983). These could either be fossil sulphides transported away from the axis, or else could have formed near the walls of the median valley where greater fracturing and permeability might have favoured hydrothermal discharge (Normark *et al.* 1983). Sulphides formed at the spreading axis are likely to be rapidly buried by later lavas and thus would be expected to be located low in a hypothetical vertical succession of axial lavas. This contrasts with the Mathiati–Margi area, where the massive sulphides are located on top of the lavas interpreted as having formed in the axial valley prior to major faulting. In this regard the sulphides seem to differ somewhat in location from the known 'black smokers' which are more axial. Constraints on the actual distance from the axis that the Cyprus massive sulphides were deposited can be inferred from modern examples, assuming that they were deposited beyond the axial volcanic zone but inside the axial valley. Maximum development of the rift-valley walls is achieved at 10 km from the axis at the FAMOUS area, *c.* 4 km at the Galapagos rift, and *c.* 1.5 km at the Juan de Fuca rift. No sulphides have been found on the slow-spreading axes, so a realistic maximum distance for sulphide formation is *c.* 4 km.

The later C and D unit lavas in the Mathiati–Margi area were erupted during a period of intense fault rotation and differential uplift which can be intrepreted as the construction of the rift-valley walls. The site of eruption would thus be at the margins of the axial graben rather than for example some distance out on the flanks of the ridge. To date, off-axis extrusion has been reported only in the FAMOUS area, but these extrusions are more evolved than their axial counterparts (Bryan & Moore 1977), in contrast with the Troodos. In many parts of the Troodos Massif the traditional Upper Pillow Lava–Lower Pillow Lava break is less marked or apparently absent which could imply either that the later lavas were more nearly axial or that the median valley was less well defined.

Off-axis hydrothermal activity is known from the TAG and the Galapagos mounds area. The TAG hydrothermal vents, now inactive, produced MnO_2 deposits which are located on the inner walls of the rift, 10–12 km from the axis, on crust *c.* 1 m.y. old (Rona *et al.* 1976). In the Galapagos area, the well-known hydrothermal mounds are sited along fractures 20–30 km away from the spreading axis on crust 500,000–700,000 years old, outside the main tectonic zone (Lonsdale 1977a). Unlike the Cyprus umbers, the hydrothermal solutions which formed the mounds percolated through 20–30 m of pelagic carbonate formed beneath a high productivity zone. The umbers are chemically rather less akin to the Galapagos mounds than they are to the EPR crestal sediments (Boström & Peterson 1969), but this may be due in part to the modifying effects of the underlying pelagic sediment at Galapagos (Corliss *et al.* 1978). However, the location is analogous, suggesting that active hydrothermal exhalation precipitating the umbers could have operated in crust up to 0.5–1 m.y. old and up to 30 km from the axis. A minimum distance, given that formation post-dated rift-valley construction, is 4 km. The overlying metal-enriched pelagic clays then formed further from the spreading axis with a hydrogenous component related to the spreading axis.

The question remains as to why the Mathiati–Margi area is one of a number of areas of the Troodos which are metal-enriched at all levels of the extrusives. Although these sediments accumulated close to a major fault, there are plenty of other highly faulted areas of the Troodos which are devoid of mineralization. Modelling of convective circulation by Spooner (1977) has demonstrated the need for local thermal anomalies to impose spatial stability, and he pointed out that large magma chambers would act in this way. Theoretical considerations of the thermal budget of the hydrothermal 'smokers' indicate that the heat source needed to sustain hydrothermal discharge at 370°C must involve magma crystallization (Strens & Cann 1982), which thus implies the existence of magma chambers under the 'smokers'. Even after freezing, magma chambers would remain thermal anomalies which could localize cooler hydrothermal circulation after they had moved off-axis. Unfortunately, no relationship between the plutonic rocks and extrusive sequence can be established in the area mapped. Regardless of the mechanism, however, the localization of hydrothermal sediments at particular sites in the Troodos ophiolite indicates a local persistence of hydrothermal metallogenesis not yet demonstrated at modern spreading axes.

A further point is that the close integration now possible of all the Troodos lavas and sediments into the evolution of spreading axis offers no obvious support for earlier suggestions that the Upper Pillow Lavas formed in some separate tectonic setting from the Lower Pillow Lavas, e.g.

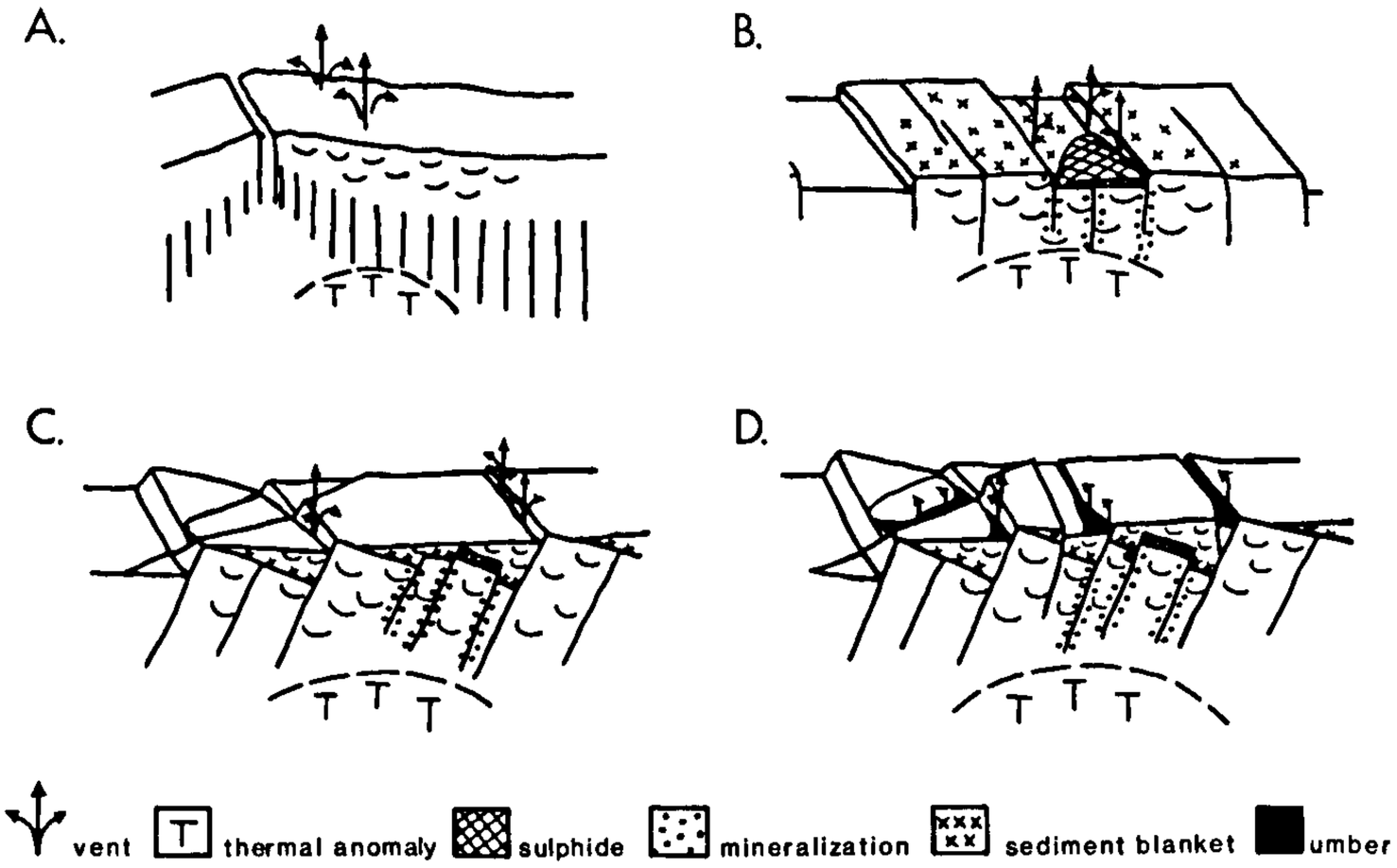

FIG. 5. Summary of evolving Troodos metallogenesis. (a) Axial volcanic zone. Rapid lava extrusion dilutes hydrothermal iron-oxide and background pelagic sediments. (b) Details of part of rift-floor towards the rift walls. Sulphides form together with volcaniclastic sediment during a pause in volcanism. (c) Rift valley wall. Here normal faulting and rotation is accompanied by renewed volcanism. (d) The ridge flanks. After cessation of faulting, the umbers accumulate in fault hollows, which later fill with metal-rich clays and more normal pelagic sediments.

as an off-axis seamount (Gass & Smewing 1973) or as an incipient island arc (Pearce 1975).

Conclusions

The combined field observations and the comparisons with the modern oceans show that the volcanic and structural development of the Mathiati–Margi area of the eastern Troodos Massif (Upper Cretaceous) is compatible with formation at an intermediate spreading rate axis with a well-defined axial graben, as illustrated in Fig. 5. The bulk of the lava pile was erupted on an area of relatively flat sea floor in the axial part of the median valley (traditional Lower Pillow Lavas). During a pause in volcanism submarine erosion produced a thin layer of volcaniclastic sediments. The massive sulphides accumulated in small fault-controlled depressions towards the walls of the axial graben, with a halo of Fe-Mn oxide-sediments. Ferruginous oxides dispersed throughout the lava pile are possibly drifted products of high-temperature sulphide vents.

The walls of the median valley were constructed by two phases of normal faulting, of which the second accompanied the eruption of the later more mafic lavas (traditional Upper Pillow Lavas). The Fe-Mn oxide-sediments, the umbers, were then precipitated in small fault-controlled hollows near the crest of the ridge flanks. Later, as the spreading axis migrated away, pelagic clays accumulated which were enriched in metals by hydrogenous processes, followed by pelagic chalk deposition.

Analogy with modern intermediate-rate spreading axes suggests an axial volcanic zone *c.* 2 km across within an 3–8 km wide rift valley. The inferred origin of most, if not all, the Cyprus massive sulphides above the highest axial lavas differs somewhat from the 'smokers' of modern Pacific spreading axes which mostly appear to have formed immediately on the axis. By analogy with the Galapagos mounds the umbers accumulated on crust of less than 1 Ma, up to several tens of kilometres from the axis. The persistence of both sulphide- and oxide-sediment formation throughout the lava pile in some areas of Cyprus implies a record of continuing hydrothermal activity from the axis to ridge flanks on particular areas of crust. This feature has not yet been reported in the oceans.

ACKNOWLEDGMENTS: The authors wish to thank G. Constantinou and the members of the International Deep Crustal Research Group for helpful discussion in the field. JFB was supported by an NERC studentship; AHFR by Edinburgh University.

References

ADAMIDES, N. G. 1980. The form and environment of formation of the Kalavasos ore deposits—Cyprus. *In*: PANAYIOTOU, A. (ed.) *Ophiolites. Proc. Int. Ophiolite Symp.*, Cyprus, 117–27.

BALLARD, R. D. & VAN ANDEL, Tj. H. 1977. Morphology and tectonics of the inner rift valley at lat. 37°50'N on the Mid-Atlantic Ridge. *Geol. Soc. Am. Bull.* **88**, 507–30.

—— & MOORE, J. G. 1977. *Photographic Atlas of the Mid-Atlantic Ridge Rift Valley*. Springer-Verlag, New York, 114 pp.

——, VAN ANDEL, Tj. H. & HOLCOMB, R. T. 1982. The Galapagos rift 86°W. Variations in volcanism, structure and hydrothermal activity along a 30-kilometer segment of the rift valley, *J. Geophys. Res.* **87**, 1149–61.

——, FRANCHETEAU, J., JUTEAU, T., RANGAN, C. & NORMARK, W. 1981. East Pacific Rise at 21°N: the volcanic, tectonic and hydrothermal processes of the central axis. *Earth Planet. Sci. Lett.* **55**, 1–10.

BEAR, L. M. 1960. The geology and mineral resources of the Akaki-Lythrodondha area, *Cyprus Geol. Surv. Dept. Mem.* **3**, 60 pp.

BOSTRÖM, K. & PETERSON, M. N. A. 1969. The origin of aluminium-poor ferromanganoan sediments in areas of high heat flow on the East Pacific Rise. *Marine Geol.* **7**, 427–47.

BRYAN, W. B. & MOORE, J. G. 1977. Compositional variations of young basalts in the Mid-Atlantic Ridge rift valley near lat. 36°49'N, *Geol. Soc. Am. Bull.* **88**, 556–70.

CONSTANTINOU, G. 1980. Metallogenesis associated with Troodos Ophiolite. *In*: PANAYIOTOU, A. (ed.) *Ophiolites, Proc. Int. Ophiolite Symp.*, Cyprus, pp. 663–74.

—— & GOVETT, G. J. S. 1972. Genesis of sulphide deposits, ochre and umber of Cyprus. *Trans. Inst. Min. met.* **81**, B34–46.

—— & —— 1973. Geology, geochemistry and genesis of Cyprus sulphide deposits. *Econ. Geol.* **68**, 843–58.

CORLISS, J. B., LYLE, M., DYMOND, J. & CRANE, K. 1978. The chemistry of hydrothermal mounds near the Galapagos Rift. *Earth Planet. Sci. Lett.* **40**, 12–24.

EDMOND, J. M., VON DAMM, K. L., MCDUFF, R. E. & MEASURES, C. I. 1982. Chemistry of hot springs on the East Pacific Rise and their effluent dispersal. *Nature, Lond.* **297**, 187–91.

FLEET, A. J. & ROBERTSON, A. H. F. 1980. Ocean ridge metalliferous and pelagic sediments of the Semail Nappe, Oman. *J. Geol. Soc. Lond.* **137**, 403–22.

FRANCHETEAU, J., NEEDHAM, H. D., CHOUKROUNE, P., JUTEAU, T., SÉGURET, M., BALLARD, R. D., FOX, P. J., NORMARK, W., CARRANZA, A., CORDOBA, D., GUERRERO, J., RANGIN, C., BOUGAULT, P., CAMBON, P. & HEKINIAN, R. 1979. Massive deep-sea sulphide ore deposits discovered on the East Pacific Rise. *Nature, Lond.* **277**, 523–8.

GASS, I. G. 1960. The geology and mineral resources of the Dhali area. *Cyprus Geol. Survey Dept. Mem.* **4**, 116 pp.

—— 1968. Is the Troodos Massif of Cyprus a fragment of Mesozoic ocean floor? *Nature, Lond.* **220**, 39–42.

—— 1980. The Troodos Massif: its role in the unravelling of the ophiolite problem and its significance in the understanding of constructive plate margin processes. *In*: PANAYIOTOU, A. (ed.) *Ophiolites, Proc. Int. Ophiolite Symp.* Cyprus, pp. 23–35.

—— & SMEWING, J. D. 1973. Intrusion, extrusion and metamorphism at constructive margins: Evidence from the Troodos Massif, Cyprus, *Nature, Lond.* **242**, 26–9.

HEATON, T. H. E. & SHEPPARD, S. M. F. 1977. Hydrogen and oxygen isotope evidence of sea-water-hydrothermal alteration and ore deposition, Troodos complex, Cyprus, *Geol. Soc. London Spec. Publ.* **7**, 42–57.

HOFFERT, M., PERSEIL, A., HEKINIAN, R., CHOUKROUNE, P., NEEDHAM, H. D., FRANCHETEAU, J. & LE PICHON, X. 1978. Hydrothermal deposits sampled by diving saucer in Transform Fault 'A' near 37°N on the Mid-Atlantic Ridge, FAMOUS area. *Oceanol. Acta* **1**, 73–86.

KIDD, R. D. W. & CANN, J. R. 1974. Chilling statistics indicate an ocean floor spreading origin for the Troodos complex, Cyprus. *Earth Planet. Sci. Lett.* **24**, 151–5.

LONSDALE, P. 1977a. Deep-tow observations at the mounds abyssal hydrothermal field, Galapagos Rift. *Earth Planet. Sci. Lett.* **36**, 92–110.

—— 1977b. Structural geomorphology of a fast-spreading rise crest: the East Pacific Rise near 3°25'S. *Mar. Geophys. Res.* **3**, 251–93.

MACDONALD, K. C. & LUYENDYK, B. P. 1977. Deep-tow studies of the Mid-Atlantic Ridge crest near lat. 37°N. *Geol. Soc. Am. Bull.* **88**, 621–36.

MOORES, E. M. & VINE, F. J. 1971. The Troodos massif, Cyprus and other ophiolites as oceanic crusts evaluation and implications. *Roy. Soc. London Philos. Trans.* **A268**, 433–66.

NORMARK, W. R., MORTON, J. L., KOSKI, R. A. & CLAQUE, D. A. 1983. Active hydrothermal vents and sulphide deposits on the southern Juan de Fuca ridge. *Geology* **11**, 158–63.

PEARCE, J. A. 1975. Basalt geochemistry used to investigate past tectonic environments on Cyprus. *Tectonophysics* **25**, 41–67.

—— 1980. Geochemical evidence for the genesis and eruptive setting of lavas from Tethyan ophiolites. *In*: PANAYIOTOU, A. (ed.) *Ophiolites, Proc. Int. Ophiolite Symp.* Cyprus, pp. 261–72.

ROBERTSON, A. H. F. 1975. Cyprus umbers: basal-sediment relationships on a Mesozoic ocean ridge. *J. Geol. Soc. Lond.* **131**, 511–31.

—— 1976. Origin of ochres and umbers: evidence from Skouriotissa, Troodos Massif, Cyprus. *Trans. Inst. Min. Met.* **85**, B245–51.

—— 1978.. Metallogenesis along a fossil oceanic fracture zone: Arakapas fault belt. Troodos Massif, Cyprus. *Earth Planet. Sci. Lett.* **41**, 317–29.

—— & FLEET, A. J. 1976. The origins of rare earths in

metalliferous sediments of the Troodos Massif, Cyprus. *Earth Planet. Sci. Lett.* **28**, 385–94.

—— & HUDSON, J. D. 1973. Cyprus umbers: Chemical precipitates on a Tethyan ocean ridge. *Earth Planet. Sci. Lett.* **18**, 93–101.

—— & —— 1974. Pelagic sediments in the Cretaceous and Tertiary history of the Troodos Massif, Cyprus. *Spec. Publ. Int. Assoc. Sedimentol.* **1**, 403–36.

—— & WOODCOCK, N. H. 1980. Tectonic setting of the Troodos Massif in the East Mediterranean. *In*: PANAYIOTOU, A. (ed.) *Ophiolites, Proc. Int. Ophiolite Symp.* Cyprus, 36–49.

ROBINSON, P. T. & GIBSON, I. L. 1983. Cyprus Crustal Study Project Hole CY-1 Lithological unit summaries. Unpublished report, University of Waterloo, Waterloo, Ontario, Canada.

RONA, R. A., HARBISON, R. N., BASSINGER, B. G., SCOTT, R. B. & NALWALK, A. J. 1976. Tectonic fabric and hydrothermal activity of Mid-Atlantic Ridge, Lat. 26°N. *Geol. Soc. Am. Bull.* **87**, 661–74.

SCHMINCKE, H. & RAUTENSCHLEIN, M. 1982. Volcanology along the Kamara Potamos. Unpublished report.

SIMONIAN, K. O. & GASS, I. G. 1978. Arakapas fault belt Cyprus: A fossil transform belt, *Geol. Soc. Am. Bull.* **89**, 1220–30.

SKIRROW, R. & COLEMAN, M. L. 1982. Origin of sulphur and geothermometry of hydrothermal sulphides from the Galapagos rift, 86°W, *Nature, Lond.* **229**, 142–4.

SMEWING, J. D., SIMONIAN, K. O. & GASS, I. G. 1975. Metabasalts from the Troodos Massif, Cyprus: genetic implication deduced from petrology and trace element composition. *Contrib. Min. Pet.* **51**, 49–64.

SPOONER, E. T. C. 1977. Hydrothermal model for the origin of the ophiolitic cupriferous pyrite ore deposits of Cyprus. *Geol. Soc. London Spec. Publ.* **7**, 58–71.

STRENS, M. R. & CANN, J. R. 1982. A model of hydrothermal circulation in fault zones at mid-ocean ridge crests. *Geophys. J. R. astr. Soc.* **71**, 225–40.

WILSON, R. A. M. 1959. The geology of the Xeros-Troodos area. *Cyprus Geol. Surv. Dept. Mem.* **1**, 73 pp.

J. F. BOYLE & A. H. F. ROBERTSON, Grant Institute of Geology, University of Edinburgh, West Mains Road, Edinburgh EH9 3JW, Scotland.